Planetary and Space Science

Volume 1 1959

Editor-in-Chief: MILTON GREENBERG

Regional Editors:

D. F. MARTYN
S. K. MITRA
M. NICOLET
A. I. LEBEDINSKY
C. E. PALMER
F. L. WHIPPLE

PERGAMON PRESS

NEW YORK · LONDON · PARIS · LOS ANGELES

Planetary and Space Science

NOTES FOR CONTRIBUTORS

1. Only papers not previously published will be accepted, and emphasis is placed upon originality of concept or observation. The text should be clear and concise, and a technical description of the methods used should be given in detail only when the methods are new.

2. The Editor-in-Chief requests that short *Research Notes* for which rapid publication is desired should be sent directly to him at Geophysics Corporation of America, 700 Commonwealth Avenue, Boston 15, Massachusetts, U.S.A. *Research Notes should be in English, without illustrations, and no longer than four double-spaced typewritten pages.*

3. Other contributions (Research Papers and Critical Surveys) should be sent initially to one of the other editors near the author: in the *Southern Hemisphere*, to Dr. D. F. Martyn, Radio Research Laboratories, CSIRO, Camden, New South Wales, Australia; in the *Far East*, to Prof. S. K. Mitra, F.R.S., Institute of Radiophysics and Electronics, University of Calcutta, India; in *Europe*, to Dr. M. Nicolet, c/o Service du Rayonnement, 3 Avenue Circulaire, Uccle, Belguim; in *Eastern North America*, to Dr. Fred L. Whipple, Astrophysical Observatory, 60 Garden Street, Cambridge 38, Massachusetts; in *Western North America*, to Prof. C. E. Palmer, Institute of Geophysics, University of California, Los Angeles 24, California; and in the *Soviet Union*, to Prof. A. I. Lebedinsky, Physical Department, Moscow State University, Moscow, U.S.S.R.

4. Submission of two typescripts (an original and a carbon copy) will facilitate refereeing; if one only is submitted, it should be the original. The author should retain a copy for his own use. The text should be ready for setting in type and should be carefully checked for errors. Scripts should be typed on one side of the paper with double or triple spacing.

5. Illustrations may accompany Research Papers and Critical Surveys but should be restricted to the minimum necessary, and must accompany the typescript mounted on separate sheets. Photographs should be enlarged sufficiently to permit clear reproduction (about 8 by 10 inches). If words or numbers appear in photographs, two copies should be sent, one with clear printing and the other without inscription. Line drawings which require redrawing should include all relevant details. Any lettering should be large and bold enough to be legible after the diagram has been reduced in size for printing. Captions or legends should be given on a separate sheet and labelled to show which illustrations each is to accompany.

6. Proofs will be sent to authors for correction, and fifty free reprints of each paper will be provided. Additional reprints should be ordered when the proofs are returned by the author. Otherwise, it may not be possible to furnish them at a reasonable price. A reprint order form will accompany the proofs.

7. References are indicated in the text by superior numbers in parentheses, and the full reference should be given in a list at the end of the paper in the following form:

1. Y. TANAKA, *J. Chem. Phys.* **22**, 2045 (1954).
2. P. MOORE, *The Planet Venus*, p. 84. Faber and Faber, London (1957).

and should include the usual abbreviated title of the journal, the volume number, the page number and year, in that order.

Footnotes, as distinct from literature references, should be indicated by the following symbols—*, †, ‡, ‡‡, commencing anew on each page; they should *not* be included in the numbered reference system.

8. The language preferred is English, but papers may be published in other languages from time to time. An abstract of not more than 200 words, giving the essential contents of the paper should be provided by the author, if possible in English; but the abstract may be submitted in the language of the paper, for translation into English by the editorial staff.

9. To conserve space, authors are requested to mark the less important parts of the paper (such as records of experimental results) for printing in smaller type. For long papers (over 12 double-spaced typewritten pages) sections which could be deleted without destroying either the sense or the continuity of the paper should be indicated as a guide for the editors.

CONTENTS

NUMBER 1

Foreword 1

International New—COSPAR 2

J. E. KUPPERIAN, Jr., E. T. BYRAM, T. A. CHUBB and H. FRIEDMAN: Far ultra-violet radiation in the night sky 3

Y. TANAKA, A. S. JURSA, F. J. LEBLANC and E. C. Y. INN: Spectroscopic study of the afterglows of N_2 and (N_2+O_2) in the vacuum region 7

V. I. KRASSOVSKY: Energy sources of the upper atmosphere 14

I. HARRIS and R. JASTROW: An interim atmosphere derived from rocket and stellite data . . 20

E. R. MANRING: Micrometeorite measurements from 1958 Alpha and Gamma satellites . . 27

G. NEWKIRK, Jr.: The airglow of Venus 32

I. HARRIS and R. JASTROW: Re-entry of the Sputnik I rocket 37

O. OLDENBERG: A short duration afterglow of nitrogen; survey of afterglows 40

J. W. WARWICK: Decay of spin in Sputnik I 43

J. P. CASTELLI, J. AARONS, C. FERIOLI and J. CASEY: Absorption refraction and scintillation measurements at 4700 mc/s with a travelling-wave tube radiometer 50

G. I. GALPERIN: Hydrogen emission and two types of auroral spectra 57

I. S. SHKLOVSKY: On hydrogen emission in the night glow 63

E. L. FIREMAN: The distribution of helium-3 in the Grant meteorite and a determination of the original mass 66

W. W. KELLOGG: IGY rockets and satellites: a report on the Moscow Meetings, August 1958 . 71

NUMBER 2

S. N. VERNOV, A. E. CHUDAKOV, E. V. GORCHAKOV, J. L. LOGACHEV and P. V. VAKULOV: Study of the cosmic-ray soft component by the 3rd Soviet Earth Satellite 86

W. G. ELFORD: A study of winds between 80 and 100 km in medium latitudes 94

L. HARANG and J. TRÖIM: An example of heavy absorption in the VHF-band in the Arctic ionosphere 102

J. V. JELLEY: Čerenkov radiation in the atmosphere 105

R. A. DUNCAN: Polarization of the red oxygen auroral line 112

H. K. PAETZOLD: Observations of the Russian satellites and the structure of the outer terrestrial atmosphere 115

E. L. MURRAY: Ambipolar diffusion of a meteor trail and its relation with height 125

A. N. KAZANTSEV: Absorption and electron distribution in the F_2 layer determined from measurements of transmitted radio signals from earth satellites 130

G. F. SCHILLING and C. A. WHITNEY: Derivation and analysis of atmospheric density from observations of Satellite 1958 Epsilon 136

DIRAN DEIRMENDJIAN and E. H. VESTINE: Some remarks on the nature and origin of noctilucent cloud particles 146

NUMBER 3

I. ESCOBAR V., N. NERURKAR and R. WEIL: Sidereal anisotrophy of high energy cosmic rays . 155

A. S. JURSA, Y. TANAKA and F. LEBLANC: Nitric oxide and molecular oxygen in the earth's upper atmosphere 161

H. NORINDER and E. KNUDSEN: The relation between lightning discharges and whistlers . . 173

J. W. SIRY: Satellite orbits and atmospheric densities at altitudes up to 750 km obtained from the Vanguard Orbit Determination Program 184

B. HULTQVIST and J. ORTNER: Strongly absorbing layers below 50 km 193

M. Bossolasco and A. Elena: On some characteristics of the E_s-layer 205
P. G. Mezger and H. Strassl: The thermal radiation of the moon at 1420 Mc/s . . . 213
F. F. Marmo, L. M. Aschenbrand and J. Pressman: Artificial electron clouds—I Summary report on the creation of artificial electron clouds in the upper atmosphere 227
W. C. Hoffman: A report on the symposium on the use of space vehicles at the fall 1958 URSI meeting 238
International News
Second meeting of the *ad hoc* Committee on Contamination by Extra-Terrestrial Exploration . 249

NUMBER 4

G. R. A. Ellis: Low frequency electromagnetic radiation associated with magnetic disturbances 253
K. W. Champion and R. A. Minzner: Atmospheric densities from satellites and rocket observation 259
K. L. Coulson: Characteristics of the radiation emerging from the top of a Rayleigh atmosphere—I 265
K. L. Coulson: Characteristics of the radiation emerging from the top of a Rayleigh atmosphere—II 272
E. H. Vestine and W. L. Sibley: Lines of force of the geomagnetic field in space 285
F. F. Marmo, J. Pressman and L. M. Aschenbrand: Artificial electron clouds—II General considerations 291
F. F. Marmo, L. M. Aschenbrand and J. Pressman: Artificial electron clouds—III Release of atomic potassium at 121 kilometers 306
K. D. Cole: Electro-hydromagnetic waves in a fully ionized gas—I 319
A. Maxwell, A. R. Thompson and G. Garmire: The association of solar radio bursts with auroral streams 325
W. E. Groth and H. Schierholz: The photolysis of nitrous oxide in the far ultraviolet . . 333
A. Rosen, P. J. Coleman, Jr. and C. P. Sonett: Ionizing radiation detected by Pioneer II . 343

AUTHOR INDEX TO VOLUME I

Aarons, J. 50
Aschenbrand, L. M. 227, 291, 306
Bossolasco, M. 205
Byram, E. T. 3
Casey, J. 50
Castelli, J. P. 50
Champion, K. W. 259
Chubb, T. A. 3
Chudakov, A. E. 86
Cole, K. D. 319
Coleman, Jr., P. J. 343
Coulson, K. L. 265, 272
Deirmendjian, D. 146
Duncan, R. A. 112
Elena, A. 205
Elford, W. G. 94
Ellis, G. R. A. 253
Escobar V., I. 155
Ferioli, C. 50
Fireman, E. L. 66
Friedman, H. 3
Galperin, G. I. 57
Garmire, G. 325
Gorchakov, E. V. 86
Groth, W. E. 333
Harang, L. H. 102
Harris, I. 20, 37
Hoffman, W. C. 238
Hultqvist, B. 193
Inn, E. C. Y. 7
Jastrow, R. 20, 37
Jelley, J. V. 105
Jursa, A. S. 7, 161
Kazantsev, A. N. 130
Kellogg, W. W. 71
Krassovsky, V. I. 14
Knudsen, E. 173
Kupperian, Jr., J. E. 3
LeBlanc, F. J. 7, 161
Logachev, J. L. 86
Manring, E. R. 27
Marmo, F. F. 227, 291, 306
Maxwell, A. 325
Minzner, R. A. 259
Mezger, P. G. 213
Murray, E. L. 125
Nerurkar, N. 155
Newkirk, Jr., G. 32
Norinder, H. 173
Oldenberg, O. 40
Ortner, J. 193
Paetzold, H. K. 115
Pressman, J. 277, 291, 306
Rosen, A. 343
Schierholz, H. 333
Schilling, G. F. 136
Shklovsky, I. S. 63
Sibley, W. L. 285
Siry, J. W. 184
Sonett, C. P. 343
Strassl, H. 213
Tanaka, Y. T. 161
Thompson, A. R. 325
Tröim, J. 102
Vakulov, P. V. 86
Vernov, S. N. 86
Vestine, E. H. 146, 285
Warwick, J. W. 43
Weil, R. 155
Whitney, C. A. 136

VO
1
19

FOREWORD

THE launching of the first Sputnik in October 1957 marked one of the greatest scientific and technological achievements of man. By providing astronomers and physicists with a means of carrying their instruments away from our earthbound environment it opened a new epoch in scientific investigations. The regions of interplanetary space with their complex of particles and radiations can now be studied directly and soon we can look forward to aequiring more intimate knowledge of the nearer planets.

The earth satellite and the space probe represent the climax of the great developments in technique for the exploration of the solar system which have occurred during the last decade. Improved astronomical techniques, rockets and radio astronomy have already increased our knowledge of our immediate environment in space to an extent which would have been unimaginable a few years ago. The vast accumulation of new data needs new openings for publication on an international scale. This new journal *Planetary and Space Science* will help to fulfil this need, by providing a medium for the publication of original work on the upper regions of the earth's atmosphere, the planets, interplanetary space and all related problems.

A. C. B. LOVELL

COSPAR

I have pleasure in bringing to your attention the following Notice concerning the International Committee on Space Research, which I have received from its President, Professor H. C. van de Hulst.

M. GREENBERG.

THE Committee on Space Research (COSPAR) set up by the International Council of Scientific Unions at its General Assembly, 2–6 October 1958, held its first meeting in London on 14–15 November 1958, as guests of the Royal Society. The following Charter was adopted:

"The purpose of COSPAR is to further on an international scale the progress of all kinds of scientific investigation which are carried out with the use of rockets or rocket-propelled vehicles. COSPAR shall be concerned with fundamental research. It will not normally concern itself with such technological problems as propulsion, construction of rockets, guidance and control.

"These objectives shall be achieved through the maximum developments of space research programs by the international community of scientists working through the ICSU and its adhering national academies and unions. Recognizing the need for international regulation and discussion of certain aspects of satellite and space probe programs, the Committee shall keep itself fully informed on United Nations or other international activities in this field, in order to assure that maximum advantage is accorded international space science research through such regulations, and to make recommendations relative to matters of planning and regulation that may effect the optimum program of scientific research.

"COSPAR shall report to ICSU those measures needed in the future to achieve the participation in international programs of space research of all countries of the world with those which are already actively engaged in research programs within the domain of COSPAR".

The composition of the Committee is as follows:

(a) A representative from each of the countries which are actually launching earth satellites, and also from those conducting fundamental researches using rockets;

(b) Three representatives, designated on an agreed system of rotation, from among countries actively participating in tracking and other aspects of space research;

(c) One representative each from the following Unions: IAU, IUGG, IUPAC, URSI, IUPAP, IUBS, IUTAM, IUPS and IUB.

The composition of the Executive Committee elected at the meeting is:

President: Professor H. C. van de Hulst, Leiden, Netherlands (IAU).

Vice-Presidents: Professor E. K. Fedorov, Moscow, U.S.S.R.
Professor W. A. Noyes, Jr., Rochester, New York, U.S.A.

Members: Professor Maurice Roy, Chatillon sous Bagneux, France (IUTAM).
Professor H. S. W. Massey, London, England (IUPAP).

A Secretariat has been established and may be addressed c/o ICSU Secretariat, Paleis Noordeinde, The Hague, Netherlands.

Both the charter and the membership show that COSPAR within its domain intends to serve science in the broadest sense of the word. Three of the Unions represented (those of the Biological Sciences, of the Physiological Sciences, and of Biochemistry) have connection with biological problems. The Charter further makes clear that COSPAR is not an agency that will initiate independent investigations in space research, nor a kind of governing body that has to approve whatever researches take place. Its main aim is to maintain the spirit of scientific co-operation that has been so fully displayed in a number of fields closely related to space research and to provide the meeting place for scientific initiatives from various sides. In order to fulfil its task COSPAR will form three working groups on "Tracking and transmission of scientific information", "Scientific experiments", and "Data and publications".

Planet. Space Sci. Pergamon Press 1959. Vol. 1, pp. 3–6. Printed in Great Britain.

FAR ULTRAVIOLET RADIATION IN THE NIGHT SKY*

J. E. KUPPERIAN, Jr., E. T. BYRAM, T. A. CHUBB and H. FRIEDMAN

U.S. Naval Research Laboratory, Washington 25, D.C.

(*Received* 2 *October* 1958)

Abstract—Rocket measurements have shown that the night sky is aglow with a diffuse Lyman-α (1216 Å) emission amounting to 10^{-2} erg $cm^{-2}sec^{-1}$ from the entire hemisphere. The glow was so bright that celestial sources of Lyman-α could not be detected through it. At wavelengths near 1300 Å discrete celestial sources were observed, which contributed 10^{-4} erg $cm^{-2}sec^{-1}$ from the entire sky in the wavelength interval 1225-1350 Å.

1. ROCKET MEASUREMENTS

SINCE the beginning of upper air research with rockets, astrophysical measurements have been confined almost exclusively to solar spectroscopy. In view of the success achieved in measuring the sun's ultraviolet and X-ray emission with photon counters we were encouraged to search for these radiations from celestial objects in the night sky. The sun is a comparatively weak star. Early blue-white stars are so much hotter than the sun that maximum brightness ought to occur in the far ultraviolet. A simple rocket experiment was attempted in November 1955 to determine the possibility of obtaining a map of stellar magnitudes in wavelengths of Lyman-α and the adjacent ultraviolet near 1300 Å. The observed fluxes were unexpectedly high and saturated the photon counters after they had penetrated only a few kilometers into the D-region. From that experiment it was possible to conclude that the major component of night-time ultraviolet fell within a wavelength band of 1050 Å to 1225 Å including the Lyman-α wavelength (1216 Å) and a lower limit of $3{\cdot}4 \times 10^{-4}$ erg cm^{-2} sec^{-1} was assigned as the flux[1]. At wavelengths between 1225 Å and 1350 Å discrete celestial sources were detected.

With these early results as a guide, a much more elaborate experiment[2] was carried out on 28 March 1957 with NRL Aerobee 31. The rocket was launched at 21.56 MST and reached an altitude of 146 km. The ultraviolet telescopes consisted of bundles of hypodermic tubings through which the sky could be viewed over an angular field of 3° by sensitive photon counters. With less sensitive detectors, such as ionization chambers, wider collimators were used providing fields as broad as 0·3 sterad. The detectors were mounted with their collimeters looking outward in directions normal to the rocket's long axis. A spatial scan of the sky was produced by the combined spin and yaw motions of the rocket. The rocket behaved in almost ideal fashion, approximating an arrow trajectory with horizontal attitude near the peak of the flight and rolling with a period of 16 sec. A broad scan of the sky was therefore obtained.

2. DISCRETE CELESTIAL SOURCES AT 1300 Å

Numerous sources were observed in the 1225 Å to 1350 Å region. The determination of the direction of view of each detector at each instant of flight is an exceedingly tedious job. It involves fitting together in a self-consistent manner the star signals from visible light photometers and positions of the visible airglow horizons. The end product of this analysis is a solution of the aspect problem with an accuracy of 1°, permitting the construction of a map of the ultraviolet sky near 1300 Å with a resolution of 3°. The brightest single source observed was the Orion complex which delivered about 2×10^{-3} erg cm^{-2} per sec at the top of the atmosphere.

* Presented at the Fifth CSAGI Assembly, Moscow, 30 July–9 August 1958.

3. LYMAN-α FROM THE NIGHT SKY

The detectors whose bandwidth included the Lyman–α line showed a very different picture of the sky. At an altitude of 75 km an intense glow, diffused over the entire sky, was seen above the rocket. At 85 km, an additional source became evident, originating in the atmosphere below the rocket. Both fluxes increased up to 120 km and then remained constant to the peak of the flight, 146 km. Both the atmospheric and extra-terrestrial sources of radiation have been identified with the Lyman–α emission of hydrogen. Furthermore, this radiation appears to be of solar origin; the flux from outside the atmosphere is scattered by atomic hydrogen in space; the flux from below the rocket is scattered a second time by hydrogen in our atmosphere. The observed albedo was about 42 per cent.

The average flux of Lyman–α from space was 3·2 erg cm^{-2} sec^{-1} per sterad. Fig. 1 is a polar plot of the intensity isophotes obtained with a detector collimated to view a field of 16° half-width. The center of the plot is the zenith. The minimum contour occurs in the anti-solar direction, i.e. looking directly away from the sun. This is a plot of the raw data and the effect of the unsubtracted 1300 Å radiation from Orion and the galactic plane can be seen in the West. From the presence of the minimum in the anti-solar direction we can conclude that the source of this radiation is the sun.

4. INTERPLANETARY AND ATMOSPHERIC HYDROGEN

That the influx of Lyman–α is scattered to the night side of the earth by neutral hydrogen in space is deduced from the high albedo of hydrogen in the earth's atmosphere. Lyman–α from the sun is a broadened emission line characteristic of the high temperature of the solar atmosphere. The scattering cross-section of the cold hydrogen for the solar line is small except for the very center of the line. As a

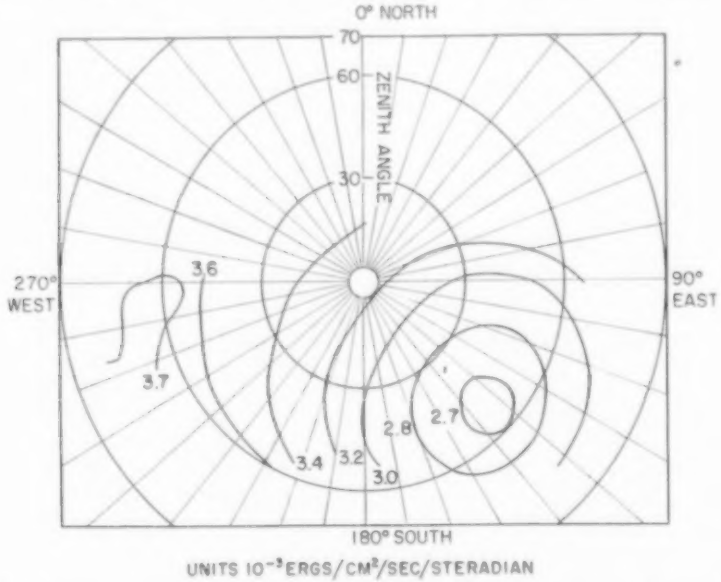

Fig. 1. Lyman-α directional intensity contours when the detector looked at the upper hemisphere. These data were obtained from the portion of the flight above 130 km and are uncorrected for the 1225 to 1350 A discrete sources. The smallest intensity contour circle contains the anti-solar direction.

consequence, the daytime albedo is barely detectable with the solar flux of Lyman–α directly incident on the atmosphere. On the other hand, if Lyman–α in the night sky is once scattered by neutral hydrogen atoms, it is monochromatized by the scattering process to include only the core of the original solar line. When this highly monochromatized radiation enters the denser hydrogen region of the earth's atmosphere near 80 km it is back-scattered with the observed albedo of 42 per cent.

Estimating the neutral hydrogen density of interplanetary space from these observations is complicated by our lack of detailed knowledge of factors such as the solar line profile and particularly its central intensity. From rocket spectrograms the half-width of the Lyman–α line appears to be less than 0·3 Å. However, the resolution of the spectrographic measurements is not adequate to define the true contour of the line or to reveal the presence of an absorption core at the line center. Since the scattering cross-section is a maximum at the line center and falls very rapidly toward the wings, the presence of an absorption core in the line center can profoundly affect the scattered intensity. The presence of a deep core can be inferred from the weak albedo (<2 per cent) of the earth's atmosphere when directly irradiated by solar Lyman–α. If the albedo of the atmosphere under direct illumination by solar Lyman–α were accurately known, the ratio of daytime and night-time albedos would permit us to estimate the effective scattering cross-section of the interplanetary gas and hence its temperature.

From the mere fact that the incoming distribution still shows a minimum when viewed from the earth (Fig. 1), one may deduce that the mean free path of a Lyman–α quantum before scattering is at least one astronomical unit (1 A.U. $= 1{\cdot}5 \times 10^{13}$ cm). If the distance were a small fraction of 1 A.U., multiple scattering would destroy any directionality in the radiation seen from the earth. If 1 A.U. reprsents unit optical depth in the core of the Lyman–α line, the neutral hydrogen density, η_H, can be estimated provided the scattering cross-section, σ, is known. The value of σ depends on the temperature of the interplanetary gas. The high albedo observed at night implies that the interplanetary gas cannot be much hotter than the hydrogen in the terrestrial atmosphere near the 85 km level. If we take $\sigma = 3 \times 10^{-13}$ cm^2 ($T \sim 400°$K) the corresponding value of η_H is about 0·2 per cm^3 which may be considered an upper limit.

Independent estimates of η_H have been made by I. S. Shklovsky[3] and by O. Struve[4] on the basis of the rocket measurement. Shklovsky, assuming a solar flux of 0·5 erg cm^{-2} sec^{-1} and the effective width of the solar line to be 0·2 Å, computes a density of 0·5 atoms per cm^3. Struve assumes a line width of 1 Å and a flux of 3 erg cm^{-2} sec^{-1} and finds $\eta_H = 0{\cdot}1$ per cm^3. If the scattering atoms originated in gas clouds emitted by the sun, we should expect a concentration toward the ecliptic plane. It was mentioned above that the scattering gas must be cold and both Shklovsky and Struve have also pointed out that the isophote contours of Fig. 1 are nearly circular. The evidence therefore does not indicate an extended hot coronal atmosphere as the scattering medium.

Shklovsky[3] has computed the flux of H_α that would be produced by excitation of the interplanetary hydrogen by Lyman–β. Absorption of Lyman–β raises a hydrogen atom to the quantum 3 state from which it may radiate H_α and Lyman–α. Taking the solar Lyman–β flux to be 1/40 Lyman–α, Shklovsky derives a ratio of the number of H_α quanta to Lyman–α quanta in the night sky. The expected intensity of H_α is 2×10^7 photons cm^{-2} sec^{-1} or 20 Rayleighs if the direct solar flux is 5 ergs cm^{-2} sec^{-1} at 1 A.U. and η_H is 0·5 cm^{-3}. The flux measured at Zvenigorod fluctuated from night to night between limits of 5 and 20 R. This agreement is as good as can be expected considering the uncertainties involved in the value of the Lyman–β flux and η_H.

5. THE PROTON DENSITY OF INTERPLANETARY SPACE

If the neutral hydrogen content and the solar flux below the Lyman limit are known, it is possible to compute the number of protons per cm^3 under conditions of ionization equilibrium.

The energy content of the ionizing solar flux may be distributed between the Lyman continuum, the He resonance lines at 304 Å and 584 Å and X-rays from 20 Å to 200 Å. At the Lyman limit the absorption cross-section is of the order of 10^{-17} cm^2. Towards shorter wavelengths the cross-section decreases inversely as the wavelength cubed. At the He II line (340 Å) the cross-section should be closer to 10^{-18} cm^2. Using the ionosphere as a gauge of the ionizing flux it can be shown that about 0·1 erg cm^{-2} sec^{-1} is adequate to produce an equilibrium density of 10^6 electrons cm^{-3} at the maximum of $F2$ region. Neglecting the possibility of electron loss by attachment to dust particles, the recombination of electrons and protons may be attributed to radiative recombination for which the coefficient, α, is about $1{\cdot}5 \times 10^{-12}$ cm^3 sec^{-1}. Accordingly, if we adopt $\eta_H = 0{\cdot}2$ cm^{-3} and a flux of 0·1 erg cm^{-2} sec^{-1}, the corresponding electron and proton densities lie between 15 and 45 depending on where the appropriate cross-section falls between the values 10^{-18} and 10^{-17} cm^2. If the true value of the solar flux is higher than 0·1 erg cm^{-2} sec^{-1} the resultant electron density will increase as the square root of the flux.

It is quite clear that much needs to be done experimentally before a more rigorous solution of the problem is possible. A measurement of the contour of the solar Lyman-α line with a resolution of about a hundredth of an Angstrom is essential. It is entirely possible to achieve this resolution in a rocket experiment. The daytime albedo needs to be accurately measured. The recent success of Rense[5] in photographing the spectrum below the Lyman limit has provided the first direct experimental evidence regarding the region from 300 Å to 910 Å. Although it may be difficult to determine absolute intensities from this spectrogram, there is little doubt that future attempts will lead to quantitative data that should permit an accurate assignment of the ionizing flux.

REFERENCES

1. Byram E. T., Chubb T. A., Friedman H. and Kupperian J. E. Jr. *The Threshold of Space*, pp. 203–209. Pergamon Press, London (1957).
2. Kupperian, J. E. Jr., Byram E. T., Chubb T. A. and Friedman H. *Bull. Amer. Phys. Soc.* Ser. II, 3, 222 (1958); *Ann. Géophys.* (In press.)
3. Shklovsky I. S. Paper presented at V General Assembly CSAGI, Moscow, August 1958.
4. Struve O. *Sky & Telesc.* 445 (1958).
5. Rense W. private communication.

Planet. Space Sci. Pergamon Press 1959. Vol. 1, pp. 7–13. Printed in Great Britain.

SPECTROSCOPIC STUDY OF THE AFTERGLOWS OF N_2 AND (N_2+O_2) IN THE VACUUM REGION

Y. TANAKA, A. S. JURSA, F. J. LeBLANC and E. C. Y. INN*

Geophysics Research Directorate, Air Force Cambridge Research Center, Air Research and Development Command, Laurence G. Hanscom Field, Bedford, Massachusetts

(*Received* 11 *August* 1958)

Abstract—Four different stages of afterglow can be observed when the O_2 partial pressure in a mixture of N_2 and O_2 is changed. A study was made of the relationship between the partial pressures of N_2 and O_2 for each individual stage. The absorption spectra of these glows in the vacuum region showed the presence of N, O, and NO, and measurements were made of the concentration of atomic nitrogen, $2p^3\ {}^4S$, $2p^3\ {}^2D$, $2p^3\ {}^2P$, in the nitrogen afterglow. The $a^1\Pi_g - X^1\Sigma_g^+$ bands of N_2 were observed in emission in the nitrogen afterglow. With consideration of both emission and absorption spectra, the reaction mechanisms are discussed briefly for each stage.

1. INTRODUCTION

As Kaplan suggested many years ago, there are similarities between the spectrum of the nitrogen afterglow and that of the aurora and night airglow. The study of the nitrogen afterglow, particularly the study of the mechanism of its excitation processes, therefore might lead to an understanding of these upper atmospheric phenomena. A brief description of the present work was presented at the conference on chemical aeronomy; however, we believe it worthwhile to report the results in detail.

Considerable experimental and theoretical work has been carried out in the last several decades concerning the nitrogen afterglow, and the reader is referred to a review of previous work presented in Mitra's book[1]. Recently, Cario and Reinecke[2] proposed a new theory for the mechanism of the afterglow, which was supported by Brook and Kaplan[3], by studying the effect of rare gases on the glow. More recently, Schiff[4], and Kistiakowsky[5] independently found atomic nitrogen in the afterglow, each using the mass spectrograph. The latter has suggested the so-called "two step process" for the glow mechanism.

The main purpose of the present work was to find active substances not only in the nitrogen afterglow but also in its modified stages produced by a condensed discharge of (N_2+O_2) by studying their absorption spectra in the vacuum region.

2. EXPERIMENTAL

The general procedure in producing the afterglow was essentially the same as described in a previous paper[6]. The tank N_2 was first allowed to flow at an arbitrary pressure ($1 \sim 13$ mm Hg); then, tank O_2 was added gradually to the flow until a desired stage of the glow filled the glow tube. The partial pressures of N_2 and O_2 were measured with a McLeod gauge attached to the glow tube about 20 cm from its inlet. Both a Hilger medium size quartz and a 2-meter vacuum spectrograph were used for recording the emission spectra.

In the absorption work, the glow was allowed to flow through the absorption cell, attached to the slit of the vacuum spectrograph, which was 8 cm in length and provided with thin LiF windows at each end. In most cases the rare gas continuum[7] was used as a background, but for the experiment on the determination of atomic nitrogen concentration, a condensed discharge of $(He+N_2)$, which is rich in NI-lines was adopted. Three groups of

* Present address: Naval Radiological and Defense Laboratory, San Francisco, California.

NI-lines at 1200, 1493, and 1743 Å were chosen for the measurement of the concentration of the N-atom in $2p^3\ ^4S$, $2p^3\ ^2D$, and $2p^3\ ^2P$ states respectively.* Because of the high concentration of the ^4S state, the cell length had to be reduced to 8 mm for an accurate absorption measurement for the 1200 Å line while for the ^2D and ^2P states an 800 mm cell was required.

Throughout the experiment, great care was taken to avoid the stray discharge from passing into the glow tube or the absorption cell.

3. RESULTS

Four stages of the afterglow, three of them known, can be produced simply by changing the partial pressure of O_2. They are distinctly different from one another in their color and their emission spectra as well. The relation between the partial pressures of N_2 and O_2

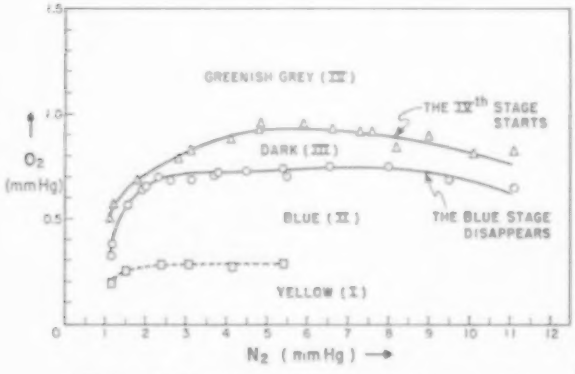

Fig. 1. Relation between the afterglow stages and partial pressure of N_2 and O_2.

required to produce the different stages is shown in Fig. 1. The observed spectra, in emission as well as in absorption, are summarized in Table 1 together with suggested reactions.

3.1. *The first stage* (*Lewis–Rayleigh afterglow; straw-yellow*)

When the N_2 was extremely pure†, its spectrum consisted only of the first positive bands exhibiting their well-known characteristic distribution of intensity. In the vacuum region, we found the $a^1\Pi_g - X^1\Sigma_g^+$ bands of N_2, but they were extremely weak.‡ The observed bands are listed in Table 2.

Table 2. The $a^1\Pi_g$–$X^1\Sigma_g^+$ Bands of N_2 Observed in the First Stage

v', v''	λ (Å)	I*	I†
1 1	1464·1	1	8
0 1	1500·7	3	7
1 2	1515·2	1	5
2 3	1529·9	1	5
0 2	1554·3	4	9
2 4	1584·4	2	5
0 3	1611·3	5	9
1 4	1626·5	1	6
0 4	1671·7	4	8
1 5	1687·3	3	9
2 6	1703·3	1	4
0 5	1736·2	3	5
1 6	1751·9	2	7
2 7	1768·1	2	6
0 6	1804·7	1	3
1 7	1820·8	2	5
2 8	1837·2	2	5

* Eye estimated intensity in the afterglow spectrum.
† Eye estimated intensity in an ordinary discharge of nitrogen by Birge and Hopfield.

Douglas and Herzberg[8] found a predissociation in the $a^1\Pi_g$, $v=6$, and suggested that the perturbing state must have a potential curve with a shallow minimum. The perturbing state is probably the $^5\Sigma_g^+$, whose dissociation products are the two normal atoms (^4S), and it also causes the predissociation of $B^3\Pi_g$ at $v=12$. The present observation of the $a^1\Pi_g - X^1\Sigma_g^+$ bands in the glow suggests that

* The measurement was carried out by means of photographic photometry using SWR plates and these lines as background.

† Tank N_2 with purity of 99·99% was not sufficiently pure to exclude NO bands. To obtain a spectrum without NO bands, special precautions are required in purification of N_2 and in seasoning the discharge tube as well.

‡ On account of the extreme weakness of the bands, special care was taken to avoid both stray discharge and reflected light originating in the main discharge. Not only that, we also took several plates of a feeble stray discharge which was intentionally introduced into the glow tube and compared them with the glow spectrum.

Table 1. Emission and Absorption Spectra in the Afterglow of ($N_2 + O_2$)

Glow	Emission spectra	Absorption spectra	Proposed reactions
(I) Straw-yellow	N_2, $B\,^3\Pi_g \rightarrow A\,^3\Sigma_u^+$, N_2, $a\,^1\Pi_g \rightarrow X\,^1\Sigma_g^+$, N_2, $^5\Sigma_g^+ \rightarrow A\,^3\Sigma_u^+$, (a)	NI, 1134Å ($^4S \rightarrow 2p^4\,^4P$) ... 1200Å ($^4S \rightarrow 3s\,^4P$) } strong ... 1493/5Å ($2p^3\,^2D \rightarrow 3s\,^2P$) ... 1743/5Å ($2p^3\,^2P \rightarrow 3s\,^2P$) } v. weak	$\{(N+N) \rightarrow N_2(^3\Sigma_g^+)\} + N_2 \rightarrow N_2(B^3\Pi_g) + N_2$. $N_2(B^3\Pi_g) \rightarrow N_2(A^3\Sigma_u^+) + h\nu$. (1)[b] $\{(N+N) \rightarrow N_2(^3\Sigma_g^+)\} + N_2 \rightarrow N_2(a^1\Pi_g) + N_2$. $N_2(a^1\Pi_g) \rightarrow N_2(X^1\Sigma_g^+) + h\nu$. (2)
(II) Blue	NO, $A\,^2\Sigma \rightarrow X\,^2\Pi$ (γ), $B\,^2\Pi \rightarrow X\,^2\Pi$ (β), (c) $C\,^2\Pi \rightarrow X\,^2\Pi$ (δ), NO, Brook [d] and Ogawa bands [e] O_2, $b\,^1\Sigma_g^+ \rightarrow X\,^3\Sigma_g^-$.	(*l*) NI, 1200Å ($4S \rightarrow 3s\,^4P$) OI, 1302Å ($^3P \rightarrow 3s\,^3S$) } strong Unidentified bands at 1487, 1482, 1442, 1413, and 1408Å .... strong	$N + O + NO \rightarrow NO + NO^*$ ($A^3\Sigma$, $B^3\Pi$, $C^3\Pi$), NO^* (A, B, C) $\rightarrow$ NO ($X^2\Pi$) + $h\nu$ (γ, β, δ). (3)[f]
(III) Dark		(*l*) OI, 1302Å ($^3P \rightarrow 3s\,^3S$) ... strong Unidentified bands at 1487, 1482, 1442, 1413, and 1408Å .... v. strong	
(IV) Greenish gray	Continuous spectrum with diffuse bands superimposed (4000–9000Å)[g] O_2, $A\,^3\Sigma_u^+ \rightarrow X\,^3\Sigma_g^-$.[h]	(*l*) OI, 1302Å ($^3P \rightarrow 3s\,^3S$) ... strong Unidentified bands at 1487, 1482, 1442, 1413, and 1408Å .... v. strong NO bands (γ,δ, and others around 1700Å) ... weak	$O + NO \rightarrow NO_2^*$ $NO_2^* \rightarrow NO_2 + h\nu$ (continuum and diffuse bands). (4)[i] $N + O_3 \rightarrow NO + O_2(A^3\Sigma_u^*)$ $O_2(A^3\Sigma_u^+) \rightarrow O_2 + h\nu$ (Herzberg bands), at low concentration of O_2. (5)[j] $O + O + O_2 \rightarrow O_2 + O_2(A^3\Sigma_u^+)$, $O_2(A^3\Sigma_u^+) \rightarrow O_2 + h\nu$ (Herzberg bands), at high concentration of O_2. (5')[k]

(a) see ref. 9. According to their recent announcement the bands are not due to N_2. (b) see refs. 2, 3, 5. (c) G. Herzberg, A. Lagerquist and E. Miescher, *Canad. J. Phys.* **34,** 622 (1956); A. Lagerquist and E. Miescher, *Helv. Phys. Acta.* **31,** 221 (1958). (d) see ref 11. (e) M. Ogawa, *Sci. of Light* **3,** 39 (1954). (f) see ref. 6. (g) see ref. 13. It seems very probable that the continuum can be extended further to the longer wavelengths. (h) see refs. 11, 12. (i) see ref. 13. (j) see ref. 14. (k) see ref. 15. (l) only observed when the partial pressure of O_2 was relatively small otherwise obscured by the absorption spectrum of O_2.

they are produced by reaction (2) (see Table 1), which is similar to reaction (1) in the same afterglow. Unlike the first positive bands however, no clear enhancement of any particular band was observed (see Table 2), and this probably is due to the metastability of the $a^1\Pi_g$. In the reaction, the radiationless transition $^5\Sigma_g^+ - a^1\Pi_g$ is highly forbidden, and this, combined with the metastability of the $a^1\Pi_g$, is compatible with the extreme weakness of the bands.

It is not clear whether the $^5\Sigma_g^+$ is a pure repulsive state or whether it has a potential curve with a shallow minimum. Broida and his co-worker[9] found new emission bands in the afterglow of solid nitrogen and attributed them to the transition $^5\Sigma_g^+ - A^3\Sigma_u^+$ of N_2 with the dissociation energy of the $^5\Sigma_g^+$ as 1060 cm^{-1} (=0·131 eV). However, according to their recent pronouncement, the bands are not due to the nitrogen molecule.

The absorption spectrum of this stage showed four groups of NI-lines as shown in Table 1, and no other absorption was observed except that of the weak $a^1\Pi_g - X^1\Sigma_g^+$ bands* of N_2[10]. Fig. 2 shows part of the spectrum which was taken by using the line source as a background. Since the N_2 was not sufficiently pure, in this case, one could see weak absorption of Lyman-α and of OI-lines at 1302 Å in addition to that of the NI-lines.

The results of the concentration measurement of the N-atom are shown in Table 3. In this phase of the experiment, the peak intensity was measured and the oscillator strength $f=0·1$† was assumed for all the lines used. The present values of concentration for N (^4S) agree with those obtained by the method of mass spectrometry[4, 5]. While there is no mention of the metastable states, ^2D, ^2P, by those who used the mass spectrograph technique, we definitely observed the existence of the two states although their concentrations were much smaller than that of the ^4S (see Table 3). It must be mentioned that the concentration of an active substance, such as an atomic species, in the glow depends largely on the excitation conditions in the main discharge, and, in particular, with a condensed discharge it depends on capacitance and spark conditions.

There is no question about the existence of a large amount of N (^4S) in the glow, and no other active substance was observed that could approximate the concentration of N (^4S). Therefore, reactions (1) and (2) can be accepted as being the main processes involved in this

* These are absorption due to N_2 normal state and not to any active substance.

† The value was estimated by Professor R. King at California Institute of Technology for which we express our appreciation.

Table 3. Concentration of N (^4S) in the First Stages of the Afterglow

Plate No.	$(P)N_2$ (mm Hg)	(P)Argon (mm Hg)	$\frac{(P)N(^4S)}{(P)N_2}\times 100$	$\frac{(P)N(^4S)}{(P)\text{ total}}\times 100$
I	3·05		0·08	
II	1·58		0·11	
III	5·55		0·09	
IV	1·20		0·11	
V	1·98		0·12	
VI	0·32	7·88	0·55	0·02
VII	0·42	8·00	0·63	0·03
VIII	0·52	7·58	0·40	0·03
IX	1·44	7·57	0·28	0·04
X	0·55	8·50	0·27	0·02
XI	0·80	8·20	0·23	0·02

$$\frac{(P)N(^2P)}{(P)N_2} \cong \frac{1}{500}\times\frac{(P)N(^4S)}{(P)N_2}, \text{ and } (P)N(^2D) \lesssim (P)N(^2P).$$

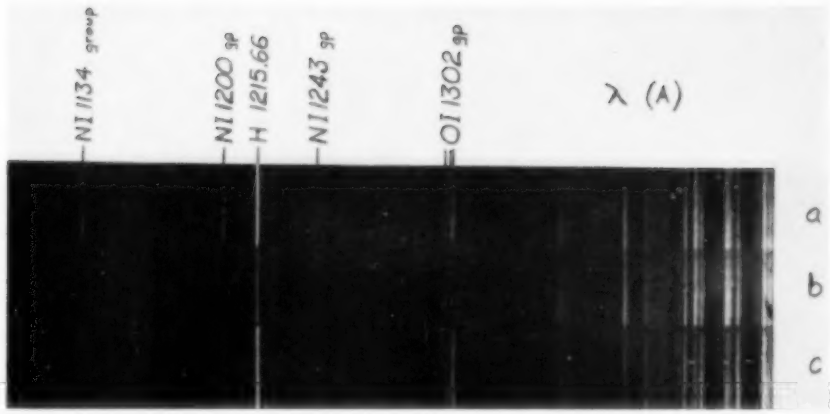

Fig. 2. Absorption spectrum of the first stage. Cell length: about 80 cm. A condensed discharge of (He + N_2) was used as a background: (a, c) without glow; (b) with glow in the cell.

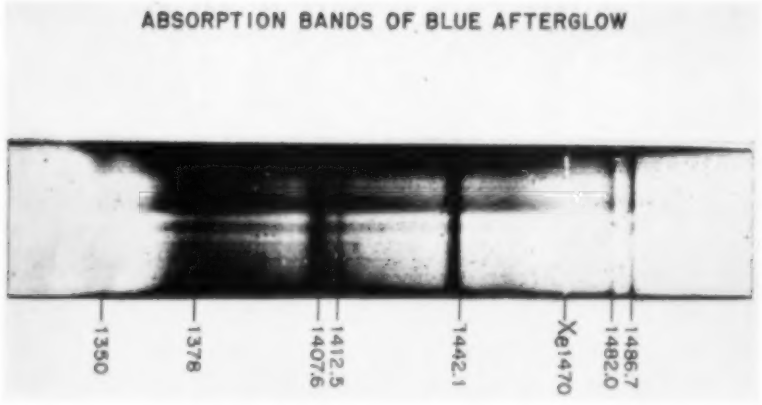

Fig. 3. Absorption bands of blue afterglow.

facing p. 10

stage of the afterglow. Because of their small concentrations, the role of the metastable atoms might be a minor one if at all.

3.2. *The second stage (blue-glow)*

When a very small amount of O_2 was introduced into the flow of pure N_2, the NO bands appeared in emission in addition to the first positive bands, but the glow color remained the same. By increasing the O_2 pressure, the color changed gradually from yellow to whitish yellow, then whitish blue, until it became pure blue at which point the nitrogen bands completely disappeared. At this point, the NO bands[6, 11, 12] occupied the entire region, 1900–8500 Å, with the atmospheric O_2 bands also present. This stage we will call the "second stage". Regarding its color and spectrum, there was no sharp boundary between this stage and the first stage.

As shown in Table 1, the absorption spectrum of this stage showed strong OI-lines and several bands in addition to the NI-lines*. The intensity of the OI-lines was as strong as that of the NI-lines in the first stage. We did not measure the intensity of the OI-lines but it might be safe to estimate that the concentration of atomic oxygen in the ground state $O(^3P)$, is of the same order of magnitude as that of $N(^4S)$ in the first stage. As will be described later, we have no adequate explanation for the origin of the absorption bands. NO molecules were not detected in absorption, but their emission spectrum appeared in the main discharge as well as in the glow. This indicates the existence of the molecule but the amount is not sufficient to allow for its observation in absorption with 8 cm of cell length.

Reaction (3), proposed for this stage, can be accepted since all the necessary elements were observed. The intermediate stage between this and the first stage is produced simply by co-existence of the three reactions, (1), (2), and (3). It should be mentioned that reaction (3) must be very strong because only a slight impurity of O_2 is sufficient to cause strong emission of NO bands in the afterglow.

3.3. *The third stage (no visible glow)*

A further increase of the partial pressure of O_2 in the second stage simply weakens the brightness of the blue glow without any change in the nature of its color and emission spectrum. At some specific amount of O_2 the glow disappears completely. This stage we will call the third stage or "the dark stage".

As shown in Fig. 1, the existence of this stage could be observed throughout the entire range of N_2 partial pressure used. No emission spectrum was observed in this stage but absorption lines of OI at 1302 Å and the absorption bands mentioned in the previous stage were observed both being intensified. It is difficult to explain how this stage is produced, but probably could be as follows: As the O_2 pressure is increased, the concentration of $N(^4S)$ will decrease while that of $O(^3P)$ and of $NO(X^2\Pi)$ will increase, and finally a condition is attained where neither reaction (3) nor (4) is sufficiently strong to result in an observable glow.

3.4. *The fourth stage (greenish-gray)*

When the O_2 pressure attains a certain value (see Fig. 1), the greenish-gray glow appears rather abruptly following the dark stage. The brightness of the glow was increased as the O_2 pressure was increased and no further stage was observed. The emission spectrum of the stage was identical with the so-called air afterglow[13]. Namely, it consists of many weak and diffuse bands superimposed with a strong continuum extending from about 4000 Å to at least 9000 Å. The existence of $O(^3P)$ and $NO(X^2\Pi)$ in the glow was confirmed by a study of its absorption spectrum (see Table 1), and the proposed reaction (4) seems to be the most likely one responsible for the glow.

Recently, Barth and Kaplan[14] observed the Herzberg bands of O_2* in the beginning of this stage. Their suggested reaction is equation (5)

* These additional absorption spectra were observed even in nitrogen in which O_2 was a slight impurity, and their intensity increased with an increase in the partial pressure of O_2.

* Very long exposures are required to record these bands and we made no attempt to observe them.

Table 4. Energy Differences between the Unidentified Bands and Characteristic O_2 Absorption Bands

Characteristic absorption bands of O_2		Unidentified absorption bands		ΔE (eV)	Excitation energy of $b\,^1\Sigma_g^+$ of O_2
λ(Å)	eV	λ(Å)	eV		eV
1244	9·96	1487	8·34	1·62	
		1482	8·36	1·60	1·626 $v=1$
1207	10·27	1442	8·60	1·67	
1172	10·58	1413	8·78	1·80	1·802
		1408	8·81	1·77	$v=1$

in Table 1. Broida and Gaydon[15] also found the same bands in their oxygen afterglow and suggested equation (5′) as its reaction mechanism. Since both observed a strong air afterglow simultaneously with the O_2 bands, there should be two different reactions in this stage; one for the air afterglow, and the other for the Herzberg bands. We tried to detect $N(^4S)$ and O_3 in absorption but did not succeed because the strong O_2 absorption was superimposed on their expected absorption spectrum†. However, since the emission spectrum of this stage was identical with that of air afterglow rather than that of chemiluminescence in the reaction between O_3 and NO,[15] the amount of O_3 in the stage should be very small. According to Schiff,[17] the production of O_3 in an oxygen discharge is extremely small when the O_2 pressure is low (~1 mm Hg), and this tends to support the above statement.

3.5. *The absorption bands*

Fig. 3 shows the absorption bands taken in the second stage with the krypton continuum as a background. The longest three are somewhat diffuse but clearly shaded toward the violet while the rest of them have no apparent shading and appear very diffuse.

An attempt was made to determine the origin of the bands. Accordingly, we studied the absorption spectrum of the discharge products* of molecules such as H_2, N_2, O_2, NO, CO, N_2O, NO_2, CO_2, and H_2O†. Of these, all the oxide molecules (including pure O_2) showed the bands with the only exception being CO. This suggests that they are probably due to an excited O_2 molecule. O_2^+, O_2^-, and O_3 are presumably contained in the discharge products but seem unlikely as the origin of the bands. The oxygen molecule has three characteristic absorption bands at 1244, 1207, and 1172 Å[18]. They are very strong and diffuse, and Price and Collins[19] suggested that their upper states are predissociated. As can be seen in Table 4, the energy differences between those and the present bands are fairly close to the excitation energy of one of the metastable states of O_2 ($b^1\Sigma_g^+$, $v=0$, 1) suggesting the observed bands may originate in the transition between that state and, probably, the perturbing states of the characteristic absorption bands mentioned above.

† We looked for the 1200Å lines of NI and the continuum maximum of O_3 at about 1350 Å.[16]

* Another discharge tube was attached to the absorption cell and the discharge products were pumped through the latter.

† We took absorption spectra of all of these gases in the vacuum region with the same instrument, but none of the present bands appeared in any of the spectra.

REFERENCES

1. Mitra S. K. *Active nitrogen*, Ind. Association for the Cultivation of Science, Calcutta (1945).

2. Cario G. and Reinecke L. *Abh. braunschw. wiss. Ges.* **1,** 8 (1949); Reinecke L. *Z Phys.* **135,** 361 (1953).
3. Brook M. Sci. Rep. No. 2. Institute of Geophysics, Univ. of California, Los Angeles (March 1953); Kaplan J. and Brook M. private communication.
4. Jackson D. S. and Schiff H. I. *J. Chem. Phys.* **21,** 2233 (1953); *Ibid* **23,** 2333 (1955).
5. Berkowitz J., Chupka William and Kistiakowsky G. B. *J. Chem Phys.* **25,** 457 (1956).
6. Tanaka Y. *J. Chem. Phys.* **22,** 2045 (1954).
7. Tanaka Y. *J. Opt. Soc. Amer.* **45,** 710 (1955).
8. Douglas A. E. and Herzberg G. *Canad. J. Phys.* **29,** 294 (1951).
9. Herzfeld C. M. and Broida H. P. *Phys. Rev.* **101,** 606 (1956).
10. Tanaka Y. *J. Opt. Soc. Amer.* **45,** 663 (1955).
11. Brook M. and Kaplan J. *Phys. Rev.* **96,** 1940 (1954)
12. Ogawa M. *Sci. of Light* **3,** 39 (1954)
13. Tanaka Y. and Shimazu M. *Sci. Pap. Inst. Phys. Chem. Res. Tokyo* **43,** 241 (1949)
14. Kaplan J. and Barth C. A. *J. Chem. Phys.* **26,** 506 (1957).
15. Broida H. P. and Gaydon A. G. *Proc. Roy. Soc. A* **222,** 181 (1954)
16. Tanaka Y., Inn C. Y. and Watanabe K. *J. Chem. Phys.* **21,** 1651 (1953)
17. Schiff H. I. *Ann. N.Y. Acad. Sci.* **67,** 518 (1957); Warren J. W. *Nature (Lond.)* **165,** 810 (1950).
18. Tanaka Y. *J. Chem. Phys.* **20,** 1728 (1952).
19. Price W. C. and Collins G. *Phys. Rev.* **48,** 714 (1935).

Planet. Space Sci. Pergamon Press 1959. Vol., 1, pp. 14–19, Printed in Great Britain.

ENERGY SOURCES OF THE UPPER ATMOSPHERE

V. I. KRASSOVSKY

Institute for Atmospheric Physics, Academy of Sciences of the U.S.S.R., Moscow

(*Received* 25 *September* 1958)

Abstract—Investigations by earth satellites indicate that the product of atmospheric density and the square root of scale height at the 220–230 km altitude is higher in daytime than at night and also higher in polar regions than in equatorial ones. Interpretation of this data indicates that density and temperature in this region are much higher than previously supposed. Various energy sources which may account for this variable heating and swelling of the atmosphere are considered. An explanation is given in terms of variable heating due to electric currents in the upper atmosphere induced by magnetic fields frozen in the corpuscular streams. It is supposed that this mechanism can accelerate atmospheric ions and electrons.

UPPER atmosphere investigations by means of the artificial earth satellites launched by the Soviet Union[1] have shown that at 220–230 km altitudes, the product of the atmospheric density and the square root of the scale height is higher in the daytime than at night. This product is also greater over high latitudes, decreasing gradually as we move to the equatorial zone. The data obtained may hardly be interpreted otherwise than to mean that at a level of 220–230 km the atmospheric density and temperature are much higher than was supposed ever before. In this connection our ideas as to the energy sources necessary for an intense variable heating and swelling of the upper atmosphere become even more hazy. Obviously the heretofore adopted view concerning the structure and dynamics of the upper atmosphere must be revised in the light of the new information.

As early as 1951, Bates[2] showed that the upper atmosphere is cooled down considerably by the microwave radiation of atomic oxygen. Thus, the known penetrating ultraviolet and X-ray radiation of the sun, absorbable by the upper atmosphere, appeared to be quite insufficient for maintaining the very high temperatures prevailing there. To obviate this difficulty, Chapman[3, 4] supposed that the intense heating of the upper atmosphere might be due to some interplanetary gas medium having as high temperatures as several hundred thousands of degrees Kelvin. According to his hypothesis, this medium is an extension of the solar corona. He believes its existence to be corroborated by some recent evidence of the high density of the interplanetary gas. However, the entire explanation is open to doubt at more than one point[5].

A few years ago, Daniels[6] advanced the assumption that the upper atmosphere might possibly be heated by infrasonic waves from the troposphere, where these waves arise by the agitation of the world ocean and atmospheric turbulence and winds. However, diurnal and latitude variations of the density can hardly be accounted for by such a source of heating, since it is hard to suppose that tropospheric infrasounds would depend on the hour and the latitude. Another explanation seems more worthy of attention; namely, the heating of the upper atmosphere can possibly be caused by the electric currents that flow in it and are responsible for the variations of the magnetic field.

Studies on whistling atmospherics indicate[7] the outer atmosphere of the earth can be considered as a system of many electrically conducting channels, following the magnetic lines of force and closed to form a circuit by the conducting layers in the lower portion of the ionosphere. Such conducting channels are

due to a nearly complete absence of electric conductivity in the direction perpendicular to the magnetic lines of force. I. S. Shklovsky was the first[8] to point out the existence of similar conditions in the solar corona where they account for sharp temperature differences between some neighbouring regions. At this time, magnetic thermal insulation is used in laboratory experiments with thermonuclear reactions[9]. Since ions and electrons collide in large numbers with the atoms and molecules of the atmosphere, the electric conductivity of the lower portion of the ionosphere is as great across the magnetic lines of force as along them. Hence the earth can be regarded as encircled by conducting rings which form a kind of tore about it, and are interconnected on the internal side of this tore. If at some part of the conducting channel its conductivity becomes low such a channel may act as an oscillating circuit.

Since the interplanetary gas and solar corpuscular streams are carrying magnetic fields frozen in them, great electromotive forces and strong currents are bound to arise in these circuits. If, for instance, a corpuscular stream moving at a rate of several thousand kilometers per second carries a magnetic field of only $1/10$ γ, whose direction changes ten–twenty times in a second, then the electromotive force may attain millions of volts in a circuit along the magnetic line of force 10^{11} cm long (the existence of such conducting channels has been established from observations of whistling atmospherics[10]). This is quite sufficient for a powerful heating of the upper atmosphere, especially its outer very rarified portion. Heating by short-period variations of the geomagnetic field will be strongest near the poles, because the cross-section of the conducting channels is much larger than in low-latitude regions. It will also be stronger during the day than at night, since the penetrating electro-magnetic radiation of the sun enhances the ionization in the lower layers of the ionosphere. The latter are good electric conductors at night only in the case of a powerful corpuscular penetration to the nocturnal side of the earth.

Apart from the short-period variations of the magnetic field, electric current producing long period variations of this field may also account for the heating of the upper atmosphere. At this juncture we can offer some considerations concerning the altitude of these currents. By observations of radar reflections from auroras at Roshchino, south of the zone of their most frequent recurrence, it has been found that at the time of weak geomagnetic disturbances the radar reflections were strictly in accordance with Chapman's ideas; i.e. reflecting were those zones where the magnetic lines of force were at right angles to the direction towards the radar (V. I. Pogorelov). From this standpoint no radar reflections may be possible at the Loparskaya station, in the auroral maximum zone, if the geomagnetic field is in normal state, since the perpendicular condition is fulfilled only at altitudes much below 100 km from the earth's surface. However, regular radar reflections from North are observed at Loparskaya during geomagnetic perturbations (J. G. Birfeld, A. I. Grachev). Primarily important is to find out their dependence on positive and negative bays in the reflection zone (J. G. Birfeld, V. I. Jarin, A. J. Grachev). The radio reflections are seldom observed during positive bays; usually only when negative bays come to replace positive bays will radio reflections make their appearance. Their number is highest during negative bays. For radio reflections to appear at Loparskaya, the magnetic lines of force must be inclined to the south. Therefore, the usual absence of reflections during positive bays and their appearance with negative bays may be taken to mean that the currents responsible for the bays flow below the reflecting zone. Should the reflecting zones be identified with the auroral maximum brightness zones, where the ionization is of the greatest importance, then it is only natural to suppose that the electric currents producing baylike disturbances flow usually below the maximum brightness zone of auroras. Thus the S_D and D variations of the geomagnetic field can heat respective layers of the upper atmosphere.

Some heating of the upper atmosphere can be ascribed to corpuscular penetrations. However, the main role of the corpuscles appears

to consist of a specific ionization of the upper atmosphere. Ordinarily, a penetrating electromagnetic radiation from solar flares fails to produce any appreciable geomagnetic disturbances. Such disturbances arise only on corpuscular penetrations. We may therefore expect the corpuscles to have some specific effect on electric conductivity. What seems to be most probable is that the corpuscles produce an intense ionization by breaking up oxygen molecules directly to positive and negative oxygen ions. This process has been observed in the laboratory[11] and it can well increase the ionic conductivity of the ionosphere, especially at night, when effective photodetachment of electrons from negative ions is impossible.

It may be remarked, moreover, that in the daytime the average life of positive ions can be lengthened by the formation about them of shielding shells made of neutral molecules (cluster ions). This factor can also prolong the life of negative ions, since a photoelectron from a negative ion will have a higher probability for attachment to one of the shell molecules. In the atomic oxygen zone the electric conductivity may possibly increase in the direction perpendicular to the magnetic lines of force owing to an increase in the number of collisions due to charge exchange by ions whose effective cross-section is larger than the gasokinetic one.

Until recently, the main interest centered about the brighest forms of auroral displays and no due attention was given to the processes in the space outside them. Radar reflections from auroras testify to an exceptionally high local ionization in the auroral zone. Yet, for large scale current systems to exist, the ionization cannot be local but should rather embrace all zones of the conducting circuit and secure a high electric conductivity in the latter. From this point of view, ray structures, which are apparently most frequently attended by radar reflections, can hardly secure a good conductivity throughout the current system circuit, since a few good conductors located at right angles to the electric current lines in the conducting medium cannot appreciably change its electric conductivity. Investigations of emissions from auroras at Loparskaya have shown, as a rule, that most of auroral energy is radiated, not from bright forms, but rather from the surrounding diffuse formations, which are considerably more uniform and are extended in space (N. V. Jorjio, M. L. Bragin). It has also been established that in general there are no bright auroral forms without some diffuse formation about them. All of this remained unnoticed until now, probably because visual observations, when bright forms appeared, were not able to detect the weak diffuse light. At the same time, investigations at Loparskaya have shown that neither is the emission of corpuscular hydrogen concentrated in bright forms alone. As a rule, indeed, it is observed about on a wide area (G. I. Galperin).

There is good ground to suppose that at the time of corpuscular penetrations, wide electrically conducting layers are created in the upper atmosphere, although the electron concentration in them may not attain the high value suggested by the existence of radar reflections from auroras. It would seem, therefore, that most essential for usual geomagnetic disturbances are the wide areas taken up by a weak diffuse light about the bright forms of auroras rather than these forms themselves.

Until now only hydrogen corpuscles were identified in auroral emission spectra from the Doppler shift. At this time, modern highly sensitive spectrographs permit hydrogen emission to be recorded practically during almost any aurora (G. I. Galperin). In cases where this emission is not identified with certainty its place is usually taken up by blending molecular bands, and so it cannot be definitely stated that it was actually absent. At the stations of this Institute, hydrogen emission was recorded during a quiet time, both before geomagnetic disturbances and when they were altogether absent; i.e. did not appear after the time of emission. Moreover, narrow hydrogen lines without the Doppler shift have been recorded at Zvenigorod (V. S. Prokudina). Similar emissions have been observed at Loparskaya too (G. I. Galperin). Recently at Zvenigorod helium emission was apparently detected in the

infrared at about 10830 Å (V. S. Prokudina, N. N. Shefov, A. V. Mironov). Very likely certain auroras, during which no hydrogen emission could be detected, were due to penetrations of helium corpuscles, or of hard electrons. At the symposium on aeronomy in Toronto in September last year, Elvey[12] reported that hydrogen emission appears usually a few hours before the outset of a bright aurora and is attended by a strengthening of terrestrial currents, noticed formerly by Störmer, as a precursor of these phenomena. This is exceptionally interesting. At Loparskaya, too, the appearance of a hydrogen emission was recorded a few hours before the advent of an auroral display (G. I. Galperin). Moreover, a simultaneous appearance of radar reflections from auroras was stated (G. I. Galperin, J. G. Birfeld, A. I. Grachev). These reflections testify to the penetration of hydrogen corpuscles in the form of dense formations which produce a high degree of ionization on their way. Sometimes the precursors of an aurora and of a geomagnetic disturbance disappear without resulting in a development of these phenomena (G. I. Galperin).

All of this appears to furnish a good confirmation of the influence which the magnetic fields frozen into solar corpuscular streams exert on the outer atmosphere of the earth while moving past it. Under the action of such a variable magnetic field the conducting channels in the atmosphere, coinciding with the magnetic lines of force, begin to acquire heat and the scale height in them grows. As a result of an intense heating, a rather dense fibre of ionized gas, stretching from one hemisphere of the earth to the other, may be formed. Thereby the power supplied to the upper atmosphere through such a channel increases sharply. The initial phase of an aurora corresponds to the time of preliminary heating. It is attended by more or less uniform penetrations of primary solar corpuscles into wide polar and near-polar regions. The time of formation of a denser fibre along a magnetic line of force corresponds to the outset of an intense aurora and a geomagnetic disturbance. The arrangement of an auroral zone along the geomagnetic parallel can easily be explained by the fact that in the regions located towards the geomagnetic pole from the auroral zone the magnetic force lines are tangled in the moving interplanetary gas medium and do not follow the shortest path to the other pole in the outer atmosphere, rigidly bound to the earth. When the magnetic fields frozen into corpuscular streams get stronger, the region taken up by the fibres which follow the direction of magnetic lines and are closed to form an electric circuit with the other hemisphere, is reduced in area, and the maximum of auroral displays is shifted toward the equator. Also the predominance of high altitude forms of type A in low-latitude auroras may be easily explained. Since the electromotive force in the circuits will be at a maximum when the direction of the magnetic field is at right angles to the trajectory of the corpuscular streams and to the planes of the circuits, the predominance of relatively quiet forms in the evening and morning hours is quite understandable.

The swellings of the terrestrial atmosphere along the magnetic force lines consist of ions and electrons. On the other hand, in the corpuscular streams neutral hydrogen atoms must be present alongside protons, as a result of charge exchange. According to Shklovsky[13] charge exchange processes can start in the interplanetary space. In the terrestrial atmosphere they cannot possibly fail to occur. Apart from neutral primary corpuscles, the outer atmosphere contains some primary corpuscles reflected from the earth that have undergone a charge exchange. Their existence is evidenced directly by the red Doppler shift, which is observed in any auroral hydrogen emission. Every spectral profile of this emission brings usually into evidence that 10 to 20 per cent of the radiating corpusles move from the surface of the earth in various directions (G. I. Galperin). All the neutral corpuscles, while travelling through the swellings of atmospheric ions along the magnetic force line, can undergo charge exchange. According to the direction of their velocity relative to the magnetic force line, such charged particles will be captured by

the latter and will move along this line to either hemisphere.

The density ρ of the stream of corpuscles thus captured can be defined as

$$\rho = n_0 v \sigma N,$$

and since $N > nl$

then $\rho > n_0 v \sigma n l,$

where n_0 is the concentration of neutral corpuscles in cm^{-3}, v is their velocity in $cm\ sec^{-1}$, σ is the effective cross-section for charge exchange in cm^2, N is the number of ion pairs in a fibre with 1 cm^2 base, n is the average concentration of ionized particles in the outer atmosphere of the earth, and l is the path length along the magnetic line of force.

As an example, put $n_0 = 1\ cm^{-3}$, $v = 2 \times 10^5$ $cm\ sec^{-1}$, $\sigma = 10^{-16}$ cm^2, $n = 10^6$ cm^{-3} and $l = 5 \times 10^9$ cm. Then $\rho > 10^8$ H^+ $cm^{-2}\ sec^{-1}$. It will be obvious that the densities of the streams captured by the swelling of neutral molecules can in fact attain or even exceed the densities of the streams of neutral hydrogen corpuscles. The corpuscles thus captured will add heat to the outer atmosphere, thereby creating an unhomogeneous density distribution in the directions perpendicular to the magnetic field. As a result, very narrow dense streams of captured corpuscles can be expected to appear. In addition to this, the outer atmosphere's own ions can be accelerated, and a change in the velocity of the captured corpuscles is possible.

The corpuscles captured to the magnetic line of force and the atmosphere's own accelerated ions and electrons will be responsible for the brightest auroral forms. The upper portions of the swelling, if present in the region illuminated by the sun, can be detected because of their fluorescence. On the different mechanisms by which light emission is excited, the discontinuties in the auroral rays at the boundary of the earth's shadow can be easily explained. Effectively fluorescent in solar radiation are ionized molecules of nitrogen only. Their spectra are most typical of auroras in regions illuminated by the sun. Other emissions observed in this type of aurora can be due to diffuse auroral light, which comprises wide extents of the upper atmosphere, and the excitation of atoms and molecules in the atmosphere swellings when there is charge exchange between their ions and neutral reflected corpuscles, and especially primary ones.

An intense heating of the upper atmosphere by short period variations of the geomagnetic field will also account for the slow decline of the electron density upwards of the F_2-layer maximum, discovered by rocket investigations in the U.S.S.R.[14]. Since the frequency of collisions above the F_2-layer maximum in the exosphere is not appreciable, the variable geomagnetic field can add acceleration to ions and electrons and put them out of thermodynamic equilibrium with neutral particles. In this case the height of the homogeneous atmosphere for ions and electrons will be greater than for neutral particles. At the time of intense auroras the outer atmosphere for ions and electrons must be heated to a very high temperature. This phenomenon has been apparently recorded at Loparskaya, where a broadening of the [OI] red line at 6300 Å was detected by means of an interferometer (T. M. Mularchik). There have been registered cases where in the course of the development of an aurora the temperature rose from an initial value of several hundred degrees up to several thousand degrees. It is worthy of note also that an increase of temperature towards the polar regions at an altitude level of 100 km is apparently indicated by the continuous increase of the rotational temperature of hydroxyl in the direction towards higher latitudes. According to the observations made at our Institute, the rotational temperature of hydroxyl grows from approximately 200°K in southern regions to 350°K in the auroral maximum zone (V. S. Prokudina, N. N. Shefov, N. I. Federova, G. I. Galperin, F. K. Shuiskaya). At Loparskaya this temperature has been observed to differ in the zenith and at the northern horizon. As the atmosphere is heated, and the thermal balance of its lower layers at about 100–150 km is disturbed, a specific circulation seems to arise in it, which results in the geomagnetic variations of S_D and D.

As was stated above, electromotive forces of

several hundred kilovolts can arise in the circuits, their electric chain being closed along the magnetic force lines in the outer atmosphere and perpendicular to them in conductive ionosphere layers. Since in the outer atmosphere, i.e. in the exosphere, charged particles travel along magnetic force lines practically without colliding with other particles, they can receive very high accelerations, sufficient for penetration into lower layers through a greater thickness of atmosphere. In this way protons, helium ions and electrons can be accelerated.

In an earlier paper[15], published before the Toronto symposium on aeronomy, the assumption was made by me that the absorption which takes place in the ionosphere at the time of auroras and geomagnetic disturbances may be due to the formation of the *D* layer. This layer may originate from two different sources: by L_α hydrogen emission, which arises on the neutralization of protons, and by X-rays emitted as a result of bombardment of the upper atmosphere by hard electrons. From the materials of the symposium it was learned later[16] that similar assumptions had been advanced by Bates and Chapman in papers that were forthcoming. By now the presence of hard electrons in the auroral zone appears to have been proved by Van Allen[17] and by Winckler and associates[18]. Yet the role of the H L_α radiation in the formation of the *D* layer remains obscure.

In my opinion, three types of fast corpuscles are possible. First, primary corpuscles which come to the terrestrial atmosphere directly from interplanetary space; secondly, primary corpuscles that receive added acceleration or are retarded on their motion to the lower layers of the atmosphere along the magnetic lines of force; thirdly, corpuscles generated owing to the ions and electrons available in the outer atmosphere, as a result of short-period variations of the geomagnetic field. To estimate the relative significance of each of these components is, of course, a matter of considerable difficulty at this juncture. An exhaustive solution of this problem will probably be obtained when the interplanetary space about the earth will be accessible for exploration by direct methods. This possibility does not appear to be very remote.

Given in parentheses are the names of the workers of our Institute whose papers are forthcoming.

REFERENCES

1. Official communication, Pravda, 27 April 1958.
2. Bates D. R. *Proc. Phys. Soc.* B **64**, 805 (1951).
3. Chapman S. *Smithsonian Contribution to Astrophys.* **2**, N 1 (1957).
4. Chapman S. *Report to aeronomy symposium at Toronto* (1957).
5. Blackwell D. E. *Observatory* **77**, 187 (1957).
6. Daniels F. B. *J. Acoust. Soc. Amer.* **24**, 83 (1952).
7. Storey L. R. O. *Trans. Roy. Soc.* **246**, 113 (1953).
8. Shklovsky I. S. *Solar Corona*, p. 382. Moscow (1951).
9. Kurchatov I. V. *Usp. fiz. nauk* **59**, 608 (1956).
10. Millman P. M. *J. R. Astr. Soc. Can.* **51**, 335 (1957).
11. Massey H. S. W. and Burhop E. H. S. *Electronic and Ionic Impact Phenomena*, p. 258. Oxford (1956).
12. Elvey C. T. *Report to aeronomy symposium at Toronto* (1957).
13. Shklovsky I. S. *Report to aeronomy symposium at Toronto* (1957).
14. Official communication, Pravda, 21 March 1958.
15. Krassovsky V. I. *Priroda* ("*Nature*"), No. 5, 59 (1957).
16. Matsushita S. *Abstracts Inter. Assoc. Geom. Aero. Toronto meeting*, 7 (1957).
17. Van Allen J. *Proc. Nat. Acad. Sci., Wash.* **43**, 57 (1957).
18. Winckler J. R. and Peterson L. *Phys. Rev.* **108**, 903 (1957).

Planet. Space Sci. Pergamon Press 1959. Vol. 1, pp. 20–26. Printed in Great Britain.

AN INTERIM ATMOSPHERE DERIVED FROM ROCKET AND SATELLITE DATA*

I. HARRIS and R. JASTROW†
Nucleonics Division, U.S. Naval Research Laboratory, Washington, D.C.

(*Received* 29 *September* 1958)

1. INTRODUCTION

THE analysis of radio tracking data obtained from the U.S. and U.S.S.R. satellites provides information on the density and temperature of the atmosphere at high altitudes. We find that by combining this information with data recently obtained from rocket flights at altitudes below 200 km, we may construct a model atmosphere which yields a relatively unambiguous determination of density up to 400 km. Above 200 km this atmosphere indicates values of temperature and density which are substantially greater than those predicted in recent extrapolations to these altitudes. They are, however, relatively close to the results of the earlier analysis by Grimminger[1].

The proposed atmosphere is based on rocket data obtained at latitude 33°N, together with orbit data from satellite 1957 Alpha 2, whose perigee was located at 39°N during the period of observation. The model therefore describes atmospheric conditions at temperate latitudes.

Additional data on the density in the equatorial belt between 33°N and 33°S are available from the U.S. satellites, 1958 Alpha (Explorer I) and 1958 Beta (Vanguard I). The results of our preliminary analysis on these satellites will be given below. Unfortunately they cannot be combined with the rocket data and the results from 1957 Alpha 2, because of the pronounced latitude dependence of density above 200 km[2].

2. ANALYSIS OF THE SATELLITE DATA

Our analysis of satellite data is based on orbital elements obtained from Minitrack observations, and in particular on the rate of change of the orbital period. This change in period is the direct result of the drag exerted by the atmosphere, which causes the satellite to lose energy continuously during its repeated circuits of the Earth. As its energy decreases the satellite falls towards the center of the Earth, reducing its average altitude and therefore the time required to complete each circuit. Detailed numerical integrations may then be used to determine the quantitative relation between the reduction in the period and the distribution of air density around the orbit. These integrations are not convenient for an extended lifetime study, and one of us (I.H.) has therefore developed an adiabatic approximation to the equations of motion, which yields a set of simple relations giving directly the time derivatives of the planar orbit elements[2].

2.1. *Adiabatic equations for the orbit elements*

We assume that the orbit is given by an osculating ellipse with time-dependent period (P) and eccentricity (e). We average the energy loss due to the drag over one period of revolution, and after some manipulations obtain the following equations for the rates of change of period and eccentricity:

$$dP/dt = a\overline{\rho v^3/B} \tag{1}$$

$$(e/1-e^2)\,de/dt = b\overline{\rho v/B} - c\overline{\rho v^2/B}. \tag{2}$$

Here ρ is the density of the atmosphere, v is the speed of the satellite, and a, b, and c are quantities defined in the Appendix. B is the conventional ballistic drag parameter, defined

* Presented at the Fifth CSAGI Assembly, Moscow, 30 July–9 August 1958.

† Present address: National Aeronautics and Space Administration, Washington, D.C.

as $C_D A/m$ where C_D is the drag coefficient, A is the satellite area projected along the direction of motion, and m is the satellite mass. The bar denotes a time average over one revolution. The details of the derivation are given in the Appendix.

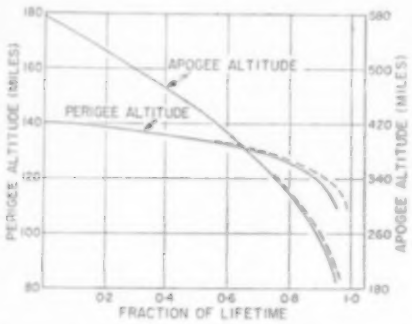

Fig. 1. Comparison between the solutions to the adiabatic equations for the orbit elements and the solutions to the equations of motion. The solid lines are the perigee and apogee altitudes for 1957 Alpha 2, calculated from equations (1) and (2). The dotted lines represent the results of a numerical integration of the equations of motion.

Fig. 1 compares the solutions to equations (1) and (2) with the results of a numerical integration of the exact equations of motion, for the particular case of the 1957 Alpha 2 orbit. In this orbit the initial perigee and apogee altitudes were 232 km and 920 km respectively. We see from Fig. 1 that the error in the approximate results is $\leqslant 2$ per cent during the first 80 per cent of the satellite lifetime.

2.2. *Relation between perigee density and rate of change of period*

The equations for the time-dependent orbit elements indicate that dP/dt is proportional to the average value of $\rho v^3/B$ over the orbit. Since the density falls off very rapidly with increasing altitude, the average of ρv^3 is heavily weighted by the contributions near perigee. Therefore to a first approximation the observed value of dP/dt determines the density at perigee[4]. However, we may expect that this result will depend to some degree on the scale height at perigee. Our calculations indicate that for reasonable scale height distributions, a given value of dP/dt actually determines the density uniquely at an altitude of the order of one scale height above perigee. Fig. 2, for example, shows four model atmospheres which

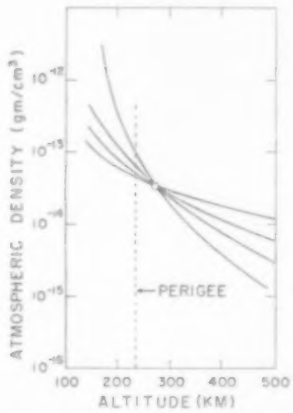

Fig. 2. Four model atmospheres which have been adjusted to fit the observed rate of change of period for 1957 Alpha 2. The atmospheres correspond to the scale height distributions in Fig. 5. All models intersect within 5 km of a point located approximately 50 km above perigee.

have been adjusted to fit the observed rate of change of period of Sputnik I, but correspond to different scale height distributions. We see that these atmospheres intersect within 5 km of a single point located approximately 50 km above perigee. Similar results are obtained for the other satellites.

3. DETERMINATION OF THE MODEL ATMOSPHERE

We construct a provisional atmosphere for temperate zones by combining the rocket data with the density datum furnished by Alpha 2. The analysis of Alpha 2 depends on orbit elements deduced from Minitrack data[5] for the period between 14 October and 25 October. The average values of the relevant elements for that interval are given in Table 1.

We also require the ballistic drag parameter for the determination of the density from the

observed rate of change of period. The present calculations are based on a ballistic drag parameter of 89 ± 11 kg/m², derived from U.S.S.R. announcements of mass and area*.

Our results are shown in Fig. 3[6]. Curves A and B represent two atmospheres with different scale height distributions, each adjusted to agree with the orbital data and observed value of dP/dt for Alpha 2. These curves intersect at 275 km, as noted above. Curve A is further determined to pass through the rocket density data of Byram, Chubb, and Friedman[7]. Curve B passes through the rocket data of Horowitz and LaGow[8]. The spread in curves A and B above 275 km indicates the probable error in the density at high altitudes corresponding to the uncertainty in the rocket data below 200 km. The dashed curves in Fig. 3 include the additional uncertainty in the density when allowance is made for the quoted probable errors in the perigee altitude and ballistic drag parameter of Sputnik I.

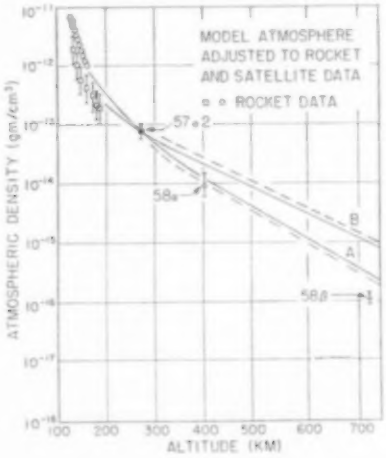

Fig. 3. Model atmosphere adjusted to agree with the rocket data below 200 km and with the density datum determined from satellite 1957 Alpha 2. The probable error in the Alpha 2 datum represents uncertainties in the perigee altitude and ballistic drag parameter of Alpha 2. Points determined by the analysis of Satellites 1958 Alpha and 1958 Beta are also shown.

* Mass = 83·4 kg; diameter = 58 cm; total antenna length = 812 cm; mean antenna radius = 1·0 ± ·3 cm (estimated). Extreme assumptions regarding the mechanism of reflection at the satellite surface lead to values for the drag coefficient, C_D, which vary from 2·0 to 2·7, hence we take $C_D = 2{\cdot}3 \pm {\cdot}3$. The ballistic drag parameter, $M/C_D A$, is then 89 ± 11 kg/m².

The proposed interim atmosphere for temperate latitudes is an average of curves A and B. We show this atmosphere in Fig. 4. The

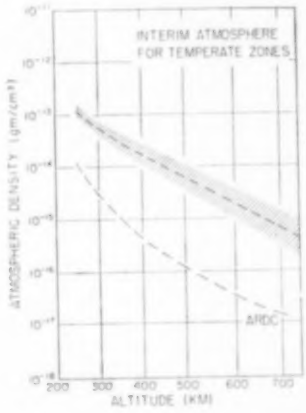

Fig. 4. Interim atmosphere for temperature latitude, constructed from rocket data and the analysis of Satellite 1957 Alpha 2. The shaded area indicates the probable error associated with uncertainties in the rocket data and the Alpha 2 result. The dashed curve shows the ARDC atmosphere.

shaded area in Fig. 4 corresponds to the spread between the dashed curves in Fig. 3, and represents our estimate of the probable errors in the interim atmosphere.

Table 1. Orbit Elements for Satellite 1957 Alpha 2, Derived from Minitrack Data for the Interval 13 October-25 October

Perigee altitude	232 ± 5 km
Eccentricity	$0{\cdot}047 \pm {\cdot}004$
Latitude of perigee	$39° \pm 6°$
Equatorial inclination	$64{\cdot}5° \pm 0{\cdot}3°$
Mean period (Oct. 19)	95·63 min
Rate of change of period	$-{\cdot}045 \pm 0{\cdot}003$ min/day

3.1. *Scale height and temperature*

Fig. 5 shows the scale height distributions for atmospheres A and B. These distributions

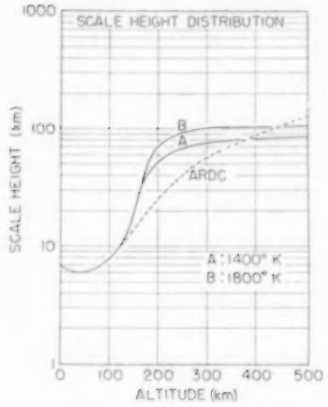

Fig. 5. Scale height distributions assumed in constructing atmospheres A and B of Fig. 3. The dashed curve indicates the ARDC scale height distribution.

are assumed to be constant above 400 km, following the arguments of Johnson[9] on the heating of the ionosphere by the absorption of solar radiation in the ultra-violet. However, there is evidence that the energy available in the ultra-violet may be inadequate, and that thermal conduction from the solar corona is the principal source of energy[10, 11]. In this event the temperature and scale height distributions will continue to rise above 400 km, and densities above that altitude will be greater than those in the present model[12].

The limiting values of the scale height and the corresponding atmospheric temperatures are given in Table 2. From Table 2 we obtain a mean scale height of (95 ± 10) km, and a mean temperature of (1600 ± 200)°K, above 300 km.

3.2. *Comparison with the ARDC atmosphere*

Fig. 4 also shows the ARDC atmosphere constructed by Mizner and Ripley in 1955 as an extrapolation of the rocket data available at that time[13].

The ARDC scale height distribution is indicated in Fig. 5. According to the present analysis, the ARDC scale heights are too small by a factor of 2 between 200 and 400 km. Above 400 km the discrepancy between the two models diminishes.

We may attempt a less drastic revision of the ARDC atmosphere, in which the temperature and scale heights of that model are preserved and the entire atmosphere is multiplied by a constant factor (~ 10) to bring it into agreement with the Sputnik I observations. The resulting atmosphere is shown as curve C in Fig. 6. We see that curve C is in disagreement with the rocket data by a factor of 5, suggesting that this is not an acceptable manner of modification of the ARDC atmosphere.

Table 2. Scale Height and Temperature Above 400 km for Atmospheres Adjusted to fit the Rocket and Sputnik 1 Data

Atmosphere	Scale height (km)	Temperature (°K)
A	85	1400
B	105	1800

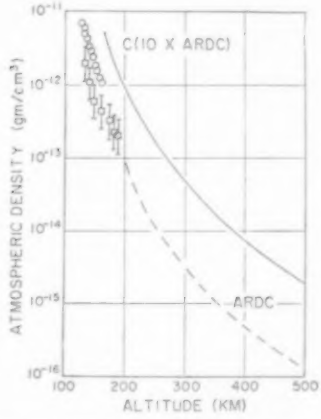

Fig. 6. Comparison of model C with the rocket data. Model C is the ARDC atmosphere multiplied by a constant factor to produce agreement with the observed rate of change of period for Satellite 1957 Alpha 2. The ARDC scale height distribution is preserved.

3.3. *Satellite lifetimes*

The densities indicated by the present analysis are 10 times larger than those of the ARDC atmosphere at 275 km, and 20 to 40 times

larger at 400 km. Estimates of satellite lifetime will therefore be reduced by the same factors for orbits with these altitudes at perigee. Fig. 7

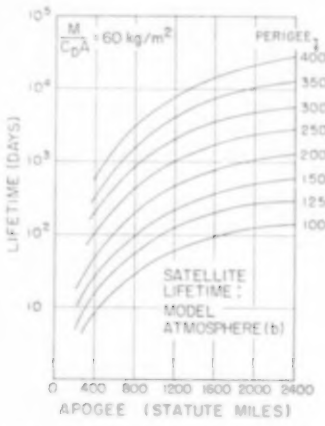

Fig. 7. Survey of lifetimes for a satellite with a ballistic drag parameter (B) of 60 kg/m², moving in the atmosphere of Fig. 4. Results for other satellites may be obtained from this graph by noting that the lifetime is directly proportional to the ballistic drag parameter.

presents a survey of lifetimes calculated for a satellite with a ballistic drag parameter of 60 kg/m², moving in the atmosphere of Fig. 7. Results for other satellites may be obtained from Fig. 7 by noting that the lifetime is directly proportional to the ballistic drag parameter.

4. ANALYSIS OF EXPLORER AND VANGUARD DATA

Minitrack observations on the orbits of satellites 1958 Alpha (Explorer I) and 1958 Beta (Vanguard I) permit us to determine the density of the atmosphere at latitudes between 33°N and 33°S[14]. Our analysis is based on the orbit elements and rate of change of period determined for these satellites by the Vanguard Computing Center.

Tables 3 and 4 list the periods and corresponding rates of change of period for the Explorer I and Vanguard I satellites. The tables also give the estimated values of the ballistic drag parameter. Referring to equation (1) we note that the observed rate of change

Table 3. Orbital Periods for 1958 α (Explorer 1), derived by the Vanguard Computing Center from Minitrack Data. The Third Column Gives the Average Value of dP/dt, obtained from the Tabular Differences in the First and Second Columns

Date	P (min)	dP/dt (min/day)
Feb. 5	114·95	
Apr. 2	114·54	·0073
May 2	114·25	·0097
May 17	114·13	·0075
Weighted average (min/day)		$(8^{+6}_{-2})\times10^{-3}$
B		(24±8) kg/m²

Table 4. Orbital periods for 1958 β (Vanguard 1), derived by the Vanguard Computing Center from Minitrack data. The third column gives the average value of dP/dt, obtained from the tabular differences in the first and second columns

Date	P (min)	dP/dt (min/day)
May 1	134·277	$(3·0\pm·5)\times10^{-4}$
June 7	134·266	$(2·8\pm·8)\times10^{-4}$
June 25	134·261	
Weighted average (min/day)		$(3·0\pm·6)\times10^{-4}$
B		(24±3) kg/m²

of period determines only the ratio of the density to the ballistic drag parameter, hence a knowledge of this parameter is essential for the density analysis. The large probable error in B indicated for Explorer I represents the uncertainty in the cross sectional area of that satellite. Explorer I has a cylindrical shape with a length of 203 cm and a radius of 7·3 cm, and the maximum and minimum values of its projected area may therefore vary by a factor of 20, depending on the orientation of the cylinder relative to the direction of motion. In our analysis the projected area is estimated by averaging over all orientations of the satellite, but a proper calculation of the effective area is extremely complicated, because the motion of

Explorer I about its center of mass cannot be properly described by either a random tumbling or a uniform precession about a fixed spin axis*. We consider our estimate of the projected area to be uncertain by a factor of 2.

Table 5 gives the densities which we obtain from the time-weighted averages of dP/dt in Tables 3 and 4, together with the altitudes to which these densities refer. The probable errors in the average density represent the combined effects of the uncertainty in the ballistic drag parameter and the variations in dP/dt during the period covered by the observations. The densities in Table 5 correspond to a mean scale height of (73 ± 10) km and a mean temperature of (1250 ± 200)°K for the region between 400 and 700 km.

Table 5. Densities Derived from Satellite Data

Altitude (km)	Density (gm/cm³)
405 (1958 α)	$9^{+6}_{-4} \times 10^{-15}$
720 (1958 β)	$(1{\cdot}2 \pm {\cdot}3) \times 10^{-16}$

Although the density value based on Explorer I has a large probable error, this result is still of substantial interest because when combined with the Vanguard I density it gives us an indication of atmospheric conditions in a latitude region not covered by the results from Sputnik I and the earlier rocket flights. The perigee of Sputnik I was located at a latitude of $39° \pm 6°$N. during the period of 12 days on which the density analysis of that satellite was based, and did not move appreciably during that interval†. The rocket data which we combined with the Sputnik value were obtained at latitude 33°N. Thus the combination of rocket and Sputnik I data describes a temperate zone atmosphere. On the other hand, the orbits of the Explorer and Vanguard satellites are confined to the region centered on the equator and lying between 33°N and 33°S. Since perigee rotates in the orbital planes of of these satellites at the rate of one revolution in 60 days, the average densities for the intervals covered in Tables 3 and 4 constitute a thorough sampling of all latitudes in this region. Therefore the Explorer and Vanguard results refer to a band of latitudes centered about the equator.

According to recent results of LaGow at 200 km², the summer daytime density at 59°N is 8 times the corresponding density at 33°N. We expect comparable differences between the present results and our provisional model for temperate latitudes, but in fact the densities of Table 3 are only 30 per cent to 50 per cent less than the lower limit of probable error in the temperate zone atmosphere. Presumably the comparison must also allow for diurnal and seasonal variations, which are as yet very poorly determined.

As a corollary to the preceding remarks, it is interesting to note that because of the strong latitude dependence of upper atmosphere densities, we cannot compare density determinations based on the orbits of the present U.S. satellites with those obtained from U.S.S.R. satellites.

* The use of the average cross section is clearly appropriate for random tumbling. If the cylinder spins about a fixed axis the average will still be applicable to observations spread over a period of one or more months, because of the rapid motion of the perigee in the orbital plane. In fact, however, the spin axis of Explorer I is not fixed. This satellite is aerodynamically stable, and air drag exerts a torque about its center of mass on each passage through perigee tending to align the spin axis with the direction of motion at perigee.

† Perigee rotates in the orbital plane at the rate of one revolution in 2 years for an orbital inclination of 65°.

ACKNOWLEDGEMENTS

We are indebted to Mr. H. E. LaGow and Drs. H. Friedman, H. E. Newell, J. A. O'Keefe, and F. C. Johnson for many valuable discussions on the properties of the upper atmosphere. We are also very grateful to Mr. W. F. Cahill of the National Bureau of Standards for the preparation of the IBM 704 programs required in the analysis, to Mr. J. H. Wegstein for his collaboration in writing the earlier forms of these programs, and to Mr. C. Wade, Jr., for his co-operation in executing the machine calculations.

APPENDIX

We assume that the drag force is small and the orbit of the satellite a quasi-ellipse. The total energy of the satellite in an elliptical orbit is given by

$$E = -\tfrac{1}{2}\frac{GMm}{R} \qquad (1a)$$

in which G is the universal gravitational constant, M and m are the masses of Earth and satellite, respectively, and R is the length of the semi-major axis. The rate of energy loss is given by the average power dissipated over one revolution, for which we take a time average of the power consumed in friction. The drag force is $-\frac{1}{2}C_D A\rho v^2$, in which C_D is the drag coefficient, A the area projected along the direction of motion, ρ the air density and v the satellite speed. Then

$$\frac{dE}{dt} = \frac{1}{2}\frac{GMm}{R^2}\frac{dR}{dt} = -\frac{1}{2}\overline{C_D A\rho v^3} \quad . \tag{2a}$$

The bar in (2a) denotes the time average over one revolution,

$$\bar{F} = \frac{1}{P}\int_0^P F(t)\,dt$$

where P is the orbital period. Since $R = (P\sqrt{GM}/2\pi)^{2/3}$, we obtain finally

$$dP/dt = -a(\overline{\rho v^3}/B) \tag{3a}$$

where $a = 3\pi(GM)^{1/3}(P/2\pi)^{5/3}$.

The second equation is derived by equating the rate of change of angular momentum to the angular impulse. Let L denote the angular momentum, R_E the radius of the Earth, e the eccentricity and ϕ the angle between the radius vector and the tangent to the ellipse, i.e., $\sin\phi = L/mvR$. Then we have

$$\frac{L^2}{m^2 g R_E^2} = R(1-e^2)$$

and

$$\frac{dL}{dt} = \frac{\partial L}{\partial R}\frac{dR}{dt} + \frac{\partial L}{\partial e}\frac{de}{dt} = -\frac{1}{2}\overline{C_D A\rho v^2 r\sin\phi} \quad . \tag{4a}$$

From (2a)–(4a) we obtain

$$\left(\frac{e}{1-e^2}\right)\frac{de}{dt} = b(\overline{\rho v/B}) - c(\overline{\rho v^3/B})$$

in which $b = \frac{1}{2}$ and $c = R/GM$.

REFERENCES

1. GRIMMINGER G. *Analysis of Temperature, Pressure and Density of the Atmosphere Extending to Extreme Altitudes.* RAND Corporation (Nov. 1948).
2. LAGOW H. *Ann. Géophys.* **5** (1958).
3. Similar equations have been derived by T. E. STERNE, *Astr. J.* (in press).
4. STERNE T. E. *Science* **127,** 1245 (1958).
5. MENGEL J. *Elec. Eng.* **76,** 666 (1957).
6. A preliminary report on these calculations has appeared in *Science* **127,** 471 (1958).
7. BYRAM E. T., CHUBB T. A. and FRIEDMAN H. *Dissociation of Oxygen at High Altitudes, Threshold of Space,* p. 211. Pergamon Press, London (1957).
8. HOROWITZ K. and LAGOW H. *J. Geophys. Res.* **62,** 57 (1957).
9. JOHNSON F. S. International Union of Geodesy and Geophysics, Toronto (1957).
10. FRIEDMAN H. *9th Report of the Council of International Scientific Unions.* Commission on Solar-Terrestrial Relationships, Paris (1957).
11. CHAPMAN S. *Smithsonian Contributions to Astrophysics* **2,** No. 1 (1956).
12. NICOLET M. *Science* **127,** 13–17 (1958).
13. MIZNER R. A. and RIPLEY W. S. *ARDC Model Atmosphere.* ASTIA Document 110233 (1956).
14. These data have also been analyzed by J. W. Siry, in a paper presented at the Fifth CSAGI Assembly (Moscow, 1958), and in the IGY reports of the Smithsonian Astrophysical Observatory by
STERNE T. E. *SAO IGY Report* **11,** p. 18; JACCHIA L. G. *SAO IGY Report* **12,** p. 30; SCHILLING G. F. and STERNE T. E. *SAO IGY Report* **12,** p. 37.

Planet. Space Sci. Pergamon Press 1959. Vol. 1, pp. 27–31. Printed in Great Britain.

MICROMETEORITE MEASUREMENTS FROM 1958 ALPHA AND GAMMA SATELLITES

EDWARD R. MANRING*

Geophysics Research Directorate, Air Force Cambridge Research Center, Air Research and Development Command, Laurence G. Hanscom Field, Bedford, Massachusetts

(*Received* 11 *July* 1958)

Abstract—Grid abrasion micrometeorite detectors mounted on 1958 Alpha and Gamma satellites give a maximum influx rate of particle 10 μ in diameter or larger for the period 1 February to 7 May 1958. On 7 May 1958 two detectors appeared to indicate impacts on 1958 Gamma. The failure within a few days of all electronics on the satellite open the possibility that a shower was encountered with meteor damage subsequently destroying electronics; or of an electronics failure which first manifested itself in the meteorite detection gear.

1. INTRODUCTION

THE direct detection of micrometeorites reaching the earth's atmosphere cannot be accomplished by the standard visual, photographic, or radio methods. Since these small particles survive their entry into the atmosphere, the possibility of gathering them at the earth's surface exists[1]. Estimates of micrometeorite influx rates from such collections are usually much higher than would be predicted from the direct observation of larger meteor trails and from the application of theory to extrapolate to small sizes.

Direct measurements of micrometeorite densities above the atmosphere have been made over very short time intervals from rocket platforms. The influx rates thus determined vary over wide limits[2, 3]. The platform provided by a satellite vehicle is very desirable in that it remains above the atmosphere for long periods of time. The IGY satellite program includes various equipments for direct measurement of these densities. The Vanguard II "package" which was transferred to the Explorer series and became 1958 Alpha and Gamma carried small wire grids which could be fractured by micrometeorite impacts. It was also possible to place a microphone in contact with the shell of 1958 Alpha which responded to the acoustical disturbances of an impacting micrometeorite upon the vehicle skin.

2. INSTRUMENTATION

The weight, power, and telemetry available impose severe limitations on equipment which may be utilized, with the inevitable results that some desired measurements must be sacrificed. The parameters of interest are:

(*a*) Influx rates of each size interval.
(*b*) Impinging velocity.
(*c*) Composition and density.

Acoustical devices respond to impacting momentum so that each recorded event is a function of both mass and velocity. Optical sensing of the amount of light admitted through an opaque film as the film is abraded is a function of number of hits as well as crater area. Measurements in general, involve such interdependence of parameters.

The micrometeorite experiment proposed by Air Force Cambridge Research Center and approved for Vanguard II by the IGY Earth Satellite Panel was composed of twelve cards mounted to the sphere's surface. Each card was wound with enamelled wire 17 μ in diameter. A micrometeorite of about 10 μ or larger impacting upon one of the wire grids would fracture it destroying electrical con-

* Present address: Geophysics Corporation of America, 700 Commonwealth Avenue, Boston, Massachusetts.

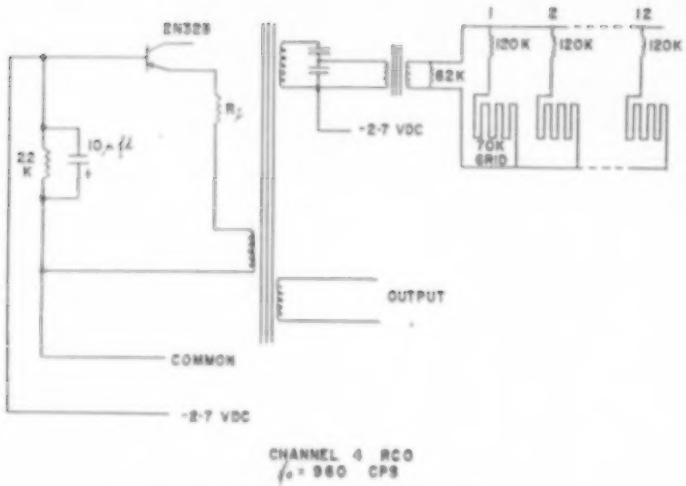

Fig. 1. Circuit diagram of sub-carrier generator and grid detectors feeding into the low power transmitter.

tinuity. The wire was a nickel alloy (Tophet C., W. B. Driver and Co.) wound with the individual turns side by side. The wire diameter was about 21 μ with the enamel insulation included. Two layers were wound on each card to insure that a total area of 1 cm × 1 cm was completely covered. Each winding presented an electrical resistance of about 70,000 Ω and had a fixed resistor of 120,000 Ω connected in series with it.

The individual cards were connected in parallel electrically. The combined resistance then became the frequency controlling element of a sub-carrier generator used to modulate the satellite transmitter. In the original circuits designed for Vanguard II, the detector combined resistance was replaced periodically with two standard resistors by means of a single pole double throw relay actuated by a slow, free running multivibrator. The detectors were connected to one terminal, a standard resistor to the second terminal, and the second standard resistor was connected to the pole so that during relay throw time it provided the second calibration check. Since the sub-carrier generator was temperature sensitive, this calibration also provided an independent measurement of the electronics chamber temperature.

At the time the Vanguard II "package" was transferred to the Explorer series, the Jet Propulsion Laboratory undertook the task of designing the sub-carrier generator due to the very short lead time, as well as the distance separating the assembly point and the Geophysics Research Directorate.

The twelve grids were mounted in a Fiberglas supporting ring attached around the six inch diameter cylinder near the back and just behind a ring or launching surface which accepted the previous stage. In this manner the grids were protected from aerodynamic forces and heating during the ascent phase.

A circuit diagram is shown in Fig. 1, mounting ring in Fig. 2, and a calibration curve of the sub-carrier generator frequency in Fig. 3. The output of the generator shown in Fig. 1 was connected in series with two temperature measuring units as well as the cosmic ray counter, and the combined outputs impressed upon the low power transmitter operating continuously on 108·00 Mc/sec with a 10 mW output.

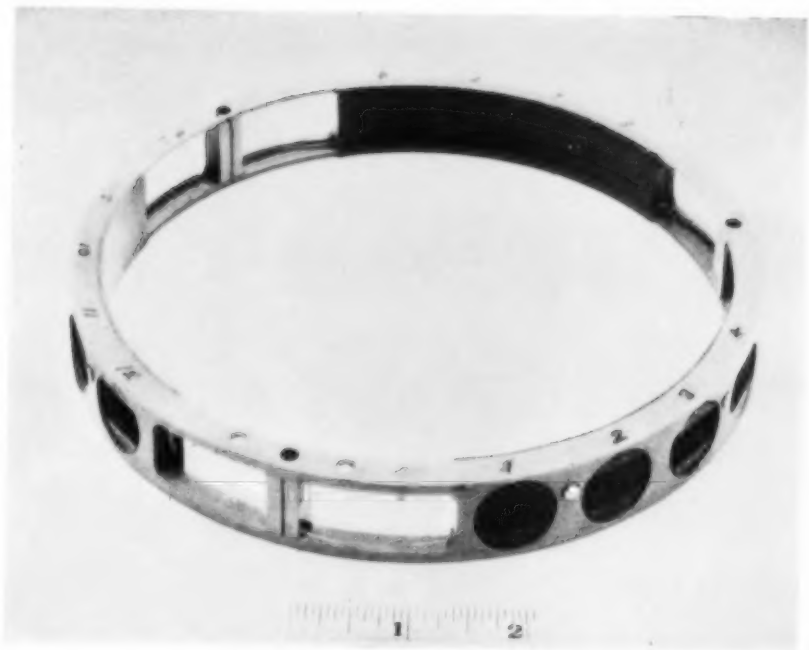

Fig. 2. Grid detector mounting ring.

Facing p. 28

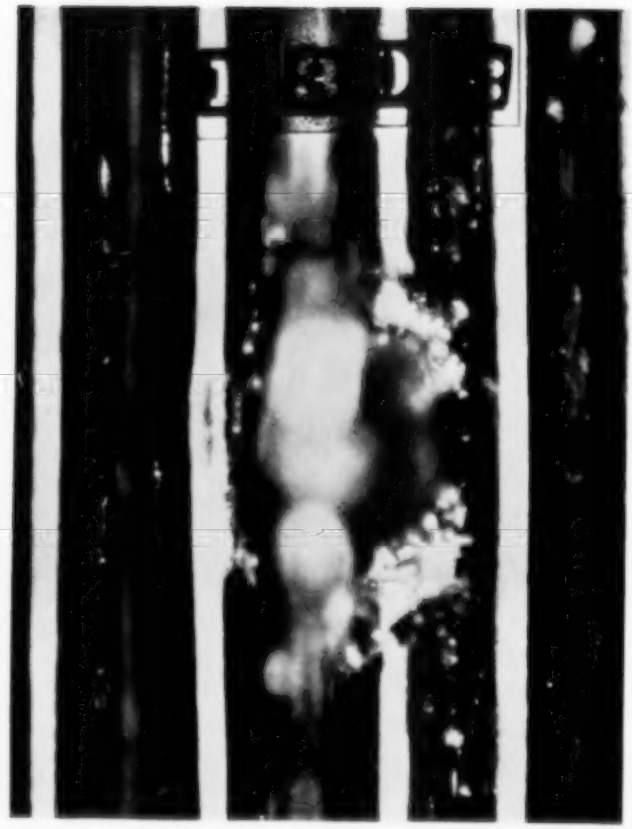

Fig. 4. Single layer of 17 μ wires. Crater produced by an impact of a steel particle less than 15 μ in diameter accelerated to between 4 and 6 km/sec. Work carried out by T. C. Poulter, Stanford Research Institute, Menlo Park, California.

facing p. 29]

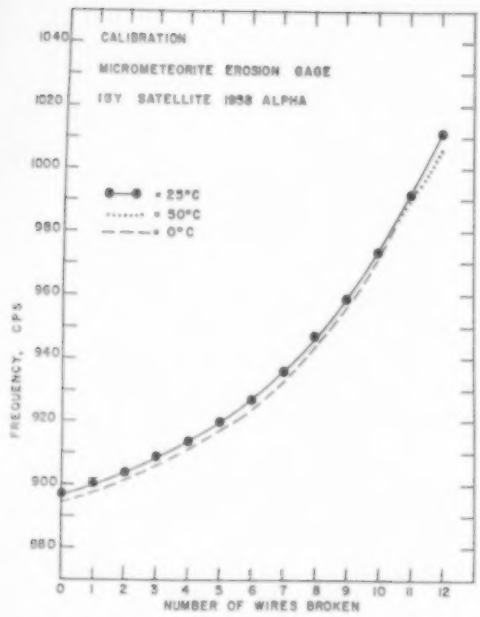

Fig. 3. Sub-carrier generator as a function of broken grid detectors.

Meteorite velocities are between about 11 and 70 km/sec. Crater diameters for particles at these velocities are two and perhaps eight to ten times the particle diameter, dependent upon the particle density and target density. Some work has been done to calibrate experimentally. Shaped charge particles of 15 μ or less in diameter (low value cannot be determined) accelerated to about 5 km/sec were noted to break at least one, and in many instances several, of the wires. Particles 5 μ or less in diameter accelerated to about 5 km/sec were observed to break the wires when the hit was direct and to pass between without breaking electrical continuity in some cases. Fig. 4 shows a micro-photograph of an impact of a particle smaller than 15 μ upon a test grid.

It became possible on 1958 Alpha to include a microphone pick-up and amplifier to detect the impact of micrometeorites upon the vehicle's skin. This work was under the direction of M. Dubin of this organization and is reported on in greater detail by him[3]. The microphone was placed in acoustical contact with the instrument or middle section skin. The nose cone and motor chambers were acoustically isolated from the middle section by Fiberglas separators. The effective area of this section was 0·075 m².

The amplifier pulses actuated a bi-stable multivibrator which modulated the high power transmitter, 60 mW, producing either a high or low tone which changed from one to the other when an impact above the equipment threshold occurred. The threshold sensitivity over the area varied from $1{\cdot}7\times10^{-3}$ to $5{\cdot}2\times10^{-3}$ g cm/sec and averaged about $2{\cdot}5\times10^{-3}$ g cm/sec. These values were determined by dropping particles of known mass and impact velocity upon various portions of the skin. To extend these sensitivity values to meteor velocities it is assumed that the acoustical response is a function only of the impinging momentum. This relation appears to hold to 300 m/sec from experimental tests, and should serve as a relative calibration even though subsequent work should indicate that acoustical response is not a function of momentum only, but perhaps some complicated function of velocity of the impacting particle. Fig. 5 shows the mounting arrangement and calibration.

3. RESULTS

1958 Alpha was launched on 1 February 1958, at 0355 GCT. The high power transmitter remained in operation until 12 February; it returned for reasons not well understood some five days later and continued to give useful data for several additional days. The low power transmitter functioned continuously until after mid-April; however, useful data of good signal to noise ratios were not taken after about 1 April. 1958 Gamma, launched on 26 March 1958, at 1738 GCT, operated normally until 7 May when various electronic components began to fail over the subsequent five days.

During the launch phase of 1958 Alpha one or two of the grid detectors were apparently broken. For the portion of the calibration corresponding to less than four grid detectors open, the sub-carrier generator frequency as a function of detectors broken cannot be determined with better precision than plus or minus

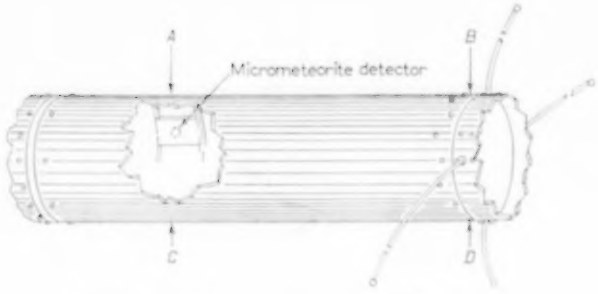

Fig. 5. Microphone position and threshold sensitivities. Micrometeorite impact calibration of cylindrical shell of Explorer I. *Threshold impulse:* A—$1{\cdot}7\times10^{-3}$ g cm/sec. B—$4{\cdot}6\times10^{-3}$ g cm/sec. C—$2{\cdot}5\times10^{-3}$ g cm/sec. D—$5{\cdot}2\times10^{-3}$ g cm/sec. *Area*—$7{\cdot}25\times10^{-2}$ mc.

one open grid when temperature uncertainties are considered. No more than one and perhaps no detectors were broken from meteor impacts on Alpha. All grids survived the launching of Gamma, and none were broken before 7 May.

The sequence of events after 7 May are:

(1) 7 May, Sub-carrier generator indicated two grids broken.
(2) 8 May, Channel 5, low power transmitter (temperature) not operating.
(3) 9 May, Modulator on low power transmitter not operating.
(4) 10 May, Command receiver misses interrogation.
(5) 11 May, High power transmitter completely silent.
(6) 12 May, Low power transmitter not functioning.

The two transmitters were independent units with separate battery supplies. They had been operating less than half of the predicted lifetime. It is difficult to account for the nearly simultaneous failure of the two independent systems by attributing them to electronic defects.

The two open grid detectors may indicate that the satellite passed through a meteor shower, damage from which caused the subsequent failures. The Aquarids shower in May occurred at about the time of the failure. If the failures were occasioned by some defect in the electronic or battery units, it may be that the first unit notably affected was the micrometeorite generator frequency. The number of recorded passes after the first hits on 7 May yielding micrometeorite readings and available at this time are not enough to preclude either of these explanations. The electronics staff at Jet Propulsion Laboratory cannot account for the sequence of events with normal electronics failures (private communication).

From 1958 Alpha the recorded grid data was good for about 60 days. Since two grids were broken during ascent and not more than one additional grid broken during the following 60 days, it is possible to compute a meaningful maximum influx rate of particles large enough to break the grid wire. Because the number of hits is not more than one, the average value has little or no statistical significance. A value of greater meaning is to ask what influx rate would produce at least one detector hit in the time interval observed with a known probability.

Where $N(A, t)$ = total number of hits on area A in time t,

$$\bar{n} = \lim_{t \to \infty} \frac{N}{At}$$

and

$$X = At\bar{n}$$

then

$$P_{r+} = 1 - \sum_{\lambda=0}^{\lambda=s-1} \frac{X^{\lambda} e^{-X}}{\lambda!}$$

is the probability that during time t, at least ν hits will be recorded on area A.

For $A=10$ detectors of 1 cm² each or 10^{-3} m², $t=60\times24\times3600$ the time recorded in seconds; then for $\nu=1$; $P_{1+}=1-e^{-X}$

P_{1+}	X	$\bar{n}$
0·99	4·6	$0{\cdot}90\times10^{-3}$/m² sec
0·999	9·0	$1{\cdot}7\times10^{-3}$/m² sec

Shielding of the satellite by the earth has not been considered in the above and would have the effect of increasing the calculated maximum influx rates of threshold size particles by a factor slightly less than two. It is important to note that these maximum rates are significant only in terms of the experiment itself. Much higher rates might be expected during the autumn showers or in the belts of defunct comets. The threshold size for particles which will fracture the wire grids at meteor velocities cannot be stated with certainty but are probably smaller than 10 μ.

The microphone experiment carried on 1958 Alpha reported impacts which occurred over a ground recording station. Due to poor signal to noise ratios the task of reducing data has proven to be a great one. M. Dubin, who directed the experiment, and F. Dearborn have developed very elaborate reduction procedures to analyze this data. The results will be reported later in greater detail. The influx rate determined from presently available data is about 3×10^{-2}/m² sec for particles larger than the instrumental threshold. Since the average sensitivity was $2{\cdot}5\times10^{-3}$ g cm/sec, assuming linear response with velocity, average velocities of 40 km/sec, and a density of 3·6 g/cm² for spherical particles; the threshold diameter is about 3 μ. This data represents only a very small amount of the total available and only positive impacts utilized. More impacts (presently obscured by noise) are probably present and will be apparent when more detailed reduction is accomplished.

ACKNOWLEDGEMENTS

Satellite experiments require co-operation from many people, groups and organizations. The original Vanguard II electronics were built by Mr. F. Dearborn, the grid winding was done very expertly by Mr. Arthur Corman. The Explorer electronics, installation, and calibration were done very thoroughly and carefully by personnel at Jet Propulsion Laboratory, California Institute of Technology. Data recording was by the Naval Research Laboratory, numerous volunteer groups and amateurs. The IGY offices organized, originated and made the experiment possible. The host experimenters at State University of Iowa co-operated in all possible detail. Special acknowledgement is also made to the Jupiter C launching and developmental groups.

REFERENCES

1. Whipple F. L. *Vistas in Astronautics*, edited by M. Alperin and M. Stern. Pergamon Press London (1958).
2. Berg O. and Meredith L. *J. Geophys. Res.* **61**, 751 (1956).
3. Dubin M. *Cosmic Debris of Interplanetary Space*. To be published (1958).

Planet. Space Sci. Pergamon Press 1959. Vol. 1, pp. 32–36. Printed in Great Britain.

THE AIRGLOW OF VENUS*

GORDON NEWKIRK, Jr.

High Altitude Observatory of the University of Colorado, Boulder, Colorado

(*Received* 28 *October* 1958)

Abstract—Low dispersion, high speed spectra of the unilluminated portion of Venus show emission features at 4415 Å and 4435 Å which agree in position with those found by Kozyrev. Kozyrev's other emission bands are not corroborated by these spectra. A previously unreported emission band may be present at 4505 Å. The radiance of the emission bands centered at 4420 Å is about eighty times that of the 5577 Å line of the terrestrial airglow. It is unknown whether the emission from the dark side of Venus is of airglow or auroral character.

1. INTRODUCTION

ONE of the earliest telescopic observations of Venus by Johannes Riccioli in 1634[1] reports that the unilluminated portion of the planet was visible with an appearance somewhat similar to the "old moon in the new moon's arms". Since that time many observers have recorded the occasional appearance of the "ashen light" on the dark side of the crescent Venus. The physical reality of the ashen light has been severely questioned, particularly because some observers of this phenomenon also claim to see the dark portion of the planet silhouetted against the bright daylight sky. Nevertheless, one should expect the occurrence of both airglow and, if Venus has a magnetic field, aurora on the dark side of the planet. A Cytherean aurora of moderate intensity would be easily visible with a telescope were it not for the background of light scattered in the terrestrial atmosphere and the telescope.

In a recent study of the spectrum of the dark side of Venus, N. A. Kozyrev[2] located some fifty emission features, most of which he identified as due to the spectrum of N_2. The oxygen line at 5577 Å, which is outstanding in the terrestrial airglow and aurora, was absent on his spectra. The examination of the spectrum of the airglow or aurora of Venus is of importance because it provides information on both the composition of the Cytherean atmosphere and the possible existence of a magnetic field on the planet.

To the end of furthering Kozyrev's study, we constructed a fast planetary spectrograph to examine possible variations in time of the intensity of the emission lines of Venus.

2. INSTRUMENTATION

Since the major difficulty in the study of the dark side of Venus is the light scattered in the atmosphere and in the telescope, we designed a system similar to a coronagraph to minimize the latter source of background light. A schematic diagram of the optics appears in Fig. 1a. A triplet, designed by Dr. James G. Baker as an achromatic coronagraph lens with a minimum of internal scattering, forms an image of Venus on a wide, polished slit. The light from the illuminated crescent is reflected from the slit jaws to an eyepiece for guiding while that from the dark side of the planet passes to a collimator-field lens. This lens both collimates the light from the slit and forms an image of the objective on an aperture stop, which eliminates the radiation diffracted by the objective aperture. A grating (600 lines/mm) and a semi-solid Schmidt camera (3 in. aperture, $f/0{\cdot}6$, manufactured by Perkin–Elmer Corporation) complete the system. The combination gives a dispersion of 350 Å/mm at H_γ. The high speed spectrograph was chosen in order to allow exposures to be made near inferior con-

* This research was carried out under Contract Nonr 393(05) with the Office of Naval Research.

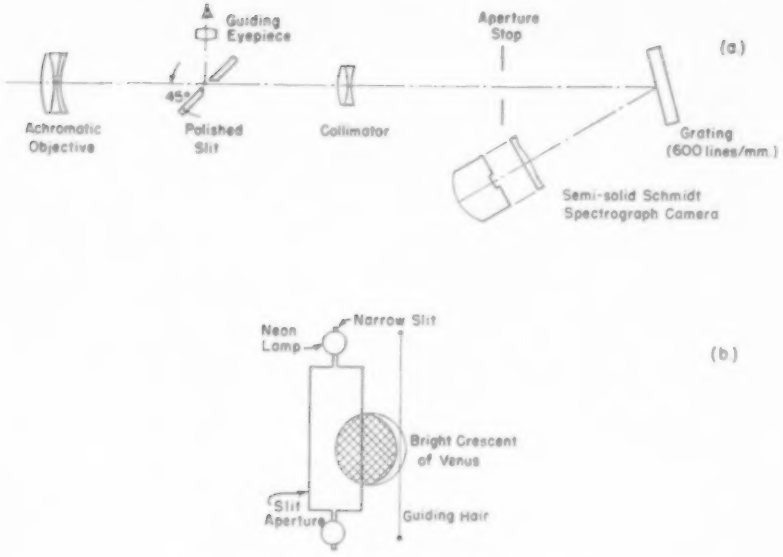

Fig. 1. (a) Schematic diagram of the optics for examining the spectrum of the dark side of Venus. (b) Arrangement of Venus on the slit during "dark side" exposures.

junction when but a few minutes elapse between the end of twilight and the setting of the planet.

The instrument seemed to contribute very little to the halo of scattered light seen about Venus. Tests on spectra taken with the planet in position (Fig. 1b) showed the radiance of the aureole in units of the radiance of the bright crescent to be

$$B/B_{\varphi} \sim 10^{-7},$$

which agrees approximately with what is to be expected from the measurements of the solar aureole. The scattered radiation was still intense enough to prevent exposures on Eastman Tri-X film longer than about 5 min under average circumstances.

To give standards of both wavelength and intensity, two small neon lamps illuminated two narrow slits at either side (Fig. 1b) of the slit aperture. An electric shutter behind the slit assembly made certain that the exposures on the standard and on Venus were of the same length.

3. OBSERVATIONS

Our efforts to obtain a long series of spectra of the dark side of Venus to compare the intensity of the emission features with geomagnetic activity were frustrated by the late arrival of the spectrograph camera from the manufacturer. Between 6 and 10 January 1958, 9 exposures on the dark side and 10 calibration exposures of the bright crescent were made. Microdensitometer tracings of the blue region of enlarged positives of some of the best spectra appear in Fig. 2. On these tracings the locations of the major Fraunhofer lines in the scattered radiation are marked by lines below the spectrum, while the locations of the brightest emission features catalogued by Kozyrev are marked by short lines above the tracings. The difficulty caused by the film grain is apparent. In the attempt to partially obviate this difficulty, we have superimposed tracings of several different spectra in Fig. 3.

For those emission bands which are not in danger of being confused with the "shoulder"

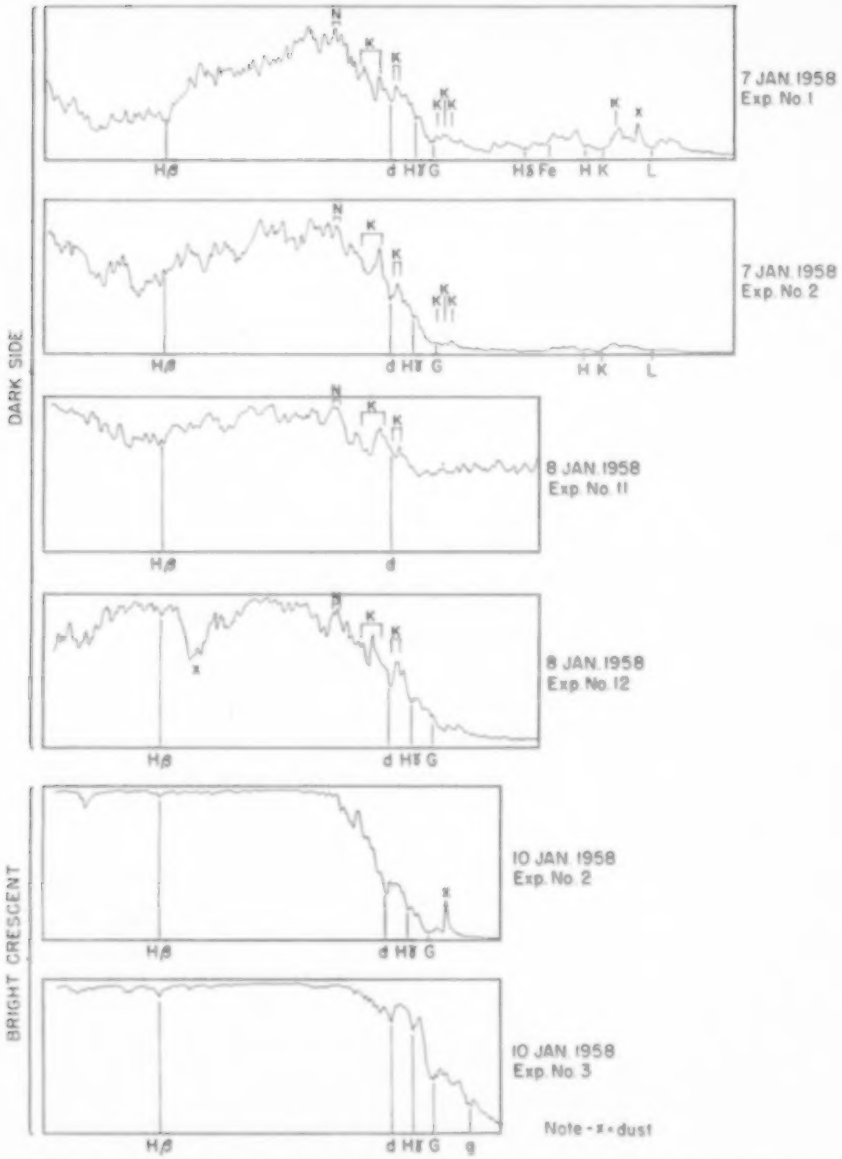

Fig. 2. Microdensitometer tracings of spectra made on the dark side and on the illuminated crescent (attenuated) of Venus. The positions of the Fraunhofer lines and the brightest emission features are marked.

between absorption lines it is possible to set up an objective criterion P for the reality of the band. Here P is the number of spurious features of a given amplitude which would be expected to appear in our superposed tracings due to the random fluctuations (plate grain) of the original tracings.

In the table appear the wavelengths of the

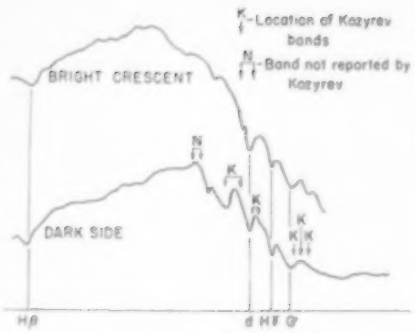

Fig. 3. Superposition of tracings of several different spectra. Note that the contrasts are not the same in the dark side and in the bright crescent tracings.

brightest bands (intensity at least 3) observed by Kozyrev, their tentative identification, the quantity P, and brief remarks. The band centered at 4505 Å, which appears on our spectra, was not reported by Kozyrev. Clearly, only the bands with $P < 0{\cdot}1$ can be regarded as being even probably established by this study. It is quite possible that Kozyrev's higher dispersion plates show the fainter emission lines; however, it is difficult to form a definite opinion of their reality since the reproduction of his spectrum is exceedingly poor and is unaccompanied by microdensitometer tracings.

4. ORIGIN OF THE EMISSION FEATURES

Kozyrev's identification of the bands at 3914 Å and 4278 Å with the heads of the negative groups of N_2^+ is of significance since there is no other spectroscopic evidence for nitrogen in the atmosphere of Venus. The two emission bands whose existence is confirmed by this study, i.e. those at 4415 Å and 4435 Å, remain unidentified. The coincidence of a forbidden molecular oxygen band

$$(3\Sigma_u^+ - 3\Sigma_g^-,\ 1\text{–}8),$$

which appears in the terrestrial airglow, with the latter feature is probably accidental since the dominant 5577 Å oxygen line of the terrestrial airglow is missing from both Kozyrev's and our spectra.

The question of whether the emission bands are of auroral or of airglow character is still unanswered. Over the short interval of observation there was no change in intensity of the bands. The geomagnetic activity was also low during this period. Our system was incapable of resolving any auroral zones on Venus so that this technique of distinguishing between airglow and aurora could not be applied.

5. INTENSITY OF THE EMISSION

The radiance of the major feature of the airglow of Venus between 4410 Å and 4440 Å can be estimated by using the neon lines on each spectrogram as an intermediate standard between the airglow exposure and the exposure made on the attenuated crescent of Venus. Since the slit of the spectrograph was large

λ (Å) ±7 Å	Identification (Kozyrev)	P	Remarks
3914	N_2^+, NG (0–0)	?	Feature may be "shoulder" of K line of Fraunhofer spectrum.
4250	—	?	These three features seem to be present, but the relative rise in intensity at this position may well be the shoulder of the G band.
4264	—	?	
4278	N_2^+, NG (0–1)	?	
4363–70	—	4	
4410–20	—	0·007	No feature which could be misinterpreted as an emission band appears in the spectrum of the illuminated crescent at the positions of the first two bands.
4430–40	—	0·007	
4450–62	—	absent	
4500–10	—	0·068	Not reported by Kozyrev.

enough to admit the full image of Venus, we can write

$$B_{4430} = \frac{i_\lambda}{i_c} t \left(\frac{r\odot}{r\,\varphi}\right)^2 \frac{1}{f} \frac{l\,\varphi}{l\odot} \frac{\Delta\lambda}{2} B\odot,$$

where i_λ = intensity of 4430 Å band on the neon scale,
i_c = intensity of the nearby continuum of the attenuated crescent on the neon scale,
$t = 2{\cdot}9 \times 10^{-4}$ = transmission of attenuating filter,
$r\odot$ = apparent radius of sun,
$r\,\varphi$ = apparent radius of Venus[2],
f = fraction of Venus entering spectrograph for "airglow" exposures (f is taken as $\frac{1}{4}$),
$l\,\varphi$ = luminosity of Venus,
$l\odot$ = luminosity of the sun,
$\Delta\lambda = 16$ Å = approximate width of 4430 Å band,
$B\odot = 2{\cdot}6 \times 10^6$ erg sterad^{-1} cm^{-2} sec^{-1} Å^{-1} = radiance of solar surface.

From the spectra we determine that $i_\lambda/i_c = 0{\cdot}7$. Since on 10 January 1958 the visual magnitude of Venus was $-4{\cdot}1$[2] and the magnitude of the sun is $m\odot = -26{\cdot}7$[4],

$$\log l\,\varphi/l\odot = -0{\cdot}4\,(26{\cdot}7 - 4{\cdot}1) = -9{\cdot}04.$$

We find

$$B_{4430} \sim 9{\cdot}6 \times 10^{-3} \text{ erg sterad}^{-1} \text{ cm}^{-2} \text{ sec}^{-1}$$

by assuming a triangular shape for the band profile. In the more conventional unit of Rayleighs[5] for airglow and auroral work

$$B_{4430} \sim 20 \times 10^3 \text{ R}.$$

We must emphasize that this value is derived on the assumption that the emission is uniformly distributed over the dark side of Venus. If the radiation is concentrated in auroral zones, the radiance from these zones must be correspondingly higher.

To compare the radiance of this feature in the Cytherean airglow with the 5577 Å line of the terrestrial airglow we note that the airglow brightness averaged over the sky is about $2{\cdot}5 \times 10^2$ R[6] and find that the ratio of the Cytherean to the terrestrial airglow is about 80. This agrees, within the accuracy of the determination, with Kozyrev's value of 50 for the same ratio.

6. VISIBILITY OF THE ASHEN LIGHT

On the five nights from 6 January 1958 through 10 January 1958 I carefully examined the dark side of Venus for emission by allowing the bright crescent to pass through the slit aperture and reflecting the dark side from the polished slit jaw. On no occasion was any radiation from the dark side visible (although Patrick Moore of the British Astronomical Association reports that the ashen light was visible under high ($\times 320$) magnification during the period). At first glance this fact seems difficult to reconcile with the radiance of 20,000 R for the emission band at 4430 Å. since a similar radiance corresponds to a Class I–II aurora. However, a source with an apparent diameter of 30′ (as seen in the eyepiece of our apparatus) with a radiance of 20,000R is only a factor of about 40 above the threshold of the eye for peripheral vision[7]. Considering the fact that the eye is some five times less sensitive at 4300 Å than at 5577 Å, we should not be surprised that the ashen light, which is superposed on a field of scattered light, is difficult to see. An increase in the intensity of the band by a factor of five would bring the ashen light well above the threshold of visibility. Such a phenomenon may account for the occasional sightings of the ashen light.

ACKNOWLEDGEMENTS

I should like to thank Dr. G. Herzberg and Dr. W. O. Roberts for suggesting a search for the airglow of Venus. Dr. F. E. Roach aided through his discussions of the problem. The construction of the apparatus was under the supervision of L. B. Lacey of the High Altitude Observatory staff.

REFERENCES

1. Moore P. *The Planet Venus*, p. 84. Faber and Faber, London (1957).
2. Kozyrev N. A. *Izv. Krym. Astrofiz. Obs.* **12**, 169 (1954).
3. Clemence G. M. *U.S. Ephemeris and Nautical Almanac*, 393 (1958).
4. Stebbins J. and Kron G. E. *Astrophys. J.* **126**, 266 (1957).
5. Hunten D. M., Roach F. E. and Chamberlain J. W. *J. Atmos. Terr. Phys.* **8**, 345 (1956).
6. Allen C. W. *Astrophysical Quantities*, p. 127. The Athlone Press, London (1955).
7. Roach F. E. and Jamnick P. M. *Sky and Telesc.* **17**, 164 (1958).

Planet. Space Sci. Pergamon Press 1959. Vol. 1, pp. 37–39. Printed in Great Britain.

RE-ENTRY OF THE SPUTNIK I ROCKET*

I. HARRIS and R. JASTROW†

Nucleonics Division, U.S. Naval Research Laboratory, Washington, D.C.

(*Received* 29 *September* 1958)

1. INTRODUCTION

OBSERVATIONS on Satellites 1957 Alpha 1 (Sputnik I rocket) and 1957 Beta (Sputnik II) provide an opportunity for a study of the behavior of artificial satellites during the final stage of re-entry into the atmosphere. In the present report we confine ourselves to a discussion of the data on Sputnik I.

Our analysis indicates that in general the determination of the impact point requires one or more observations of altitude during the final pass. The observations on the Sputnik I rocket include a late radar echo obtained by

* Presented at the Fifth CSAGI Assembly, Moscow, 30 July–9 August 1958.

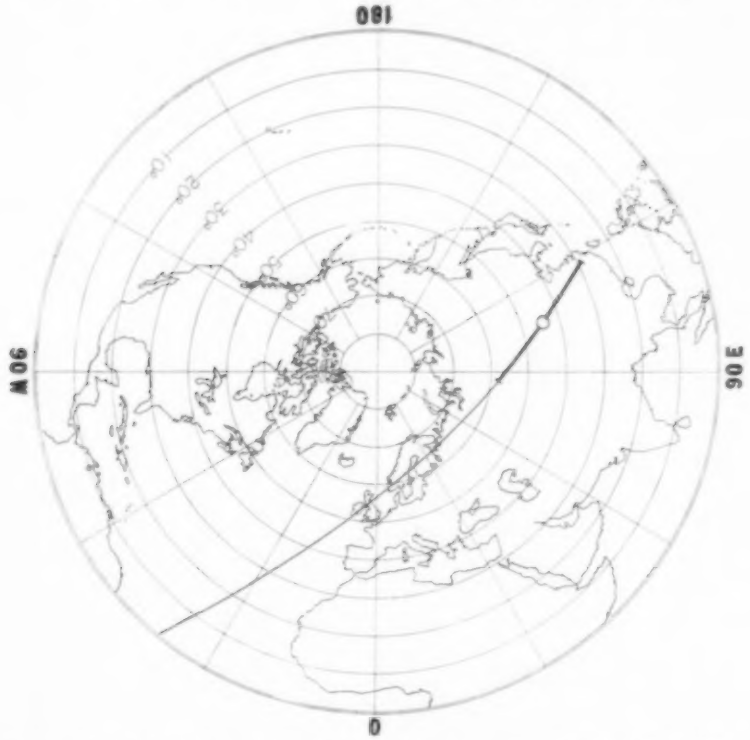

Fig. 1. Polar projection of the northern hemisphere showing the trajectory of Satellite 1957 Alpha 1 during its final pass. The calculated impact point is indicated by a circle at latitude 45° N and longitude 106° E. The probable error in the impact point due to uncertainties in (i) the altitude over Malvern, England and (ii) the drag coefficient is indicated with heavy lines to either side of this circle.

† Present address: National Aeronautics and Space Administration, Washington, D.C.

the staff of the Royal Radar Establishment at Malvern, England. The Malvern datum, combined with other radar observations on 1957 Alpha 1, leads us to the conclusion that this satellite fell on 1 December at 0846 GMT, approximately 8 hr after the last sighting made on it in the United States. We place the probable point of impact at latitude 45°N and longitude 106°E, in Outer Mongolia. The result of our investigation is shown in Fig. 1, which represents the trajectory of 1957 Alpha 1 during its final pass over the northern hemisphere. The probable impact point is marked by a circle in Fig. 1, and the uncertainty in the impact point by heavy lines to either side of this circle.

2. DETAILS OF THE ANALYSIS

We start the numerical integration of the satellite equations of motion at an epoch prior to the re-entry, checking our results against available observations as the integration proceeds. When significant discrepancies develop we adjust the value of the drag coefficient and repeat the integration until agreement is obtained. In the final stage of the calculation the drag adjustments are made most conveniently by integrating backwards in time from the last observation.

In the course of the calculations it was noted that the orbits maintained an appreciable eccentricity down to the final passes. Fig. 2 shows the difference between apogee and perigee altitudes for a typical integration in the calculations on 1957 Alpha 1.

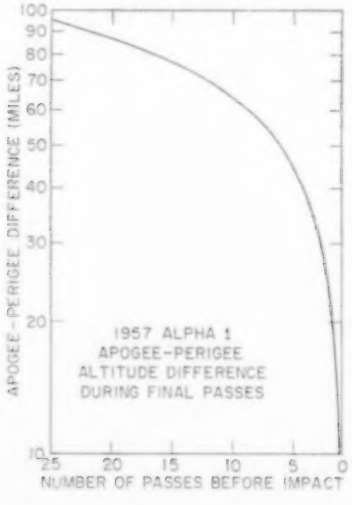

Fig. 2. Difference in apogee and perigee altitudes for the final passes of Satellite 1957 Alpha 1.

2.1. *Satellite 1957 Alpha 1*

The investigation of Alpha 1 starts from the orbital data provided by the Smithsonian Astrophysical Observatory for the date of 11 November 1957. Our analysis of the re-entry is based on several observations of the altitude of the satellite during the last 5 days of its lifetime. These altitudes were deduced from radar data on 1957 Alpha 1 obtained by: (*a*) the Lincoln Laboratory[1] on 27 November at 2153 GMT, 29 November at 2137 GMT, and 30 November at 1944 GMT and 2114 GMT; (*b*) the Stanford Research Institute[2] on

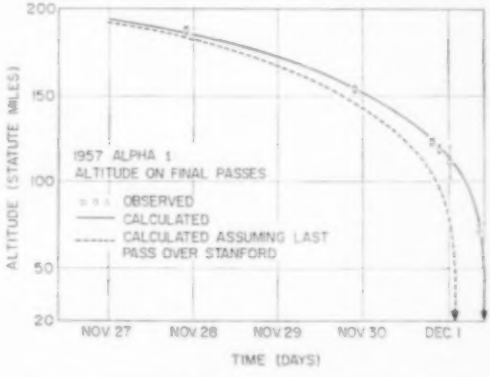

Fig. 3. Comparison of observed and calculated altitudes during the final days of Satellite 1957 Alpha 1. ○ Lincoln Laboratory; □ Stanford Research Institute; △ Royal Radar Establishment (Malvern, England). The solid curve indicates the calculated altitudes. The dashed curve represents the calculated altitudes on the assumption that the satellite fell during its last pass over the United States.

1 December at 0011 GMT; and (*c*) the Royal Radar Establishment[3] at Malvern, England, on 1 December at 0828 GMT. The altitudes

obtained from these radar sightings are indicated in Fig. 3. Fig. 3 also shows the calculated altitudes resulting from the numerical integrations. The calculated altitudes are seen to be in good agreement with the observed altitudes for all passes.

The penultimate measurement shown in Fig. 3 was taken on the Stanford radar during the final pass of the satellite over the United States. The last measurement in Fig. 3 is that of the RRE radar at Malvern, obtained, as already noted, at 0828 GMT. It is interesting to note that even if both of these data are omitted, the comparison of the remaining observations with our calculated altitudes indicates that the satellite could not have fallen during its last pass over the continental United States, nor in fact for several passes thereafter. For if we assume the last pass in the lifetime of the satellite to be that in which it crossed the western United States, the calculated altitudes then fall on the dashed curve of Fig. 3. The differences between this curve and the data are well outside the probable errors for the observations. In our view Fig. 3 provides conclusive evidence that the satellite continued on for approximately 8 hr beyond the pass over the west coast of the United States.

ACKNOWLEDGEMENTS

We wish to thank Mr. W. F. Cahill of the National Bureau of Standards for the preparation of the IBM 704 programs used in the analysis. We are grateful to Mr. Cahill and also to Messrs. C. Wade, Jr., P. O'Hara, and G. Galler of the National Bureau of Standards for their co-operation in executing the machine calculations.

REFERENCES

1. Pettengill G. H., private communication.
2. Peterson A. M. and Jaye W. E., private communication.
3. Hey J. S. and Hughes V. A., private communication.

Planet. Space Sci. Pergamon Press 1959. Vol. 1, pp. 40–42. Printed in Great Britain.

A SHORT DURATION AFTERGLOW OF NITROGEN; SURVEY OF AFTERGLOWS*

O. OLDENBERG

Geophysics Research Directorate, Air Force Cambridge Research Center, Air Research and Development Command; and Lyman Laboratory of Physics, Harvard University

(*Received* 15 *July* 1958)

Abstract—When an electron beam of more than 10·5 eV energy traverses low pressure nitrogen the beam is surrounded by a diffuse glow emitting the first positive bands[1]. This light is interpreted as an afterglow. It is attributed to metastable molecules, $a^1\Pi$, which diffuse out of the space occupied by the beam, are thrown by collisions with normal molecules into the unstable state $B^3\Pi$ and then emit the first positive bands. The time required for diffusion is of the order 5×10^{-5} sec. This afterglow is compared with four other types of nitrogen afterglow.

1. NEW TYPE OF AFTERGLOW

We want to call attention to a new type of nitrogen afterglow which has a duration shorter than those of the well established types. Thompson and Williams[1] describe the light excited in nitrogen of low pressure (3×10^{-3} mm Hg) by a beam of electrons. When the energy of the electrons exceeds 10·5 eV, the sharply defined beam is surrounded by a diffuse glow which emits the first positive bands limited by $v'=12$. However, this radiation is not simply identical with the Lewis–Rayleigh afterglow in which an isolated emission from the vibrational quantum numbers $v'=11$ and 12 is predominant. Here the quantum numbers from $v'=12$ down are well represented. Also theoretically we should not expect the Lewis–Rayleigh afterglow since the triple collisions required for its excitation hardly occur at a pressure as low as 3×10^{-3} mm.

The authors explain the diffuse light as fluorescence. The electron beam certainly excites among others the singlet level $a^1\Pi$, that is, the upper level of the Lyman–Birge–Hopfield bands. The radiation from this level is assumed to produce fluorescence, that is, excite the same level in the gas surrounding the beam. Collisions throw this level into the triplet level $B^3\Pi$, which then radiates the first positive bands.

This mechanism, however, is not acceptable since it is incompatible with the metastable character of the level $a^1\Pi$. Herzberg[2] discovered this metastability and confirmed it by reference to the absorption spectrum of nitrogen investigated by Birge and Hopfield[3]. This spectrum shows only very weak absorption of the Lyman–Birge–Hopfield bands. Even when photographed with one full atmosphere of nitrogen and a path length of 40 cm (quoting Herzberg) "the bands do not appear particularly strong". In the experiment of Thompson and Williams, assuming $p=3\times10^{-3}$ mm, we estimate the absorption to be smaller than in the experiment of Birge and Hopfield by the factor 2×10^{-7}. Hence no observable fluorescence can be expected.

We suggest that many metastable molecules, $a^1\Pi$, produced in the electron beam, diffuse out of the beam and then either emit their spontaneous radiation (the Lyman–Birge–Hopfield bands) or, as suggested by Thompson and Williams, are thrown by collisions with normal molecules into the unstable state $B^3\Pi$, and thus emit the first positive bands. This hypothesis changes the character of the radiation observed from fluorescence to an afterglow and suggests

* Work supported by the Air Force Cambridge Research Center under Contract A.F. 19(604)—1041.

the comparison with the other types of nitrogen afterglow. At the pressure of 3×10^{-3} mm Hg the mean free path is about 2 cm. Here the diffusion takes only slightly more time than that required to travel the distance of, say, 2 cm with gas-kinetic speed, that is, 5×10^{-5} sec. This then is an estimate of the lifetime of the metastable state as it is limited by collisions with N_2 molecules†.

The process here considered (energy transfer from $a^1\Pi$ to $B^3\Pi$) is different from the process responsible for the Lewis–Rayleigh afterglow (excitation of $^5\Sigma$, energy transfer to $B^3\Pi$). Hence it may appear as a mere coincidence that the highest vibration excited ($v'=12$) is in both cases the same. This, however, is well explained. In both cases the limit is given by the energy of dissociation of the N_2 molecule, although in the Thompson–Williams afterglow this limitation enters indirectly as follows. Herzberg[7] discovered that the level $a^1\Pi$ predissociates above its vibrational quantum $v'=6$ (9·76 eV); that is, it suffers a radiationless transition to a pair of free atoms. Hence, at low pressure, this level cannot contain higher vibrational quanta and is unable to generate vibration of the B level beyond the same energy limit; that is, beyond $v'=12$ of the B level. The various vibrational quanta of the B level, v' from 12 down to 4, are presumably generated by the various quanta of the a level. Moreover, in any transfer from a to B some of the energy may be diverted to translation or rotation.

The interpretation here given leaves one difficulty unsolved. In the collision of the second kind, a transfer takes place from a singlet to a triplet state without a compensating transfer in the other molecule. This process violates the Wigner spin conservation rule. However, the rule is by no means rigorous as is evident from several other violations discussed by Massey and Burhop[8]. More recent evidence is presented by Aynard[9].

† W. Lichten[4] measured the natural life time of the $a^1\Pi$ level to be $1{\cdot}7 \times 10^{-4}$ sec. It is worth noting how insensitive the other metastable state of nitrogen, $A^3\Sigma$, is to collisions with normal N_2 molecules. This is the initial state of the Vegard–Kaplan bands which even in one full atmosphere of pure nitrogen are emitted with remarkable intensity.[5] In a wide tube filled with an atmosphere of pure nitrogen they survive an appreciable fraction of a second.[6]

2. SURVEY OF NITROGEN AFTERGLOWS

These then are the fundamental processes responsible for the various types of nitrogen afterglow which differ by their durations and spectra.

(*a*) The *Lewis–Rayleigh afterglow* is excited in the low pressure discharge. It is distinguished by its long duration. It emits the first positive bands with a great preference for $v'=12$ or 11. It receives its energy from *recombining normal atoms*[10].

(*b*) Noxon[6] investigated a related afterglow in *pure nitrogen of atmospheric pressure*. There the late stages of the afterglow represent a unique light source in which with increasing age the forbidden radiations become increasingly predominant. Presumably the metastable levels survive from the early stages of the afterglow.

(*c*) *Kaplan's*[11] *auroral afterglow* is excited by a low pressure discharge through very pure nitrogen. Its spectrum shows higher excitation, even bands of N_2^+. Only its early stages may be supplied by recombining electrons and ions. But principally it must be due to recombination of atoms, partly in metastable levels. No detailed explanation can be given.

(*d*) *The recombination of ions and electrons*, which takes place within milliseconds after a discharge, produces an afterglow whose spectrum is similar to that emitted by the auroral afterglow but in the red and infrared shows intense characteristic features[12].

(*e*) The *Thompson–Williams afterglow* discussed above is of short duration and is due to the diffusion of metastable molecules ($a^1\Pi$) from a beam and their later conversion to the level $B^3\Pi$.

REFERENCES

1. Thompson N. and Williams S. E. *Proc. Roy. Soc.* A **147**, 583 (1934).

2. HERZBERG G. *Phys. Rev.* **69**, 364 (1946).
3. BIRGE R. T. and HOPFIELD J. J. *Astrophys. J.* **68**, 257 (1928).
4. LICHTE W. *J. Chem. Phys.* **26**, 306 (1957).
5. JANIN J. *Ann. Phys., Paris*, **1**, 548 (1946).
6. NOXON J. F. Ph.D. Thesis, Harvard University (1957).
7. HERZBERG G. *Canad. J. Phys.* **29**, 294 (1951).
8. MASSEY H. S. W. and BURHOP E. H. S. *Electronic and Ionic Impact Phenomena*, pp. 428, 537. Clarendon Press, Oxford (1952).
9. AYNARD R. Thèse présentée a la Faculté des Sciences de l'Université de Paris (1956).
10. BERKOWITZ J., CHUPKA W. A. and KISTIAKOWSKY G. B. *J. Chem. Phys.* **25**, 457 (1956).
11. KAPLAN J. *Phys. Rev.* **42**, 807 (1932); *Ibid.* **45**, 671 (1934); *Ibid.* **51**, 143 (1937); *Ibid.* **54**, 176 (1938).
12. BRYAN R. B., HOLT R. B. and OLDENBERG O. *Phys. Rev.* **106**, 83 (1957).
BRYAN R. B. Ph.D. Thesis, Harvard University (1951).

Planet. Space Sci. Pergamon Press 1959 Vol. 1, pp. 43-49. Printed in Great Britain.

DECAY OF SPIN IN SPUTNIK I

J. W. WARWICK

High Altitude Observatory, University of Colorado, Boulder, Colorado

(*Received* 31 *July* 1958)

Abstract—A secular change took place in the spin-fading rate during the three weeks of observation of the radio transmissions from Sputnik I, between 4 October 1957 and 24 October 1957. This effect allows a determination of atmospheric density near the perigee point. For an assumed atmospheric scale height of 30 km, we derive a value $3{\cdot}8\times10^{-13}$ g cm^{-3} for the density at 220 km. Some fluctuations in the spin decay appear to be real, and may result from small changes in the orientation of the spin axis within the satellite. An alternative interpretation in terms of charged drag resulting from motion of the satellite through the ionospheric plasma, requires a charge of at least 10^4 volts on the satellite. This charge might be acquired in the auroral zone.

1. IDENTIFICATION OF THE SPIN

SPIN-FADING showed most clearly on our records of south-going Sputnik I passages near Boulder. Fig. 1 shows records covering a week of observation during these morning passes, in which the spin-fading stands out from a rapid, ionospheric fading. We have attempted to align the spin-fading minima carefully, so that their basic periodicity will be evident from one record to the next. The period is about 4½ sec for successive minima, and about 9 sec for alternate minima. The latter is probably the correct period, as shown by the top strip of Fig. 1.

The morning passes here were characterized by appearance of the satellite first at an elevation of some 45° above the northern horizon, and a prolonged trailing-off of the signals as the satellite passed beyond the southern horizon. Depending on the orientation of the spin axis, the satellite will appear to rotate at a fixed rate (axis parallel to the orbital plane), or more rapidly (axis of rotation positive, in the right-handed sense, to the west), or less rapidly (axis of rotation to the east) than the true rate, observed in an inertial system fixed to the satellite. If the axis points towards the west, the phase of fading minima, predicted from the true period, will decrease by about one-eighth of a rotation from first appearance of the satellite to the point of closest approach. As the satellite passes the point of closest approach and moves to the south, the phase will at first continue decreasing at about the rate it showed before closest approach and then level off at some constant phase as the satellite passes beyond the southern horizon.

Fig. 2 illustrates the observed variation in phase of fading minima, computed for three possible true periods of spinning, for the close passage on 14 October 1958, at 1330 U.T. Clearly, the longest period, $P=8{\cdot}975\pm0{\cdot}002$ sec, satisfies the criteria for a spin axis positive towards the west, and opposite in sense to the satellite's orbital angular momentum. The precision of this determination follows from the fact that the phase, at the end of the passage, should be constant within 0·1 rotations.

A second requirement of the spin-fading is that it should show a nominally constant period from day to day. Fig. 3 illustrates our observations of the spin period from the beginning of Sputnik I to the failure of its radio on about 24 October 1957. Exclusive of the first day of flight, the satellite obviously spun at a more-or-less constant rate.

During the first 24 hr, our observations of Sputnik I were virtually complete, because of the ease of identification of the keyed signal in the midst of noise, and probably also because

of the initial strength of the transmissions. At this time, a change in the spin period, so sharp as to be almost discontinuous over two revolutions of the satellite about the earth, took place. We identify this initial slowing of the spin rate as the result of a discontinuous increase in the moment of inertia of the satellite about the axis of spin. One possible origin of such an effect might be the opening of the antenna system, initially stowed, before separation of satellite and launcher, within the body of the rocket. A second possibility may be that Sputnik I behaved like Explorer I (1958 α), and shifted about its constant direction of angular momentum, until the spin axis lay in the direction of maximum moment of inertia[1]. We cannot decide between these alternatives on the basis of the present evidence.

2. DETERMINATION OF ATMOSPHERIC DENSITY

Of more immediate interest is the secular decrease in the spinning rate from 5 October through 24 October. The only points failing to

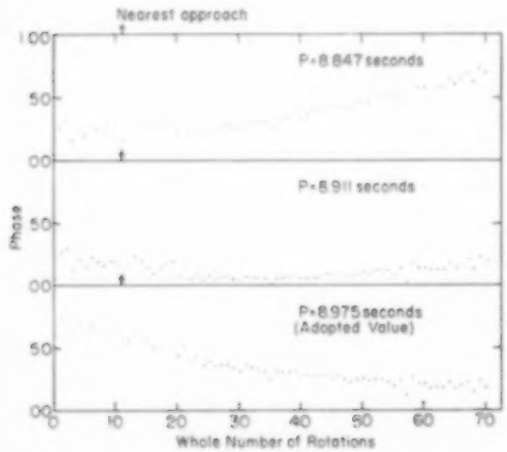

Fig. 2. Phases, reckoned from an arbitrary zero-point, of fading minima, plotted against number of spin rotations, also from an arbitrary initial value.

show the decrease are those for 10, and possibly 9 October 1957. These points appear to be real discrepancies, in view of the precision of the determinations.

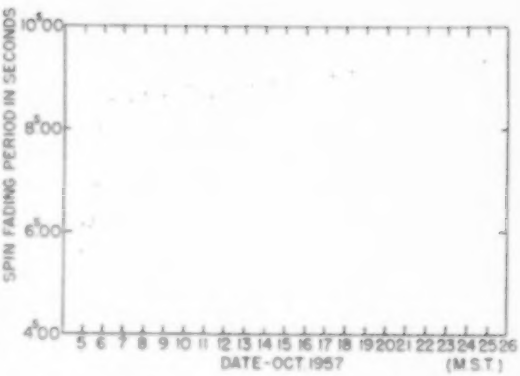

Fig. 3. The period of spin-fading as a function of epoch in the life of Sputnik I.

The systematic effect results from aerodynamic drag between the rotating antenna system and the residual atmosphere near perigee in the orbit. The change in the spin rate is sufficiently small so that the angular rate of spin is substantially constant throughout a given passage. There will also be a dissipative torque on the spherical body of the satellite, but this is minute in comparison with the torque on the antennas. If we assume that the system is two 7·5 m dipoles made of tapered stubs, then it is likely that the dipole frontal area is comparable to the frontal area of the 58 cm sphere of the satellite body.

The element of torque on a section of antenna s cm from the center of rotation (the center of the satellite body) is

$$\delta L = \delta D(V)\frac{\mathbf{V}}{V} \cdot (\boldsymbol{\Omega} \times \mathbf{R})\, s. \qquad (1)$$

Here, $\mathbf{V}$ is the vector velocity of the element of antenna on which a drag force $\delta D(V)$ is exerted. $\boldsymbol{\Omega}$ is the unit vector in the direction of spin, and $\mathbf{R}$ is the unit vector (a function of time) directed out from the satellite body along the antenna. Where $\mathbf{V}_0$ is the orbital velocity of the satellite, and ω is the magnitude of the angular velocity, in radians per second, we have

$$\mathbf{V} = \mathbf{V}_0 + s\omega\boldsymbol{\Omega} \times \mathbf{R}. \qquad (2)$$

Also, letting $t(s)$ be the thickness of the antenna

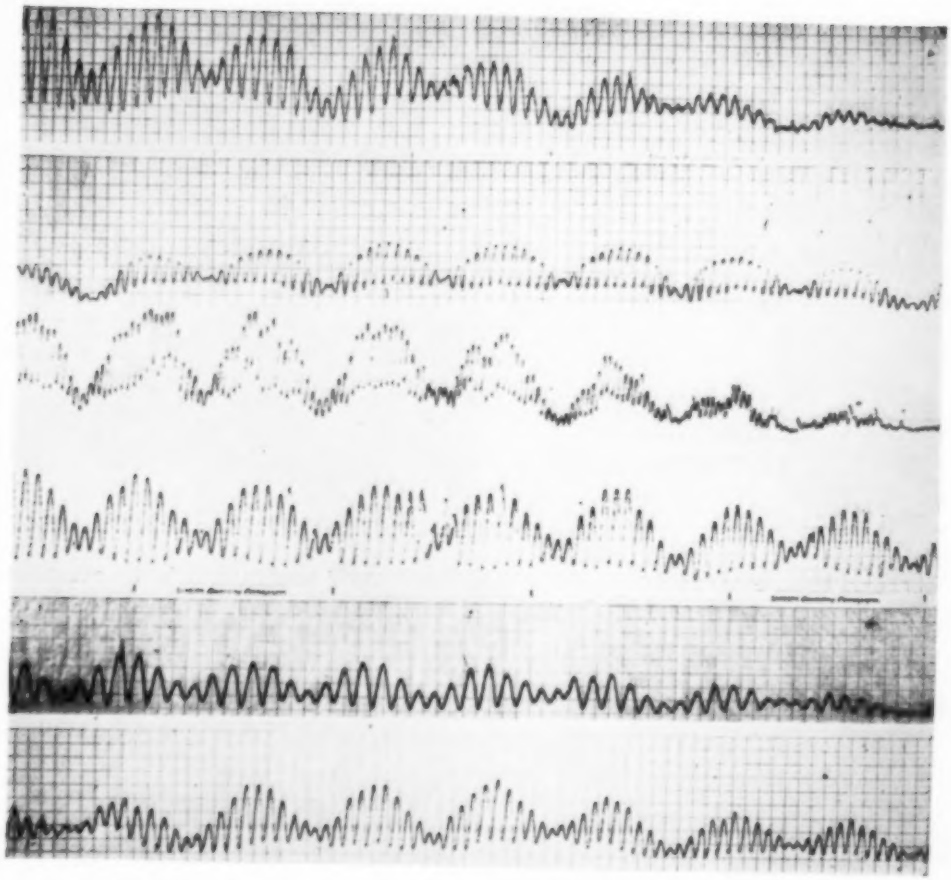

Fig. 1. Amplitude-fading in the 20 Mc/s signals from Sputnik 1 (1957 ε 2). The vertical divisions are at intervals of 0·5 sec. The satellite was high and to the south of Boulder. These strips show the synchronization of the spin-fading on morning passes, over an interval of one week (12 October through 18 October 1957, 15 October missing). Note also the double periodicity of the top strip.

Facing p. 44

VO
1
19

s cm from the satellite body, we write the aerodynamic drag in the form

$$\delta D(V) = C_D t(s) \left| \frac{\mathbf{V}}{V} \times \mathbf{R} \right| \rho V^2 ds. \qquad (3)$$

In equation (3), C_D represents the drag coefficient, of order unity, and ρ is the local atmospheric density at the position of the satellite. The torque has the sign of $\mathbf{V} \cdot (\boldsymbol{\Omega} \times \mathbf{R})$. If the satellite antenna is s_1 cm long, then the total torque exerted by the antenna is

$$L = C_D \rho \boldsymbol{\Omega} \cdot \mathbf{R} \times \int_0^{s_1} \mathbf{V} t(s) \, | \, \mathbf{V} \times \mathbf{R} \, | \, s ds. \qquad (4)$$

When we substitute equation (2) in equation (4), there results

$$L = C_D \rho \boldsymbol{\Omega} \cdot (\mathbf{R} \times \mathbf{V}_0) \int_0^{s_1} t(s) \, | \, \mathbf{V} \times \mathbf{R} \, | \, s ds +$$

$$+ C_D \rho (\boldsymbol{\Omega} \times \mathbf{R})^2 \omega \int_0^{s_1} t(s) \, | \, \mathbf{V} \times \mathbf{R} \, | \, s^2 ds, \qquad (5)$$

where

$$| \, \mathbf{V} \times \mathbf{R} \, | = [V_0^2 - (\mathbf{V}_0 \cdot \mathbf{R})^2 + 2\boldsymbol{\Omega} \cdot (\mathbf{R} \times \mathbf{V}_0)\omega s +$$
$$+ (\boldsymbol{\Omega} \times \mathbf{R})^2 \omega^2 s^2]^{\frac{1}{2}}. \qquad (6)$$

We now expand the square-root in terms of the small quantity $\frac{\omega s}{V_0}$. Let $\frac{\mathbf{V}_0}{V_0} \cdot \mathbf{R} = \cos\delta$; then

$$| \, \mathbf{V} \times \mathbf{R} \, | = V_0 \sin\delta + \frac{\omega s}{V_0 \sin\delta} \boldsymbol{\Omega} \cdot (\mathbf{R} \times \mathbf{V}_0) + \ldots, \qquad (7)$$

where the expansion is valid only when $\frac{\omega s}{V_0 \sin\delta} \ll 1$, and $\sin\delta > 0$. This condition will be satisfied unless the spinning antenna comes within a degree of the orbital direction, and is therefore quite unrestrictive. When equation (7) is substituted in equation (5), we find three terms, inclusive of first order terms in $\frac{\omega s}{V_0}$,

$$L = C_D \rho \mathbf{V}_0 \cdot (\boldsymbol{\Omega} \times \mathbf{R}) V_0 \sin\delta \int_0^{s_1} t(s) s ds$$

$$+ C_D \rho [\mathbf{V}_0 \cdot (\boldsymbol{\Omega} \times \mathbf{R})]^2 \frac{\omega}{\sin\delta} \int_0^{s_1} t(s) s^2 ds$$

$$+ C_D \rho \mathbf{V}_0 (\boldsymbol{\Omega} \times \mathbf{R})^2 \omega \sin\delta \int_0^{s_1} t(s) s^2 ds. \qquad (8)$$

We now develop the vector function $\mathbf{R}(t)$.

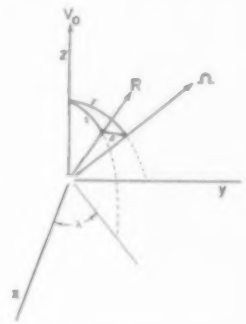

Fig. 4. Cartesian co-ordinate system for representing the components of $\mathbf{R}(t)$.

We introduce a cartesian co-ordinate system (see Fig. 4), with z-axis lying along the orbital velocity, and the y–z plane containing the spin axis, $\boldsymbol{\Omega}$. The instantaneous direction of the antenna is defined by spherical co-ordinates δ, λ. Let γ be the angle between the spin direction and the orbital velocity. We measure time from the moment that the instantaneous antenna direction lies in the y–z plane, within 90° of the orbital velocity. Finally, let β represent the angle between the antenna and the spin axis. $180° > \beta > 0$, and β is assumed to be a fixed angle. Then

$$\mathbf{V}_0 = (0, \; 0, \; V_0), \qquad (9)$$

$$\boldsymbol{\Omega} = (0, \; \sin\gamma, \; \cos\gamma), \qquad (10)$$

$$\mathbf{R} = (\sin\delta\cos\lambda, \; \sin\delta\sin\lambda, \; \cos\delta)$$
$$= (-\sin\beta\sin\omega t, \cos\beta\sin\gamma - \sin\beta\cos\gamma\cos\omega t,$$
$$\cos\beta\cos\gamma + \sin\beta\sin\gamma\cos\omega t). \qquad (11)$$

Substitute equations (9), (10), and (11) in the first term of equation (8). Then

$$C_D \rho V_0 \sin\gamma \sin\beta \, . \, V_0 \sin\delta \sin\omega t \int_0^{s_1} t(s)\, s\, ds. \quad (12)$$

This term is an oscillating function of time, which does not contribute to the decay of the spinning. The second and third terms of equation (8) become

$$C_D \rho V_0 \frac{\sin^2\beta}{\sin\delta} (\sin^2\gamma \sin^2\omega t + \sin^2\delta)\, \omega \int_0^{s_1} t(s)\, s^2 ds. \quad (13)$$

Therefore, the integral of the torque over one spin period becomes

$$\int_0^P L dt = C_D \rho V_0 \sin^2\beta\, A(\beta,\gamma) \int_0^{s_1} t(s)\, s^2 ds, \quad (14)$$

where

$$A(\beta,\gamma) = \int_0^{2\pi} (\sin^2\gamma \sin^2\theta + \sin^2\delta) \frac{d\theta}{\sin\delta}, \quad (15)$$

and

$$\cos\delta = \cos\beta\cos\gamma + \sin\beta\sin\gamma\cos\theta.$$

The integral, equation (15), is unfortunately elliptic, owing to the presence of the square-root, $\sqrt{1-\cos^2\delta}$, in the denominator. In order to proceed further, we expand the root (to the first order) in a series in $\cos\delta$,

$$A(\beta,\gamma) \simeq \int_0^{2\pi} (\sin^2\gamma \sin^2\theta + \sin^2\delta)(1 + \tfrac{1}{2}\cos^2\delta)\, d\theta. \quad (16)$$

This approximation limits the accuracy of the remaining work to values of δ greater than about 20°. With the notation

$$\mu = \cos\gamma, \quad \nu = \cos\beta, \quad (17)$$

$$A(\beta,\gamma) = 2\pi\left[\frac{9}{8} - \frac{1}{8}\mu^4 + \left(\frac{9}{16} - \frac{9}{4}\mu^2 + \frac{25}{16}\mu^4\right)\nu^2 + \left(-\frac{3}{16} + \frac{15}{8}\mu^2 - \frac{31}{16}\mu^4\right)\nu^4\right]. \quad (18)$$

We have now to relate the drags produced by each of the four antennas. Assume that the antennas occur in orthogonal pairs, and therefore define a plane. For a single antenna and its opposite, we have θ, β and $180° + \theta$, $180° - \beta$, respectively. The opposite antenna simply doubles the effect of a single antenna. To relate the effects of the pairs, we introduce the azimuthal angle, α, between the conjugate antenna and the spin axis, as measured with the first antenna pair as a pole. Denoting the pairs by subscripts, we find that

$$\cos\beta_2 = -\sin\beta_1 \cos\alpha. \quad (19)$$

The sum of the effects of all four antennas is then

$$\Sigma \int_0^P L dt = 4\pi C_D \rho V_0 \int_0^{s_1} t(s)\, s^2 ds \times \left[\left(\frac{9}{8} - \frac{1}{8}\mu^4\right)(1 + (1-\nu_1^2)\sin^2\alpha) + \left(\frac{9}{16} - \frac{9}{4}\mu^2 + \frac{25}{16}\mu^4\right)(1-\nu_1^2) \times (\cos^2\alpha - \cos^4\alpha + (1+\cos^4\alpha)\nu_1^2) + \left(-\frac{3}{16} + \frac{15}{8}\mu^2 - \frac{31}{16}\mu^4\right)(1-\nu_1^2)(\cos^4\alpha - \cos^6\alpha - (\cos^4\alpha - 2\cos^6\alpha)\nu_1^2 + (1-\cos^6\alpha)\nu_1^4.\right] \quad (20)$$

The angles α, β are not known for Sputnik I. On the other hand, we showed in Section 2 that the spin axis lay to the west on at least one morning passage of the satellite near Boulder. Therefore, we assume $\gamma = 90°$. Without, for the moment, justification, we take $\cos^2\alpha = \nu_1^2 = \frac{1}{2}$. Then equation (20) becomes

$$\Sigma \int_0^P L dt = 20{\cdot}4\, C_D \rho V_0 \int_0^{s_1} t(s)\, s^2 ds. \quad (21)$$

The first integral, over the arbitrary time interval $(t_a - t_b)$, of the angular equation of motion of the spinning satellite is

$$\omega(t_a) = \omega(t_b) - \frac{1}{I}\int_{t_b}^{t_a} L\,dt, \tag{22}$$

where I is the satellite's moment of inertia about the spin axis. This moment is the sum of the moment of the satellite body proper, which we shall neglect, and the antenna moment, which takes the form

$$I = \Sigma(\boldsymbol{\Omega} \times \mathbf{R})^2 \int_0^{s_1} m(s)\, s^2 ds. \tag{23}$$

$m(s)$ is the mass distribution per unit length of the antennas. Suppose that the antennas consist of thin-walled aluminum tubing, with walls 0·15 cm thick. If the tubing is of constant skin thickness, the detailed configuration of the antennas cancels from the expression for the change in period. For thin-walled tubing

$$m(s) \simeq 1{\cdot}273\, t(s)\ \mathrm{cm}^{-1}, \tag{24}$$

where we assumed that the antenna material had a density 2·7 g cm^{-3} (aluminum). Equation (22) becomes, for a constant value of ρ in the interval $(t_a - t_b)$

$$\omega(t_a) = \omega(t_b) - 16{\cdot}0\,\frac{C_D \rho V_0}{\Sigma(\boldsymbol{\Omega} \times \mathbf{R})^2}. \tag{25}$$

We return to the assumption that

$$\nu_1^2 = \cos^2 \alpha = \tfrac{1}{2}.$$

Equation (25), in the denominator, has the term

$$\Sigma(\boldsymbol{\Omega} + \mathbf{R})^2 = 2\,(1 + (1 - \nu_1^2)\sin^2 \alpha), \tag{26}$$

which is 5/2 under the assumed values of α and β_1. These are only probable, or average values; however, the leading term of equation (20) contains the same dependence on these angles as equation (26). The exact values of α and β_1 therefore do not enter the problem sensitively. Assume that $V_0 = 8 \times 10^5$ cm sec^{-1}; then equation (25) becomes

$$\omega(t_a) = \omega(t_b) - 5{\cdot}02 \times 10^6 C_D \rho, \tag{27}$$

per spin period, where ρ is in g cm^{-3}, and ω is in rad sec^{-1}.

Before we can compare this result with the observations, we must compute the total decrease in spin rate over one perigee passage. Since the satellite moved in a slightly elliptical orbit, the density at the position of the satellite varied with time. We therefore rewrite equation (27) in the form

$$\omega(t_a) = \omega(t_b) - 5{\cdot}02 \times 10^6 C_D \int_{t_b}^{t_a} \rho(t)\,\frac{dt}{P}. \tag{28}$$

The integrand is effectively non-zero only when t is quite close to t_0, the time of perigee passage. The radial motion in an elliptical orbit for eccentricity, e, even as small as 0·05 (the value for Sputnik I), is large in comparison with the few tens of kilometers over which the atmospheric density varies exponentially. We therefore may write the height of the satellite as a quadratic function of time near perigee passage.

$$h = h_0 + \tfrac{1}{2} r\,(t - t_0)^2. \tag{29}$$

r, equation (29), is the radial component of the acceleration of the satellite in its orbit, and is given in terms of the orbital elements by

$$r = \frac{4\pi^2}{T^2} ae \left(\frac{1 + e^2}{1 - e^2}\right)^2, \tag{30}$$

at the perigee point. h_0 is the perigee altitude of Sputnik I (about 220 km), T, the period (5760 sec), and a, the semi-axis major ($6{\cdot}6 \times 10^8$ cm). We represent $\rho(h)$ by the exponential function

$$\rho = \rho_0 e^{\frac{-(h - h_0)}{H}}, \tag{31}$$

where H is the scale height of the atmosphere at the perigee point, and ρ_0 is the density of the atmosphere at that point. We shall assume that $H = 30$ km.[2] Substituting equations (29), (30), and (31) in equation (28), and letting the values t_a and t_b extend to $\pm\infty$, we find that the change in spin rate for one perigee passage is

$$\Delta\omega = -3{\cdot}8 \times 10^6 C_D \rho_0. \tag{32}$$

The measured value of $\Delta\omega$ (see Fig. 3) corresponds to 1·02 sec in 18 days. Since the satellite made nearly 15 revolutions of the earth each day, this value implies a deceleration of $2{\cdot}9 \times 10^{-4}$ rad sec^{-1}, per passage. Dividing equation (32) into this value, we find that

$$C_D\rho_0 = 7{\cdot}6 \times 10^{-13} \text{ g cm}^{-3}. \quad (33)$$

For a drag coefficient $C_D = 2$[3]

$$\rho_0 = 3{\cdot}8 \times 10^{-13} \text{ g cm}^{-3}. \quad (34)$$

3. FLUCTUATIONS IN SPIN DECAY

As noted earlier in Section 2, several of the experimental points on the curve of spin decay (Fig. 3) depart from a smooth curve by amounts exceeding by a considerable margin the experimental errors of a single determination of the period. Furthermore, the points suggest that the spinning may even increase in frequency over short intervals of time. Possibly the simplest explanation of such effects is that the orientation of the satellite about the constant direction of spin angular momentum changes slightly from time to time. Such an internal dynamical mechanism would allow any shift away from the direction of greatest moment of inertia and to some faster spinning rate, to be cancelled by a shift back to the stable condition. On the other hand, if the satellite already spins about the direction of greatest moment of inertia, the additional sharp decrease in spinning rate, such as occurred on 10 October 1957, then cannot be easily explained.

What is required is an external mechanism which, for brief intervals of time, is capable of increasing the drag by considerable amounts, as well as, after a brief interval, decreasing the effect by correspondingly large amounts. Although we will not, in this report, develop a detailed theory of the anticipated effects, it may be useful to set an upper limit to the conditions required for the ionospheric, or plasma, drag on the satellite's spinning to be commensurable with the ordinary, aerodynamic effects considered in Section 2.

One mechanism is suggested by the work of Jastrow and Pearse[4] on "charged" drag on a spherical satellite. Here, the drag results from the fact that the satellite tends to become negatively charged by the rapidly moving electrons of the ionosphere. As the satellite moves through the relatively stationary positive ions, the ions are attracted to the satellite, and momentum is transferred from the satellite to the ions. The question of the sign of the transferred momentum depends, in their work, on an integral over all colliding ions, which impinge on the spherical satellite at various points over its surface. An ion acquires an electron just before impact, and therefore may reflect from the satellite at energy including not only the relative kinetic energy but also the additional potential energy of the negative charge on the satellite. This additional energy may conceivably result in an acceleration of the satellite at the ultimate expense of the energy of the ionospheric electrons.

We shall set an upper limit to the magnitude of the effect. The largest potentials acquired by the satellite are likely to result from the streams of high-energy electrons responsible for the 10 to 100 kV X-radiation observed in the auroral zone.[5] Suppose therefore that the satellite acquires a potential of 10^4 V.

The most efficient acceleration will occur when an ion encounters the preceding antenna (moving in the direction of the satellite's motion through the ionosphere), is neutralized, and recoils in the direction opposite to the direction of satellite motion, with the full energy corresponding to the satellite's potential of 10^4 V. Let the satellite's potential be φ, and introduce the velocity

$$V_1 = \sqrt{\frac{2\varepsilon\varphi}{m_i}}, \quad (35)$$

where ε is the charge, and m_i, the mass of the ion. The change of momentum, under these optimistic conditions, for an ion encountering the preceding side of the antenna system is

$$\Delta p_{pre} = m_i[\sqrt{(V_0 + \delta V_0)^2 + V_1^2} - \delta V_0 - V_0], \quad (36)$$

where δV_0 is the increment of velocity due to the spinning of the antenna system. Similarly, an encounter with the receding side of the antenna system produces a change of momentum

$$\Delta p_{rec} = m_i[\sqrt{(V_0 - \delta V_0)^2 + V_1^2} + \delta V_0 - V_0]. \quad (37)$$

The pressures on the two sides are, respectively,

$$N_i(V_0 + \delta V_0)\Delta p_{pre},$$
$$N_i(V_0 - \delta V_0)\Delta p_{rec}. \quad (38)$$

where N_i is the number of ions per cubic centimeter. The differential pressure, across the antenna system, then is

$$\delta P_i = 2m_i N_i \frac{2V_0^2 + V_i^2}{\sqrt{V_0^2 + V_i^2}} \delta V_0. \quad (39)$$

Equation (39) should be compared with the similar expression derivable from aerodynamic drag, that is,

$$\delta P = 4mNV_0 \delta V_0. \quad (40)$$

In equation (40), m is the mass of an average air molecule, and N is the number of such particles per cubic centimeter.

The ratio of these two pressures is

$$\frac{\delta P_i}{\delta P} = \frac{1}{2}\frac{m_i}{m}\frac{N_i}{N}\frac{1}{V_0}\frac{2V_0^2 + V_i^2}{\sqrt{V_0^2 + V_i^2}} f\left(\frac{H_e}{H}\right) g(\mp), \quad (41)$$

where we have introduced two additional factors, f, and g; f to represent the increased scale height, H_e, of the ions over the scale height of the neutral atmosphere, and g to represent the larger cross-section of the charged satellite antennas for collisions with ions.

Roughly speaking, we may evaluate f and g as follows. From equations (28), (29), and (31) we conclude that effects of scale height go as the square-root of the scale height. Assume that H_e, the scale of the ionosphere, is about 300 km. Then, $f \simeq 3$. From Jastrow and Pearse's[4] equation (7), we estimate g to be roughly 20, for a satellite potential of 10^4 V, the potential of auroral zone electrons. Then $V_i = 2{\cdot}6 \times 10^7$ cm sec^{-1}, and $\frac{\delta P_i}{\delta P} \simeq 1$. The energetics of the problem do not rule out the possibility that charged drag played a role in the decay of spin in Sputnik I.

4. CONCLUSIONS

We identify the spin of Sputnik I (1957 $\alpha 2$), and determine its orientation in space from the nature of the phase variations of the fading curves near point of closest approach. Apparently, at least on 14 October 1957 at 1330 U.T., the satellite spun with its spin angular momentum directly opposite to its orbital angular momentum. The spin, studied as a function of epoch in the life of Sputnik I, slows down, or decays, at a more-or-less steady rate of $2{\cdot}9 \times 10^{-4}$ rad sec^{-1}, per orbital revolution. This decay may be interpreted, without any strong assumptions on the satellite geometry, as a result of aerodynamic drag between the satellite's antenna system and the residual atmosphere near the perigee point, 220 km above the surface of the earth. The derived density value, $3{\cdot}8 \times 10^{-13}$ g cm^{-3} agrees with values[3] derived from the change in period of revolution.

On the other hand, the density values derived from spinning depend on an easily measured quantity, the spin-fading period as a function of time. Fluctuations in this quantity can be studied in greater detail than fluctuations in the period of revolution. Fluctuations in spin rate exist and make attractive the possibility of using spin-fading to study the dynamical effects of the interaction of the satellite with the ionospheric plasma. Our rudimentary approach to this problem concludes that such interactions may occur for Sputnik I, but must in any event take place in the highly energetic electron streams of the auroral zone.

The launching of future satellites, with different perigee distances, offers possibility of further observations of atmospheric density from spin rates. We suggest that for this purpose at least a spinning satellite is desirable; the orientation of the antennas, and consequently, the polarization of the emitted waves, can be inferred without any stabilization apparatus being carried aboard the satellite.

This research was supported by the Electronics Research Directorate, of the Air Force Cambridge Research Center.

REFERENCES

1. WHITNEY C. A. *IGY Satellite Report Series* No. 3, p. 6. IGY World Data Center A, Rockets and Satellites, Washington, D.C. (1958).
2. MINZNER R. A. and RIPLEY W. S. *Air Force Surveys in Geophysics* No. 86. Geophysics Research Directorate, Air Force Cambridge Research Center, Massachusetts (1956).
3. STERNE T. E. and SCHILLING G. F. *Special Report* No. 3. IGY Project No. 30.10, Smithsonian Astrophysical Observatory, Cambridge.
4. JASTROW R. and PEARSE C. A. *J. Geophys. Res.* **62**, 413 (1957).
5. VAN ALLEN J. A. and KASPER J. E. *Bull. Amer. Phys. Soc.* (II), **1**, 230 (1956).

Planet. Space Sci. Pergamon Press 1959. Vol. 1, pp. 50–56. Printed in Great Britain.

ABSORPTION, REFRACTION, AND SCINTILLATION MEASUREMENTS AT 4700 Mc/s WITH A TRAVELING-WAVE TUBE RADIOMETER

JOHN P. CASTELLI, JULES AARONS, CARL FERIOLI and JOSEPH CASEY

Air Force Cambridge Research Center, Electronics Research Directorate, Air Research and Development Command, United States Air Force, Laurence G. Hanscom Field, Bedford Massachusetts

(*Received* 26 *September* 1958)

Abstract—By means of radio astronomy techniques, measurements of atmospheric absorption, refraction, and scintillation were made at C band (4700 Mc/s), with the sun as a source of radiofrequency energy. The equipment, a comparison-type radiometer, used traveling-wave tubes, a tuned radio frequency receiver, and an altazimuth antenna mount. The average solar temperatures recorded for the period varied from 22,000°K at zero elevation to 26,000°K at 60° of elevation. Individual readings ranged between 18,000°K and 30,000°K. The mean absorption, based on average solar temperatures at the various elevations for the period, was 0·00348 dB/km. Refractive errors were approximately the same as optical although deviations from the mean during any day were large. Atmospheric scintillation for periods ranging fom 0·5 sec to 90 sec were recorded. Scintillation amplitudes ranged from 2 per cent to 20 per cent of antenna signal temperature at low angles. At high elevation angles, scintillations rarely reached 10 per cent and were generally less than 1 per cent.

1. INTRODUCTION

DURING the month of July 1957, measurements were made at 4700 Mc/s on atmospheric absorption, refraction, and scintillation, with the sun as the source of radiofrequency energy. The equipment used was a new type of radiometer utilizing traveling-wave tubes in a tuned radiofrequency receiver instead of the usual superheterodyne circuit.

The equipment was set up at Ipswich, Massachusetts, on a site overlooking the ocean. Measurements were taken at sunrise during the month of July 1957, and approximately 19 days of data recorded and analyzed. As in the study at other microwave and meter wavelengths[1], the drift technique was used whereby the sun was allowed to pass through the center of the antenna at a series of arbitrarily chosen altitudes. Time signals from WWV were recorded on the charts to indicate the time of passage of the radio center of the sun through the antenna pattern.

2. EQUIPMENT

The receiver was a radiometer of the Dicke type, using a three-stage traveling-wave tube amplifier receiver. The frequency of the tubes built by Federal Telecommunications Laboratories is centered on 4700 Mc/s. A filter of 800 Mc/s bandwidth and a detector followed the TRF sections. The noise figure of the first stage was 14 dB.

A block diagram is shown in Fig. 1.

The antenna on a altazimuth mount was a 6 ft parabola with Cutler feed and horizontal polarization. Its measured half-power beam angle was 2·69°.

A 30 c/s mechanical chopper wheel arrangement furnished the switching between antenna and the 300°K black body matched load signal. A 16 dB noise tube and suitable precision attenuator were used to check system operation and furnish temperature calibration for signals.

The output from the filter and synchronous detector was fed through the integrator unit to

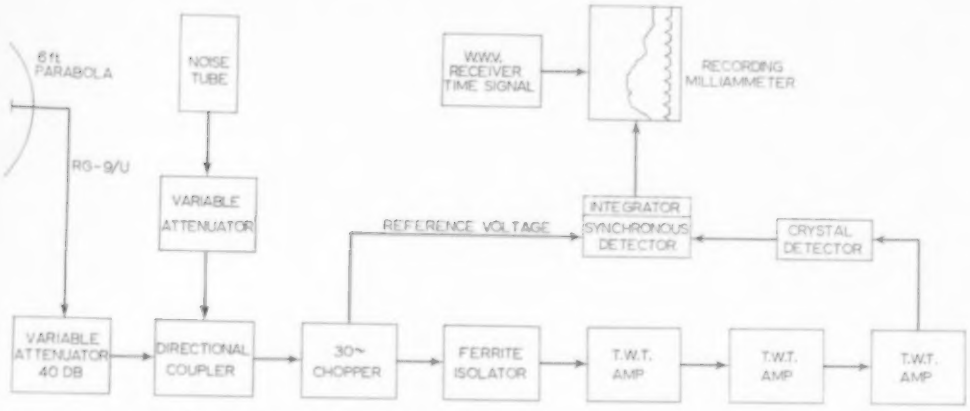

Fig. 1. Block diagram of C-band traveling-wave tube radiometer.

a recording milliammeter with a 0·5 sec time constant.

The basic advantage of the traveling-wave tube radiometer lies in its wide band. Since the minimum detectable signal is inversely proportional to the square root of the bandwidth, the sensitivity of this unit was five times that of a 10 Mc/s superheterodyne (effectively 20 Mc/s since both sidebands are normally used in the microwave superheterodyne).

In initial equipment tests in June 1955, the Dicke system was found necessary since without the comparison technique the long term drift was considerable. In this first series of tests taken with the TWT radiometer, a peak-to-peak power fluctuation of the equipment corresponded to temperature changes of about 1°K for a response time of 4 sec as compared with about 5°K for a superheterodyne radiometer having the same noise figure and response time. When the gain stabilization features (signal chopper and synchronous detector) are deactivated the long term drift becomes severe but the device maintains its short term sensitivity.

3. ABSORPTION

Although theoretically it is not possible to simultaneously measure refraction and absorption by means of the drift technique described, fairly good atmospheric absorption data can be obtained. The measured antenna temperature when the sun sweeps across the antenna pattern consists of two components, the solar and the sky temperatures. Since the angle subtended by the suit at 4700 Mc/s is approximately 35′ and the antenna beam angle is 2° 41′, the contribution of the sky must be subtracted from the total reading obtained.

The ratio of the solar temperature thus obtained at an elevation angle of 60° to that obtained at an elevation of 1° 30′ is the attenuation. To obtain the difference in the length of path, the solar signal has at 1° 30′ been transmitted through a path length of 152 statute miles while at 60° of elevation the path length is only 8 statute miles. The ratio of the resultant solar temperature values for the various elevation angles is plotted in Fig. 2.

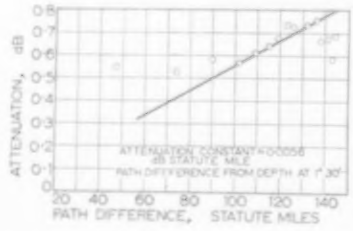

Fig. 2. Attenuation $\left(10 \log_{10} \frac{T_{el}}{T_{1° 30'}}\right)$ as a function of path difference.

The effective height of the atmosphere used was 6·9 statute miles. The 1° 30′ value was

chosen because the solar temperature recorded could be read more accurately than the zero elevation horizon signals. The mean absorption recorded was 0·0056 dB per statute mile. This value is lower than that extrapolated from shorter wavelength measurements by Van Vleck[23]. However, the extremely long path lengths inherent in radio astronomy techniques yields more accurate results for determining total atmospheric absorption.

Fig. 3. Zero elevation angle drift curves of the sun. a—presunrise sky noise followed by drift curve, 30 July 1957. Scintillations 15% of antenna temperature. b—low scintillation drift curve, 15 July 1957. Scintillations 6% of antenna temperature. c—large scale long period scintillations, 19% of antenna temperature, 20 July 1957.

4. APPARENT SKY TEMPERATURE

Each day, to determine the percentage of signal contribution from the ambient surroundings and the sky, background temperatures were recorded at the same elevations and azimuths as the solar recordings. The average value ranged from 106°K with the antenna pointed at the over-water horizon to 80°K at an elevation of 60°. The deviations from this mean were plus and minus 4°K at 60° of elevation.

The term, apparent sky temperature, is applied to the measurements because of the difficulty in evaluating the side lobe contribution, particularly at low angles of elevation. Equivalent ground temperatures vary as a function of weather conditions as well as of the composition of material (roads, roofs, water, hills). Since the azimuth of the antenna pointing is changing during a single day's run and from day to day at a constant elevation, a constant term cannot be used as the antenna side lobe and back lobe contributions.

While the small range of high angle antenna temperatures given in this section are not absolute sky temperatures, they do indicate the relative constancy with weather of the reflectivity, absorptivity, and emission of the sky in this frequency region. The day-to-day variations were not greater than the detection sensitivity of the radiometer. For each day the sky measurements were relatively constant from 10° to 60° of elevation. This may be contrasted to the data at K_a band where the temperature fluctuations at high angles varied from 38°K to 120°K. At 9300 Mc/s the range was from 54°K to 67°K at the same elevations.

5. SCINTILLATIONS

For the purposes of illustrating the types of scintillations present during the movement of the sun across the antenna pattern, several records are reproduced. Fig. 3 is a series of records taken at zero elevation. In Fig. 3a a run is shown just before the edge of the sun has appeared. The stability of the sky-ground temperature and the equipment is evident by the straight line from 0423 to 0430. As the edge of the sun appeared a deflection to the right was recorded at 0430. As the sun signal increased the milliammeter was switched to a reverse direction and the sun swept across the antenna pattern. The quiet background signal at zero elevation is ample proof of the scintillation cause being a source, point or extended, acting on the atmospheric screen. At this wavelength, individual blobs in the atmosphere do not produce selective or periodic absorption of the sky background. Scintillations are present only when a source is present.

Throughout the recordings a time constant of 0·5 sec was used. Each record is taken at a different gain scale; therefore the illustrations must not be compared on the amplitude scale presented in the figures. In Fig. 3a the scintillation peak to peak amplitudes were 15 per cent of the maximum antenna signals. Periods of the order of 10 to 15 sec predominated. A heavy fog was over the area.

Fig. 3b illustrates a quiet run with peak-to-peak scintillations of 6 per cent of the amplitudes. Long periods of the order of 20 to 25 sec predominate. The weather conditions were overcast.

The longest period scintillations observed are shown in Fig. 3c. Fluctuations longer than a minute in period are shown between 0425 and 0428. A peak-to-peak variation was 19 per cent of the antenna signal during the fair weather solar scan.

In the range of elevations 3° to 7·5°, three illustrations have been taken from the records. The first two, Figs. 4a and 4b, were drift curves at 3° of altitude. In Fig. 4a moderate scintillations of 13 per cent of the antenna temperature are observed. Both fast fluctuations of periods 1 to 3 sec are seen as well as the longer period scintillations of 15 to 40 sec period. During that period on 31 July when the drift curve was taken, a fog was over the antenna site. A second curve, made at the same elevation of 22 July, showed extremely deep fades of the order of 20 per cent of antenna temperature or greater. Only the long period scintillations were seen and the fast fluctuations of Fig. 4a are not present.

Normally, at an elevation angle of 7·5°, the scintillation amplitudes are decreasing with only

5 of 20 periods analyzed having detectable fluctuations. A high amplitude example is shown in Fig. 4c where the prevalent period is 1 sec but longer period fluctuations are also evident.

Typical high elevation drift curves are shown in Fig. 5a. Fluctuations in signal were less than 1 per cent of the antenna temperature. Calibration signals are seen at 0823. The antenna elevation was 40°.

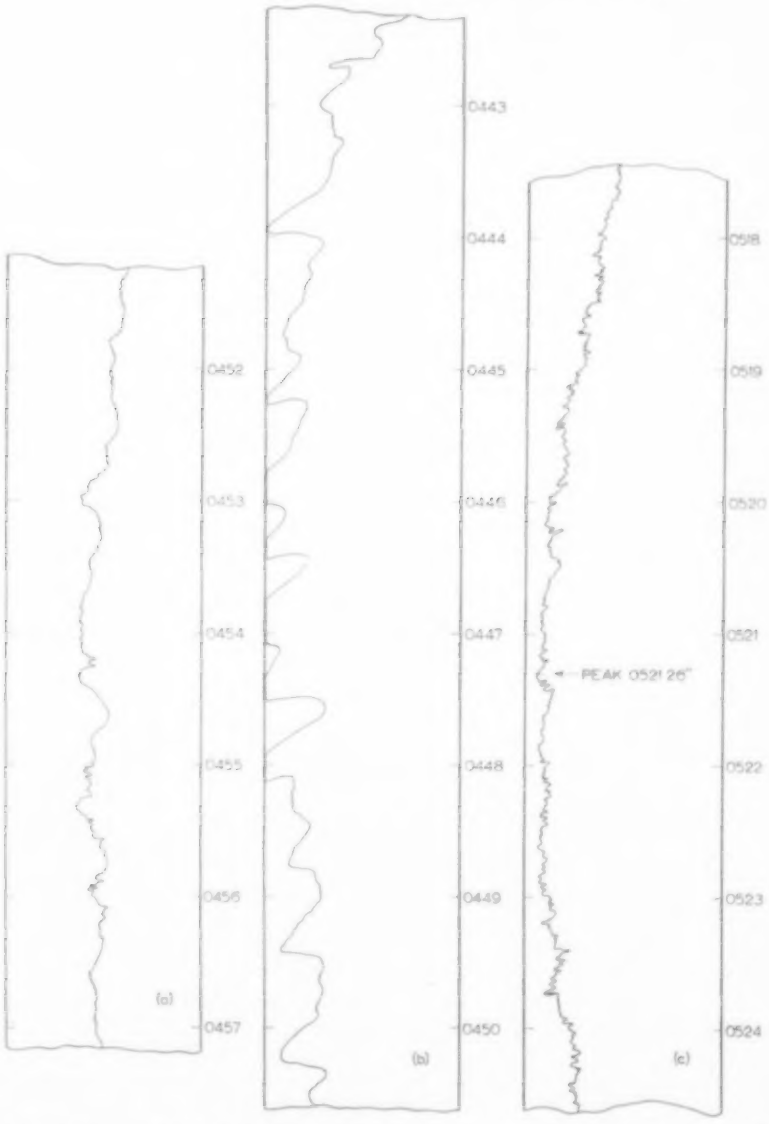

Fig. 4. Scintillations at 3° and 7° 30′ of elevation. a—moderate amplitude scintillations at 3° of elevation, 31 July 1957. b—large amplitude, long period scintillations at 3° of elevation, 20% of antenna temperature, 22 July 1957. c—relatively large (4%) short period fluctuations at 7½° of elevation, 1 August 1957.

On 2 August 1957, at the antenna elevation of 15°, sudden fluctuations were seen at the beginning of the drift curve (Fig. 5b). They stopped abruptly and a normal quiet run commenced. These short period fluctuations were of the order of 7 per cent of the antenna signal. Similar high angle scintillations are seen in Fig. 5c where the burst activity rises to 11 per cent of the antenna signal, falls to a quiet level and repeats this pattern several times. Periods of 1 sec predominate.

Fig. 6 summarizes the data on scintillation

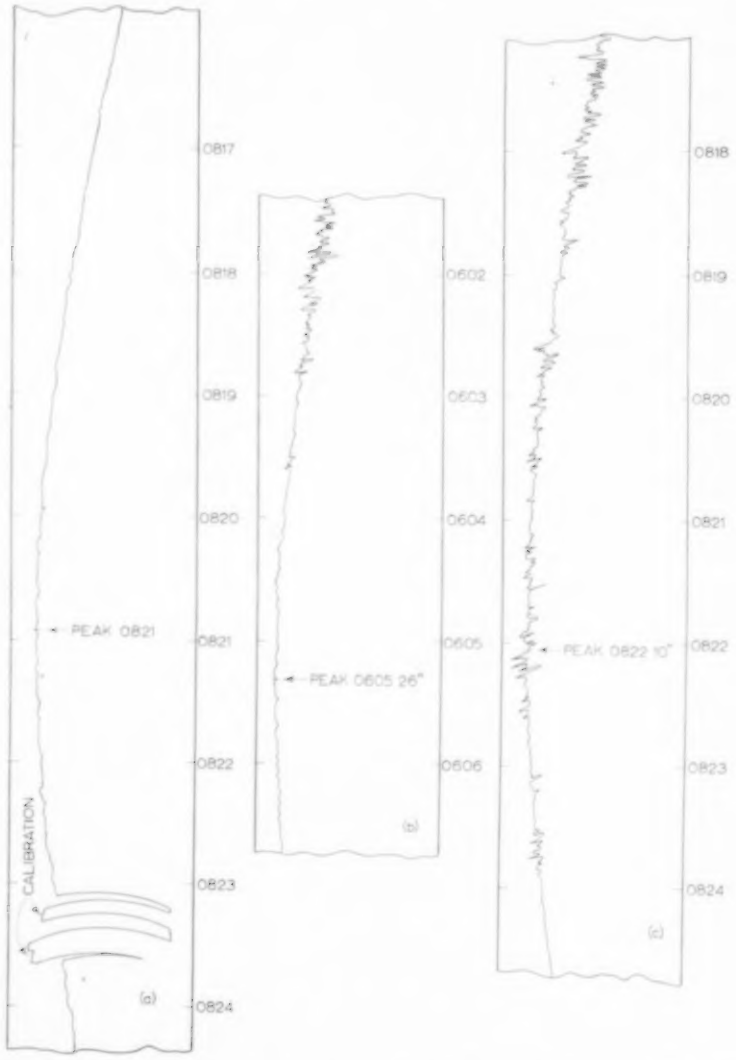

Fig 5. High elevation angle drift curves. a—quiet reading with scintillations less than 1% of the antenna signal. Calibration signals are illustrated. Angle of elevation 40°, 31 July 1957. b—sporadic fluctuations at an elevation angle of 15° on 2 August 1957. Fluctuations are 7% of antenna temperature. c—sporadic fluctuations at an elevation angle of 40° on 1 August 1957. Fluctuations are 11% of antenna temperature.

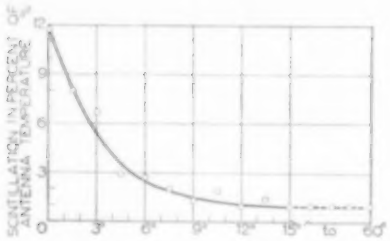

Fig. 6. Antenna elevation. Peak-to-peak fluctuation (percentage of antenna temperature) as a function of antenna elevation.

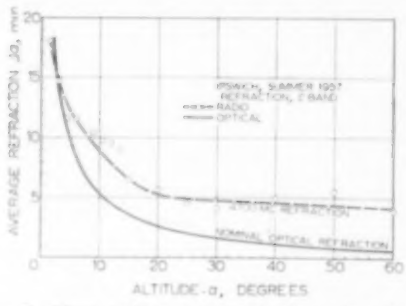

Fig. 7. Mean refractive error (radio and optical) as a function of altitude of the sun.

amplitude as a function of elevation angle. Above 12° the fluctuations were less than 1 per cent of the signal. The data reveals that the peak-to-peak fluctuation varies with the cosecant of the angle of elevation.

In all likelihood the scintillations are due to many factors. The evidence is that at high elevations we are observing short solar bursts. Pointing to the solar origin of these bursts are the rapid onset and decay of the fluctuation plus the correlation between days of high solar activity and high elevation short-period bursts.

The low angle scintillations are always present, indicating their atmospheric origin. Correlation between scintillation amplitude and many meteorological parameters at ground level (barometric pressure, wind speed and direction, etc.) were unsuccessful.

6. REFRACTION

Utilizing the drift technique, refraction is measured by comparing the time of transit of the sun through the antenna pattern (the apparent as refracted position) with the astronomically calculated position of the center of the sun's disk for this time. The difference between the true position and the apparent position of the sun as a function of antenna elevation is graphed in Fig. 7. The nominal astronomical refraction utilized by various almanacs was used for the optical curve.

7. SUMMARY

The evidence on refraction on this and on the previous experiments conducted by the group[1] are that in the microwave region, the average refraction is the same as in the optical region. Experimental results indicate that during a particular day there might be considerable fluctuations about this average.

Low angle amplitude scintillations are always present and can be of large amplitude with longer periods prevailing. At higher angles the fluctuations are probably solar in origin and are of short period and small amplitude. While the origin of the scintillations is probably meteorological no correlation of scintillation amplitude at low angles and commonly measured meteorological parameters was noted.

The absorption measurements yield a value of 0·00348 dB/km. The extremely long path lengths used in radio astronomical techniques perform an unusual method for propagation measurements at wavelengths that undergo relatively low atmospheric absorption.

ACKNOWLEDGEMENTS

This investigation was carried out under the general supervision of Dr. P. Newman. Mr. W. Barron assisted greatly with the calculations and data analysis.

REFERENCES

1. Aarons J., Barron W. R. and Castelli J. P. Radio Astronomy Measurements at VHF and Microwaves. *Proc. Inst. Radio Engrs.* **46**, No. 1, 325 (1958).
2. Van Vleck J. H. in *Propagation of Short Radio Waves* MIT Rad. Lab. Ser., Vol. 13, p. 641. McGraw-Hill, New York (1951).

Planet. Space Sci. Pergamon Press 1959. Vol. 1, pp. 57–62. Printed in Great Britain.

HYDROGEN EMISSION AND TWO TYPES OF AURORAL SPECTRA

G. I. GALPERIN

Institute for Atmospheric Physics, Academy of Sciences of the U.S.S.R., Moscow

(*Received* 25 *September* 1958)

Abstract—Various characteristics of auroral activity have been correlated with the hydrogen emission. This emission has been studied with the CII–48 and CII–47 spectrographs having dispersions of 85–95 and 200 Å/mm respectively. The observations were made at the Loparskaya station of this Institute where the geomagnetic latitude is 64°. The correlations include the intensity of H_α with:

(1) *K*-index.
(2) The atomic lines of OI, OII, NI, and NII.
(3) The molecular bands 1 NG and 2 NG of N_2^+ and 1 NG of O_2^+.
(4) The intensities of H_β and H_γ as well as their profiles.
(5) Radio reflections.

THE formation mechanism of auroras can be studied directly by investigating their hydrogen emission. Investigations by Vegard[1], Gartlein[2] and Meinel[3] revealed some important properties of the latter: considerable intensity variations relative to the brightness of auroras, the Doppler character of its line widening, and the dependence of the line profiles upon the angle formed by the line of sight of the spectrograph and the magnetic force line. Later evidence points to the absence of a definite relation between the appearance of a hydrogen emission and the *K*-index of the magnetic disturbance, so that hydrogen emission is apt to appear at the initial stage of an aurora, especially when the latter has the shape of a homogenous arc and some more data. However, the accumulation of experimental evidence, especially that bearing on hydrogen line profiles, has been greatly hampered by the weakness of hydrogen emission from auroras and by the small resolving power of the instruments used.

During 1955–1958 at the Loparskaya station of this Institute, located in the auroral zone (geomagnetic latitude, $\phi = 64°$), spectrograms of auroras were taken using a CII-48 spectrograph with a dispersion of 85–95 Å/mm.

The spectra thus obtained can be distributed between two extreme types[4]. The first type is

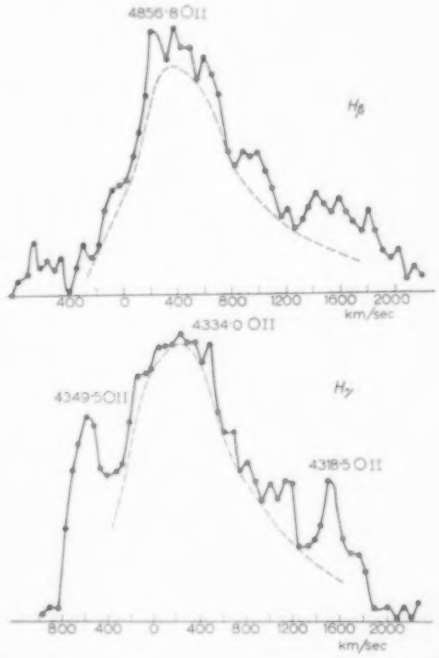

Fig. 1. H_β and H_γ profiles in the magnetic zenith on 16–17 February 1958, CII-48, dispersion 87 and 95 Å/mm respectively. These profiles are typical for a series of hydrogen line profiles obtained at Loparskaya ($\phi = 64°$), Roshchino ($\phi = 57°$) and Zvenigorod ($\phi = 51°$). The measured value of decrement $I_{H_\beta} : I_{H_\gamma} = 0{\cdot}80$.

peculiar to high red auroras of type A. Its atomic lines OI, OII, NI, and NII and its [OI] emission at λ 6300–6364 Å are relatively strong, while its molecular bands 1 PG and 2 PG of N_2 and 1 NG of O_2^+ are weakened. This type of spectrum is also characteristic of low latitude auroras, where the bands 1 PG of N_2 may be absent altogether[5]. The second kind of spectrum is peculiar to low yellow greenish auroras and is characterized by intense molecular bands 1 PG and 2 PG of N_2 and 1 NG of O_2^+ and by an [OI] emission at λ 5577 Å. The 1 NG bands of N_2^+ can attain a considerable intensity in either type. Further details will be published elsewhere by A. B. Korotin.

Hydrogen emission is much more often observed in the first type of spectrum than in the second. More than once it was obtained when the spectrograph was directed solely to high red auroral forms. Thus, hydrogen emission appears to be correlated somehow with emission at λ 6300–6364 Å and with the permitted lines OI and OII. Its correlation with NI and NII lines is less pronounced and sometimes even entirely absent.

Besides high dispersion studies of auroral spectra, spectrograph CII-47 with a dispersion of 200 Å/mm and 1 hr exposure was used at Loparskaya in 1956–1958 for patrol observations for appearance of hydrogen emission. Its slit was divided into three parts, directed respectively to the magnetic horizon, magnetic zenith, and the white diffuse surface which gave the average luminosity of the sky. Later the third part of the slit was directed to the south. A considerable amount of successive spectrograms for auroras, part of which was taken in clouds, has been studied, and by now it is possible to make some conclusions on the character of the appearance of hydrogen emission.

The intensity of the H_α emission is rarely above 200 rayleighs, though sometimes it attains several thousands rayleighs (24–25 March 1958). Most of the earlier estimates were based on such unusually high values. Our results are in agreement with the spectroelectrophotometric measurements made by Hunten[6]. The intensity of the emission varies slowly, and generally the H_α line is observed on several successive 1 hr exposures, though sometimes it may disappear during the night, reappear again, and so on. Once it was observed on nine successive nights (18–28 January 1958), and its appearance on two or three successive nights was very often, though it did not continue throughout the night. The intensity of the hydrogen emission is not correlated with the intensity of auroras. A rather faint aurora may sometimes follow an intense and long emission of hydrogen (16–17 February 1958).

Most often the H_α line is observed simultaneously on all three parts of the spectrogram during several hours on end, but the relative intensity of the emission in the different directions varies throughout the night. This is because the region of hydrogen emission moves across the sky. At the outset of a polar display it ordinarily appears in the north and moves to the south, and by the end of the night sometimes the reversed motion may be observed (16–17 February 1958). In the middle of the night the character of the variations is not defined clearly, though hydrogen emission has been rather frequently observed at that time.

In general, hydrogen emission is observed very often, and nearly half of the spectrograms, taken from most varied auroral forms and phases, reveal its presence. The most frequent, however, is its appearance with quiet forms without the ray structure, and especially with red forms of type A characterized by enhanced lines at λ 6300–6364 Å.

Several different investigators have noticed the tendency of hydrogen emission to appear in early phases of an aurora. The present observations showed that in a number of cases it appeared simultaneously with a faint auroral light and attained a maximum intensity one to two hours ahead of full auroral development. What is more, in some cases hydrogen emission has been stated to start before any auroral forms could be observed visually, and only one to two hours later did an intense yellow greenish auroral light burst into view. By that time the hydrogen emission may cease almost completely, as it did, for instance, on 21–22 November 1957 and on 11–12 December 1957.

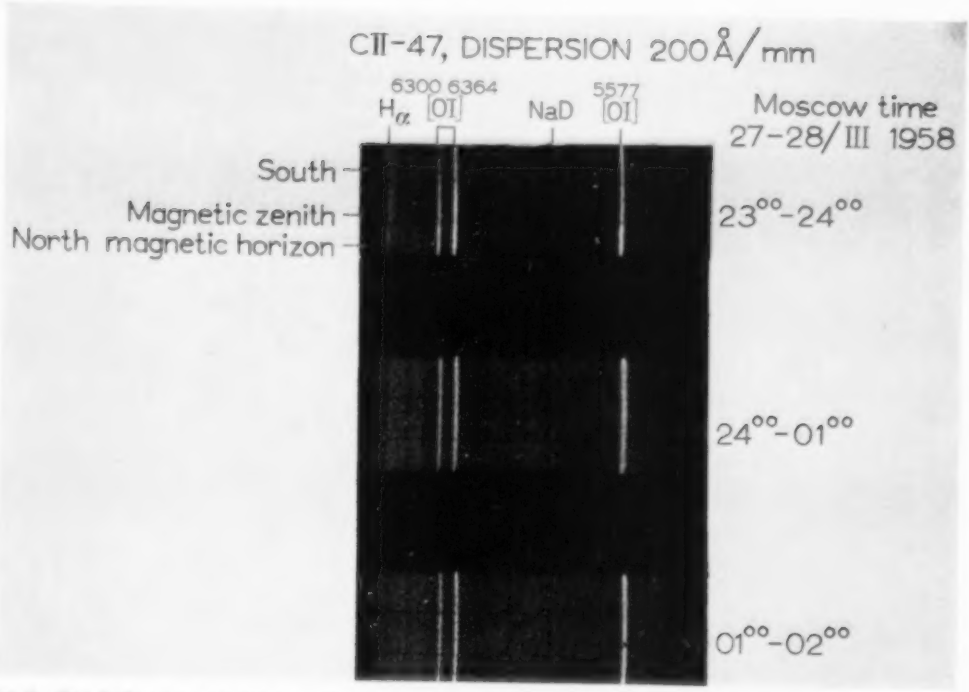

Fig. 2. The hydrogen emission is simultaneously observed in the northern, zenith and southern directions in the absence of aurora. During subsequent hours an intensive auroral display takes place.

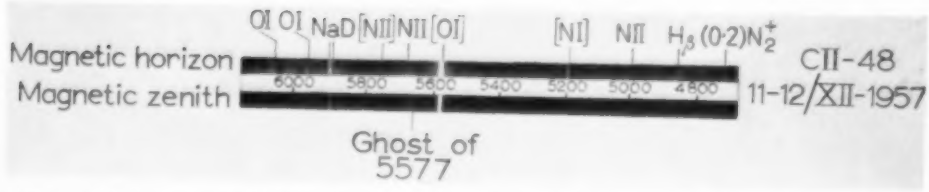

Fig. 3. The spectrum obtained under a clear sky and complete absence of a visual aurora. There can be seen the emission of H_β and of NI, NII, OI and N_2^+.

Facing p. 59

Recently, Romick and Elvey[7] came to similar conclusions from observations south of the auroral zone.

The very faint emission that appears simultaneously with hydrogen emission, preceding any visual auroral form, has a spectrum characteristic to the first, "atomic", type (spectrograms with a dispersion of 85 Å/mm). On this ground it may be supposed that the spectra of high auroral forms, having atomic lines with high excitation potentials, which we have referred empirically to the first type[4], are excited by interactions with stream corpuscles. The main energy of light emission from bright auroras is evolved in later phases of their development and is not necessarily connected with the presence of hydrogen emission.

The average estimate of the emission altitudes can be obtained on the following considerations. We may assume that the growth of the λ 6300 to λ 5577 Å intensity ratio in the average is related to increase in altitude (it can also be related to intensity). Then, from the value of this ratio as measured on the spectrogram, the light emission altitude can be determined statistically. Such estimates of average emission altitudes have been made from the plotted ratio of red line to green, as recently published by Seaton[8] on the basis of some observations. Although Seaton's curve is far from being quite certain, it may still be inferred from the obtained estimates that in many cases hydrogen emission is connected with light emission altitudes higher than 120 km.

After three years of observation with the CII-48 spectrograph, we have a considerable number of spectrograms with a resolution limit of 2–3 Å, which permit the profiles of H_α, H_β and H_γ lines to be determined reliably. The accuracy of the profiles obtained is impaired by blends, but recurring blends can be revealed by superimposing several records. Moreover, only slightly blended hydrogen lines are obtained on occasion. When reduced to a single scale, the profiles of H_α, H_β and H_γ are very similar. The shift of the maximum within the profile in the magnetic zenith does not reach outside 300–400 km/sec; towards the violet side the emission can be followed up to about 2000 km/sec; and there is a slight "red shift" reaching +300–500 km/sec.

In the intermediate directions the aspect of the profile varies smoothly from one extreme case to the other. Within the observational error no appreciable differences have been noticed either between profiles referring to equal distances from the magnetic horizon or between different hydrogen lines. Similar results have been obtained at other stations of this Institute; viz. at Roshchino[9] and at Zvenigorod[10]. Decrement measurements for the Balmer series lines gave the following results: $H_\beta : H_\gamma = 1 : 0{\cdot}80$. The decrement value for $H_\beta : H_\gamma$ is widely different from that calculated by Chamberlain[11]. As early as 1951, I. S. Shklovsky[12] has inferred from the results obtained by Meinel[3] and Gartlein[2] that the aspect of the hydrogen line profile in the magnetic zenith directly testifies to a dispersion of the velocities of hydrogen corpuscles, since the profile observed is sharply different from the way in which the effective cross-section for the excitation of H_α varies with the velocity. In my published paper[13] the available data on this variation were analyzed. According to the experimental data secured by Fan and Meinel[14], as well as from Chamberlain's computations[11] and from estimates based on the adiabatic theory[15], the velocity corresponding to the maximum effective cross-section turns out to be about 1700 km/sec.

Uncertainty is due only to the absence of experimental data on the interaction between the streams of hydrogen corpuscles and the atomic oxygen. If such an interaction in the atmosphere modifies this velocity only slightly, Chamberlain's formula[11] can be made use of. Furthermore, computations show that to explain at once the small shift of the maximum within the profile in the magnetic zenith and the small half-width in the magnetic horizon is impossible, if we will not relinquish the assumption that the corpuscles enter the atmosphere with a constant velocity. Recently, Chamberlain[16] came to similar conclusions. B. A. Bagariatsky[17] has shown that on this assump-

tion it is also hard to account for the observed value of the "red shift" within the profile in the magnetic zenith. Since at high speeds the scattering of protons is slight, it may be supposed that the "red shift" will be accounted for satisfactorily if the considerable dispersion of the velocities with which the corpuscles enter the atmosphere is taken into account. The effective cross-sections for the processes by which the H_α line is excited (charge exchange by protons in excited levels, excitation of hydrogen atoms by collisions with atmosphere molecules) depend on the velocity in such a way that the dispersion of velocities cannot appreciably affect the profile's aspect unless the velocities are about one or two thousand km per second or less. The hydrogen line profiles obtained in different places at different times* are all similar.

On the standpoint set forth here, none of these profiles will directly reveal any appreciable number of hydrogen corpuscles with velocities equal to or higher than 2000 km/sec. If, however, the smallness of the maximum shift

* by Meinel[3], Vegard[1], Gartlein[2], and Chamberlain[16], and at three station of this Institute with identical instruments[9, 10, 18, 19].

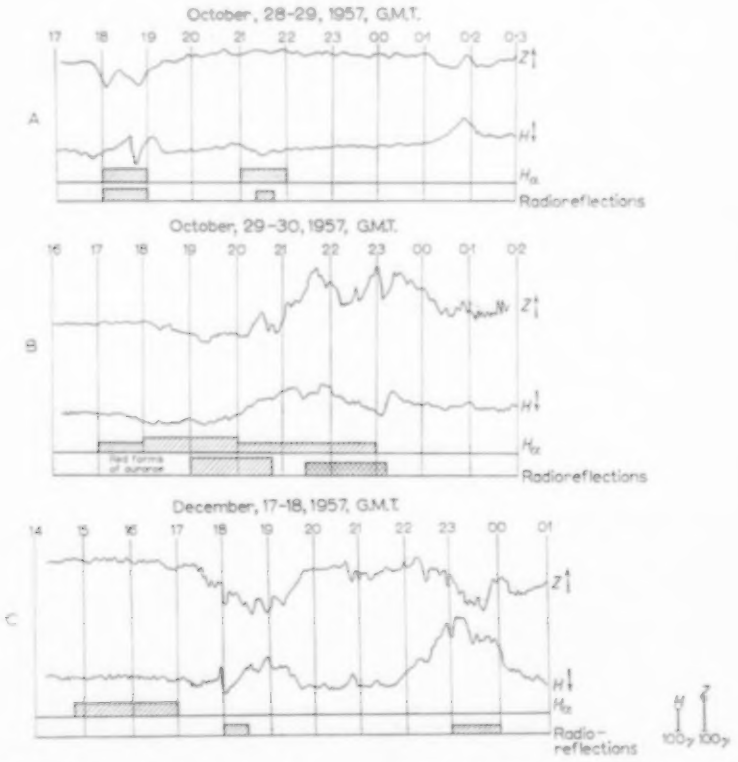

Fig. 4. The relations between the hydrogen emission, radio reflections from the aurora (λ—4·2 m) and the Earth magnetic field.

A. Synchronous appearance and disappearance of the H_α emission and radio reflections. 65 per cent of cases. B. The absence of radio reflections when the H_α emission is taking place. 26 per cent of cases. C. The absence of correlation between the H_α emission and radio reflections. 9 per cent of cases. It seems from such comparisons that for the occurrence of radio reflections two conditions must be fulfilled: the presence of hydrogen emission and disturbance of the Earth magnetic field.

in the observed hydrogen emission profile is due to the dispersion of the velocities of corpuscles, then the observed constancy of this shift and of the entire profile is difficult to explain. One of the possible explanations is that during the exposure, which lasts 1 hr or more, the velocities of the radiating corpuscles have time to vary again and again with the result that an average profile in respect to time is obtained. The penetration depth of the corpuscles can vary quickly even in an homogeneous quiet arc, as is obvious from a set of four successive spectrograms with a dispersion of 200 Å/mm, taken within the exposure range of 5 to 15 min. A vertical section of the homogeneous arc was projected on the slit of the spectrograph. In one of these spectrograms, the maximum of the H_α emission stands higher in the arc than in others. On the other spectrograms the intensity maximum of the H_α emission lies under the arc. So it is not advisable to rely on the analysis of the hydrogen emission luminosity curve until a great deal more observational data has been accumulated.

An array of independent facts seem to show that a considerable proportion of stream corpuscles enter the terrestrial atmosphere at small speeds, not above 1000–2000 km/sec; viz. (1) recurrence of hydrogen lines in many different spectrograms taken from high red auroral forms; (2) the investigations of profiles of hydrogen lines, as described here; (3) the direct observation of hydrogen emission above an homogeneous arc; (4) differences between the spectrum of direct excitation by protons previous to the appearance of visible auroral forms and the spectrum of low bright auroral forms. These corpuscle velocities are in agreement with statistical data on the delay of a magnetic storm behind solar activity phenomena[20, 21].

There is no strong connection between hydrogen emission and the variations of the terrestrial magnetic field. Hydrogen emission was often observed when the magnetic field was quiet. Sometimes with a fairly quiet magnetic field a displacement of the region of hydrogen emission can be noticed. On the other hand, an absence of hydrogen emission is sometimes concomitant with a strong magnetic storm. Spectrograms from 24 magnetic storms reveal that there was no hydrogen emission during four of these storms (one very strong storm, two strong ones, and one weak storm), although during the other 20 storms, hydrogen emission was definitely present.

Contrary to this, correlation with radio reflections from auroras is quite pronounced. The observations of radio reflections were carried on at a 4-meter wave length no less frequently than every 15 min.[22]. For the sake of comparison about 130 patrol spectrograms taken with a CII-47 spectrograph were used. Of these spectra, 65 per cent have shown that there is time coincidence between the appearance of radio reflections and hydrogen emission. In 26 per cent the H_α line was observed in the absence of radio reflections (in several cases H_α appeared when the magnetic field was quiet and in several more when red forms of type A were present with which no radio reflections occur usually, and there were a number of other cases also). In 9 per cent of the spectra the H_α line was absent at the time of radio reflections, yet part of these spectrograms were strongly blended by 1 PG bands of N_2 (dispersion ~ 200 Å/mm) which made them unfit for comparison.

Radio reflections from auroras, therefore, like the emission of hydrogen, seem to furnish direct evidence of the penetration of corpuscular streams into the atmosphere, and this evidence is more definite than the visually observed auroral forms. If so, radio reflections may be conveniently used as an indicator of the appearance of hydrogen corpuscles at any time of the day, even when the sky is covered with clouds.

REFERENCES

1. VEGARD, L. *Geofys. Publ., Oslo* **18**, No. 15 (1952).
2. GARTLEIN C. W. *Trans. Amer. Geophys. Un.* **31**, 18 (1950); *Phys. Rev.* **81**, 463 (1951); *Mém. Soc. Roy. Sci. Liége* **12**, 195 (1952).
3. MEINEL A. B. *Astrophys. J.* **113**, 50 (1951).
4. KRASSOVSKY V. I. *et al. Report to aeronomy symposium at Toronto* (1957).
5. MIRONOV A. V., PROKUDINA V. S. and SHEFOV N. N. in press (1958).

6. HUNTEN D. M. *J. Atmos. Terr. Phys.* **7**, 141 (1955).
7. ROMICK G. J. and ELVEY C. T. in press (1958).
8. SEATON M. J. *Astrophys. J.* **127**, 67 (1958).
9. SHUISKAIA. F. K. in press (1958).
10. MIRONOV A. V., PROKUDINA V. S. and SHEFOV N. N. *Izv. Akad. Nauk*, in press (1958).
11. CHAMBERLAIN J. W. *Astrophys. J.* **120**, 360 (1954); *Ibid.* **120**, 566 (1954).
12. SHKLOVSKY I. S. *Dokl. Akad. Nauk SSSR* **81**, 367 (1951); *Izv. Krym. Astrofiz. obs.* **8**, 51 (1952).
13. GALPERIN G. I. *Astro. J., Moscow* **35**, 382 (1958).
14. FAN C. Y. and MEINEL A. B. *Astrophys. J.* **118**, 205 (1953).
15. GILBODY H. B. and HASTED J. B. *Proc. Roy. Soc.* A **238**, 334 (1957).
16. CHAMBERLAIN J. W. *Astrophys. J.* **126**, 245 (1958).
17. BAGARIATSKY B. A. *Astro. J., Moscow* **35**, 101 (1958).
18. GALPERIN G. I. *Astro. J., Moscow* **34**, 131 (1957).
19. GALPERIN G. I. in press (1958).
20. NEWTON H. W. *Mon. Not. R. Astr. Soc.* **103**, 244 (1943).
21. MUSTEL E. R. *Astro. J., Moscow* N 1 (1958).
22. BIRFELD J. G. *Izv. Akad. Nauk SSSR, geofiz. ser.* N 4, 543 (1957)

Planet. Space Sci. Pergamon Press 1959. Vol. 1, pp. 63–65. Printed in Great Britain.

ON HYDROGEN EMISSION IN THE NIGHT GLOW

I. S. SHKLOVSKY

Institute for Atmospheric Physics, Academy of Sciences of the U.S.S.R., Moscow

(*Received 25 September* 1958)

Abstract—H_α emission has been observed at the Zvenigorod Station of the Institute for Atmospheric Physics. The width of the observed emission does not exceed the instrumental width of 2 Å. It is shown that the recombination of protons and electrons can not account for this emission, and that a probable source is the resonance scattering of solar L_α radiation by interplanetary neutral hydrogen atoms. The possibility that L_α radiation arises from a "geocorona" is considered as is the effect of resonance scattering of L_β radiation and the intensity at H_α resulting from flourescence when L_α and L_β are absorbed.

At the Zvenigorod Station of the Institute for Atmospheric Physics an H_α line has been discovered recently in the night sky spectrum without any appreciable geomagnetic disturbance[1]. Another feature of this H_α line is its narrowness. Its width does not exceed the instrumental width; i.e. lies within 2 Å. From this the spread in velocity, ΔV, of the radiating hydrogen atoms is found to be $\Delta V < 50$ km per second. On the other hand, the widths of H_α lines in auroral spectra are known to attain tens of angstroms, and the spread of velocities of the radiating atoms (for observations in the magnetic horizon) attains some hundred kilometers per second. The H_α emission observed at Zvenigorod may differ essentially from the hydrogen emission of auroras. We are inclined to connect this Balmer line with the diffuse L_α emission of the night sky, observed recently at high altitudes[2].

According to reference (2), the average intensity of the diffuse L_α radiation coming from the upper hemisphere, at heights starting with 120 km, is

$$I_{L_\alpha} = 3{\cdot}2 \times 10^{-3} \frac{\text{erg}}{\text{cm}^2\,\text{sec sterad}} = 2 \times 10^{8} \frac{\text{photon } L_\alpha}{\text{cm}^2\,\text{sec sterad}} \qquad (1)$$

As has been emphasized in reference (2), the observed L_α radiation is most likely to be due to interplanetary gas. Nevertheless, no preference has been given to either of the two possible hypotheses on the origin of Lyman's emission of the interplanetary gas; viz. (1) recombination of protons and free electrons, (2) scattering of solar L_α quanta by interplanetary neutral hydrogen atoms.

Hypothesis (1) is untenable. Suppose that the concentration of free electrons in the interplanetary space is $n_e = n_i$, where n_i is the concentration of protons. Making use of the well-known formulae from the theory of light emission by gaseous nebulae, determining n_e when I and the extension of the radiating region l are known, let $l = 10^{13}$ cm, then $n_e = 2 \times 10^4\ \text{cm}^{-3}$. But this concentration of free electrons in the interplanetary space seems impossibly high and is strikingly at variance with the photometric and polarization observations of the zodiacal light.

By far more effective is the mechanism of resonance scattering of solar L_α quanta on interplanetary neutral hydrogen atoms. In this case the concentration of the latter, n_{II}, can be determined from the relation

$$I_{L_\alpha} = \frac{I}{4\pi} n_{\text{II}} B_{12} u_{21} w l = \frac{I}{4\pi} n_{\text{II}} A_{21} w \frac{g_2}{g_1} e^{\frac{-h\nu_{12}}{kT}} \qquad (2)$$

Here ν_{12} is the frequency of the L_α line, $w = 6 \times 10^{-6}$ is the dilution coefficient, $g_2/g_1 = 4$ is the ratio of statistical weights, and T can be determined if the flux of solar L_α quanta and the profile of the solar L_α line are known.

According to the observations reported in (3), the flux of solar L_α quanta varies within a rather wide range; viz. from 0·1 erg/cm² sec to 5 erg/cm² sec, being apparently correlated with solar activity. A month before the flight of the rocket by means of which Lyman emission in the night sky was investigated, daylight rocket measurements of the flux of direct solar L_α radiation had given $F^\circ_{L_\alpha}=0{\cdot}6$ erg/cm² sec.[3] On this basis we put $F^\circ_{L_\alpha}=0{\cdot}5$ erg/cm² sec in further calculations. On the other hand, the width of the solar L_α line is $\Delta\lambda<0{\cdot}3$ Å[4]. Making allowance for the high thermal velocities of the hydrogen atoms and for turbulent velocities in the upper chromosphere (wherefrom apparently the solar L_α is radiated), we find that the breadth of this line is hardly below 0·15 Å. Taking 0·2 Å for the true value of the breadth of L_α in the sun's spectrum, and putting $F^\circ_{L_\alpha}=0{\cdot}5$ erg/cm² sec, we find $T\sim 7000^\circ$ for the equivalent temperature. Substituting this value of T in the second equation gives $n_{\mathrm{H}}\sim 0{\cdot}5\,\mathrm{cm}^{-3}$. Suppose that there is ionization equilibrium in the interplanetary gas and that the flux of solar radiation in the Lyman continuum is $\sim 0{\cdot}3$ erg/cm² sec; then, knowing n_{H}, we can use the formulae of the theory of gaseous nebulae to find that the concentration of ionized hydrogen atoms, which is equal to the concentration of free electrons, will be $\sim 200\,\mathrm{cm}^{-3}$ one astronomical unit away from the sun. This value is much lower than that obtained by Seidentopf and Behr[5] from polarization observations of the zodiacal light. So the observed polarization of the zodiacal light appears to be due to dust particles rather than free electrons[6].

Even if the observed diffuse L_α radiation should be accounted for by some reason other than the interplanetary gas, e.g. by a "geocorona" extending over several thousands or tens of thousands of kilometers (this hypothesis cannot be excluded entirely for the time being), then, all the same, the results obtained are of exceptional importance for the study of the nature of the interplanetary medium. In this case the values of n_{H} and n_e found from these observations must be considered the *upper boundary* of the content of neutral and ionized hydrogen in the interplanetary space.

If the scattering of solar L_α quanta by interplanetary (or "geocoronal"—this makes no difference here) neutral hydrogen atoms is the casual mechanism of the L_α radiation from the night sky, we may expect that other solar Lyman lines, and in the first instance the L_β line, will be scattered too. Owing to fluorescence this must lead to a Balmer emission, possibly of an interplanetary origin. Let us estimate this effect quantitatively.

The intensity of the solar L_β line, obtained in the rocket flight of 21 February 1955, is 0·01 erg/cm² sec, if allowance for absorption by O_2 and N_2 molecules in the higher layers of the atmosphere is made. This is 1/60 of the L_α line intensity. Alongside the absorption of L_β by O_2 and N_2 molecules its resonance absorption by oxygen atoms on the transition $^3P_2$–$^3D^\circ_{1,2,3}$ should be expected[7]. If the oscillator strength for this transition is 0·01[8], we may state from the computations made in reference (7) that the atomic oxygen of the earth's atmosphere will absorb as much as 30 per cent of the L_β radiation flux*. Thus the flux of L_β radiation liberated from absorption by the atmosphere is 1/40 of the L_α radiation flux.

After the absorption of a L_β quantam, an interplanetary hydrogen atom can pass to the second level with the emission of an H_α quantum. Let us estimate the number N of H_α quanta thereby scattered:

$$N_{\mathrm{H}_\alpha}=N_{\mathrm{L}_\alpha}\times\frac{F^\circ_{\mathrm{L}_\beta}}{F^\circ_{\mathrm{L}_\alpha}}\times\frac{A_{31}}{A_{21}}\times\frac{g_3}{g_2}\times\frac{A_{32}}{A_{32}+A_{31}} \quad (3)$$

N_{L_α} being the number of scattered L_α quanta. Substituting the quantities in equation 3 by their value gives

$$N_{\mathrm{H}_\alpha}\approx 3\times 10^{-3}N_{\mathrm{L}_\alpha} \quad (4)$$

If the flux of L_α radiation from the night sky is $F_{L_\alpha}=10^{-2}$ erg/cm² sec $=6\times 10^8$ photons/cm²

* This gives rise to a fluorescence of the terrestrial atmosphere in lines λλ 8446 and 11294 Å which can be observed during twilight.[7]

sec, then the flux of interplanetary (or "geocoronal") H_α will be

$$F_{H_\alpha} \approx 2 \times 10^6 \text{ photons/cm}^2 \text{ sec.} \quad (5)$$

As a matter of fact, this value must be several tens per cent higher owing to the scattering of the higher Lyman lines and the subsequent cascade transitions.

Thus the presence of the diffuse L_α radiation in the night glow must necessarily have for its consequence the presence of a weak but yet measurable field of H_α radiation. This emission is likely to arise in the interplanetary space, although there is no sufficient argument for the present to refute the "geocoronal" hypothesis. It should be emphasized that our conclusion on the presence of an H_α emission does not depend on either "interplanetary" or "geocoronal" location of the scattering hydrogen atoms.

As has been stated above, the flux of solar L_α quanta is variable within a fairly wide range. At the end of 1955 this flux, according to reference (3), was about 5 erg/cm² sec, which may be connected with increase in the general activity of the sun. In 1957–1958, when the observations at Zvenigorod were being conducted, the general level of solar activity was higher on the average than in 1955. The flux of L_β may also be supposed to be correlated with solar activity. If so, the flux of H_α quanta in the night glow can be an order of magnitude higher than the computed value, reaching 2×10^7 photons/cm² sec, or 20 R, and even more perhaps. The flux of H_α measured at Zvenigorod fluctuated from night to night within 5 to 20 R, which is in fair agreement with the concepts developed above.

An interesting experiment, decisive for the evolved theory, may be suggested. Namely, if the H_α emission in the night glow is due to scattering by hydrogen atoms, it should be considerably polarized. The observations which might verify this point are not easy in view of the slight intensity of the H_α emission. Still, they can be fulfilled.

REFERENCES

1. PROKUDINA V. S. *Astro. J., Moscow* **35**, (1958) (in press).
2. KUPPERIAN J. E., BYRAM E. T., CHUBB T. A. and FRIEDMAN H. preprint *N.R.L.* (1958).
3. BYRAM E. T., CHUBB T. A., FRIEDMAN H. and KUPPERIAN J. E. *Astrophys. J.* **124**, 480 (1956).
4. JOHNSON F. S., MALITSON H. H., PURCELL J. D. and TOUSEY R. *Astrophys. J.* **127**, 80 (1958).
5. SIEDENTOPF H., BEHR A. and ELSASSER H. *Nature, Lond.* **171**, 1066 (1953).
6. BIERMANN L. *Observatory* **77**, 110 (1957).
7. SHKLOVSKY I. S. *Astro. J., Moscow* **34**, 127 (1957).
8. OMHOLT A. *J. Atmos. Terr. Phys.* **9**, 28 (1956).

Planet. Space Sci. Pergamon Press 1959. Vol. 1, pp. 66–70. Printed in Great Britain.

THE DISTRIBUTION OF HELIUM-3 IN THE GRANT METEORITE AND A DETERMINATION OF THE ORIGINAL MASS

E. L. FIREMAN

Smithsonian Astrophysical Observatory, Cambridge, Massachusetts

(*Received* 18 *June* 1958)

Abstract—The distribution of helium-3 in a slice of the Grant meteorite was determined by exposing it to slow neutrons and counting the converted tritium. The measured values ranged from $6{\cdot}5\times10^{-6}$ cm³/g to $5{\cdot}1\times10^{-6}$ cm³/g, with the highest value occurring near one edge of the slice. The helium-3 isopleths corresponding to $5{\cdot}7\times10^{-6}$ cm³/g or less form closed loops which are not circles. This indicates that the meteorite was not spherical when it was exposed to extraterrestrial cosmic radiation. The variation of the helium-3 content with depth indicates that the average energy of the cosmic radiation to which it had been exposed was close to 6 BeV. These measurements also indicate that the Grant meteorite, before it struck the earth's atmosphere, was a pear-shaped object with a mass of approximately 880 kg; and that 400 kg ablated from the meteorite in its plunge through the atmosphere.

1. INTRODUCTION

THE Grant meteorite, found in New Mexico about 1929, is an iron meteorite with a mass of 480 kg, and is now the property of the U.S. National Museum. Work[1] done on isotopes produced in long iron targets when they are bombarded by high energy protons suggested that the distribution of helium-3 in a meteorite could be used to estimate the average energy of the incident cosmic rays to which it had been exposed as well as the size and shape of the meteorite before it struck the earth's atmosphere. The distribution of helium-3 in the Carbo meteorite had been measured[2, 3], and the results were applied to estimate the average energy of the incident cosmic rays and the original shape of the Carbo meteorite.

2. EXPERIMENTAL PROCEDURE

A slice was taken from the center of the Grant meteorite. The helium-3 content of the slice was measured by the method of neutron activation[4] whereby the helium-3 is converted to tritium which is extracted and counted. Several bars $\frac{1}{4}$ in. wide and $\frac{1}{2}$ in. thick were cut*† from the slice as indicated by the fine lines in the drawing of Fig. 1. Samples weighing 1·2 to 1·5 g were taken from the bars at the positions indicated by crosses in the drawing. Surface material and troilite nodules were avoided. After the sharp edges were removed from the samples they were etched down to 1·0 g. Twelve to fifteen of the samples were packaged in a small plastic container, which was irradiated in the Brookhaven reactor for 16 hr at a location where there were very few fast neutrons. The slow neutron flux was about 10^{12} neutrons/cm² sec. A sample of terrestrial iron and a sample of either the Harvard Bethany‡ or of the Cape York meteorite, which are known to have less than 10^{-9} cm³/g of helium-3, were also in each package.

In two similar irradiations done in earlier work[3] with samples of the Carbo meteorite, a gas standard with a known amount of helium-3 in an aluminum container had been included with the plastic containers. The gas

* The slice was cut at the Battelle Memorial Institute, Columbus, Ohio.

† Dr. E. P. Henderson kindly loaned the author the bars.

‡ A fragment of the Gibeon meteorite fall.

standard served as an absolute calibration. The uncertainty in this calibration was about 10 per cent; however, relative measurements are accurate to better than 5 per cent. The Grant samples reported here were calibrated by including two Carbo samples in the same package.

The irradiated sample was placed in an alumina crucible with 5 cm^3 of hydrogen carrier and melted with an induction heater. The gas was extracted, and the hydrogen was purified and counted in the manner described in the previous publication[4]. In the work referred to, graphite crucibles were used. The use of alumina crucibles made the removal of tritium from the sample more complete. No tritium was detectable in second extractions done by remelting the samples which is an improvement over the use of graphite crucibles. The electromagnetic stirring action on the molten iron and gas from the alumina serving as an additional carrier probably assists in the tritium extraction. Preparation of the sample is also important in achieving reproducible results. Samples which are less than one-half gram and meteorite chips gave lower tritium yields per gram than did the one-gram samples. This is thought to be caused by a loss of tritium produced near the surface during the irradiation. The one-gram samples were etched to 0·7 g after the irradiation, and before the tritium was extracted.

To test the reproducibility of the measurements, five adjacent Carbo and four adjacent Grant samples were irradiated together and processed to determine their helium-3 content. The largest observed differences in the measurements of the helium-3 content of the five Carbo samples was 5 per cent; the largest difference with the four Grant samples was 3 per cent. The counting errors should give less than one per cent difference. The additional fluctuation may be real; that is, caused by variations in the helium-3 content due to inhomogenieties in the meteorite itself, or it may be a spurious experimental effect. Possible experimental sources of the fluctuation are the variation in the neutron flux over the dimensions of the package, or the variation in the loss of tritium near surfaces. The samples of terrestrial iron of the Cape York and the Harvard Bethany meteorites gave less than one per cent of the activity measured in the Grant samples; it is therefore believed that traces of lithium are not the cause of the fluctuation. The fluctuations in any case are not large enough to affect seriously the validity of the experiment.

3. RESULTS

Table 1. The Measured He^3 Values and their Locations

Bar	Distance* (in.)	He^3 (10^{-6} cm^3/g)
S	+1·6	6·5, 6·6
	−1·3	6·3, 6·4
O	−0·5	5·8, 6·0
	−1·5	5·9
	+3·0	5·9, 5·7
	+6·0	6·1, 6·0
	+9·0	6·3, 6·5
	+12·0	6·5
K	−0·5	5·5, 5·3
	−1·5	5·6, 5·5
	−3·5	5·9
	+3·0	5·4, 5·6
	+6·0	5·6
	+9·0	5·9, 5·7
	+12·0	6·0, 6·2
G	−0·5	5·4, 5·2
	−4·0	5·8
	−6·0	6·1
	+3·0	5·1, 5·2
	+6·0	5·1, 5·0
	+9·0	5·2
	+12·0	5·5, 5·5
C	−0·5	5·6
	−1·0	5·6
	−2·0	5·7
	−3·5	5·9
	−4·5	6·0, 6·0, 5·9, 5·8
	−5·0	6·0
	+3·0	5·5, 5·4
	+6·0	5·5
	+9·0	5·7, 5·9
	+12·0	5·9, 6·0

* The distance is from the reference line which is shown perpendicular to the lettered bars in Fig. 1. The (+) distances are to the left and the (−) distances are to the right of the reference line.

The measured helium-3 values together with the locations of the samples from which they were obtained are given in Table 1 and are shown in Fig. 1. The helium-3 determinations ranged from $6{\cdot}5 \times 10^{-6}$ cm^3/g to $5{\cdot}1 \times 10^{-6}$cm^3/g. These values are very high for a meteorite the size of the Grant. Although the meteorite itself is almost symmetrical about the arrow line in Fig. 1, the helium-3 isopleths, or contours of equal helium-3 content, appear to be symmetrical about bar G, where the lowest values were observed. The contours of constant helium-3 follow approximately the outline of the slice near two of its four sides. The highest value, $6{\cdot}5 \times 10^{-6}$ cm^3/g, parallels one of these sides. The region of lowest helium-3 content is an elongated region well inside the slice. This indicates that the body as it existed in space was not a sphere, and that its central region has remained the central region of the present body.

Fig. 2 sketches a reconstruction of the parent body of the Grant meteorite and shows that it probably was a pear-shaped body before it entered the earth's atmosphere. The incomplete contour lines of constant helium-3 were completed by an extrapolation. The greatest distance between the edge of the slice and the contour line of $6{\cdot}5 \times 10^{-6}$ cm^3/g helium-3 determines the original perimeter of the meteorite. The helium-3 isopleths are almost symmetrical about an axis through the bar giving the lowest helium-3 value. If the parent body had been symmetrical about this axis, then it would have had a mass of 880 kg, and must have lost 400 kg in its plunge through the atmosphere. If the entrance velocity of the Grant were known, a basis for the calculation of ablation loss for bodies entering the earth's atmosphere would exist. The best estimated value for a velocity of a meteorite in the earth's upper atmosphere is 17 km/sec[5].

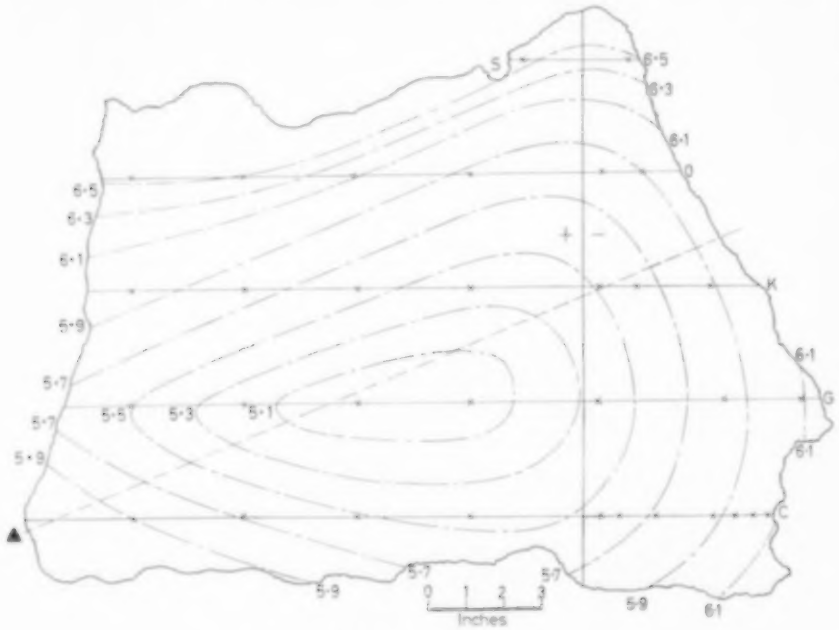

Fig. 1. Drawing of the slice of the Grant meteorite with the distribution of helium-3 in units of 10^{-6} cm^3/g.

If all meteorites were exposed to the same cosmic ray intensity and for the same length of time before entering the earth's atmosphere, then the helium-3 content of a small sample compared with the values observed in the Grant meteorite would give some information about the original mass of the body from which the sample was taken. If the helium-3 content of the sample is higher than $6{\cdot}5 \times 10^{-6}$ cm^3/g, the maximum measured in the Grant meteorite, then the original mass of the meteorite under study must have been less than 880 kg. If the helium-3 content is less than the minimum value in the Grant, $5{\cdot}1 \times 10^{-6}$ cm^3/g, then the original mass of the meteorite under study must have been greater than 880 kg. Since most of the measured samples show helium-3 values less than $5{\cdot}1 \times 10^{-6}$ cm^3/g, we may conclude that most meteorites are the remnants of bodies that in space were larger than 880 kg.

An interesting metallurgical feature that can be correlated with the helium-3 distribution is the heat-altered layer near the edge of the slice. Examination of the Carbo slice showed a region where the metal had been altered by heat and a second region not showing this effect. In the first region the helium-3 content was $5{\cdot}0 \times 10^{-6}$ cm^3/g while only $3{\cdot}5 \times 10^{-6}$ cm^3/g for the second region. In the Grant meteorite this relationship is more pronounced[6, 7]. A very wide heat altered layer lies along the edge parallel to the helium-3 contour of $6{\cdot}5 \times 10^{-6}$ cm^3/g; and at one place the iron is completely melted to a depth of almost one centimeter. The correlation between high helium-3 content and heat alteration of the surface metal can be interpreted as follows: During a meteorite's flight through the atmosphere heat generated at the surface can affect the metal to a depth of almost one centimeter if there is little ablation; if the ablation is rapid, however, the heat cannot affect more than a very thin surface layer.

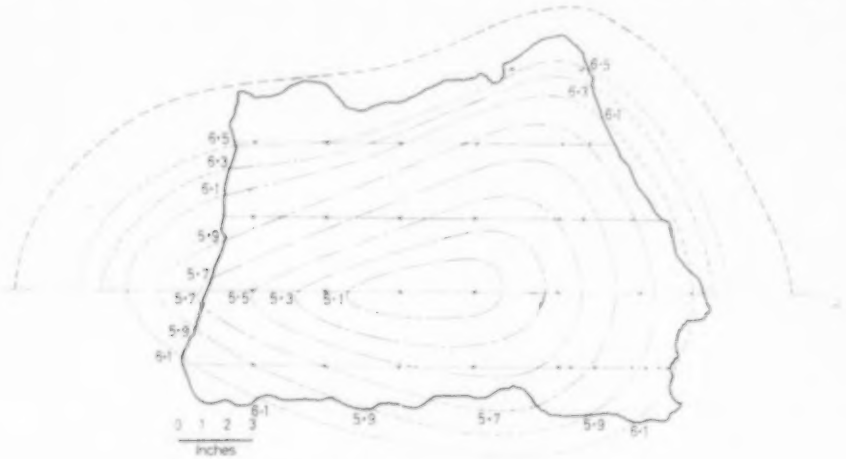

Fig. 2. Sketch showing parent body of the Grant meteorite, reconstructed from measurements of helium-3 content.

4. DISCUSSION OF RESULTS

The measurement of the distribution of helium-3 allows us to reconstruct the original shape and mass of the Grant meteorite and to make estimates for other specimens. Since a large meteorite must be sliced if we are to measure the helium-3 distribution, probably very few specimens will be made available for such a complete study. However, for many meteorites the helium-3 in small samples can

be measured with very little damage to the specimen.

Experiments[1] with long iron targets bombarded by 6 BeV protons have shown that the helium-3 production in a sphere of 30 cm radius is 1·36 times greater near the surface than at the center. In the Grant slice the largest helium-3 value is 1·28 times the smallest one. The distance between the edge having the highest helium-3 content and the position of lowest helium-3 content varies from 19 cm to 27 cm. This fact indicates that the average energy of the incident cosmic rays was about 6 BeV, and that very little material was ablated from this edge. If the energy were greater than 6 BeV, the depth variation of helium-3 would be smaller than the measured value. On the other hand, if the average energy of the rays were 3 BeV or less, then the measured helium-3 gradient could be explained if more than 10 cm of additional material covered the edge with the highest helium-3 content. However, it would then be difficult to account for the fact that the $6{\cdot}5 \times 10^{-6}$ cm^3/g contour is parallel to this edge and that the $5{\cdot}1 \times 10^{-6}$ cm^3/g contour is not more circular. The absolute value of the helium-3 content also gives evidence for the average cosmic ray energy of 6 BeV, and supports the conclusion that less than 10 cm of material was ablated from the side of the slice with the highest value of helium-3. The target measurements with 6 BeV protons indicate that the helium-3 production near the surface of the 30 cm sphere would be 83 per cent of the production in small spheres.

The highest helium-3 content measured in any meteorite is $8{\cdot}8 \times 10^{-6}$ cm^3/g, found in the Mt. Ayliff meteorite[8], which has a mass of 13·6 kg. The ratio of 6·5 to 8·8 is 73 per cent. However, there is a 10 per cent uncertainty in the absolute values. If the edge of the Grant slice with the highest helium-3 value were covered with more than 10 cm of material, iron meteorites with helium-3 content greater than $8{\cdot}8 \times 10^{-6}$ cm^3/g should have been found.

In samples of Harvard's Bethany and of the Cape York meteorite the helium-3 content approaches 10^{-10} cm^3/g, the lowest amount detectable by present methods. These samples therefore derive from the interior of very large bodies. From the spallation rate, which is reduced by a factor of e for each 150 g/cm^2 of shielding, we deduce that these two samples must have come from bodies whose masses were greater than 500 tons.

ACKNOWLEDGEMENTS

The author is indebted to Prof. Fred. L. Whipple for several valuable discussions, and to the U.S. Atomic Energy Commission for a grant.

REFERENCES

1. Fireman E. L. and Zahringer J. *Phys. Rev.* **107**, 1695 (1957).
2. Paneth F. A., Reasbeck P. and Mayne K. I. *Nature (Lond.)* **172**, 200 (1953).
3. Fireman E. L. *Nature (Lond.)* **181**, 1725 (1958).
4. Fireman E. L. and Schwarzer D. *Geochim et Cosmochim. Acta* **11**, 252 (1957).
4. Fireman E. L. and Schwarzer D *Phys. Rev.* **107**, 1695 (1957).
5. Whipple F. L. and Hughes F. F. *J. Atmos. Terr. Phys.* **2**, 149 (1955).
6. Henderson E. P. private communication.
7. Maringer R. E., Manning G. K. and Jackson L. R. *Battelle Third Quarterly Report* (1957).
8. Dalton J. C., Paneth F. A., Reasbeck P., Thomson S. J. and Mayne K. I. *Nature (Lond.)* **172**, 1168 (1953).

Planet. Space Sci. Pergamon Press 1959. Vol. 1, pp. 71–84. Printed in Great Britain.

IGY ROCKETS AND SATELLITES: A REPORT ON THE MOSCOW MEETINGS, AUGUST 1958

WILLIAM W. KELLOGG

The Rand Corporation, 1700 Main Street, Santa Monica, California

(*Received 9 October* 1958)

INTRODUCTION

THE Fifth Meeting of CSAGI (Committee Speciale de l'Annee Geophysique Internationale) was held at Moscow from 31 July to 9 August 1958. The most urgent matters to be considered by the two hundred and twenty assembled scientists had to do with the organization of the programs for international cooperation which would continue the work of the IGY in many fields of geophysics. However, with the period of the International Geophysical Year drawing to a close, this was also an occasion for a first review of the geophysical and astrophysical research which had been achieved with rockets and satellites.

The purpose of this report is to summarize the proceedings of the Technical Symposia on Rockets and Satellites. Since these symposia occupied the better part of four days and consisted of 77 papers on nearly all phases of the subject, a summary must necessarily be somewhat superficial, and apologies are due to the authors of the many excellent papers for reviewing their work so tersely. Fortunately for posterity, all of the papers presented will appear in the Annals of the IGY.

A report on the Moscow meetings would not be complete without some mention of the activities of the Working Group on Rockets and Satellites of CSAGI. Working in parallel with working groups in each of the other IGY disciplines, this Working Group spent the opening days of the meeting trying to arrive at a plan for international working arrangements for the co-ordination of research and the efficient and rapid exchange of observations and results. In the absence of Dr. Lloyd V. Berkner, the designated chairman, Dr. Homer E. Newell, Jr., was acting chairman. The nations actively represented in this Rockets and Satellites Working Group were the U.S.A., the U.S.S.R., Great Britain, Japan, Australia, and South Africa. Although some progress was made in obtaining a better understanding of the achievements and aims of the various programs in each of the countries represented, Chairman Newell was forced to admit, in his address to the closing plenary session, that the international agreements which had existed were too general to be workable, and that the Working Group had not been able to arrive at more detailed agreements in the area of rocket and satellite research.

Nevertheless, as demonstrated by the material presented at the technical symposia, it was clear that tremendous strides had been made in the exploration of the upper atmosphere and the space beyond by our new vehicles. The fact that satellites, by their very nature, cross national boundaries and signal their messages to all parts of the world makes them uniquely international—a sort of symbol of worldwide scientific endeavor. So it seems inevitable that working arrangements for the international use of these scientific tools will eventually be made.

In the summary which follows the *subject matter* being studied rather than the *vehicle* is the central theme. Satellites are, in a sense, just a very high performance rocket—"a long-playing rocket", to quote J. Kaplan. In tracing this theme of the planet Earth and its environment the original order in which the papers appeared has been lost, but the story should be a good deal more coherent.

In identifying the various papers the names of the original authors are used, even though

these authors were in many cases not able to attend the meeting and a colleague had to present the paper.

1. ATMOSPHERIC STRUCTURE

1.1. *Pressure, density, and temperature distribution*

Prior to the launching of the first satellite in October 1957, the structure of the upper atmosphere had been repeatedly measured by rockets, and two summaries of these rocket measurements in the U.S. are still widely quoted. The older one is the "Rocket Panel Atmosphere"[1], and a somewhat more recent one is referred to as the "ARDC Model"[2], based on a study by the U.S. Working Group on Extension to the Standard Atmosphere. These two models agree to within a few per cent in pressure up to about 220 km. There were no rocket data above 220 km (and only one measurement at this height), but the ARDC Model extends to 500 km by a theoretical extrapolation. All the data used for these models were from White Sands Proving Ground (WSPG), N.M., Lat. 31°N. This is mentioned at the outset, since so many of the IGY results were presented in relation to these earlier summaries.

A fairly large portion of the rocket programs of the U.S., U.S.S.R., Great Britain, Japan, and Australia have been or will be devoted to measurements of pressure, density, or temperature at various altitudes and latitudes, using a variety of measuring techniques.

The IGY measurements have shown some highly significant differences between the mid-latitude and arctic upper atmospheres. Spencer (U.S.) La Gow, Horowitz, and Ainsworth (U.S.), Jones, Fischbach, and Peterson (U.S.), and Stroud, Bandeen, Nordberg, Bartman, Otterman, and Titus (U.S.) reported results from Ft. Churchill, and Shvidkovsky (S.U.) reported on the measurements with the Soviet Meteorological rocket at central and Arctic U.S.S.R. stations (exact locations unspecified).

The Soviet observations of temperature by thin wire temperature elements strung along a nose probe were quite extensive up to 50 km, and showed that the seasonal change of temperature occurred earlier at the higher altitudes, following the change in insolation with less lag than at the surface. Thus, at 50 km the temperature maximum is in late June, the temperature minimum in late December. (This is a trend which was pointed out by Dobson, Brewer, and Cwilong[3] in 1938 on the basis of balloon observation, though of course they did not have data to such high altitudes.)

In comparing mid-latitude and Arctic results, Jones, La Gow, and Stroud all concluded, on the basis of separate sets of measurements, that up to 80 km in the Arctic the density is about the same or a trifle higher in summer, but in winter it is significantly lower by 10 to 20 per cent. This corresponds to a lower wintertime temperature in the Arctic between 30 and 80 km. The day-to-day variation in this altitude range at Ft. Churchill appears to be much greater than at WSPG, especially in winter.

It is important to note the wind measurements in this altitude range, determined at WSPG and Ft. Churchill as reported by Stroud (U.S.), in Australia as reported by Massey (U.K.), and in Japan as reported by Hatanaka. All made use of the propagation of sound from grenade explosions, and the Australian rockets also combined radar observations of drifting chaff or "window". The results were essentially the same from all three locations: Strong west winds in winter, reaching a peak velocity in the 70 to 80 km region, and weaker east winds in summer. Note that west winds imply higher pressure towards the equator, while east winds mean higher pressure towards the poles. At 60 to 80 or 90 km the pressure and density gradients are roughly in the same direction, so the wind observations tend to verify the latitudinal density differences reported between WSPG and Ft. Churchill.

Above 80 km the trend is different. Both Jones and La Gow agreed that the temperature (or scale height) was higher at 80 to 90 km in the Arctic in summer and during the winter day, though it is about the same during the winter night. La Gow, who got two successful flights to 250 km last winter, found that this general trend continued upwards, but with an ever-increasing diurnal effect. Thus, the winter

daytime temperatures are apparently higher in the Arctic, and at 200 km and above the resulting density is ten times greater. During the winter night the upper atmosphere appears to cool off, and densities at 200 km are about the same as at WSPG.

The Soviet studies of atmospheric densities and pressures by rockets and satellites were reviewed by Michnevich (S.U.). Using magnetic manometers, pressures have been measured by rockets, presumably at a higher latitude than WSPG, and his results are as follows:

100 km	$4{\cdot}0 \times 10^{-10}$ g cm^{-3}
150	$4{\cdot}7 \times 10^{-12}$
200	$2{\cdot}7 \times 10^{-13}$
220	$1{\cdot}6 \times 10^{-13}$
260	$6{\cdot}9 \times 10^{-14}$

Of particular interest were the results from a magnetic manometer in a Sputnik, which gave a value of 1×10^{-13} at 260 km, and $8{\cdot}8 \times 10^{-15}$ at 355 km (same units). The pressure observed by the Sputnik magnetic manometer apparently decreased over the first few days, which was interpreted as due to gas leaving the Sputnik. (This explanation, however, would seem to be at odds with Mirtov's theoretical treatment of gases around a satellite—see below.)

Above 200 km a new and powerful density measuring technique comes into play: The earth satellite drag effect. All three Sputniks and Explorers I and III had perigees at altitudes which were sufficiently low for the drag to have an observable effect on the orbit, and the effect is a function of perigee density and the scale height just above perigee. The theory of hypersonic drag is in a somewhat unsatisfactory state still, and the fact that the satellites are in most cases non-spherical and spinning in a complex way further complicates the analysis. Sedov (S.U.), Whipple (U.S.), and Cornford (U.K.) each reviewed this matter, and there seemed to be little difference of opinion on the essentials of the theory of orbits and atmospheric drag, but some confusion when it came to details.

Applying the satellite drag observations to atmospheric density determinations, the following conclusions were reached: Previous atmospheric models based on rocket observations at middle latitudes underestimated densities at 220 km and above, which implies that temperatures in the 100 to 200 km region must be higher [Sedov (S.U., Lidov (S.U.), Whipple (U.S.), Aoki (Japan), Warwick (U.S.), and Jastrow (U.S.)]; the density apparently increases as perigee moves from the dark (night) hemisphere into the light (day) hemisphere (Sedov and Lidov); the drag increases as perigee moves toward the equator, due to the equatorial bulge of the earth and its atmosphere [Siry (U.S.)]. The various density determinations were treated in different ways by the authors, but there was no apparent disagreement in the general results. It was apparent that the satellites launched so far are not very well suited for this type of determination because of their shape and complex motions, and therefore exact agreement in such an analysis could hardly be expected.

It is significant that the Sputniks, which were most often treated in these analyses, had high inclination orbits (about 65°), and therefore their perigees were at latitudes of greater than 40° a large fraction of the time. Thus, Sputnik densities may refer to higher latitudes than rocket densities at WSPG, and the results would then be more consistent with the Ft. Churchill rocket findings reported by La Gow, showing much higher densities in the Arctic day. Note that the day–night change indicated by the satellites is also consistent with the two Ft. Churchill rocket observations, which showed higher density by day.

1.2. *Molecular and ion distribution*

From sea level up to 50 or 60 km the atmosphere is essentially well mixed, and only certain constituents such as ozone and water vapor are variable. At higher altitudes two strong effects come into play which alter the composition of the atmosphere: The sun causes ionization and dissociation, and molecular diffusion becomes effective enough to cause a gravitational separation between the light and heavy constituents.

Both Soviet and U.S. rockets have successfully measured these changes in composition. Kupperian, Byram, Friedman, and Unzicker (U.S.) reported observations of the distribution

of the O_2 molecule (relative to atomic oxygen) at Ft. Churchill by measuring the change in absorption of sunlight in the ultraviolet (1000–2000 Å) by this gas as the rocket moved vertically. It was found that at noon in the spring dissociation of O_2 into atomic oxygen begins at 86 km, and that dissociation is rapid above this level. Berning (U.S.) reported that a similar method was being developed to measure water vapor distribution by absorption of infrared from the sun.

Newell (U.S.) and Townsend, Johnson, Holmes, and Meadows (U.S.) summarized the observations of atmospheric composition at Ft. Churchill on three flights using mass spectrographs for the neutral particles. The diffusive separation between light and heavy constituents was clearly observable, but the level at which this separation started varied from about 100 to 120 km. Townsend suggested that this day-to-day variation might be due to large scale circulation changes. Wenzel, Loh, Nichols, and Jones (U.S.), reporting on a series of flights at WSPG in which air samples were taken at various altitudes and measured in the laboratory, indicated that definite diffusive separation began at 90 km, and that there was slight separation on some occasions as low as 60 km. Wenzel referred to some previously reported rocket observations by Mirtov (S.U.), which also showed some slight separation at 60 to 90 km. Thus, there appears to be a latitudinal difference in the mixing processes which control the level at which this separation begins.

The same three flights at Ft. Churchill also gave results on the relative abundance of various ions at each level, which were summarized by Newell and given in some detail by Townsend. The main conclusions can be stated as follows, where the various ions are rated in terms of their relative abundance:

	100 km	150 km	200 km
Night	NO^+, O_2^+	NO^+, O_2^+, O^+	O^+, NO^+, O_2^+
Day	O_2^+, NO^+	NO^+, O_2^+, O^+	O^+, NO^+, O_2^+

Also observed in the records were such ions as N_2^+ and OH^+, but in very small quantities. The dominant negative ion was NO_2^-.

Some preliminary results of ion sampling from Sputnik III were also reported. Krassovsky (S.U.) described the ion traps, which are spherical grids or cages, separated from the main body by an arm and surrounding a charged probe. The probe-to-grid and grid-to-satellite voltages are changed stepwise, and the flow of current due to ions being collected by the probe is measured. The data are still being analyzed, but one sample result showed $1{\cdot}8 \times 10^5$ ions$^+$/cm^3 at an altitude of 795 km, at a time two hours before local noon. A significant auxiliary measurement, based on the grid-to-satellite voltages and currents, was a potential of the satellite relative to the ambient plasma of $-6{\cdot}4$ V (same time and place). At night and at lower altitudes the satellite potential was less than one volt. Istomin (S.U.) reported some preliminary results from radio-frequency mass spectrometers on sounding rockets and on Sputnik III which were designed to sample the relative abundance of molecules between mass units 6 and 50. At altitudes between 105 and 206 km mass 30, which is NO^+, predominated. On other samplings at altitudes from 230 to 820 km mass 16, or O^+, was predominant. This is roughly consistent with the U.S. rocket results at Ft. Churchill, shown above.

An interesting finding of the Sputnik III ion analysis was the presence at first of a positive ion of mass 18, apparently ionized water vapor. There was considerable discussion of this from the floor (much of which was lost on the audience due to the difficulties of translating the exchanges). Istomin maintained that water vapor under ultraviolet radiation from the sun would dissociate more readily than it would ionize, so there must be some other mechanism for ionization. Mirtov (S.U.), in a separate theoretical paper, concluded that above 150 km the mean free paths in the atmosphere are so large and the satellite speed so great relative to the molecular speeds that a molecule being desorbed or leaking from a satellite would have a low probability of being scattered back to the satellite and detected. However, he concluded

that the observed ions of water vapor must be from the Sputnik itself, since the concentration decreased with time, even though the explanation is still not clear. He suggested that the ionization might be due to the plasma of "terrestrial radiation" particles. Krassovsky stated that there was no real mystery about the water vapor being ionized, and referred to a "recharging process".

2. ELECTROMAGNETIC PROPERTIES OF THE IONOSPHERE

2.1. *Free electron distribution*

For several years the electron distribution has been measured by rockets, using the general principle that a high frequency radio wave, just above the "critical frequency" of the ionsphere, will be progressively more retarded than a VHF radio wave as the rocket penetrates the ionosphere. The difference between the mean speed of travel of the two waves from rocket to ground depends uniquely on the total number of free electrons along the path (one can ignore the small effects of the atmospheric ions). Thus, by keeping track of this difference as the rocket moves upward through the inosphere one can measure the free electron distribution.

A number of variations of this technique have been undertaken during the IGY. Newell (U.S.), in his rapid-fire review of U.S. rocket work, mentioned that the results showed that the ionosphere above Ft. Churchill had the same general character as at WSPG, with no clearly defined minimum in electron density between the *E*- and *F*-regions. This was elaborated on by Seddon and Jackson (U.S.), who described the two-frequency phase-comparison method, and indicated how differential absorption could also be measured. They made some flights during a polar blackout, and observed the increased ionization in the *D*-region at this time. They also detected a sharp sporadic *E*-layer, and observed a peculiar perturbation in the *F*-region called "spread-*F*". Krassovsky (S.U.) reported on similar observations with rockets at an unspecified location in the U.S.S.R., and his results showed the same general character as those from the U.S.—a rapid increase at about 100 km, the base of the *E*-region, and a continuous slowly increasing background above this on which were superimposed some smaller scale variations. The Soviet rocket on 21 February 1958, which reached 473 km, showed that even to this altitude there was little or no decrease in electron density above the *F*-region maximum, it still being about 10^6 electrons/cm^3.

Massey (U.K.), in reviewing the British "Skylark" rocket program, described a successful flight with a different technique for measuring electron densities. The nose of the rocket is electrically insulated from the body, and the inductance-capacity of this system is used to set the frequency of an oscillator. As the conductivity and dielectric constant of the ambient air changes, so does the frequency of the rocket oscillator. Apparently the response of this system is very rapid, since Massey showed an observation of fine structure in the *E*-region in which there were rapid changes in electron density in less than 1 km—fine structure which did not show up on the ground-based ionospheric recorder records.

The transmissions from satellites on 20, 40, and 108 Mc/s have also been studied extensively in order to learn about the ionospheric structure. Actual values of electron density can be obtained from satellite transmissions, but apparently with a good deal of strain and much less accurately than with rockets. Nevertheless, a number of approaches to this problem were described, and a great deal of interest was expressed, since it is a phase of satellite work in which all countries can participate. Berning (U.S.) reviewed the difficulties inherent in the use of satellites for precise ionospheric work, and pointed out that errors can be due to ionospheric inhomogeneities, lack of frequency stability in the satellite transmitter, and weak signals at long ranges. To overcome the last source of error, frequency filters with very low bandwidth have been developed which can permit reading a CW signal when the signal-to-noise ratio is as low as 1/4000. Observations of 20·040 Mc/s transmissions from Sputniks have been made in the U.S. with this equipment, observing the change in lag of the radio wave due to the ionosphere as the satellite

passes from horizon to horizon. The results applied to the determination of electron distribution above the *F*-region maximum appear to be erratic—Berning showed one case where electron density apparently continued to increase all the way to 1100 km, and other cases where there was a decrease, with various unexplained bumps on the curves. Another approach was reported by Kazanyev (S.U.), in which observed field strengths as a function of satellite range were compared with computed field strengths using various assumptions or "models" of electron distribution above the *F*-region maximum. (He stated that the lower layers could be disregarded in the analysis when the satellite was above the *F*-region maximum.) The best fit to the observations at 20 Mc/s for ranges up to 2500 km was obtained when a very gradual decrease of electron density was used in the theoretical model, thus confirming the Soviet rocket results. However, it was noted by Kazanyev that beyond 2500 km the observed field strengths were markedly higher than the computed ones, suggesting that the fine structure in the ionosphere must be giving some "wave-guide propagation" over the horizon.

The curious effects of the ionosphere on the 20 and 40 Mc/s Sputnik transmission over long distances were the subject of several papers. Bain and Shearman (U.K.) made a detailed study of the Doppler records combined with bearing and angle-of-elevation measurements, in an attempt to explain the curious effects at the ends of the records when the Sputniks were over the horizon from the British Isles. Two examples were shown in which the Sputnik, many thousands of kilometers away, climbed through the *F*-region maximum, and the mode of transmission abruptly changed from a skip transmission (a bounce off the ground and back to the ionosphere) to a direct transmission. The assumption of a simple broad parabolic layer for the *F*-region can apparently explain this effect satisfactorily. They ended with an appeal on behalf of their colleagues for more information on satellite orientation, modulations of transmitters, antenna characteristics, power, etc., as well as on orbits. Another study, by Warwick, Lawrence, and Schiffmacher (U.S.), of the Doppler records from Sputniks showed that the irregularities in these records, referred to as "residuals" from the smoothed curve, were due to ionospheric irregularities. Furthermore, these residuals showed no apparent relation to zenith angle or to magnetic orientation, and it was deduced that the irregularities responsible for them must lie in a thin layer in the ionosphere.

2.2. *Magnetic fields and electric currents*

The latest set of measurements by the U.S. of the earth's magnetic field at high altitudes was mentioned by Newell and described in more detail by Cahill and Van Allen (U.S.) and Meredith, Davis, Heppner, and Berg (U.S.). Cahill's report referred to the rockoon flights with magnetometers from the U.S.S. Glacier last winter at a number of locations in the northern and southern hemispheres, with emphasis on the flights near the equator. Three of these flights penetrated the electric current sheet in the *E*-region, or "equatorial electrojet", and there is evidence to indicate that there may be two distinct levels of current flow, one at about 100 km and the other at over 110 km. In fact, at the peak altitude of 120 km in one case the rocket appeared to still be within the region of the upper electrojet. These currents were fairly stable, since the ascent and descent records agreed quite well. Meredith reported on rocket firings at Ft. Churchill, in which magnetometers were able to measure the currents in the *E*-region associated with various phases of an aurora. (There were also various kinds of particle detectors on these rockets, as described below.) The general conclusion was that electric currents in the auroral zone are extremely variable in time (or space), since there were marked differences between the ascent and descent records. Berning (U.S.) reported that additional magnetometer measurements at Ft. Churchill were planned for the IGY.

Dolginov (S.U.) described the equipment for measuring the earth's magnetic field in Sputnik III. Apparently there is a problem due to stray magnetic fields from other pieces of equipment in the Sputnik, but the records show very

clearly the effects of rotation and precession of the vehicle—suggesting that it is a good device for determining the vehicle motion. This was a preliminary report, and Dolginov hopes to be able to use the data for a harmonic analysis of the earth's field at high altitudes.

3. COSMIC AND AURORAL PARTICLES

It is clear that there are two rather distinct kinds of charged particles in the earth's upper atmosphere (and even beyond). Those called "cosmic rays" are nuclei of various atomic species, protons being the predominant cosmic ray particle. The energies of these particles is measured in millions or billions of electron-volts. The origin of the cosmic rays is not well understood, but presumably most of them are truly cosmic, in that they come directly from distant star systems.

The auroral particles, or "terrestrial rays", are electrons and protons, most of which have energies of the order of 100 kilo-electron-volts (keV) or less. These particles, although they may originate elsewhere, are semi-permanent residents in the vicinity of the earth, being trapped in orbits outside the atmosphere by the earth's magnetic field.

In practice, it is sometimes difficult to distinguish the two types, since some detectors will respond to either. Much of the recent research in this area, however, deals with detectors which are sufficiently sophisticated to sort out the various kinds of particles according to energy, mass, penetrating power, etc., and this was an important phase of the meeting.

Cosmic rays have been under direct observation for many years, and recently these observations have been extended in altitude by means of balloons and rockets. Van Allen and Cahill reported on the U.S. program, which began before the IGY, to sample high altitude cosmic rays at a wide range of latitudes using rockets, mostly rockoons. They found, as predicted by theory, that the fluxes were the same to within 5 per cent at corresponding north and south geomagnetic latitude, and at high latitudes they were about 15 per cent higher than over the equator. In the course of this work some of the firings in the auroral zone had carried the cosmic ray detectors into a region where they recorded a very large counting rate. The exact explanation for this large counting rate has been sought by a number of investigators. Van Allen (U.S.) summarized the high latitude rocket research on auroral particles, carried on since 1953, and McIlwain (U.S.) and Meredith, Davis, Heppner, and Berg (U.S.) reported separately on some of the recent work at Ft. Churchill with special instruments for identifying the energy and type of particle. (Meredith's rockets also made magnetometer measurements, as previously mentioned.) The results of McIlwain's flight through a Class I aurora showed that the electrons of 50 to 100 keV energy began to show up at about 80 km (as had happened in other flights with ordinary cosmic ray detectors), while protons of somewhat higher energies were detected starting at higher altitudes. Meredith indicated that on other flights at Ft. Churchill the results for both electrons and protons were variable with time, and there was an indication on one flight that the ion counting rate and ion energy remained constant from 130 to 178 km. By noting the type and phase of aurora through which each rocket passed Meredith concluded that electrons of over 1 keV energy are only in the aurorae (at these altitudes below about 200 km), but that the energetic protons existed throughout the auroral region.

These same energetic electrons, which penetrate down into the *E*-region in the auroral zone during auroral displays, have also been detected by satellites at much higher altitudes. Van Allen (U.S.) reviewed the results of cosmic ray research with Explorers I and III, results which had been previously announced in May 1958. The main features of his report: Cosmic ray counts showed an altitude and latitude dependence which agreed very well with theoretical predictions, i.e. a slow and steady increase with increasing altitude and increasing geomagnetic latitude; at about 1000 km altitude the U.S. satellites' counters showed an anomalous behaviour, which was interpreted as due to a very large flux of X-rays at the Geiger tubes due to auroral electrons striking

the skin of the vehicle. ("Bremsstrahlung" is the term usually applied to such X-rays.) During the Symposium a telegram was received from Van Allen, McIlwain, and Ludwig offering a brief preliminary report on results from Explorer IV (1958 Epsilon), launched on 26 July. It reads in part: ". . . All detectors are operating properly and outputs are remaining within their dynamic ranges for quantitative measurement. General situation similar to that previously reported . . .[4] Radiation intensity increases by a factor of several thousand between 300 and 1600 km with rapid rise beginning about 400 km . . . Total energy scintillator gives 10 ergs cm^{-2} sec^{-1} per sterad. at 1600 km . . . On basis this fact and our previous rocket and balloon flight data in auroral zones, consider it reasonable to suppose that most of energy flux is due to electrons whose energy is typically 50 keV. Total flux of such low energy electrons is order of magnitude 10^8 cm^{-2} sec^{-1} per sterad. No evidence for marked temporal fluctuations during three day period. High intensities extend to lower altitudes at high latitude. Exposure level at 1600 km of the order of 2 r per hr . . ." In this same communication the discovery of a flux of some 10^3 cm^{-2} sec^{-1} per sterad. of a much more energetic particle, either 6 MeV electrons or 40 MeV protons, was reported. This was taken to be evidence in favor of Neher's suggestion that the reflected or scattered cosmic rays may be stored in the "geomagnetic mirror", i.e. trapped in the earth's magnetic field. The more numerous low energy electrons, it was tentatively suggested, may be due to the decay of upward moving mu-mesons.

The Soviet satellites also made extensive cosmic and auroral particle measurements. The first report on this subject was by Vernov (S.U.) at a special evening session devoted to his paper alone. He reviewed the Soviet work in this area, which started with rockets in 1947, described the various types of detection systems, including those in Sputniks II and III, and summarized the results. The flux of primary cosmic rays was shown to increase with altitude and geomagnetic latitude in a regular way, on the basis of Sputnik II measurements, due to the change of magnetic field, and they also saw an apparent shift of the "cosmic ray equator" relative to the geomagnetic equator in these observations (a phenomenon, as Vernov pointed out, which had been detected by Simpson from low level observations). Both Sputniks II and III encountered the sudden increase of counting rates as they penetrated the regions of the trapped auroral electrons. Due to the high inclination of the Sputniks (about 65° to the equator), they were able to see these at lower altitudes than the first two Explorers—in fact, the Sputniks *only* encountered them, apparently, at latitudes in excess of 50°, which does not seem to be entirely consistent with the U.S. results just described.

Chudakov, Kurnessova, and Krassovsky each gave preliminary reports in more detail on the cosmic ray observations in Sputnik III. Chudakov described the NaI scintillation counters and the system for continuously telemetering the observations, and showed how the counting rate increased rapidly as the Sputnik approached higher latitudes, the transition occurring sooner when the altitude was greater. Although Chudakov reported some modulation of the counting rates with roll, and also a diurnal effect, there were apparently no correlations of these with solar flares. He ended with a plea for recordings of Sputnik III telemetry from other places outside the Soviet Union, since, he said, with his system of direct telemetry he had limited geographic coverage and nothing from the southern hemisphere. Krassovsky gave very much the same story, as a result of various scintillation counters using fluourescent screens with thin metallic coverings, and elaborated on several interesting theoretical implications of the particles trapped in the earth's magnetic field. Kurnessova described the results of Sputnik observations based on the Vairlov–Cherenkov effect, the purpose being to count the flux of heavy nuclei in the primary cosmic rays. The two alternative thresholds were set for nuclei of mass number (Z) greater than 15 or 16 and greater than 30. Preliminary results, based on 1·5 hr of observation over a 10 day period, indicate

an average of $1{\cdot}2 \pm 0{\cdot}1$ counts per minutes for Z greater than 16, and only one count in the entire period for Z greater than 30.

Another evaluation of the Explorer I observations was by Aono (Japan), which served to emphazise the potentially international character of an artificial satellite when the launching agency makes information on the telemetry system and satellite characteristics available to scientists in other countries. Aono compared counting rates in the first U.S. satellite over Japan and over California and found evidence for a "soft component" in the counting rate, and a strong correlation between counting rate and F_2 critical frequency, which are also evidences for a soft cosmic ray component. Finally, he found that, although low altitude counts are unaffected by changes in the world index for magnetic activity (the so-called "K-index"), the counts at higher altitudes tend to increase with increasing geomagnetic activity.

4. SOLAR AND STELLAR ULTRAVIOLET AND X-RAY RADIATION

Because rockets and satellites can rise above the atmosphere, which absorbs all incoming radiation with wavelengths shorter than about 3000 Å (in the ultraviolet), scientists have recently been able to explore a previously unobservable part of the solar spectrum. The short wavelength part of the sun's spectrum is of considerable practical interest, since it is well established that changes in this radiation cause important changes in the earth's upper atmosphere, often accompanied by magnetic storms, radio blackouts, auroral displays, etc.

Newell touched on the U.S. work in this field, and this was elaborated upon by subsequent speakers. Byram, Chubb, Friedman, and Kupperian (U.S.) reviewed the studies of the intensities of the solar Lyma-α, Lyman-β, and other adjacent lines in the ultraviolet between 1050 and 1340 Å, using photon counters. The Lyman-α line of hydrogen (at 1210 Å) is by far the strongest in this region, and as previously reported contains about 6 ergs cm^{-2} per sec, apparently unchanged during periods of solar activity. Purcell, Boggess, and Tousey (U.S.) described high resolution photographic spectra of the sun in the ultraviolet, down to a little under 1000 Å, in which most of the lines have been identified.

Kupperian, Byram, Chubb, and Friedman (U.S.) also reported on a survey of Lyman-α radiation in the night sky, using a field of view of about 3°. It was found that this radiation was nearly isotropic, but with a measurable minimum in the antisolar direction. This radiation is due to emission by the hydrogen in interplanetary space, and it is estimated on the basis of these observations that there must be about 1 neutral hydrogen atom and 100 to 1000 protons per cm^3 in space. (Professor Schlovsky (S.U.), reporting in the Airglow and Aurora Symposium, came to the same theoretical conclusion on the basis of these same rocket observations.) The albedo of the earth's atmosphere for this Lyman-α of interplanetary origin is much higher than for solar Lyman-α, since its line width is narrower, and atmospheric hydrogen can therefore scatter it back more effectively. Finally, although this radiation is several hundred times weaker than the corresponding daytime radiation, it may contribute one-tenth to one-fifth as much ionization to the lower ionosphere and could explain a large part of the nocturnal ionization in the E-region. By a further analysis of the inhomogenieties of this Lyman-α radiation, and also of radiation at 1300 Å, Kupperian, Boggess, Milligan, and Friedman (U.S.), in a separate paper, concluded that there are definite stellar sources of ultraviolet emission giving some 10^{-3} ergs cm^{-2} per sec in these wavelengths.

Turning to the X-ray radiation from the sun, Friedman, Chubb, Kupperian, and Lindsay (U.S.) reported on the rocket observations of solar radiation in various wavelength intervals below 100 Å. The significant conclusion was that X-ray radiation from the sun at about 2·5 Å does increase with solar flare activity, whereas Lyman-α radiation does not. The authors argued in favor of a solar X-ray change as an explanation for the increased ionization in the D-region (70–90 km) which accompanies radio blackouts.

Kupperian and Friedman (U.S.) gave some results of observations of "gamma rays" from rockets, giving the flux and energy distribution for various altitudes. The energy range is from 20 to 260 keV (mostly below 50 keV), and the total energy flux is of the order of 10^{-6} ergs cm^{-2} per sec. There is no particular evidence suggesting that these come from the sun. To Simpson's inquiry as to whether these might be due to bremstrahlung formed in the atmosphere from energetic electrons, Friedman replied that under certain assumptions this could be a possible explanation.

5. MICROMETEORITES

Rockets, satellites, and would-be satellites have all been used to detect the tiny solid particles which inhabit the solar system. Since they are fairly few and far between, it is usually necessary to have long records in order to get a really meaningful sample, and so satellites are the preferable vehicle for this purpose.

Richter (U.S.), in reviewing the results from Explorer I and III (published previously)[5] suggested that Explorer III may have been hit by some larger meteors when two of the wire meteor detectors were severed almost simultaneously, followed by erratic behaviour in the high-power transmitter. This event coincided with the eta Aquarids, one of the regularly occurring meteor showers.

Nazarova (S.U.) summarized both rocket and satellite meteor observations, using ballistic piezoelectric pickups, made of ammonium phosphate, capable of recording down to a meteor of mass about 10^{-9} g. Comparing rocket and satellite results, referred to a nominal 1 m^2 area, the average impact rate observed with rockets between 150 and 300 km was 31 impacts/sec, while for Sputnik III it was 38 ± 10 impacts/sec at 500 to 600 km and 90 ± 34 impacts/ sec at 1700 to 1880 km. (These values would appear to be 10^3 to 10^4 higher than previously reported for Explorers I and III by Dubin.)[5]

La Gow, Schaeffer, and Schaffert (U.S.) described the micrometer observations on the 27 May 1958, firing of a 20-in. sphere which was intended as a satellite but ended as an excellent high altitude rocket flight, going to 2500 km altitude. The counting rates, on a crystal microphone which gave a fairly uniform response over the whole sphere, were erratic. After the end of third-stage burning there was a period with no impacts. Then, between 1450 and 1550 km there was a flurry of impacts, followed by 9 more counts at irregularly spaced intervals to the end of the record at an altitude of 2500 km. Curiously enough, at the time of the rapid counting rate on the microphone there were positive signals in a number of separate optical or photon detectors, a coincidence which is difficult to explain. (Following this talk, and also following her own talk, there was a lively discussion between La Gow and Nazarova, which was largely lost in a muttering of interpreters. Central issues were apparently the methods of calibrating meteor detectors, correspondence between momentum and energy of meteors, and size of sample needed to obtain a measure of the total flux of meteors into the earth's atmosphere.)

6. BIOLOGICAL EXPERIMENTS

Although the Rockets and Satellites Symposia were devoted primarily to geophysical and astrophysical matters, it was inevitable that some report be made on the Soviet experiments with dogs. Yazdoosky (S.U.) described the early experiments in which rockets were used to carry the subjects to high altitudes, after which they were recovered (alive) by parachute, and went on to review the well publicized experiment with Laika in Sputnik II. The purpose of these flights was to test the effects of cosmic rays, acceleration, and zero-gravity on living mammals, and to develop ways of providing a liveable environment in space with a minimum of weight. Dogs were used primarily since their normal physiology is so well known.

In Sputnik II the complex changes in respiration and heartbeat observed during take-off apparently did not have a pathological character, and the animal returned to a state where its physiological functions were essentially normal.

7. ROCKET AND SATELLITE INSTRUMENTATION AND SPECIAL APPLICATIONS

In addition to the scientific instruments aboard a rocket or satellite, there is, of course, a variety of other instrumentation concerned with guidance, telemetry, power supply, etc. The emphasis in the Symposia being on observational results, there were relatively few papers in the area of auxiliary instrumentation.

However, in addition to the papers already reported, in which instrumentation was sometimes described in great detail, Spencer (U.S.) gave a review of the development at the University of Michigan of radioactive ionization gauges for measuring pressures from rockets. Due to large mean free paths and the layer of gas surrounding the rocket, static pressures cannot be effectively measured above about 90 to 100 km. However, advantage can be taken of the "ram effect" at high speeds, and with the rockets used at Ft. Churchill a twenty-fold increase in pressure can be obtained. He pointed out the wide dynamic range of such radioactive ionization gauges, extending from 1 to 10^{-4} mm. This paper was supplemented by that of Michnevich (S.U.) who discussed the Soviet development of thermo-ionization gauges, capable of measuring from 10^{-5} to 10^{-9} mm, and magnetic manometers measuring down to 10^{-5} mm. Michnevich also went into the serious problems involved in sampling air at such low pressures or densities due to ionization of the gas, behavior at the inlet, etc.

Two of the satellites still in orbit have special devices, known as solar cells, for converting sunlight directly into electricity. These represent one of the most promising sources of power for space vehicles. Zahl and Ziegler (U.S.) reviewed the general question of power sources and compared the three potential contenders: chemical cells, radiactive power units, and solar cells. The silicon cells used in the Vanguard were developed by Bell Telephone Labs, and have been extensively tested in the laboratory as well as in the satellite. The Vanguard cells are apparently still effective and the transmitter running off them is being heard whenever the satellite is in the sunlight. Vavilov (S.U.) went into the theory of silicon solar cells and some of the factors controlling their efficiency, such as thickness of film, chemical action at the surface, etc. The Soviet cells were tested in a vacuum and under electron bombardment before being used in Sputnik III. So far, there has apparently been no adverse effects observed from cosmic rays or meteors. Like the Vanguard cells, the Sputnik cells are covered with a protecting glass plate.

A special application of rockets for a not-necessarily geophysical purpose is the use of rocket flashes for surveying in widely separated points. Atkinson (U.K.) described how the theory had been worked out and the scheme appears to be entirely practical. (Whipple (U.S.) commented that this useful technique had indeed been used to survey in the meteor cameras in New Mexico.)

8. REVIEWS OF ROCKET PROGRAMS

One of the aims of the Symposia being to report to the scientific community on the scope and the goals of each country's rocket sounding program, there were a number of review papers devoted to this more general end.

Massey (U.K.) described the British "Skylark" rocket program. The Skylark is a solid propellant rocket capable of carrying 150 lb to better than 170 km. It was developed at the Royal Aircraft Establishment, Farnboro, and has been fired at Woomera, Australia. After a number of test flights, three successful flights have been made with instrumentation. (Results of these were given by Massey, and are summarized above.) Future flights will continue the grenade experiments to determine winds and temperatures, the foil "window" to give winds, and the electron density determinations. In addition, it is planned to study micrometeors, Lyman-α, airglow, and possibly composition and ionization by means of mass spectrographs and electrical probes.

Newell (U.S.) gave a comprehensive review of U.S. rocket results from the first twelve months of the IGY. In this period some 116 upper air sounding rockets were fired, of which 41 were at Ft. Churchill, Canada, 54 were rockoons from shipboard at locations from the

Arctic to the Antarctic, and the remainder were at White Sands (New Mexico) and San Nicolas Island (California). The emphasis was on extending geographic coverage and on exploring the hitherto inaccessible Arctic upper atmosphere. A variety of rocket combinations were used, such as the Nike–Cajun, Nike–Asp, and Nike–Deacon, in addition to the well known Aerobee and the rockoons. Future firings will include a new rocket called the Spaerobee. The total number of future firings during the remainder of the IGY will be 70, of which more than half will be at Ft. Churchill. The results of the rocket program to date, as described by Newell, have already been covered for the most part and so will not be repeated here.

Hatanaka (Japan) described the Kappa, Type 6, sounding rocket developed recently in Japan. It is a two-stage solid propellant rocket, 5·3 m in overall length and weighing 255 kg. It uses a mobile launcher. It is capable of carrying a payload of 4·5 kg to 45 or 50 km. After some early development troubles, the Kappa has now flown a number of times successfully, and the grenade experiment to determine winds and temperatures has been tried. Future firings will continue to use grenades, and the Japanese program will also include cosmic ray and ionospheric measurements.

The Australian rocket program was reported on in a paper by Webster (Australia). In addition to supporting the U.K. program, the Australians have their own "Long Tom", a two-stage missile capable of going to 100 km. They plan to study winds, ionization densities, and micrometeors.

The past results of the Soviet rocket program were reviewed piecemeal by Krassovsky, Yazdovsky, Shvidkovsky, Istomin, and Michnevich. These papers have already been treated. There was no mention of the future plans for the Soviet rocket program.

9. SATELLITE PROGRAMS

Beyond the papers which have already been mentioned, there were no general reviews of satellite programs in the U.S. or in the S.U. Furthermore, any discussion of future satellites or satellite experiments was conspicuous by its absence—though the U.S. satellite program for the IGY has been reported elsewhere in some detail, and some general reports have also been issued on the Soviet program.

There was one phase of satellite work, however, which received more attention than any other single subject: Satellite tracking and orbit theory. As mentioned earlier, the process of observing satellites as they pass overhead by various means has occupied scientists in many countries, since satellites obviously know no international boundaries. Moreover, the effort to obtain good orbit parameters requires observers in many places who can report their observations to central computing facilities where the observations can be combined.

The opening paper of the Symposium was by Sedov (S.U.), who reviewed the fundamentals of orbit theory and the effects of drag, and he was followed by Whipple (U.S.) who described the U.S. IGY optical tracking and computation systems with its international network of co-operative satellite cameras, which is directed by the Smithsonian Astrophysical Institution. Hynek (U.S.) in a later paper went into more detail on the Smithsonian's program, and told about the moonwatch teams and their visual observations. Siry (U.S.) discussed the U.S. minitrack radio tracking system and the Vanguard computing facility, which is also an international effort, and Cormier (U.S.) explained the U.S. National Academy's simplified satellite prediction procedure, which could be used to predict times and locations of passes by a hand computation using certain basic orbital parameters. The activities in other countries which support the U.S. optical and radio tracking programs were reported separately: Miyada for Japan, which has three moonwatch teams and a Smithsonian satellite camera for optical tracking, and its own radio tracking facility for observing the U.S. satellites at 108 Mc/s, and Webster for Australia, which has five moonwatch teams, a Smithsonian camera, and a prime minitrack station which feeds information to the Vanguard computer center. Both of these countries have also made

recordings of the telemetered data from both U.S. and Soviet satellites.

The Soviet moonwatch program, using a network of observing teams dotted about over the Soviet Union, was treated by Masevich (S.U.). This program also uses various kinds of satellite cameras, of which 25 are specially designed for this purpose, and others are modified astronomical telescopes. These observations are all processed at a central computing facility, which (like both the Vanguard and Smithsonian systems) sends out predictions of satellite passage to the many co-operating stations. The Soviet scientists did not mention any precision radio or radar tracking, but Shachovsky (S.U.) talked about the amateur radio stations which make Doppler measurements on the Sputniks. There are some 28 of these, mostly in western Russia or in a straight line along the 55th parallel.

So much for the large scale efforts. There were many papers on various observational techniques and on orbit theory. Cornford (U.K.) discussed some refinements to the orbital theory, and showed how both radio and visual tracking methods had been applied in Great Britain; Harris and Jastrow (U.S.) presented a short program for determining an approximate satellite ephemeris from a small number of radio tracking observations, including the effects of atmospheric drag. Many facets of optical tracking were treated: Tousey (U.S.) on studies of limiting visual magnitudes for satellites; Shklovsky (S.U.) on the angular (and timing) errors involved in the various optical methods, ranging from moonwatch (manned) observations to the most advanced photographic and/or photoelectric systems; Smyth (U.K.) on the use of 35 mm cameras with a special arrangement for applying time markers; and Hynek (U.S.) on the Smithsonian cameras designed by Baker and Nunn. On the subject of radio, radar, and Doppler analysis, there were papers by Cornford (U.K.) and Siry (U.S.), already mentioned, by Blackband (U.K.), who reviewed the use of Doppler and interferometric methods in Great Britain and showed how Doppler records at 20 and 40 Mc/s could be corrected for ionospheric effects, by Haywood (U.K.), who described amateur Doppler measurements on the Sputniks I and II, and by Berning (U.S.), Warwick, Laurence, and Schiffmacher (U.S.), Kotelnikov (S.U.), and Kitchen (U.K.) on refinements in the use of Doppler techniques. Evans (U.K.) reported on results with the 80 m diameter radio telescope at Joddrell Bank converted to a radar (on 100 and 36 Mc/s). There was considerable discussion in this paper on the large fluctuation of the radar cross-sections of satellites and sputniks, presumably due to changes in orientation.

Finally, there were several papers on a most dramatic part of a satellite's career, its final plunge back into the atmosphere. Harris and Jastrow (U.S.), Jacchia (U.S.), and Cornford (U.K.) each reported on the spectacular demise of Sputnik II (1957 β) over the Caribbean on 13 April. According to the collected reports, this Sputnik was visible as a glowing object with a short tail over Long Island, N.Y., and a few minutes later it was sighted over Barbados as a bright object of -6 to -9 magnitude with a tail estimated to be 100 km long. Shortly thereafter it faded rapidly and appeared to break up. Harris and Jastrow also presented some observations and calculations of the final plunge of the Sputnik I rocket body (1957 α_1) on 1 December. Its last days were accurately observed optically, so that its decaying orbit could be computed. A last pass was observed by the Malvern radar in Great Britain, at which time it was at only 74 miles altitude. The impact point must have been somewhere along a NW to SE line extending from north-central U.S.S.R. across Outer Mongolia and into China near Hongkong. There was apparently no published report by the Soviets or Chinese that this object had been observed, and Jastrow suggested that an enquiry in this region might be fruitful.

In conclusion, it is the feeling of this author that the CSAGI Rockets and Satellites Symposia held in Moscow in August 1958 were for the most part highly interesting and successful. Although much remained to be told, there is no question about the value of the scientific information in this rapidly moving field which

was discussed. Our Soviet hosts are also to be thanked for their hospitality and the care with which they treated their guests from many countries. It is unfortunate that more of our colleagues could not be there to take part—perhaps this report will at least partially make up for their loss.

REFERENCES

1. The Rocket Panel, Harvard College Observatory. *Phys. Rev.* **88**, 1027 (1952).
2. Minzner R. A. and Ripley W. S. *The ARDC Model Atmosphere 1956*. Surveys in Geophysics No. 86, Geophysics Research Directorate, Air Force Cambridge Research Center (December 1956).
3. Dobson G. M. B., Brewer A. W. and Cwilong B. M. *Meteorology of the Lower Stratosphere* (Bakerian Lecture). *Proc. Roy. Soc.* A **185**, 144–175 (1946).
4. Van Allen J. A., Ludwig G. H., Ray E. C. and McIlwain C. E. *Observation of High Intensity Radiation by Satellites 1958 Alpha and Gamma*. State University of Iowa, Research Report 58-5, 1 May 1958. (Also contained in World Data Center A, IGY Satellite Report Series No. 3.)
5. Manring E. and Dubin M. *Satellite Micrometeorite Measurements*. Geophysics Research Directorate, Air Force Cambridge Research Center, 1 May 1958. (Also contained in World Data Center A, IGY Satellite Report Series No. 3).

AVANT-PROPOS

Les Astres et l'Espace qui nous en sépare conditionnent la vie humaine sur la Terre et l'évolution de notre monde. Aussi ont-ils, de temps immémorial, tenté non seulement les rêveries des poètes et les méditations des philosophes, mais aussi le désir de connaissance des hommes et suscité les premières Sciences, l'Astronomie fournissant dès l'origine le moyen le plus commode et le plus précis de définir et de repérer le Temps.

Jusqu'à ces dernières années, la connaissance des Astres et de l'Espace restait entravée par l'impossibilité d'éloigner notablement du sol terrestre observateur et instruments d'observation.

En réalisant la première expérience humaine de Mécanique céleste, le lancement réussi en octobre 1957 du premier SPOUTNIK a marqué pour cette connaissance le début d'une ère nouvelle.

Au premier satellite terrestre artificiel vient de succéder, à quinze mois seulement de distance, la première planète solaire artificielle.

Désormais, la route est donc largement ouverte à l'exploration de l'Espace, d'abord par instruments puis par observateurs, et à une étude infiniment plus large et plus détaillée du milieu spatial et des Astres.

Le progrès de toutes les sciences qui s'y rattachent en sera très rapidement accéléré, et l'importance vitale des problèmes que ces sciences concernent y attirera de plus en plus l'intérêt de milieux scientifiques très divers.

C'est donc à l'heure opportune qu'apparaît une publication à caractère international, vouée à diffuser et à propager les nouvelles connaissances relatives aux Astres et à l'Espace, Terre et Atmosphère terrestre comprises.

Puisse donc *Planetary and Space Science* remplir pleinement ce rôle et contribuer ainsi, en faveur de l'humanité tout entière, aux progrès les plus utiles de la connaissance scientifique!

MAURICE ROY.

Planet. Space Sci. Pergamon Press 1959. Vol. 1, pp. 86–93. Printed in Great Britain.

STUDY OF THE COSMIC-RAY SOFT COMPONENT BY THE 3rd SOVIET EARTH SATELLITE

S. N. VERNOV, A. E. CHUDAKOV, E. V. GORCHAKOV, J. L. LOGACHEV and P. V. VAKULOV
Academy of Sciences of the U.S.S.R., Moscow

(*Received* 17 *January* 1959)

Abstract—Measurements made with a scintillation counter installed on the 3rd Soviet earth satellite are presented. By this instrument the counting rate corresponding to the energy greater than 35 keV and the total ionization in the scintillator were measured. Two zones of high intensity radiation are observed. The first one is observed on latitudes greater than 60° and altitudes above 300 km. Radiation in this "polar zone" consists of electrons of energy about 100 keV and flux rate of 10^3 to 10^4 particles/cm^2 sec sterad (increasing with altitude). The second zone is observed on altitudes about 1000 km and latitudes not exceeding 50°. In this "equator zone" the ionization in the scintillator is 3 orders of magnitude greater than that due to cosmic-rays. Strong dependence on latitude and longitude is assumed to be consistent with the symmetry of the zone relative to the inclined and displaced geomagnetic axis. Lower limits are given for the γ-radiation from the Sun.

1. APPARATUS

In order to obtain data on photons at high altitudes, the 3rd Soviet earth satellite was equipped with a scintillation counter. This counter has a high efficiency for photon recording (about 2 orders of magnitude greater than the efficiency of Geiger counters). The counter consists of a cylindrical crystal of sodium iodide, 40 × 39 mm in size, and a photomultiplier with a photocathode diameter of 40 mm.

The following measurements were carried out with this instrument:

1. The counting rate of these events producing pulses corresponding to energy release in the crystal of 35 keV or more.
2. The value of the photomultiplier anode current.
3. The value of the intermediate dynode current.

The last two parameters characterize the total energy release in the crystal per time unit.

The simultaneous measurement of anode and dynode currents makes possible the determination of total ionization produced in the crystal (dynode current), as well as an evaluation, on the average, of the energy spectrum of this ionization. This is possible by utilizing the effect of non-linearity in the region of the last photomultiplier electrodes. Hence, the relation between the currents of the anode and intermediate dynodes depends on the value of separate pulses.

In order to measure relatively small anode and dynode currents, a circuit was worked out which operated on the principle of charge storage by a capacitor. After charging to the break-down potential of a neon bulb, the condenser discharges through the bulb until the bulb extinguishes. This method made it possible to measure currents of 10^{-10} A. The pulse produced by the discharge operates the trigger which controls the relay; the position of the connections of this relay is transmitted by radio.

To measure the counting rate, pulses arising on the last photomultiplier dynode are amplified by the two-stage amplifier and come to the input of the binary scaler having a scaling factor of 4096. The threshold of the scaler corresponds to an energy of 35 keV. The last trigger of the scaler controls the position of a proper relay. All electronic components were made of semiconductors. The total power supplied to the instrument was equal to 0·15 W.

For telemetering the transmitter "Majak" was used (frequency 20 Mc/s). This transmitter operated during the satellite flight without interruption. The transmission of information by the "Majak" was carried out by varying the duration of telegraph signals. We used the second and third signals (second and third channels).

Fig. 1 gives the block-scheme and shape of telegraph signals emitted by the transmitter. The duration of the signals depends on the resistance applied to the entrance of the corresponding channel:

at $R=0$	$\tau=50$ msec
$R=10\,\mathrm{k}\Omega$	$\tau=100$ msec
$R=\infty$	$\tau=150$ msec

Change of the relay position takes place after storage of a certain charge (relay 1 and 2) or at storage of a certain number of pulses (relay 3). Thus the intensity can be calculated by the formula $J=K/T$, where T is the time during which a given relay is kept in one position.

In the case of measuring the counting rate, $K_c=2048$.

In the case of measuring ionization by the anode current, $K_A=2\times10^9$ eV.

In the case of measuring ionization by the dynode current, $K_D=18\times10^9$ eV.

Coefficients K_A and K_D were measured by means of calibration by γ-rays of the mercury isotope Hg^{203} (energy 279 keV). In this case the dependence between the energy and pulse amplitude is still linear. The maximum output pulse amplitude occurs at an energy of 1 to 2 MeV or greater. Thus, if the instrument is irradiated by primary cosmic rays only (in this case the energy of pulses exceeds 20 MeV), one can expect that measurements of the anode current would give values of ionization at least 10 times less than the measurements determined by dynode current, for which the effect of non-linearity is practically negligible.

2. DATA TREATMENT

Information is obtained for the most part as transmitted "Majak" signals recorded by ground-based receivers on magnetic tape. At present the collection of information is not finished, and only a small part of the data is analysed. Time intervals corresponding to satellite flight over the territory of the U.S.S.R. for 15–20 May and also 13–16 June 1958 have been studied more completely. Separate records from the Southern Hemisphere for 7, 17 and 18 June and also numerous separate records of the territory of the U.S.S.R. were also studied.

This analysis showed that the instrument was giving complete information during more than

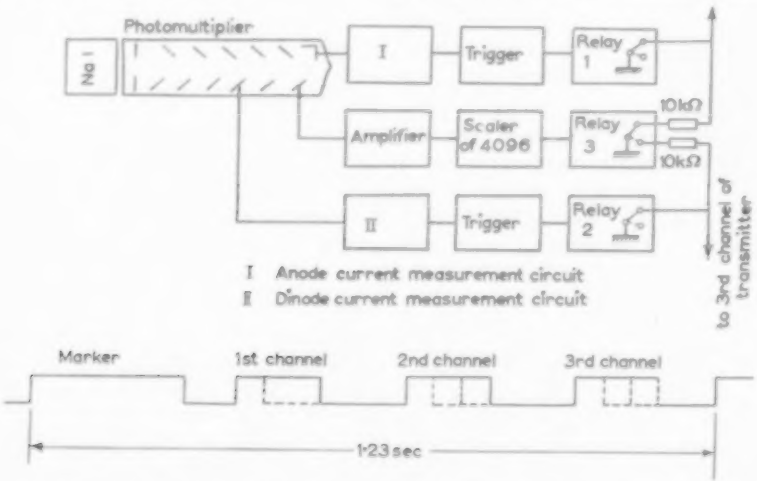

Fig. 1. Block-scheme of the apparatus and shape of telegraph signals.

a month of flight. Information on ionization currents was obtained during more than 3 months, since the power consumption by these elements of the instrument was small and since a large power supply had been provided. Measurements of the counting rate showed that the number of pulses in all cases exceeds by 10 or more times the counting rate expected from the primary cosmic rays. This means that photon registration is the main contribution to the counting rate.* At least a part of these photons must depend on the photon albedo arising in the atmosphere under the action of cosmic rays.

Figs. 2a and 2b show typical examples of recording performed by a single receiving station (Fig. 2a) and by two receiving stations (Fig. 2b) in the U.S.S.R. The lower curve shows the counting rate, the two upper curves —ionization (complete energy release in the crystal per sec). The measured ionization exceeds by several times the ionization expected due to cosmic rays. The fact that a large part of ionization is not connected with cosmic rays follows also from the small difference between the records of dynode and anode currents. This phenomenon proves that at least some "excess ionization" takes place.

However, the relation between the counting rate and ionization does not make it possible to explain this phenomenon at any energy of incident radiation. The point is that even if the energy of incident photons is lower than the threshold of registration by the counting channel, the counting rate would be 1 order larger than the observed one, since at the intensity necessary for the production of the observed anode current, time pulse overlap plays its role. This fact was checked during X-ray irradiation of the instrument in the laboratory.

It happened that the observed relation between the counting rate and anode current can be obtained only when the photocathode is

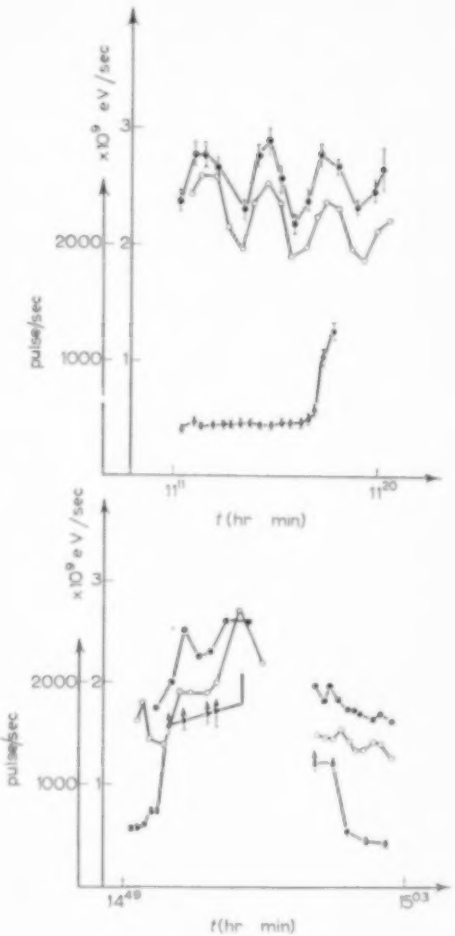

Fig. 2. Characteristic recording of counting rate and ionization by the data of the scintillation counter for 19 May 1958.
Abscissa: Moscow time
● Ionization by measurements of dynode current.
○ Ionization by measurements of anode current.
• Counting rate.

illuminated by a steady light source. Thus "excess ionization" can be explained only as a long afterglow-phosphorescence of NaI (Tl) crystal.

The study of the crystals used by us has shown that this phenomenon really takes place. Fig. 3 shows one of the afterglow curves. In

* This conclusion follows from a comparison of these results with the data obtained by Geiger counters. It should also be taken into account that a scintillation counter was placed inside the aluminum envelope of the Sputnik, so that the detector was surrounded by a layer of matter at least 1 g cm^{-2}.

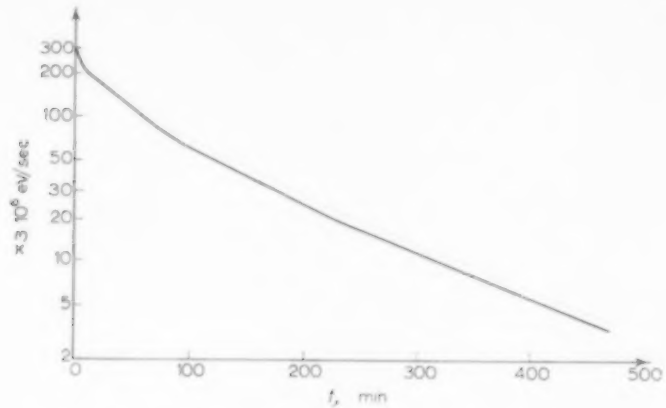

Fig. 3. NaI afterglow curve. Ionization in the crystal necessary to produce the observed afterglow J_3^t intensity is shown on the ordinate axis.

this case the irradiation of the crystal by X-rays with an energy of 80 keV was continued for 40 min, and the intensity of irradiation corresponded to an energy release in the crystal of $1{\cdot}4 \times 10^{12}$ eV per sec. Just after the X-ray tube was switched off, the current in the photomultiplier decreased by 140 times. The law of the afterglow can be approximated by a sum of three exponents with $\tau = 15$, 75 and 150 min. The total energy of the long light emission is about 1 per cent of the short light emission. Thus "excess ionization" over the territory of the U.S.S.R. recorded during the satellite flight can be explained for the most part, not by the radiation available in that region, but by some "memory" of the crystal, irradiated as will be shown below, in the region of the equator.

In Fig. 2a one can see oscillations of the anode and dynode currents during a period of about 2·5 min and modulation of the order of 10 per cent. The period of these oscillations coincides with the period of the satellite rotation. Obviously, current oscillations are caused by the influence of the earth's magnetic field on the sensitivity of the photomultiplier. This magnitude of the effect was expected on the basis of laboratory measurements. The fact that the counting rate has no such oscillations proves that only a small part of the photon spectrum has energies close to the threshold energy of 35 keV.

3. ELECTRONIC COMPONENT OF COSMIC RAYS IN THE POLAR REGION

As one can see from Fig. 2a, the counting rate increases sharply at a certain moment. This effect is observed in all cases when the satellite is flying in the region of approximately 60°N. When the satellite moves from north to south, one can observe a decrease of the counting rate. Fig. 2b shows one of the cases, when the beginning of increase as well as decrease are recorded on the same path.

In the region of increased counting, it is not always possible to make an exact measurement of this counting rate, since the intensity often exceeds the potentialities of radio-telemetering and of the scaler. In these cases one can only state that the intensity exceeds some limit. In Fig. 2b, arrows are used just for this purpose.

Fig. 2a shows that a considerable increase of counting rate is not followed by an appreciable increase of ionization. Consequently, the energy of separate particles is very small, and, taking into account the screen thickness ($1\ \mathrm{g\,cm^{-2}}$), one can conclude that in this case photons are registered. On the other hand, the observable strong dependence of the intensity on geo-

graphic coordinates may take place only for charged particles.

If one assumes that the counter records a bremsstrahlung radiation of electrons absolutely absorbed in the satellite envelope, it becomes possible to explain the observed facts. The analysis of many records similar to Fig. 2a and Fig. 2b permitted us to determine that in the region of increased counting rate a slight increase of ionization is, on the average, observable. Comparing this increase of ionization and increase of the counting rate, one can estimate photon energy of the bremsstrahlung radiation and, consequently, the energy of electrons. The photon energy will be of the order of 100 keV or less. The sign "less" arises due to the fact that in some cases only a low limit of counting rate is known. However, the photon energy cannot be significantly lower than 100 keV, since the threshold is 35 keV. Thus, the most probable value of the energy of electrons responsible for the effect is about 100 keV.

A flux of these particles is characterized by considerable fluctuations; sometimes the increase of ionization is absolutely negligible. However, the counting rate strongly increases in every case.

Thus, the polar region is characterized by a permanent electron flux, the intensity of which varies in a wide range. Taking into account the efficiency of electron registration by the bremsstrahlung radiation, we estimate the electron flux as 10^3 to 10^4 particles/cm^2 sec sterad.

Fig. 4 shows a geographic diagram on which points indicate the places where the satellite was flying in a region of a large intensity, and crosses indicate the places where the satellite was leaving this region. The map is prepared in accordance with the date for 15–22 May 1958. The fact that the crosses are located somewhat southward, apparently, points out the dependence of the effect on altitude, since the crosses correspond to "opposite paths" (the motion from north to south) and, consequently, to a higher altitude of flight.

The region of high intensity is not located symmetrically to the magnetic field. In order to illustrate this fact, a geomagnetic parallel is given as a dashed line. Further treatment must give additional information concerning the longitude dependence and also must clear up the dependence on the solar time. It would also be of interest to establish the correlation between the intensity of electron radiation and other geophysical phenomena.

At present it is difficult to give a complete

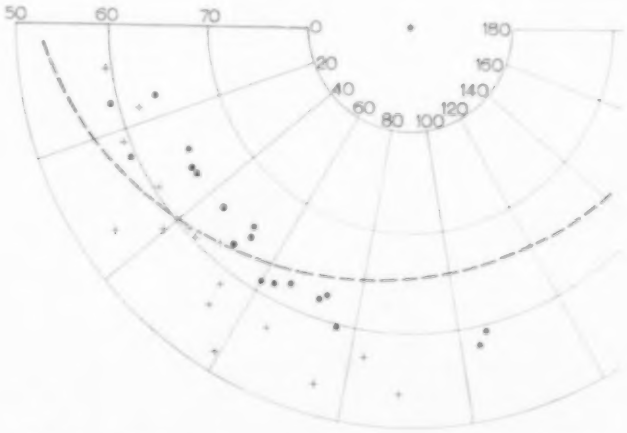

Fig. 4. Map of the location of points in which a sharp increase of the counting rate arises (circles). Crosses correspond to the satellite coming out of the polar zone, where an increased counting rate was observed.

interpretation of the electron component observed. It is not excluded that these electrons are accelerated near the earth by electric fields similar to those assumed to be in the aurora. But it is possible also that the electron component comes from far away, for example, from the sun; and penetrates, despite the small amount of energy of the particles, through the earth's magnetic field due to the difference between the field and that of an ideal dipole.

4. ZONE OF HIGH INTENSITY IN THE EQUATOR REGION

Van Allen and others, with the help of Geiger counters placed on the American satellites α and γ, determined that at a high altitude (more than 1000 km) a very high intensity of charged particles is observed. At present we have no exact information about the nature and origin of these particles. The main fact determined by these experiments is a sharp increase of intensity with altitude (the number of pulses in the Geiger counter increased at high altitudes by 1000 or more times).

In our measurements the altitude of the flight was as great as 1850 km. Since the part of the orbit corresponding to high altitudes is in the Southern Hemisphere, and since we have received records from that region only with great delay, only a small part of these records has been studied. These data show that at the altitude of 1200 km a very large intensity is really observed (ionization in the crystal exceeds by three orders of magnitude the ionization produced by cosmic rays). However, it was found that this phenomenon depends not as much on altitude as on latitude.

Fig. 5 shows one of the records made in the southern region of South America. The abscissa axis gives the latitude, and the ordinate axis gives the ionization in the crystal by measurement of the dynode current. One can see from this figure that during the motion towards the equator the intensity sharply increases, in spite of the fact that the altitude of the flight decreases from 1600 to 1100 km. Independently of the mechanism of production of particles in the equatorial zone, it is obvious that the main role in this effect is played by the factor of

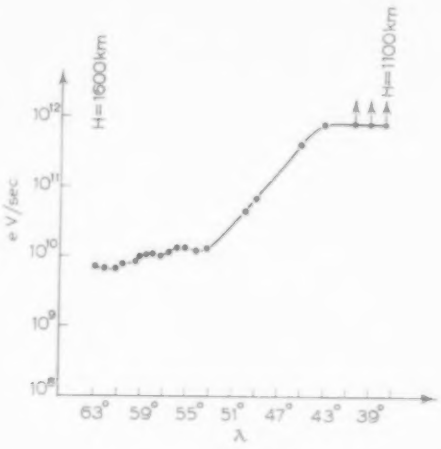

Fig. 5. One of the records made in the southern hemisphere in the altitude range of 1600–1100 km. Geographic latitude (southern) is shown on the abscissa axis. Ionization in the crystal by measurements of dynode current is shown on the ordinate axis.

storing. This fact is proved by the concentration of particles in the equatorial zone where, at a sufficient altitude, they can oscillate for a very long period of time.

It is natural to expect that the plane of the geomagnetic equator must serve as the plane of symmetry. At present we have no data along the whole length of the equator to answer this question, but it is possible to use the phenomenon of a long afterglow of the crystal NaI, that permits us, with the help of measurements performed in the U.S.S.R., to get information concerning the energy released in the crystal during the flight through the equatorial zone. Indeed, direct measurements given in Fig. 5, and measurements of the energy of afterglow made in the U.S.S.R., are in good agreement with the afterglow characteristics obtained experimentally. Thus, one can use numerous measurements over the territory of the U.S.S.R. in order to obtain equatorial data.

First, we obtain a complete quantity of energy which is released in the crystal for one orbit of the satellite (a predominant part of this energy is released in the equatorial zone). This

energy is 2×10^{15} eV for one rotation or on the average 3×10^{11} eV sec^{-1}. If one assumed the time period of 10 min for an average duration of the flight in the maximum intensity zone, the average intensity in this zone will be 3×10^{12} eV sec^{-1}.

Second, it is possible to obtain information about the constancy of this value. It will be found that if one speaks about the constancy of the intensity in the equatorial zone measured by satellite flights over the same points of the globe (such flights are practically repeated every twenty-four hours), a rather high constancy will be noted, with deviations no greater than 30 per cent. However, during twenty-four hours, when the orbit changes its position relative to geographic coordinates because of the earth's rotation, variation of the intensity takes place. Fig. 6 shows the dependence of

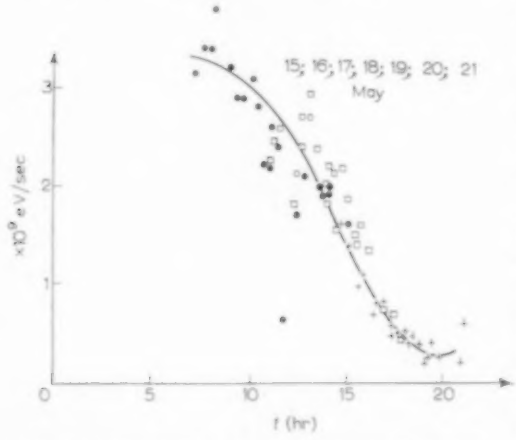

Fig. 6. Dependence of "excess ionization" on time. Moscow time (hr) is shown on the abscissa axis.

the intensity on the respective position of the earth. Since during one week the position of the satellite's orbit can be regarded as sufficiently constant in space, one can characterize the position of the orbit relative to the globe by solar time. The abscissa axis of Fig. 6 gives Moscow time. The value of "excess ionization" (that is, the value proportional to the irradiation energy on the equator) is put on the ordinate axis. In preparing this diagram, data for the time interval from 15 to 21 May were used.

It is observed from the diagram that systematic intensity variations take place, and that the minimum intensity occurs at 7 p.m. Moscow time. This intensity is at least 10 times less than the maximum intensity. If one looks at the orbit position at the time when a minimum variation in intensity is observed, one finds that at this time a southern part of the orbit is positioned at the minimum distance from the magnetic pole. In this case, the southern part of the orbit passing through high altitudes happens to be at the farthest distance from the magnetic equator.

If one assumes that particle concentration sharply increases when approaching the geomagnetic equator, as well as with altitude, the dependence of the effect on the rotation of the earth can be explained at least qualitatively. Under more detailed consideration it will be necessary to take into account not only the inclination of the direction of magnetic dipole relative to the axis of the earth's rotation, but also displacement of the dipole center relative to the center of the earth.

It is possible now to make a hypothesis that the equatorial zone of high intensity is placed symmetrically to the earth's magnetic field and is characterized by a strong concentration of the density of particle flux in the plane of magnetic equator. Such an equatorial zone provides, apparently, ideal conditions for particle oscillations in a magnetic field, and leakage is determined probably only by ionization losses and losses for radiation. In this case such a long lifetime of particles is possible (of the order of a year) that even such a weak mechanism of injection as the decay of neutrons leaving the atmosphere under the action of cosmic rays appears to be sufficient to explain the observed intensity.

5. SEARCH FOR γ-RADIATION FROM THE SUN

The existence of a great intensity of secondary photons leaving the atmosphere under the action of cosmic rays, as also the existence of intensive electron fluxes in separate regions of the satellite trajectory, make it difficult to discover a weak γ-radiation of the sun and

other astronomical bodies. In order to find γ-radiation of the sun, we studied the variations of photon intensity during the solar flares of 6 June 1958. We also studied the moments when the satellite crossed the boundary of the earth's shadow, when it would have been possible to observe the existence of a quiet solar radiation. In both cases the effect was not discovered. One can say that in these few cases the photon flux from the sun did not exceed some definite value.

These limits depend on the supposed photon energy:

Photon energy (keV)	Energy flux (erg cm^{-2} sec^{-1}) is less than
10	1
30	10^{-4}
50	10^{-6}

It is impossible to state that these limits are always valid, since statistics are still few. However, one can say that systematic study of the problem depends, apparently, on an increase of the sensitivity of instruments, probably by establishing a detector of sensitivity in a small solid angle and automatically directed toward the sun.

Planet. Space Sci. Pergamon Press 1959. Vol. 1, pp. 94–101. Printed in Great Britain.

A STUDY OF WINDS BETWEEN 80 AND 100 km IN MEDIUM LATITUDES

W. G. ELFORD

Department of Physics, University of Adelaide, South Australia

(*Received* 30 *December* 1958)

Abstract—Results of a systematic investigation of winds in the upper atmosphere by the radio observation of drifting meteor trails are described. It is shown that in medium latitudes the diurnal behaviour of the winds in this region can be described in terms of three horizontal components of comparable magnitude; a prevailing component and two oscillatory components with periods of 24 and 12 hr.

The prevailing winds are predominantly zonal and are directed toward the East during most of the year. Large wind gradients are present in summer and winter.

In general the periodic components represent anticlockwise rotation of the wind vectors. The seasonal variations in the magnitude and phase of the 24-hr oscillation suggest a direct thermal origin for this component. The amplitude and phase of the 12-hr component vary in a complex manner throughout the year, but the mean amplitude increases with height.

1. INTRODUCTION

In recent years the radio observation of drifting meteor trails has been developed as a technique of considerable precision for studying the motion of the atmosphere in the height range 80–100 km above the ground. Two methods, developed independently, one at Adelaide[1] and the other at the Jodrell Bank Experimental Station[2, 3] have been used. Both systems enable the diurnal variations and height gradients of the wind to be determined.

In this paper results of observations of winds obtained over a period of more than two years are presented and it is shown that, at medium latitudes, the motion of the air in the meteor region of the atmosphere can be described in terms of three components; a constant term, a 24-hr periodic component and a 12-hr periodic component. All three components exhibit seasonal changes and variations with height.

2. TECHNIQUE

The radio system used at Adelaide for measuring the velocity of drift and position of meteor trails has already been described in detail.[1, 4] Continuous wave radiation on a frequency of 27 Mc/s is emitted vertically within a cone of semi-angle 40°, and a meteor trail suitably oriented within this cone reflects radiation back to an aerial array on the ground by means of which the direction of the reflection point can be determined. The component of the velocity of drift in the direction of observation is derived from the doppler frequency change of the reflected wave, while the range of the reflection point is found by the radar technique using pulses superimposed on the C.W.

The effective scattering region of a trail is of the order of length of a Fresnel zone about the point of intersection of the trail and a perpendicular from the observer. For a trail at a slant range of 200 km and a radio frequency of 30 Mc/s the length of the first zone along the trail is of the order of 2 km.

An estimate of the overall accuracy of the system can be given in terms of the accuracy of the height measurement which includes errors in the measurements of both direction and range. The probable error in the height of an individual reflection point is ± 2 km.

3. ANALYSIS OF THE DATA

The equipment was operated continuously from October to December 1952 and thereafter one month in every three until February 1955. During this period approximately 47,000 meteor echoes were recorded of which 9700 gave a measurement of drift.

Since each observation can only give a measure of the radial component of the motion of the trail relative to the station, reflections from a minimum of three trails occurring at approximately the same height and time but at different azimuths are required to give the magnitude and direction of the actual wind. The extension of this method to determine the behaviour of the wind over the full extent of the meteor region would require 100–200 usable records per hour, a rate which is attained only during periods of meteor showers. Hence the measurement of the instantaneous amplitude and direction of the wind is in general not possible.

Preliminary observations[5] showed that, although the wind changes greatly in strength and direction in the course of a day, the diurnal pattern of the winds repeats very closely on successive days. This repetition in day to day behaviour makes it possible to determine the average wind for some particular hour of the day by grouping together all observations which occurred during the same selected hour on 10–20 successive days. In this way the data from a particular sequence of days selected for analysis are grouped into 24 hourly intervals. To examine the height variations of the wind the data in each hourly interval are further arranged in three groups according to the height ranges 75–84, 85–94 and 95–104 km.

The magnitude and direction of the mean wind which gives the best fit to the observed components of the velocity of drift is determined by the method of least squares. It is found that the mean winds are effectively horizontal.

In order to study the diurnal behaviour of the winds the mean wind vector for each hour is resolved along the E–W and N–S directions and the components plotted as a function of time. A typical amplitude-time plot is shown in Fig. 1. Fourier analysis of all the component plots has confirmed the preliminary observation[5] that the winds in this region can be described in terms of three components; a constant term, a 24-hr periodic component and a 12-hr periodic component. The dotted curves in Fig. 1 represent the first three terms of the Fourier series.

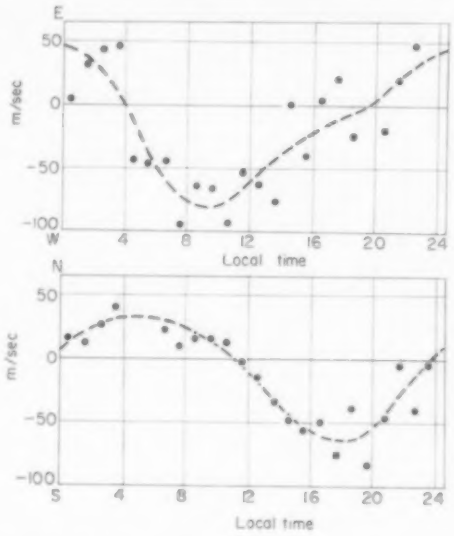

Fig. 1. Plot of components of mean wind for each hourly interval, March 16th–24th, 1953, 85–94 km. Dashed curves represent sum of first three terms of Fourier series.

The E–W and N–S components of the winds for each month are given in Table 1. The greatest proportion of meteor trails which gives usable echoes occurs in the height range 85–94 km, and in general it has been possible to obtain wind components in this height range for two sequences of days each month.

4. RESULTS

4.1. *Prevailing winds*

The average prevailing winds for all months are predominantly in the E–W directions and during summer and winter exhibit large vertical gradients. In Fig. 2 the prevailing components are plotted as a function of height for the months December, March, June and September.

The outstanding feature of these curves is the large and opposite wind gradients which existed in the E–W directions during December and June and the almost complete absence of the gradients during September and March. It can be seen that the prevailing wind would reverse direction from East to West at a height of 100 km in June and at about 70 km in December, while in March it was directed toward the East and in September toward the West over the total height range. The average wind gradient in December was $+2{\cdot}3\ \mathrm{m\,sec^{-1}\,km^{-1}}$ and in June $-3{\cdot}3\ \mathrm{m\,sec^{-1}\,km^{-1}}$.

The annual variation of the prevailing winds is illustrated in Fig. 3 and Fig. 4 where the amplitudes of the E–W and N–S components

Table 1

Period	Height (km)	North–South and East–West wind components Amplitudes (m sec^{-1})
October 1952	85– 94	$V_{NS} = +\ 0{\cdot}4 + 32{\cdot}3\cos\pi/_{12}(t-17{\cdot}5) + 20{\cdot}7\cos\pi/_{6}(t-\ 2{\cdot}4)$
		$V_{EW} = +\ 8{\cdot}6 + 36{\cdot}9\cos\pi/_{12}(t-11{\cdot}8) + \ 7{\cdot}5\cos\pi/_{6}(t-\ 2{\cdot}4)$
November 1952	85– 94	$V_{NS} = +16{\cdot}6 + 12{\cdot}4\cos\pi/_{12}(t-17{\cdot}9) + 19{\cdot}2\cos\pi/_{6}(t-10{\cdot}4)$
		$V_{EW} = +38{\cdot}0 + 28{\cdot}1\cos\pi/_{12}(t-\ 9{\cdot}9) + 18{\cdot}8\cos\pi/_{6}(t-\ 6{\cdot}5)$
December 1952	75– 84	$V_{NS} = +\ 0{\cdot}7 + 15{\cdot}3\cos\pi/_{12}(t-\ 0{\cdot}8) + 10{\cdot}1\cos\pi/_{6}(t-11{\cdot}4)$
		$V_{EW} = +28{\cdot}1 + 33{\cdot}4\cos\pi/_{12}(t-\ 9{\cdot}6) + 19{\cdot}7\cos\pi/_{6}(t-\ 6{\cdot}4)$
2nd–11th	85– 94	$V_{NS} = +14{\cdot}7 + 26{\cdot}4\cos\pi/_{12}(t-23{\cdot}0) + \ 9{\cdot}7\cos\pi/_{6}(t-\ 1{\cdot}4)$
		$V_{EW} = +54{\cdot}9 + 19{\cdot}9\cos\pi/_{12}(t-10{\cdot}4) + \ 1{\cdot}6\cos\pi/_{6}(t-\ 4{\cdot}4)$
12th–20th		$V_{NS} = +10{\cdot}7 + 32{\cdot}1\cos\pi/_{12}(t-17{\cdot}7) + 18{\cdot}1\cos\pi/_{6}(t-10{\cdot}9)$
		$V_{EW} = +34{\cdot}6 + 42{\cdot}6\cos\pi/_{12}(t-11{\cdot}4) + 18{\cdot}6\cos\pi/_{6}(t-\ 6{\cdot}4)$
	95–104	$V_{NS} = +16{\cdot}4 + 18{\cdot}1\cos\pi/_{12}(t-22{\cdot}9) + 31{\cdot}1\cos\pi/_{6}(t-\ 1{\cdot}3)$
		$V_{EW} = +56{\cdot}0 + 26{\cdot}6\cos\pi/_{12}(t-\ 5{\cdot}6) + \ 5{\cdot}9\cos\pi/_{6}(t-\ 8{\cdot}3)$
March 1953	75– 84	$V_{NS} = -\ 7{\cdot}7 + 35{\cdot}7\cos\pi/_{12}(t-17{\cdot}4) + \ 9{\cdot}1\cos\pi/_{6}(t-\ 7{\cdot}9)$
		$V_{EW} = +32{\cdot}3 + 32{\cdot}4\cos\pi/_{12}(t-14{\cdot}0) + 14{\cdot}7\cos\pi/_{6}(t-\ 7{\cdot}3)$
8th–15th	85– 94	$V_{NS} = -\ 5{\cdot}0 + 22{\cdot}4\cos\pi/_{12}(t-16{\cdot}8) + 16{\cdot}8\cos\pi/_{6}(t-\ 7{\cdot}0)$
		$V_{EW} = +38{\cdot}8 + 27{\cdot}8\cos\pi/_{12}(t-11{\cdot}2) + 20{\cdot}3\cos\pi/_{6}(t-\ 3{\cdot}8)$
16th–24th		$V_{NS} = +10{\cdot}1 + 48{\cdot}3\cos\pi/_{12}(t-17{\cdot}4) + \ 6{\cdot}5\cos\pi/_{6}(t-\ 6{\cdot}4)$
		$V_{EW} = +18{\cdot}5 + 54{\cdot}5\cos\pi/_{12}(t-10{\cdot}7) + 19{\cdot}0\cos\pi/_{6}(t-\ 8{\cdot}0)$
	95–104	$V_{NS} = +\ 5{\cdot}2 + 29{\cdot}7\cos\pi/_{12}(t-\ 8{\cdot}7) + 40{\cdot}0\cos\pi/_{6}(t-\ 2{\cdot}2)$
		$V_{EW} = +38{\cdot}4 + 29{\cdot}5\cos\pi/_{12}(t-11{\cdot}3) + \ 6{\cdot}5\cos\pi/_{6}(t-\ 4{\cdot}0)$
June 1953	75– 84	$V_{NS} = -\ 6{\cdot}9 + 12{\cdot}0\cos\pi/_{12}(t-\ 7{\cdot}0) + \ 4{\cdot}5\cos\pi/_{6}(t-11{\cdot}2)$
		$V_{EW} = +64{\cdot}6 + 32{\cdot}0\cos\pi/_{12}(t-22{\cdot}2) + 15{\cdot}9\cos\pi/_{6}(t-\ 7{\cdot}8)$
	85– 94	$V_{NS} = -19{\cdot}8 + 10{\cdot}2\cos\pi/_{12}(t-10{\cdot}6) + \ 4{\cdot}0\cos\pi/_{6}(t-\ 5{\cdot}9)$
		$V_{EW} = +30{\cdot}1 + 12{\cdot}4\cos\pi/_{12}(t-23{\cdot}6) + 31{\cdot}0\cos\pi/_{6}(t-\ 8{\cdot}5)$
	95–104	$V_{NS} = -\ 3{\cdot}6 + 32{\cdot}5\cos\pi/_{12}(t-16{\cdot}8) + \ 2{\cdot}8\cos\pi/_{6}(t-\ 3{\cdot}2)$
		$V_{EW} = +10{\cdot}4 + 14{\cdot}6\cos\pi/_{12}(t-15{\cdot}7) + 54{\cdot}2\cos\pi/_{6}(t-\ 8{\cdot}0)$
September 1953	75– 84	$V_{NS} = -\ 3{\cdot}1 + 16{\cdot}1\cos\pi/_{12}(t-18{\cdot}9) + 18{\cdot}4\cos\pi/_{6}(t-\ 6{\cdot}3)$
		$V_{EW} = -\ 5{\cdot}3 + 14{\cdot}0\cos\pi/_{12}(t-11{\cdot}9) + 10{\cdot}6\cos\pi/_{6}(t-\ 4{\cdot}7)$
8th–18th	85– 94	$V_{NS} = +12{\cdot}9 + 19{\cdot}2\cos\pi/_{12}(t-15{\cdot}1) + \ 3{\cdot}6\cos\pi/_{6}(t-10{\cdot}6)$
		$V_{EW} = +\ 3{\cdot}5 + 25{\cdot}0\cos\pi/_{12}(t-\ 8{\cdot}4) + 15{\cdot}9\cos\pi/_{6}(t-11{\cdot}4)$
20th–30th		$V_{NS} = +\ 5{\cdot}4 + \ 9{\cdot}0\cos\pi/_{12}(t-18{\cdot}7) + 14{\cdot}8\cos\pi/_{6}(t-\ 2{\cdot}9)$
		$V_{EW} = -24{\cdot}3 + 13{\cdot}4\cos\pi/_{12}(t-\ 6{\cdot}3) + 14{\cdot}1\cos\pi/_{6}(t-\ 2{\cdot}7)$
	95–104	$V_{NS} = +\ 0{\cdot}3 + 26{\cdot}3\cos\pi/_{12}(t-18{\cdot}0) + 25{\cdot}1\cos\pi/_{6}(t-10{\cdot}9)$
		$V_{EW} = -14{\cdot}3 + 15{\cdot}9\cos\pi/_{12}(t-14{\cdot}8) + 27{\cdot}6\cos\pi/_{6}(t-10{\cdot}7)$

Table I. *Continued*

Period	Height (km)	North-South and East-West wind components Amplitudes (m sec^{-1})
December 1953	75- 84	$V_{NS} = +1{\cdot}7 + 11{\cdot}3 \cos \pi/_{12}(t-23{\cdot}6) + 15{\cdot}8 \cos \pi/_{6}(t-0{\cdot}1)$
		$V_{EW} = +26{\cdot}7 + 24{\cdot}4 \cos \pi/_{12}(t-13{\cdot}2) + 24{\cdot}4 \cos \pi/_{6}(t-7{\cdot}8)$
	85- 94	$V_{NS} = +5{\cdot}2 + 31{\cdot}5 \cos \pi/_{12}(t-21{\cdot}0) + 12{\cdot}7 \cos \pi/_{6}(t-11{\cdot}7)$
		$V_{EW} = +46{\cdot}5 + 25{\cdot}8 \cos \pi/_{12}(t-10{\cdot}9) + 12{\cdot}6 \cos \pi/_{6}(t-5{\cdot}6)$
	95-104	$V_{NS} = +2{\cdot}9 + 22{\cdot}1 \cos \pi/_{12}(t-0{\cdot}9) + 10{\cdot}8 \cos \pi/_{6}(t-0{\cdot}4)$
		$V_{EW} = +70{\cdot}4 + 20{\cdot}4 \cos \pi/_{12}(t-9{\cdot}5) + 20{\cdot}8 \cos \pi/_{6}(t-7{\cdot}3)$
May 1954	75- 84	$V_{NS} = -5{\cdot}5 + 18{\cdot}8 \cos \pi/_{12}(t-17{\cdot}5) + 11{\cdot}6 \cos \pi/_{6}(t-2{\cdot}1)$
		$V_{EW} = +37{\cdot}7 + 19{\cdot}0 \cos \pi/_{12}(t-16{\cdot}4) + 5{\cdot}1 \cos \pi/_{6}(t-8{\cdot}7)$
1st-14th	85- 94	$V_{NS} = +3{\cdot}2 + 12{\cdot}2 \cos \pi/_{12}(t-13{\cdot}4) + 18{\cdot}0 \cos \pi/_{6}(t-2{\cdot}7)$
		$V_{EW} = +26{\cdot}6 + 24{\cdot}3 \cos \pi/_{12}(t-7{\cdot}3) + 17{\cdot}0 \cos \pi/_{6}(t-10{\cdot}4)$
15th-28th		$V_{NS} = +6{\cdot}0 + 30{\cdot}0 \cos \pi/_{12}(t-16{\cdot}6) + 15{\cdot}1 \cos \pi/_{6}(t-4{\cdot}6)$
		$V_{EW} = +14{\cdot}7 + 14{\cdot}4 \cos \pi/_{12}(t-8{\cdot}1) + 23{\cdot}1 \cos \pi/_{6}(t-0{\cdot}1)$
	95-104	$V_{NS} = -15{\cdot}8 + 14{\cdot}5 \cos \pi/_{12}(t-7{\cdot}0) + 14{\cdot}8 \cos \pi/_{6}(t-1{\cdot}4)$
		$V_{EW} = -6{\cdot}3 + 15{\cdot}1 \cos \pi/_{12}(t-21{\cdot}0) + 51{\cdot}4 \cos \pi/_{6}(t-9{\cdot}9)$
July 1954	75- 84	$V_{NS} = -14{\cdot}6 + 6{\cdot}5 \cos \pi/_{12}(t-18{\cdot}4) + 10{\cdot}7 \cos \pi/_{6}(t-6{\cdot}2)$
		$V_{EW} = +31{\cdot}4 + 21{\cdot}6 \cos \pi/_{12}(t-13{\cdot}0) + 19{\cdot}5 \cos \pi/_{6}(t-2{\cdot}1)$
1st-20th	85- 94	$V_{NS} = -9{\cdot}9 + 16{\cdot}6 \cos \pi/_{12}(t-19{\cdot}2) + 43{\cdot}5 \cos \pi/_{6}(t-5{\cdot}4)$
		$V_{EW} = +19{\cdot}1 + 10{\cdot}1 \cos \pi/_{12}(t-17{\cdot}4) + 32{\cdot}1 \cos \pi/_{6}(t-2{\cdot}1)$
21st-Aug. 7th		$V_{NS} = -18{\cdot}9 + 22{\cdot}3 \cos \pi/_{12}(t-16{\cdot}2) + 20{\cdot}7 \cos \pi/_{6}(t-3{\cdot}6)$
		$V_{EW} = -5{\cdot}8 + 6{\cdot}1 \cos \pi/_{12}(t-14{\cdot}0) + 34{\cdot}7 \cos \pi/_{6}(t-1{\cdot}2)$
	95-104	$V_{NS} = -22{\cdot}8 + 27{\cdot}7 \cos \pi/_{12}(t-15{\cdot}7) + 28{\cdot}1 \cos \pi/_{6}(t-3{\cdot}0)$
		$V_{EW} = +9{\cdot}5 + 15{\cdot}4 \cos \pi/_{12}(t-19{\cdot}6) + 39{\cdot}6 \cos \pi/_{6}(t-11{\cdot}4)$
October 1954		
3rd-16th	75- 84	$V_{NS} = -4{\cdot}3 + 22{\cdot}4 \cos \pi/_{12}(t-16{\cdot}6) + 8{\cdot}2 \cos \pi/_{6}(t-2{\cdot}3)$
		$V_{EW} = -23{\cdot}0 + 30{\cdot}0 \cos \pi/_{12}(t-13{\cdot}5) + 15{\cdot}2 \cos \pi/_{6}(t-11{\cdot}6)$
17th-Nov. 3rd		$V_{NS} = +11{\cdot}8 + 8{\cdot}6 \cos \pi/_{12}(t-17{\cdot}9) + 5{\cdot}0 \cos \pi/_{6}(t-3{\cdot}0)$
		$V_{EW} = -6{\cdot}3 + 31{\cdot}5 \cos \pi/_{12}(t-16{\cdot}5) + 49{\cdot}5 \cos \pi/_{6}(t-2{\cdot}6)$
3rd-16th	85- 94	$V_{NS} = +6{\cdot}5 + 34{\cdot}9 \cos \pi/_{12}(t-14{\cdot}9) + 9{\cdot}1 \cos \pi/_{6}(t-1{\cdot}1)$
		$V_{EW} = -8{\cdot}1 + 28{\cdot}1 \cos \pi/_{12}(t-10{\cdot}4) + 32{\cdot}1 \cos \pi/_{6}(t-11{\cdot}1)$
17th-Nov. 3rd		$V_{NS} = +9{\cdot}4 + 35{\cdot}5 \cos \pi/_{12}(t-18{\cdot}6) + 13{\cdot}5 \cos \pi/_{6}(t-10{\cdot}6)$
		$V_{EW} = +16{\cdot}6 + 26{\cdot}4 \cos \pi/_{12}(t-11{\cdot}0) + 4{\cdot}5 \cos \pi/_{6}(t-6{\cdot}7)$
	95-104	$V_{NS} = 0 + 23{\cdot}6 \cos \pi/_{12}(t-7{\cdot}6) + 35{\cdot}1 \cos \pi/_{6}(t-11{\cdot}8)$
		$V_{EW} = +1{\cdot}6 + 30{\cdot}0 \cos \pi/_{12}(t-14{\cdot}2) + 44{\cdot}1 \cos \pi/_{6}(t-8{\cdot}5)$
February 1955	75- 84	$V_{NS} = +1{\cdot}6 + 16{\cdot}1 \cos \pi/_{12}(t-19{\cdot}2) + 19{\cdot}0 \cos \pi/_{6}(t-1{\cdot}3)$
		$V_{EW} = +22{\cdot}0 + 27{\cdot}3 \cos \pi/_{12}(t-14{\cdot}7) + 9{\cdot}2 \cos \pi/_{6}(t-8{\cdot}7)$
3rd-13th	85- 94	$V_{NS} = +11{\cdot}0 + 35{\cdot}6 \cos \pi/_{12}(t-19{\cdot}6) + 26{\cdot}1 \cos \pi/_{6}(t-0{\cdot}7)$
		$V_{EW} = +25{\cdot}7 + 58{\cdot}4 \cos \pi/_{12}(t-12{\cdot}1) + 15{\cdot}8 \cos \pi/_{6}(t-7{\cdot}1)$
14th-28th		$V_{NS} = +12{\cdot}8 + 44{\cdot}3 \cos \pi/_{12}(t-19{\cdot}0) + 15{\cdot}7 \cos \pi/_{6}(t-3{\cdot}3)$
		$V_{EW} = +21{\cdot}4 + 52{\cdot}1 \cos \pi/_{12}(t-11{\cdot}8) + 4{\cdot}6 \cos \pi/_{6}(t-8{\cdot}8)$
	95-104	$V_{NS} = +29{\cdot}3 + 36{\cdot}2 \cos \pi/_{12}(t-18{\cdot}1) + 47{\cdot}0 \cos \pi/_{6}(t-1{\cdot}2)$
		$V_{EW} = +18{\cdot}1 + 58{\cdot}7 \cos \pi/_{12}(t-10{\cdot}2) + 15{\cdot}1 \cos \pi/_{6}(t-9{\cdot}2)$

are plotted for each of the height intervals. There is no significant change in the pattern from one year to the next and the dotted curves represent the approximate mean behaviour of the prevailing components throughout the year. These curves indicate that the winds in this region of the atmosphere are toward the East for the greater part of the year. Westward

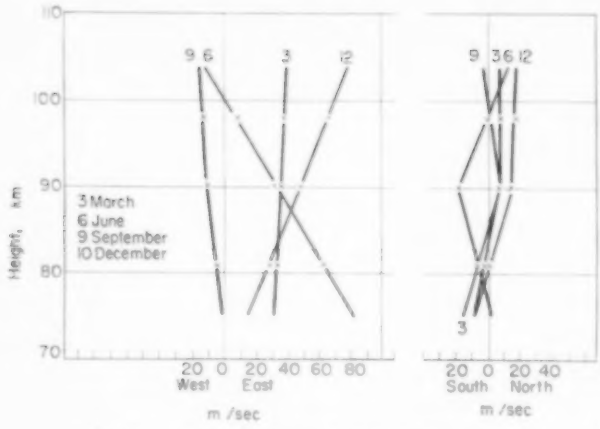

Fig. 2. Gradients of zonal and meridional prevailing winds.

winds occurring only during the spring months. With the onset of summer there is a rapid change back to the Eastward pattern at all levels. This rapid reversal is most marked in the upper height interval where a total change of wind speed of nearly 100 m sec^{-1} occurred during the period October to December.

The annual variation of the N–S component of the prevailing wind is much smaller but more regular than the E–W component. In summer the wind is directed towards the North and in winter towards the South. The maximum speeds increase with height from approximately ± 5 m sec^{-1} at 80 km to ± 20 m sec^{-1} at 100 km.

4.2. *Periodic components*

In Fig. 5 and Fig. 6 the 24- and 12-hr periodic components for five months are plotted in polar form. In general the end of the wind vector traces out an ellipse and the phase of the oscillation is indicated by the direction of the wind vector at 0000 hr local time. The sense of rotation of the vectors is predominantly anti-clockwise as would be expected for periodic winds in the Southern Hemisphere.

The amplitude of the diurnal component is approximately independent of height but exhibits large annual variations. This is shown in more detail in Fig. 7a where the amplitude of the oscillation, represented by the length of the major axis of each ellipse, is plotted for each period of observation. Maximum wind speeds (40–50 m sec^{-1}) occur in summer and autumn, and minimum speeds (20–30 m sec^{-1}) in winter and spring. The phase of the diurnal oscillation also varies from month to month but between the heights of 75 and 94 km there is a tendency for the wind to be directed North at about 1800 hr local time during summer, autumn and spring, while the phase of the weak oscillation during winter is approximately reversed compared with the other seasons. Between 95 and 104 km the behaviour of the 24-hr component is irregular with regard to both sense of rotation and phase.

In comparison with the 24-hr components the 12-hr oscillations shown in Fig. 6 behave in a very complex manner. The annual variations of the amplitude of the semi-diurnal winds for the three height intervals are shown in Fig. 7b.

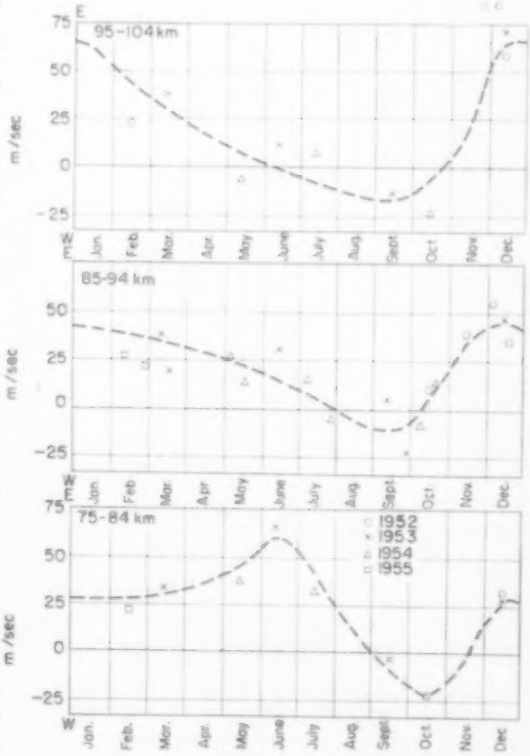

Fig. 3. Annual variation of zonal winds.

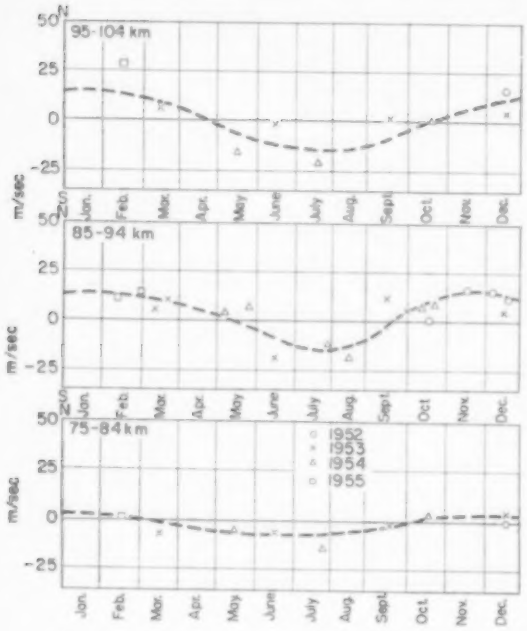

Fig. 4. Annual variation of meridional winds.

There is an increase of 20 m sec^{-1} in the average amplitude of this component over the height range 80 to 100 km, and evidence that the maximum value of this oscillation occurs during winter at the higher level and during summer at the lower level. Thus during June the amplitude gradient of this component is 2·5 m sec^{-1} km^{-1}, while in December the gradient is almost zero. The phase of the 12-hr oscillations varies irregularly from month to month.

5. DISCUSSION

5.1. *Prevailing winds*

It is evident from Fig. 2 that the prevailing winds are predominantly zonal and are characterized by large seasonal changes. The summer and winter components are complementary to measurements of winds between 0–70 km carried out in similar latitudes in the Northern Hemisphere.[6] These measurements have been obtained from balloon flights and from the explosions of grenades carried on rockets and the mean winds are reproduced in Fig. 8 together with the meteor results. In summer the agreement is remarkably good and the reversal at approximately 70 km appears conclusive. The winter results are consistent and indicate that the maximum wind speed occurs at about 60 km.

The only comparable meteor wind observations are those made at Manchester (53°N) by Greenhow and Neufeld[7]. The prevailing winds measured at Manchester exhibit seasonal variations which are similar in form during summer, autumn and spring to the wind variations depicted in Figs. 3 and 4, although the scale of the variations of the zonal component at Adelaide is three times as large as that at Manchester.

The amplitude of the N–S components are comparable at both places and the direction of motion is such that when the sun is north of the equator the meridional component is directed toward the south in both hemispheres and vice versa. In addition, at the equinoxes the meridional components observed at Adelaide and Manchester are approximately zero over the total height range.

It is of interest to compare winds measured by means of meteors with a zonal wind field suggested by Murgatroyd[8] from a survey of winds and temperatures up to 100 km. The gradients of the summer and winter winds agree closely with the proposed wind field but the absolute values differ by 20–30 m sec^{-1}. This discrepancy can be removed by shifting the zonal wind field at 90 km, 10° of latitude.

5.2. *Periodic components*

A feature of the winds observed at Adelaide is the comparable magnitude of the 24- and 12-hr components, the amplitude of both varying between 20 and 50 m sec^{-1}. Semi-diurnal winds of similar magnitude have been reported by Greenhow and Neufeld from meter observations, and by a number of workers from the observation of *E*-layer drifts. However, diurnal winds are rarely detected in the ionospheric drift measurements, and are only just detectable in twelve months observations of meteor winds at Manchester. It appears, therefore, that there is a strong latitude dependence of diurnal winds at heights of 80–100 km.

If the presence of the diurnal winds is attri-

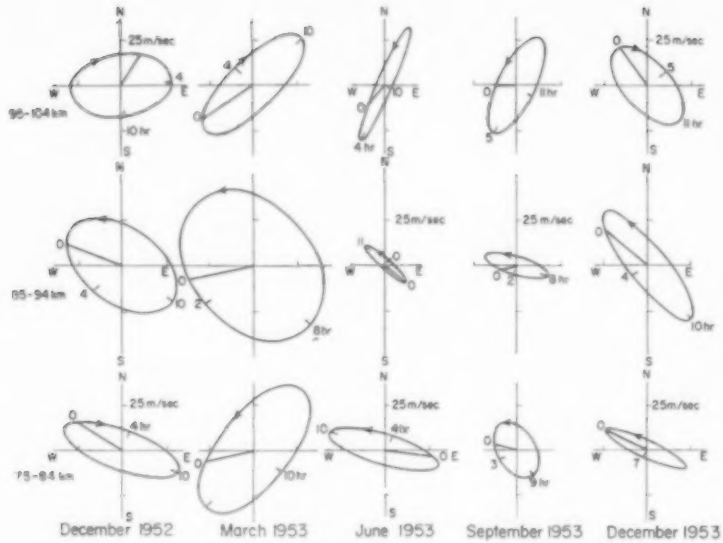

Fig. 5. Polar representation of the 24-hr periodic wind components.

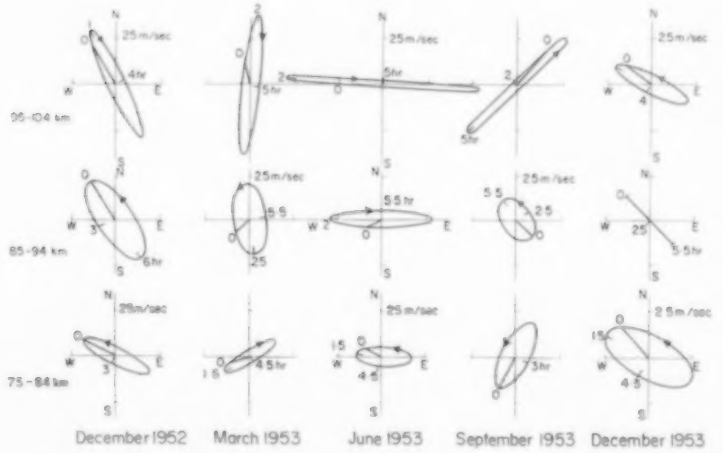

Fig. 6. Polar representation of the 12-hr periodic wind components.

buted to the daily heating and cooling of the atmosphere it is to be expected that the 24-hr component will show evidence of direct solar control. This argument is supported by the observed annual variation shown in Fig. 7a where the maximum amplitude occurs in late summer and the minimum about six months later. The phase of the diurnal winds also suggests that these winds are produced by direct solar heating. In the height range 75–94 km the associated pressure oscillation has a minimum value at approximately midday during summer, autumn and spring and a maximum value at midday in winter.

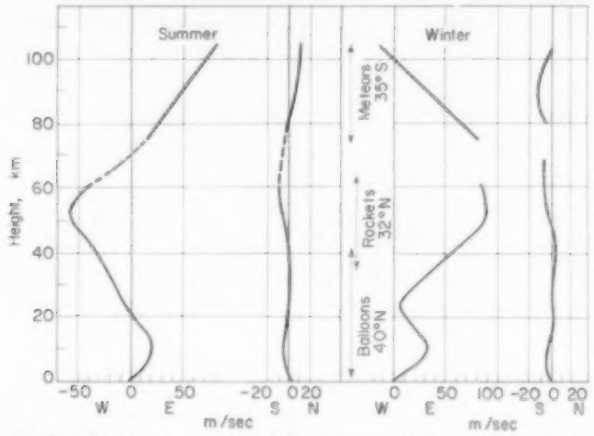

Fig. 6. Zonal and meridional components of the prevailing winds measured by means of balloons, rockets and meteors at medium latitudes.

The presence of diurnal winds in the dynamo region of the ionosphere has been deduced by Kato[9] from the earth's S_q variations. The magnitude and seasonal variations of the winds are similar to the Adelaide results but the phases are reversed.

The semi-diurnal wind components vary from month to month in a complex manner but the mean amplitude and the average gradient of $+1\ \mathrm{m\,sec^{-1}\,km^{-1}}$ are consistent with winds predicted by the theory of tidal oscillations of the atmosphere. Greenhow and Neufeld find a mean gradient of the same value in the semi-diurnal component of the winds measured at Manchester. These workers also find that this gradient has a maximum value in winter and is approximately zero in summer. This seasonal feature is also common to the Adelaide results and is apparent in Fig. 7b.

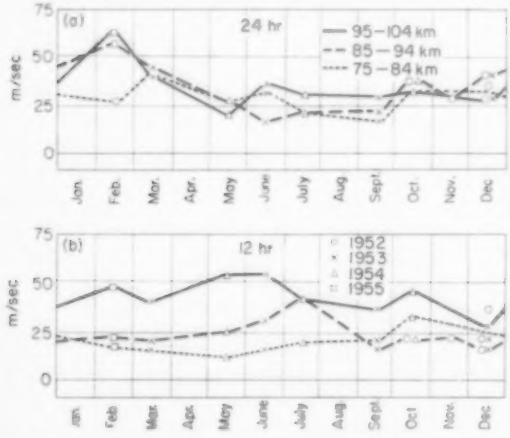

Fig. 7. Annual variation of the amplitude of (a) the 24-hr components, and (b) the 12-hr components.

Acknowledgements—This work forms part of the upper atmosphere research programme of the University of Adelaide. The project is financed jointly by the University of Adelaide and the Radio Research Board. The author wishes to thank Professor L. G. H. Huxley for his constant encouragement and the many members of the upper atmosphere research group who have assisted in the operation of the equipment and in data reduction.

REFERENCES

1. D. S. Robertson, D. T. Liddy and W. G. Elford, *J. Atmos. Terr. Phys.* **4**, 255 (1953).
2. J. S. Greenhow, *Phil. Mag.* Ser. 7, **45**, 364 (1954).
3. J. S. Greenhow and E. L. Neufeld, *Phil. Mag.* Ser. 7, **46**, 549 (1955).
4. L. G. H. Huxley, *Annals of the IGY*, Vol. III, 250 (1957).
5. W. G. Elford and D. S. Robertson, *J. Atmos. Terr. Phys.* **4**, 271 (1953)
6. C. J. Brasefield, *J. Geophys. Res.* **59**, 233 (1954).
7. J. S. Greenhow and E. L. Neufeld, *Phil. Mag.* Ser. 8, **1**, 1157 (1956).
8. R. J. Murgatroyd, *Quart. J. R. Met. Soc.* **83**, 417 (1957).
9. S. Kato, *J. Geomagn. Geoelect., Kyoto* **9**, 107 (1957).

Planet. Space Sci. Pergamon Press 1959. Vol. 1, pp. 102–104. Printed in Great Britain.

AN EXAMPLE OF HEAVY ABSORPTION IN THE VHF-BAND IN THE ARCTIC IONOSPHERE

L. HARANG and J. TRÖIM

Norwegian Defence Research Establishment, Kjeller (Oslo), Norway

(*Received November* 1958)

Abstract—From records of meteor echoes on 40 Mc/s and of scintillations from the Cassiopeia source on 45 Mc/s it is shown that on 7 July 1958 in the early morning hours a very heavy absorption appeared. The meteor echoes disappeared completely and the radiation from Cassiopeia diminished to less than 1/5 of its normal value. The observations were made at Tromsö ($\phi = 70°$ N) and in the direction towards the auroral zone. A great geomagnetic storm appeared with a sudden commencement at 08·40 MET, the geomagnetic storm started about 5 hr *after* the absorption effect of the ionosphere had started.

1. INTRODUCTION

The strong absorption of radio waves in the HF-band during disturbances along the auroral zone has been the subject of numerous investigations. During strong disturbances there may be a complete cessation of echoes reflected at vertical incidence and usually it is not possible to measure quantitatively the absorption during the blackout phase. In order to estimate the amount of absorption during strong disturbances in the Arctic ionosphere the field-strength of the galactic radio waves in the VHF-band has been studied. Little and Leinbach[1] have shown that during strong disturbances there may be an increase in the absorption of the order 3–6 dB measured on 30 Mc/s.

In the following an example of extraordinary strong absorption in the 40–45 Mc/s band will be given based on records of meteoric reflections and records of radio noise from the Cassiopeia source. The observations were made at Tromsö ($\phi = 70°$) lying close to the southern edge of the auroral zone.

2. OBSERVATIONS OF METEORS

In order to study the auroral echoes a two-channel radar operating on 40 and 80 Mc/s was in continuous operation. On the photographic records normally a great number of meteor echoes were simultaneously appearing. During the early morning hours on 7 July 1958 the number of meteors observed on 40 Mc/s decreased continuously and the reflections disappeared completely at 0800 MET. At 0840 MET a sudden commencement of a very great geomagnetic storm appeared during which no meteor reflections could be observed. The observations were made with the aerials, Yagis, pointing towards the North and at low elevation angle. Peak power was 25 kW.

A closer inspection of the records revealed the following details in this process of continuously increasing absorption. Dividing the ranges of the meteoric reflections into three intervals, $R > 500$ km, $500 > R > 250$ km and 250 km $> R > 0$, it appeared that there was a time lag in the time of disappearance. The meteor reflections having the greatest ranges disappeared first. Fig. 1 shows the records and Fig. 2 the gradual disappearance of the number of meteoric reflections.

3. OBSERVATIONS OF SCINTILLATIONS

The radiation from Cassiopeia source on 45 Mc/s was simultaneously recorded by means of a phase-switching interferometer having a base-length of 9λ. Fig. 3 shows the record from the preceding day of the disturbance,

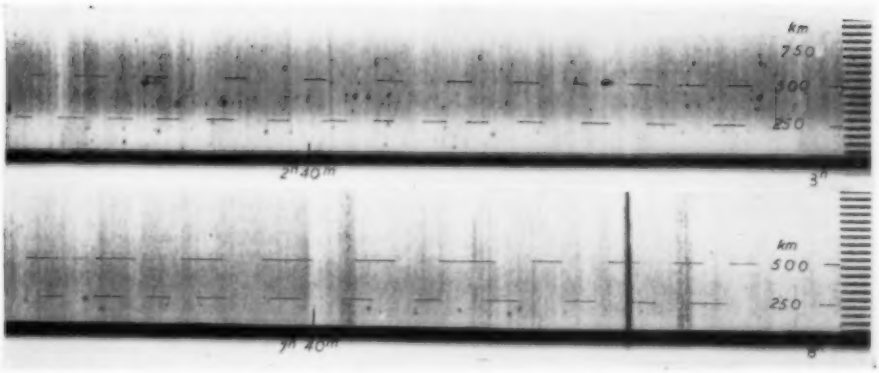

Fig. 1. Meteor echoes on 40 Mc/s. Upper part: before the disturbance, the meteor echoes appear with normal rate of occurrence. Lower part: during the first phase of the disturbance, meteor echoes having greater ranges than 250 km completely disappeared.

[Facing p. 102

6 July, which showed the normal features of heavy scintillations on the sinusoidal trace usually occurring even on a quiet day at the Arctic station Tromsö. The records from the following day, 7 July, show that the amplitude of the sinusoidal interference pattern has decreased to less than 1/5 of the value appearing on the preceding day. At this time of recordings, 0500–0700 MET, the Cassiopeia source was in the North approximately at lower culmination. The meteor reflections and the radiation from the Cassiopeia source were thus

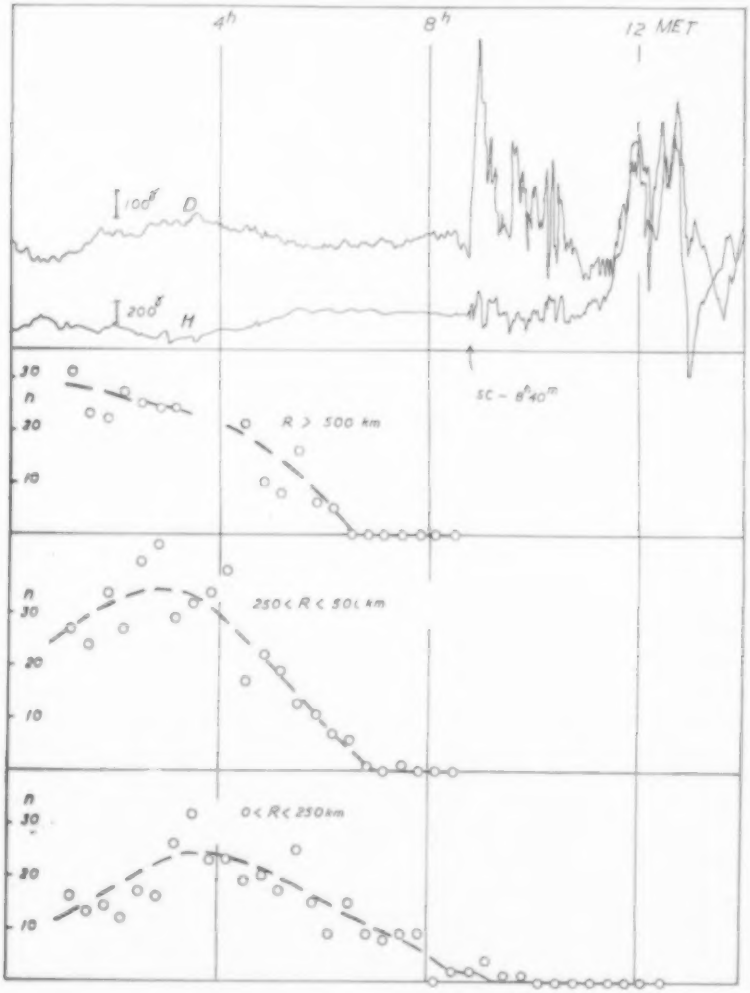

Fig. 2. Upper part: geomagnetic records from Tromsö. Lower part: number of meteor reflections in different range intervals. n is the number counted per twenty minutes.

both received from the Northern sky at low elevation, and would have had to cross the auroral zone before being received.

4. GEOMAGNETIC AND SOLAR OBSERVATIONS

The great geomagnetic storm appeared with a sudden commencement at 0840 MET on 7 July, i.e. 4–5 hr *after* the strong absorption of the 40–45 Mc/s waves had started. During the first hours of the period of absorption the geomagnetic conditions were even quiet. At Tromsö there was midnight sun and the ionosphere was therefore completely sunlit. The strong absorption, which must be due to increase in electron density at the lower edge of, or below, the *E*-layer, may in this case therefore most presumably be due to increased solar short wave emission. The sudden commencement of the geomagnetic storm, appearing after the start of the absorption process, could be interpreted as the time of arrival of the charged particle cloud.

Solar observations show that during the interval 039–324 GMT solar flares of the highest intensity (3+) were observed at the observatories at Honolulu, Tokyo and Sydney. During the same time major radio bursts on frequencies up to 10,000 Mc/s were recorded. Due to the midnight sun this disturbance was noticeable even shortly after midnight at the high-latitude station at Tromsö. The absorption effect of the ionosphere started at about 0330 MET and was complete at about 0800 MET.

The well defined sudden commencement of the geomagnetic disturbance at 0840 MET, which we interpret as the time of arrival of the ion cloud, indicate a time difference of about five hours between the arrival of the ultraviolet emission and the particle emission, which should give a velocity of the ion cloud about 8000 km/sec.

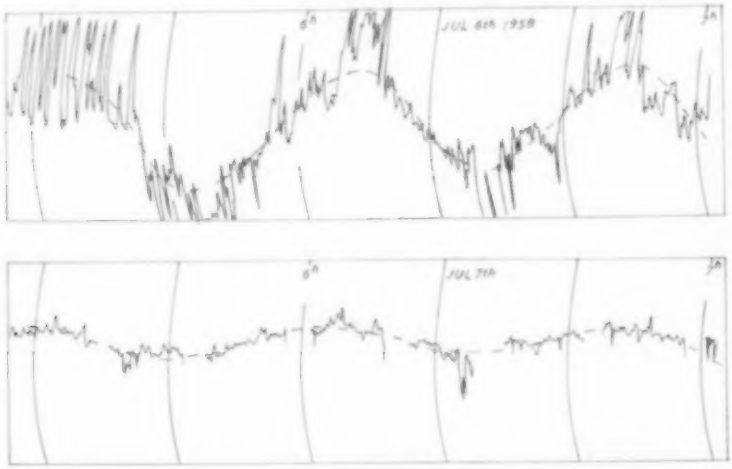

Fig. 3. Records of the radiation from the Cassiopeia source on 45 Mc/s. Upper record: during the undisturbed day 6 July. Lower part: During the day of heavy disturbance, 7 July 1958.

The authors wish to express their sincere thanks to the director of the Auroral Observatory at Tromsö, Mr. E. Tönsberg for putting the facilities of the observatory to our disposal and to Mr. K. Malmjord and R. Larsen for valuable assistance during the observations.

REFERENCE

1. C. G. Little and H. Leinbach, *Proc. Inst. Radio Engrs.* **46**, 334–348 (1958); C. G. Little and S. Chapman, *J. Atmos. Terr. Phys.* **10**, 20–31 (1957).

Planet. Space Sci. Pergamon Press, 1959. Vol. 1, pp. 105–111. Printed in Great Britain.

ČERENKOV RADIATION IN THE ATMOSPHERE

J. V. JELLEY*

Atomic Energy Research Establishment, Harwell, England
(*Received* 27 *January* 1959)

Abstract—The bursts of large numbers of electrons produced in the atmosphere by cosmic-ray air showers, give rise to Čerenkov radiation in the air. The showers are therefore accompanied by light pulses of short duration; these may be detected quite easily with simple apparatus on a clear dark night. This phenomenon, which was discovered by the author and his colleagues in England in 1953, has been studied in more detail by two groups, one in the U.S.S.R. and one in Australia.

In this article, the writer reviews the theoretical and experimental work that has been done up to the present time, and discusses the potentialities and limitations of the technique as a new tool for cosmic-ray research. The paper concludes with a few remarks on the future possibilities in this field, and the likely technical developments.

1. INTRODUCTION

In 1948 Blackett[1] suggested that there should be a small contribution to the light of the night sky from Čerenkov radiation produced by cosmic-ray particles traversing the atmosphere. From a knowledge of the flux of particles, the rate of production of light by the Čerenkov effect, and some early measurements of the average intensity of the light of the night sky, Blackett showed that the contribution due to Čerenkov radiation would amount to $\sim 10^{-4}$ of the total light.

It was obvious that such a low light intensity could not be detected by normal methods, nor could it be correlated with the intensity of the general cosmic-radiation, which is remarkably constant with time. If, however, individual cosmic-ray events of the highest energy were isolated, namely the so called Extensive Air Showers, in which there are bursts of great numbers of particles, there would be momentary pulses of light of an intensity considerably greater than the mean intensity produced by the general cosmic-radiation, indeed probably strong enough to be detected against the much more intense steady background light of the sky. It was with these ideas in mind that Galbraith and Jelley[2] first discovered light pulses from the night sky associated with large cosmic-ray showers.

It is necessary at this stage to digress from the main theme, to discuss some of the essential features of the cosmic-ray air showers, for those readers not familiar with this field. The primary particles of the cosmic radiation, now believed to be mostly protons, cause nuclear disintegrations at the top of the atmosphere. These disintegrations lead to the emission of further particles, which in turn themselves produce disintegrations. Among the products of these nuclear disintegrations are neutral π-mesons, which decay into high energy γ-rays. These in turn produce a cascade of electrons and further γ-rays, by the processes of electron pair-production and Bremsstrahlung; such a cascade is known as an electron–photon shower. When the energy E_0 of the primary particle is sufficiently high, the shower reaches down to sea-level and is then known as an Extensive Air Shower, since the particles are then found at considerable distances from the main axis of the shower.

The multiplication of the number of particles in the shower increases with atmospheric depth

* At present on leave of absence from Harwell, at the Harvard College Observatory, Cambridge, Massachusetts, U.S.A.

until their individual energies are reduced to ~ 100 MeV; below this energy the processes of pair production and Bremsstrahlung lose in competition with Compton scattering and ionization energy-loss, and the shower then dwindles. There is thus some level at which there is a maximum number of electrons, N_{max}, for a given E_0; this is shown in the sketch, Fig. 1, where N is plotted against h, the height above the ground.

Fig. 1. To show the general trend in the distribution of the number of particles N in an air shower, as a function of the height h above the ground.

Air showers are observed by conventional counter techniques over a range of values of E_0 from $\sim 10^{13}$ to 10^{18} eV, there being a frequency distribution of the type

$$n(>E_0) \propto E_0^{-1\cdot 5}$$

which holds over most of the range. To give some numerical data for specific cases, showers of energy $E_0 > 10^{14}$ eV arrive at the earth's surface at a rate $\sim 300\,\text{km}^{-2}\,\text{sec}^{-1}\,\text{sterad}^{-1}$, and those with $E_0 > 10^{15}$ eV at a rate $\sim 0{\cdot}2\,\text{km}^{-2}\,\text{sec}^{-1}\,\text{sterad}^{-1}$; these showers have approximately 10^5 and 10^6 electrons respectively, when they arrive at sea-level.

There is a very extensive literature on cosmic-ray air showers, and the reader is referred to the review articles by Rossi and Greisen[3], the proceedings of the IUPAP conference at Varenna, Italy, in (1957), and the recent monograph by Galbraith[4]. Other salient features of these showers which should be mentioned in this very brief account of a most intricate field, are added for completeness: (1) There is a very well-established law of variation for the particle density as a function of the lateral distance from the shower core, for given values of E_0; typical results of measurements of this function may be found in the work of Cranshaw *et al.*[5] (2) The angular distribution of the axes of showers is a steep function of the zenith angle Z, and is of the form $n(Z)\,dZ \sim \cos^6 Z$. (3) The rate of arrival of showers, at a given E_0, occurs at random and at a mean rate that is remarkably constant in both solar and sidereal time. (4) A feature particularly important to an understanding of the Čerenkov effect in the atmosphere, is the extremely short duration of the event as experienced by detectors at a given level in the atmosphere or on the ground. Measurement by Bassi *et al.*[6] showed that the vertical spread of the "sheet" of particles when they reach sea-level is ~ 1 m, so that the particles all arrive within a time interval $\sim 10^{-8}$ sec; this will also be the order of magnitude of the duration of the associated light pulses.

2. THE DISCOVERY OF LIGHT PULSES FROM THE NIGHT SKY

Until 1953, studies and applications of the Čerenkov effect had been restricted to solid and liquid media. For those unacquainted with the phenomenon, the reader is referred to the original papers by Čerenkov[7], the theoretical interpretation by Frank and Tamm[8], and a recent monograph on the entire field by Jelley[9].

Returning now to the subject of Čerenkov radiation in the atmosphere, it was with the very simple apparatus shown in Fig. 2 that Galbraith and Jelley[2] first discovered that light pulses associated with cosmic-ray air showers could be very easily detected against the background light of the night-sky. In these experiments a photomultiplier was used as light detector, set up with its cathode in the focal plane of a parabolic mirror; the phototube was connected to a pulse-amplifier, pulse-height discriminator and recording oscilloscope. In their first experiments a 5 cm dia. phototube was used, with a 25 cm dia. f/0·46 mirror, working into an amplifier with cut-off frequency ~ 5 Mc/s. The field of view of this simple

telescope was 0·11 steradians, determined by the area of the photocathode and the focal length of the mirror. This instrument, when directed to the zenith on a dark clear moonless night, detected light pulses at a rate $\sim 1\ \text{min}^{-1}$, when the discriminator was set at a bias level of twice the "noise" level from the background light of the night sky. It was soon proved that the pulses indeed originated from the night-sky, that they were directly correlated with extensive air showers, and that they were not associated with other types of events, such as distant lightning or faint meteors.

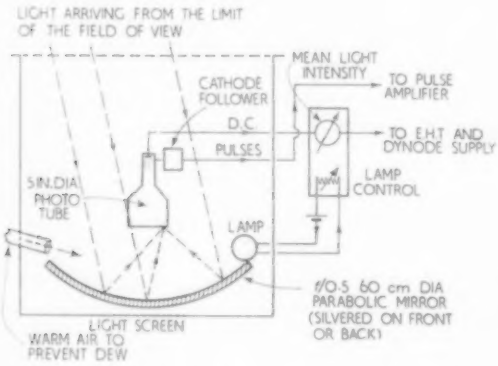

Fig. 2. The essential features of the light receivers used throughout the work carried out by Galbraith and the author.

It soon became clear that a new technique was available for studies of cosmic-ray air showers, the new instrument having two unique characteristics. First, since the "pool" of light associated with the shower has a diameter comparable with the lateral extent of the shower, a single light receiver has an effective area large compared with its physical dimensions. Secondly, the instrument is highly directional, its field of view being governed by the optics of the system, the characteristic cone-angle for the light emission, and the spread in the directions of the shower particles (caused by Coulomb scattering). Further work in the field has since shown that although the basic potentialities of the technique remain, it is not likely that light receivers by themselves will replace existing techniques, but may well supplement them, for particular investigations.

2.1. *Sensitivity of the instrument and background "noise"*

The absolute sensitivity of a light receiver is limited by the background light from the night sky which produces a "noise" output on the recording equipment. This "noise", which arises from fluctuations in the number of photoelectrons at the photocathode, exceeds the natural dark-current of the phototube by a large factor, $\sim 10^4$, even on the darkest night, with a receiver of the type we have described. This "noise" from the night sky is estimated as follows: —

If A is the collecting area of the light receiver and Ω is its field of view (i.e. the solid angle of the acceptance cone), the mean current flowing from the photocathode of the multiplier is given by:

$$i = \phi_B A \Omega \varepsilon \text{ photoelectrons sec}^{-1} \qquad (1)$$

where ε is the quantum conversion efficiency of the cathode (in photoelectrons per photon), and ϕ_B is the mean flux for the background light of the night sky. The average number $\bar{\nu}$ of photoelectrons emitted per unit resolving time $\Delta\tau$ of the amplifier (where $\Delta\tau = 1/f_c$, if f_c is the cut-off frequency) is thus $\bar{\nu} = \phi_B A \Omega \varepsilon \Delta\tau$, so that the noise-level, due to fluctuations on this number, is given by:

$$N = \sqrt{(\phi_B A \Omega \varepsilon / f_c)} \qquad (2)$$

Taking an average value for the brightness of the night sky as measured by Babcock and Johnson[10] and by Chuveyev[11], we have $\phi_B = 6{\cdot}4 \times 10^7$ photons cm^{-2} sec^{-1} sterad^{-1} (4300–5500 Å). Inserting values for the original light receiver, $A = 510$ cm^2, $\Omega = 0{\cdot}11$ sterad, $f_c = 5$ Mc/s and $\varepsilon = 10$ per cent, we obtain $N = \pm 9$ photoelectrons per unit resolving time. In the early experiments the discriminator bias was set at a level equal to $4N$, so that the light pulses detected with this arrangement gave a pulse at the photocathode of ~ 36 photoelectrons, and the light *flux* ϕ_L, during the pulse, would be given by $\phi_L = 4N/\varepsilon A = 360/510 = 0{\cdot}7$ photons cm^{-2} per flash. (This agreed within a

factor of 4 with direct measurements of the light intensity.)

3. THEORETICAL CONSIDERATIONS

From the established relationship for the Čerenkov effect

$$\cos\theta = 1/\beta n \tag{3}$$

where θ is the angle for the emission of coherent radiation, n is the refractive index and βc is the velocity of the particle, we find for air at sea-level (for which $n = 1{\cdot}00029$) that, for electrons, the threshold kinetic energy is 21 MeV, and the maximum emission-angle for ultra-relativistic electrons ($\beta = 1$) is $1{\cdot}3°$.

For the radiation yield, expressed in photons per centimeter path for a single particle,

$$\frac{dN}{dl} = \frac{2\pi}{137}\int (1 - 1/\beta^2 n^2)\,\frac{1}{\lambda^2}\,d\lambda \tag{4}$$

we also find, for air at sea-level, $(dN/dl) = 0{\cdot}23$ photons cm^{-1} (between wavelength limits of 3500 and 5000 Å). These figures, it will be seen, are very different from those encountered in solid and liquid media. For example, in water, the corresponding figures are: $E_{\min} = 0{\cdot}26$ MeV, $\theta_{\max} = 41°$ and $(dN/dl) \sim 200$ photons cm^{-1}.

Let us now consider a single fast electron traversing the atmosphere vertically, and for simplicity let us neglect slowing-down and Coulomb scattering. If we write, for the refractive index of air at sea-level, $n_0 = 1 + \eta_0$ where $\eta_0 = 2{\cdot}9 \times 10^{-4}$, the refractive index at height h will then be obtained from

$$\eta_h = \eta_0 \exp(-h/\lambda)$$

where $\lambda = 7{\cdot}1$ km for the standard atmosphere. We wish to know first, what is the lateral distribution of the light on the ground resulting from the passage of this single particle vertically through the atmosphere? Light generated at height h will fall at a radial distance r on the ground, given by $r = h\theta$. Since θ is small, $\beta \approx 1$ and n is close to unity, (3) may be rewritten $\theta \approx \sqrt{(2\eta)}$. It follows therefore that:

$$r = (5{\cdot}8 \times 10^{-4})^{1/2} h \exp(-h/2\lambda) \tag{5}$$

Since the refractive index decreases with altitude, we find from (5) that r has a maximum value, $r\,(\max) = 126$ m; this occurs when $h_{\max} = 14$ km, at which the air pressure is 140 g cm^{-2}, $\eta = 4 \times 10^{-5}$, $\theta = 9 \times 10^{-3}$ rad and $E\,(\text{threshold}) = 56$ MeV. It can likewise be shown that the intensity distribution of the light on the ground is given by:

$$I(r) \propto (1/r) \exp(-h/h_{\max}) \tag{6}$$

3.1. *Extension to showers*

To extend the arguments to electrons in showers, expressions (5) and (6) must be severely modified. First we have to allow for the vertical distribution of the numbers of electrons at different heights. This effect, by itself, is straightforward. Rather more difficult, however, is to allow for the lateral distribution of the particles. Most difficult of all is the problem of Coulomb scattering. The scattering angles are in general much greater than the Čerenkov angle; this factor, and the wide *distribution* of the angles of scatter, are of such magnitudes that most of the characteristics of the Čerenkov effect are obliterated in observations of the light flashes associated with the showers. A rigorous solution of the problem has not yet been attempted. A preliminary attack has, however, been made by Goldanskii and Zhdanov[12] and a further, and different, approach has been made by Brennan[13].

3.2. *Alternative processes for light production*

Although all the observational evidence points in favour of Čerenkov radiation as the origin of the light flashes from the night sky, it is reasonable to enquire what other processes might also contribute to radiation in the optical region of the spectrum. There are at least three processes. First there is the possibility of the emission of ionization or recombination radiation. This may be discounted, for the production rate is very low, $(dN/dl) < 3 \cdot 10^{-3}$ photons/cm, according to laboratory measurements of Barclay and Jelley[14], and, moreover, since such radiation would be emitted isotropically, the light received by an instrument placed on the ground would be a very much smaller fraction of the light produced. Secondly, there

will be Bremsstrahlung in the optical band. This, however, will be quite negligible compared with the Čerenkov radiation. For example, in the case of 100 MeV electrons in nitrogen at atmosphere pressure, it is calculated that the production-rate for radiation in this narrow slice of the spectrum is only of the order of 4×10^{-6} photons/cm. Lastly, there is the possible emission of Schwinger radiation, arising from the deflection of the shower electrons in the earth's magnetic field; this too is quite negligible, being weaker than the Bremsstrahlung by a few orders of magnitude.

3.3. *Counting rates and threshold energies of different receivers*

Since the background light of the night sky determines the threshold sensitivity of a light receiver, see equation (2), and this in turn varies with the two parameters of the optical system (the aperture D, and the field of view α), it is found that the counting-rate does not vary very rapidly with these parameters (for a given bias level relative to the noise level). Taking the accepted spectrum of the numbers of light pulses for a given primary energy of the showers E_0, namely $n(>E_0) \propto E_0^{-1.5}$, and assuming there is always complete "pile-up" of the noise pulses, it can be shown that the counting-rates R and the limiting primary energies E_{min}, are related to D, α and the amplifier cut-off frequency f_c by the following relations, which have been derived by Jelley[9]:

$$\begin{aligned} &R(D) \propto D^{1.5} && \text{(with } \alpha \text{ and } f_c \text{ constant)} \\ &R(\alpha) \propto \alpha^{0.5} && (\ ,,\ D\ ,,\ f_c\ ,,\ ) \\ &R(f_c) \propto f_c^{0.75} && (\ ,,\ D\ ,,\ \alpha\ ,,\ ) \\ \text{and } &E_{min}(D) \propto (1/D) && (\ ,,\ \alpha\ ,,\ f_c\ ,,\ ) \\ &E_{min}(\alpha) \propto \alpha && (\ ,,\ D\ ,,\ \alpha\ ,,\ ) \\ &E_{min}(f_c) \propto 1/\sqrt{f_c} && (\ ,,\ D\ ,,\ f_c\ ,,\ ) \end{aligned} \quad (7)$$

Thus, for a high counting rate, regardless of primary shower energy, an optical system of large aperture and wide field is required, working into a broad-band amplifier. Such a receiver will count mostly showers of relatively low primary energy. In order to detect only showers of extremely high energy, quite small light receivers are adequate and one may even dispense with the mirror. Results obtained with a variety of light receivers are summarized in the following table, together with figures calculated from the relations in (7), and normalized to those for the first instrument.

4. EXPERIMENTAL WORK AND PRACTICAL APPLICATIONS

After the initial discovery of the light flashes, a number of preliminary experiments were carried out at the Pic du Midi observatory in France, where the observing conditions were very good. The results of these experiments[13], which were aimed primarily at studies of the radiation itself, revealed the essential features of the phenomenon; the work included measurements of polarization, the directional character of the light, the pulse-height spectrum, an absolute measurement of the light flux, the zenith-angle distribution, and a search for possible "point" sources of showers. Shortly afterwards, some of these experiments were repeated by Nesterova and Chudakov[16], who obtained very similar results, with the same type of equipment. During the succeeding two years very little work was carried out, though mention should be made of experiments by Barclay and Jelley[17] who first showed that the lateral distribution of the light on the ground far exceeded that of the simple theory outlined in Section 3, revealing immediately the import-

Light collector	Photo-cathode diameter (in.)	D (cm)	α (deg.)	Ω (sterads) $=\pi\alpha^2$	Calc. R (min^{-1})	Obs. R (min^{-1})	ϕ_{min} (Photons cm^{-2})	E_{min} (eV)
10 in. diam. mirror	2	25	12	0·15	1·5	1·5	3	10^{14}
2 ft. diam. mirror	2	61	5·8	0·032	3·9	5	0·57	2×10^{13}
2 ft. diam. mirror	5	61	14	0·20	6·0	7	1·4	5×10^{13}
5 ft. diam. searchlight	5	150	4·9	0·022	14	11	0·2	7×10^{12}
No mirror	5	12·7	30	0·85	0·84	1·0	14	5×10^{14}

ance of Coulomb scattering of the shower particles.

The first serious attempt to apply the technique to a specific problem in the studies of showers occurred when Chudakov and Nesterova[18] set out to obtain information on the vertical structure of showers from the lateral distribution of the light. In this experiment, which was conducted at 3800 m altitude in the Pamir mountains, the locations of the shower cores, and the particle densities, were determined with some precision, using a large array of Geiger counters. Eight light receivers were combined in such a way that only vertical showers were selected, and, of these, only those for which the light intensity could be measured, were used in the analysis. From the results of this experiment, see Fig. 3, in which the light flux ϕ (as a

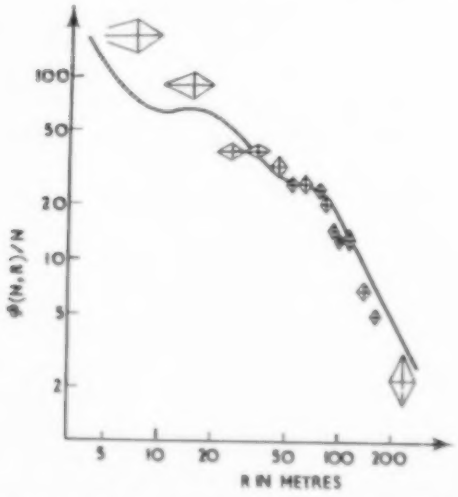

Fig. 3. The lateral distribution of light observed by Chudakov and Nesterova, using eight light receivers and a large counter array.

function of the number of particles N in the shower and the distance of the core from the light receiver R) is plotted as a function of R, Chudakov concluded that information could be deduced about the height of the point of origin of the showers.

More recently, work by Brennan *et al.* in 1958, at sea-level in Sydney, has revealed that the effects of Coulomb scattering of the shower particles play an even more influential rôle than had been suspected; that this is such an important factor became evident from experiments in which two or more light receivers were used whose optic axes were skewed both with respect to each other, and with respect to the axes of the shower cores, determined simultaneously with other instruments. From the results of their experiments, see Fig. 4, it is

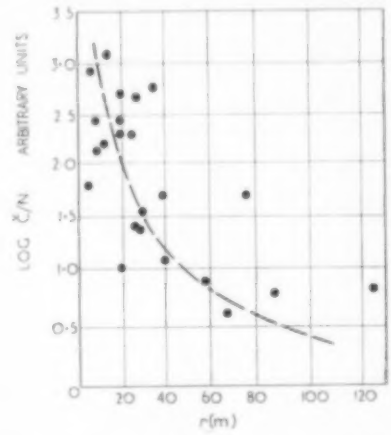

Fig. 4. The ratio of the intensity $\breve{C}$ of light flashes, to the number of particles N in the showers causing the flashes, as a function of the range r from the light receiver at which the shower cores struck the ground. Results obtained by Brennan *et al.* (1958).

evident that although the light intensity falls off with distance from the shower core, it is seen there is a very large spread in pulse height, for a given r; this, which amounts to nearly two orders of magnitude, is attributed to the wide range of scattering angles.

5. FUTURE POSSIBILITIES

In view of the stringent observing conditions required, and the very indirect nature of the information obtained by light receivers in their present form, it is unlikely that their use will seriously compete with the more conventional methods for studying showers. Nevertheless, a large array of light receivers operated in

conjunction with other types of detectors would undoubtedly provide much supplementary information on individual showers, e.g. the vertical density distribution of the particles, the Coulomb scattering itself, the time-spread among the various components of the showers, and possibly the solution of the problem of multiple cores, if these exist. If the largest showers only are selected, i.e. those with energies $> 10^{16}$ eV say, the light receivers can be quite simple, consisting merely of a single photomultiplier and a light screen, with no optical system.

On the technical side, a very attractive possibility is that of measuring the light distribution across the image in the focal plane of a light receiver having a wide field and low distortion, e.g. some form of crude Schmidt telescope used with a pulsed image converter. In this connection it might be mentioned that if the sensitivity of television storage tubes were materially improved, the light distribution over the Čerenkov image might be obtained with such a device, the night sky noise "pile-up" on the storage plate being periodically wiped off at a suitable scanning frequency.

It may be tempting to consider the possibility of detecting the Čerenkov radiation from showers in the microwave region of the spectrum, thereby developing a radiation detector which would not be restricted to operation at night. For this it would be essential to operate at the highest possible frequency, with the widest bandwidth, in a region of the spectrum which coincides with a trough in the atmospheric absorption bands. Although sufficient energy exists in the mm-wave regions, and receivers of adequate sensitivity may soon be available with travelling-wave Masers, one of the main problems is that large collecting areas are associated with narrow beam-widths.

Finally, it must be emphasized that by far the most important single factor which limits expansion of the technique, is the vexed question of atmospheric visibility and climate. Although mountain stations have been found to provide good sites for work of this kind, it would seem that plateaux of moderate altitude situated at low latitudes would provide the optimum conditions. The advantages of such a site may be listed as follows: A plateau provides adequate flat space for a large counter array, the instruments are free from low-level haze, and the twilight periods are of short duration.

REFERENCES

1. P. M. S. Blackett, *Rep. Conf. Gassiot Comm. Phys. Soc.*, p. 34. Physical Society, London (1948).
2. W. Galbraith and J. V. Jelley, *Nature, Lond.* **171** (4347), 349 (1953).
3. B. Rossi and K. Greisen, *Rev. Mod. Phys.* **13** (4), 240 (1941).
4. W. Galbraith, Extensive Air Showers. Butterworths, London (1958).
5. T. E. Cranshaw, W. Galbraith and N. Porter, *Phil. Mag.* **2**, 891 (1957).
6. P. Bassi, G. Clark and B. Rossi, *Phys. Rev.* **92**, 441 (1953).
7. P. A. Čerenkov, *Dokl. Akad. Nauk SSSR* **2**, 451 (1934); *Phys. Rev.* **52**, 378 (1937).
8. I. M. Frank and Ig. Tamm, *Dokl. Akad. Nauk SSSR* **14**, 109 (1937).
9. J. V. Jelley, *Čerenkov Radiation and its Applications*. Pergamon Press, London (1958).
10. H. W. Babcock and J. J. Johnson, *Astrophys. J.* **94**, 271 (1941).
11. K. Chuveyev, *Dokl. Akad. Nauk SSSR* **87**, 551 (1952).
12. V. I. Goldanskii and G. B. Zhdanov, *Zh. eksp. teor. fiz.* **26**, 405 (1954).
13. M. H. Brennan, Ph.D. Thesis, The University of Sydney, Australia (1958).
14. F. R. Barclay and J. V. Jelley, *Nuovo Cim.* **2**, [1], 27 (1955).
15. W. Galbraith and J. V. Jelley, *J. Atmos. Terr. Phys.* **6**, 250 (1955); *Ibid.*, **6**, 304 (1955).
16. N. M. Nesterova and A. E. Chudakov, *Zh. eksp. teor. fiz.* **28**, 384 (1955). *Sov. Phys., J.E.T.P.* **1**, 388 (1955).
17. F. R. Barclay and J. V. Jelley, *The Oxford Conference on Extensive Air Showers*, p. 74. A.E.R.E., Harwell (1956).
18. A. E. Chudakov and N. M. Nesterova, Paper read at the *IUPAP Conference*, Varenna, Como, Italy (1957).

Planet. Space Sci. Pergamon Press, 1959. Vol. 1, pp. 112–120. Printed in Great Britain.

POLARIZATION OF THE RED OXYGEN AURORAL LINE

R. A. DUNCAN

Upper Atmosphere Section, Commonwealth Scientific and Industrial Research Organization, Camden, N.S.W., Australia

(*Received* 29 *December* 1958)

Abstract—During an aurora on 8 July 1958 the zenith 6300 Å oxygen emission was found to be about 30 per cent plane polarized with the magnetic vector North-South. It is shown that such polarization would be expected if the aurora was excited by electrons whose predominant motion was gyration about the geomagnetic field lines.

1. OBSERVATIONS AND GENERAL DISCUSSION

During an aurora, observed near Sydney, Australia, (geomagnetic latitude–42°) on 8 July 1958, the zenith red oxygen emission at 6300 Å was found to be about 30 per cent plane polarized with the magnetic vector North-South.

The record showing this is reproduced in Fig. 1. It was obtained by pointing the photometer, which has an inbuilt polaroid, at the zenith and rotating it back and forth about its vertical axis. At the end of each 360° movement a shutter was closed to give a zero level.

There appears to be no mention in the literature of such polarization having been previously observed.

The green airglow (5577 Å) on the same night was unpolarized, and no other examples of polarization have been found in the course of 280 nights' observation of the green (5577 Å) and 30 nights' observation of the red (6300 Å) airglow since March 1957. It therefore seems unlikely that the polarization on 8 July could have been due to some secondary effect such as atmospheric scattering.

It will be shown that the polarization, with the sense observed, would be expected if the aurora were excited by electrons whose predominant motion was gyration about the field lines.

2. THEORY OF AURORAL POLARIZATION

The red (6300 Å) emission on 8 July was about 60 times as intense as the green (5577 Å). Indeed aurorae seen here are always predominantly red, and it is well known that this is the case at all middle and low latitude stations. This fact suggests a low energy excitation process. Middle latitude red aurorae have been discussed by Seaton[1] and Chamberlain[2]. From their work it would seem that they are excited by electric discharges containing electrons with energies less than 10 eV.

Collisions of such low energy electrons with oxygen atoms will produce excited atoms with spin, and hence magnetic moments, about axes lying mainly in planes normal to the collision direction. If therefore the electron velocities are aligned the excited atoms will be largely aligned and the resultant radiations polarized. The effect has been studied experimentally by Skinner[3] and theoretically by Oppenheimer[4] and Bethe[5].

In the upper atmosphere we must consider the geomagnetic field also. Simple aligned electron beams cannot exist except parallel to the field lines; in general the electrons will travel along helical paths. It is always true however that the electron motion, and consequently the distribution of the magnetic dipoles of the collision excited atoms, is axially symmetrical about the field lines.

As the energy level responsible for the red oxygen emission has a half life of 110 sec (Garstand[6]) the excited atoms will precess about the geomagnetic field many thousands of times before radiation occurs. This will further ensure that the distribution of atomic alignments is axially symmetrical about the field lines.

An excited oxygen atom ($1D_2$) radiates at 6300 Å by means of a magnetic dipole transition, and hence the radiation is emitted predominantly in a direction perpendicular to the magnetic dipole of the atom, and with a magnetic vector parallel to this dipole. The distribution of the polarization of photons observed at the ground therefore corresponds to the distribution of the projections of the atomic magnetic dipoles on a plane normal to the line of sight.

It is clear from this, and from what we have said about the axial symmetry of the distribution, that no polarization will be observed on looking directly up the field. On looking perpendicular to the field lines polarization may be detected. We wish to discover where maxima and minima intensities will be observed as a polaroid is rotated about the line of sight.

Let the distribution of the alignments of the emitted photons in the plane normal to the line of sight be represented by the function $f(\theta)$. That is, let the number of photons with magnetic vectors making angles of between θ and $(\theta+d\theta)$ with the geomagnetic field be

$$I = f(\theta)\, d\theta. \tag{1}$$

Polarization measurements do not distinguish between direct and reversed orientations so that θ is restricted to the range $-\pi/2 < \theta < \pi/2$.

A polaroid with its "magnetic" axis at an angle ϕ to the geomagnetic field transmits a proportion I' of the photons aligned in the direction θ, where to a good approximation

$$I' = \cos^2(\phi - \theta). \tag{2}$$

The total light transmitted will therefore be

$$I'' = f(\theta) \int_{-\pi/2}^{+\pi/2} \cos^2(\phi - \theta)\, d\theta \tag{3}$$

$$\text{i.e.} \quad I'' = \tfrac{1}{2} \int_{-\pi/2}^{+\pi/2} f(\theta)\,[1 + \cos 2(\theta - \phi)]\, d\theta \tag{4}$$

$$\text{i.e.} \quad I'' = K + \cos 2\phi \int_{-\pi/2}^{+\pi/2} f(\theta) \cos 2\theta\, d\theta + \sin 2\theta \int_{-\pi/2}^{+\pi/2} f(\theta) \sin 2\theta\, d\theta. \tag{5}$$

Now the distribution of photon alignment must be symmetrical about the field lines and hence can be expressed as a cosine series

$$f(\theta) = A_0 + A_1 \cos\theta + A_2 \cos 2\theta + \ldots \tag{6}$$

and hence from Fourier's Theorem

$$I'' = K + \pi/2 A_2 \cos 2\phi. \tag{7}$$

Hence maximum intensity will be observed, nowhere, or at polaroid orientations $\phi = 0$ or $\phi = \pi/2$ as A_2 is zero, positive or negative respectively. That is the light will appear to be unpolarized, polarized parallel to the field, or polarized perpendicular to the field, depending on the actual pattern of atomic alignment.

This conclusion has a simple physical interpretation. The polaroid used in our photometer has transmission characteristics close to that represented by equation (2). It thus selects the second harmonic of the photon alignment distribution and there can therefore be only one maximum intensity observed as the polariod is rotated between $\pm 90°$. The only position for this maximum compatible with the symmetry of the phenomena about the field lines is 0° or 90°.

It should be realized however that this result depends on the characteristic of the analysing polaroid. A more selective polaroid might have a transmission law.

$$I' = \cos^4(\phi - \theta)$$

and in this case two maxima could conceivably be observed, i.e. at both 0° and 90°.

It is clear that along lines of sight which are not perpendicular to the geomagnetic field, the amount of polarization will be less; on looking up the field lines it will be zero; but, assuming again now that equation (2) is correct, the direction of polarization will still be parallel or perpendicular to the projection of the field in the plane normal to the line of sight.

We now relate the sense of the observed polarization, i.e. parallel or perpendicular to the field, to the pattern of electron bombardment. Simple classical arguments will be adequate for present purposes. In general the electrons will move along helical paths up or down the field. If the kinetic energy parallel to

the field is a third of the total kinetic energy we may consider the electron velocities to be unaligned. There are two possible departures from such a pattern. The electron motion may be predominantly longitudinal up or down the field, or it may be predominantly gyration about the field.

If the electron motion is along the field lines, electron collision will produce excited atoms with spin axes and hence magnetic dipoles distributed in a plane normal to the field. The resultant radiation will therefore appear to be polarized with its magnetic vector perpendicular to the field.

In the case of electron gyration about the field lines, collision with unexcited atoms will produce excited atoms with spin axes (and hence magnetic dipoles) half of which will be parallel to the field lines. For random orientation only a third of the spin would be parallel to the field. On looking in a direction perpendicular to the field therefore we will see 50 per cent of the atoms with spin parallel to the field but only 25 per cent with spin perpendicular to the field. The remaining 25 per cent will have spin perpendicular to the field but parallel to the line of sight and hence will be ineffective in producing visible radiation. We should therefore expect at the most 60 per cent polarization with the magnetic vector parallel to the field.

This was the sense of the polarization observed on 8 July so it is concluded that the aurora on this night was excited by electrons gyrating around the magnetic field.

Acknowledgements—This work forms part of the research program of the Upper Atmosphere Section of the Commonwealth Scientific and Industrial Research Organization and was undertaken at the initiative of Dr. D. F. Martyn. The photometer was loaned by the U.S. Bureau of Standards as an I.G.Y. contribution. I am indebted to Drs. S. T. Butler, G. R. Ellis and J. H. Piddington for helpful discussions.

REFERENCES

1. M. J. Seaton, *The Airglow and the Aurorae*, p. 225. Pergamon Press, London (1955).
2. J. W. Chamberlain, *The Airglow and the Aurorae*, p. 206. Pergamon Press, London (1955).
3. H. W. Skinner, *Proc. Roy. Soc.* A **112**, 642 (1926).
4. J. R. Oppenheimer, *Z. Phys.* **43**, 27 (1927).
5. H. Bethe, *Handb. der Physik*, 24, Part 1, p. 508. Springer, Berlin (1933).
6. R. H. Garstang, *Monthly Not. R. Astr. Soc.* **111**, 115 (1951).

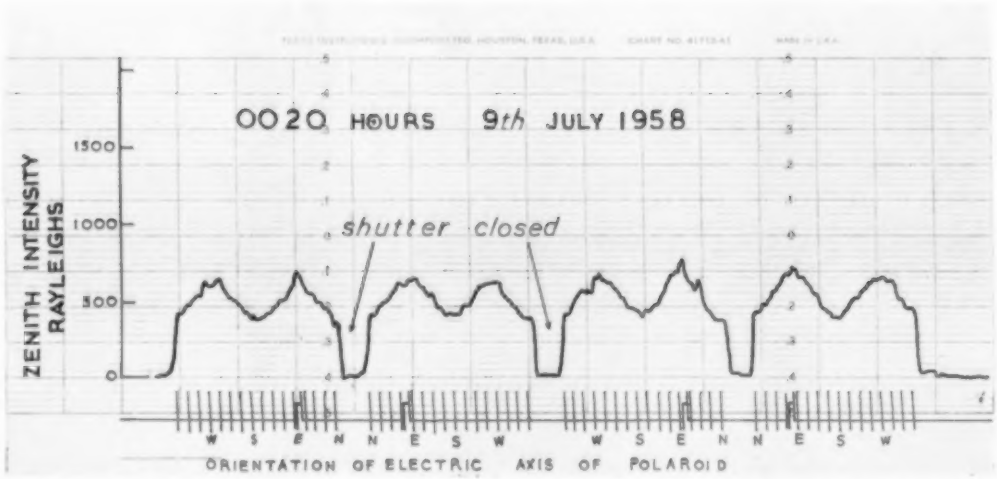

Fig. 1. Record of zenith red (6300Å) airglow intensity. As the photometer with its inbuilt polaroid was rotated a sinusoidal trace was obtained showing that this airglow was plane polarized with the electric vector East-West.

[facing p. 114

Planet. Space Sci. Pergamon Press, 1959. Vol. 1, pp. 115–124. Printed in Great Britain.

OBSERVATIONS OF THE RUSSIAN SATELLITES AND THE STRUCTURE OF THE OUTER TERRESTRIAL ATMOSPHERE

H. K. PAETZOLD

Max-Planck-Institute of Aeronomie, Institute of Physics of the Stratosphere, Weissenau/Württ., Germany

(*Received* 26 *December* 1958)

Abstract—The launching of the artificial earth satellites gave the opportunity to gain some direct information about the outer region of the earth's atmosphere. Our radio observations were mostly made on 20 MHz with a new direction-finder developed by the firm Telefunken in Ulm. This instrument uses three pairs of adcock-antennas. The direction of the wave front and the amplitude of the received signals can be measured at the front of a television tube. A movie-camera registers the pictures with a time resolution of 0·1 sec. The accuracy of the measured azimuths is about 0·5°. For 1957 α_1, 1957 β and 1958 δ_1 optical observations of the German Moonwatch-groups were used. Further orbit data were obtained from the Moonwatch Headquarters, Cambridge, Mass., the Air Force Cambridge Research Center, Bedford, Mass., and the Vanguard Computing Center, Washington.

1. WAVE PROPAGATION AND THE STRUCTURE OF THE IONOSPHERE

A transmitting satellite moving in and above the ionosphere gives information about the vertical and horizontal structure of the latter by studying the propagation of the radio waves. One of the most astonishing facts was the excellent audibility of Sputnik I far beyond the optical horizon in autumn 1957 as shown in Fig. 1a.[1] In general the satellite could be heard when it was over the Northern Hemisphere. On the average audibility was better when the satellite was to the south of the observation point than when it was to the north. An audibility far beyond the optical horizon was also observed at 40 MHz and 108 MHz. In contrast to Sputnik I the third Russian satellite Sputnik III was much less audible in summer 1958 (Fig. 1b).

The nature of this extraordinary wave propagation could be studied by the observations with the direction finder.[2] As an example, in Fig. 2 the observed azimuths are plotted for comparison with the calculated values. Even at great distances a good agreement exists. So the wave propagation must have followed the great circle between the satellite and the receiving station. It is important that in general only one well-defined wave front could be observed. So it is probable that the observed propagation is not caused by reflections but by a lead in the ionosphere due to the refraction. This mechanism only works well if the electron density is sufficiently high and if its decrease with altitude is slow. For the F_2-layer an electron density of 1×10^6 electrons/cm^3 results and a decrease by the factor 2–3 for a step of 200 km upwards is in good agreement with other authors.[3] This propagation works only over large distances if the horizontal structure of the ionosphere is sufficiently homogeneous. In Fig. 1 it is striking that the satellite could not be heard in general beyond the magnetic equator apart from single cases. Very probably the well-known deep valley of the electron density over the geomagnetic equator cuts off the leading effect of the radio waves.

On the other hand, great disturbances were also observed if the satellites were northwards and eastwards of the observation point, very probably due to the more disturbed polar ionosphere. In Fig. 1a the satellite sometimes disappeared abruptly after passing northward, although it could be heard much further away

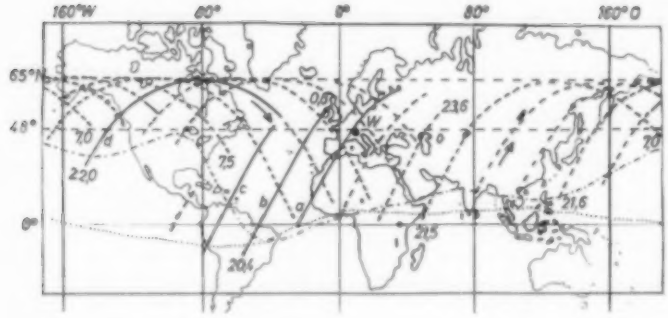

a) Sputnik I, 6/7.10.1957 (20 MHz)

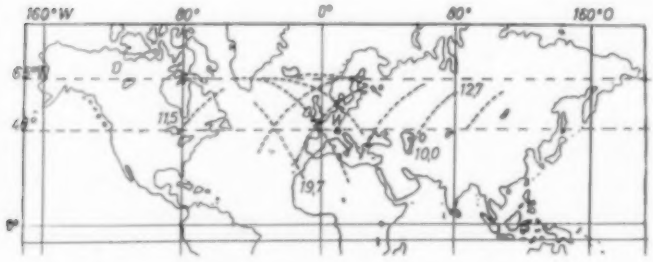

b) Sputnik III, 18/19.5.1958 (20 MHz)

Fig. 1. Audibility of Sputnik I and III. The full and the broken curves give the track, where the satellites could be heard. The dotted curve represents the geomagnetic equator. The figures give the local time.

when in the south. On the other hand, the ionosphere was much more disturbed generally in summer 1958 than in autumn 1957 (Fig. 1b). Finally the audibility was in general better if the orbit was in the night hemisphere. Horizontal gradients of the electron density could be determined by differences between the observed and calculated azimuths as is demonstrated in Fig. 3. In this case the electron density must change by the factor 5 at a horizontal range of 500 km. The scattering of the measured azimuths varies considerably with time and place. Sometimes very strong deviations occur up to 30° for a time of about 30 sec. On account of these irregularities sufficient measurements of the directions on 20 MHz are necessary during the passage of the satellite to avoid significant errors in the determination of time. From our experience the systematic error in time will not be greater than 2 sec if the mean is taken from several passages eastwards and westwards of the place of observation.

These ionospheric inhomogeneities could also be observed by the irregular fadings of the received signals. Their time scale reaches from several minutes down to several seconds, corresponding to inhomogeneities from a few thousand kilometers down to 100 km in size. A very fast fluctuation of the directions could be observed with only 0·3 sec duration as can be seen in Fig. 4. This is the same scale as that of the scintillation of the radio stars.

On the other hand, the regular fadings were of considerable interest; they are shown for a northward passage in Fig. 5 and southward

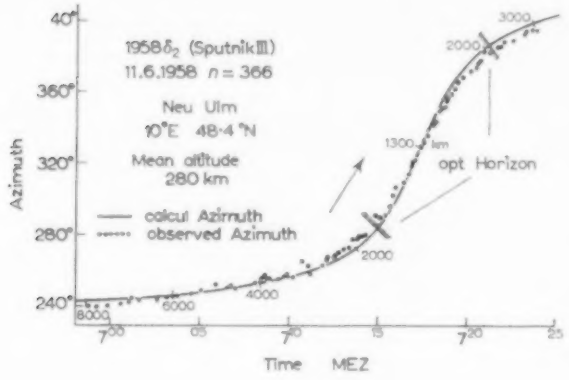

Fig. 2. Bearings of Sputnik III. The figures give the distance in km between the satellite and the observation point.

passage in Fig. 4. For the amplitude a constant period of 4·2 sec and a variable can be distinguished.[4] The constant fading of the signals is combined with a simultaneous fluctuation of the observed direction with a period of 8·4 sec. So the constant fading is very probably due to the spinning antenna-system of the satellite. For the periodical variation of the azimuth the double refraction of the ionosphere is responsible perpendicular to the lines of force in the terrestrial earth field, the so-called Cotton–Mouton effect. The splitting of the refraction parallel to the magnetic lines—the Faraday effect—is represented very probably by the second fading with variable period.[5] It produces a rotation of the polarization plane on account of the displacement of the satellite from the observation place. The frequency f_{Fa} of this Faraday-rotation is given by:

$$f_{Fa} \approx [N_e] \frac{dL}{dt} \frac{f_H \cos\theta}{f^2 - f_H^2 \cos^2\theta} \frac{e^2}{2\pi cm} \qquad (1)$$

$[N_e]$ is the electron density, L the distance

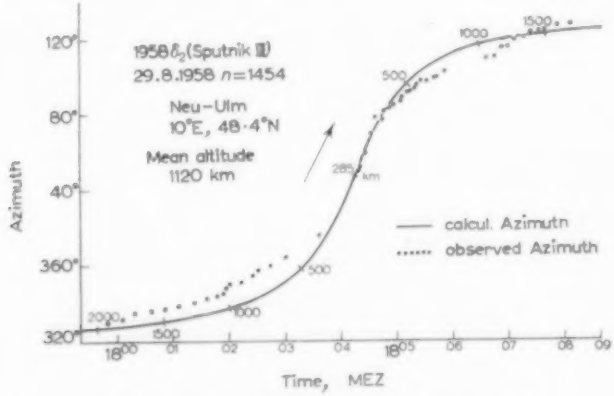

Fig. 3. Discrepancies between the observed and the calculated azimuth.

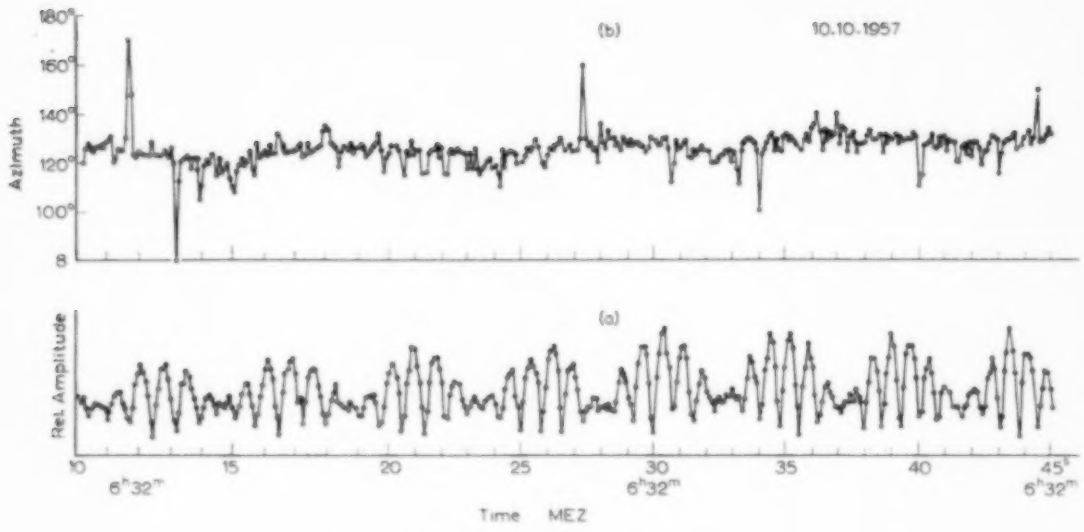

Fig. 4. Fadings of Sputnik I. The satellite is located in the southwest of the observation point going southwards.

between the satellite and the receiving station, θ the angle between the satellite's track and the magnetic lines, f_H the electronic gyro-frequency in the terrestrial magnetic field and f the radio frequency. From this Faraday rotation an electronic density could be derived of 5×10^5 electrons/cm³ at 470 km height in Fig. 1a. From Russian measurements with Sputnik III a value of $1{\cdot}5 \times 10^5$ ions/cm³ was found for an altitude of 790 km.[2] These figures are in good agreement with the above mentioned slow vertical decrease of the electron density.

2. THE DENSITY AND THE STRUCTURE OF THE ATMOSPHERE

From radio measurements with the direction-finder it was possible to determine the deceleration of the satellites $1957\alpha_2$ and $1958\delta_2$ on account of the air drag. For $1957\alpha_1$, 1957β and $1957\delta_1$ optical observations were used.

Let $\overline{F}$ be the effective mean cross-section of the satellite, M its mass, $\overline{h}$ the mean height, e the eccentricity of the satellite's orbit and $\rho(h)$ the air density. In the case of the Sputniks' orbits with their small eccentricity the following good approximation is valid for the decrease of the revolution time P

$$\frac{dP}{dn} = -3P\frac{\overline{F}}{M}\int_{\text{Orbit}}\rho(h)\,ds \tag{2}$$

After the observations the period P can be given by a quadratic formula for the first half of the life time of a satellite:

$$P = P_0 - an - bn^2 \tag{3}$$

The linear coefficient a is determined by:

$$\left(\frac{dP}{dn}\right)_{n=0} = -a = -3P_0\frac{\overline{F}}{M}c(e)\,\rho(h_{Pe})\,2\pi(R+h_{Pe}) \tag{4}$$

with

$$c(e) = \frac{\int\rho(h)\,ds}{\rho(h_{Pe}) < \pi(R+h_{Pe})}$$

where R is the earth's radius and h_{Pe} the perigee's height. The factor $c(e)$ gives the influence of the eccentricity e of the satellite's orbit on the total effective air mass which is hit by the satellite during one revolution[7]. In the possible boundary conditions $c(e)$ does not

depend very strongly on the assumed atmospheric model. So a first approximation can be derived for the atmospheric density $\rho(h_{Pe})$, at the height of the perigee h_{Pe} from equation (4).

The analysis of the quadratic coefficient b in equation (2) is somewhat more difficult because different influences have to be taken into account. Firstly, the height of perigee

In summarizing, the rate of descent of the perigee's height can be written as:

$$\frac{dh_{Pe}}{dh} = \frac{3}{2}\frac{P}{R+\bar{h}} H(h_{Pe}) \frac{1}{a}\left\{\frac{2b}{a} - \frac{1}{c(e)}\frac{dc(e)}{dn} - \frac{df(\varphi)}{dn}\right\} \quad (6)$$

where $H(h_{Pe})$ means the atmospheric scale

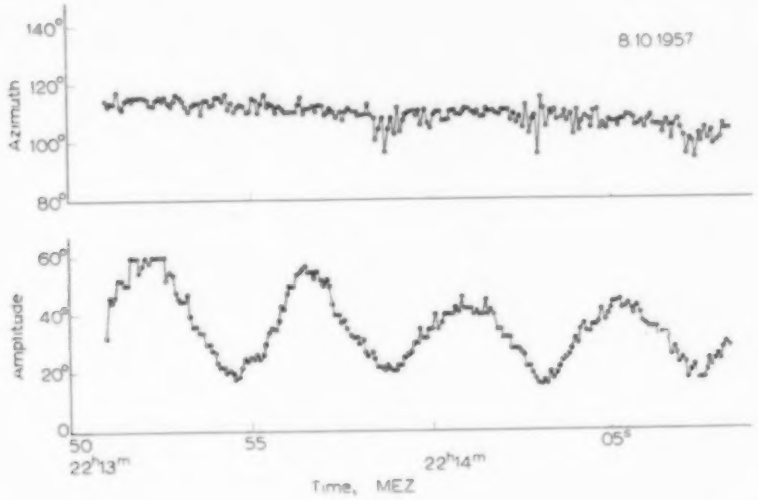

Fig. 5. Fadings of Sputnik I. The satellite is located in the southeast as in Fig. 4, but now going northwards.

decreases slowly by the resistance of air in the vicinity of the apogee so that the air density (h_{Pe}) in equation (4) increases. With sufficient accuracy we can write for the ratio of the rate of descent of the perigee to that of the mean height $\bar{h}$.

$$\frac{dh_{Pe}}{d\bar{h}} = \frac{\int \rho(h)(1-\cos\gamma)\,ds}{\int \rho(h)\,ds} \quad (5)$$

where γ is the angle between the perigee and the satellite. Further, the eccentricity of the orbit decreases and therefore $c(e)$ increases. Finally, the perigee shifts along the orbit and therefore its geographical latitude varies gradually. The effect is a variation of the air density $\rho(h_{Pe})$ on account of the earth's oblateness.

height for the perigee and $f(\varphi)$ the relative variation of the air density $\rho(h_{Pe})$ due to the shifting of the perigee. The second term in the brackets can be calculated with good accuracy. It is small compared with the first term. In Table I the coefficients a and b are given for the Russian satellites following from the mean decrease of the revolution time P for the first half of the life time. With these figures the term $df(\varphi)/dn$ is small relative to the value of $2b/a$ for all Russian satellites except $1958\delta_2$. There are two reasons for this result. First, the shift of the perigee of the Russian satellites is very slow with a rate of only about $0{\cdot}025°$/rev. On the other hand, the perigees moved from northern to lower latitudes where the air density seems to be smaller for a given altitude. (See also

Table 1

Satellite	a (sec rev^{-1})	b (sec rev^{-2})	dh_{Pe}/dh	
			observed	calc. ARDC 1956
1957 α_1	0·220	0·00016	0·21	0·075
1957 α_2	0·140	0·000080	0·19	0·075
1957 β	0·185	0·000053	0·076	0·035
1958 δ_1	0·140	0·000030	0·083	0·031
1958 δ_2	0·050	0·0000065	0·093	0·031

Fig. 7.) So the ratio $2b/a^2$ in equation (6) represents mainly the decrease of the height of perigee due to the deceleration near the apogee.

In equation (5) some uncertainty exists about the scale height $H(h_{Pe})$. The values given by different authors lay between 28 and 45 km. Here a mean value of 35 km was assumed.

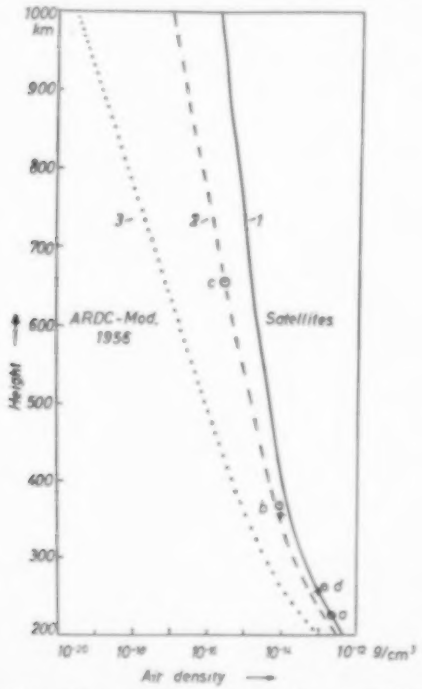

Fig. 6. The air density derived from satellites observations. Curve 1: Russian satellites, Curve 2: American satellites. The points a, b, c, d give the air density at the perigee's height for Sputnik I, III, Explorer I, Vanguard and Explorer IV. The crosses represent values after direct measurements of Sputnik III.

This figure is in good agreement with the air density of $7{\cdot}6 \times 10^{-9}$ g cm^{-3} at 100 km given by the rocket measurements and an air density of $2{\cdot}5 \times 10^{-13}$ g cm^{-3} at 225 km given by the satellites.[2, 7–9] With this value for $H(h_{Pe})$ the velocity of the perigee descent is nearly 3 times greater than follows from the ARDC model (Table 1). It seems impossible to decrease the scale height $H(h_{Pe})$ by such a factor. On the other hand, we have to consider the effect of electrical forces upon the satellite.[10] But after the observed charge accumulation obtained with 1957·δ_2[2] it seems unlikely that this effect will be of great influence. To take it into account the mean effective cross-section, $\bar{F}$ was enlarged by 20 per cent for 220 km and by 60 per cent for 800 km altitude, supposing the influence of the electrical forces will somewhat increase with altitude. These figures do not affect the following results in any way. In Fig. 6 (curve 1) the air density is plotted which results from equations (4) and (6) with the values in Table 2. It is evident that the air density decreases much more slowly with altitude than given by the ARDC model 1956 (curve 3). The curve 1 agrees well with the values of 1958 δ_2 obtained directly with ionization manometers.[2] It is nearly impossible to explain in a reasonable way the rapid descent of the perigee of the Russian satellites with the lower densities formerly adopted.

Above 300 km a somewhat lower air density seems to follow from the deceleration of the American satellites (Fig. 6, curve 2).[11–13] From recent rocket observations there is some evidence that the air density increases towards the poles.[14] This could also be observed by the deceleration of 1958 δ_2 in Fig. 8. As already mentioned the increase of the air drag by the

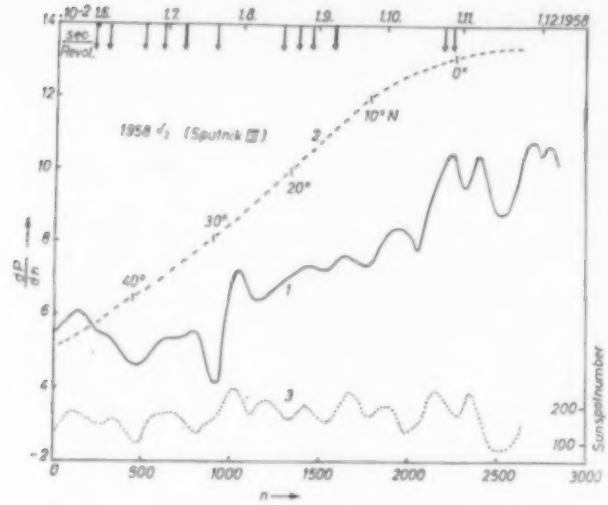

Fig. 7. Fluctuations of the deceleration of Sputnik III. The full curve gives the observed fluctuations, the dotted curve represents the calculated increase of the acceleration, if the density of air were to show no latitudinal variation. Arrows: Magnetic and ionospheric storms. Points: The sunspot number.

shifting of the perigee southwards was much smaller than expected. After Fig. 8 the air density in 225 km at 50°N in May 1958 was nearly 50 per cent greater than at 20°N in October 1958. Regarding the fact that the orbits of the Russian satellites reach much further to the poles than those of the American satellites, the meridian differences in Fig. 6 look quite reasonable. So for mean conditions a polar and an equatorial atmosphere seem to have been distinguished.

In Fig. 8a are given the air temperatures which result from the vertical density distributions. While for an altitude of 1000 km a value of about 1800°K results for the equatorial regions, the temperature seems to climb up to 2500°K in higher latitudes. From this meridional temperature gradient a considerable heat flux must exist from the poles to the equator.

The results above only concern the *mean* conditions of the upper atmosphere. But also considerable variations of the decelerations with time have been observed by several satellites such as 1957 β, 1958 α, 1958 β_2, 1958 δ_1 and 1958 δ_2.[13, 15–19] There is one complication due to the fact that, except 1957 α_2 and 1958 β_2, no satellites are spherical in shape. So the effective cross-section $\bar{F}$ will depend upon the angle between the axes of the satellites and the direction of the track. From the fadings of the radio signals it is very probable that some satellites (1957 α_2, 1958 α)[1] have shown a precession besides spinning. So the effective cross-section will vary in a complicated manner and may show regular periods in time as has been found for 1958 α.[17] But the main part of the variations of the acceleration seems to be irregular. In Fig. 7 the fluctuations of dP/dn are shown for 1958 δ_2 as derived from our radio observations on 20 MHz with the direction finder. It is very interesting that the pronounced decrease during the first half of June 1958 and the following increase at the end of July have been also found for 1958 β_2.[18] Further, 1958 δ_1 with the same orbit but with a different shape shows the same fluctuations as 1958 δ_2. Therefore these irregularities in the main part seem not to be genuine for the

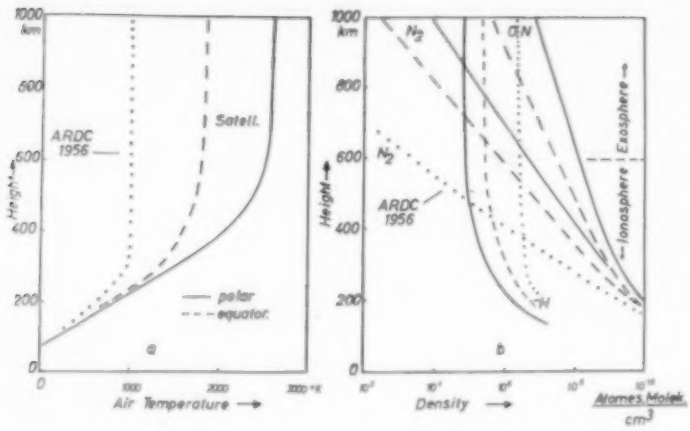

Fig. 8. The composition of the upper atmosphere. The full, dotted and broken curves represent the different atmospheric models.

satellites but are caused by the atmosphere itself. It does not seem plausible that the influence of the electrical forces will vary in such a degree. For all these reasons it is probable that the observed irregularities of the accelerations are caused primarily by variations of the air density itself in the vicinity of the perigee's height. For 1958 δ_2 in Fig. 7 the amplitude amounts nearly to the factor 2 for an altitude of 225 km. For 1958 β_2 air drag was observed to fluctuate by a factor of 4 at 658 km altitude. For still greater altitudes of 1000 km the density may vary in the range 10–100. Assuming an established vertical equilibrium according to the barometric formula the variations of temperature would amount to ± 50 °K for 225 km in Fig. 7. No direct correlations could be found with special events such as magnetic and ionospheric storms (Fig. 7). But there may be a correlation with the sunspot number. For this to have been found valid the density and the temperature of the upper atmosphere must show a considerable variation during the solar cycle. It may be that during the sunspot minimum the atmospheric polar model would look like the equatorial during the solar maximum and that the latter approximates to the ARDC-model 1956.

3. THE STRUCTURE OF THE UPPER ATMOSPHERE

In Fig. 8 the density of the O,N atoms and of the N_2 molecules are given for the two models. It was assumed that the nitrogen is dissociated to 75 per cent. With the new higher temperatures a sufficient density of the N_2 molecules results at 1000 km altitude to explain the strong spectral emission of negative N_2 bands of the high sunlit auroras which was impossible with the ARDC model. A further indication for the higher temperatures is the helium problem.[20, 21] Compared with the amount of production by radioactive decay in the earth's crust a far too small concentration of helium exists. The only way to explain this discrepancy is to assume that a considerable amount of helium escapes to free space. The number of escaping atoms is given by:

$$n_{esc} = n_c \sqrt{\frac{g_c}{2\pi}} \frac{R + h_c}{\sqrt{H_c}} e^{-\frac{R+h_c}{H_c}} \left(\frac{\text{atoms}}{\text{cm}^2 \text{ column sec}} \right) \quad (7)$$

where n_c is the number of atoms per cm^{-3}, g_c the gravitation, H_c the scale height in the critical level with the altitude h_c. The critical level is defined by the condition that the mean free path length shall be equal to the scale height. For a sufficient rate of escape for the

helium component a temperature of about 2000°K results for the critical level in a much higher value than given by the ARDC model.

For the density in Fig. 8 the exosphere will begin at an altitude of about 600 km for the neutral gases. In the outer part of the exosphere the atomic hydrogen will be the predominating part. The strong infra-red emission of OH bands is very probably explained by the reaction:

$$H + O_3 \rightarrow (HO) + O_2$$

From the intensity of OH bands the concentration of the atomic hydrogen results in 10^{-4} for 80 km height.[22] Due to the great difference between the scale height of hydrogen and that of the air a diffusive flux of hydrogen upwards must exist of about $10^9 \frac{\text{H atoms}}{\text{sec cm}^2 \text{ column}}$, which must be equal to the rate of escape according to equation (7). In Fig. 8 the resulting H concentration is also given. We have named this region "outer exosphere", where the H density exceeds that of the heavier gases.[20] In the polar region this outer exosphere would begin at 1600 km while it lies deeper at 1000 km at lower latitudes. Obviously the height where the outer exosphere starts must be very sensitive to the temperature of the exosphere. For the ARDC model with its low temperature the outer exosphere would already begin at 600 km.

But we have to consider that these estimations only give the lower limit of the possible H concentration in the exosphere. There may be a considerable influx of protons from space into the terrestrial atmosphere. One part will come directly from the sun, the other may originate from the interplanetary matter. According to recent observations of the zodiacal light the density of the interplanetary hydrogen can be estimated to about 500 protons cm^{-3} with a temperature of 5000 to 10,000°K.[23, 24] The mechanism of influx of these protons is somewhat complicated on account of the terrestrial magnetic field. The distance r to which the magnetic field influences the interplanetary protons is given by the condition that the density of kinetic energy of the protons relative to the earth shall be equal to the density of the energy of the magnetic field:

$$\frac{H_0}{16\pi}\left(\frac{R}{r}\right)^6 = V_{Pr}^2 m_{Pr} n_{Pr} \qquad (9)$$

where H_0 is the terrestrial magnetic field, V_{Pr} the velocity and n_{Pr} the number per cm^3 of the interplanetary protons. If we assume V_{Pr} to be 30 km sec^{-1}, r is equal to 10 R, so that the effective cross-section of the earth is enlarged by the factor 100. Most of the protons hit by the earth and its magnetic field will be reflected and only a small part may enter the outer atmosphere along the magnetic lines near the poles. This amount may be estimated by the heat balance of the upper atmosphere. It is well known that there exists a heat loss in the upper atmosphere by heat conduction downwards to the lower layers. With the new higher temperatures this flux amounts to 0·4 erg cm^{-2} sec^{-1}.

This value seems to be too large to be balanced by the influx of solar electromagnetic radiation according to the degree of ionization in the F layer. Half of this deficit can be balanced by the influx of interplanetary protons of 10^{10} protons/cm^2 column sec. This is only one-tenth of the total number of protons which are in interaction with the terrestrial magnetic field. The variable corpuscle streams coming directly from the sun will probably partly cause the observed irregular fluctuation of the air density. That there must exist a considerable influx of charged particles in the upper atmosphere is demonstrated by the fact that a pronounced heat flux from the poles to the equator has been established by the observed meridional gradient of air density. The incoming protons will go over the neutral H component beneath the critical layer. So the upper limit of the H concentration may be about 10 times greater than given in Fig. 9. The distance where the number of the neutral H atoms equals the interplanetary protons will vary considerably. The mean value may amount to once or twice the earth's diameter.

There is another interesting point, the ionization of the outer atmosphere. According to the observed wave propagation and the satellite measurements of ions the density of charged

particles decreases much more slowly than that of the neutral components. On the average, the proportion of charged particles is 0·03 per cent at 500 km and 2 per cent at 1000 km. It seems probable that this increase will gradually continue with height up to the total ionization in the interplanetary space. So there may exist also a considerable influx of electrons from outwards.

REFERENCES

1. H. K. Paetzold, *Telef. Hausmitt.* **31,** 100 (1958).
2. V. I. Krassovsky, *Ninth Astronautical Congress,* Amsterdam (1958).
3. H. K. Paetzold, *Umschau* **58,** 1 (1958).
4. J. W. Warwick, *IGY Satellite Rep.* No. 5 (1958).
5. The staff of the Mullard Radio Observatory, Cambridge *Nature, Lond.* **180,** 879 (1957).
6. The staff of the Royal Aircraft Establishment, Farnborough *Nature, Lond.* **180,** 937 (1957).
7. H. K. Paetzold, *Raketentechnik u. Raumfahrtforschung* **2,** 50 (1958).
8. W. Priester, H. K. Bennewitz and P. Lengrüsser, *Radiobeobachtungen der ersten künstlichen Erdsatelliten, Köln* (1958).
9. G. F. Schilling and T. E. Sterne, *IGY Satellite Rep.* No. 4, 30 (1958).
10. R. Jastrow and C. A. Pearse, *J. Geophys. Res.* **62,** 413 (1957).
11. C. A. Whitney, *IGY Satellite Rep.* No. 4, 22 (1958).
12. G. F. Schilling and C. A. Whitney, *Smithson. Inst. Spec. Rep.* No. 18, 13 (1958).
13. H. K. Paetzold and H. Zschörner, *Naturwissenschaften* **45,** 485 (1958).
14. H. E. Lagow, R. Horowitz and J. Ainsworth, *IGY Rocket Report* No. 1, 38 (1958).
15. King-Hele *Nature, Lond.* **181,** 1762 (1957).
16. L. G. Jacchia, *IGY Satellite Rep.* No. 4, 23 (1958).
17. C. A. Whitney, *IGY Satellite Rep.* No. 3, 6 (1958).
18. L. G. Jacchia and R. E. Briggs, *Smithson. Inst. Spec. Rep.* No. 18, 9 (1958).
19. G. Hergenhahn, *Naturwissenschaften* **45,** 434 (1958).
20. H. K. Paetzold, *Tangungsbuch Deutsche Phys. Gesellschaft* 63, München (1956).
21. M. Nicolet, *Ann. Géophys.* **13,** 1 (1957)
22. H. K. Paetzold, *Z. Naturf.* To be published (1958).
23. A. Behr and H. Siedentopf, *Z. Astrophys.* **32,** 19 (1953).
24. E. Elsässer, *Z. Astrophys.* **33,** 274 (1953).

Planet. Space Sci. Pergamon Press, 1959. Vol. 1, pp. 125–129. Printed in Great Britain.

AMBIPOLAR DIFFUSION OF A METEOR TRAIL AND ITS RELATION WITH HEIGHT

E. L. MURRAY

Physics Department, University of Adelaide

(*Received* 30 *December* 1958)

Abstract—Investigation of the relation between the ambipolar diffusion coefficient, D, of a meteor trail and height shows that considerable random fluctuations occur. It is however possible to obtain a statistical relation between these parameters. Regression lines have been derived for the relation between $\log D$ and height and it is shown that care must be exercised in the correct choice of the two possible regression lines.

1. INTRODUCTION

Weiss[1], and Greenhow and Neufeld[2] have shown how the ambipolar diffusion coefficient, D, of an ionized meteor trail may be obtained from the amplitude records of radio detection equipment. If the height of each meteor is known, it is easy to obtain a relation between D and height, and Greenhow and Neufeld have shown how the height of a meteor trail may be estimated from the decay time of the echo, by carrying out a calibration test in conjunction with the height measuring system described by Clegg and Davidson[3] and Evans[4]. Because of the inherent scatter in the results the calibration is statistical in nature and it is important to remember the fundamental limitations of the data presented. Essentially, Greenhow and Neufeld present their data as the regression of height on the logarithm of the echo duration, and because of the relation between echo duration and diffusion coefficient this same relation gives, with a change of scale, the regression of height on the logarithm of the diffusion coefficient.

Because of the theoretical interest in the variation of diffusion coefficient with height, such measurements are of considerable importance, but in this case the required regression is that of $\log D$ on height. The difference between the two regression lines lies in the choice of the dependent and independent variables. In discussions of the variation of D with height, height is the independent variable. In contrast, the analysis given by Greenhow and Neufeld takes the duration as the independent variable so that height becomes the dependent variable. This procedure is quite correct for their particular application where the duration is known and the best estimate of the height of reflection is required, but it is not correct to interpret the same relation as giving the best estimate of the diffusion coefficient as a function of height. It is more appropriate to follow the method of Weiss[1] who derived a relation between $\log D$ and height from the records of the Adelaide meteor wind equipment. In the present paper a larger sample of Adelaide data is presented and the difference between the two regression lines is demonstrated.

2. METHOD OF MEASUREMENT

It is now generally accepted that the decay of the radio echo from a meteor trail is mainly due to ambipolar diffusion[5, 6]. Herlofson[7] has shown that the decay of the echo amplitude is given by

$$A = A_0 \exp(-16\pi^2 Dt/\lambda^2) \qquad (1)$$

where A_0 is the initial amplitude at time $t=0$, and A is the amplitude at time t. Thus with a given radio equipment operating at a wavelength λ, the echo duration is determined by the diffusion coefficient D. We may express the diffusion coefficient in terms of τ, the time for the amplitude to decay to $1/e$ of its initial value:

$$D = \lambda^2/16\pi^2\tau \qquad (2)$$

While the above applies only to the short, decay type echoes, it can be made a general relation if the time origin for A_0 is chosen appropriately.

Throughout this paper the decay time of the meteor echo has been interpreted directly as a diffusion coefficient, according to relation (2). Since there is no reason to doubt this relation, the units of diffusion coefficient have been used in order to stress the fundamental concept rather than the less meaningful unit of decay time. It must be stressed, however, that it is really the decay time which is measured and the direct interpretation of this in terms of diffusion coefficient is merely one of convenience. Should the validity of this relation be questioned, it is then necessary to consider the variable to be $1/\tau$ rather than D.

The method of analysing the meteor echoes follows that detailed by Weiss[1]. The diffusion coefficients are deduced from the records obtained at Adelaide using a C.W. technique at a wavelength of 11·2 m, as described by Robertson, Liddy and Elford[6]. Including those from the work of Weiss,* a total of 1800 echoes have been measured for diffusion coefficients and the combined data have been subjected to a more extensive analysis. The regression lines have been recomputed to give a more complete picture of the relations between diffusion coefficient and height. The rate of decay is determined by measurement of the amplitudes of successive maxima and minima of the doppler beat pattern. While this method of measurement is much more tedious than simply measuring the decay time to half amplitude, it permits the rejection of those echoes which do not show a true exponential decay. Some disturbing influences, such as wind shear, give rise to multiple reflections which modify the simple exponential decay law. Often such echoes are not easily detected by visual inspection of the echo waveforms.

3. THE ANALYSIS OF THE DATA FOR REGRESSION

Plotting of the corresponding values of diffusion coefficient and height for a large number of meteor echoes gives a scatter diagram which shows that while the trend is for high values of the diffusion coefficient to be associated with the greater values of height, there is a considerable scatter in the individual points. Such a plot is given in Fig. 1 which details the diffusion coefficients for more than 500 sporadic echoes which were recorded during September 1953. Since the height is measured to an accuracy of ± 1 km the scatter due to this source of error is at least an order of magnitude below that necessary to explain the scatter in the observations. Since the results quoted in Section 3 show significant linear correlation between $\log D$ and h, we must look for some other explanation of the scatter. The possibilities may be summarized: —

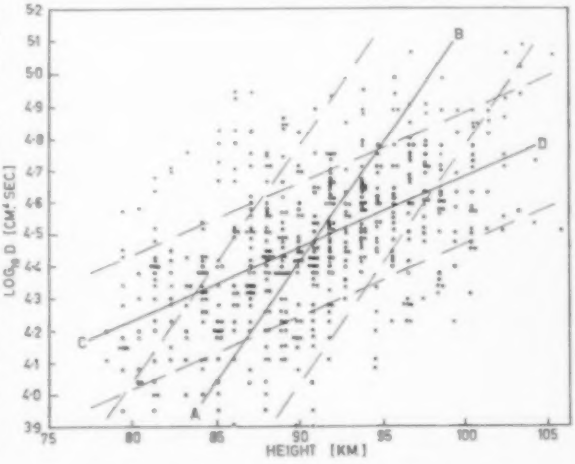

Fig. 1. The distribution of the diffusion coefficient D as a function of height for sporadic meteor echoes recorded during September 1953. The regression of height on $\log D$ (AB) and the regression of $\log D$ on height (CD) are shown together with the appropriate standard deviation limits.

* An error was made in some of the results tabulated in Table 1 of Weiss' paper. The slopes given for the regression of $\log_e D$ on height are all too high by a factor e. This error was introduced during the final reduction for publication and apart from the fact that it reduces the agreement between the slope of the measured and theoretical curves of his Fig. 3, the general conclusions of that paper are not affected.

1. That the scatter may be due to the dependence of D on some factor which varies independently with height, for example, small scale atmospheric variations or magnetic effects,
2. That instrumental errors are involved in the measurement of D.

Considering the first possibility, we have from the existing theory, vide Weiss[1],

$$D = 1{\cdot}13 \times 10^{-3} T^2 / p \text{ cm}^2 \text{ sec}^{-1} \qquad (3)$$

where T is the temperature of the region in °K and p is the pressure in mm Hg. Thus D actually depends fundamentally on the value of T and p but since the variations of T and p with height are reasonably well known, we may interpret this as a dependence of D on h directly. However, appreciable departures from the assumed temperature and pressure profiles will be reflected as a scatter in the measured values of D. This possible source of scatter was kept in mind during the analysis since it is known that hour by hour values of temperature do fluctuate, especially in the region of the temperature minimum at 80 km[9]. If this were a source of scatter then two echoes which occurred within a minute or so of each other at approximately the same height should show good agreement in their values of D. In fact, there appears to be just as large a scatter between such echoes and others which are further apart in time. This suggests that either the temperature and pressure fluctuations are not the main cause of scatter or else that an almost unbelievably fine scale of detail exists in the upper atmosphere. Magnetic effects have been suggested as a possible cause of scatter but it has not been possible to isolate any scatter as due to magnetic influence. One would expect that the magnetic influences on meteor trails with the same radiant and in the same position in the sky should be identical, yet under these conditions there is no indication of reduced scatter. There is also a significant diurnal variation in the values of diffusion coefficient which is not predicted by the existing theory. In general the highest values of the diffusion coefficient occur between 0200 and 0400 hr local time and the lowest between 1600 and 2000 hr, but it is difficult to trace a pattern from one season to the next. For example, in June and September 1953, the effect becomes more pronounced at the greater heights whereas December 1952 shows very little diurnal variation at the greater heights and March 1953 does not show any clearly defined pattern. Thus it still remains to establish whether this variation is due to a seasonal effect or to some random influence.

The above suggests that errors in recording should be considered as a source of scatter, but a careful evaluation of possible errors involved can neither explain nor reduce the scatter. Even the most rigorous selection of "perfect" echoes does not effect the scatter.

Because of the scatter it is obvious that the interdependence of D and h must be established on a statistical basis. The theory of regressions is applicable to this case if it is assumed that the variations from the regression line are random and are approximately normally distributed. It is not necessary to assume a rigidly normal distribution and the distribution of $\log D$ is sufficiently close to normal for the purpose of a regression analysis. Because of the relatively small error inherent in the height measurement it is not necessary to consider the height measurements as subject to random fluctuations. If we wish to find the variation of $\log D$ with height, we must take height as the independent variable and $\log D$ as the dependent variable in order to find the regression of $\log D$ on height. In terms of the usual statistical notation[10], we have for the regression of $\log D$ on h: —

$$(\log D - \overline{\log D}) = b\,(h - \bar{h})$$

where

$$b = \frac{\Sigma\,\{(\log D - \overline{\log D})\,(h - \bar{h})\}}{\Sigma\,(h - \bar{h})^2}$$

As an alternative procedure we have the regression of height on $\log D$: —

$$(h - \bar{h}) = b'\,(\log D - \overline{\log D})$$

where

$$b' = \frac{\Sigma\,\{(\log D - \overline{\log D})\,(h - \bar{h})\}}{\Sigma\,(\log D - \overline{\log D})^2}$$

The latter assumes that $\log D$ is the independent variable and that h is the dependent variable.

Thus the value of $\log D$ is assumed to be accurate and the variation is considered to be due to an uncertainty in the height. This approach is without basis unless it is necessary to estimate the height only from the knowledge of the diffusion coefficient. Such is the case of the experiment described by Greenhow and Neufeld.

Plotted in the $\log D$–h plot of Fig. 1, the slopes of the regressions of $\log D$ and h and of h on $\log D$ have respectively slopes of b and $1/b'$. The ratio of the slopes b and $1/b'$ is the square of the correlation coefficient r.

$$r^2 = bb'$$

It will be seen that when the correlation coefficient is unity the two regression lines are identical, but for a scatter such as that shown in Fig. 1 the correlation coefficient is approximately 0·55 and the ratio of the regression slopes is 0·30. Clearly there is a significant difference between these two regression lines and it is important to choose the correct line for a particular application.

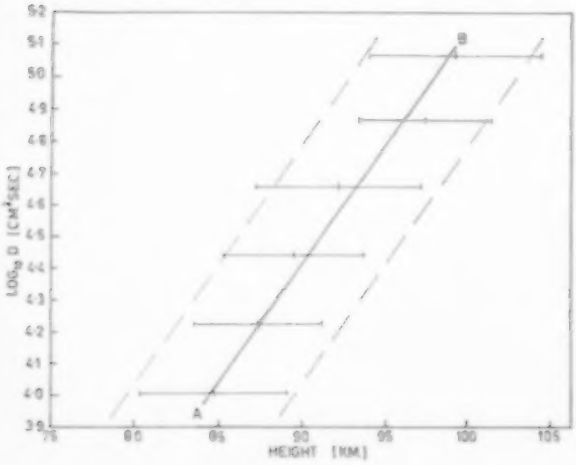

Fig. 2. The regression of height on log D (AB) is compared with the individual results of Greenhow and Neufeld's height-duration experiment at a wavelength of 8·27m. Greenhow and Neufeld's mean height spread (horizontal bars) argees well with the standard deviaton of the Adelaide resuits.

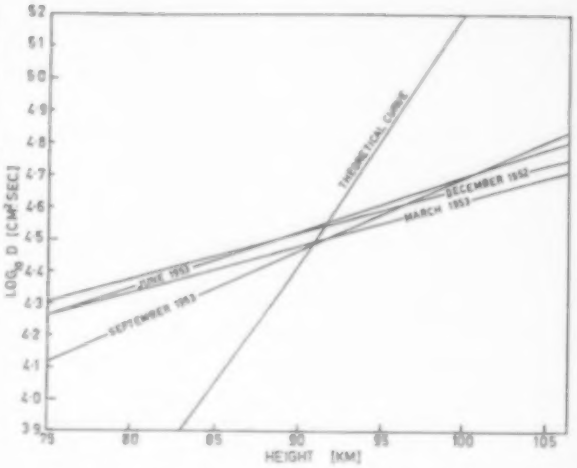

Fig. 3. The results of Table 1 are compared with the theoretical curve derived from the ARDC Model Atmosphere (1956) according to equation (3).

4. RESULTS

The regression of $\log D$ on h for sporadic echoes during the months of December 1952 and March, June and September 1953 have been analysed and results are contained in Table 1. Fig. 3 compares the experimental results with the theoretical relation of equation (3). Values of temperature and pressure were obtained from the ARDC Model Atmosphere (1953). Because the records for September contain more useable echoes than the other months, this month was chosen for a more detailed investigation. Both regression lines for this month are shown in Fig. 1. While the regression of h on $\log D$ is of little general interest, it does afford a good confirmation of the results obtained by Greenhow and Neufeld. In Fig. 2 the regression of h on $\log D$ for September 1953 is compared with the results quoted in their paper for the 8·27 m equipment. In both Figs. 1 and 2 the standard deviation limits are indicated on each side of the regression lines and it will be seen that there is excellent agreement with the results of Greenhow and Neufeld. This fact lends weight to the assumption that if Greenhow and Neufeld's results had been analysed for the dependence

Table 1. Regresssion Analysis for Sporadic Echoes

$$\mathrm{Log}_{10} D - \overline{\mathrm{Log}_{10} D} = b(h - \bar{h})$$

Month	No. of echoes	$\overline{(\log_{10} D)}$ log (cm^2 sec^{-1})	$\bar{h}$ (km)	b Regression slope of $\log_{10} D$ on height	Standard deviation of $\log_{10} D$ about regression
December 1952	370	4·546	91·1	0·0144 ± 0·0016	±0·172
March 1953	322	4·501	91·1	0·0147 ± 0·0022	±0·221
June 1953	372	4·522	89·6	0·0173 ± 0·0021	±0·208
September 1953	539	4·485	90·7	0·0233 ± 0·0019	±0·210

Additional information for September 1953

Regression of h on $\log_{10} D$: $b' = 12{\cdot}9$
Slope of regression of h on $\log_{10} D$: $1/b' = 0{\cdot}0777 \pm 0{\cdot}0019$
Correlation coefficient: $r = 0{\cdot}55$
Standard deviation of h about the regression of h on $\log_{10} D = 4{\cdot}9$ km

of D on h, the results would have been in agreement with those quoted here for the Adelaide data.

The effects of the meteor showers which were present during the months of December and June have been eliminated by neglecting the times when shower meteors were superimposed on the sporadic background. Weiss has recorded the fact that the Geminid meteor echoes for December 1952 showed a significantly higher regression slope than do the non-shower meteors. This effect has also been found again in 1953 records by comparing the Geminid echoes with the sporadic background.

5. CONCLUSIONS

A larger sample of echoes and careful selection for echoes showing pure exponential decay has confirmed the reality of the scatter found by Weiss[1]. The source of the scatter is still unexplained although a small part is due to the diurnal variation. Because of the scatter extreme caution must be exercised in applying the measured diffusion coefficients to physical problems of the atmosphere.

Acknowledgements—The author wishes to thank Professor L. G. H. Huxley for the facilities to carry out this work, Dr. A. A. Weiss for valuable discussion and advice and both Dr. Weiss and Dr. W. G. Elford for making available their records.

REFERENCES

1. A. A. Weiss, *Aust. J. Phys.* **8**, 279 (1955).
2. J. S. Greenhow and E. L. Neufeld, *J. Atmos. Terr. Phys.* **6**, 133 (1955).
3. J. A. Clegg and I. A. Davidson, *Phil. Mag.* **41**, 77 (1950).
4. S. Evans, *Mon. Not. R. Astr. Soc.* **114**, 63 (1954).
5. L. G. H. Huxley, *Aust. J. Sci. Res.* A **5**, 10 (1952).
6. T. R. Kaiser, *Advanc. Phys.* **2**, 495 (1953).
7. N. Herlofson, *Rep. Progr. Phys.* **11**, 444 (1948).
8. D. S. Robertson, D. T. Liddy and W. G. Elford, *J. Atmos. Terr. Phys.* **4**, 255 (1953).
9. Rocket Panel, *Phys. Rev.* **88**, 1027 (1952).
10. R. A. Fisher, *Statistical Methods for Research Workers* (12th ed). Oliver and Boyd, London (1954).

Planet. Space Sci. Pergamon Press, 1959. Vol. 1, pp. 130–135. Printed in Great Britain.

ABSORPTION AND ELECTRON DISTRIBUTION IN THE F_2 LAYER DETERMINED FROM MEASUREMENTS OF TRANSMITTED RADIO SIGNALS FROM EARTH SATELLITES

A. N. KAZANTSEV

Academy of Sciences of the U.S.S.R., Moscow

(*Received* 17 *January* 1959)

Abstract—Comparison is made between measured field strengths of transmitted signals from earth satellites and those theoretically predicted when the transmitter position is in the region of maximum electron concentration of the F_2 layer, below it, and above it. The observed absorption value agrees best for a biparabolic distribution with exponential continuation with $K = 8 \times 10^{-3}$ where the electron concentration is given by $N = N_0 e^{-kh}$. The number of electrons per column in the upper region of the F_2 layer is deduced to be $1{\cdot}5 \times 10^{13}$ electrons per cm^2. This value is compared to the findings of Burgess. Curves are given of field strengths at distances greater than 10,000 km. At distances of 16,000 km the formation of ionospheric wave guides make possible the transmission of radio signals.

1. FORMULATION

The present paper is concerned with one of the methods used in the treatment of results of radio observations from the artificial earth satellites. This method consisted in determining the absorption coefficients of radio waves according to the electric field strength measurement data provided by the comparator centers.

Analysis of the results of measuring the field strength of the radio signals from the satellites and of the absorption coefficients calculated on the basis of these measurements makes it possible to draw a number of conclusions concerning the ways of short wave propagation and their absorption in the whole thickness of the ionosphere as well as in its separate regions. In analyzing the results of measurements, a method of comparing the experimentally-found absorption coefficients with those calculated theoretically by the methods of Kazantsev[1] was employed.

To estimate the absorption coefficients in the F_2 layer a height of 300 km and a kinetic temperature of 1000°K were used. Above 300 km a temperature gradient of 3·5°C per km was assumed. The same gradient has been observed in the lower regions of 100 to 300 km[2]. Comparison of the experimentally obtained and calculated data makes it possible to attain a more specific understanding of the ionosphere structure.

Using the analysis of Kazantsev[1] for electric field strength measurements at 20 Mc/s, a detailed analysis was made of the data obtained during the first three days of the artificial satellite's flight (5, 6 and 7 October), since these data are the most complete and reliable. As far as the second artificial satellite is concerned, the analysis was made of the data received from the Moscow comparator center for the 3, 7 and 8 November. For each time corresponding to a field strength measurement, the geographic location, height, and distance of the satellite from the comparator center were determined. On the analysis of the results of the field-strength measurements, it is necessary to consider three kinds of distances from the satellite to the observation station:

(1) Short distances, at which the observation station was in the zone of direct visibility determined by the height of the satellite's flight.

(2) Medium distances (from the boundary of direct visibility range up to about 6000 km), over which the waves propagate by way of successive reflections from the ionosphere and the earth's surface.

(3) Long distances (more than 6000 or 8000 km) involving the region of the waveguide-type radio propagation.

Fig. 1 shows experimental data on the field strength measurements as well as the calculated curve for relatively short distances.

2. ANALYSIS OF THE DATA RELATED TO THE DIRECT VISIBILITY REGION

As is generally known, the orbit perigee of the artificial earth satellites is in the Northern Hemisphere. Therefore, at certain time intervals in this hemisphere, the satellite was below the electron concentration maximum of the F_2 layer; at other times it was above; and at still others, near it.

Thus an opportunity arises to detail the absorption suffered by radio waves during their passage through the whole thickness of the F_2 layer and even in its separate regions, which are located lower or higher than the electron concentration maximum, and to draw conclusions on the upper half of the layer which is inaccessible for radio probing from the ground. Such an analysis is feasible only by means of measurements relating to the zone of direct visibility, since at greater distances conditions become considerably complicated due to the reflections from the ionosphere and the ground.

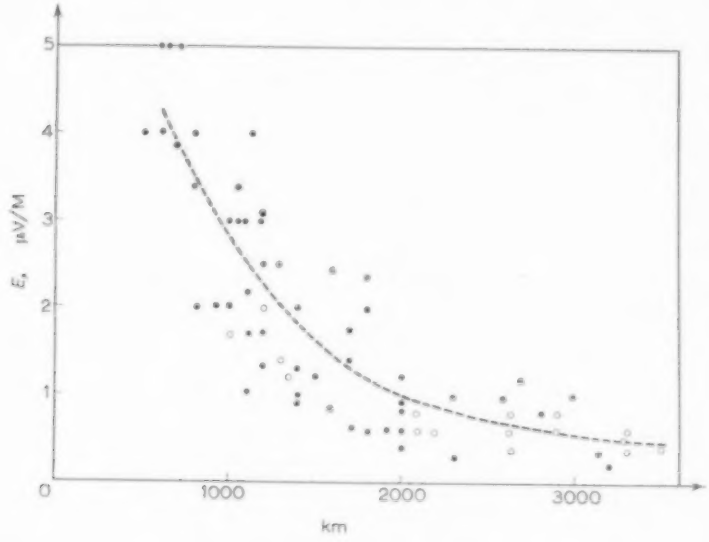

Fig. 1. Field strength of the transmitters of the first and second satellites. The satellites below F_2 layer; f=20 Mc/sec.

Experimental data
- Moscow, satellite I
- Khabarovsk, satellite I
- Moscow, satellite II

calculated

To determine the absorption in the F_2 layer and its separate parts it is necessary to have three curves drawn on the basis of experimental data:

(1) A curve of field strength as a function of distance when the satellite was below the F_2

maximum electron concentration by approximately one half-thickness (h_m) of this layer, i.e. at the base of the layer.

(2) A curve of field strength as a function of distance when the satellite was above the F_2 maximum by approximately a half-thickness. The half-thickness (h_m) is to be determined as in (1) above.

(3) A similar curve for the case when the satellite was near the maximum of electron concentration.

The curves for the median values of the field strength as a function of distance for all the three indicated positions of the satellite are given in Fig. 2.

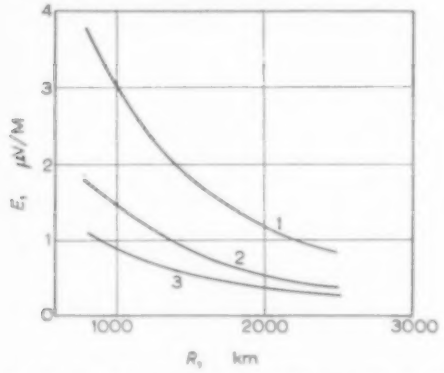

Fig. 2. Median curves of the field strength, f=20 Mc/sec. 1—satellite below F_2 layer, 2—satellite near the F_2 layer maximum, 3—satellite above the F_2 layer maximum.

Absorption coefficients were determined from these three curves according to the formula

$$E = E_0 e^{-\Gamma} \qquad (1)$$

where E is the value of the measured field strength taken from each of the curves in Fig. 2 for various distances; E_0 is the "unabsorbed field strength" determined for the range "by the beam" (taking account of the distance over the major circle arc and of the satellite's altitude); and Γ is the integral absorption coefficient of radio waves in the ionosphere.

The results available were compared for distances ranging from 800 up to 1600 km over the surface of the earth, because at greater distances the reception point is outside the zone of direct visibility for the satellite's position at the lower base of the F_2 layer. The curves in Fig. 3 show the results of determining the

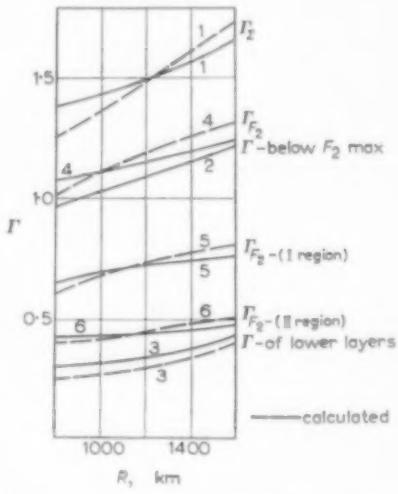

Fig. 3. The absorption coefficients of different layers of the ionosphere:—experimental data, — — — calculated.

absorption coefficients for different ionosphere regions at distances from the reception points to satellites lying within the limits of 800 to 1600 km.

Curve 1 gives a summarized absorption coefficient for the whole ionospheric region, i.e. from its lower boundary to the height exceeding the electron concentration maximum level in the F_2 layer by a half-thickness of this layer.

Curve 2 represents the overall absorption coefficient for the whole ionospheric region below the electron concentration maximum of the F_2 layer (i.e. absorption in the lower half of the F_2 layer and underlying layers).

Curve 3 determines the absorption in the region lying beneath the origin of the F_2 layer (i.e. in the layers F_1, E, and D).

Curve 4, representing the difference between curves 1 and 3, gives the value of radio wave absorption in the F_2 layer (determined as the region lying within heights from $h_{max} - h_m$ to

$h_{max}+h_m$, where h_{max} is the height of the electron concentration maximum).

Curve 5, the difference between curves 2 and 3, indicates the value of absorption in the lower half of the F_2 layer.

Finally, curve 6 (which is the difference between curves 1 and 2) gives the magnitude of absorption in the upper half of the F_2 layer (from h_{max} to $h_{max}+h_m$).

It should be noted that absorption of the radio waves passing through the F_2 layer is considerably higher than the absorption in lower layers, which depends on the effective number of collisions (generally between electrons and neutral molecules) and on the electron concentration of these layers (to put it differently, by the critical frequency). But the critical frequencies of lower layers in October and November during the morning hours (from 8 to 9 a.m., local time), were not high and could not effect a greater absorption, especially at such a high operating frequency as 20 Mc/s.

On the contrary, absorption in the F_2 layer, conditioned by collisions of electrons with ions, was relatively very great, since it is determined by the electron and ion concentrations. In other words, absorption in the F_2 layer is determined by critical frequencies of the F_2 layer which were exceptionally high during these months, especially as the observed maximum of solar activity was extremely high. In addition to the absorption coefficients obtained from experimental data, Fig. 3 represents curves obtained theoretically (dashed curved 1′, 3′, 4′, 5′, 6′). For the purpose of comparison, Fig. 4 displays curves calculated on the basis of different distribution laws of electron concentration in the F_2 layer.

Thus, curve 2 is calculated on the basis of the law governed by the formula

$$N=N_{max}\left(\frac{2h}{h_m}-\frac{h^2}{h_m^2}\right)^2 \qquad (2)$$

For short, we shall call the curve of the fourth order, determined by this formula, a "biparabola". Curves 3 and 4 in Fig. 4 are calculated on the basis of the assumption that the F_2 layer is biparabolic within the altitude range from $h=0$ to $h=3/2\,h_m$ (starting from the lower boundary of the layer), and then continues according to the exponential law:

$$N=N_0e^{-Kh} \qquad (3)$$

The values of K were taken equal to 2×10^{-2} for curve 3 and 8×10^{-3} for curve 4.

Fig. 4 also shows curve 5 drawn on the assumption that electron concentration in the lower half of the F_2 layer varies with altitude

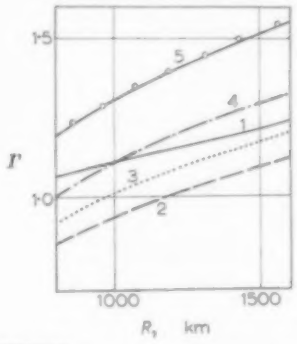

Fig. 4. The absorption coefficients of the F_2 layer. 1—experimental curve, 2—Biparabola, 3—Biparabola with exponential, continuation at $K=2\times10^{-2}$, 4—Biparabola with exponential continuation at $K=8\times10^{-2}$, 5—Bipatabola with exponential continuation at $K=4\times10^{-3}$.

according to the biparabolic law, while in the upper part it follows the exponential law ($K=4\times10^{-3}$). Patterns corresponding to the curves 2, 3, 4, and 5 of Fig. 4 are shown in Fig. 5.

After consideration of the curves shown in Fig. 4, it is evident that the absorption value observed in the F_2 layer agrees closest with the biparabolic pattern with exponential continuation at $K=8\times10^{-3}$ (curve 4 in Fig. 4). On the basis of this pattern, calculations were also made for dashed curves in Fig. 3, which show a good agreement with the absorption coefficient curves drawn on the basis of experimental data for different regions of the ionosphere.

Let us estimate, according to this pattern, the number of electrons in the vertical column of the ionosphere with a cross-section of 1 cm². In doing so we would mean the F_2 layer, as the lower layers play a minor rôle in this case.

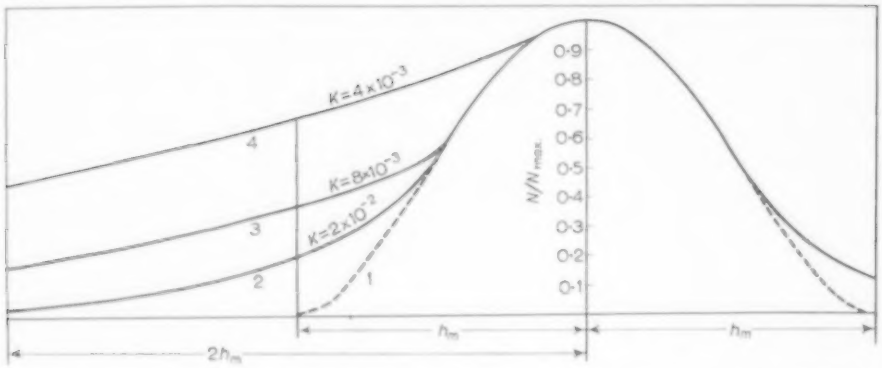

Fig. 5. F_2 layer patterns. 1—Biparabola, 2—Biparabola with exponential continuation at $K=2\times10^{-2}$, 3—Biparabola with exponential continuation at $K=8\times10^{-3}$, 4—Biparabola with exponential continuation at $K=4\times10^{-3}$.

For the lower half of the F_2 layer, where the distribution of electron concentration is assumed to follow the biparabolic law, we shall obtain

$$\int_0^{h_m} N dh = N_{max}\int_0^{h_m}\left(\frac{2h}{h_m}-\frac{h^2}{h_m^2}\right)^2 dh = \frac{8}{15}N_{max}h_m \quad (4)$$

According to the data of ionospheric measurements, the average value of electron concentration maximum during measurements can be taken equal to

$$N_{max} = 16\times10^5 \text{ electrons/cm}^3$$

and the half-thickness of the F_2 layer

$$h_{max} = 120 \text{ km} = 1{\cdot}2\times10^7 \text{ cm}$$

consequently:

$$\int_0^{h_m} N dh = 10^{13} \text{ electrons/cm}^2$$

Now we shall find the number of electrons for the region above the F_2 layer maximum. We have assumed that within the interval of heights from h_m to $3/2h_m$ the layer remains biparabolic. It follows consequently:

$$\int_{h_m}^{3/2h_m} N dh = N_{max}\int_{h_m}^{3/2h_m}\left(\frac{2h}{h_m}-\frac{h^2}{h_m^2}\right)^2 dh =$$

$$= \frac{203}{480}N_{max}h_m \cong 7\times10^{12} \text{ electrons/cm}^2 \quad (5)$$

For an exponential continuation of the F_2 layer at heights above $3/2h_m$ which we take as zero height, to the height H over this level, we shall get

$$N_0\int_0^H e^{-Kh}dh = \frac{N_0}{K}(1-e^{-KH}) \quad (6)$$

where $N_0 = 0{\cdot}5625\,N_{max}$.

With $H = 120$ km (500 km above the ground):

$$\frac{N_0}{K}(1-e^{-KH}) \cong 8\times10^{12} \text{ electrons/cm}^2. \quad (7)$$

Consequently, in the upper region of the F_2 layer (up to the indicated height) the number of electrons in the air column with a cross-section of 1 cm^2 is equal to $\sim 1{\cdot}5\times10^{13}$ electrons/cm^2.

It is of interest to compare these results with those obtained by Dr. B. Burgess[3] who employed the method based on recording rhythmical field fadings of the first Soviet Sputnik caused by rotation of the polarization plane of radio waves. Burgess found that the overall number of electrons in the vertical ionospheric column up to the altitude of the satellite (450–500 km) was $1{\cdot}9\times10^{13}$ electrons/cm^2. He considers that for the region below the F_2 layer maximum this figure is equal to 4×10^{12} electrons/cm^2, while for the region above the maximum it equals $1{\cdot}5\times10^{13}$ electrons/cm^2.

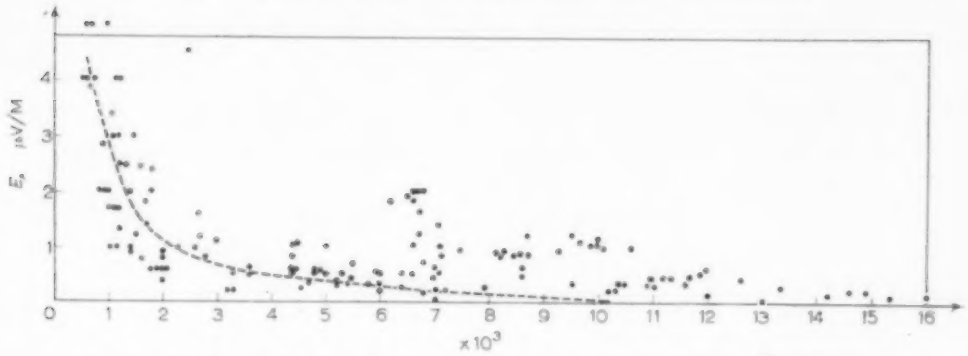

Fig. 6. Field strengths of I satellite as a function of distance, f—20 Mc/s, ●—Moscow, ○—Khabarovsk, – – – –calculated.

The latter of these figures exactly coincides with the one obtained by us, while the former is considerably less, which probably may be explained by the earlier hours (local time) of observations made in Great Britain.

If in equation (6) one takes the magnitude of H, at which e^{-kH} may be ignored in comparing with unity, we shall obtain, for the upper region of the F_2 layer (with $N_{max} = 16 \times 10^5$ electrons/cm³), the number of electrons in the 1 cm² cross-section column equal to $\sim 2 \times 10^{13}$ electrons/cm², i.e. double the value for the lower region. Of course, the results obtained are preliminary and will be checked during successive launchings of the artificial earth satellites.

3. ANALYSIS OF THE DATA RELATING TO MEDIUM AND LONG DISTANCES

Radio wave propagation over medium distances exceeding the range of direct visibility determined by the altitude of the satellite, occurred by way of successive reflections from the F_2 layer and from the surface of the earth. When the satellite was above the ionization maximum of the F_2 layer, radio waves, after passing through the thickness of the ionosphere and undergoing a certain refraction, were reflected from the surface of the earth and propagated further by way of a single or multiple reflection from the F_2 layer in those regions where its critical frequencies were of sufficiently great magnitude.

For medium distances, generally, a rather good agreement has been achieved of the experimental and calculated values of the field strength as well as the integral absorption coefficients, which testifies to the correctness of the considered views on the propagation of radio waves. However, at longer distances, beginning from 6000 or 8000 km, the mechanism of radio wave propagation proves to be unlike that for medium distances.

Analysis of the regularities governing changes in the field strength as a function of distance has shown that at longer distances the field strength during reception of radio signals from the satellite exceeded the values provided by the idea radio transmission formula. Fig. 6 shows the measured values of the field strength of the radio transmitter of the first satellite at 20 Mc/s as a function of distance. It is seen that signals were received and measured at distances of 10,000 to 12,000 km, and in some cases 14,000 to 16,000 km. The examined data provides grounds for considering that at longer distances the electromagnetic energy propagated due to formation of ionosphere radio waveguides, which made it possible to receive signals at greater distances, reaching 16,000 km.

REFERENCES

1. A. N. KAZANTSEV, T. S. ROMANOVA and A. Y. KLIMENTENKO, *Radiotekh. elektron.* No. 9 (1958).
2. A. N. KAZANTSEV, *Trud. IRE Akad. Nauk SSSR* No. 2, 36 (1956).
3. B. BURGESS, *Proc. Inst. Elect. Engrs.* B. **105**, 81 (1958).

Planet. Space Sci. Pergamon Press, 1959. Vol. 1, pp. 136–145. Printed in Great Britain.

DERIVATION AND ANALYSIS OF ATMOSPHERIC DENSITY FROM OBSERVATIONS OF SATELLITE 1958 EPSILON

G. F. SCHILLING* and C. A. WHITNEY

Smithsonian Astrophysical and Harvard College Observatories, Cambridge, Massachusetts

(*Received* 20 *December* 1958)

Abstract—The orbital behavior of Satellite 1958 Epsilon has been analyzed to derive average upper atmosphere densities in the altitude interval of 257 km to 270 km between latitudes 50°N and 50°S. The method of computation and possible errors in the calculations are discussed in detail.

At an altitude of 262·5 km above intermediate northern latitudes, the most probable value of mean density was found to be $1{\cdot}3 \pm 0{\cdot}4 \times 10^{-13}$ g/cm³. All numerical results showed a high degree of internal consistency, but gave no evidence of any appreciable variation of average density between latitudes 49°N and S during the time interval July to November, 1958. The data did not warrant firm interpretation of small deviations which could be ascribed to either a day-night effect or slightly higher mean densities in the northern hemisphere.

At about 50°N and S latitudes, however, a sharp discontinuity was found, with the average density value in the northern hemisphere about twice that in the southern hemisphere. Assuming this to be a real phenomenon, the authors present tentative conclusions about the physical and dynamical state of the upper atmosphere.

In addition, an explanation is offered for some of the apparent discrepancies between mean density values obtained from satellite observations and many of the measurements by means of high-altitude research rockets.

1. INTRODUCTION

Various investigators have derived values of upper atmosphere density from the observed variations of the orbital elements of artificial earth satellites launched prior to May, 1958. A summary and review of this work[1, 2] has shown that all density values obtained from satellites to date appear to be about an order of magnitude greater than most of those measured or extrapolated from rocket experiments.[3] However, the internal scatter in the rocket data amounts to two or three orders of magnitude, and it is difficult from rocket data alone to determine mean atmospheric conditions at high altitudes.

A number of complex phenomena can affect the reliability and accuracy of upper atmosphere densities inferred from satellite observations.[1, 4, 5] We therefore consider it important to detail here the basic assumptions as well as the computational techniques that we used to obtain density values from the orbital behavior of Satellite 1958 Epsilon (Explorer IV), launched on 26 July 1958.

This satellite was selected for a rigorous treatment because of a number of advantages with regard to its orbital characteristics in comparison with those of the other artificial satellites launched to date. The initial orbital inclination of 50·33° causes a daily advance of about 3° of the perigee, and a daily nodal regression of roughly 3·7°. In consequence, the perigee point sweeps the latitude range from 50·33°N to 50·33°S within a time interval of approximately 60 days. Such a range in latitude should be sufficient to detect variations in average atmospheric density, whereas the time interval is still brief enough to avoid

* Consultant, Rand Corporation, Santa Monica, California.

confusion due to the seasonal variation of the sub-solar latitude. In addition, the perigee point passed slowly from the sunlit side into the earth's shadow during the investigation period, permitting a study of possible day–night variations of density.

It should be noted, however, that we have placed primary emphasis in this critical analysis on the optimum reliability and absolute accuracy which can be achieved in determining drag effects and, hence, atmospheric densities. The simultaneous application of the method described, and used here, to a number of satellites in orbits at the same time should eventually yield definitive answers to various problems of upper atmosphere physics.

2. SATELLITE PARAMETERS

From published descriptions of the technical characteristics of Satellite 1958 Epsilon[6], we derived the following parameters for our calculations:

Total superficial area:	$a = 10{,}400\ \text{cm}^2$
Area of longitudinal cross-section:	$A_L = 3220\ \text{cm}^2$
Area of transverse cross-section:	$A_T = 196\ \text{cm}^2$
Effective cross-sectional area, assuming completely random orientation:	$\bar{A} = \frac{a}{4} = 2600\ \text{cm}^2$
Minimum effective cross-sectional area, assuming random orientation about a transverse axis of tumble:	$A' = 2170\ \text{cm}^2$

In our analysis, we shall refer to the numerical values of these additional parameters:

Effective mass–area ratio, assuming completely random orientation:	$m/\bar{A} = 6{\cdot}42\ \text{g/cm}^2$
Maximum possible mass–area ratio:	$m/A_T = 85{\cdot}2\ \text{g/cm}^2$
Maximum probable mass–area ratio:	$m/A' = 7{\cdot}68\ \text{g/cm}^2$
Minimum possible mass–area ratio:	$m/A_L = 5{\cdot}18\ \text{g/cm}^2$

The minimum possible cross-sectional area, A_T, is the area of a circular cross-section of the cylindrical satellite. However, to obtain a minimum probable cross-sectional area, we must consider the question of angular rotation of the satellite. MOONWATCH reports and precision photographs taken with the Baker-Nunn satellite tracking cameras have been analyzed to obtain data concerning the photometric behavior of the satellite.

Numerous visual observers have noted considerable variation in brightness, and have consistently reported intervals of about 3 sec between maxima. Five photographic images taken with exposure times of 0·8 and 1·6 sec (with short timing-breaks superposed) all show significant variations of brightness consistent with the periodicity reported by the MOONWATCH teams.

For the cylindrical shape of Satellite 1958 Epsilon, these data indicate a rotational period of approximately 6 sec. This period is consistent with conservation of angular momentum if the rotation has changed from the initial longitudinal spin imparted during launching to a transverse tumble.

Therefore, we have calculated a minimum probable cross-sectional area, A', on the assumption that the satellite tumbles with a period that is small relative to the time of appreciable drag near perigee. In this case, the minimum effective value is attained when the cylinder flies through perigee with its axis of tumble perpendicular to the flight trajectory. For any other angle between the axis of tumble and the flight trajectory, the effective area will be larger. For a right circular cylinder, this effective minimum has the value

$$A' = \frac{2}{\pi}(A_L + A_T) = 2170\ \text{cm}^2.$$

This argument considerably reduces the range of uncertainty in later derived densities, caused by the geometry of the satellite.

3. ORBITAL DATA

The computed variations of the orbital elements for Satellite 1958 Epsilon between 26 July and 16 November 1958, have been used

to determine a number of values of upper atmosphere density at altitudes between 257 km and 270 km above the earth's surface, and latitudes 50°N to 50°S. The initial orbit calculations were based on reductions of photographs made with the Baker-Nunn satellite cameras, radio observations by Minitrack and Microlock stations, visual sightings by MOONWATCH teams, and radar observations. The basic ephemeris and elements, distributed at roughly weekly intervals by the Smithsonian Astrophysical Observatory, were computed by Dr. D. A. Lautman.

Table 1. Variable Orbital Elements

Epoch (Aug. 1958)	Anomalistic period (days)	Argument of perigee	Right ascension of ascending node
−4·44643	0·07657337	47·5°*	63·6°*
0·909560	0·0765637	63·2°*	44·3°*
7·021655	0·0763475	81·07°	22·28°
11·21821	0·0762501	93·10°	7·23°
15·40983	0·0761712	105·24°	352·30°
23·78067	0·07601620	129·47°	322·48°
30·47689	0·0758786	145·96°	302·02°
40·84007	0·07563587	178·86°	260·98°
47·03737	0·07551520	196·94°	238·49°
64·59515	0·07518727	250·92°	174·20°
69·47950	0·07509993	265·81°	156·17°
73·98365	0·07504373	−80·41°	139·66°
78·48448	0·07497110	−66·58°	123·02°
97·17858	0·07457130	352·00°*	53·31°*
103·13977	0·07445225	10·66°*	30·88°*
108·71958	0·07433856	28·22°*	9·81°*

* Extrapolated.

In Table 1, we list the orbital elements that formed the basis of our calculations. In addition to these variable quantities, we took a constant orbit inclination of 50·33°, and a perigee distance of 1·0403 earth's equatorial radii, measured from the center of the earth.

Table 2 gives the quantities derived from the basic orbital elements under the following assumptions: Between the individual epochs, the anomalistic period is assumed to change linearly with time, resulting in an average change in period for the epoch intervals, and a mean period for a reference date halfway between the epochs. The perigee altitudes for the reference dates are computed from the international ellipsoid and are given in kilometers above the mean sea level. Note that the perigee distance remains constant, while this perigee altitude decreases when the subperigee point approaches the earth's equator, solely because of the flattening of the earth. Table 2 also lists the solar time at the subperigee point, computed from the difference between the right ascension of perigee and the right ascension of the sun.

4. COMPUTATIONS

Sterne's simplified formula[7] was used to calculate upper atmosphere densities for the reference dates and perigee altitudes given in Table 2. His formula relates the atmospheric density near perigee to the aerodynamic drag coefficient, C_D, an effective satellite mass–area ratio, m/A, and the orbital acceleration, $\dot{P}$, in the following way:

$$\rho_\pi \propto \frac{1}{C_D}\,\frac{m}{A}\,\frac{\dot{P}}{P}F(a,e),$$

where $F(a, e)$ is a slowly-varying function of the orbital parameters (semi-major axis and eccentricity). The factor of proportionality depends on an assumed gradient of density at the perigee altitude. We adopted the gradient given by the Smithsonian Interim Atmosphere No. 2[8]. Since the resulting numerical values of absolute density are insensitive to reasonable variations of the density gradient, no appreciable error would be introduced, if the *a priori* assumed gradient were to be based on other model atmospheres. The value of $C_D=2$ was used for the aerodynamic drag coefficient. A discussion of possible errors introduced by a number of independent effects is given in subsequent sections.

5. NUMERICAL RESULTS

The numerical results obtained are shown in Table 3. The reference numbers correspond to the listing in Table 2, and the range limits for altitude and latitude correlate with the

Table 2. Orbital Characteristics

Reference number	Reference date (datum)	Mean period (days)	Average period change (sec/day)	Sub-perigee point geo-centric latitude (deg)	Perigee altitude (km-MSL)	Solar time at sub-perigee point
1	Jul. 29.276	0·07651855	−1·769	39·5°N	265·9	09:36
2	Aug. 3.966	0·0764056	−1·643	47·0°N	268·7	09:42
3	Aug. 9.12	0·0762988	−2·005	50·2°N	269·8	09:38
4	Aug. 13.31	0·0762106	−1·63	49·5°N	269·6	09:38
5	Aug. 19.59	0·0760937	−1·60	43·3°N	267·3	09:22
6	Aug. 27.13	0·0759474	−1·78	30·2°N	262·5	08:34
7	Sept. 4.658	0·0757572	−2·02	14·4°N	258·4	07:18
8	Sept. 12.939	0·0755755	−1·682	6·0°S	257·4	05:41
9	Sept. 24.816	0·07535124	−1·614	31·2°S	262·9	03:43
10	Oct. 6.037	0·07514360	−1·545	49·2°S	269·4	03:01
11	Oct. 10.731	0·07507183	−1·078	50·2°S	269·8	03:02
12	Oct. 15.234	0·07500742	−1·394	47·5°S	268·8	03:04
13	Oct. 26.832	0·07477120	−1·848	27·7°S	261·8	02:08
14	Nov. 8.159	0·07451178	−1·725	1·0°N	257·2	00:01
15	Nov. 13.930	0·07439541	−1·760	14·8°N	258·5	23:00

original epochs. The values of average atmospheric density within these limits are computed from the value of the orbital elements at the corresponding reference dates. Note that perigee passed through the northern and the southern apex of the orbit during intervals 3 and 11, respectively. The earth's equator was passed during intervals 8 and 14.

The column labelled "Most probable" is based on the use of an effective mass–area ratio $m/\bar{A} = 6{\cdot}42\,\mathrm{g/cm^2}$, and assumes that orientation was completely random during the

Table 3. Range of Values of Atmospheric Density for $C_D = 2$ and Various Mass-Area Ratios

Reference number	Range of perigee altitudes (km-MSL)	Range of geographic latitudes (deg.)	Average atmospheric density			
			Most probable $\bar{\rho}$ (g/cm³)	Possible minimum $\rho_{\min}$	Probable maximum ρ'	Possible maximum $\rho_{\max}$
1	264·1-267·3	35° N-44° N	$1{\cdot}35\times10^{-13}$	$1{\cdot}09\times10^{-13}$	$1{\cdot}61\times10^{-13}$	$17{\cdot}9\times10^{-13}$
2	267·3-269·5	44° N-49·4°N	$1{\cdot}25\times10^{-13}$	$1{\cdot}01\times10^{-13}$	$1{\cdot}50\times10^{-13}$	$16{\cdot}6\times10^{-13}$
3	269·5-269·9	49·4°N-50·3°N	$1{\cdot}52\times10^{-13}$	$1{\cdot}23\times10^{-13}$	$1{\cdot}82\times10^{-13}$	$20{\cdot}2\times10^{-13}$
4	269·8-269·1	50·2°N-48·3°N	$1{\cdot}24\times10^{-13}$	$1{\cdot}00\times10^{-13}$	$1{\cdot}48\times10^{-13}$	$16{\cdot}5\times10^{-13}$
5	269·1-264·7	48° N-36° N	$1{\cdot}21\times10^{-13}$	$0{\cdot}98\times10^{-13}$	$1{\cdot}45\times10^{-13}$	$16{\cdot}1\times10^{-13}$
6	264·7-261·1	36° N-25° N	$1{\cdot}35\times10^{-13}$	$1{\cdot}09\times10^{-13}$	$1{\cdot}61\times10^{-13}$	$17{\cdot}9\times10^{-13}$
7	261·1-257·2	25° N- 1° N	$1{\cdot}53\times10^{-13}$	$1{\cdot}23\times10^{-13}$	$1{\cdot}83\times10^{-13}$	$20{\cdot}3\times10^{-13}$
8	257·1-258·2	1° N-13° S	$1{\cdot}27\times10^{-13}$	$1{\cdot}05\times10^{-13}$	$1{\cdot}52\times10^{-13}$	$16{\cdot}9\times10^{-13}$
9	258·2-268·5	13° S-46·5°S	$1{\cdot}21\times10^{-13}$	$0{\cdot}98\times10^{-13}$	$1{\cdot}45\times10^{-13}$	$16{\cdot}1\times10^{-13}$
10	268·5-269·7	46·5°S-50·1°S	$1{\cdot}16\times10^{-13}$	$0{\cdot}94\times10^{-13}$	$1{\cdot}39\times10^{-13}$	$15{\cdot}4\times10^{-13}$
11	269·9-269·5	50·3°S-49·3°S	$0{\cdot}81\times10^{-13}$	$0{\cdot}65\times10^{-13}$	$0{\cdot}97\times10^{-13}$	$10{\cdot}7\times10^{-13}$
12	269·5-267·8	49·3°S-45° S	$1{\cdot}04\times10^{-13}$	$0{\cdot}84\times10^{-13}$	$1{\cdot}24\times10^{-13}$	$13{\cdot}8\times10^{-13}$
13	267·8-257·4	45° S- 6° S	$1{\cdot}38\times10^{-13}$	$1{\cdot}11\times10^{-13}$	$1{\cdot}65\times10^{-13}$	$18{\cdot}3\times10^{-13}$
14	257·1-257·6	6° S- 8° N	$1{\cdot}28\times10^{-13}$	$1{\cdot}03\times10^{-13}$	$1{\cdot}53\times10^{-13}$	$17{\cdot}0\times10^{-13}$
15	257·6-260·0	8° N-21° N	$1{\cdot}30\times10^{-13}$	$1{\cdot}05\times10^{-13}$	$1{\cdot}56\times10^{-13}$	$17{\cdot}2\times10^{-13}$

passages of the satellite through the perigee. The other columns assume that the above condition has not been fulfilled and give the possible extreme values of density which would result under non-random orientation. If the satellite had passed the perigee in a broad-side position on each revolution, the use of the minimum possible mass–area ratio,

$$m/A_L = 5{\cdot}18\,\mathrm{g/cm^2},$$

would indicate a possible minimum density ρ_{min}. Conversely, if the long axis of the satellite had been aligned, on every passage through perigee, parallel to the flight trajectory, the maximum possible mass–area ratio,

$$m/A_T = 85{\cdot}2\,\mathrm{g/cm^2},$$

would be applicable, resulting in a high density, ρ_{max}. The probable maximum density, ρ', based on m/A', is considerably below this value, however.

For a satellite whose axis is not aligned in inertial space by rotational momentum, aerodynamic torques during perigee passage may cause an alignment of the body axis, leading to systematic deviations from completely random orientation. For example, if the center of mass is sufficiently far from the center of volume, the assumption of completely random orientation at perigee may result in an overestimate of the average presentation area and lead to consistent underestimates of density.

However, this argument does not apply to Satellite 1958 Epsilon. The photometric evidence cited earlier shows that this satellite tumbles about a transverse axis. Therefore, we do not admit the applicability of the possible maximum, and we believe that reasonable limits are given by the probable maximum and possible minimum values of density listed in Table 3.

We have thus estimated the probable range of densities introduced by uncertainties in the effective presentation area of the non-spherical Satellite 1958 Epsilon. Numerically, this range covers a factor of 1·48, the ratio A_L/A'. Note that the upper limit, A_L, is a definite one that results in a minimum possible mass–area ratio, m/A_L, and in the lowest possible values of density, ρ_{min}.

6. UNCERTAINTIES IN THE DENSITY DERIVATIONS

Three types of criticisms can be levelled at the direct application of Sterne's formula to the data for Satellite 1958 Epsilon. The first, that the orientation of the object at perigee cannot be precisely specified, has been shown above to introduce uncertainties of ±25 per cent in the geometrically effective cross-sectional area, with a definite upper limit, A_L. In turn, this value specifies a definite lower limit for derived densities, leaving open only the possibility that the true densities are higher than the computed minimum values.

Second, a major uncertainty is introduced by the variation of the drag coefficient with altitude and attitude[9]. Recently a study group at the RAND Corporation thoroughly investigated this phenomenon. Available evidence[10], both experimental and theoretical, indicates tentatively that a better value of the drag coefficient, at the altitude with which we are concerned here, and for the shape and surface characteristics of Explorer IV, might be $C_D = 2{\cdot}3$, with probable limits of 2·0 and 2·5 depending primarily on the degree of dissociation of nitrogen. Since the values listed in Table 3 are based on the use of $C_D = 2$, multiplication of all entries in the density columns by factors of 0·87 and 0·80, respectively, would give reasonable corrections due to deviations of C_D from the value used.

Finally, we can safely neglect electrostatic[11] and electrohydrodynamic[12] drag effects as additional sources of possible error, for the perigee altitudes of Satellite 1958 Epsilon. Re-evaluation[13, 1] of the early theoretical considerations by Jastrow and Pearse[11], and experimental data on charge accumulation obtained by Soviet scientists with Sputnik III[14], make it appear extremely unlikely that such additional drag effects would alter our derived densities by more than five per cent.

We have neglected any additional drag effects due to the presence of the earth's magnetic field and ionization of the atmospheric gases

for the perigee altitude and configuration of Satellite 1958 Epsilon. While such effects may become appreciable at portions of the orbit near apogee, theoretical arguments suggest that they would be negligible in comparison with the atmospheric drag force acting near perigee.

Further, there is an empirical justification for ruling out the possibility of severe drag effects not considered in our discussion above. Warwick[15] has derived an atmospheric density from the observed damping of the rotation of Satellite 1957 $\alpha 2$, on the assumption that aerodynamic drag on the antennae produced the damping. The density thus derived agrees very well with those derived from observed changes of the orbital period of the same satellite[16]. Since completely different regimes are involved, non-aerodynamic effects changing the orbital period would not affect rotational motions to the same degree. Therefore, the agreement in densities strongly suggests that aerodynamic drag is, indeed, the only force acting to dissipate energy.

Our calculations did not consider rotational velocity of the earth's atmosphere. For the orbital characteristics of Satellite 1958 Epsilon, this neglect may lead to an underestimate of density by perhaps as much as 10 per cent.

We now consider possible errors due to inaccuracies in the orbital elements. We have reproduced in Tables 1 and 2 the orbital data to the precision with which they were known or could be reasonably calculated. Uncertainties in these data cannot affect the density results by more than one or two per cent, with one important exception: the perigee altitudes may possibly be accurate only to ± 5 km above the geoid, and hence the absolute altitudes to which these densities refer are uncertain by the same amount. The relative altitudes or altitude differences, on the other hand, are accurate to several tenths of a kilometer.

7. NUMERICAL ESTIMATES OF PROBABLE ERRORS

By assuming that all effects discussed above may possibly, although not necessarily, introduce accumulative errors, we can derive the numerical limits of accuracy. We have chosen Reference Interval Number 6 at the altitude of 262·5 km between latitudes 25°N and 36°N for this purpose, but the analogous calculations can, of course, be carried out for all values of density listed in Table 3. In Table 4, possible values of density for different presentation areas and drag coefficients at this perigee altitude are shown. All density values are given in g/cm^3, C_D is dimensionless, and m/A is in g/cm^2.

A quantitative evaluation of the various other effects which can contribute possible errors is attempted in Table 5. Correction factors are listed which represent maximum probable deviations from the computed density values shown in Table 4.

If we now take the highest and lowest possible density values shown in Table 4, and multiply with the appropriate accumulative correction factor, we can place absolute limits on the true value of the average upper atmosphere density inferred from Satellite 1958

Table 4. Possible Density Values at 262·5 km Altitude as a Function of Mass–Area Ratio and Aerodynamic Drag Coefficient

m/A / C_D	Maximum possible 85·2	Maximum probable 7·68	Probable random 6·42	Minimum possible 5·18
2·0	$17{\cdot}9\times10^{-13}$*	$1{\cdot}61\times10^{-13}$	$1{\cdot}35\times10^{-13}$	$1{\cdot}09\times10^{-13}$
2·3	$15{\cdot}6\times10^{-13}$	$1{\cdot}40\times10^{-13}$	$1{\cdot}17\times10^{-13}$	$0{\cdot}94\times10^{-13}$
2·5	$14{\cdot}3\times10^{-13}$	$1{\cdot}29\times10^{-13}$	$1{\cdot}08\times10^{-13}$	$0{\cdot}87\times10^{-13}$†

* Highest possible value.
† Lowest possible value.

Epsilon at a perigee altitude of 262·5 km above geographic latitude 25°–36°N, as follows:

$$6{\cdot}8 \times 10^{-14}\,\mathrm{g/cm^3} < \rho_{262{\cdot}5} < 2{\cdot}3 \times 10^{-12}\,\mathrm{g/cm^3}.$$

We think that this procedure takes into account all *possible* accumulative errors, and it illustrates and places reasonable limits on the errors which lack of knowledge could introduce into derivations of density from satellite observations. We feel inclined, however, to believe that the most *probable* limits for the accuracy of our average density point at 262·5 km, in accordance with the earlier discussions, would be:

$$\rho_{262{\cdot}5} = (1{\cdot}3 \pm 0{\cdot}4) \times 10^{-13}\,\mathrm{g/cm^3}.$$

Table 5. Estimates of Probable Error Corrections in Addition to Uncertainties in Mass-Area Ratio and Drag Coefficient

Possible effect	Decrease in ρ	Increase in ρ
Electrostatic and electrohydrodynamic drag	5%	—
Rotation of atmosphere	—	10%
Inaccuracies of orbital elements	2%	2%
Uncertainty in perigee height	14%	14%
Accumulative effect	22%	28%

8. DISCUSSION

The variation of average atmospheric density with altitude between 250 km and 275 km above the earth's surface is shown in Fig. 1. The most probable values of density derived from Satellite 1958 Epsilon are plotted for the reference dates and altitudes given in Table 2. We have indicated the range of probable accuracy for Reference Interval Number 6 at the altitude 262·5 km as estimated in the preceding section. For easy orientation, the figure contains also portions of model atmospheres[17, 18, 9, 19].

Examination of Fig. 1 evidences a striking consistency and surprisingly little spread of the derived values. Otherwise, the data presented in this form are insufficient to allow any firm conclusions, because all deviations fall within the limits of uncertainty and probable errors.

From extrapolations of rocket data, on the other hand[20, 21, 5, 22], we would have expected to find substantial evidence for rather large latitudinal as well as diurnal variations of density at these altitudes. Fig. 2 shows the results of an attempt to investigate our data further in this respect.

First, we tried to eliminate the variation of density produced by ellipticity of the geoid. The normalized quantity $\bar{\rho}/\rho_s$ represents the ratios between the most probable density values, from Table 3, and corresponding density values given by the Smithsonian Interim Atmosphere Number 2[8] for each reference altitude (see Table 2). If we assume the applicability of the scale heights, or density gradients of this model atmosphere, any observed variation of $\bar{\rho}/\rho_s$ should be independent of height changes. Further, it will be proportional to the atmospheric density at a fixed, standard height within the interval 257 km to 270 km at all latitudes, regardless of the flattening of the earth. It should be noted, however, that this procedure would be incorrect, if the true atmosphere is formed of concentric spherical shells and does not follow a quasi-ellipsoidal distribution of geopotential surfaces at higher altitudes.

Fig. 2 is a plot of the quantity $\bar{\rho}/\rho_s$ for each reference interval against geographic latitude and shows an interesting phenomenon. With the sole exception of two intervals, Numbers 3 and 11, the variation from latitude 49°N to latitude 49°S is less than 25 per cent. Intervals 3 and 11, however, represent the passes of perigee through the most northern and most southern latitudes reached, slightly beyond 50°. The probability of a coincidence due to chance appears rather low to us. It does not seem possible that orbital phenomena or inaccuracies associated with the perigee location near the orbit apices could be responsible either. Assuming that the phenomenon is real, we can interpret the results as an indication of a true variation of density with latitude or time.

9. CONCLUSIONS

It will be noted that the points in Fig. 1 fall sufficiently close to the Smithsonian Interim Atmosphere[8] that it was not necessary to fit

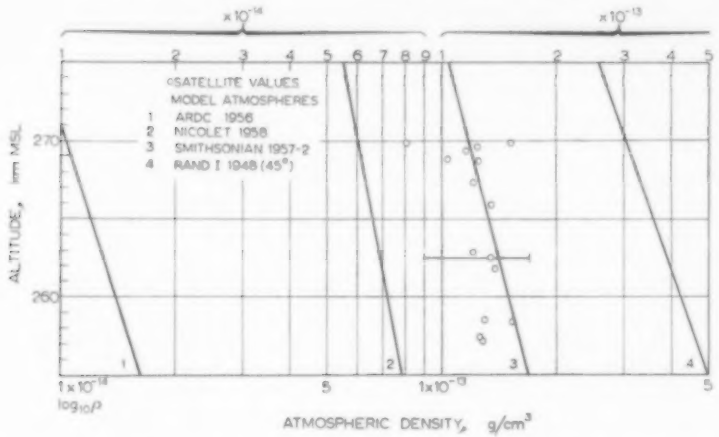

Fig. 1. Atmospheric densities derived from Satellite 1958 Epsilon. (Perigee distance of 6635·5 km from earth's center assumed constant.) Portions of model atmospheres are inlcuded for comparision.

another curve to the determined values. It will also be noted that all densities derived with any one set of assumptions show a remarkable consistency with each other. Taking into account the probable errors and uncertainties, we conclude that satellite observations provide a consistent means of deriving the ambient density of the upper atmosphere.

While it would be unreasonable to base any firm conclusions on deviations from standard values that do not fall significantly beyond an area of probable errors, the implications could be of such importance to upper atmosphere physics as to warrant some speculative deductions. From the evidence shown in Fig. 2, we may reach thus the following tentative conclusions:

Between 26 July and 16 November the average atmospheric density, as derived from observations of Satellite 1958 Epsilon between the heights of 257 km and 270 km above the earth's surface, showed no appreciable variation as a function of latitude from 49°N to 49°S. The present data give a very slight indication that the mean densities in the southern hemisphere were somewhat lower by perhaps 10 per cent to 20 per cent, than those in the northern hemisphere, before the sun dropped considerably below the equator. However, there is a possibility that at least part of this slight difference, if real, may have been due to a day–night effect. The variations of $\bar{\rho}/\rho_s$ against solar time at the sub-perigee points have not been plotted here, but can be inferred from Table 2. Intervals 1 through 7 were determined while the area of perigee passage was illuminated by the sun. For intervals 8 through 15, the sub-perigee point was located in the earth's shadow.

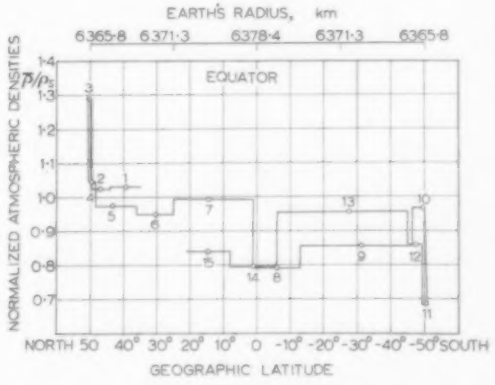
EARTH'S RADIUS, km
6365·8 6371·3 6378·4 6371·3 6365·8
EQUATOR
NORMALIZED ATMOSPHERIC DENSITIES
NORTH 50° 40° 30° 20° 10° 0 -10° -20° -30° -40° -50° SOUTH
GEOGRAPHIC LATITUDE

Fig. 2. Variation, with latitude, of normalized densities in the neighborhood of 260 km altitude as derived from Satellite 1958 Epsilon. (Normalized densities are ratios of derived densities to model densities at perigee height, and are thus essentially free of perigee-height variations.)

Hence, the apparently higher densities in the northern hemisphere before October may be representative of a true though small diurnal variation, with somewhat higher densities occurring in the sunlit parts of the earth's atmosphere.

There are indications that the average atmospheric density showed a considerable discontinuity in the vicinity of latitudes 50°N and S, the northern value being almost twice as high as the southern value. If this proves to be a real phenomenon, we would be led to deduce a dynamic behavior[23] of the atmospheric region above 250 km, that may be analogous to the large-scale wind circulation in the stratosphere between some 30 km and 80 km altitude[24].

The apparent density discontinuities at 50°N and 50°S, if representative of higher and lower ambient densities at high northern and southern latitudes, respectively, could logically be associated with circumpolar vortices of mean air flow pattern above both the north and the south polar regions. As a consequence, there would be a large-scale mean meridional flow from high northern latitudes to high southern latitudes at these altitudes. The Coriolis force on such flow would cause predominantly east wind components in the northern hemisphere, and predominantly west wind components in the southern hemisphere. Again, in analogy to the average stratospheric circulation, we would expect a reversal of this basic pattern twice a year, if the causative agent is absorption of solar energy by an atmospheric constituent as a function of concentration and solar zenith angle, with subsequent dissociation and heating, or the downward flux of thermal energy from outside the atmosphere. Diurnal as well as sporadic changes could be superimposed on this general circulation, frequently masking the localized picture, but not radically affecting the average large-scale density system.

The above argument is, of course, a truly speculative one, suggesting that the dynamic scheme above some 200 km altitude may be different from the flow patterns which we believe to operate in the lower ionosphere[25, 26], i.e. solar heating primarily above tropical latitudes and resultant flow patterns generally similar to tropospheric circulation systems.

Finally, we can use the density data analyzed here to propose a partial explanation of the fact that, as opposed to satellite measures, the measurements by means of high-altitude research rockets have shown a large scatter of density and pressure values, with results from individual ascents frequently differing by orders of magnitude[1, 3, 2]. Although rocket measurements necessarily represent exceedingly short-lived, practically instantaneous probings, they consistently give the impression of widely diverse and rapidly changing conditions. Not a single measurement appears to be reproducible and we seem to be faced with large changes of density and temperature from season to season, and day to day. Naturally, a rather confused picture of average conditions evolves.

Satellite data, on the other hand, are truly long-period integrated measures of the ambient atmospheric density over wide ranges of time and latitude. These results appear to give us a quiet and consistent picture of average conditions of the high atmosphere.

When making the plausible assumption that the basic discrepancies between rocket and satellite results are not solely caused by instrumental errors or large inaccuracies, but are due, at least in part, to the actual atmospheric situation, we are finally led to a conclusion which by now will be rather obvious. We can express it best in these simple terms: Rockets measure the weather of the upper atmosphere; satellites measure the climate as far as atmospheric density is concerned. In consequence, it appears to us that the physical and dynamical state of the high atmosphere must be studied from the point of view of meteorological research. However, while this picture can explain density changes by perhaps factors of two or three, we are unable to interpret variations, of orders of magnitudes, as indicated by some rocket measurements.

With the simultaneous existence of a number of satellites in different orbits, extension of our present method of analysis may soon result in a wealth of reliable information on the dependence of average upper atmosphere density on

latitude, season, and time of day. Continued probings by means of research rockets will provide the information needed to study the fine structure and to further our understanding of the physical state and behavior of the earth's atmosphere.

Acknowledgements—We wish to express our appreciation to the many members of photographic, radio and visual satellite tracking stations, whose efforts furnished the basic observational data. We were stimulated to undertake our calculations as the result of an informal conference on satellite drag phenomena at the RAND Corporation, arranged by Drs. C. Gazley, Jr., H. K. Kallmann-Bijl, D. J. Masson, and others. Special thanks are due Drs. A. F. Charwat, University of California at Los Angeles; F. C. Hurlbut and S. A. Schaaf, University of California at Berkeley; H. W. Liepmann, California Institute of Technology; L. Kraus, Convair; H. C. Chang, M. C. Smith and E. H. Vestine, RAND Corporation, for valuable thoughts and ideas freely given during many fruitful discussions. For the present interpretations and use, right or wrong, of some of the results of these discussions, we are solely responsible, of course. For very pertinent comments and suggestions, we are indebted to Dr. Marcel Nicolet, Secretary General, CSAGI; Dr. W. S. Ripley, Air Force Cambridge Research Center, and Dr. H. E. La Gow, Naval Research Laboratory. Dr. R. E. McCrosky, Harvard University, has provided us with helpful criticism of our manuscript.

REFERENCES

1. T. E. Sterne, *Phys. of Fluids* **1**, 165 (1958).
2. G. F. Schilling and T. E. Sterne, *J. Geophys. Res.* **64**, in press (1959).
3. H. E. La Gow, R. Horowitz and J. Ainsworth, *IGY Rocket Report Series*, No. 1, pp. 38–46. National Academy of Sciences (1958).
4. I. Harris and R. Jastrow, *Science* **127**, 471 (1958).
5. R. Jastrow and I. Harris, *Trans. Amer. Geophys. Un.* **39**, 519 (1958).
6. J. Boehm, Orbital Data Series, Issue 1, p. 2, Army Ballistics Missile Agency and Smithsonian Astrophysical Observatory (1958).
7. T. E. Sterne, *Science* **127**, 1245 (1958).
8. T. E. Sterne, B. M. Folkart and G. F. Schilling, Special Report No. 7 (re-printed in *Smithsonian Contrib. Astrophys.* **2**, 275 (1958). Smithsonian Astrophysical Observatory (1957).
9. R. M. L. Baker, Jr. and A. F. Charwat, *Physics of Fluids* **1**, 73 (1958).
10. S. A. Schaaf, A. F. Charwat and F. C. Hurlbut, private communication (1958).
11. R. Jastrow and C. A. Pearse, *J. Geophys. Res.* **62**, 413 (1957).
12. L. Kraus and K. M. Watson, *Report* ZPh–016. Physics Sections, Convair, San Diego (1958).
13. Naval Research Laboratory. Conference Proceedings, *Interaction of Satellites with the Ionosphere*. Naval Research Laboratory (1958).
14. V. I. Krassovsky, Presented at the General Assembly of CSAGI, Moscow (1958).
15. J. W. Warwick, *IGY Satellite Report*, No. 5. National Academy of Sciences (1958).
16. T. E. Sterne and G. F. Schilling, *Smithsonian Contrib. Astrophys.* **2**, 207 (1958).
17. G. Grimminger, *RAND Report* No. R–105 (1948).
18. R. A. Minzner and W. S. Ripley, *Air Force Surveys in Geophysics*, No. 86. Geophysics Research Directorate, AFCRC, ARDC (1956).
19. M. Nicolet, *Scientific Report* No. 102, Contract No. AF19 (604)-1304. Ionosphere Research Laboratory, Pennsylvania State University (1958).
20. L. M. Jones, F. F. Fischback and J. W. Peterson, *IGY Rocket Report Series* No. 1, pp. 47–57. National Academy of Sciences (1958).
21. H. E. La Gow, R. Horowitz and J. Ainsworth, *IGY Rocket Report Series* No. 1, pp. 26–37. National Academy of Sciences (1958).
22. J. W. Townsend and E. B. Meadows, *IGY Rocket Report Series* No. 1, pp. 14–25. National Academy of Sciences (1958).
23. E. H. Vestine, *J. Geophys. Res.* **58**, 539 (1953). E. H. Vestine, *J. Geophys. Res.* **59**, 93 (1954).
24. W. W. Kellogg and G. F. Schilling, *J. Met.* **8**, 222 (1951).
25. D. G. Yerg, *J. Met.* **8**, 244 (1951).

Planet. Space Sci. Pergamon Press, 1959. Vol. 1, pp. 146–153. Printed in Great Britain.

SOME REMARKS ON THE NATURE AND ORIGIN OF NOCTILUCENT CLOUD PARTICLES*

DIRAN DEIRMENDJIAN and E. H. VESTINE
The Rand Corporation, Santa Monica, California

(*Received* 18 *November* 1958)

Abstract—Continuous spectra of the light from noctilucent clouds, recently obtained by N. I. Grishin near Moscow, U.S.S.R., are analysed after accounting for the selective attenuation of the lower atmosphere and the spectrum of sunlight. It is found that the spectra may be explained in terms of primary scattering of direct sunlight by dielectric spheres with a maximum radius of 0·4 μ, and certain night sky emissions. The apparent absence of any nocturnal ozone layers above 35 km is also noted.

The possibility of an ice composition of the clouds formed by condensation of terrestrial water vapor is examined and found unjustified on physical grounds. Rather a silicaceous or similar composition and an interplanetary origin for the cloud particles is favoured and a close relation with the Martian "blue haze" is suggested.

1. INTRODUCTION

In recent years and during the IGY the investigation of noctilucent clouds has been receiving renewed attention. Systematic new observations have been carried out in Sweden[1, 2] and in the Soviet Union[3]. These already permit some testing of various theories concerning the nature and origin of the particles responsible for this interesting visual phenomenon.

It will be the purpose here to present new analyses of the continuous spectrum of the light from the clouds, by considering the scattering of sunlight by the cloud particles and its transmission through the atmosphere. Some inferences are drawn respecting the size of the particles as well as the nature and origin of the clouds.

2. THE CONTINUOUS SPECTRUM OF NOCTILUCENT CLOUDS

2.1. *Method of reduction*

N. I. Grishin[3] has recently provided especially interesting observations including the first published continuous spectra of noctilucent clouds. Fig. 1 gives some of the original unreduced spectra obtained by that author[3] by means of photographic spectrophotometry in June and July 1951 from a station 19 km NW of Moscow. The topmost spectrum is that of the night sky without noctilucent clouds. The remaining three spectra correspond to noctilucent clouds at an elevation 8° to 9° above the horizon. Observations were conducted after local midnight. The traces reveal considerable spectral detail and the added luminosity of the clouds in the green and blue region, above that of the clear sky, is evident. By a careful reduction of these observations Grishin has shown some interesting characteristics of the relative spectra of the twilight sky and noctilucent clouds for which details the reader is referred to the original publication[3].

It is fairly certain that the visibility of these clouds is mainly due to the scattering of sunlight at small angles ($\theta < 90°$) by layers of particles just above the earth's shadow. It is therefore important to study the intensity distribution for various wavelengths and its variations with the scattering angle in order to obtain as much information as possible regarding the size, nature, and concentration of the cloud particles.

Since the height of the clouds is known to be well above the main scattering part of the molecular atmosphere (e.g. the layer up to 30 km

* Originally presented at a symposium on noctilucent clouds during the Fifth CSAGI meeting at Moscow, U.S.S.R., 30 July–9 August 1958.

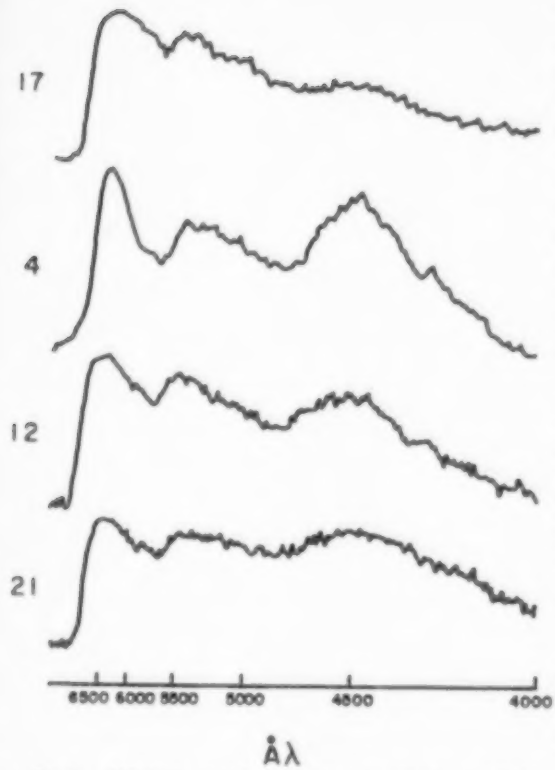

Fig. 1. Original unreduced spectra of the twilight sky (top curve) and noctilucent clouds (remaining curves) after N. I. Grishin (3).

above sea level) the nature of the true spectrum can be deduced from that observed at the ground by using certain simplifying assumptions: (1) that the observed intensity is the sum of singly scattered sunlight from the clouds and the twilight (multiply scattered light) received from the same portion of the clear sky and at the same solar depression, in the absence of noctilucent clouds; (2) that the clouds are illuminated only by direct sunlight whose path lies entirely above the main scattering layer of the lower atmosphere.

In Table 1 below are listed pairs of observations of the noctilucent cloud and clear sky, marked A, B, C, D, chosen from the original data[3] in such a way that the sun's depression h_0 and angular elevation h of the point of observation are closely equivalent for each pair. The values of the scattering angle θ in column 6 of Table 1 represent the angle between the forward direction of direct solar radiation at the cloud and the direction of the light from the clouds scattered toward the observer. The values shown, obtained by setting $\theta = h_0 + h$, will be strictly correct only if the plane determined by the sun, the point of the sky observed and the observer passes through the local zenith. In any other case the scattering angle will exceed the sum $h_0 + h$. Astronomical refraction and atmospheric dispersion have been neglected.

Under the assumption (1) above, the relative spectrum of the noctilucent clouds proper can be found by subtracting the intensities of the clear sky from those of the clouds in each pair of Table 1. Thus, using the intensities i' and i'' for clouded and clear skies, respectively, as listed for various wavelengths by Grishin[3], and applying the calibration factors $E_{\lambda T}$ also listed by that author, we have,

$$I'_c(\theta) = (i' - i'')\, E_{\lambda T} \qquad (1)$$

where $I'_c(\theta)$ represents the light of the noctilucent clouds only, after passage through the atmosphere.

Under assumption (2) above and according to the appropriate theory of particle scattering of sunlight[5], the directional scattered intensity at each wavelength is proportional to the incident solar flux density, to the concentration of the particles per unit volume, and the normalized scattering function which is determined by the size and nature of the particles. It is these last two quantities which are unknown, whereas the extraterrestrial solar flux spectrum and the transmission characteristics of the clear atmosphere are known with good accuracy. One may therefore reduce the data further by means of the expression

$$I_c(\theta) = \frac{I'_c(\theta)}{F_s}\, e^{\tau_a \csc h} \qquad (2)$$

where for any given wavelength, $I'_c(\theta)$ is given by equation (1), F_s is the extraterrestrial flux of solar radiation taken from recent data[4], τ_a is the normal optical thickness of the slightly hazy atmosphere according to a realistic

Table 1. Noctilucent Clouds

Pair No.	Film No.	Date (1951)	h_o	h	θ (Approximate)
A	19	23 June	10·5°–10·3°	7°	17·5°
B	14	28 June	10·7°	9°	19·6°
C	29	28 June	9·8°–9·6°	12°	21·5°
D	28	7 July	7·6°–7·1°	15°	22·4°
		Clear Sky			
A	17	22 June	10·6°	7°	
B	15	22 June	10·6°	9°	
C	58	29 June	9·4°–9·2°	12°	
D	55	28 June	7·3°	17°	

model[3] and $\csc h$ represents the usual "air mass" given by the secant of the zenith angle of the point of observation. The quantity $I_o(\theta)$ on the left of equation (2) then represents the true normalized intensity (i.e. with uniform illumination at all wavelengths) of the scattered light from the noctilucent clouds that would be observed in the absence of the lower atmosphere.

2.2. *Analysis and interpretation of the spectra*

The values of $I_o(\theta)$ obtained by means of equations (1) and (2) are plotted logarithmically against the wavelength in Fig. 2, where for clarity the individual points of each pair, listed under Table 1, are joined by straight lines without any attempt to fit smooth curves. Although the curves A, B, C, and D are in *relative units*, they are intercomparable since the same method of reduction was used throughout. As a guide, Fig. 2 also includes the straight dash lines representing the Rayleigh λ^{-4} law, multiplied by an arbitrary constant. The most salient feature of the reduced spectra is that they all exhibit a higher intensity in the blue end than in the red end of the spectrum. Furthermore, considering curves A, B, and C only, the intensity generally decreases with increasing apparent scattering angle θ. Thus, broadly speaking, the cloud particles show a scattering pattern similar to that given by the Rayleigh law, except that the intensity diminishes considerably more with scattering angle than indicated by this law.

On the basis of these few observations, it would appear that the particles are not strictly speaking within the Rayleigh size range. However, the spectra shown in Fig. 2 may not be comparable with each other because the scattered intensity is proportional to the number density of cloud particles in each case and this may have varied from day to day. Temporal variations in the optical thickness of the lower atmosphere would present a further complication. Barring such variations, we must assume that the noctilucent particles are of a size comparable to or slightly larger than the wavelength of visible light. For example, if we assume that the curve C corresponds to a true scattering angle of say 30° instead of 21·5°, then according to the Mie theory of scattering by spherical dielectric particles of a real refractive index 1·33, the normalized intensity should decrease by a factor of 10 between the angles of 17·5° and 30°, provided the radius a of the particle is such that $2\pi a/\lambda = 6$. From Fig. 2 we note that at $\lambda 420\,\mathrm{m}\mu$ the intensity ratio is indeed 10 : 1 between the curves A and C, and this would give a particle radius of $0{\cdot}4\,\mu$. This is a reasonable estimate close to values proposed in the recent literature[1], as well as an earlier estimate of $0{\cdot}2\,\mu$ given by one of us[6]. It is interesting to note that the above mentioned anisotropy should decrease with decreasing values of $2\pi a/\lambda$, that is with increasing wavelength, and such a trend is also evident in Fig. 2.

A better explanation of the observed spectral intensity gradient, for example in the 430 to $500\,\mathrm{m}\mu$ region (curve A), as well as of the angular anisotropy would perhaps result if,

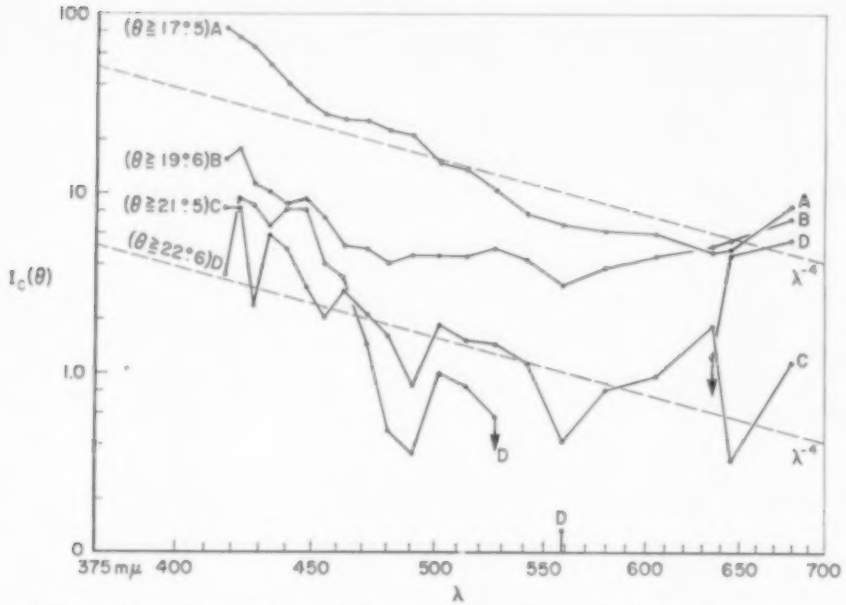

Fig. 2. Normalized extraterrestrial spectra of noctilucent clouds at various scattering angles θ (see text and Table 1.)

instead of a constant radius, one were to assume a *size spectrum* in which the concentration of particles greatly increases with decreasing size.

As for the increase in intensity beyond $\lambda 600$ mμ shown in curves A and B of Fig. 2, this could be explained by the fact that we have not taken into account the filtering action of the atmosphere above 30 km on the direct sunlight incident on the noctilucent clouds. The normal optical thickness of this portion of the atmosphere is very small[6], and it is governed by molecular scattering. However, it is not negligible in the present case, since parallel radiation grazing the 30 km level would be reduced to 78 per cent at $\lambda 450$ mμ and to 95 per cent at $\lambda 650$ mμ of its original flux due to attenuation by scattering.

Another interesting feature of the plots in Fig. 2 is the fact that no minimum appears in the vicinity of $\lambda 600$ mμ. This is the region of maximum absorption by ozone in the Chappuis bands. A calculation shows that if the noctilucent cloud is illuminated by direct sunlight passing through only 1/4th of the total ozone content in the vertical, the light received at the ground at $\lambda 600$ mμ should be reduced to about 30 per cent of its original flux due to ozone absorption alone. This is based on a total ozone content of 24 mm s.t.p. above the observer, and includes the absorption of the scattered light which must pass through the whole ozone layer.

A consideration of the geometry of the situation corresponding to curve B in Fig. 2, for which the clouds were about 400 km away from the observer according to the original report[3], shows that the point of closest approach to the earth of the illuminating solar rays was some 35 km above sea level. The same applies to curve C. Since in neither of these curves is there an appreciable reduction at $\lambda 600$ mμ, we must conclude that, during these observations at least, *there was a negligible amount of ozone (much less than 0·6 mm s.t.p.) above 35 km.* This may be a significant result since very little is known about ozone variations during and after sunset, especially above the level of maximum concentration. Theoretical considerations seem to be of little help here (cf. recent articles by Bates

and by Nicolet[11]). One might tentatively conclude that in the region where ozone is governed by photochemical equilibrium, say above 30 km, it disappears during the night. This of course must be checked by further observational and theoretical evidence. At any rate, the study of the continuous spectrum of noctilucent clouds would provide a rather sensitive tool in the investigation of night time ozone amounts and variations with height, on account of the long path of the incident solar radiation through the layers of interest.

Some remarks are in order regarding the irregularity in the continuous spectra of Fig. 2, especially those in curves C and D. Some of the maxima mentioned but not explained by Grishin[3], in the vicinity of λ423, 448, 463, 500, and 635 mμ appear also in some of the curves of Fig. 2. Instead of these maxima we are inclined to consider the *minima* appearing around λ428, 455, 558, and 645 mμ as more significant. In effect these might be explained if we remember that in our reduction we have *subtracted* the intensity spectrum of the clear night sky from that of the noctilucent clouds appearing on other nights at the same elevation angle. If the clear twilight and night sky has emission lines or bands at these wavelengths, originating from atmospheric layers above the level of noctilucent clouds, one would expect minima in the resulting curves at the same wavelengths. The minima at λ428 mμ (curve C) are in the vicinity of the strongest Kaplan–Vegard emission systems of N_2[7] and the one at 558 mμ almost coincides with the auroral green line at λ557·7 mμ. The curve D in Fig. 1 shows negative values between λ527 and 635 mμ except at 558 mμ. This might be an indication that on this occasion (7 July 1951) the auroral green line was strong enough to penetrate the noctilucent clouds. Furthermore the broad minimum appearing in the green region of the spectrum could be attributed to a green continuum in the twilight (scattered) light of the clear sky.

2.3. *Further remarks on the spectra*

The foregoing analysis shows that the spectra of noctilucent clouds can be explained primarily in terms of single scattering at small angles of direct sunlight falling on minute particles. The observed white or silvery color with the "reddening" closer to the horizon is clearly the result of the selective transmission of the underlying atmosphere.

The relatively high luminosity of the clouds, despite their tenuous character, indicates that the particles are highly efficient, non-absorbing scatterers, composed entirely of, or coated by, a dielectric material. The angular distribution of the scattered light indicates a size comparable to the wavelength and a moderate index of refraction. Although the clouds are mostly visible at low elevations above the horizon, there are exceptions. For example according to Jesse's observation of 19 July 1885, as quoted by Vestine[8], the clouds were visible over the entire sky including the antisolar portion. Geometrically it is quite possible for direct sunlight passing above the 30 km level to illuminate the noctilucent cloud level as far as 17° above the antisolar horizon, provided the sun's depression does not exceed 6°. Therefore the above mentioned observation cannot be discounted as an error of judgment. This means that the clouds can scatter with considerable intensity also at large angles or with $\theta > 90°$, which supports the assumption that there must be large amounts of particles with a radius $a < 0{\cdot}1\,\mu$. The high degree of polarization reported in the literature[1, 2] offers additional evidence of this.

The constant height of 82 km found by most observers is of course significant. However, this does not necessarily mean that the clouds are concentrated in a thin layer at that altitude. According to theory, the amount of scattered light is, in the first approximation, determined by the optical thickness of the layer, that is the mass of scatterers in a unit column, regardless of the degree of concentration. The layer may thus occupy a depth of several kilometers and still appear as a reflecting surface at 82 km, and this should be considered as a *virtual height* of the clouds rather than the true height.

Additional information about the character of noctilucent clouds should become available from further spectro-photometric observations.

The monochromatic optical thickness of the clouds at several wavelengths should be sought and this could be determined by star observations through the clouds. Of particular interest would be any spectra taken from higher elevations above the main atmosphere, including the spectral attenuation through the clouds in a horizontal direction. Additional ground observations similar to those discussed above, would be very helpful in a more detailed analysis, especially with regard to the angular distribution of the light from a given cloud, and simultaneous measurements of the degree of polarization.

3. ORIGIN OF NOCTILUCENT CLOUDS

It has been noted above that the spectrum of the clouds provides interesting information respecting the nature of the particles in the clouds. Precise knowledge of the nature of the particles, if available, would of course be of high interest with regard to their possible origin. Unfortunately such precise information is not available but it was noted that one possibility worth considering is that the clouds are likely to consist of nuclei coated with a dielectric material such as water, possibly in droplet or hydroscopic form, or as ice, which might provide the observed scattering of sunlight. On the other hand, since the dielectric constant for silicaceous materials is not very different, dust particles of silicaceous composition would also fit the data equally well. Since the particles exist on either side of the earth's shadow, the temperature of particles may be different on either side of this shadow, which may be a factor of some interest in connection with attempting to decide whether the particles are ice-coated particles or dust particles. It is hence desirable to estimate the possible temperatures in the atmosphere acquired by particles of characteristic absorbtivity α and emissivity ε, (1) within the earth's shadow and (2) in sunlit regions.

It is found experimentally that a value of bulk absorbtivity $\alpha=0{\cdot}5$ may be appropriate to many materials at modest temperatures. The emissivity, on the other hand, is harder to estimate usefully. For instance, it may vary from 0·08 for clean metals, to 0·3 for average substances, to 0·8 for oxides or ice. In the temperature estimates use was made of typical curves giving the temperature of spinning spheres for various values of α/ε[9]. Also used were additional curves for the case when the particle is in darkness near the earth, and also for the case of direct sunlight, the albedo of the earth being taken here as about 0·5, which is high ordinarily but may serve in the infrared. Actually the equilibrium temperature decreases with distance from the sun and also with increasing α/ε on the dark side of a planet. Expressed otherwise if the temperature of space is taken as $T_0=279°K$ when $\alpha/\varepsilon=1{\cdot}0$, the temperature T for other values of α/ε will be given by $T=(\alpha/\varepsilon)^{1/4}T_0$. Using these considerations it is found that for oxide-coated particles or ice a suitable value may be roughly $\alpha/\varepsilon=0{\cdot}625$, in which case $T=248°K$ in space, 283°K near the earth in sunlight, and 166°K near the earth on the dark side. For average materials ($\alpha/\varepsilon=1{\cdot}7$) these temperatures become roughly $T=320°K$ in space, 360°K near the earth in sunlight, and 166°K near the earth on the dark side. For clean or polished surfaces a typical value of α/ε is about 6·2, so that in space (at earth distance) $T=440°K$, 490°K near the earth in sunlight, and 166°K near the earth on the dark side. It is reasonably clear therefore that even on the dark side near the earth it will be difficult to form a water deposit on particles above the level of noctilucent clouds. However, it would be desirable to examine the heating of small spheres of diameter comparable with the wavelength, in order to estimate the thermal error in these initial approximations.

The history of a cosmic particle contributing to the formation of noctilucent clouds is of course unknown. Since from the calculated radiation effects above the night temperature is about 166°K, the same as that of the upper atmospheric gas, there would obviously be no thermal changes due to the atmospheric gases in contact with the particle. In sunlight the particle may achieve a higher temperature, and of interest here is the fact that a particle drifting across the boundary of the earth's shadow

may heat up at a certain rate with time, as it moves into the sunlit region. If this rate is very slow and if an ice coating had formed in the darkness, the particles might remain ice coated for some time. On the other hand, the particle would lose its ice coating if solar heating is communicated at a sufficiently rapid rate.

It is shown in treatises on the kinetic theory of gases that the energy communicated as heat to the particle by an atmospheric molecule colliding with it is of order $4kT$ per second where k is Boltzmann's constant. If a is the radius of the particle its surface of cross-section is of area πa^2. The number of molecules at 82 km is about 3×10^{14}, and if $\bar{v}$ is the mean velocity of a molecule the total flux of energy to the particle is roughly $n\bar{v}(4kT)\pi a^2$ or about $2 \times 10^{-8} \pi a^2$ ergs/sec or

$$2 \times 10^{-8} \times 3 \times 10^{14} a^2 = 6 \times 10^6 a^2 \text{ ergs/sec.}$$

Since the flux of incident solar radiation is about 10^6 ergs/cm^2 sec, the temperature of the particle should be about the same as that of the local atmosphere in which it is suspended. But less than 15 km above, at 95 km, the influence of radiation alone may be dominant.

At any rate as Ludlam[1] has noted, it is difficult to deposit water vapour in significant amounts in cloud form at these levels. The warming action of sunlight, at least at higher levels, will accentuate these difficulties, and make the hypothesis of dust particles the more likely one. The latter, incidentally, is the simplest hypothesis since particles of the sizes we have mentioned are needed in any case as nuclei for the deposit of water vapour. Since particles of size $0{\cdot}1\,\mu$ to $0{\cdot}4\,\mu$ radius are ordinarily needed as nuclei in order to form a cloud ascribed to water vapour, these nuclei alone would collectively appear as a cloud of the same number density of particles per unit volume. Moreover, from the scattering considerations indicated above it is clear that a cloud of cosmic or other dust needed to form nuclei could be seen just about as readily as would these nuclei coated with ice. For the foregoing reasons the discussion of temperature of these nuclei, though interesting, is probably largely academic.

The vapour pressure of ice at $-107°$C is so low that it would take a long time for a film of water to evaporate off a droplet at a pressure of about 10^{-5} atm. Conversely, it would also take a long time for condensation to take place. Hence it appears likely that if the clouds consist of dust particles, they will be mainly of silicaceous or similar dielectric composition, as inferred from the optical properties. But if the particles are metallic, for example, an ice coating would provide suitable dielectric action. In an earlier paper one of us has suggested that a cosmic origin of such particles is likely[8]. A water source from comets may be possible, as well as a supply of dust from meteoric streams.

In this connection it is interesting to note that an analysis of recent spectra of the Martian atmosphere during the blue clearing, obtained by A. G. Wilson[10], shows certain similarities with those of noctilucent clouds. In particular these spectra, after reduction, show a maximum intensity in the blue region and generally resemble those of noctilucent clouds, except that the positions of the secondary maxima and minima are reversed. Assuming that particles of the same size and nature are responsible for both types of spectra, this reversal is reasonable in view of the fact that the Martian spectra represent back-scattered sunlight whereas the terrestrial cloud spectra correspond to scattering in the forward direction. This may be the first indication of the existence of haze layers of the same interplanetary origin existing in the atmosphere of both planets.

It will also be noted that except for particles very near the sun, which might have an iron content and subsequently cool, it will be unlikely that the particles will become magnetic on cooling through the curie point in the geomagnetic field. The temperatures estimated are too low for this to happen ordinarily. Although it seems likely that some magnetized dust particles may preferentially enter the terrestrial polar regions, there appears to be no evidence that the geomagnetic field exerts an important diverting influence upon such particles.

REFERENCES

1. F. H. Ludlam, *Tellus* **9**, 341–364 (1957).
2. G. Witt, *Tellus* **9**, 365–371 (1957).

3. N. I. GRISHIN, *All-Union Astr. Geod. Soc. Bull.* **19** (26), 3–16 (1956).
4. F. S. JOHNSON, *J. Met.* **11**, 431–439 (1954).
5. D. DEIRMENDJIAN, *Ann. Geoph.* **13**, 286–306 (1957); *Ann. Geoph.* **15**, No. 2, in press (1959)
6. D. DEIRMENDJIAN, *Arch Met., Wien* B **6**, 452–461 (1955).
7. P. SWINGS and A. B. MEINEL, The Spectra of the Night Sky and the Aurora, *The Atmosphere of the Earth and Planets*, edited by G. P. KUIPER, pp. 159–210. University of Chicago Press, Chicago (1952).
8. E. H. VESTINE, *J. Roy. Astr. Soc., Canada*, 249–272, 303–317 (1934).
9. C. GAZLEY, JR., W. W. KELLOGG and E. H. VESTINE, submitted for publication in *J. Aero Space Sci.* Institute of Aeronautical Sciences, New York.
10. A. G. WILSON, Spectrographic Observations of the Blue Haze in the Atmosphere of Mars, Moscow Meeting, IAU (1958).
11. *The Earth as a Planet*, edited by G. P. KUIPER, University of Chicago Press, Chicago (1954).

Planet. Space Sci. Pergamon Press 1959. Vol. 1, pp. 155–160. Printed in Great Britain.

SIDEREAL ANISOTROPY OF HIGH ENERGY COSMIC RAYS*

I. ESCOBAR V., N. NERURKAR† and R. WEIL

Laboratorio de Fisica Cosmica de Chacaltaya, U.M.S.A., Bolivia
Centro Brasilero de Pesquisas Fisicas, Brazil

(*Received* 13 *December* 1958)

Abstract—An experiment detecting extensive air showers responding to primary energies greater than 10^{14} eV is being conducted at Chacaltaya, Bolivia (Elevation 5220 m; geographic latitude 16° S) with counter trays separated at least by 20 m. There is evidence of a sidereal anistropy of about 1·6 per cent with the time of maximum at 1400 LST (Local Sidereal Time). The barometric coefficient is discussed in connection with the absorption curve for extensive showers.

1. INTRODUCTION

The cosmic ray intensity measured by instruments installed on a fixed point on the earth may indicate a variation due to the fact that, as the earth rotates on its axis, the instruments point to different parts of the interstellar space. Studies made over the past few years of data obtained with instruments responding to primary cosmic rays of low and medium energies have shown a significant variation of intensity with solar time, while the intensity appears to be almost constant over a sidereal day. These facts have been generally interpreted in the sense that the solar variation arises partly due to terrestrial atmospheric changes following solar time, and partly due to the diverse electro-magnetic structure of the interplanetary space in different directions. The high degree of isotropy in sidereal time could then be due to the large scattering of primaries while they pass through the magnetic fields in the interplanetary space; thus, these particles would lose completely all correlation with their original directions. All this would suggest that, if there is anisotropic distribution of primary cosmic radiation in our galaxy, it could only be detected by measuring high energy cosmic rays, which would only be slightly affected by the magnetic fields in the earth's neighbourhood. A study of the sidereal time variation is therefore related to the search for a galactic anisotropy in the primary cosmic radiation.

In the energy range from 10^{14} to 10^{15} eV, measurements made in the northern hemisphere by Hodson[1] indicated an amplitude of $(1{\cdot}15 \pm 0{\cdot}61)$ per cent with a maximum at 2330 LST (Local Sidereal Time) while Daudin and Daudin[2], whose measurements were more precise, reported several variations, but all with negligible amplitudes, suggesting that it would always be difficult to separate them from the atmospheric effects. With energies about 10^{16} eV, Cranshaw and Galbraith[3] first found an amplitude of $(4{\cdot}9 \pm 1{\cdot}5)$ per cent with maximum at 1030 LST, but their later results are in contradiction with the earlier ones, so that the total data do not show any significant variation. This removes the discrepancy that appeared between the earlier results of both Daudin and Daudin[2] and Cranshaw and Galbraith[3], both experiments having been conducted at the same latitude.

In the Southern hemisphere, Farley and Storey[4] in the beginning reported an amplitude of $(1{\cdot}5 \pm 0{\cdot}23)$ per cent with the maximum at 1700 LST. However, their later results also

* Supported in part by the joint program of the O.N.R. and U.S. A.E.C. through the L.N.S.E. of M.I.T., Cambridge, Mass.

† On leave of absence from the Physical Research Laboratory, Ahmedabad, India, under a UNESCO post doctoral fellowship.

failed to confirm the earlier ones, thus indicating negligible sidereal variation. A recent report by Chapman and Ryder[5] shows a variation of $(0{\cdot}88 \pm 0{\cdot}65)$ per cent with the maximum at 1700 LST, which can also not be said to be significant.

It is to be noted that in 1956, the results of Hodson, Daudin and Daudin, and Farley and Storey showed that the maximum intensity appeared within half an hour of the passage overhead of the galactic plane. The galactic center being 23°S, anisotropy bearing relation with the galactic center is expected to show up more favourably in the observations made in the southern hemisphere. In addition, most of the above mentioned experiments were conducted at sea level.

In view of these facts, an experiment was planned in 1956 and was set up in Chacaltaya (Geomagnetic Latitude 4°S, Geographic Latitude 16°S and Longitude 68°W) which is located at 5220 m elevation with a mean annual pressure of 407 mm of mercury. It is somewhat advantageous to conduct these experiments at high altitudes in order to have large counting rates to improve the statistical significance of the data. This station has an additional advantage in that, being situated near the equator, the seasonal temperature changes are quite small and regular compared to those at intermediate latitudes. The purpose of this paper is to give an account of the sidereal variation in high energy primaries observed at Chacaltaya during 230 days scattered over a period of 18 months.

2. EXPERIMENTAL ARRANGEMENT*

The sensitive part of the equipment consists of 4 trays of GM counters placed in a horizontal plane, as shown in Fig. 1. Trays I, II and III consist of 8 counters each, while tray IV has only two counters. All counters are 1 in. in diameter and 22 in. in length with brass walls 0·02 in. thick and are filled with a mixture of petroleum ether and argon (composition ratio 1 : 10) to a total pressure of 8·4 cm Hg. The counters in each tray are connected in parallel making the sensitive area 1136 cm² for each of the first three trays and 284 cm² for the fourth one.

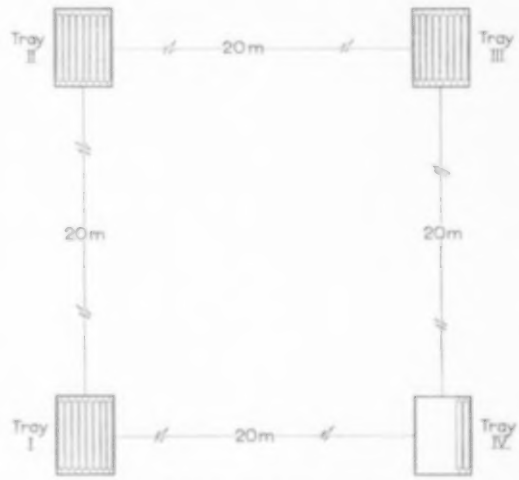

Fig. 1. Experimental arrangement.

Trays II and III are housed in the main laboratory building where the temperature changes from 17° to 22°, while the other two trays are placed outside in thermally insulated boxes whose inside temperature is controlled thermostatically. Above the first two trays there is 3 g cm^{-2} of absorbing material while the last two have negligible absorbing material over them and are placed on the mountain side which has a slope of 28°. The trays are in a horizontal position.

Threefold coincidences between trays I, II, and III and fourfold coincidences are registered separately. The resolving time of the coincidence circuit is less than 3 μs. The single tray rates of the first three trays are of the order of 7,200 counts/min, and the threefold and fourfold coincidences give about 340 and 100 counts/hr, respectively. The accidental coincidences for the threefold are of the order of 3 counts/hr and for the fourfold coincidences 0·04 counts/hr. Each coincidence output is registered by two separate recorders, one of which self-clears every hour; in addition, the

* The complete details of the equipment and its operation are described in *Resumen de Labores* 1956-1957 U.M.S.A.-C.B.P.F. publication.

counting rates of trays I and II are monitored continuously. All the mechanical recorders are photographed every hour together with two altimeters, a thermometer indicating the temperature of the instruments room, and a 24 hr electric clock which is driven by a frequency standard together with the timer which triggers the camera control circuit.

Counting rates of all the trays are checked five times a week while a quick check of the whole equipment is done from the hourly rates of triple and fourfold coincidences. The operating points of each counter are checked every second day, and, if necessary, adjusted. Approximately once a month, a general check of the operating conditions of the equipment is made. In the beginning, failures of the main power source shut down the whole equipment requiring manual restart. This caused the loss of many hours of data. Later on, an automatic reset mechanism was provided which reconnected the unit after a power failure.

3. SELECTION OF THE DATA

The data were rigorously selected. First it was made sure that the information corresponded to periods when all the equipment was operating normally. This was determined mainly from the log book notes. Another check was provided by the level of counting of the monitored trays; all the data were rejected for those hours during which any recorder showed large departures from the statistical fluctuations. Thus, whenever there was any doubt of the reliability of the data, or when there was a factor which could have falsely affected the diurnal variation of intensity, the information was rejected. Only after this selection had been made did the statistical analysis follow.

It has been mentioned earlier that out of 18 months of operation only 230 days were used. Five months, or 150 days, of data were rejected outright. They were considered unreliable since replacement counters were not available when needed. Furthermore, a total of 50 days was lost because of photographic registration difficulties. The balance of lost information corresponds to days when the equipment was checked, main power failures, and the critical data selection described in the previous paragraph.

Although the data were read every hour, only two-hourly intensities were used to facilitate computation. This also permitted the use of the instantaneous pressure values of the hours on which the intensities were centered.

4. DISCUSSION

The energies of the primary cosmic rays originating the showers which produce the threefold and the fourfold coincidences were calculated by the method given by Greisen[6]. These energies were found to be 5×10^{14} and 2×10^{15} eV for the threefold and fourfold coincidences respectively.

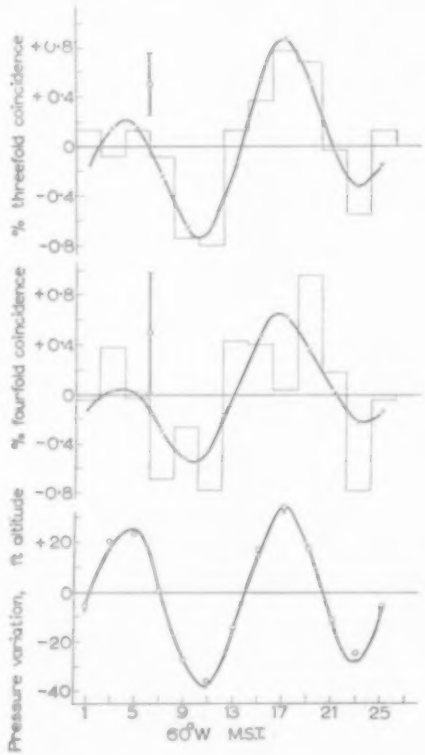

Fig. 2. Diurnal variation in solar time without any correction. Note for the lowest curve only: x—three fold; o—four fold.

Table. 1. First and Second Harmonic Coefficients of 3-fold, 4-fold Coincidences and the Corresponding Pressure Variation on Solar Time.

	First harmonic		Second harmonic	
	Amplitude	Angle of maximum	Amplitude	Angle of maximum
3-fold coincidences	0·38%	−78°	0·51%	+137°
4-fold coincidences	0·34%	−86°	0·34%	+129°
Pressure for 3-fold	4·5 ft	−43°	28·5 ft	+147°
Pressure for 4-fold	8·0 ft	−46°	29·7 ft	+140°

Fig. 2 shows the uncorrected variation of threefold and fourfold coincidences as well as the corresponding pressure plotted against Local Standard Solar Time. The pressure is expressed in feet of altitude given by the mean reading of two aircraft altimeters. At the altitude of Chacaltaya, 608 ft of altitude variation are equivalent to a pressure change of 1 cm Hg.

It can be seen from Fig. 2 that there exists a very good correlation between cosmic ray variation and pressure variation. The harmonic components of these variations are expressed on harmonic dials in Fig. 3 and Table 1. Considering the phases of these components, cosmic ray and pressure variation vectors are very well correlated, but there does not exist a unique relation between them. If the second harmonic of the cosmic ray intensity variation arises due to that of the pressure variation only, the first harmonic of the pressure variation is too small to account for that of the cosmic ray variation vector. On the other hand, if the first harmonic of the cosmic ray variation is supposed to arise completely due to that of the pressure variation, there will be a large residual second harmonic whose cause would be rather difficult to ascertain. Furthermore, there is no known cause, except semi-diurnal oscillations of pressure, which can give rise to a large semi-diurnal component in cosmic ray variation, whereas the first harmonic can arise from a diurnal temperature variation. We therefore assumed that the second harmonic in the variation of threefold and fourfold coincidences arises only because of that of pressure variation, between which the correlation is greater than 0·96, and the following equation was used:

$$B = -CR_2\,100/P_2\cos\theta$$

where B = pressure coefficient

CR_2 = amplitude of second harmonic cosmic ray intensity vector

P_2 = amplitude of second harmonic pressure vector (cm Hg)

θ = angle between CR_2 and $-P_2$.

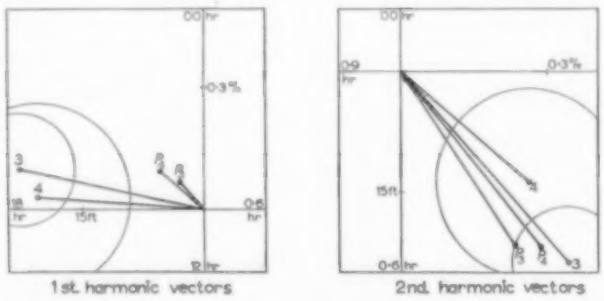

Fig. 3. 60° W mean solar time harmonic dials. P_3, P_4—pressure vectors; 3, 4—coincidence vectors.

The coefficients thus obtained are the following:

For 3-fold coincidences

$(-11{\cdot}05 \pm 2{\cdot}38)$ per cent/cm Hg

For 4-fold coincidences

$(-\ 7{\cdot}08 \pm 3{\cdot}96)$ per cent/cm Hg

A check was made of these coefficients by using the least squares method on the total intensity and pressure curves. This method yielded the results given below:

For 3-fold coincidences

$(-10{\cdot}75 \pm 2{\cdot}85)$ per cent/cm Hg

For 4-fold coincidences

$(-\ 7{\cdot}95 \pm 3{\cdot}70)$ per cent/cm Hg

It can be seen that, within the experimental errors, both results agree. As it was felt that the assumptions of the first method are more justified in the present case, the results thus obtained were used in the calculations to follow.

Considering the experimental errors, our results are also consistent with those found by other workers.[2–4] Furthermore, from the experimental absorption curve given by Greisen[6], to which our fourfold coincidence geometry corresponds, we expect a 15 per cent reduction in the pressure coefficient of the fourfold coincidence variation. Although the experimental errors do not allow the confirmation of these results, the nature of the curves given in Fig. 2, showing an extremely good correlation between pressure and cosmic ray intensity, gives a strong indication that the lower coefficient observed in the fourfold coincidence variation may have genuine significance.

5. SIDEREAL VARIATION

Since the intensities were averaged over two hour intervals, it was impossible to convert the data to sidereal time every day. Hence the monthly averages, corrected for pressure, were shifted by two hours every month starting from September so as to obtain every month's data in terms of Local Standard Sidereal Time. This procedure smoothed the sidereal variation but this effect was corrected in the final value by the method suggested by Chapman and Bartels[7].

Fig. 4 (full line curves) shows the sidereal variation of threefold and fourfold coincidences obtained after correction for pressure only. Since all the fourfold coincidences were registered also as threefold coincidences, it was deemed interesting to remove the contribution of these events from the threefold coincidences. The dotted curve in Fig. 4 (a) shows the time variation of the events that were responsible for threefold but not for fourfold coincidences. Thus it appears that the sidereal variation of primaries in the range of 5×10^{14} to 2×10^{15} eV is extremely small and could be considered as negligible within our statistical errors. We have, therefore, concentrated our attention to the fourfold variation only in further investigation on sidereal time.

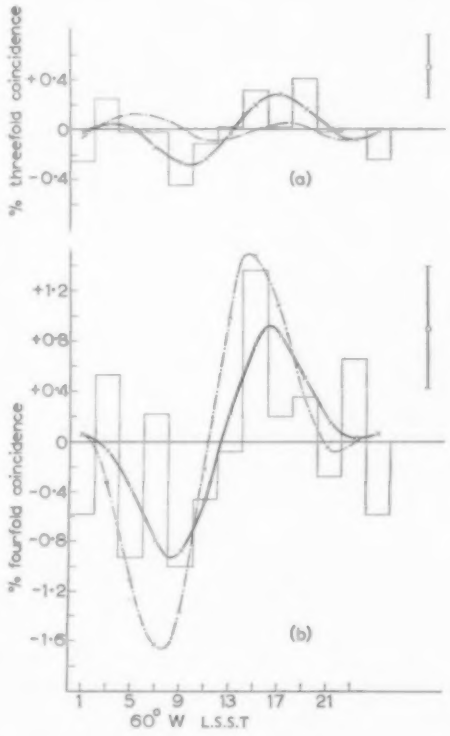

Fig. 4. Diurnal variation in sidereal time.
(a) ——— with pressure corrections only;
—·—·— fourfold contribution subtracted;
(b) ——— with pressure correction only;
—·—·— with all corrections.

The solar component may have a seasonal modulation. This, together with the necessarily incomplete meteorological correction, may give rise to an apparent sidereal variation. In order to correct for these effects, the method described by Farley and Storey[4] has been used. Fig. 4 (b), dotted curve, shows the resulting variation of fourfold coincidences after effecting this correction and the correction for the smoothing effect mentioned earlier. As can be seen from this curve, there appears to be a sidereal variation in the fourfold coincidences with a maximum of 1·6 per cent at 1430 Local Standard Sidereal Time (LSST), that is, 1400 Local Sidereal Time (LST).* The harmonic coefficients from which this curve arises are the following:

Harmonic	Amplitude	Hour of maximum LSST	Hour of maximum LST
1st	(1·10 ± 0·28)%	17·37 ± 0·96	16·84 ± 0·96
2nd	(0·71 ± 0·28)%	2·17 ± 0·72	1·10 ± 0·72

The time of maximum of the first harmonic at about 1700 LST, together with the large second harmonic, would be quite consistent with the interpretation of Davis[8] in which he suggests the possibility of a sidereal anisotropy arising both by the acceleration of cosmic rays by the Fermi mechanism and by the inhomogeneities in cosmic ray densities normal to the interstellar magnetic field lines. However, the fact that isotropy is found in the range of primaries of energies from 5×10^{14} to 2×10^{15} eV implies that the sidereal anisotropy exists only in energies higher than 2×10^{15} eV and this is difficult to explain in terms of the present theories.

* Local Standard Sidereal Time = UST − 4·000 hr; Local Sidereal Time = UST − 4·533 hr. The difference arises from the fact that Local Standard Sidereal Time is 60° W time, while Chacaltaya is located at 68° W.

6. CONCLUSION

The barometric coefficient of the extensive air showers at an altitude of 5·220 m near the equator was found to be (−11·05 ± 2·38) per cent/cm Hg and (−7·08 ± 3·96) per cent/cm Hg for two different geometries responding to primary energies of 5×10^{14} eV and 2×10^{15} eV, respectively. The latter coefficient is suggestive of a smaller value than that found for those energies at intermediate latitudes and at sea level. In the energy range above 2×10^{15} eV there appears to be a sidereal variation of about 1·6 per cent with maximum at about 1400 LST.

ACKNOWLEDGEMENTS

We are grateful to Dr. R. W. Williams for his invaluable assistance, to Mr. R. Palmeira for helping to set up the equipment and to Prof. J. Hersil and Messrs. A. Lazo and J. Saavedra for their cooperation in running the equipment. Our thanks are due to Miss I. Argandoña for computational assistance.

REFERENCES

1. A. L. Hodson, *Proc. Phys. Soc.* A **64,** 1061 (1951).
2. A. Daudin and J. Daudin, *J. Atmos. Terr. Phys.* **3,** 245 (1953).
3. T. E. Cranshaw and W. Galbraith, *Phil. Mag.* Ser. 7, **45,** 1109 (1954); *ibid.* Ser. 8, **2,** 804 (1957).
4. F. J. M. Farley and J. R. Storey, *Proc. Phys. Soc.* A **67,** 996 (1954); *ibid.* B **70,** 843 (1957).
5. N. G. Chapman and N. V. Ryder, *J. Atmos. Terr. Phys.* **11,** 291 (1957).
6. K. Greisen, *Progress in Cosmic Rays,* Vol. III. North Holland Publishing Co., Amsterdam (1956).
7. S. Chapman and J. Bartels, *Geomagnetism,* Vol. II. Oxford University Press (1940).
8. L. Davis, *Phys. Rev.* **96,** 743 (1954).

Planet. Space Sci. Pergamon Press 1959. Vol. 1, pp. 161–172. Printed in Great Britain.

NITRIC OXIDE AND MOLECULAR OXYGEN IN THE EARTH'S UPPER ATMOSPHERE

A. S. JURSA, Y. TANAKA and F. LeBLANC

Geophysics Research Directorate, Air Force Cambridge Research Center, Air Research and Development Command, L. G. Hanscom Field, Bedford, Massachusetts

(*Received November* 1958)

Abstract—As a result of a rocket-borne experiment performed in New Mexico on 18 March 1958 at sunset, data were obtained which led to conclusions concerning the concentrations of nitric oxide and molecular oxygen in the altitude range 60 to 87 km.

The technique used was that of absorption spectroscopy. A specially designed spectrograph, mounted in a biaxial pointing control, was flown in an Aerobee Rocket. Seven spectrograms were obtained.

It was determined that the concentration of nitric oxide in the altitude interval 63 to 87 km cannot exceed 10^8 molecules/cm^3. The molecular oxygen concentration in the same region was found to be essentially the same as derived from the assumption that the composition of the atmosphere, below 90 km does not change with height.

A comment is made concerning the solar continuum and solar Lyman-α radiation.

1. INTRODUCTION

The fact that nitric oxide exists in the upper atmosphere and that it plays an important role in the formation of the *D*-layer is, today, quite well accepted by those who are engaged in the study of the Earth's atmosphere.

In 1939, Kaplan[1] suggested, based on his laboratory study of nitrogen afterglow, that nitric oxide bands are present in the light of the night sky but are not observed because of absorption by ozone. Soon after, Elvey[2] showed coincidences between bands in the spectrum of the night sky and nitric oxide bands; and Price[3] discussed processes that could lead to the production of nitric oxide in the upper atmosphere.

In 1945, Nicolet[4] suggested that the ionization below 100 km, which is the *D*-region, could be explained by photoionization of nitric oxide by solar radiation. From that time there has been increased interest in the importance of nitric oxide in the upper atmospheric phenomena. Bates[5] has presented theoretical arguments showing how nitric oxide could be formed in the *D*-region, why it must be a constituent of the atmosphere at those altitudes, and speculating as to its concentration and distribution in the upper atmosphere. Nicolet[6–8] has given additional theoretical support to his original suggestion[4] while Watanabe[9] and others presented laboratory results on the ionization cross-section of nitric oxide which support the theory that the observed electron density in the *D*-region is produced by the process

$$NO + h\nu\,(\text{Lyman-}\alpha) \rightarrow NO^+ + e$$

However, to this time, no direct determination of the presence of nitric oxide in the upper atmosphere has been made and its concentration and distribution remain uncertain. Mitra[10] has presented tentative models of equilibrium height distribution of nitric oxide in which he states the concentration of nitric oxide to be of the order of 10^{10} molecules/cm^3 at 90 km and 10^{12}/cm^3 at 82 km. Nicolet[7, 8] has stated that the nitric oxide concentration is considerably less, of the order of 10^8 molecules/cm^3 at 80 km and 10^9/cm^3 at 65 km.

In 1949, Durand[11] and others, reporting on solar spectra obtained from a rocket, stated that broad absorption observed at approximately 2264 Å might be caused by atmospheric nitric oxide. Later, Johnson[12] and others, reporting on additional solar spectrograms obtained from rockets, withdrew the earlier suggestion and stated there was no evidence of nitric oxide absorption occurring either in the terrestrial or solar atmosphere. Nicolet[8] interpreted the results in Johnson's paper as setting the upper limit of nitric oxide concentration at 10^{11} molecules/cm^3. In 1952, Migeotte and Nevan[13], using infrared absorption techniques from a European mountain top, were unable to detect absorption by atmospheric nitric oxide, and they set an upper limit of 0·02 cm (n.t.p.) for the nitric oxide concentration, which is equivalent to 5×10^{17} molecules/cm^2-column. In 1953, Byram[14] and others, reporting on the results of a rocket experiment concerned with Lyman-α radiation in the solar spectrum, stated that the concentration of nitric oxide above 75 km does not exceed an upper limit of 0·007 cm (n.t.p.).

In addition, in rocket experiments for the purpose of determining the composition of the upper atmosphere by mass spectrometer techniques, nitric oxide ions have been reported as found over an extremely large altitude range (but no quantitative results have been stated). Johnson[15] reported ions of mass number 30 (nitric oxide?) recorded between 100 and 200 km. And, in the "Soviet Bloc IGY Information"[16] it is stated that data obtained between the altitudes of 105 and 206 km indicate that ions of mass number 30 predominate and are presumed to be nitric oxide ions. In our opinion, until more positive evidence is available, the detection of nitric oxide ions in the upper atmosphere by mass spectrometer techniques from rockets should be accepted with reservation because of the possibility of contamination of the atmosphere, at least in the vicinity of the measuring instrumentation, by nitric oxide from the rocket engine, fuel and combustion products,[17] and because of the possibility of the formation of NO within the measuring instrumentation.

It has been our purpose, in the present experiment, to attempt to detect the presence of nitric oxide in the altitude range 60 to 90 km and to possibly determine its concentration or to set an upper limit on that concentration by means of absorption spectroscopy in the vacuum ultra-violet region.

This experiment has been a part of the official IGY effort.

2. EXPERIMENTAL

The technique used in this attempt to make a direct determination of the NO concentration was that of absorption spectroscopy in the vacuum ultra-violet region. We have used this technique extensively in the laboratory to study the structure of various gas molecules such as N_2, O_2, H_2, NO, NO_2, N_2O, CO_2 and others, and, consequently, are quite familiar with the absorption spectrum of NO. In the present case, the sun was used to provide the background radiation, the atmosphere was the absorbing medium and the rocket spectrograph the recording instrument.

2.1. *Field*

The experiment was performed at sunset. This permitted the use of long atmospheric pathlength while still maintaining the condition that only radiation passing through layers above, and including the one in which the instrument is located, is recorded at any given moment. A maximum atmospheric pathlength was considered to be necessary because of the low concentration of NO assumed to exist at those altitudes.

The rocket spectrograph used in this experiment is similar to one previously described.[18] It is shown with the covers off in Fig. 1 with the pencil pointing at the film cassette. It is basically a concave grating instrument utilizing a 40 cm radius of curvature, 600 grooves/mm replica grating with a ruled area of approximately 2 × 4 cm. The instrument is 22 in. long, 8½ in. wide and 4 in. deep. It is extensively baffled throughout to eliminate stray and reflected light and to allow for the use of a relatively large air evacuation port at the rear. The slit, 1 cm in height, was set at a width of

Fig. 1. Rocket spectrograph. The top plates have been removed to reveal the baffles, slit holder, grating holder and air evacuation ports. The pencil indicates the armoured film cassette.

Facing p. 152

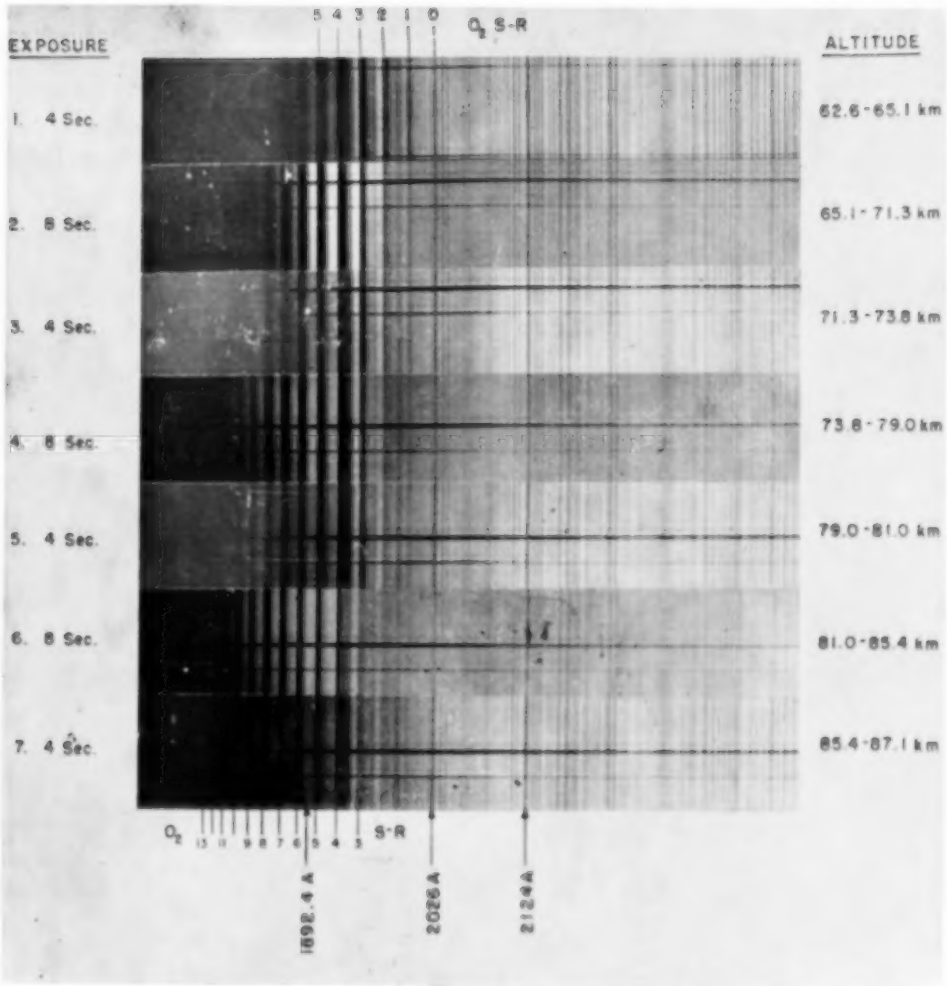

Fig. 2. Spectrograms obtained during rocket flight. Seven spectrograms obtained between the altitudes of 62·6 and 87·1 km are shown. The Schumann–Runge absorption bands of atmospheric O_2 are identified as are a solar emission line at 1892·4 Å and two strong solar absorption lines at 2026 Å and 2124 Å.

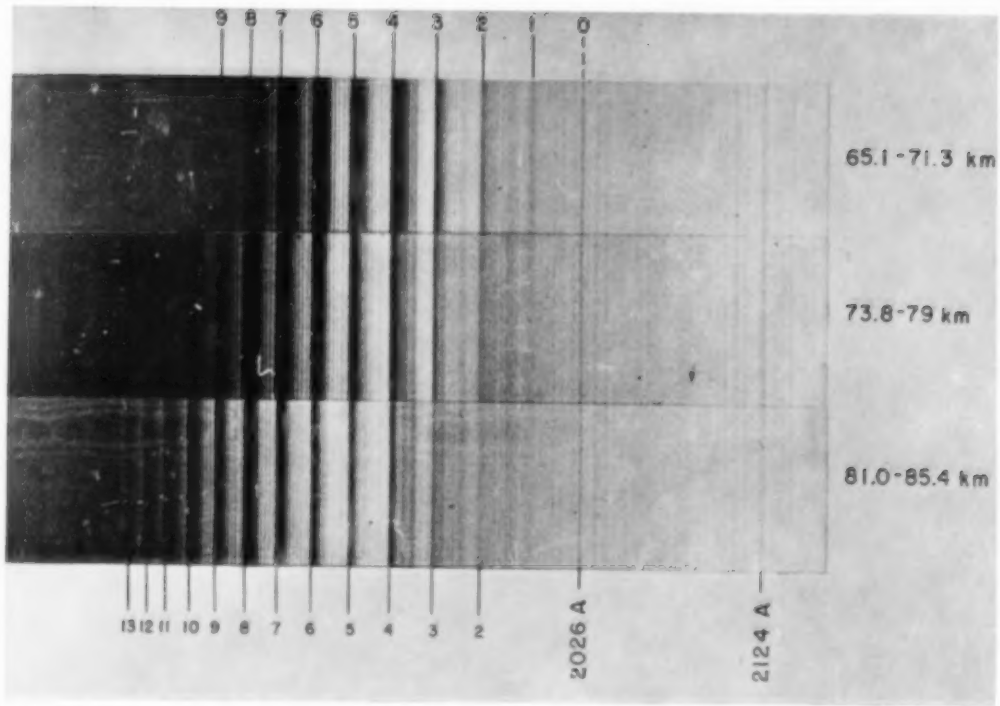

Fig. 3. Rocket-flight spectrograms. The well defined rotational structure in the atmospheric O_2 Schumann –Runge absorption bands shows the relatively good resolution obtained in the spectrograms from the rocket.

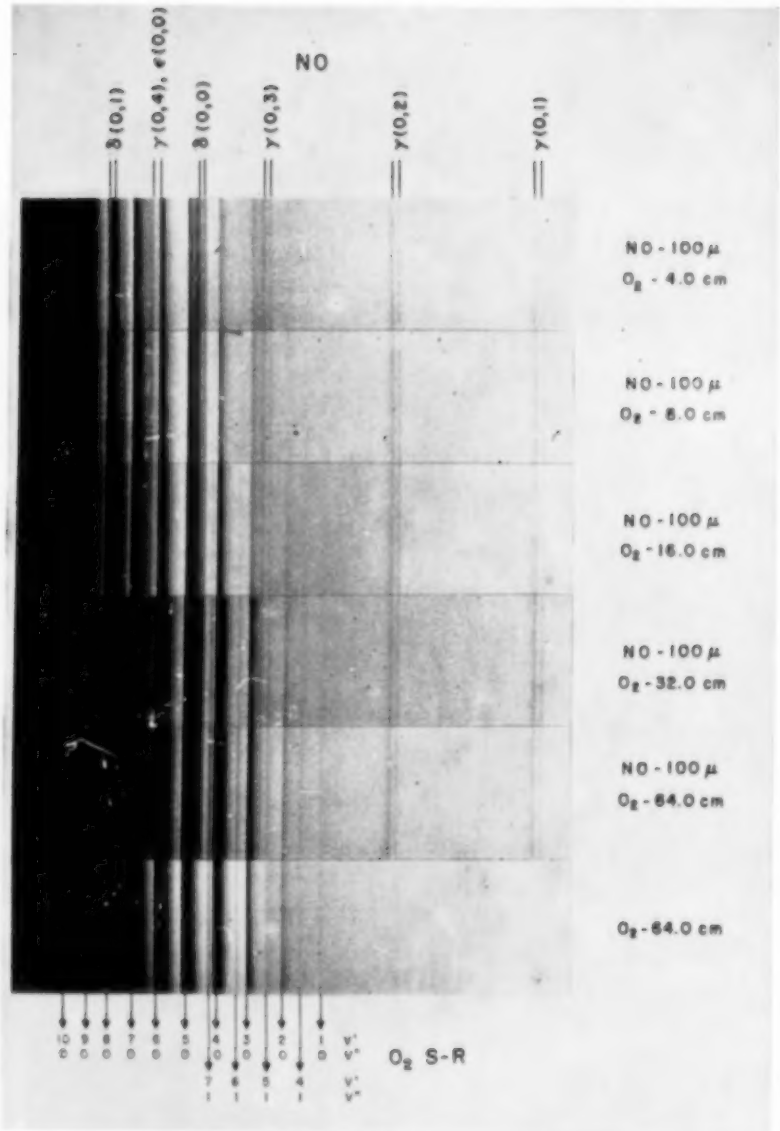

Fig. 4. Laboratory spectrograms. Superimposed absorption spectra of NO at 100μ pressure with O_2 at various pressures as obtained in the laboratory.

facing p. 153)

15 μ for this experiment. Seven strips of film, $\frac{3}{8}$ in. $\times 2\frac{1}{2}$ in., were mounted in slots on a drum which was enclosed in an armoured cassette. The wavelength region covered approximately 1000 to 3000 Å. The film was SWR type which we use regularly in the laboratory.

One of the major problems in solar spectroscopy from rockets has been, and is, that of scattered light (longer λ) from the grating surface. In lieu of undertaking a research project in grating rulings and their effects on scattered light, we investigated several reflecting materials as coatings for the grating surface. As a result of those tests, the grating we used in the experiment was coated with germanium.* Although this coating did not solve the scattered light problem completely, it did help noticeably by reducing the reflected visible and near ultraviolet radiation and by showing an improvement in reflectivity in the 2000 Å region and below when compared with an aluminium coating. Our purpose, in this case, was to choose a reflecting material which would allow for a sufficient exposure time without introducing any apparent scattered light in the wavelength region of interest. This was accomplished in the present experiment with a Ge coated grating and exposure times of four seconds.

The spectrograph was oriented at the sun during the rocket flight by a biaxial pointing control which is a photoelectric servo-mechanism. This device† has been used successfully in solar spectroscopy experiments from rockets for several years. The rocket was a standard or relatively low altitude Aerobee, AF 10-25.

USAF Aerobee number 93 was launched at the Holloman Missile Development Center in New Mexico (32° 53′ N, 106° 08′ W) at 1812 hr (2 min before sunset) on 18 March 1958. The rocket flight was normal and well behaved. The pointing control functioned well as did the spectrograph. The first exposure began at $X+75$ sec and the seventh, and final, exposure ended at $X+115$ sec. Recovery was by parachute and all equipment was recovered in excellent condition. The SWR film was developed, four hours after rocket launching, in ice-cooled D-19, which was diluted 4–1, for 2 min.

Fig. 2 shows enlargements of the seven spectrograms, the altitudes at which they were obtained and the exposure times of each. The spectrograms are composed of the Fraunhofer absorption spectrum superimposed with the Schumann–Runge absorption bands of atmospheric O_2. Because the resolution was very good, as evidenced by the rotational structure in the O_2 bands, Fig. 3, we were able to make a thorough analysis of the spectrograms.

2.2. *Laboratory*

In order to estimate the NO concentration in the upper atmosphere, we took absorption spectrograms of NO, O_2 and $(NO+O_2)$ under various conditions in the laboratory, with the same spectrograph used in the flight, prior to the actual flight. Because the recovery was perfect, this work was repeated again after the flight. The spectrograms taken in this laboratory work were used as a reference for evaluation of the flight spectrograms.

We set up a system with the hydrogen continuum as a source, an absorption cell of 19·5 cm length fitted with lithium fluoride windows for NO, and a vacuum chamber to contain the rocket spectrograph and to act as an absorption "cell" of 94·4 cm pathlength for O_2. The pressures in the cell and in the tank were measured with a McLeod Gauge before and after each exposure. The ranges of pressure were 0·1 to 76 cm Hg for O_2 and 1·0 to 500 μ for NO. The exposure times were about four minutes. A closed system was adopted for the absorption cell, and we did not notice any change of pressure between readings before and after the exposures. The minimum pressure of NO at which the $\delta(0,0)$ band was detectable with the rocket spectrograph without O_2 present was 3 μ. (Although there is a possibility that there was photo-decomposition of some of the NO in such a closed system, we feel that this effect was negligible mainly because of the weak laboratory light source which we used. In addition, if such decomposition were present,

* Experimental coatings were produced for us by Mr. Max Troesch.

† developed by the University of Colorado for the AFCRC.

then our instrument was capable of detecting less NO than we believed to be the case.) However, for convenience and ease of analysis, we did not take superimposed spectra at this extreme limit of detectability, but we held the NO pressure constant at 20 μ while varying the O_2 pressure over the range 1 mm to 73 cm. Fig. 4 shows a series of additional spectra taken with the NO at 100 μ and with various O_2 pressures in the tank.

3. RESULTS AND DISCUSSION

3.1. *Nitric oxide*

NO has several band systems, β, γ, δ, ε, etc., that appear in absorption in the vacuum ultraviolet region,[19] but, as may be seen in Table 1, only a few relatively strong bands fall in the wavelength region 1800–2100 Å. We chose that region in which to work because, first, the solar continuum provides sufficient radiation for absorption studies and, second, that region in the solar spectrum is least cluttered with solar absorption lines. The strongest NO bands which fall in this wavelength region are the $\delta(0,0)$, $\delta(1,0)$, $\gamma(4,0)$ and $\gamma(5,0)$ (see Table 1). However, for the purpose of our experiment, only one band, the $\delta(0,0)$, is appropriately situated with respect to a Schumann–Runge absorption band to allow for a meaningful analysis; the other bands mentioned are very strongly masked by the S–R bands and are not detectable when the quantity of O_2 present is such as that which we encountered in the upper atmosphere.

The band at approximately 2264 Å which Durand[11] and others mentioned is the relatively weak $\gamma(0,0)$ with heads at 2269·4 Å and 2262·8 Å, and it falls in a region of relatively strong Fraunhofer absorption which makes its detection difficult unless the NO concentration is considerable. Certainly, if any of the bands in this region appeared and were detectable, the

Table 1. NO Absorption Bands in the Region: 1800—2100 Å

β-bands			γ-bands			δ-bands		
v', v''	$(\text{Å})_{\text{head}}$	*Absorption coefficient	v', v''	$(\text{Å})_{\text{head}}$	*Absorption coefficient	v', v''	$(\text{Å})_{\text{head}}$	*Absorption coefficient
3,0	2062·55	1	2,0	2053·87	7	0,0	1914·91	21
				2052·62			1913·88	
4,0	2024·28	1		2048·45			1910·33	
	2020·82			2047·44			1909·45	
5,0	1985·19	2	3,0	1961·91	7	1,0	1833·67	40
	1981·93			1960·74			1832·59	
6,0	1948·24	—		1957·03			1829·46	
	1945·17			1956·12			1828·63	
7,0	1913·65	—	4,0	1882·00	18			
	1910·26			1880·75		†E-bands		
8,0	1879·79	—		1877·24				
	1877·00			1876·56		0,0	1881·63	
9,0	1848·08	3	5,0	1804·38	22		1880·77	
	1845·48			1803·50			1877·26	
10,0	1817·57	—		1800·30			1876·60	
	1815·10			1799·60		1,0	1804·34	
							1803·51	
							1800·26	
							1799·58	

All the wavelength data were obtained from ref. (20).

* This is the value estimated in Fig. 2 in the paper by F. F. Marmo, *J. Opt. Amer.* **43**, 1186 (1953).

† These are values observed in emission. The two (0,0) and (1,0), superimpose with the $\gamma(4,0)$, and $\gamma(5,0)$, respectively.

$\delta(0,0)$, with four heads:[20] P_{21} – 1909·45 Å, P_{11}–1910·33 Å, P_{22}–1913·88 Å, P_{12}–1914·91 Å, should appear.

First we determined exactly what effect the $\delta(0,0)$ band of NO would have on the appearance of the (5, 0) band ($\lambda_{head} = 1902{\cdot}49$ Å) of the S–R system with which it coincides when the spectra are superimposed. Fig. 5 shows the relative positions of the heads of the $\delta(0,0)$ and the rotational lines of the S–R (5, 0) band.[21] It can be seen, because the $\delta(0,0)$ shades to shorter wavelengths, that the rotational lines $P(17)$, $R(15)$ ($v = 52374{\cdot}1\ cm^{-1}$) of the (5, 0) band will be most noticeably affected because of the proximity of the P_{21} head of the $\delta(0,0)$ band ($\Delta v = 3{\cdot}0\ cm^{-1}$)*. Also affected, but not to so large a degree, will be the rotational lines $P(21)$; $R(19)$ ($v = 52271{\cdot}2\ cm^{-1}$, by the P_{22} branch ($\Delta v = 21{\cdot}4\ cm^{-1}$)*; this is noticeable only at relatively higher pressures of NO. Because the rotational structure of the NO bands was not resolved, the effect in the superimposed spectra is an increase in the intensity of absorption and a broadening of the rotational lines of O_2 involved.

By studying microphotometer tracings of the spectra concerned, we were able to establish limits of detectability of NO absorption when superimposed with O_2 absorption for the same instrumentation which we used in the rocket experiment. With 20 μ pressure in the NO absorption cell, which corresponds to a concentration of $1{\cdot}38 \times 10^{16}$ molecules/cm²-column, we were still able to detect clearly the small effect of the $\delta(0,0)$ band on the rotational lines $P(17)$, $R(15)$ of the (5, 0) band in the S–R absorption produced by the O_2 pressure of 8 cm in the tank or $2{\cdot}67 \times 10^{20}$ molecules/cm²-column. At O_2 pressures of less than 8 cm, the effect of the NO absorption was much more pronounced. When the NO pressure was maintained at 100 μ or $6{\cdot}9 \times 10^{16}$ molecules/cm²-column, we could detect clearly the same effect even at an O_2 pressure of 64 cm or $2{\cdot}14 \times 10^{21}$ molecules/cm²-column. At O_2 pressures of less than 64 cm, the effect was very noticeable.

Fig. 6 shows microphotometer tracings of three of the spectra obtained in the rocket flight compared with laboratory spectra of NO and O_2 absorption superimposed and with O_2 absorption spectra. In the figure, "×" represents the rotational lines $P(17)$, $R(15)$ in the (5, 0) S–R band, "O" the rotational lines $P(19)$, $R(17)$, and "Δ" the rotational lines $P(21)$, $R(19)$. "×" is most noticeably affected when NO is present. "Δ" is also noticeably affected but only when the pressure of NO is consider-

* The Δv represents the separation between the head of the P-branches of the $\delta(0,0)$ and the rotational lines affected by those branches. Actually, the rotational structure of the δ-bands was not resolved because of its close spacing. The closest lines to $P(17)$, $R(15)$ and $P(19)$ are, respectively, $P_{21}(6\frac{1}{2}) = 52373{\cdot}4\ cm^{-1}$, and $P_{11}(18\frac{1}{2}) = 52373{\cdot}4\ cm^{-1}$, and $P_{22}(12\frac{1}{2}) = 52272{\cdot}1\ cm^{-1}$, $R_{12}(4\frac{1}{2}) = 52270{\cdot}0\ cm^{-1}$.

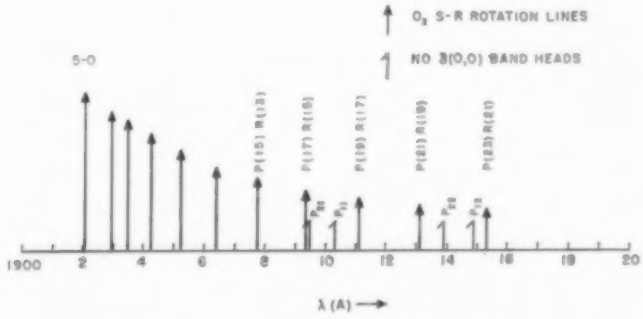

Fig. 5. Fine structure of O_2 Schumann–Runge band 5,0 superimposed with NO δ (0,0) band heads.

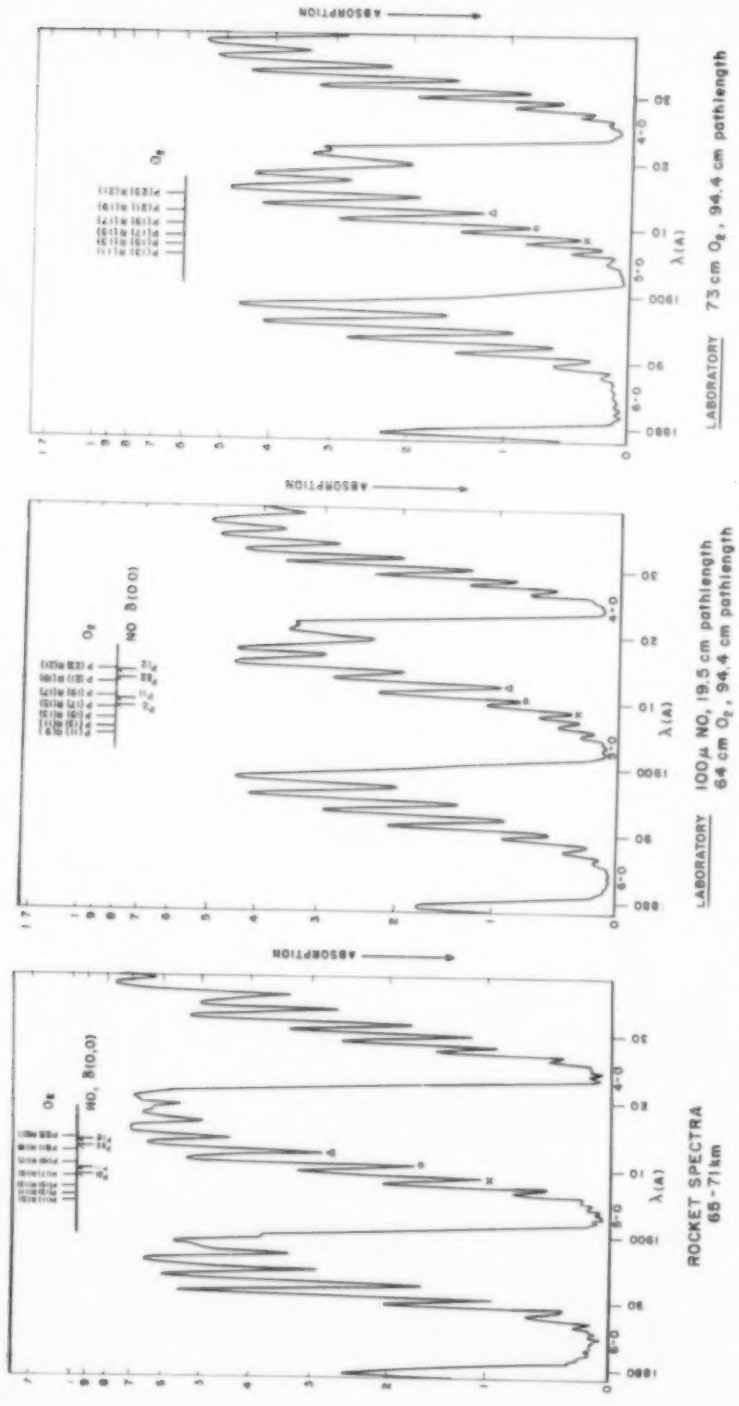

Fig. 6. Comparisons of microphotometer tracings of rocket spectrograms and laboratory spectrograms.
A. Rocket spectrogram obtained between 65 and 71 km.

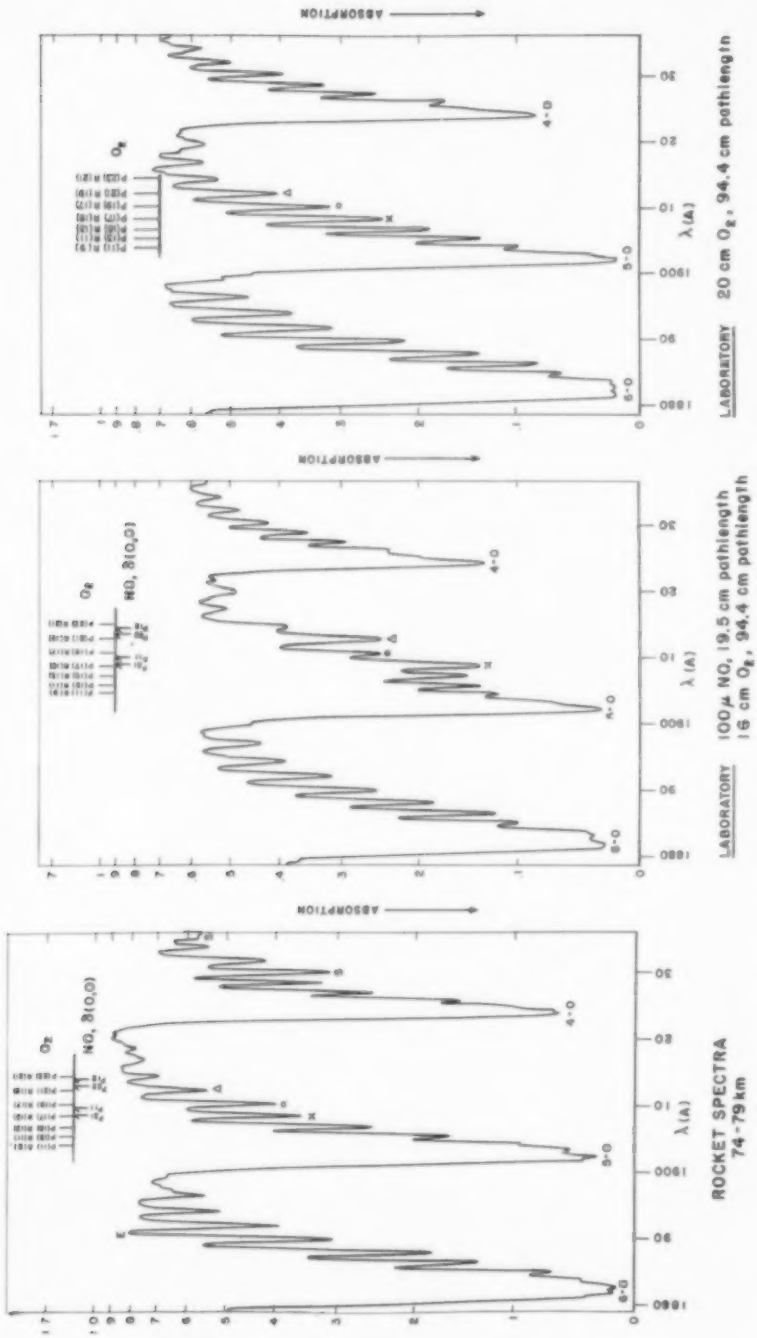

Fig. 6. B. Rocket spectrogram obtained between 74 and 79 km.

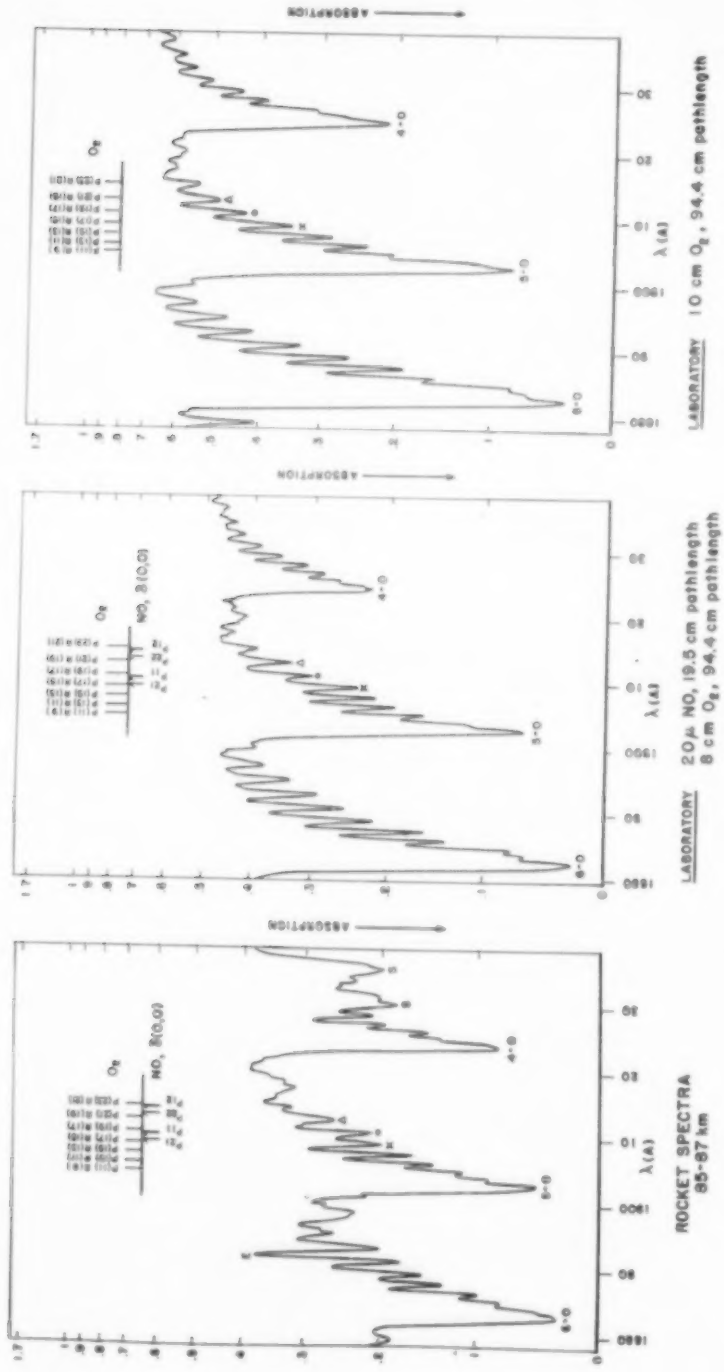

Fig. 6. C. Rocket spectrogram obtained between 85 and 87 km.

ably higher than that required to produce an effect on "×" (by higher pressure, we mean $6{\cdot}9 \times 10^{16}$ molecules/cm^2-column in our experiment). "O" is not affected in appearance by the $\delta(0,0)$ band, but it shows an anomaly in the traces of the flight spectra because it is superimposed with an absorption line in the solar spectrum. "E" is the solar emission line at 1892·4 Å,[18, 22] and "S" is strong absorption[18] in the solar spectrum.

In none of our flight spectrograms could we find an intensity anomaly in the rotation lines $P(17)$, $R(15)$ of the $(5,0)$ S–R band which could compare, even in the slightest, with the anomaly appearing in the same rotation lines in the comparable superimposed laboratory spectrogram.

Therefore, at no time, under the experimental conditions that existed*, were we able to detect a concentration of NO molecules equal to or more than 10^{16} molecules/cm^2-column between the spectrograph and the sun. Because the concentration 10^{16} molecules/cm^2-column is a *detectable* limit in our case, and because we were unable to detect any NO absorption from the rocket, we feel that it can safely be stated that a concentration of not more than 10^{15} molecules/cm^2-column of NO could have been present at the time of our experiment. If one assumes a pathlength of 100 km†, in the altitude range under consideration and in a direction similar to that in the experiment (there is virtually no change in altitude over that distance), 10^{15} molecules/cm^2-column is then equal to 10^6 molecules/cm^3. Therefore, if one assumes that nitric oxide does exist in this region of the upper atmosphere, its concentration cannot exceed 10^8 molecules/cm^3.

In arriving at the conclusion stated above, we have taken into consideration two additional factors which enter into our experiment. One is the difference in temperature between the absorbing gases in the laboratory with which we obtained our reference spectra and those in the upper atmosphere which produced the spectra obtained in the rocket flight. The other is the difference in background sources; the hydrogen lamp in the laboratory, the sun in the rocket experiment.

A change in the temperature of an absorbing gas results in a shift in the intensity distribution of the rotational lines in a band. We calculated the shift that would result in the $\delta(0,0)$ band of NO for a temperature change of 100°C (300°K in the lab., 200°K at 60–90 km in the upper atmosphere‡) and found that it was of no important consequence in forming our conclusion.

In the case of the different background sources, it is known that both are continuous in nature without any sharp intensity gradients in the wavelength region in which we were interested, although, as has already been stated, the solar continuum is superimposed with relatively weak Fraunhofer lines in this region. Also, we were careful to match background densities when comparing spectra.

If we wish to be very precise, it is also necessary to consider a pressure effect, because the gas pressures used in the laboratory to obtain our reference spectra were higher than those in the upper atmosphere which produced our flight spectra, although the pressures were low in both cases. However, the effect is not significant in our present experiment, because of the low resolution of the spectrograph used. In order to comment on the pressure effect, we must have much more accurate quantitative measurements, at higher resolution, both in the laboratory and in the actual rocket flight. We did not intend to do this in our present effort.

3.2. *Molecular oxygen*

The primary purpose of our experiment was the detection of and the measurement of the

* Altitude range: 63–87 km. Direction of view through atmosphere: toward the sun, parallel to the tangent to the earth's surface at a point directly beneath the rocket.

† We suggest 100 km as a conservative pathlength for the absorbing NO. For all practical purposes, the pathlength is contained in an atmospheric layer 1 km or 2, thick and any NO included in layers above is ignored.

‡ We chose 200° K as the temperature in the 60–90 km region of the upper atmosphere as suggested in the ARDC Standard Model Atmosphere.

concentration of NO. However, the spectra have yielded, in addition, data concerning atmospheric molecular oxygen, and we are able to make preliminary comments in regard to its concentration in the altitude range 63–87 km.

The Schumann–Runge absorption bands appear strongly in all the flight spectrograms (Figs. 2, 3). At the lowest altitude the bands can be traced down to the (1, 0) band. The (0, 0) band may also appear, but this is uncertain because, in addition to being naturally very weak, its head, at 2025·8 Å, coincides with a strong solar absorption line. The bands can be seen to extend farther to the shorter wavelength as the altitude increases, and, at 87 km, the bands extend $v' = 13$. We expect to extend the system even farther to shorter wavelengths when, in the near future, we will perform further composition experiments from rockets using the same techniques.

In order to make a determination of the O_2 density in the region under consideration we compared microphotometer tracings of the flight spectra with those of absorption spectra of pure O_2 obtained in the laboratory. The lab. spectra of O_2 were obtained with the same spectrograph used in the flight and with the experimental procedure described earlier. Absorption spectra were obtained with O_2 pressures from 2 to 75 cm Hg in a pathlength of 94·4 cm. We then calculated the number of molecules/cm²-column for each pressure used which, in turn, was related to a S–R absorption spectrum with a particular vibrational intensity distribution. Keeping in mind that the background sources were different, we compared the microphotometer tracings of the flight and the lab. spectra (to give approximately equal intensity distribution), and were able to relate number of molecules/cm²-column to S–R absorption obtained at any given altitude.

For numerical comparison purposes we used values of O_2 density at various altitudes as listed by Miller[22]. Miller assumes that the composition of the atmosphere does not change with height up to about 90 km. In order to convert from number of O_2 molecules/cm³, as listed by Miller, to molecules/cm²-column at a specific altitude we integrated the density over a 600 km pathlength* in 6 steps. The density of O_2 in the first 100 km we took to be constant and as listed by Miller for that specific altitude. The density in the next 100 km we took as the density listed for an atmospheric layer 2·5 km higher, which represents the average density in that pathlength; the density for the third 100 km, that of an atmospheric layer higher by an additional 5 km (again the average density for that pathlength), and so on for the fourth and fifth segments. For the sixth 100 km pathlength, the average density is equivalent to that

* in the direction in which the instrument was pointed at the sun.

Table 2. Density of O_2 in the Altitude Range 64—87 km

Our values		Miller[22]			Difference
Altitude interval (km)	Number of molecules of O_2/cm²-column from lab. and flight spectra	Altitude (km)	O_2 molecules/cm³ at that altitude	Number of O_2 molecules/cm²-column over a 600 km pathlength*	Factor by which our values are lower
63-65	$>3{\cdot}0\times10^{21}$	64·0	$9{\cdot}4\times10^{14}$	$2{\cdot}2\times10^{22}$	—
65-71	$2{\cdot}7\times10^{21}$	68·0	$5{\cdot}7\times10^{14}$	$1{\cdot}32\times10^{22}$	4·9
71-74	$2{\cdot}3\times10^{21}$	72·5	$3{\cdot}1\times10^{14}$	$6{\cdot}8\times10^{21}$	3·0
74-79	$1{\cdot}0\times10^{21}$	76·5	$1{\cdot}7\times10^{14}$	$3{\cdot}5\times10^{21}$	3·5
79-81	$6{\cdot}7\times10^{20}$	80·0	$9{\cdot}5\times10^{13}$	$2{\cdot}1\times10^{21}$	3·1
81-85	$3{\cdot}3\times10^{20}$	83·0	$6{\cdot}1\times10^{13}$	$1{\cdot}2\times10^{21}$	3·6
85-87	$2{\cdot}0\times10^{20}$	86·0	$3{\cdot}7\times10^{13}$	$7{\cdot}2\times10^{20}$	3·6

* Derivation of these values explained in text.

in an atmospheric layer 8 km higher than that used for the fifth because of the rapidly increasing curvature of the atmospheric layers at that distance. Beyond 600 km, the density of O_2 has fallen to negligible values for our purposes at these altitudes. The values of number of molecules of O_2/cm^2-column based on densities listed by Miller are compared with similar values which we determined from our laboratory and flight spectra in Table 2.

It can be seen that our values of number of molecules/cm^2-column are consistently lower at all altitudes than those derived from Miller's densities by factors of 3 to 5. Nevertheless, the agreement is surprisingly good considering that the values of O_2 molecules/cm^2-column which we used as a standard for comparison were obtained by a method of rough integration and that each of our flight spectrograms was obtained not at a specific altitude but over an altitude range of 2 to 6 km because of rocket motion during each exposure. This good agreement may be considered a justification of our experimental method or technique, and it strengthens our conclusions in regard to the NO concentration in the upper atmosphere.

3.3. *Solar continuum and Lyman-α radiation*

A short comment may be worthwhile concerning these two components of the solar radiation. The extent of and the intensity of the solar continuum in the vacuum ultra-violet region has been of considerable interest to those who have been engaged in studying the solar spectrum. Rense[23] has stated that the continuum is detectable with certainty to as far as 1750 Å. We can say, qualitatively, that the continuum must certainly extend, with "reasonable" intensity, to 1780 Å because we were able to observe, with certainty, the S–R absorption bands to (13, 0) whose head is at 1782 Å. It is probable that the continuum does extend farther to shorter wavelengths, but this is difficult to determine in our present case because when the S–R bands are well developed, as in the present case, the strong S–R continuum, which is always associated with them, absorbs the radiation below about 1750 Å.

Previously, Lyman-α radiation has been detected from rockets with photon counters at altitudes as low as 74 km.[14] That was accomplished with the sun's elevation at about 20° above the horizon. We performed our experiment at sunset, as has been stated, and did not record Lyman-α on any of the seven spectrograms taken over the altitude range 63–87 km. Although our exposure times were short, 4 and 8 sec, we were able previously,[18] to record Lyman-α easily at an altitude of 94 km with similar instrumentation, similar film and similar exposure times but with the sun above the horizon (0947 MST, 29 March 1955, 33°N, 106°W). Even though the absorption coefficient of O_2 at Lyman-α is small, 0·27 cm^{-1},[24] we attribute our inability to record that solar emission line primarily to absorption by the long pathlength of O_2.

REFERENCES

1. J. KAPLAN, Nature, Lond. **144**, 125 (1939).
2. C. T. ELVEY, P. SWINGS and W. LINKE, *Astrophys. J.* **93**, 337 (1941).
   C. T. ELVEY, *Rev. Mod. Phys.* **14**, 140 (1942).
3. W. C. PRICE, *Rep. Progr. Phys.* **9**, 10 (1942-43).
4. M. NICOLET, *Mém. Inst. Mét. Belg.* **19**, 124 (1945).
5. D. R. BATES and M. NICOLET, *J. Geophys. Res.* **55**, 306 (1950).
   D. R. BATES and M. J. SEATON, *Proc. Phys. Soc.* B **63**, 129 (1950).
   D. R. BATES, *Proc. Phys. Soc.* B **64**, 805 (1951).
   D. R. BATES, *Solar Eclipses and the Ionosphere*, p. 184. Pergamon Press, London (1956).
6. M. NICOLET and P. MANGE, *Ionospheric Res. Sci. Rep.* No. 35, State College, Penn., Contract No. AF19(122)-44 (1952).
7. M. NICOLET, *Ionospheric Res. Sci. Rep.* No. 52, State College, Penn., Contract No. AF19(122)-44 (1953).
8. M. NICOLET, *Earth as a Planet*, p. 691. University of Chicago Press (1954).
9. K. WATANABE, F. MARMO and E. C. Y. INN, *Phys. Rev.* **90**, 155 (1953); *Ibid.* **91**, 436 (1953).
   K. WATANABE, F. MARMO and J. PRESSMAN, *J. Geophys. Res.* **60**, 513 (1955).
10. A. P. MITRA, *Ionospheric Res. Sci. Rep.* No. 46, State College, Penn., Contract No. AF19(122)-44 (1953).
    A. P. MITRA, *J. Atmos. Terr. Phys.* **5**, 28 (1954).
11. E. DURAND, J. OBERLY and R. TOUSEY, *Astrophys. J.* **109**, 1–16 (1949).
12. F. S. JOHNSON, J. PURCELL, R. TOUSEY and N. WILSON, *Gassiot Meeting*, August 1953, Oxford, England.
13. M. MIGEOTTE and L. NEVAN, *Mem. Soc. Sci. Liége*, Ser. 4, **12**, 165 (1952).
14. E. T. BYRAM, T. CHUBB, H. FRIEDMAN and N. GAILAR, *Phys. Rev.* **91**, 1278 (1953).

15. C. Y. JOHNSON and E. B. MEADOWS, *J. Geophys. Res.* **60**, 193 (1955).
16. Soviet Bloc IGY Information, U.S. Dept. of Commerce, 18 April 1958, Office of Technical Services, Washington, D.C.
17. L. E. BENITEZ and S. S. PENNER, *J. Appl. Phys.* **21**, 907 (1950).
18. A. S. JURSA, F. LEBLANC and Y. TANAKA, *J. Opt. Soc. Amer.* **45**, 1085 (1955).
19. G. HERZBERG, *Spectra of Diatomic Molecules*. Van Nostrand, New York (1957).
L. G. SUTCLIFFE and A. D. WALSH, *Proc. Phys. Soc.* A **66**, 209 (1953).
Y. TANAKA, M. SEYA and K. MORI, *J. Chem. Phys.* **19**, 979 (1951).
20. Y. TANAKA, *J. Sci. Res. Inst., Tokyo* **43**, 160 (1949).
A. LAGERQUIST and E. MIESCHER, *Helvet. Phys. Acta* **31**, 221 (1958).
21. H. P. KNAUSS and S. S. BALLARD, *Phys. Rev.* **48**, 796 (1939).
22. L. E. MILLER, *J. Geophys. Res.* **62**, 351 (1957).
23. W. A. RENSE, *Astrophys. J.* **127**, 676 (1958).
24. K. WATANABE, M. ZELIKOFF and E. C. Y. INN, *Geophys. Res. Papers* No. 21, Geophys. Res. Directorate, AFCRC, ARDC (1953).

Planet. Space Sci. Pergamon Press 1959. Vol. 1, pp. 173–183. Printed in Great Britain.

THE RELATION BETWEEN LIGHTNING DISCHARGES AND WHISTLERS

HARALD NORINDER and EDGAR KNUDSEN

Institute of High Tension Research, University of Uppsala, Sweden

(*Received* 22 *January* 1959)

Abstract—A station for analysis of relations between lightning discharges and whistlers was operated near Uppsala. After preliminary tests in 1956-57 a definite programme was realized during the thunderstorm season of 1958. It was found that whistlers occur in groups—whistler situations—with periods often of ½–2½ hr, exceptionally of 5–6 hr. Whistlers sometimes occurred in great numbers for shorter periods of time between total cessations. These extended over hours, days and even weeks. Whistler situations on days with thunderstorms were located by a c.r.o. direction finder. It was found that whilst a thunderstorm in one direction produced whistlers, a simultaneous thunderstorm in another direction at about the same distance sometimes did not. Investigation of variations in the same thunderstorm of the electric field force from atmospherics related to whistlers or not so related showed that atmospherics with the highest field force were always followed by whistlers. This was explained partially by facilitated propagation for wave-packets in the low-frequency band around 5 kc/s and partially by high initial energy in the discharges causing whistlers. A comparison in the same thunderstorm of waveforms from atmospherics not producing whistlers showed typically irregular variational forms and one single discharge in the lightning path. Waveforms of whistler-producing atmospherics showed regular variational forms with frequencies around 5 kc/s. In several cases the waveforms indicated multiple discharges in the lightning path.

1. INTRODUCTION

Lightning discharges give rise in radio receiving sets to the special kinds of disturbances known as atmospherics. When observing atmospherics at very low and audible frequencies, special types of a musical (tonal) quality are heard on rare occasions. One type is classified as a whistler and consists of a steadily decreasing whistling tone from the upper limit of hearing, the frequency of which falls first rapidly and then more slowly.

A historical review of whistlers was given by Helliwell[1], and the connexion between whistler atmospherics and non-whistler atmospherics was given by Helliwell *et al.*[2]

The relations between the mechanism of lightning discharges and whistlers still constitute a problem not yet solved in important respects. This was the reason why, in 1956, there were started at a special station outside Uppsala some preliminary investigations transformed into a definite research programme in 1958, the results of which will be presented in this paper.

That a whistler starts from lightning discharges was first mentioned by Eckersley, who stated that Tremellen in a nocturnal thunderstorm (Morgan[3]) observed that lightning flashes were accompanied by whistlers. In a local thunderstorm in 1957 Morgan himself observed that every visible flash was producing strong whistlers with several echoes, and that each flash was followed in a few seconds by thunder.

At the Swedish whistler station, described later, two thunderstorm centres were observed at 2030 on 9 August 1956 at a c.r.o.d.f. bearing of 140° above the Baltic and at 220° above the Swedish inland, respectively. Atmospherics recorded from an antenna and a c.r.o. were followed by whistlers 80 per cent of the time. From the centre of the Swedish mainland the whistlers occurred frequently but were weaker than those from the Baltic.

At the station there were observed on 6 August 1957 several passing thunderstorm centres with local lightning discharges followed by whistlers. The vertical magnetic field components of the discharges (Norinder[4]) were recorded on the c.r.o. system. Simultaneously with the records it was possible to obtain a daylight picture of a vertical lightning flash followed by whistlers and with a crest current value of 7 kA, calculated from oscillograms by a method described by Papet-Lépine[5]. In the latest passing storm Norinder had opportunities to observe with excellent visibility for 45 min typical vertical lightning flashes followed by thunder. All vertical flashes were accompanied by very strong whistlers.

It has been established by the investigations of the last thunderstorms quoted that local vertical lightning paths generate whistlers. Numerous observations during neighbouring thunderstorms have also established that the occurrence of whistlers is a hazardous phenomenon. From this it follows that investigations of whistlers in connexion with lightning discharges must not only be directed within the immediate vicinity in order to give results but must also be concentrated on what occurs at greater distances. This method has been followed in the investigations described in this article.

2. LOCATION OF FIELD STATION FOR WHISTLERS

Having regard to Sweden's geographical extension north and south, a place in the neighbourhood of Uppsala with geomagnetic latitude Φ 58·4 and longitude Λ 107·0 was considered suitable for a whistler station. On preliminary investigations in 1956 it proved very difficult to avoid man-made interference, and after several tests a place called Kaptensudden 17 km east of Uppsala was chosen. The station is situated on the shores of a lake in an area where houses and electric transmission line systems are few and far away.

3. EQUIPMENT OF STATION

In 1956 preparatory observations of whistlers were made by a 0·3 km long antenna of plastic-insulated copper wire placed on the lake bottom in a north–south direction. In 1957 a frame aerial set up in a north–south direction with a quadratic section of 3×3 m and with 200 turns of insulated copper wire was used with strikingly good reception.

During the International Geophysical Year (IGY) a newly constructed antenna and other equipment were used chiefly in connexion with the experiments described by Helliwell[1]. Waveforms of atmospherics were recorded by the *E*-method (Norinder[6]) and their directions were observed by a c.r.o. sense direction finder (Stoffregen[7].)

4. RESEARCH PROGRAMME

Preliminary researches were carried out in the autumn of 1956 and in the following winter. Observation periods were arranged for several hours in combination with very favourable thunderstorm activities. Nevertheless, whistler results failed, with the inference that whistlers only occurred during special rare periods. From this experience there followed a limited research programme during the thunderstorm season of 1957. Then it was possible to receive lightning discharges within the sensitivity range of the station and to control thunderstorms on the c.r.o. direction finder.

On the experience and results obtained, the following more extended research programme of 1958 was based:

(1) Observations and notations of whistlers and thunderstorm situations for 10 min every $\frac{1}{2}$ hr between 0830 and 2130 had to be carried out.

(2) If whistlers happened to occur it was under all circumstances necessary to start continuous observations.

(3) In the event of sufficiently intense whistler activity it was necessary to undertake simultaneous records on: (a) tape recorder, (b) c.r.o. direction finder, and (c) c.r.o. recorder of waveforms and multiple discharges.

(4) After the latest whistler had been heard during an observation period it was necessary to continue observations for about $\frac{1}{2}$ hr in order to ascertain that the activity had definitely ended.

5. OCCURRENCE OF WHISTLERS

From the observations it has been found that whistlers occur in groups during periods up to several hours. Between these periods whistlers are entirely absent. In the routine observations made every ½ hr no occasion of isolated whistlers occurred. Throughout the rest of the article cases in which groups of a number of whistlers occur have been designated as "whistler situations".

A noteworthy point is that several whistler situations may occur on the same day. In Fig. 1, 2 days occur with three whistler situations and 2 days with two. It can hardly be considered as a pure coincidence that of 12 days with whistlers more than one whistler situation occurs in 5 days. It probably is not chance either that on four occasions there occur 2 days with whistler situations in succession. The whistler observations have been accompanied

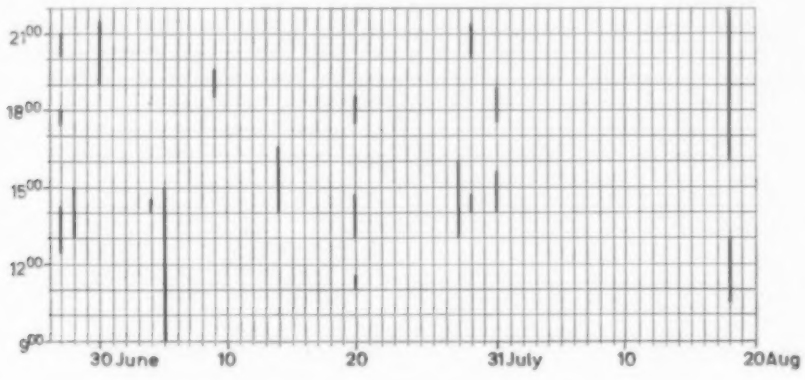

Fig. 1. General survey of whistler situations.

In Fig. 1 a survey is given of the whistler situations encountered during the observation period 27 June to 20 August 1958, during a period of 46 days. From Fig. 1 it is clear that there occurred 12 days with whistlers which comprised eighteen whistler situations. It further appears that whistlers as a rule appear for periods of several hours. Between these there is total cessation and the possibility of isolated whistlers occurring between the whistler situations is very small.

Since the observations of whistler situations did not encompass the whole 24 hr, the variation of the situations cannot be judged in relation to the time of day.

by simultaneous observations with the c.r.o. direction finder, and only in a couple of exceptional cases has the ending of the whistler situation been dependent on the cessation of the thunderstorm activity.

The duration of whistler situations is variable, which is already apparent from the comparison in Fig. 1. In Table 1 the duration of whistler situations from the results of 1957-58 is reproduced. It appears that they most commonly last for periods of between ½ and 2½ hr. Values of 5-6 hr have been obtained only in two cases. In the question of the distribution of whistler durations the 2 years show the same tendency.

Table 1

Duration (hr)	0–½	½–1	1–1½	1½–2	2–2½	2½–3	3–3½	3½–4	4–4½	4½–5	5–5½	5½–6
Number	2	3	5	4	3	2	1				1	1

A summary of the frequency of whistlers occurring in whistler situations is reproduced in Fig. 2, where the whole body of records has been divided up into 5 min intervals and the number of whistlers in the intervals is 56. One whistler situation on 28 June 1958 is not included in the statistical comparison, as this situation diverges. From the comparison in Fig. 2 it appears that two to four whistlers in 5 min is the most common, with about 70 per cent of the cases in this range. When, according to Fig. 2, only one whistler has occurred during the 5 min interval, the records show that five of these lie at the end of a closing whistler situation.

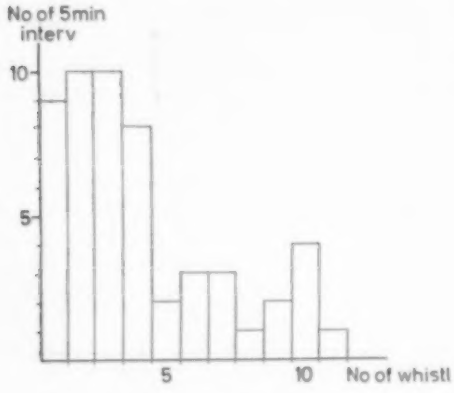

Fig. 2. Frequency of whistlers.

The distribution of individual whistlers may change for two different days even though they are consecutive. The two dates of 27 and 28 June 1958 form a striking example (see Tables 2 and 3) where the number of whistlers in a 5 min interval is reproduced. The first date must be considered as a normal day; three whistlers per 5 min interval is the most common. This number applies for about ½ hr, whilst the highest number goes up to ten. On 28 June, a considerable difference appears from the previous day. The activity is considerably higher. During a 30 min interval in the middle of the recording there occur groups of more than twenty whistlers with a maximum number of twenty-five. The activity is such that it was a typical whistler storm. Besides the great diffusion in the occurrence of whistlers on different days, there is also a great diffusion in activity within the same whistler situation to be taken into account.

Table 2. 27 June 1958

20^h10	15	20	25	30	35	40	45	50	55	21^h00	05
−15	20	25	30	35	40	45	50	55	60	−05	10
4	7	4	10	3	3	3	3	3	2	1	1

From observational reports and recordings it appeared that whistler activity can conclude in two different ways. In the majority of cases it ceases in spite of the fact that discharge activity in the simultaneous thunderstorm is still continuing. On two occasions whistlers ceased simultaneously with the thunderstorm, but these cases are exceptional. The most usual conclusion is that during a period of 10-20 min the whistler activity changes from being normal to gradually terminating. These results have been obtained from the continuous observations of whistler activity simultaneously with the observations with the c.r.o. direction finder. Such observations have been carried out and records kept up to ½ hr after the whistler situation has ceased.

From the observations of whistlers and their analysis the following general conclusions can be drawn:

(1) Whistlers occur in great numbers during short periods of time between which there occurs a total cessation. This may extend over hours, days and, in isolated cases, even weeks.

(2) Several whistler situations occur on the same day or on consecutive days.

Table 3. 28 June 1958

12^h00	05	10	15	20	25	30	35	40	45	50	55	13^h00	05	10	15	20	25	30	35	40	45	50
−05	10	15	20	25	30	35	40	45	50	55	60	−05	10	15	20	25	30	35	40	45	50	55
20	7	7	9	10	18	16	17	20	25	24	24	21	22	22	21	14	16	12	10	15	7	2

(3) A cessation of whistler activity cannot be connected with a general cessation of thunder activity.

By the investigation of whistlers and their occurrence carried out as described above, it is confirmed that, besides lightning discharges, there are required certain other, locally manifested, geophysical conditions which are necessary for whistlers to be generated at all.

6. WHISTLER SITUATIONS ON DAYS WITH THUNDERSTORMS

During the preliminary investigations in 1957 it was discovered that whistler activity was bound up with thunderstorms of limited range situated in definite directions. Thunderstorms in other directions and at about the same distance were not accompanied by whistlers. Such situations could easily be investigated, and this could be done by simultaneous recording of whistlers and a c.r.o. direction finder in combination with thunderstorm observations from synoptic charts and from meteorological stations. In the following figures such recordings are graphically reproduced with indications of time and distance. Open circles indicate no whistlers; half-open circles, an average number of whistlers; closed circles, a high number.

The investigations begun in 1957 have been continued on an extended scale in 1958 and they have confirmed earlier results. An interesting case on 28 July 1958 appears in the map in Fig. 3. The meteorological observations show two thunderstorm centres, partly over north-east Sweden and partly over the Gulf of Finland.

The thunderstorm situation in Sweden could be observed with the direction finder from 0800 with deviations of bearing from 10° to 20°. According to local observations, this thunderstorm situation during the course of the day is apparent from the graphical summary in Fig. 4. In this are to be noted very weak whistlers from both thunderstorms at the observation periods of 1300 and 1330. Not until 1400–1440 were the whistlers stronger in both directions and records made at distances of 550–850 km and 500–750 km, respectively. In the observation periods of 1500 and 1530 the whistlers became weaker and then ceased entirely, in spite of the fact that the thunderstorms, and especially the one in north-east Sweden, were still very intense.

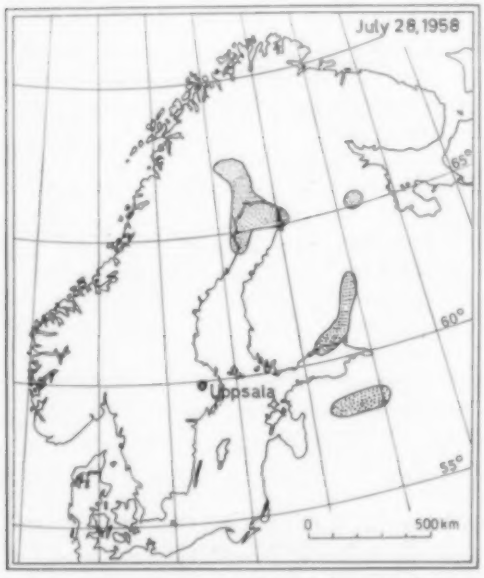

Fig. 3. Thunderstorm regions producing whistlers.

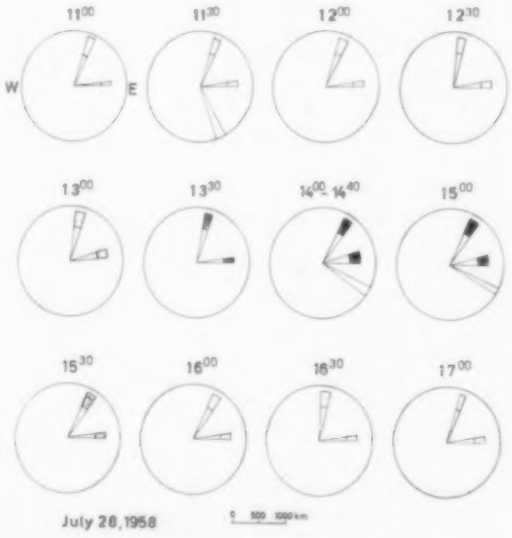

Fig. 4. Variation of thunderstorm regions.

In this case the whistler situation ceased whilst the thunderstorms continued.

The following day, 29 July, a thunderstorm was still active in north-east Sweden within the sector 0°–10°. This thunderstorm was located by the direction finder early in the morning and continued all day. A second area with thunderstorms was located on a bearing from 180°–190°. This thunderstorm area was located southwards over Germany and Central Europe.

According to the graphic summary in Fig. 5, whistlers began at 1400 and recordings were taken between 1400 and 1440. On the latter

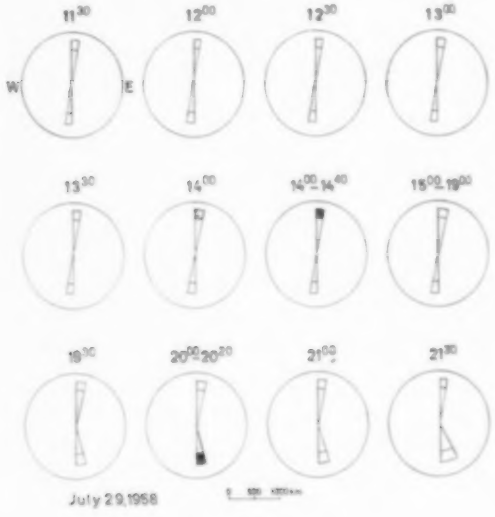

Fig. 5. Variation of thunderstorm regions.

occasion the whistlers which emanated from the thunderstorm in north-east Sweden ceased. On the other hand, the thunderstorm region in the southerly direction gave no whistlers. One gets the impression that this case shows that it is not primarily the distance from the receiving station which decides whether whistlers are received or not. The thunderstorm centre which gave whistlers was at distances of 700–800 km, whilst the distances to the southerly thunderstorm which gave no whistlers at this time were 500–700 km.

According to Fig. 5, no whistlers appeared from this southerly thunderstorm before 2000. Recordings of whistlers in this case were taken from 2000 until 2020. As is seen from Fig. 5, only a slight change had ensued in the position of the southerly thunderstorm activity, the bearings changing from 180°–190° to 165°–180°. Furthermore, whistlers were not observed from the southern area in spite of the fact that the thunderstorm continued.

Samples of other cases have been analysed with satisfactory agreement and with variations in a similar fashion to those exemplified. In doing so it has sometimes ensued that whistler activity can be typically connected to a limited thunderstorm. From our experience not all lightning discharges in such a thunderstorm will produce whistlers. As explained later, the final cause of the production of whistlers will be closely linked with some features of the discharge mechanism in lightning flashes.

In the investigations carried out hitherto with the aid of one direction finder, synoptic charts and meteorological stations, there has been no possibility of determining accurately the local position within a thunderstorm region of such lightning discharges as were accompanied by whistlers. This task is by no means easy, but it is important and it will be tried in subsequent investigations.

7. DISCHARGE MECHANISM IN LIGHTING FLASHES AND WHISTLERS

The occurrence of a thunderstorm is only one of several necessary conditions for the development of whistlers.

From our experience hitherto, the development of whistlers is bound to the direction of the lightning paths. From direct observations, as well as from unique daylight photography of a lightning flash, it has been verified that whistlers are produced by typical vertical lightning paths between the thunderstorm cloud and the earth's surface.

The current variations in lightning flashes are of importance for the development of whistlers. A calculation of the available photographed lightning path resulted in a crest current value of the same magnitude as the most frequent crest current values of vertical flashes striking vertical objects on the earth (Norinder[8]). This

does not preclude the fact that lightning discharges with very low current values may produce whistlers. Because of their low energy content such whistlers will not propagate with such amplitudes that they will be observed at greater distances.

Special conditions in the lightning mechanism are necessary for producing whistlers. In the gradual progress of the discharge such low-frequency bursts must be generated which are necessary for the development of whistlers. The actual frequency region is, as we know, between 1 kc/s and 15 kc/s, with an optimal value at 5 kc/s. A preliminary analysis of the frequency distribution of lightning discharges has shown (Norinder[4]) that these actual frequencies are occurring in vertical lightning strokes. These frequencies are not dominating. If the reverse should be the case, whistlers should occur more frequently than is actually the case. An analysis of the magnetic field variation of a considerable number of vertical lightning strokes showed that the low-frequency waves are mainly generated on the frontal but also to some extent on the decreasing parts of lightning currents.

The development of the low-frequency variations is enhanced by an intensification of the ionization in the lightning path (especially in the branches) and the volumes of the thunderstorm atmosphere which carry the charges. From this follows a decreased resistance in the discharge region which must excite the development of the wave-packets.

The analysis by oscillograms of local lightning flashes to detect the causal relations between the lightning mechanism and the whistlers produced depends on the very hazardous occurrence of whistlers. To arrive at results within a reasonable time the observational area must be substantially enlarged, and one no longer deals with lightning discharges at their source, but with their transformation with distance, i.e. with atmospherics. This transformation with distance has been analysed only to a limited extent (Norinder[6]). When what is called the waveform of atmospherics in the following discussion is related to the generated lightning discharges, it must be with reservation and caution.

The activity of whistlers may be connected with a limited thunderstorm region and it is evident that not all lightning discharges indicated by atmospherics give rise to whistlers. This is shown in Fig. 6, in which the filled piles represent percentages of atmospherics with whistlers and the empty ones atmospherics lacking whistlers. The relation shows very pronounced variation with time. The whistler situation described in Fig. 6 was unusually intense. Otherwise, in the general character of its variations, it is quite in keeping with the majority of other whistler situations observed.

The material which has been forthcoming up to now is very comprehensive with regard to oscillograms of atmospherics with and without subsequent whistlers. Further analysis will be

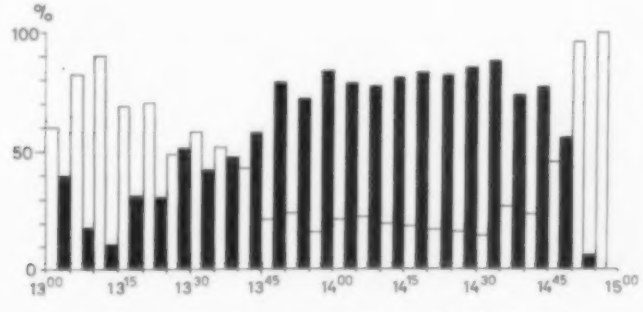

Fig. 6. Atmospherics productive of whistlers versus non-productive.

carried out according to the following principles:

(1) Comparison between the peak values of the electric field force of the atmospherics.
(2) Comparison between the waveforms of atmospherics.

8. VARIATIONS OF ELECTRIC FIELD OF ATMOSPHERICS IN RELATION TO WHISTLERS

In a comparison between the peak values of the electric field force of atmospherics, whether followed by whistlers or not, the whistler situation reproduced in Fig. 1 affords remarkable material for comparison of the phases of development following each other in whistler situations. For practical reasons the field force or field values have been directly determined by measurements from the original oscillograms in such a way that the values represent the highest amplitude difference between the two polarities. During the first ½ hr of the whistler situation, about 30 per cent of all oscillographic recordings gave subsequent whistlers within the actual sector fixed by the direction finder. During a later period (1350–1425) the occurrence of atmospherics with subsequent whistlers reached about 85 per cent. The measured field values are graphically reproduced in Fig. 7, where (a) indicates the first period (79 observations) and (b) the second (119 observations). The field in volts/metre accompanied by whistlers is represented by closed circles and those without whistlers by open circles.

In Fig. 7 there is a very clear tendency to be found for the relation of the field values to whistlers. In the area of the lowest field values atmospherics are not accompanied by whistlers. In an intermediate area on the scale atmospherics occur with and without whistlers. At the higher values on the scale all atmospherics are accompanied by whistlers.

It was natural to assume that the relation clearly shown in Fig. 7 between field values and whistlers only applied to the particularly intense whistler situation on 28 June 1958. With a view to checking this, similar investigations of field variations in atmospherics have been carried out in several other whistler situations.

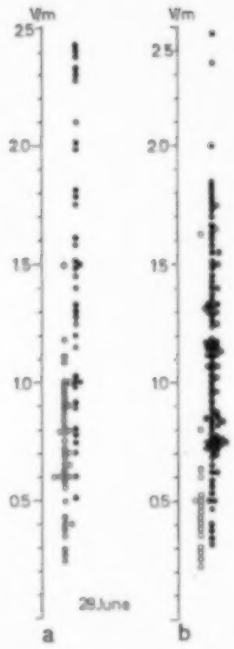

Fig. 7. Electric field of atmospherics related to whistlers.

The result is given in Fig. 8. A difference in the mean level of field values for the different whistler situations is noticeable. This is explained by the fact that the oscillographic recordings have been carried out at different times on different days and at different distances from the thunderstorm regions. Fig. 8 clearly shows the same tendency as Fig. 7.

It therefore appears to be fully established following Figs. 7 and 8 that atmospherics with the highest field values are accompanied by whistlers.

From the established amplitude distribution of atmospherics in relation to whistlers it is natural to try to find out whether the amplitude constitutes the deciding factor as to whether atmospherics are to be accompanied by whistlers or not. Should this hypothesis be correct, there should have been not three different areas on the field scale in Figs. 7 and 8 but only two, all lightning discharges with field values over a

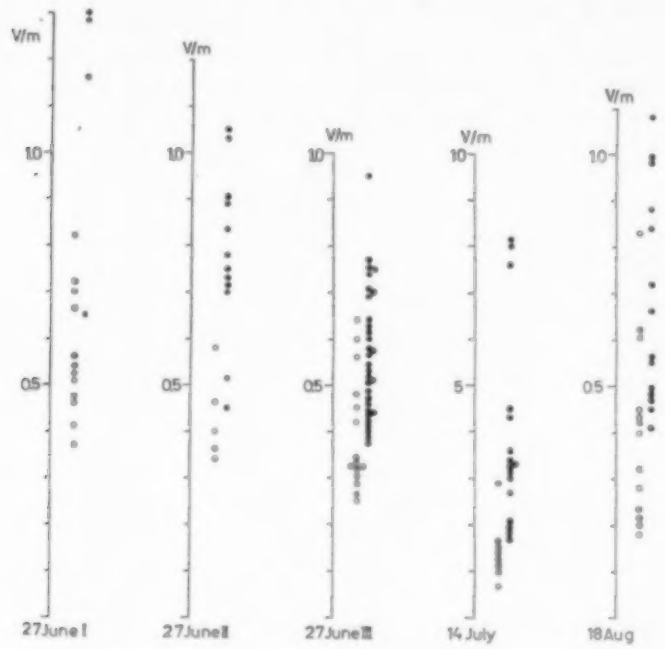

Fig. 8. Electric field of atmospherics related to whistlers.

certain limit giving whistlers, and all those with lower field values giving no whistlers.

The predominant occurrence of atmospherics producing whistlers at the groups of higher field-force values in Figs. 7 and 8 might to some extent be related to intensified current variations in the whistler-generating lightning discharges as compared with those lacking whistlers. Another plausible explanation is related to the transmission coefficient of the ionosphere in the very low-frequency band from 1 to 5 kc/s (Wait[9]). This transmission coefficient has a maximum at the quoted frequencies, a circumstance that will facilitate the propagation of the amplitudes of atmospherics followed by whistlers as compared with those without whistlers and thus lacking the above-mentioned prevalent low frequencies.

9. WAVEFORMS OF ATMOSPHERICS IN RELATION TO WHISTLERS

During the 1958 observation period nearly 700 oscillograms of atmospherics have been obtained from whistler situations. It has not yet been possible to treat this comprehensive material and especially to carry through an important harmonic analysis dealing with the occurrence of frequencies.

On account of the large number of oscillograms, it appeared especially suitable to divide up the material with the help of the amplitude values of the field force in conjunction with Fig. 8 (III). Three characteristic groups of amplitude variations in atmospherics were noted: (1) oscillograms of atmospherics not producing whistlers; (2) oscillograms of atmospherics productive and unproductive of whistlers; (3) oscillograms of atmospherics which produced whistlers. Group (2), which contains atmospherics both productive and unproductive of whistlers, is especially suitable for comparative purposes.

According to Fig. 8, there developed on 27 June 1958 three whistler situations. The latest in the day, between 2000 and 2109, gave, according to simultaneous observations with the

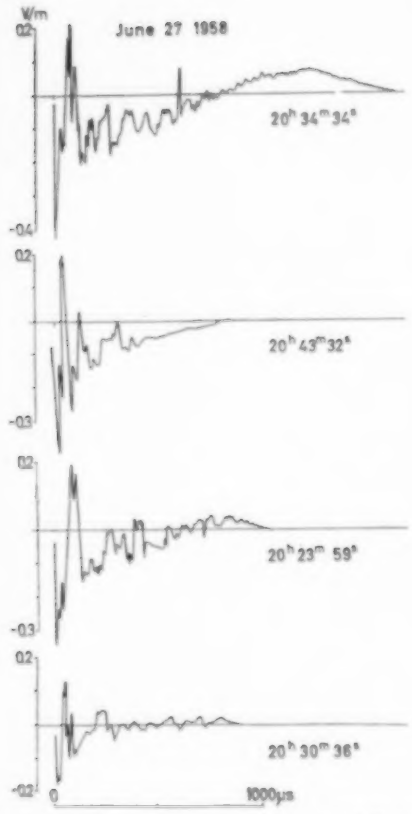

Fig. 9. Oscillograms of atmospherics not followed by whistlers.

c.r.o. direction finder, the whistlers' deviations in bearing between 40° and 65°. The thunderstorm centre was spread out, with a mean distance of about 450–550 km.

Within the observation area were received a number of atmospherics in Group (2) not producing whistlers; this is illustrated in Fig. 9. The oscillograms show typically irregular variational forms, and particularly regular frequencies are absent. The atmospherics have this in common—that they have been generated by single lightning strokes, and so high resistance in the lightning path must be taken into account.

In Fig. 10 are illustrated a number of whistler-producing atmospherics in Group (2) from the same observation area. Except in the initial stages, these atmospherics show very regular variational forms so that they can immediately be recognized as waveforms where the frequencies most nearly correspond to 5 kc/s or to the band nearest this frequency. This is in full agreement with what has been discussed earlier.

The intention is to publish in a later report the results of a harmonic analysis of the comprehensive oscillographic material. Some preparatory tests show already that the wave spectrum will be characterized by an intense energy peak at 5 kc/s.

The oscillograms reproduced in Fig. 10 are characterized, with one exception, by multiple discharges recorded by the method reported by Norinder and Vollmer[10]. It is, moreover, not out of the question that in this exceptional case also multiple discharges occurred, but did not appear in the recording on account of their low amplitude.

Multiple discharges often occurring in the lightning path presuppose, in contrast to single discharges, increased ionization both in the path and in the volume within the thunderstorm atmosphere from which the large quantities of electricity transformed into the lightning discharge are fed. The consequence is, on the whole, a smaller resistance in the lightning path than in the cases characterized by only a single discharge. To what extent this may contribute to particularly favourable conditions in the frequency ranges which are specially characteristic of whistlers will be investigated more closely in a coming treatment of the comprehensive oscillographic material already referred to.

Acknowledgements—The authors wish to thank their former collaborator Mr. B. Vollmer who, in a very skilful manner, constructed the necessary electronic devices for recording whistlers in the researches. Mr. Vollmer also participated in the preliminary researches until March 1958.

Special cathode-ray recording oscillographs and a direction finder were used in this investigation. The instruments were constructed with the help of grants from Statens naturvetenskapliga forskningsråd (The Swedish Natural Science Research Council) and Statens tekniska forskningsråd (The State Council of Technical Research). The authors are very grateful for this valuable help with the necessary instrumental equipment.

The Geophysics Research reported in this article was sponsored by Contract AF 61(052)-07, Electronics

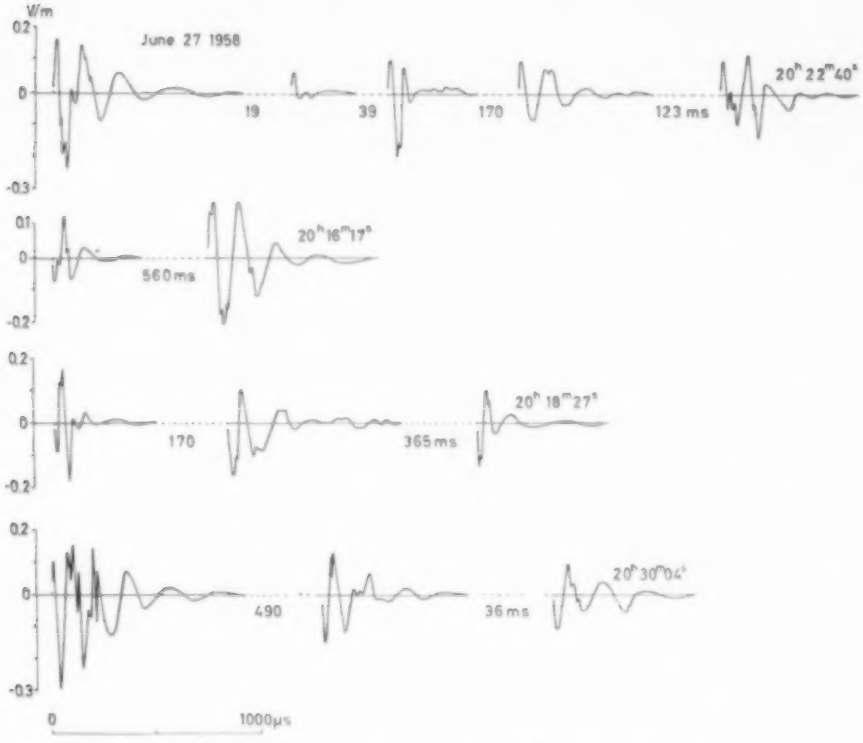

Fig. 10. Oscillograms of atmospherics followed by whistlers.

Research Directorate, Air Force Cambridge Research Center of the Air Research and Development Command, United States Air Force, through its European Office.

REFERENCES

1. R. A. HELLIWELL, Whistlers and related phenomena. *Low-Frequency Propagation Studies*, Part I. Radio Propagation Laboratory, Stanford University, Calif. (1956).
2. R. A. HELLIWELL, A. G. JEAN and W. L. TAYLOR, *Proc. Inst. Radio Engrs., N.Y.* **46**, 1760 (1958).
3. M. G. MORGAN, *Nature, Lond.* **182**, 332 (1958).
4. H. NORINDER, *Ark. Geofys.* **2**, 423 (1956).
5. J. PAPET-LÉPINE, *Ark. Geofys.* **3**, 79 (1958).
6. H. NORINDER, *Ark. Geofys.* **2**, 161 (1954).
7. W. STOFFREGEN, *Ark. Mat. Astr. Fys.* A, **34**, (1947).
8. H. NORINDER, *J. Franklin Inst.* **253**, 492 (1952).
9. J. WAIT, *Symposium on Propagation of VLF Radio Waves, Boulder, Colorado*, Vol. 4, p. 23 (1957).
10. H. NORINDER and B. VOLLMER, *Ark. Geofys.* **2**, 515 (1957).

Planet. Space Sci. Pergamon Press 1959. Vol. 1, pp. 184–192. Printed in Great Britain.

SATELLITE ORBITS AND ATMOSPHERIC DENSITIES AT ALTITUDES UP TO 750 km OBTAINED FROM THE VANGUARD ORBIT DETERMINATION PROGRAM*

JOSEPH W. SIRY†

U.S. Naval Research Laboratory, Washington, D.C.

(*Received* 10 *January* 1959)

The objectives of the Vanguard Orbit Determination Program have been to use Minitrack and other observational data to acquire and determine the orbits of artificial earth satellites, to make appropriate predictions to facilitate further observing, to determine interim definitive orbits for researchers conducting experiments with instrumentation in the satellites, to determine definitive orbits, and to conduct analyses of orbits for geophysical and other research purposes.

The Vanguard Orbit Determination Program has been developed under the direction of the Vanguard Working Group on Orbits whose members are Dr. G. M. Clemence, President of the American Astronomical Society and Scientific Director of the Naval Observatory Dr. R. Duncombe, Assistant Director of the Nautical Almanac, Dr. P. Herget, Director of the Cincinnati Observatory, Mr. J. J. Fleming, Head of the Operational Research Branch of the Naval Research Laboratory, and the author who serves as Chairman of the Group. The program utilizes the facilities of the Vanguard Computing Center which has been established in Washington, D.C., under a contract with the International Business Machines Corporation.

The prime Minitrack network was established and is operated under the technical direction of a Project Vanguard group under J. T. Mengel. It has made more than 1250 precision 108 Mc/s radio observations of the satellite 1958 α, Explorer I, and nearly 1000 observations of the satellite 1958 γ, Explorer III. It had already made about 1000 observations of the Vanguard satellite, 1958 β_2, when this satellite's orbit first came around to a position in full sunlight on 22 June 1958. One of the radio transmitters of this satellite is powered with solar cells. Hence, it may continue to transmit and be observed for a long time to come. Table 1 gives a typical set of orbital elements issued for this satellite by the Vanguard Computing Center of the Naval Research Laboratory.

Table 1. Orbit Elements for 1958 β_2, VANGUARD I, as Issued on 2 April 1958

The following are the orbital elements of 1958 Beta (Vanguard) issued at 022000 U.T. by the Vanguard Computing Center of the U.S. Naval Research Laboratory.

Epoch	17 March 1958 12 hr 27 min UT
Anomalistic period	134·29 min
Eccentricity	0·1906
Inclination	34·30°
Longitude of ascending node	154·59° (motion −3·04°/day)
Argument of perigee	128·08° (motion −4·43°/day)
Mean anomaly at epoch	5·11°
Semi-major axis	1·3619 earth radii
Perigee	405·1 statute miles
Apogee	2463·6 statute miles

* Presented at the Tenth General Assembly, International Astronomical Union, Moscow, 12 August to 21 August 1958.

† Present address: Goddard Space Flight Center, Washington 25, D.C.

The satellites 1958 β_2, Vanguard I, and 1958 γ, Explorer III, represent the extremes from the orbit determination standpoint. The absolute fluctuations in the mean motion were smallest for the former, and largest for the latter, among the satellites for which precision radio observations were available. Accordingly, the orbit of the former was determined with the greater precision. Even in the case of 1958 γ, Explorer III, however, reasonably good fits have been obtained for 2 day arcs. The results obtained with this satellite are of interest since they indicate what can be done in the way of determining the orbits of satellites having very low perigees and very high fineness ratios.

The discussion of the observations for the first score of arcs covering the first half of this satellite's lifetime has yielded a piecewise continuous representation of the orbit extending over about 15 million miles. Certain characteristics of this orbit representation are summarized in Table 2. Shown there are the standard deviations of fit for the twenty 2 day arcs which cover this portion of the orbit. These can be thought of as root-mean-square measures in radians of the residuals of the observations which were used to determine the respective arcs. The numbers listed are also approximately a measure, in miles, of the corresponding linear deviations at the mean distance of the satellite, which was about 1000 miles. The radial distances between adjacent arcs at the times for transferring from one arc to the next are seen to be of the same order as the residuals within the individual arcs. Each arc is based upon a dozen or more observations. Some of

Table 2. Interim Definitive Orbit for Satellite 1958 γ
Summary of Certain Position Information For Arcs Extending From 17·45 UT 26 March 1958 to 05·59 UT 6 May 1958

Arc number	Interval (d-h-m) UT	Standard deviation of fit ($\times 10^5$)	Coordinate differences and corresponding distances between points in adjacent arcs at transfer times. Distances are in nautical miles, angles in nautical miles at sea level			
			Long.	Lat.	Height	Radial distance
1	26-17-45 to 28-23-57	5·5				
			4·51	0·09	6·42	8·6
2	28-23-57 to 30-23-47	9·8	4·25	0·35	4·25	6·3
3	30-23-47 to 02-01-03	3·4	9·30	6·76	6·16	17·0
4	02-01-03 to 04-01-00	7·0	4·69	0·52	6·33	8·3
5	04-01-00 to 06-00-52	4·6	1·73	3·63	2·44	5·1
6	06-00-52 to 08-01-54	4·5	0·92	1·60	0·01	1·9
7	08-01-54 to 10-02-55	8·4	2·17	3·05	0·25	3·9
8	10-02-55 to 11-21-52	2·4	1·65	0·02	2·05	2·8
9	11-21-52 to 14-02-23	6·4	0·95	1·78	0·22	2·1
10	14-02-23 to 16-02-36	6·2	1·80	4·18	1·48	5·3
11	16-02-36 to 17-23-35	4·6	1·81	2·27	0·19	3·1
12	17-23-35 to 19-21-28	3·6	0·85	0·18	2·10	2·3
13	19-21-28 to 22-01-02	1·4	0·03	0·93	3·25	3·4
14	22-01-02 to 24-02-45	1·3	0·53	1·13	1·01	1·7
15	24-02-45 to 26-00-33	3·4	1·49	1·87	0·61	2·5
16	26-00-33 to 28-01-46	4·1	1·84	1·70	0·05	2·6
17	28-01-46 to 30-04-51	2·0	1·53	2·82	1·09	3·7
18	30-04-51 to 02-04-58	4·8	1·62	0·07	3·77	4·2
19	02-04-58 to 04-00-39	5·9	4·68	4·35	3·87	7·6
20	04-00-39 to 06-05-59	5·1				

the observations, usually one or two per arc, were removed in the discussion of the observations. The differences between the observed and computed times of meridian passage for a typical set of observations are shown in Table 3. The root-mean-square value of the residuals for the entire 40 day period is less than 6 milliradians and less than 20′ of arc.

At the present time, the best estimate of the overall performance of the entire orbit determination system, including the Minitrack observing system and the orbit computing system, is obtained by analysis of the orbit of the Vanguard satellite, 1958 β_2. Errors only about half the size of the smallest ones appearing in Table 2 have been obtained for some of the arcs of the Vanguard satellite. Hence, it is now possible to state that the overall orbit determination system, including the Minitrack system and the orbit computation system, is capable of accuracies of better than 1 mrad or about 3′ of arc. Analyses of the data for systematic station residuals, ionospheric effects, etc., have not yet been completed. These analyses may make it possible further to improve the accuracy of the overall Vanguard satellite orbit determination system.

Various orbit determination methods are used at the Vanguard Computing Center. These results just cited for the satellite 1958γ, Explorer III, were obtained using the general perturbation method developed by Herget and Musen[1]. It is based upon the method of

Table 3. Meridian Crossing Time Residuals For Arc No. 14 of the Interim Definitive Orbit For the Satellite 1958γ

Pass No.	Minitrack station	Residual (observed − computed)
338	Ft. Stewart	−0·53 sec
339	San Diego	−0·54
339	Havana	+0·09
340	San Diego	+0·12
340	Havana	+0·24
341	Quito	+0·21
342	Antofagasta	+0·40
343	Santiago	+0·12
344	Santiago	−0·07
348	Quito	−0·13
348	Antigua	−0·01
349	Havana	+0·22
350	Havana	+0·33
350	Ft. Stewart	+0·12
351	San Diego	+0·54
351	Ft. Stewart	−0·39
352	San Diego	−0·16
353	San Diego	−1·01
356	Santiago	−0·20

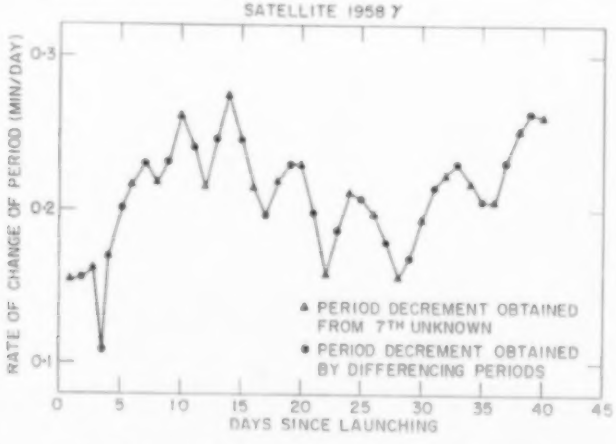

Fig. 1. Rate of change of period of the satellite 1958γ, EXPLORER III as a function of time during the first 40 days of its lifetime.

Hansen's lunar theory. It was used in conjunction with the Eckert–Brouwer Method of differential corrections.[2] The atmospheric drag effects were accounted for by identifying them with a corresponding linear change in the mean motion. This rate of change became a seventh unknown which was solved for in the differential correction program.

The period decrement was also determined by differencing the periods obtained for adjacent arcs. Details of the relationships between these two methods are being studied. In view of the importance and interest attaching to this subject, however, the preliminary results of Fig. 1 are included. There appear to be at least two periods present in the 1958 γ, Explorer III, data shown there. The longer period of the two has a length which corresponds with that of the motion of perigee. The ratio of the period decrement at the maximum and minimum amplitudes is about 4 : 3. An effect of this type is expected as a result of the variation with latitude of the height of perigee above the ellipsoid. If the scale height were 40 km, the amplitude ratio would be about 1·2. This is somewhat smaller than the observed effect. The effect would be still smaller if the scale height were larger. The variation of density with latitude, which is implied by other data, would tend to decrease the amplitude still further. Nevertheless, the observed long period variation in the period decrement for 1958 γ, Explorer III, does appear to correspond approximately to that which is expected as result of a latitude variation of the height of perigee above the ellipsoid. The variation having the shorter period is probably due to a variation in the orientation of the velocity vector relative to the satellite axis. The motion probably represents a combination of the aerodynamic effects and the rigid-body dynamical effects.

A significant measure of air density at a very high altitude was obtained from the orbital data for the satellite 1958 β_2, Vanguard I. Dynamic pressure, ρv^2, is conveniently measured in terms of the characteristic unit, $w/C_D A$, where w, C_D and A denote, respectively, the weight, the drag coefficient and the corresponding reference, projected frontal area of the satellite. For the satellite 1958 β_2, Vanguard I, this characteristic unit, often called the drag parameter, has the value 3·25 g/cm^2, assuming diffuse reflection with no accommodation. The observed rate of change of period for this satellite was $3{\cdot}1 \times 10^{-4}$ min/day. This is the average value for the first 3 months of its life-

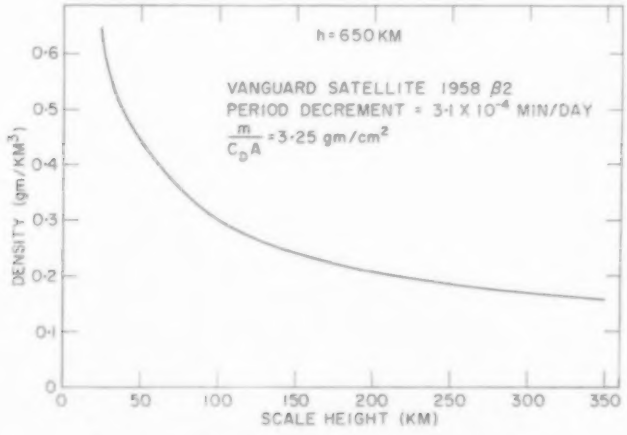

Fig. 2. Density vs. scale height at the 1958 β_2, VANGUARD I, perigee altitude of 650 km as implied by the orbital data for this satellite. An isothermal atmosphere is assumed.

time. During this period, the perigee advanced a little more than one revolution. Hence the value cited represents a sampling of all the latitudes traversed by this satellite, i.e. up to 34·3°.

If the atmosphere over the entire orbital range is considered to be isothermal, these data imply the relation between perigee density and scale height which is shown in Fig. 2. An assumption about scale height allows one to arrive at an estimate of the density at this altitude. Similar curves exist for other altitudes. For example, the same Vanguard satellite data also imply the curves of density versus scale height shown in Figs. 3 and 4. It is seen that the 750 km level is of particular interest. At this height any assumption as to scale height in the range from 125 to 350 km yields very nearly the same implication concerning the density. This height can thus be regarded as a pycnometric level, i.e. a level at which the density is separated relatively well from the other atmospheric parameters, and hence can be determined by means of the satellite observations on the

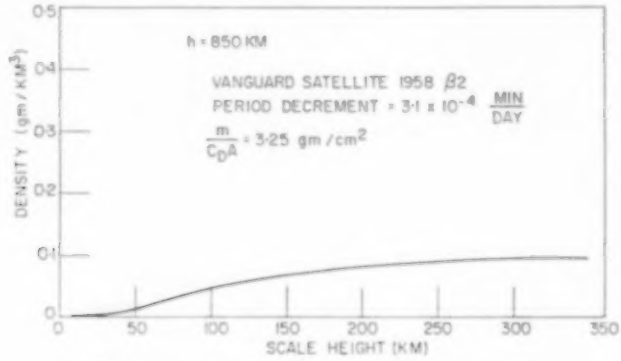

Fig. 3. Density vs. scale height at an altitude of 850 km as implied by the orbital data for 1958 β_2, VANGUARD I. An isothermal atmosphere is assumed.

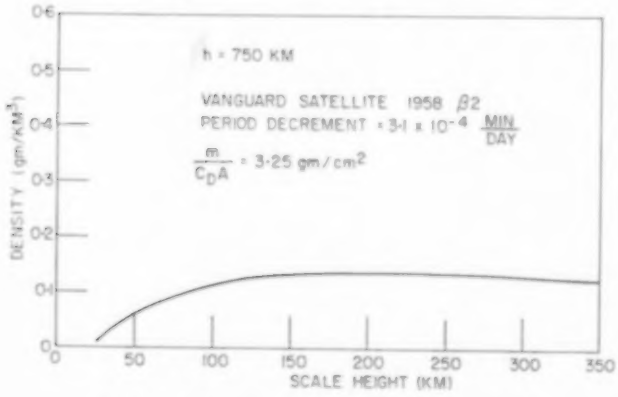

Fig. 4. Density vs. scale height at an altitude of 750 km as implied by the orbital data for 1958 β_2, VANGUARD I. An isothermal atmosphere is assumed.

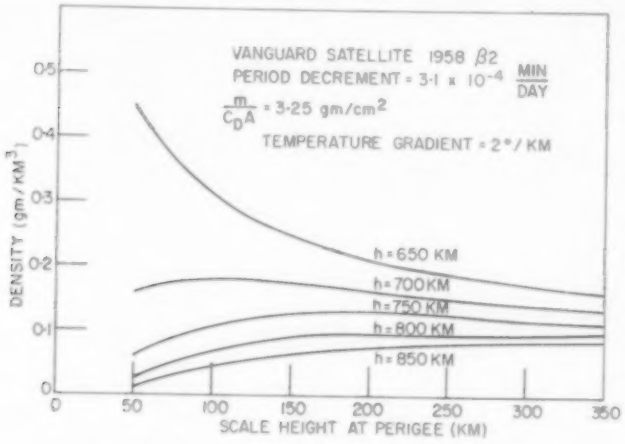
VANGUARD SATELLITE 1958 β2
PERIOD DECREMENT = 3·1 x 10⁻⁴ MIN/DAY
m/C_DA = 3·25 gm/cm²
TEMPERATURE GRADIENT = 2°/KM
h = 650 KM
h = 700 KM
h = 750 KM
h = 800 KM
h = 850 KM
DENSITY (gm/KM³)
SCALE HEIGHT AT PERIGEE (KM)

Fig. 5. Graph illustrating certain pycnometric properties of the orbit of the satellite 1958 β_2, VANGUARD I. Shown are curves of density vs. scale height at several altitudes as implied by the orbital data for this satellite. An isothermal atmosphere is assumed.

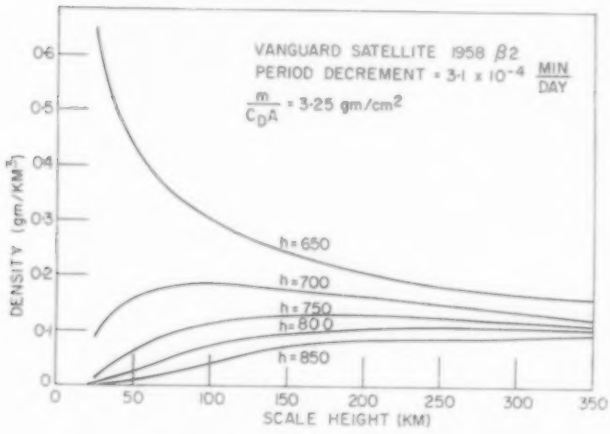

Fig. 6. Graph illustrating certain pycnometric properties of the orbit of the satellite 1958 β_2, VANGUARD I. Shown are curves of density vs. scale height at several altitudes as implied by the orbital data for this satellite. A temperature gradient of 2° K/km is assumed.

basis of assumptions which are not very restrictive. The behavior of the surface $\rho(h, H)$ in the neighborhood of the pycnometric level is indicated in Fig. 5.

This type of analysis has also been conducted for two other cases, corresponding to temperature gradients of 2°/km and 4°km, respectively. Again, curves of density versus scale height were obtained for a number of heights of interest. They are shown in Figs. 6 and 7.

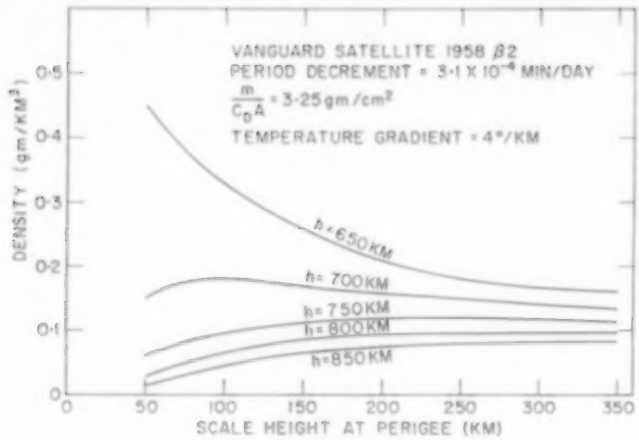

Fig. 7. Graph illustrating certain pycnometric properties of the orbit of the satellite 1958 β_2, VANGUARD I. Shown are curves of density vs. scale height at several altitudes as implied by the orbital data for this satellite. A temperature gradient of 4° K km is assumed.

The 750 km level again has useful pycnometric properties. The atmospheric density is seen to lie within about 8 per cent of $1{\cdot}2 \times 10^{-16}$ g/cm³ for all scale heights between 125 and 350 km and all temperature gradients from 0°K/km to 4°K/km.

An analysis of the same general type has been made for the satellites 1957 α_2 and 1958 α.[3] The results for all three satellites are shown in Fig. 8. Related analyses have also been conducted by other workers.[4, 5] The point shown for the satellite 1958 α, Explorer I,

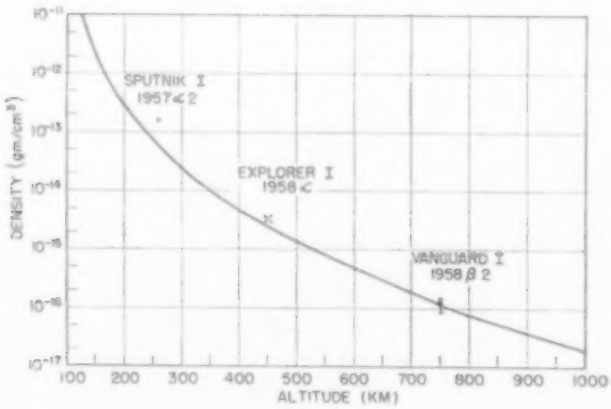

Fig. 8. Atmospheric densities based on observations of certain IGY satellites.

was based on the period decrement of 0·065 min/day which was observed during the first 4 days of its orbital journey. According to Jet Propulsion Laboratory estimates, the minimum value of the drag parameter was assumed by 1958 α at the beginning of its orbital journey.[6] On this basis, and assuming diffuse reflection with no accommodation, the value of the drag parameter was taken to be 3·6 g/cm^2. The latitude of perigee associated with the 1958 α observation shown in Fig. 8 is about 20°N. The latitude of perigee associated with the 1957 α_2 observation shown there is about 50°N.

The analysis of the pycnometric level made above in connection with the Vanguard satellite was primarily mathematical in approach. It sought to determine the pycnometric level which is optimum for a given orbit, without regard, *a priori*, to physical considerations.

An analysis of the Vanguard satellite orbital data can also be made by means of an approach in which an appeal to the physical theory is made. Nicolet[7] has studied atmospheric models in which the mechanism of heat conduction plays an important role in determining the temperature gradient, and hence the atmospheric structure at high altitudes. He considers several cases, each corresponding to an effective temperature at the 500 km level. Variations of this model which he considered thus form a one-parameter family of atmospheres. It was found that the Vanguard satellite orbital data implied that the reference temperature at 500 km is about 1600°K. The corresponding temperature gradient and energy flux are about 2°K/km and 0·3 erg/cm^2 sec, respectively. For this atmosphere the scale height and the temperature gradient at the 750 km level are about 140 km and 2°K/km, respectively. These values fall within the pycnometric region at this altitude which was described earlier. The density implied by this atmosphere at the pycnometric level of 750 km is $1{\cdot}2 \times 10^{-16}$ g/cm^3. The temperature at this level is about 2100°K. The lifetime of the Vanguard satellite determined on the basis of this atmospheric model is about 200 years.

Variations of about 25 per cent were observed in the period decrements for the different arcs in the 90 day period covered by this study. These variations are larger than the standard deviations of the period decrements, themselves. These observed period-decrement variations correspond to variations of about 25 per cent in density and to variations of about 100°K in the reference temperature at the 500 km level.

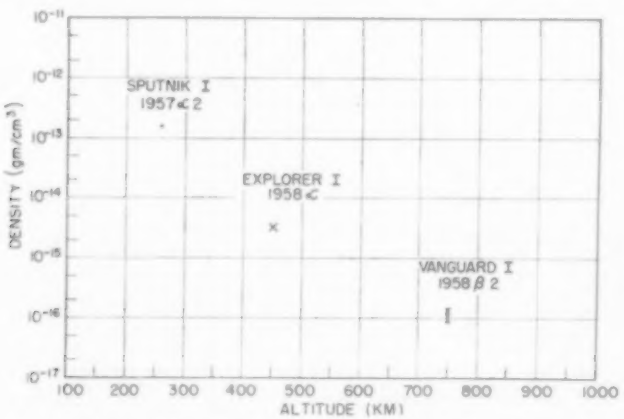

Fig. 9. Density vs. altitude for an atmospheric model of the Nicolet thermal conduction type adjusted to agree with the orbital data for the satellite 1958 β_2, VANGUARD I. Other satellite density values are also shown.

Correlations with other geophysical and solar parameters are being sought in further analyses.

The effect of contributions of charged particles to the drag would be to decrease the corresponding value of the total mass density.[8] Estimates based upon moderate assumptions about the charged-particle drag indicate that it may contribute perhaps 10 per cent of the total drag effect. More drastic assumptions, about the electron temperatures, say, could increase the corresponding charged-particle contributions considerably. This would have the effect of decreasing the corresponding values of the density and the temperature.

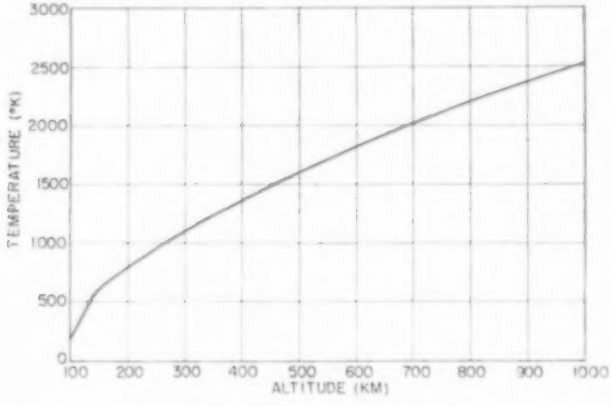

Fig. 10. Temperature vs. altitude for an atmospheric model of the Nicolet thermal conduction type adjusted to agree with the orbital data for the satellite 1958 β_2, VANGUARD I.

The atmospheric density profile which follows Nicolet's theory and is adjusted to fit the Vanguard satellite observations is shown in Fig. 9. It is extrapolated there to the 1000 km level. The corresponding temperature profile is shown in Fig. 10. This atmospheric model is consistent with the satellite observations made at the higher altitudes in the 68·6° latitude belt centered on the equator.

Acknowledgements—It is a pleasure to acknowledge the contributions of the many individuals, in addition to those already mentioned, who have participated in various phases of the effort. In particular, Mr. H. Hancock has prepared a number of NAREC programs and performed numerous calculations using this computer in connection with the atmospheric density analyses. Messrs. N. Bonavito, E. Doll, J. Hayes and R. K. Squires have also performed many calculations in this connection. Messrs. R. Bryant, C. H. Chrisman, M. Lecar and Miss A. Eckels have made many calculations concerning the satellite orbital parameters. The author enjoyed valuable discussions with Drs. R. Jastrow, P. Mange, H. E. Newell, Jr., M. Nicolet and C. Pearse and Mr. H. LaGow concerning the upper atmosphere.

REFERENCES

1. P. Herget and P. Musen, General theory of oblateness perturbations. *American Mathematical Society Symposium on Orbit Theory* (1957).
2. W. Eckert and D. Brouwer, *Astr. J.* **46**, 125 (1937).
3. J. W. Siry, The Vanguard IGY earth satellite program, *Proc. 5th General Assembly of CSAGI, Moscow, 30 July to 10 August, 1958*. In press.
4. I. Harris and R. Jastrow, *Science* **127**, 471 (1958).
5. T. Sterne and G. F. Schilling, *Special Report No. 3, IGY Project No. 30.10*. Smithsonian Astrophysical Observatory, Cambridge (1957).
6. A. Hibbs and H. Richter, Jet Propulsion Laboratory Staff, private Communication.
7. M. Nicolet, *Science* **127**, 1317 (1958).
8. R. Jastrow and C. Pearce, *J. Geophys. Res.* **62**, No. 3 (1957).

Planet. Space Sci. Pergamon Press 1959. Vol. 1, pp. 193–204. Printed in Great Britain.

STRONGLY ABSORBING LAYERS BELOW 50 km

BENGT HULTQVIST and JOHANNES ORTNER

Kiruna Geophysical Observatory, Kiruna C., Sweden

(*Received 5 April* 1959)

Abstract—In a few cases of very strong absorption of very long duration observed at Kiruna Geophysical Observatory during the summer of 1958, the height of the upper boundary of the ionized layer has been found to be about 50 km. It is shown that this height value accords well with what is to be expected if the ionizing agent consists of protons. Earlier proposed interpretation is discussed with regard to this new height information.

1. INTRODUCTION

Within 1 hr after the strong solar flare of 23 February 1956 very strong absorption of radio waves was observed at several ionospheric observatories to the north of 60° geomagnetic latitude (Shapley and Roberts[1]). One exceptional characteristic of the effect was that it was not accompanied by any geomagnetic disturbances or auroral phenomena. It seems to have been the first time that such an effect had been reported. A large number of reports appeared in the literature concerning various geophysical effects of the flare in various regions of the earth, most of them occurring less than 1 hr after the flare outbreak. Several of the reports indicated that unusually deep layers of the atmosphere were influenced (cf. Aarons and Barron[2]; Belrose *et al.*[3]; Gold and Palmer[4]; Pierce and Moritz[5]; Ehmert and Revellio[6]). However, no quantitative height determinations of the absorbing ionization seem to have been made.

Similar absorption without geomagnetic or auroral effects was observed a few times in the summer of 1958 at Kiruna Geophysical Observatory (geographic co-ordinates 67·8°N, 20·4°E; geomagnetic co-ordinates 65·3°N, 115·5°E) (see Hultqvist *et al.*[7]; Hultqvist[8]). The purpose of this paper is to report height determinations of those ionized layers and to discuss the effect of the low heights obtained (less than 50 km) on the interpretation proposed earlier.[8]

The existence of ionized layers (the *C*-layers) in the lower and middle atmosphere (between 5 and 60 km altitude) was proposed more than 20 years ago by several authors (Colwell and Friend[9]; Watson Watt *et al.*[10]; Mitra and Bahr[11]). Short-range echoes (20–50 km) have also been reported in recent years (cf. Okamota *et al.*[12]; Brice[13]). According to Berkner[14], Major[15], Dowden[16] and others it is, however, doubtful if the short-range reflections reported were produced by ionization (probably sea reflections). Landmark[17] has recently obtained a few echoes from 65 km height, which seem to have been of ionospheric origin. They appeared during periods of strong solar disturbances. During polar blackouts at Churchill, Canada, Seddon and Jackson[18] have found measurable electron density down to 55 km altitude from rocket measurements.

2. OBSERVATIONS AND THE PREVIOUS INTERPRETATION

A riometer (relative ionospheric opacity meter) has been in operation at Kiruna Geophysical Observatory since the end of March 1958 (see Little and Leinbach[19] for equipment details).

Very strong absorption starting 2–4 hr after the outbreak of strong solar flares was observed at Kiruna Geophysical Observatory during the summer of 1958 on four occasions: 7 July, 16, 22 and 26 August.

On 8 July and 26 August the maximal absorptions recorded surmounted 20 dB (the signal

strength was so near zero that only a lower limit can be stated with any certainty), which, as far as we are aware, are the highest absorption values reported for vertical radiation around 30 Mc/s. Fig. 1 shows as an example the absorption as function of time for 26 August.

tories at Lycksele (geomagnetic latitude 62·5°N) and Uppsala (geomagnetic latitude 58·4°N).

Characteristic features of the absorption effect being discussed, as compared to absorption effects caused by magnetically disturbing beams, and which also are requirements for application of the method of height determina-

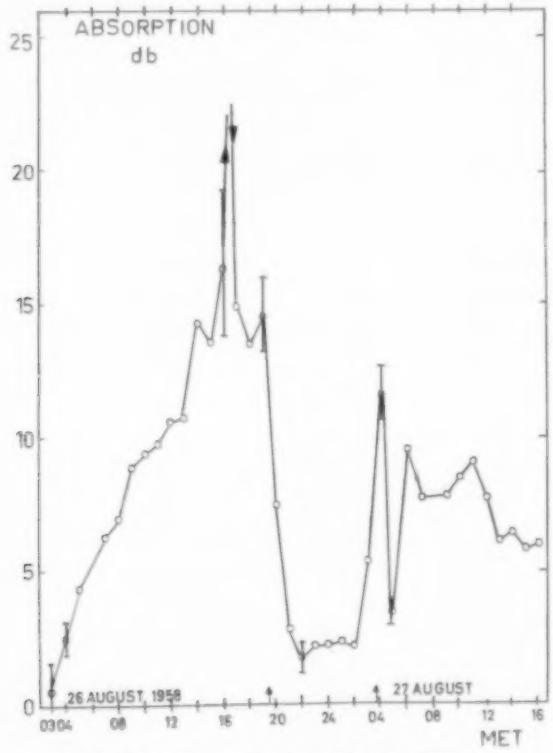

Fig. 1. Absorption as function of time for the period 26–28 August 1958. The maximum limits of errors due to reading of the record are given for a few points to indicate the order of magnitude. The uncertainty in the relative position of neighbouring points is far less.

The most remarkable feature of the whole phenomena was the absence of magnetic effects before the sudden commencement of the magnetic storm.

The restriction of the absorption to geomagnetic latitudes greater than approximately 60° was found from the ionosounder records obtained at the Swedish ionospheric observation described in this paper, are the strength of the effect, the long duration and the smooth time variation, indicating a homogeneous ionization over a large area. Therefore drift motions, turbulence and diffusion seem to play unimportant roles.

The decrease of the absorption was extremely slow. It took some 3 days for the cosmic noise

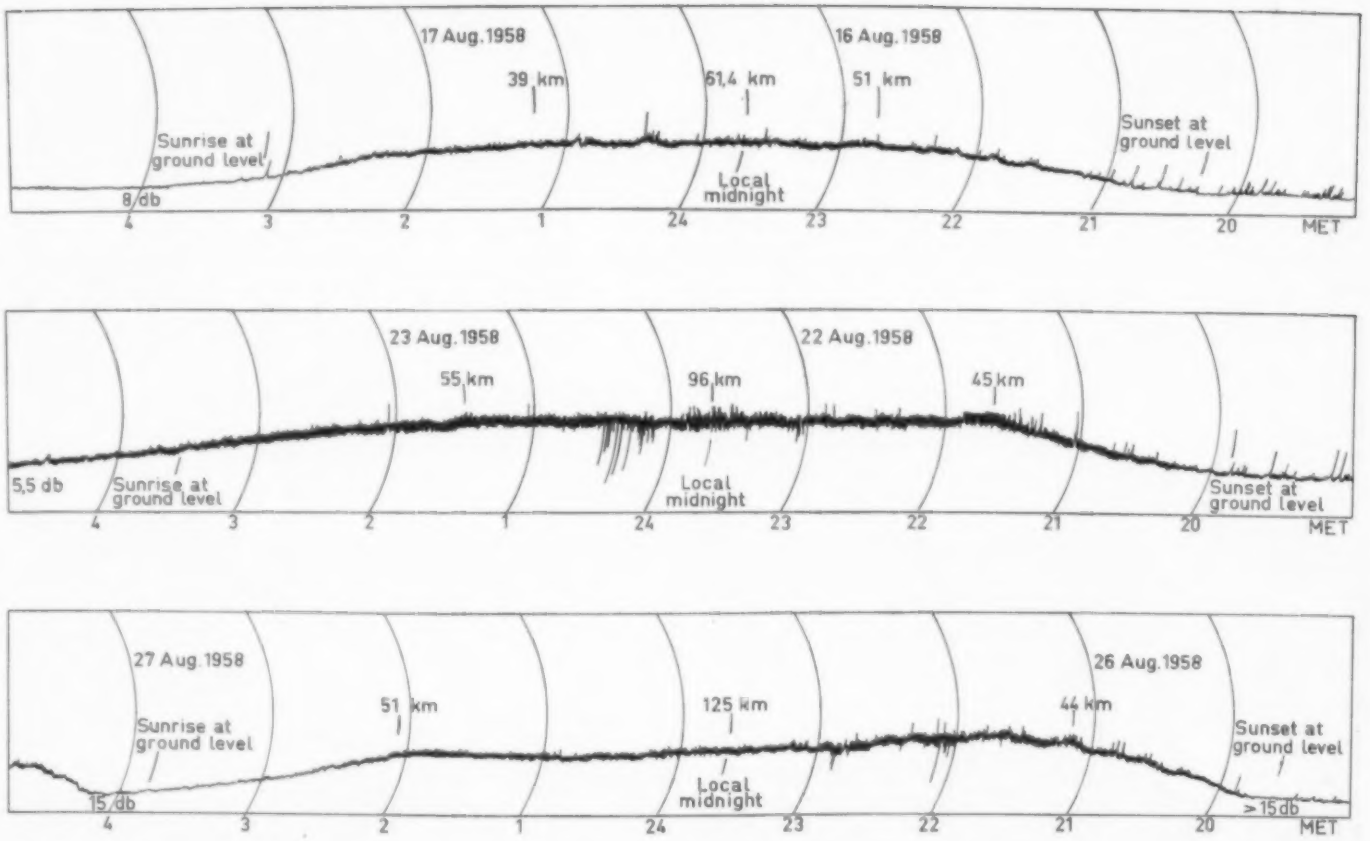

Fig. 2. Increase of cosmic-noise signal strength during the night hours of 16–17, 22–23, and 26–27 August 1958. The figures in km above the curves give the upper limit of the solid earth's shadow vertically above Kiruna for every hour, at local midnight, and at the estimated beginnings and ends of the periods of night-time absorption.

signal strength to reach its predisturbance value again (see Hultqvist[20]).

During the absorption periods of August mentioned, very marked night-time decreases of absorption occurred (cf. Fig. 2). From the records of those decreases the heights of the absorbing layers have been obtained in the way described in paragraph 3 below.

It was shown by Hultqvist[8] that the ionization may be caused by ions—most probably protons of energy up to a few hundred MeV for the lowest magnetic latitudes where the effect has been observed. The necessary number density of the beam was shown to be extremely small, so small that one-particle theory can be used. As no quantitative data concerning the height of the absorbing layer were known when the report of the interpretation mentioned above was prepared, it was supposed that the ionization was situated in the ordinary *D*-layer.

3. HEIGHT DETERMINATIONS

Fig. 2 shows the variation of the cosmic noise signal strength during the nights 16–17, 22–23 and 26–27 August.

The most important types of reactions determining the balance between free electrons, N, and negative ions, N^-, are the following (cf., for example, Bates and Massey[21]):

electron attachment:

$$e^- + X \rightarrow X^- + h\nu, \quad \text{coefficient } \eta, \qquad (1)$$

collision detachment:

$$X^- + Y \rightarrow XY + e^-, \text{ coefficient } \kappa, \qquad (2)$$

photo detachment:

$$X^- + h\nu \rightarrow X + e^-, \quad \text{coefficient } \rho. \qquad (3)$$

In the night when no light reaches the layer the photodetachment reaction is inoperative and therefore N/N^- is less than in the day.

The electron affinity of the O_2 molecule, to which electrons mainly attach in the lower ionosphere and the mesosphere, is approximately 1 eV, which means that the photons of almost the whole solar emission spectrum have sufficient energy for the photodetachment reaction.

The rate of the photodetachment reaction is a function of the solar zenith angle, but as the atmosphere is very transparent for most of the radiation producing the detachment the solar angle dependence is small (cf. Chapman and Davies[22]), as is also indicated by the records of Fig. 2.

From what has been said above about the energy requirements of the photodetachment reaction it seems to be very probable that the effective shadow for the reaction in question is that of the solid earth—or possibly of the cloud layer a few kilometres outside the earth's surface. Direct experimental evidence for that exists. It has, for example, been found at Stanford[23] that the intensity of reflections on 325 kc/s tends to increase when the solar rays tangent to the earth strike the lower *E*-region, and the height of the lowest observed *E*-region reflections on 100 kc/s has been found to drop appreciably at the time when the region leaves the shadow of the solid earth. These effects are attributed to electron photodetachment, as in the cases under discussion here. Furthermore, the investigations of the ozone distribution with height, using the eclipsed moon as the reflecting surface (Götz[24]; Barbier *et al.*[25]), are based on the fact that visible radiation even in the Chappuis diffuse absorption bands of ozone penetrates the earth's atmosphere in the ozone levels, reaches the partially eclipsed moon, and is reflected back to the spectrometer on the earth's night side.

On the basis of these facts and the additional one that the time constant for changes in the N/N^- ratio is certainly less than 1 min, it is evident that the absorption should reach its constant night-time value as soon as the whole layer contributing appreciably to the absorption has come into the shadow of the solid earth (or of the cloud layer). This permits the height of the absorbing layer to be determined for those few cases of unusually strong absorption being discussed in this report.

The values of the height of the limit of the solid earth's shadow above Kiruna at the times of the beginning and the end of the periods of night-time absorption, together with the shadow's height at local midnight are presented in Table 1.

In the morning of 24 August the geomagnetic sudden commencement started before sunrise, and therefore no observations could be made.

Table 1.

Date in August 1959	Beginning of period of night absorption		End of period of night absorption		Height of shadow of solid earth at local midnight (km)
	Time (MET)	Height of shadow of solid earth (km)	Time (MET)	Height of shadow of solid earth (km)	
16–17	2245	51	0115	39	62
22–23	2138	45	0130	55	96
23–24	2141	53	—	—	102
26–27	2110	44	0205	51	125
Average		48·3		48·3	

In two of the seven cases the record is concave upwards during the whole transition periods between daytime and night-time conditions. In those cases the times of beginning and ending, respectively, of the transition is estimated to be in error by as little as ± 3 min. This corresponds to an uncertainty of the height of about ± 2 km. In the remaining five cases the uncertainty is of the order of 5 km, which is less than the highest deviation of any one value from the average ($\leqslant 9$ km).

A possible complete opacity of the lowest or lowest few kilometres of the atmosphere does not increase the upper limits of the absorbing layers, as determined above, by more than the same amount, approximately (one or a few kilometres).

It will be shown below that the very low heights found—the lowest ever reported (except for the sea reflections, mentioned in the introduction)—are in good accordance with what is to be expected if protons constitute the ionizing agent.

4. IONIZATION OF PROTONS AS FUNCTION OF HEIGHT FOR ENERGIES BETWEEN THOSE OF ORDINARY AURORA PRODUCING PROTONS AND COSMIC-RAY PROTONS

The upper geomagnetic colatitude limit, θ, as function of proton energy, according to one-particle theory (see, for example, Störmer[25]) is shown in Fig. 3. The θ-region of special interest here is from $\theta \simeq 20°$ to $\theta \simeq 30°$. For θ less than approximately 20° the protons, for which that colatitude is the upper limit, are stopped already in the D-layer, and for θ greater than about 30° the absorption effect has hitherto not been observed.

Numerical calculations have been made of the energy release as function of height for protons with the following energies outside the atmosphere: 29·5, 49·3, 60·0, 67·7, 97·2, 181·1, 360·3 and 1690 MeV corresponding to $\theta = 21·0°$, 22·5°, 23·1°, 23·5°, 24·7°, 27·1°, 30·3° and 41·2°, respectively.

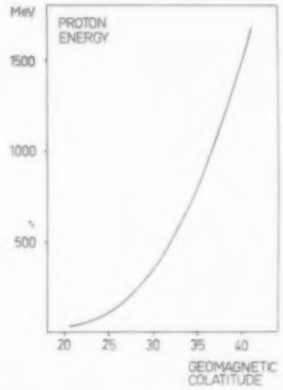

Fig. 3. Upper geomagnetic colatitude limit in the earth's magnetic dipole field as function of proton energy, according to one-particle theory.

The energy decrease during the passage of a proton through the atmosphere has been calculated numerically by taking height intervals of a depth so small that the energy release in every interval is only a few per cent of the remaining energy, except in the very last part of the proton path, where the particle is loosing all its rest

energy. For the last few intervals a depth of 0·2 km has been adopted, and for the very last ones 0·1 km. The total number of intervals for one proton has varied around twenty. The "stopping cross section" for protons in air given in diagram form by Segré[26] and the rocket measurements of the density of the upper atmosphere published by La Gow and Ainsworth[27] have been used as basic data. For the lowest 20 km the density data for the INA atmosphere as found in Landolt-Börnstein[28] have been used. The atmospheric composition has been assumed to be that of the bottom region over the whole interval, as in all cases of interest here the protons penetrate to below 60 km.

Some results of the calculations are presented in Figs. 4 and 5.

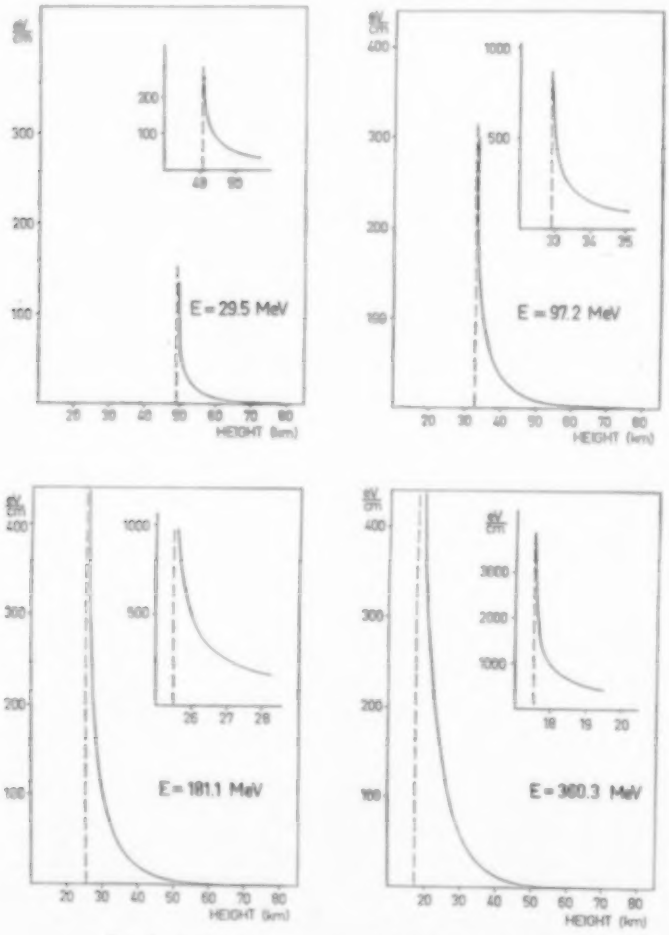

Fig. 4. Energy release per unit length as function of height for protons of energies 29·5, 97·2, 181·1 and 360·3 MeV, corresponding to geomagnetic colatitudes 21·0°, 24·7°, 27·1° and 30·3°, respectively.

The uncertainty due to method of calculation in the obtained height distributions has been roughly estimated by making the calculations with the double number of intervals for the proton energy 97·2 MeV, corresponding to Kiruna's latitude. It was found that the penetration depth is in error by a fraction of one kilometre only. Such an accuracy is quite sufficient for our purposes.

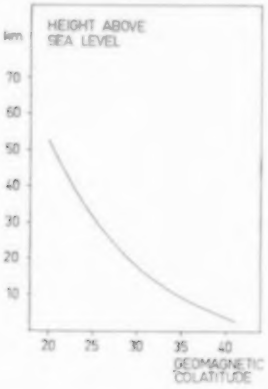

Fig. 5. Lower boundary of the proton ionization as function of geomagnetic colatitude. Concerning basic assumptions, see text.

It has been assumed above that the paths of the protons are straight vertical lines and that the distance from the earth's centre to the level where the protons are stopped is 6400 km (in the numerical calculations of the energy-colatitude dependence the level of appreciable interaction with the atmosphere has been put at 40 km for all proton energies, an approximation which affects the results in a negligible way). It is evident that in this way a lower limit of the lower boundary of the ionization is obtained.

The assumption of vertical paths does not introduce any appreciable error, as for the high latitudes of interest the inclination has values between 70° and 80°.

For Kiruna's geomagnetic latitude (65·3°N) the radius of curvature for protons of lower limit energy is 25 km before any considerable amount of energy has been released in the atmosphere. As the protons, which reach the lower magnetic latitude limit along Störmer trajectories, have quite small pitch angles with regard to the geomagnetic field lines, and as 90 per cent of the energy release occurs over a height interval of only some 12 km, it is evident that the curvature does not increase the penetrated mass of air by any considerable amount. Therefore the position in height of the ionized layer is probably too low by an amount of the order of 1 km or less for Kiruna's latitude and by still less for lower latitudes. Even for the highest geomagnetic latitudes considered in this report (up to 70°) the error in the depth of penetration due to used approximations is assumed to be unimportant.

5. THE ABSORPTION CROSS-SECTION FOR VERTICAL h.f.-RADIATION IN HIGH LATITUDES

For vertical radiation in the h.f.-band and above, the propagation is quasilongitudinal in the latitude range of interest here. For that case the absorption cross-section, σ, can be written

$$\sigma = \frac{k}{N} = \frac{2\pi e^2 \nu}{mc\,\{(p + H_L e/mc)^2 + \nu^2\}} \qquad (4)$$

where k is the absorption coefficient (cm^{-1}), N is the electron density (cm^{-3}), $p = 2\pi f$ is the angular frequency of the wave, ν is the electron collision frequency, H_L is the component of the earth's magnetic field in the direction of propagation, c is the velocity of light and e and m refer to electrons. There are three variables in the expression: p, ν and H_L.

Below the 90 km level the electron collision frequency is a function of pressure, P, and temperature, T:

$$\nu = 5{\cdot}22 + 10^9 P/\sqrt{T} \qquad (5)$$

where P is measured in mm Hg (Nicolet[29]).

The influence of the variations in H_L is very small. Over the geomagnetic latitude range 53°–75° the variation of the term

$$(p + H_L e/mc)^2$$

of (4) amounts to only 3 per cent even for a frequency of 18 Mc/s, and still less for higher frequencies, which means that σ varies with the same amount in the higher levels of the

atmosphere and not at all in the lowest ones. Such variations are negligible compared to the uncertainty of the constant in (5), for instance.

The variation of σ with height has been computed for the four frequencies 18, 27, 36 and 45 Mc/s for Kiruna's latitude, using the P and T information given by La Gow and Ainsworth[27]. The results are shown in Fig. 6, where it can be seen that the absorption cross-section has its maximum far below the ordinary ionospheric layers, and that the height of maximum cross-section only varies between 55 and 49 km over the frequency range 18–45 Mc/s.

6. ABSORPTION DUE TO PROTON IONIZATION

The product $\sigma dE/dh$ is a measure of the absorption coefficient per proton per cm^2. If we want to measure the absorption in dB we have to multiply the product with $20/Q$ ln 10, where Q is the energy required for production of one electron–ion pair. The resulting expression represents the absorption in dB/cm, which would exist in the atmosphere if one proton of vertical direction had traversed every square centimetre of a plane in the upper atmosphere parallel to the earth's surface, and if no recombination occurred.

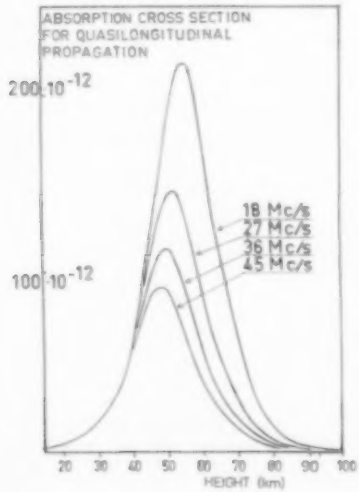

Fig. 6. Absorption cross-section for quasilongitudinal propagation as function of height for the frequencies 18, 27, 36 and 45 Mc/s.

Fig. 7 shows the relative variation with the height of the absorption per cm caused by mono-energetic protons of various energies for vertical trajectories, if the curvature of their orbits and the variation of recombination rate with height within the ionized layer are neglected. These simplifications make the layers too thin but the influence of the omissions is certainly not important. Protons of energy higher than the lower limit for any latitude will mainly ionize at still greater depths than those derived above.

According to the experimental height determinations, the results of which are collected in Table 1, the average height above Kiruna of the limit of the shadow of the solid earth was 48·3 km. Taking into account a complete opacity due to clouds of, say, the lowest 3 km, it increases the height mentioned to 51 km. Approximately 14 per cent of the calculated total absorption due to proton ionization occurs at levels higher than 51 km, as can be estimated from Fig. 7b. It should be remembered that the contribution to the absorption of the layers directly above 51 km altitude is certainly considerably less when the radiation from the sun is reaching the region from angles below the horizon as compared to daytime conditions. Remembering also the uncertainty in the measured height values, which is estimated at a few kilometres—even for the averages—it seems to be possible to state that there exists good agreement between calculated and experimental upper boundaries of the ionization causing the unusually strong absorption. Not more than 20 per cent of the absorption seems to occur at altitudes above the values of Table 1, and still smaller proportion of the ionization is situated at those height levels.

Fig. 8 shows the variation of the total absorption per proton per cm^2 per sec with the geomagnetic colatitude. The absorption per proton has a maximum in the auroral zone (between $\theta = 22°$ and 23·5°). As the maximum height of σ (cf. Fig. 6) varies fairly slowly with

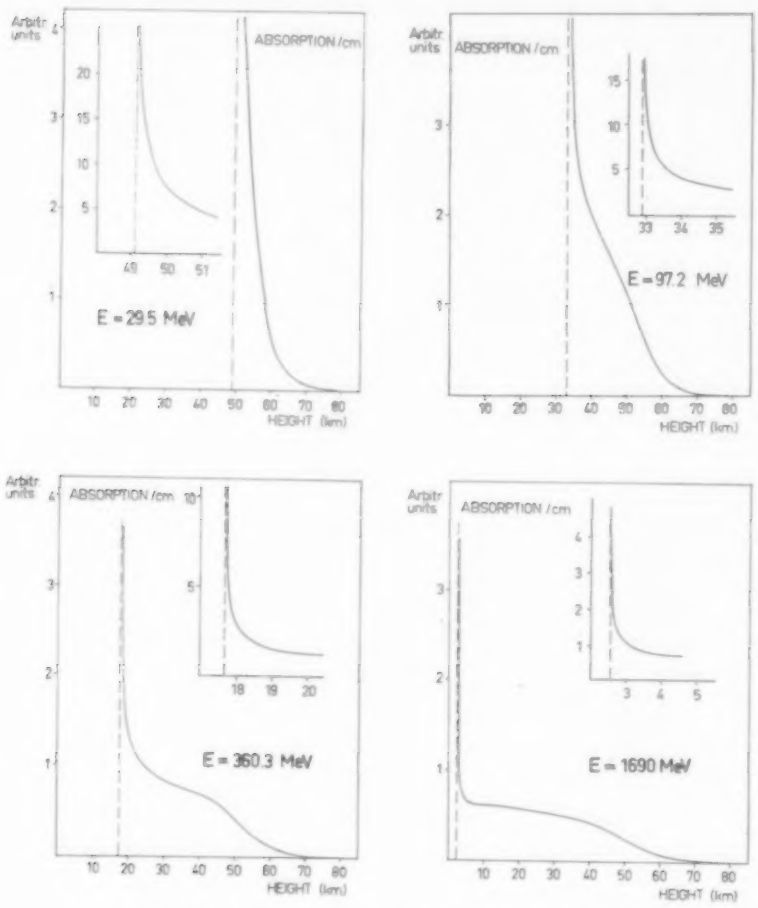

Fig. 7. Relative variation with height of the absorption per cm caused by monoenergetic protons of vertical direction, for the four energies 29·5, 97·2, 360·3 and 1690 MeV, corresponding to upper colatitude limits of 21·0°, 24·7°, 30·3° and 41·2°, respectively.

frequency the absorption effect per proton has a maximum in the auroral zone over a fairly broad frequency range.

7. ESTIMATION OF THE REQUIRED NUMBER DENSITY OF THE PROTON STREAM

In order to find quantitative values of the absorption per cm per proton/cm² sec, the recombination, of course, must be taken into account.

The following relation is valid between the rate of electron production, nq (electrons/cm³ sec) and the electron content, N (electrons/cm³):

$$\frac{nq}{1+\lambda} = \frac{dN}{dt} + (\alpha_e + \lambda \alpha_i) N^2 \qquad (6)$$

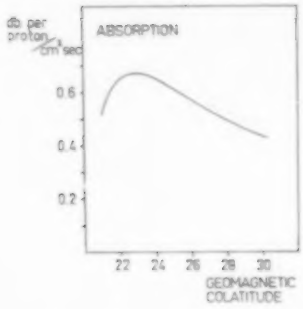

Fig. 8. Variation of the total absorption per proton with geomagnetic colatitude. The ordinate scale gives the absorption, A, in dB per proton/cm^2 sec corresponding to a stationary electron content ($dA/dt=0$).

where n is the vertical influx of protons/cm^2 sec, q is the electron production per cm per proton, $\lambda = N^-/N$ is the ratio of the contents of negative ions (N^-) and free electrons (N), α_e is the coefficient of the electron–ion recombination and α_i is the coefficient of ion–ion recombination.

For the layers of the atmosphere of interest here $\lambda\alpha_i \gg \alpha_e$. Multiplication of all terms with the factor $0{\cdot}459\,\nu/(3{\cdot}32\times10^{16}+\nu^2)$ and integration with regard to height, h, gives

$$n\times 0{\cdot}459\int\frac{\nu q}{(1+\lambda)(3{\cdot}32\times10^{16}+\nu^2)}\,dh=\frac{dA}{dt}+$$
$$+\int(\alpha_i N^-)\frac{dA}{dh}\,dh=\frac{dA}{dt}+(\alpha_i N^-)_{h_1}A \qquad (7)$$

where A is the absorption, measured in dB, and ν is the electron collision frequency.

We know approximately how ν and q vary with height (cf. (5) and Fig. 4) but it is not known how λ varies or the value of h_1.

It can be shown that when recombination can be neglected $\lambda=\eta m/(\kappa m+\rho)$,* where m is the number density of neutral particles to which electrons attach, and η, κ and ρ are the coefficients of reactions (1), (2) and (3) (cf., for example, Hultqvist[20]). The value of λ in the mesosphere is unknown. With all probability $\lambda=100$ is, however, an upper limit especially for daytime conditions even for the low levels being discussed (cf. Bates and Massey[21] concerning the value of η in the lowest ionosphere, Mitra and Jones[30] for a κ-value for the lowest D-region and Hultqvist[20] for $\rho/\kappa m$-values of the absorption cases under discussion). If this value of λ is used for the calculation of the proton flux the obtained flux will certainly be an upper limit.

From the observations that constitute the experimental basis of the height determinations reported above, an average value of $\alpha_i N^-$ has been determined (cf. Hultqvist[20]). The obtained value is $1{\cdot}6\times10^{-5}\,\mathrm{sec}^{-1}$. It is not known for which height this value is typical. The error introduced in using this numerical value for $(\alpha_i N^-)_{h_1}$ in (7) is, however, probably not great compared to other sources of uncertainty. Introduction of the values of λ and $\alpha_i N^-$ mentioned above and putting $q=(1/Q)\,dE/dh$ gives for n:

$$n=\left(\frac{dA}{dt}+1{\cdot}6\times10^{-5}A\right)\Big/\left(1{\cdot}15\times10^{-4}\int\frac{\nu\,dE/dh}{3{\cdot}32\times10^{16}+\nu^2}\,dh\right) \qquad (8)$$

if the value 40 for Q, used earlier, is adopted.

With $dA/dt=1$ dB/hr and $A=20$ dB, which values are typical for the cases of very strong absorption reported in this paper, an upper limit, corresponding to the presumed value of λ, of the n-value of 63 protons/cm^2 sec is obtained. As the velocity of 97·2 MeV protons is $1{\cdot}27\times10^{10}$ cm/sec the required number density of protons in the beam is found to be as low as 5×10^{-9} protons/cm^3. This is within the limits given by Hultqvist[8] before any quantitative estimations of the height had been made. As probably only a small part of the total number of protons in the beam reaches down into the atmosphere in the way sketched above, the total number density of the proton beam is assuredly several orders of magnitude higher, but even then the trajectories are with

* There is some uncertainty concerning the parameter m in the term κm. In adopting the same value for m in this term as in the term ηm of the expression for λ we have followed Mitra and Jones[30] and Bailey[31].

all probability of the Störmer types, as the marginals for use of one-particle theory are wide.

8. DISCUSSION

(1) The deep penetration into the atmosphere is a very strong support for the hypothesis that the ionization is produced by protons of energy between that of ordinary auroral protons on one hand and cosmic-ray protons on the other, as proposed by Hultqvist[8]. It rules out the possibility of heavy ions (like calcium ions) being the ionizing agent.

From the time interval between solar flare outbreak and start of increase of absorption and the velocity corresponding to the energy of those protons, for which Kiruna's latitude is the lower limit, it can be found that the distance, sun to earth, along the real proton orbits is 6 times longer than the straight line distance, which is not unreasonable according to Block's[32] calculations.

(2) From Fig. 8 it can be seen that the absorption due to a proton of energy 360 MeV reaching 60° geomagnetic latitude is about 60 per cent of that produced by a proton one-sixth as energetic reaching the auroral zone. The efficiency per unit energy is thus 10 times greater in the auroral zone than 7° further south. This fact contributes to the decrease of the absorption effect with decreasing geomagnetic latitude. It can, however, not alone explain the observed lack of any effect to the south of 60° geomagnetic latitude. The main reason for that must be that the number density of the proton beam as a function of energy decreases rapidly with increasing energy.

Measurements of the latitude-dependence of the absorption effects, described in this paper, would give valuable information about the proton number density vs. energy curve for the energy range of, say, 20 or 30 to 350 MeV.

(3) The exceptionally low height in the atmosphere explains the remarkable fact that the absorption was not accompanied by geomagnetic disturbance. If the ionization responsible for the geomagnetic effects is situated in the *E*-layer, the absorption per electron is some 2500 times less than if it is localized in the 30–50 km levels. Taking into account the fact that the ratio of the cross-conductivities per electron (proportional to $\nu/(\nu^2+\omega^2)$, where ω is the gyrofrequency) for the 40 and 115 km levels is 6 to 7 and that a reasonable value of the ratio of average wind velocities in the two levels mentioned is 1/3 (cf. Crary[33] and Harang[34]), it is found reasonable that the electric current due to winds is some 50 times or more higher in the 115 km level for an absorption localized there of the order of 1 dB than an electron content at 40 km height producing some 20 dB absorption, which seems to be sufficient to explain the lack of measurable currents associated with the low layers.

(4) A very low decay rate—several orders of magnitude less than is expected on theoretical basis—has been found for the type of ionization discussed (see Bailey[31] and Hultqvist[20]). It may have something to do with the fact that the ionization, according to our measurements, is situated in the ozonosphere, or the low rate of decay may be due to continuous bombardment of particles from corpuscular radiation stored in the earth's magnetic field.

(5) The observed decrease of absorption in connexion with the start of the geomagnetic storm, reported earlier (Hultqvist *et al.*[7]; Hultqvist[8]) can evidently not be due to thermal expansion of the atmosphere, which has been proposed, as an expansion would increase the absorption at Kiruna's latitude due to the shape of the absorption cross-section curve of Fig. 6. The sudden occurrence of an electrical field directed upwards seems then to be the most simple explanation.

The experimental material on which the interpretation and discussion of this paper are based is very small. The results are therefore to be considered as preliminary until more data have been collected. As the occurrence of the special type of extremely strong absorption of long duration seems to be intimately correlated with very strong solar flares it may, however, take several years to collect good material.

Acknowledgement—The authors are indebted to Mr. W. Stoffregen for furnishing information concerning the absorption effects recorded at the ionospheric observatories at Uppsala and Lycksele.

This work has been supported in part by the European Office of Air Research and Development Command (contract 61(514)-1314) and by the Swedish Natural Science Research Council.

REFERENCES

1. A. H. Shapley and W. O. Roberts, *Nat. Bur. Stand. Rep.* No. 5062 (1957).
2. J. Aarons and W. R. Barron, *Nature, Lond.* **178,** 277 (1956).
3. J. S. Belrose, M. H. Davenport and K. Weekes, *J. Atmos. Terr. Phys.* **8,** 281 (1956).
4. T. Gold and D. R. Palmer, *J. Atmos. Terr. Phys.* **8,** 287 (1956).
5. J. A. Pierce and E. M. Moritz, *Cruft Lab. Progr. Rep.* 39 (1956).
6. A. Ehmert and K. Revellio, *Z. Geophys.* **23,** 113 (1957).
7. B. Hultqvist, J. Aarons and J. Ortner, *Tellus*, in press (1959).
8. B. Hultqvist, *Tellus*, in press (1959).
9. R. C. Colwell and A. W. Friend, *Nature, Lond.* **137,** 782 (1936).
10. R. A. Watson Watt, L. H. Bainbridge-Bell, A. F. Wilkins and E. G. Bowen, *Nature, Lond.* **137,** 866 (1936).
11. Mitra and Bahr, *Sci. & Cult.* **1,** 782 (1936).
12. H. Okamota, M. Ose and K. Aida, *Rep. Ionosph. Res. Japan* **11,** 50 (1957).
13. N. M. Brice, *J. Atmos. Terr. Phys.* **13,** 179 (1958).
14. L. W. Berkner, *Terrestrial Magnetism and Electricity* (Edited by Fleming) McGraw-Hill, New York (1939).
15. G. Major, *Nature, Lond.* **175,** 862 (1955).
16. R. L. Dowden, *J. Atmos. Terr. Phys.* **11,** 111 (1957).
17. B. Landmark, *J. Atmos. Terr. Phys.* **12,** 79 (1958).
18. J. C. Seddon and J. E. Jackson, *Ann. Géophys.* **14,** 456 (1958).
19. C. G. Little and H. Leinbach, *Proc. Inst. Radio Engrs., N.Y.* **47,** 315 (1959).
20. B. Hultqvist, *Ark. Geofys.* in press (1959).
21. D. R. Bates and H. S. W. Massey, *J. Atmos. Terr. Phys.* **2,** 1 (1951).
22. S. Chapman and K. Davies, *J. Atmos. Terr. Phys.* **13,** 86 (1958).
23. *Interim Progress Report, Electronics Research Lab., Stanford Univ.* Bur. Stand. Contract No. Cst.-10751. (1951).
24. F. W. P. Götz, *Ergebn. kosm. Phys.* **3,** 253 (1938).
25. D. Barbier, D. Chalonge and E. Vigroux, *Ann. Astrophys.* **5,** 1 (1942).
C. Störmer, *The Polar Aurora.* Oxford University Press (1955).
26. E. Segre (Editor), *Experimental Nuclear Physics* Vol. 1. New York (1953).
27. H. E. La Gow and J. Ainsworth, *J. Geophys. Res.* **61,** 77 (1956).
28. Landolt-Börnstein, *Zahlenwerte und Funktionen* (6th Ed.) Vol. 3, *Astronomie und Geophysik* p. 579. Berlin (1952).
29. M. Nicolet, *J. Atmos. Terr. Phys.* **3,** 200 (1953).
30. A. P. Mitra and R. E. Jones, *J. Geophys. Res.* **59,** 391 (1954).
31. D. K. Bailey, *J. Geophys. Res.* **62,** 431 (1957).
32. L. Block, *Ark. Fys.* **14,** 161 (1958).
33. A. P. Crary, *J. Met.* **7,** 233 (1950).
34. L. Harang, *J. Atmos. Terr. Phys.* Spec. suppl. p. 26 (1957).

Planet. Space Sci. Pergamon Press 1959. Vol. 1, pp. 205–212. Printed in Great Britain.

ON SOME CHARACTERISTICS OF THE E_s–LAYER

M. BOSSOLASCO and A. ELENA

Istituto Geofisico e Geodetico, Università di Genova, Italy

(*Received 5 February* 1959)

Abstract—Some aspects of the dependence of the E_s–ionization on the geomagnetic field are derived; further, an attempt is made to deduce the mean world-wide drift direction of E_s in summer, using the time displacement that occurs for the daily maxima of the hourly median values of f_0E_s.

1. E_s AND THE GEOMAGNETIC FIELD

It is generally assumed that some of the chief properties of the E_s–layer are intimately related with the geomagnetic field, but this bond is still supported only on isolated results rather than on results collected and discussed on a world-wide basis. With the data gathered during the IGY a better knowledge of the same bond will be possible, allowing us to deduce the true nature of the ionization processes responsible for the E_s–layer.

For some years it has been known, first for Huancayo and later for Kodaikanal,[1] that on the geomagnetic equator E_s is generally so regular that the diurnal variation of its critical frequency follows roughly the $\cos\chi$–law, with midday maxima mainly very much higher than the corresponding values occurring in other latitudes. The symmetry between the forenoon and the afternoon behaviour of f_0E_s is then characteristic for these equatorial stations.

The same results, together with the seasonal variation of the f_0E_s suggest that the solar radiation is certainly the chief factor controlling the ionization of E_s in the equatorial regions and, as we shall see, everywhere.

Among the new ionospheric stations raised in the equatorial regions in the last few years, the most interesting ones are the African. Of these only Ibadan and Djibouti present a behaviour in the diurnal and seasonal variations of the f_0E_s similar to those that are recorded in Huancayo and Kodaikanal, *i.e.* over these places the E_s–layer is also prevailingly of the equatorial type.

Ibadan and Djibouti have the geomagnetic latitude of 10·6°N and 7·0°N, respectively, latitudes calculated in the assumption that the geomagnetic field is an approximation of an eccentric dipole. Therefore, these two places cannot be considered as properly lying on the magnetic equator of the eccentric dipole. Instead, Ibadan and Djibouti are nearly situated on the equator of 0° magnetic dip (of the present epoch), crossing the African continent 7–10° north of the geographic equator, while the geomagnetic dipole equator crosses from WSW to ENE the same geographic equator near Stanleyville.[2]

Since in South America and in India the 0° dip equator coincides roughly with the dipole equator the importance of the former has been neglected.

According to what Rawer[3] has pointed out, from the data now available it results that the 0° dip equator is effective in generating the equatorial type of E_s only in a narrow band around the same 0° dip equator.

Another proof, though indirect, that only the 0° dip equator is decisive in producing the ionization of the equatorial E_s–type, is given by the behaviour of E_s resulting from the ionospheric stations located in the Belgian Congo. The Lwiro station (geomagnetic latitude 4·0°S), with the data of 1952–53, reveals diurnal and seasonal variations of normal type, as recorded

in middle latitudes. The same occurs at Bunia (Ruampara, geomagnetic latitude 0·3°S), a station which was active in the IGY 1957–58.

We shall return later to the equatorial E_s-type, that we consider as belonging only to the localities placed on the narrow band around the 0° dip equator. Now we shall examine the E_s-data from observations made by ionospheric stations lying outside the band around the 0° dip-equator, and up to latitudes of nearly ±60°, where the polar type of E_s that we are not considering here begins to appear.

Since the critical frequency of a region is related to the maximum electronic density, $N \propto f_0^2$, it is clear that the highest ionization of the E_s-layer does occur with the maximum of f_0E_s. In the part of the earth we are considering, between the latitudes of −60° and +60°, these maxima always occur in the diurnal hours, *i.e.* when the sun is over the horizon, a result which confirms that the chief cause of the E_s-ionization is due to the sun's influence.

Of course, isolated f_0E_s maxima values are not significant from a statistical standpoint. Instead, we have considered the hourly median values of f_0E_s for each month and for each ionospheric station active in the IGY period (from which data have been received). Although the electrical characteristics of the sounding instruments used are often different, we have found that such medians are useful and therefore comparable.

For nearly all ionospheric stations active during the IGY we have plotted the isopleth representation of such f_0E_s hourly medians (time in MLT or of the nearest $n \times 15°$ meridian as abscissa, versus months). This representation lets us immediately infer the chief features of the diurnal and seasonal variations of the median E_s.

Before discussing such variations, we shall examine the *absolute* maximum of the same hourly median values, that we call $M(f_0E_s)$. Of course, this maximum appears in summer (generally in June–July in the northern hemisphere and December–January in the southern).

Figure 1 represents these maxima $M(f_0E_s)$ graphically, dependent on the geomagnetic latitude (this last is sufficient in this respect).

In the majority of the stations used in the northern hemisphere we have indicated the two maxima, one relative to summer 1957 and the other to summer 1958, that generally are not coincident. The corresponding differences are also sometimes great, but, as we shall demonstrate, these differences should be ascribed generally to intensity-changes of the prevailing ionospheric winds in the E_s-layer. For the southern hemisphere only one summer (December 1957–January 1958) was available, and therefore only one maxima is indicated.

At the same geomagnetic latitude the least values of $M(f_0E_s)$ are more representative of the effective maximum ionization of the E_s-layer, independent of the variation that might occur in wind intensity. Thus, in Fig. 1 we have drawn a dotted line giving the limits of the minimum values of $M(f_0E_s)$ and this smoothed curve should approximately indicate the maxima ionization in the E_s-layer, locally originated without or with little contribution of mass transport, that is, the change due to the mean magnetic field. Analysing the figure we can deduce:

(1) Although the number of ionospheric stations in the southern hemisphere is considerably less than in the northern one, it seems that by deduction of wind effect the maxima of the mean E_s-ionization are sensibly greater in the southern hemisphere.

(2) The behaviour of the same maxima in function of the geomagnetic latitude reveals:
   (a) a minimum near the equator;
   (b) two maxima near ±15°–20°;
   (c) a sharp minimum at about −35° in the southern hemisphere, while the corresponding one in the northern hemisphere seems not at all so clear.

Although for other ionospheric layers a dissymetry between the southern and the northern hemisphere has been exhibited, more stations in the southern hemisphere are needed to assure a general validity of the result.

We should remember that the mean solar daily geomagnetic variation on quiet days (S_q)

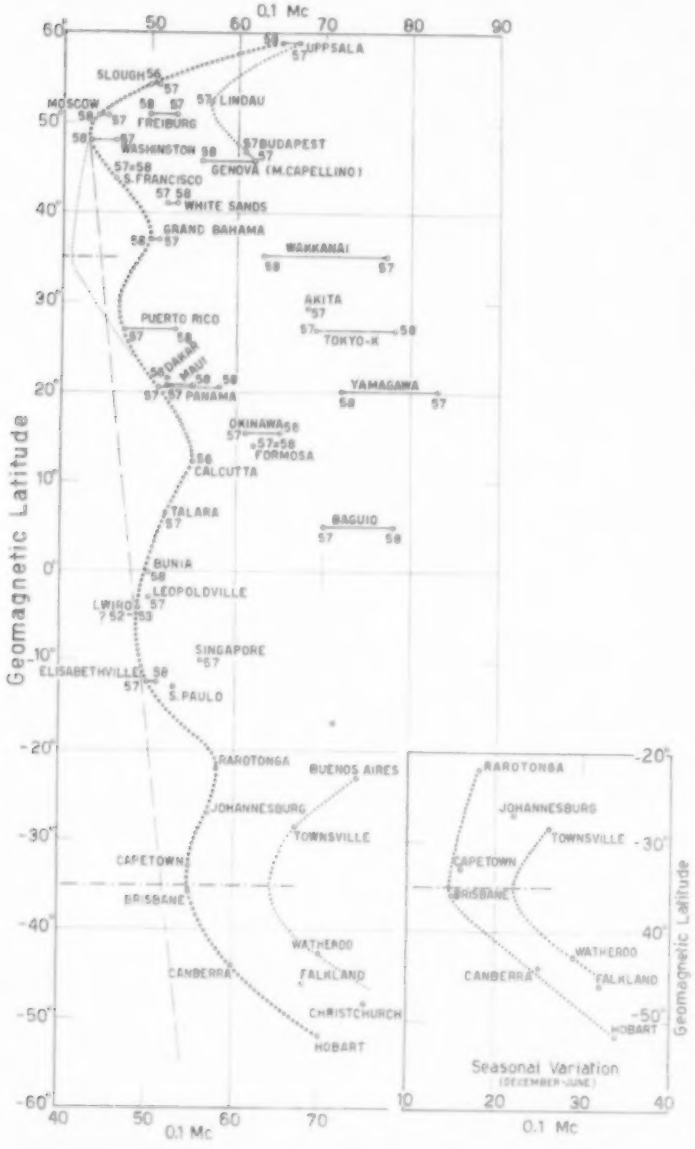

Fig. 1. Behaviour of the absolute maxima of the median hourly critical frequency $M(f_o E_s)$ dependent on the geomagnetic latitude (generally obtained from IGY data). The dotted line at the left side joins the minima values of $M(f_o E_s)$, the values that are more independent of the high speeds in the E_s- drift.

is generated by a current system in the ionosphere, one in the northern and the other in the southern hemisphere, each of them flowing around two foci, placed at latitude of ± 35–40°. In low latitudes the currents are both eastward. The two foci explain the minimum of $M(f_0E_s)$, particularly evident in the southern hemisphere during the summer. This result is also confirmed by the corresponding mean seasonal variation of the same quantity expressed in function of the latitude, since we obtain a similar picture, as the right side of Fig. 1 shows. That the situation in the northern hemisphere is not so clear should be ascribed probably to more irregular induction effects of earth currents on the ionosphere. Nevertheless, it is proved that the mean characteristics of the E_s–layer are controlled by the normal current distribution responsible for the S_q.

It is known that in some equatorial places (Huancayo, Kodaikanal, etc.) lying on the 0° dip equator, the quiet day solar magnetic variation S_q in H (horizontal magnetic intensity) is abnormally large. This fact can be explained by the daily rise and decrease of a concentrated eastward electric current, named *electrojet*, superposed on the normal current distribution responsible for the daily magnetic variation S_q.[4]

Since the mean f_0E_s in the same equatorial places has a similar abnormally large solar daily magnetic variation (S_q), also the electrojet should be the cause of the equatorial type of E_s. Indeed, if we suppose that the electrojet flows at a height less or little less than the E_s–layer, since the geomagnetic field is horizontal (0° dip), by deflection an upward movement of electrons is originated and the process continues during the solar hours when the electrojet is active. Following McNicol and Gipps[5], E_s might be formed due to the ionization of pre-excited atoms by the radiations in the visible part of the solar spectrum; and by the upward movement just mentioned this ionization increases chiefly vertically, causing accumulation that can explain the high or very high values recorded for f_0E_s.

As clearly pointed out by S. Chapman[6], "the abnormal band of eastward current superposed on normal current flow does not encircle the earth; . . . a few hours of longitude to the east and west of the focal meridian, $S_q(H)$ has sunk almost to its night time value, indicating that there the abnormal *eastward* current is only just beginning to flow, or has just ceased. As the current must complete a circuit, there must also be a westward abnormal flow (presumably both to the north and south of the abnormal band of eastward current), turning towards the equator in the forenoon to flow eastward, and away from the equator in the afternoon to flow westward. On the diagram of current intensity along the focal meridian, the return flow will correspond to depressions *below* the normal curve, to the left and right of the superposed abnormal peak, the combined curve being equal to the peak area above the normal curve." (See Fig. 6 of the quoted paper[4]).

Therefore, where the 0° dip equator differs sensibly from the geomagnetic equator, on and near it during the sun hours we have a depression, *i.e.* the current intensity is below normal value. And if we simultaneously consider different stations at low latitudes (between -10° and $+10^\circ$ geomagnetic latitude), but not those on the 0° dip equator or in the band of $\pm 4^\circ$ around them, the corresponding current intensity drawn in function of the geomagnetic latitude leads to a smoothed curve presenting a minimum near the geomagnetic equator.

Because of the total electric current system resulting during the sunlight hours by the superposition of the electrojet on the normal system responsible for S_q, we see that in low latitudes also the mean $M(f_0E_s)$ as controlled by these currents should have a minimum near the geomagnetic equator. Since the ionospheric stations being considered here are mostly in Africa south of the geomagnetic equator, the corresponding minimum of $M(f_0E_s)$ obtained by a smoothed curve going through a limited number of points, is placed somewhat south of the geomagnetic equator, but the result is qualitatively confirmed.

For the two maxima of the mean $M(f_0E_s)$ at the geomagnetic latitudes of nearly $+13^\circ$ and -22°, obtained from Fig. 1, the agreement with

the corresponding maxima of the total electric current flowing eastward during the sunlight hours should be regarded sufficient because of the very scarce data used.

Furthermore, considering the isopleth representation of the hourly median values of f_0E_s, it should be noted that some stations at low latitudes reveal a somewhat irregular behaviour in the seasonal variation of the same f_0E_s-median. This occurs in Central Africa, south of the 0° dip equator (Bunia, Lwiro, Léopoldville, Elisabethville), as well as in Central America, north of the same equator (Talara, Panama, Puerto Rico, Grand Bahama), where we have one of the following seasonal behaviours (Fig. 2):

(1) The seasonal variation is contrary to that expected; so too in Lwiro and Bunia, though to a lesser degree, the maximum of f_0E_s occurs in June (and not in December). Analogously in Talara the seasonal maximum of f_0E_s is recorded in December (instead of in June).

(2) In the stations at Léopoldville, Elisabethville, Grand Bahama, Puerto Rico and Panama the seasonal variation of f_0E_s is generally of *mixed* type, *i.e.* in these places the maxima of f_0E_s occur mainly each six months (nearly at June and December) or are more or less irregularly distributed. Effectively, Léopoldville seems to have maxima in June somewhat more sharply than the other stations, and from this point of view it belongs more appropriately to the first group; while Puerto Rico is less irregular, having maxima generally in June.

The explanation of these results can be outlined as follows: We consider, for instance, Central Africa, where the 0° dip-equator is situated several degrees north of the geographic and geomagnetic equators. Referring to the picture of the electrojet given in[4], this abnormal eastward current flowing in the sun hours over the 0° dip band provokes a compensating westward abnormal current that (contrary to what happens in the places where the equators are not so distant, *i.e.* where the flow occurs both to the north and south) should *flow only to the south* of the 0° dip equator, turning towards the magnetic equator in the forenoon to flow eastward and away from the equator in the afternoon to flow westward. Herewith the westward compensating current of the electrojet transports the properties of this electrojet to the south part, *i.e.* including its maximum seasonal activity (June), that will be superposed on the normal current system. The proposed explanation seems satisfactory, particularly because of the dissymetry of the 0° dip equator and its bending over Africa and America. Similarly, over Central America the irregular seasonal types of f_0E_s might be explained with the penetration of the abnormal westward electric current towards the north.

2. THE ZONAL MOVEMENTS OF THE E_s LAYER

For some years it was found—by the fading method or by "reflection" of radio waves at a frequency of 20 Mc/s or more[6]—that the ion clouds forming the E_s-layer are submitted generally to translational movements; directions and speed values have been estimated, although they are not always in good agreement.

Without attempting to investigate the true physical nature of these movements, more presumably generated by the electromagnetic forces causing the charged particles to move relative to the neutral particles, we introduce here a new method for obtaining the prevailing monthly direction of the zonal E_s-drift, making use of the time-displacement (advance or delay) presented by the diurnal maxima of the f_0E_s-medians, as revealed by the isopleth representation.

This procedure can clearly be justified considering, for instance, the isopleth representation of the f_0E_s-medians for Baguio (Philippine Islands, Fig. 3). The figure shows that in summer at Baguio the maximum of the f_0E_s-medians occurs very sharply in the forenoon, at about 7–10 a.m. (MLT), *i.e.* nearly 5–2 hr before noon. A similar advance appears also, though not so obviously, in Formosa, Okinawa and in Japan and is to be explained as an effect of very strong E-winds transporting the ion clouds of the E_s-layer at a speed nearly

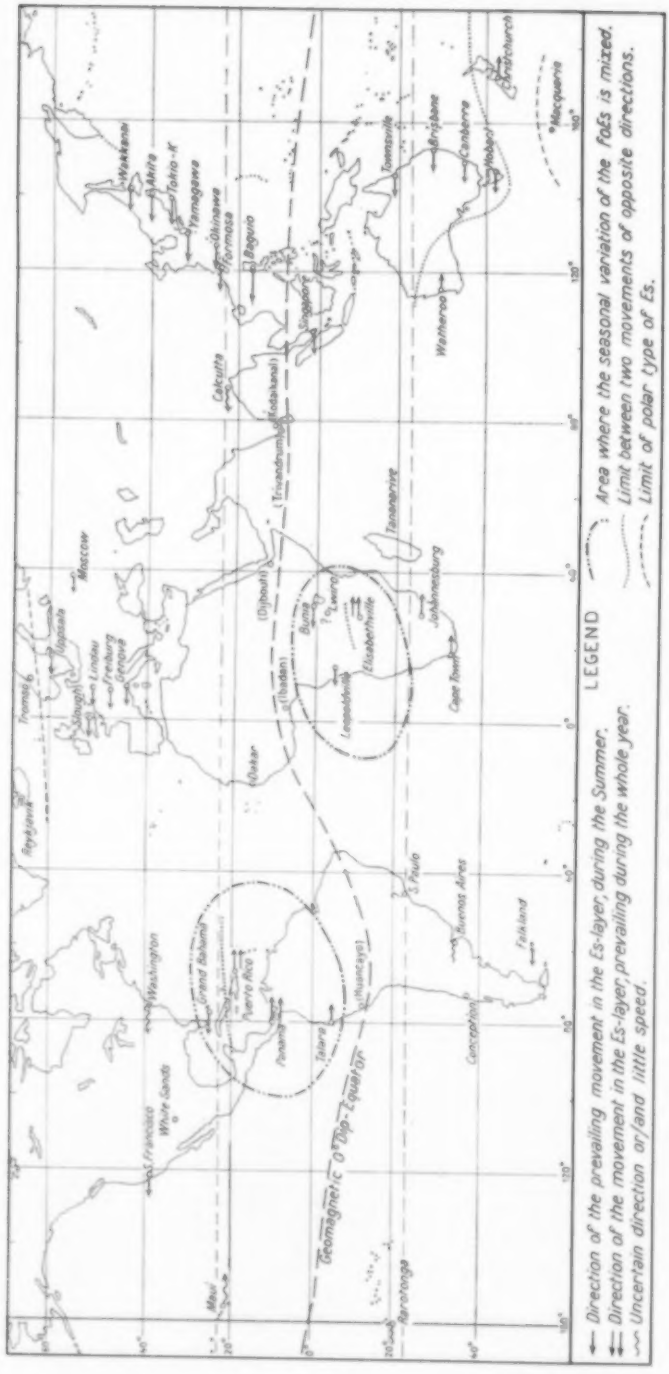

Fig. 2. Prevailing directions of the E_s-drift in summer.

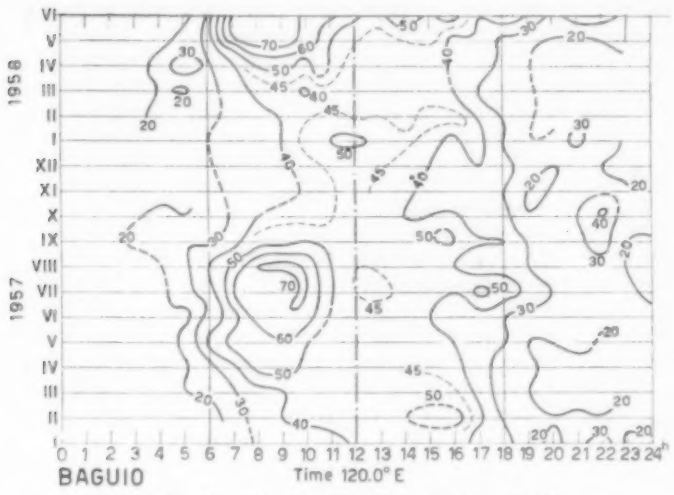

Fig. 3. Isopleth representation of the median hourly values of $f_0\,E_s$ at Baguio (Philippine Islands).

equal to the apparent speed of the sun and of the subsequent vertical growth of the same clouds. Indeed, as the greatest increase of ionization in the E_s-layer occurs generally in the hours just after sunrise,* if we have E-winds transporting this effect with the apparent speed of the sun movement over Baguio, we obtain a concentration of the ionization in the same hours, *i.e.* a maximum of the f_0E_s-medians a few hours after day break, as indicated in Fig. 3.

Of course, the method, as based on median values, is appropriate only for deducing the prevailing *zonal* winds in the season when the maxima of the f_0E_s-medians occur very clearly. As the example of Baguio shows, the agreement between the maxima relative to different months of the same season also reveals the stability of such zonal currents.

An attempt to deduce a rough value of the speed of these *zonal* winds can be made as follows. Denoting with v_0 the speed of a point over the equator at 110 km height rotating with the earth, it is, approximately, $v_0 = 1696$ km/hr and at latitude φ the speed will be $v = v_0 \cos\varphi$.

The sun's rays first contact the 110 km height in advance of the corresponding points on the earth's surface; if τ is the time between this first contact of the sun's rays and the local noon, we have, approximately[7]:

$\varphi =$	0°	10°	20°	30°	40°	45°
$\tau \cong$	6·7 hr	7·0 hr	7·5 hr	7·9 hr	8·5 hr	9·0 hr

Now, denoting with a the number of hours between the maximum in advance of f_0E_s and the local noon, it should be:

$$\tau v = (\tau - a)(v + x)$$

where x is the *zonal* wind speed acting in the sense of the earth rotation, the effect of which is just in advance of the ionization maxima in the forenoon. We have, therefore:

$$x(a, \varphi) = \frac{v_0 \cos\varphi}{(\tau/a) - 1}$$

and numerically in km/hr:

$\varphi =$	10°	20°	30°	40°	45°
$a = 1$ hr	278	245	209	153	149
2 hr	669	569	490	406	342
3 hr	1286	1063	918	723	601
4 hr	2092	1771	1470	1183	923

* Contrary to what happens at a station on the 0° dip equator where a symmetric effect occurs around local noon (when only upward winds prevail), at low and middle latitudes the horizontal movements in the E_s-layer, which during the day mix the ionization generated at sunrise, lead generally to a poorly defined effect of the sunset and, likewise, the nightly E_s-ionization does not diminish to very low values. The mixing seems mainly due to turbulence and recombination processes.

Therefore, assuming $a = 3$ hr for Baguio ($\varphi = 16^\circ 25'$) we deduce that in summer the *zonal* westward drift of the E_s–layer in the forenoon reaches mean values of the order of 1100 km/hr.

This result is confirmed with nearly progressive decrease by the stations of Formosa, Okinawa and those of Japan, lying roughly along the same meridian. Obviously, because of longer sunshine in summer at higher latitudes, the meridional disequilibrium of the ionization processes is greater in the higher than in the lower latitudes, which also occurs in the mean intensity of the meridional winds.

The very high speed of the mean zonal wind deduced for Baguio and the near stations, compared with the results obtained in other parts of the earth, reveals that in summer over the Far East the E_s–layer is presumably under the influence of this stronger drift*. In this regard it is to be remembered that for some Japanese stations (*i.e.* Akita and Tokyo-Kokubunji) a strong meridional wind has been found[5] that should be logically coupled with a similar strong *zonal* E_s–movement.

As pointed out by N. C. Gerson[6] "the strongest evidence indicating that E_s–movements represent true wind motions comes from the fact that sporadic E-winds agree very well with those determined by other means."

Similarly, the validity of our method is indirectly proved by the good agreement with the results gathered in stations or regions where other procedures have been applied.

The first attempt undertaken with the maxima–displacement method was made using the median f_0E_s–values of the ionospheric stations active in the IGY. Generally for each of these it was possible to deduce the prevailing direction of the zonal current flowing during the day and mainly in the forenoon (as E-winds) in summer (June–July for the northern hemisphere and December–January for the southern hemisphere). The results are reported in Fig. 2, and from these it appears that *in the northern hemisphere the westward drift is generally prevailing during summer and in the forenoon.* Only over Maui (Hawaii) a weak W-drift occurs in the afternoon.

For North America (USA) this is in good agreement with the summer conditions deduced by N. C. Gerson[6] using the "reflection" of radio waves at frequencies exceeding 20 Mc/s.

In Europe, if we suppose that the drift of E_s involves the normal E–layer, it should be noted that by the fading method E. Harnischmacher and K. Rawer[9] have recently obtained the same westward movement with maxima of speed just in the forenoon. The mean intensity of such currents seems greater in Europe than over the USA, but far less than the mean speed of the zonal currents prevailing in summer over the Far East.

Although in the southern hemisphere a smaller number of stations is available, Fig. 2 shows that the directions of the mean E_s–movement are grouped more irregularly. Our findings are in agreement with results in eastern Australia (Sydney), where the mean *zonal* drift in summer (December–January) occurs from E, as given by J. A. Harvey[10], who used a system of spaced pulse transmitters and a central recorder.

By our interpretation of the time displacement for the $M(f_0E_s)$ we are led to assume that very high values of f_0E_s in non-equatorial latitudes are generally generated by strong winds.

* From another standpoint this anomalous behaviour of the E_s–occurrence over the Far East appears already in the Figs. II F-9 to F-14 of paper *Worldwide Occurrence of Sporadic E* by E. K. Smith, Jr. (National Bureau of Standards Circular 582, Washington D.C., 1957).

REFERENCES

1. S. Rangarajan, *J. Geophys. Res.* **59**, 239 (1954).
2. E. H. Vestine *et al.*, The geomagnetic field. Its description and analysis. *Publ. Carneg. Instn.*, 580 (1947).
3. K. Rawer, *Geofis. pura appl.* **32**, 170 (1955).
4. S. Chapman, *Arch. Met., Wien*, **4** (A), 368 (1951).
5. R. W. E. McNicol and G. de V. Gipps, *J. Geophys. Res.* **56**, 17 (1951).
6. N. C. Gerson, *J. Met.* **12**, 74 (1955).
7. J. Lugeon, *Tables crépusculaires, Warszawa* (1934).
8. S. Matsushita, *J. Geomagn. Geoelect., Kyoto*, **3**, 119 (1951).
9. E. Harnischmacher and K. Rawer, *J. Atmos. Terr. Phys.* **13**, 1 (1958).
10. J. A. Harvey, *Aust. J. Phys.* **8**, 523 (1955).

Planet. Space Sci. Pergamon Press 1959. Vol. 1, pp. 213–226. Printed in Great Britain.

THE THERMAL RADIATION OF THE MOON AT 1420 Mc/s

P. G. MEZGER and H. STRASSL

Department of Radioastronomy, Bonn University Observatory

(*Received* 6 *April* 1959)

Abstract—Measurements of the thermal radiation of the moon at 1420 Mc/s have been made with the continuum receiver of the 25 m radio telescope of Bonn university. The measurements cover about 3 lunations (30 April to 22 July 1958). The observations and their reduction are described in detail. It is found that —within the working accuracy of about ±2 per cent relatively—the radiation temperature of the moon at 1420 Mc/s shows no variation with the phase of the moon. This may be explained by the fact that the observed radiation has its origin at some depth underneath the moon's surface where the periodic variations of heating from the sun have become insignificant.

The mean value of the radiation temperature at 1420 Mc/s is found to be 250·2° with an estimated absolute uncertainty of about ±12 per cent.

1. INTRODUCTION

For an observer of the optical radiation the moon works as a reflector of sunlight. As opposed to this, at long infra-red and radio wave lengths the moon radiates more or less exactly as a black body, corresponding to its surface temperature. Here, the amount of solar radio radiation reflected by the moon is negligible compared with its thermal radio radiation.

One-half of the moon's surface is continually heated by radiation from the sun; that part of the surface that is exposed to the radiation moves round the moon in 29·53 days. Owing to the lack of a thermally compensating atmosphere, the shadow area will cool very quickly. Part of the heat which is generated immediately at the moon's surface by absorbed solar radiation will be re-radiated into space—mainly at infra-red and radio wave lengths; the rest will penetrate into the moon's interior as a strongly attenuated wave. For quantitative treatment of this problem, a solution of the equation of heat conduction is to be found for the boundary values at the moon's surface which are given by the insulation on one hand, and by re-radiation of surface heat according to Stefan–Boltzmann's law on the other. By appropriate selection of thermal conductivity k, density ρ, and specific heat capacity s of the moon's surface—in the solution these constants appear combined to $(k\rho s)^{-\frac{1}{2}}$—Wesselink[1] reached a good agreement between the computed temperature variation and that variation of long-wave infra-red radiation temperature that was observed during a lunar eclipse, or during a lunation, respectively.[2, 3, 4]

The variation of temperature distribution, the period of which is the synodic month (29·53 days), will, in the stationary case, cause periodically varying temperatures in the deeper layers below the moon's surface, too. Mathematically, the connexion between the temperature distribution $T(\theta, t)$ at the moon's surface and the temperature distribution $T(x, t)$ at a depth of x cm below the surface is expressed by the Fourier series

$$T(x,t) = T_0 + \sum_{n=1}^{\infty} T_n \exp(-\beta_n x) \cos(n\Omega t - \beta_n x) \tag{1}$$

where $2\pi/P = \Omega = 2{\cdot}66 \times 10^{-6}\ \mathrm{sec}^{-1}$

$$\beta_n = \sqrt{n}\beta = \sqrt{n}\left(\tfrac{1}{2}\frac{s\rho}{k}\Omega\right)^{\frac{1}{2}}$$

The surface temperature variation, therefore, propagates into the moon's interior in the form of strongly attenuated heat waves with a phase lag of $\beta_n x$ against the original temperature distribution at the surface. Amplitude attenuating and phase shift are much more pronounced for the higher waves; accordingly, from a certain depth inwards the temperature distri-

bution will be given by the fundamental wave $n=1$ exclusively. At a depth of $l=2\pi/\beta$, even the amplitude of the fundamental wave is reduced to 0·2 per cent; thus, the constant temperature $T=T_0$ will occur there. From the values given by Wesselink $k=1{\cdot}6\times10^{-4}$, $\rho=2{\cdot}0$, $s=0{\cdot}2$ this so-called "heat wavelength" for the period of a synodic month is found to be 14·5 cm.

A quantitative interpretation of the thermal radio radiation is much more complicated than the interpretation of the infra-red radiation. Since the upper layers of the moon's surface are partially transparent for radio waves, the observed radio radiation temperature is composed of amounts from all layers according to

$$T=\alpha\int_0^\infty e^{-\alpha x}T(x)\,dx \qquad (2)$$

where α is the electric absorption coefficient of the lunar material for the observed radio wavelength. The longer the radio wavelength, the greater the depth of the layer which contributes most to the observed radiation temperature. This explains why the infra-red radiation varies strongly during a lunar eclipse, whereas the thermal radio radiation remains constant at the wavelength of 8 mm[6] as well as of 21 cm.[7]*

Jaeger[8, 9], using Wesselink's method of calculation, and taking into account equation (2) has computed a series of curves for the variation of the thermal radiation of the moon in the vicinity of the moon's centre. He considered two possible models of the lunar surface:

(1) A homogeneous surface layer with $(k\rho s)^{-\frac{1}{2}}=1000$ (Wesselink),

(2) A surface layer of better heat conductivity, superposed by a thin dust layer of bad heat conductivity.

The results of his calculations are given as series of curves, with the electric absorption coefficient as parameter in case 1 and, besides, the thickness of the dust layer in case 2. This second model had for the first time been proposed by Piddington and Minnett[10], who tried therewith to explain the results of their measurements at $\lambda=1{\cdot}25$ cm. Recent measurements by Gibson[6], however, made at 8 mm, are more in favour of model 1 with a value of $(k\rho s)^{-\frac{1}{2}}=1000$, in good agreement with Wesselink's results from the infra-red observations.

Unfortunately, a comparison of the variation of the microwave radiation temperature (which was calculated by Jaeger for the next vicinity of the moon's centre) with observations is severely handicapped by the fact that, apart from millimetre waves, the angular resolving power of the radio telescopes is so bad that the observed antenna temperature corresponds to a value

$$T_A=\frac{G_0}{4\pi}\int f(\phi,\theta)\,T_s(\phi,\theta)\,d\omega \qquad (3)$$

integrated over the whole disk of the moon.

Here $f(\phi,\theta)$ gives the aerial diagram, $T_s(\phi,\theta)$ is the distribution of radiation temperature over the moon's disk, G_0 is the antenna gain. As to the distribution $T_s(\phi,\theta)$, Piddington and Minnett used a formula with symmetry to the moon's equator:

$$T_s=T_0\cos^{\frac{1}{2}}\phi\,[1+\sum_{m=1}^{\infty}a_m\cos m\Omega(t-t_m)] \qquad (4)$$
$$=T_0\cos^{\frac{1}{2}}\phi\,[1+a_1\cos\Omega(t-t_1)+\ldots]$$

The formula had been suggested by infra-red observations. Here Ωt is the selenographic longitude of the centre of the moon's disk, reckoned from the subsolar point, ϕ is the selenographic latitude. The phase shifts Ωt_m, the amplitudes a_mT_0 and T_0 itself are to be found from the observations. For the radiation temperature at the wavelength 1·25 cm, reduced to the moon's equator, Piddington and Minnett found*

$$T_{eq}=249+52{\cdot}0\cos(\Omega t-\pi/4)^\circ\mathrm{K} \qquad (5)$$

Later on, Troitzky[5] (3·3 cm), Seeger[11] (400 Mc/s), and Denisse and Le Roux[12] (900 M/cs) obtained the result that, within the accuracy of measurement, there is no variation of the

* According to Wesselink, the wavelength of the heat wave at a lunar eclipse is found to be 1·3 cm for $n=1$.

* Furthermore, the radiation temperatures were reduced for an emission coefficient of 0·9.

moon's radio radiation with phase. The radiation temperatures, as given by the various authors, differ considerably from one another; perhaps this may be caused by differing methods of reduction.

Most of the observations of the moon's thermal radio radiation have been made with relatively small radio telescopes; variations of the radiation temperature of less than 10 per cent could, therefore, not have been observed. With the 25 m Bonn telescope a determination of the moon's radiation temperature at 21 cm should be possible with an uncertainty of $\pm 1{\cdot}5$ per cent.

2. THE 25 m RADIO TELESCOPE AND ITS CALIBRATION

Our observations of the moon's thermal radio radiation were made with the continuum receiver of the 25 m telescope of the Stockert radio observatory; the bandwidth is 0·9 Mc/s. We took the central band frequency of 1419 Mc/s. A band filter between antenna and receiver input suppresses harmonics and the image frequencies. A detailed description of the whole radio telescope and, especially, of the receiver is given in references 13 and 14. The aerial temperature is calibrated by means of a noise diode; this, via a directional coupler, can be connected to the receiver input simultaneously with the antenna; calibration, therefore, takes place at the working point of the temperature–voltage characteristic of the receiver. The noise diode itself is calibrated by a heatable absorber, this calibration being independent of the temperature–voltage characteristic.

The aerial diagram of the 25 m paraboloidal reflector can be approximated by its main lobe diagram f_m and a stray lobe diagram, which is homogeneously distributed over the sphere. For the main lobe we have the very good approximation

$$f_m = \exp\{-\xi^2/\alpha^2 - \eta^2/\beta^2\} \quad \begin{matrix}\alpha = 24{\cdot}6' \\ \beta = 19{\cdot}5'\end{matrix} \text{ at 1419 Mc/s} \tag{6a}$$

Fig. 1 shows the position of the ξ, η co-ordinate system with respect to the dipole, and to the azimuthal co-ordinate system a, h, respectively. The stray factor had been found to be

$$\beta_s = 0{\cdot}25\ (\pm 8 \text{ per cent}) \tag{6b}$$

For the total gain of the antenna we get, therefore,

$$G_0 = (1-\beta_s)\frac{4\pi}{\pi\alpha\beta} = 7{\cdot}38 \times 10^4\ (\pm 8 \text{ per cent}) \tag{7}$$

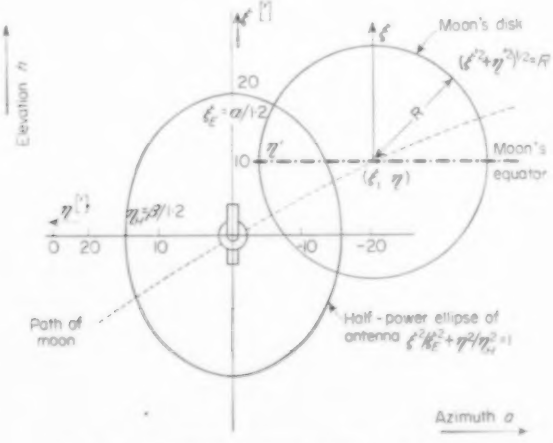

Fig. 1. Position of antenna, moon, and azimuthal co-ordinate system during a passage of moon. For simplicity of calculation, the moon's path is assumed parallel to η-axis at passage.

The calibration of the antenna temperature and the absolute calibration of the antenna have been thoroughly explained in reference 15.

3. METHOD OF OBSERVATION AND MEASURED AERIAL TEMPERATURES

Neither the main lobe diagram (6a) nor the distribution of radiation temperature over the moon's disk (4) are functions of rotational symmetry. The value of the integral (3) which gives the observed aerial temperature will, therefore, depend on the angle between the moon's equator and the main axes of the aerial diagram (Fig. 1), too. But for every day (with very few exceptions) there will be one moment when the moon's equator is parallel to the horizon and, therefore, to the magnetic plane ($\xi = 0$) of the antenna. This point of the daily path of the moon does generally not coincide with the moon's upper transit; it is determined by the condition that the position angle of the moon's rotational axis shall be equal to the parallactic angle of the moon; for our geographic latitude this can occur within about $2\frac{1}{2}$ hr before and after upper transit. For the observations, the moon's position (a and h) was calculated for this moment as well as for the moments 15 min before and after, and the radio telescope was pointed accordingly and fixed. Seventy-three sets of observations covering approximately three lunations were made from 30 April to 22 July 1958, each of the 3×73 observations consisting in recording a drift curve of the passage of the moon.

The low-pass filter has a time constant of $\tau = 3$ sec; the maximum value of antenna temperature will, therefore, be diminished by less than 0·5 per cent, and the time shift of the central ordinate in the drift curve will be about 3 sec,[16] which is of negligible influence on the results. The mean square scattering of the measurements, corresponding to $\tau = 3$ sec, is $\Delta T = \pm 0{\cdot}5$°K; for an observed average antenna temperature of 73°K this means about 0·75 per cent. From an estimation of the errors resulting from the limited positional accuracy of the radio telescope, we get $-1{\cdot}5$ per cent; the total error of the *relative* results of the measurements is, therefore, expected to be between $-2{\cdot}25$ and $+0{\cdot}75$ per cent. In Fig. 2 a typical recording of a passage of the moon is given. At that moment, when the principal direction of the antenna coincided with the centre of the moon's disk, a mark was put on the drifting curve. In Fig. 3 the main content of Table 1 is given in graphic form.

4. REDUCTION OF ANTENNA TEMPERATURE TO RADIATION TEMPERATURE AT THE CENTRE OF THE MOON'S DISK

Assuming the above-mentioned approximate representation of the aerial diagram—which, as has been said, is highly satisfactory—we get from (3)

$$T_A = \frac{(1-\beta_s)}{\pi\alpha\beta} \int_{-\infty}^{+\infty}\int d\xi d\eta T_s(\xi,\eta) \exp\left\{-\frac{\xi^2}{\alpha^2}-\frac{\eta^2}{\beta^2}\right\} \quad (8)$$

Here the spherical co-ordinates ϕ, θ have been replaced by the cartesian co-ordinates ξ, η, expressed in minutes of arc; this can be done since we are dealing with small angles only. As infra-red observations have shown, the isothermal curves on the moon's surface are concentric circles around the subsolar point, the surface temperature varying according to the law $T = T_s \cos^{\frac{1}{4}}\phi$ where T_s = radiation temperature at subsolar point, ϕ = angle between normal line at subsolar point and normal line of surface element under observation. Even Piddington and Minnett's formula (4) is an approximation for the results of infra-red observations. In order to make the evaluation of the integral (8) as simple as possible, we take a co-ordinate system $\xi'\eta'$ on the moon's disk in such a way that its origin coincides with the centre of the disk, and the η'-axis with the moon's equator. Formula (4) for the temperature distribution on the disk is modified as follows:

$$T_s(\xi'\eta') = T_0\left(1-\frac{\xi'^2}{R^2}\right)^{\frac{1}{4}} \left\{1 + a\left[\cos\Omega(t-t_0)\times\right.\right.$$
$$\left.\left.\times\left(1-\frac{\eta'^2}{R^2}\right)^{\frac{1}{4}} + \sin\Omega(t-t_0)\cdot\frac{\eta'}{R}\right]\right\} \quad (8a)$$

where R = the moon's semidiameter (minutes of arc), $\Omega = 2\pi/P$ with P = synodic month, t = time

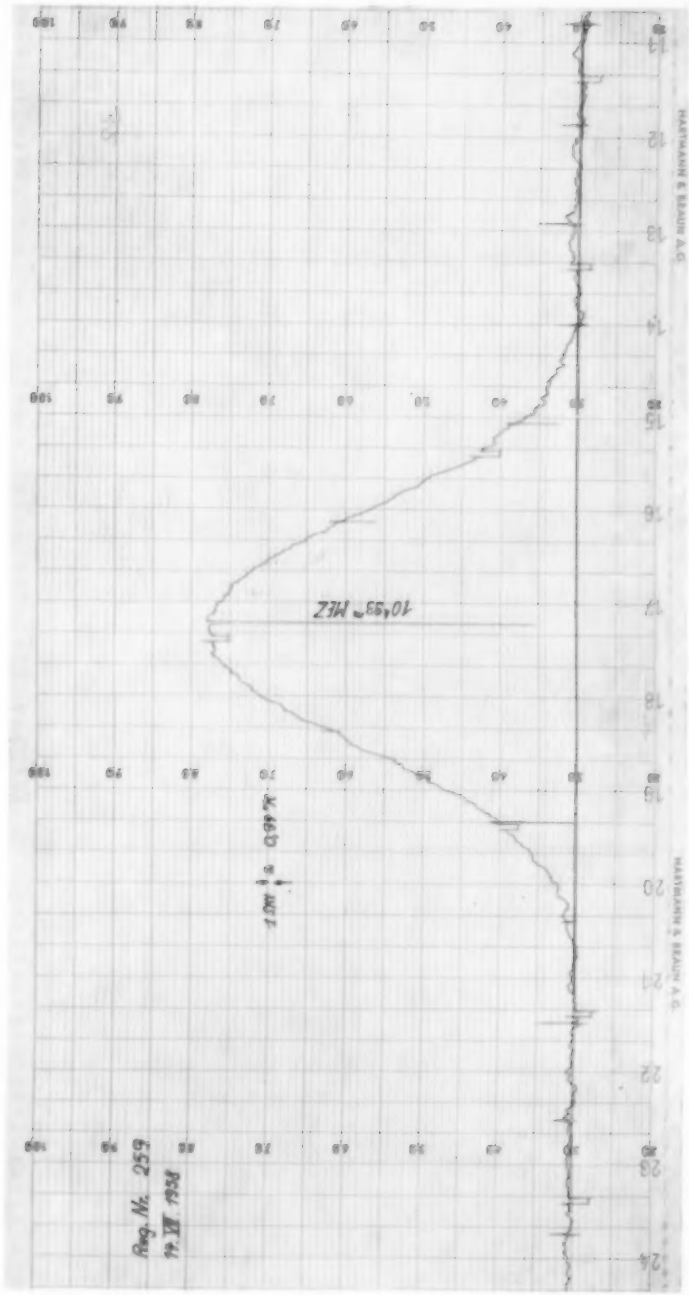

Fig. 2. Example of a drift curve of the moon through the stationary antenna beam.

(to face p. 216

Table 1. List of the observations (see p. 219 for explanation)

(1) 1958	(2) *UT* hr/min	(3) *t* hr/min	(4) *h* deg./min	(5) *q* deg.	(6) T_A °K	(7) *R* min	(8) $\psi(R)$	(9) T_M °K	(10) $T_M/\bar{T}_M$	(11) *P* deg.
April 30	23 36	2 23	26 27	24·8	77·3	16·68	3·22	248·9	0·995	+ 35·4
May 1										
2	0 30	2 22	22 12	23·6	77·7	16·71	3·22	250·2	1·000	20·9
3	1 13	2 08	19 36	20·9	79·6	16·68	3·23	257·1	1·028	+ 6·5 F.M
4	1 42	1 39	18 46	16·6	80·2	16·57	3·25	260·6	1·041	− 7·7
5	2 09	1 08	18 33	11·2	—	16·39	3·29	—	—	21·6
6	2 30	0 32	19 02	5·2	—	16·17	3·35	—	—	35·0
7	2 47	23 54	19 50	358·9	—	15·91	3·41	—	—	48·1
8	3 05	23 19	20 47	353·0	70·7	15·66	3·48	246·0	0·984	60·7
9	3 23	22 47	21 52	347·8	69·3	15·43	3·57	247·4	0·990	72·9
10	3 44	22 22	23 14	343·3	69·8	15·23	3·62	252·7	1·010	84·7 L.Q.
11	4 09	22 02	25 02	339·8	67·6	15·07	3·66	247·4	0·989	96·5
12	4 40	21 50	27 30	337·3	68·1	14·96	3·70	252·0	1·007	107·5
13	5 17	21 45	30 38	335·7	—	14·90	3·73	—	—	118·7
14	6 04	21 50	34 47	335·3	—	14·89	3·73	—	—	129·9
15	6 59	22 02	39 37	335·9	(62·5)	14·92	3·73	(233·1)	—	141·2
16	7 59	22 18	44 32	337·4	—	14·98	3·72	—	—	152·6
17	9 07	22 40	49 31	340·3	65·3	15·07	3·66	239·0	0·956	164·2
18	10 15	23 00	53 27	344·2	74·2	15·18	3·62	268·6	1·074	− 175·9 N.M.
19	11 25	23 21	56 19	348·9	70·8	15·30	3·60	254·9	1·019	+ 172·1
20	12 36	23 40	57 49	354·4	70·2	15·44	3·57	250·6	1·002	160·0
21	13 49	0 01	57 46	0·3	70·4	15·58	3·51	247·1	0·988	147·5
22	15 04	0 23	56 04	6·2	72·7	15·71	3·47	252·3	1·009	134·8
23	16 19	0 44	52 49	11·8	73·8	15·87	3·43	253·1	1·012	121·8
24	17 38	1 11	47 50	16·8	73·8	16·01	3·39	250·2	1·000	108·6
25	18 58	1 39	41 37	20·9	75·3	16·15	3·36	253·0	1·011	95·1 F.Q.
26	20 14	2 03	34 58	23·4	76·4	16·28	3·32	253·6	1·014	81·3
27	21 23	2 20	28 45	24·7	75·0	16·39	3·29	246·8	0·986	67·4
28	22 21	2 24	23 50	24·3	78·6	16·46	3·28	257·8	1·030	53·5
29	23 06	2 15	20 42	22·4	78·0	16·49	3·27	255·1	1·019	39·4
30	23 41	1 54	19 03	18·8	78·7	16·48	3·27	257·3	1·029	25·5
31										

Table 1. (Continued) List of the observations (see p. 219 for explanation)

(1) 1958	(2) UT hr/min	(3) t hr/min	(4) h deg./min	(5) q deg.	(6) T_A °K	(7) R min	(8) $\sqrt{(R)}$	(9) T_M °K	(10) $T_M/\bar{T}_M$	(11) P deg.
June 1	0 08	1 24	18 34	14·0	78·7	16·41	3·28	258·1	1·032	+ 11·7 F.M.
2	0 30	0 49	18 46	8·2	76·3	16·28	3·31	252·6	1·010	0·0
3	0 49	0 11	19 22	1·9	72·0	16·10	3·36	241·9	0·967	− 15·4
4	1 07	23 34	20 12	355·7	72·0	15·88	3·43	247·0	0·988	28·4
5	1 25	23 00	21 10	350·0	72·4	15·67	3·48	252·0	1·007	41·0
6	1 47	22 33	22 30	345·1	69·8	15·45	3·55	247·8	0·990	53·2
7	2 12	22 11	24 14	341·3	69·1	15·26	3·61	249·5	0·998	65·1
8	2 40	21 55	26 22	338·2	68·4	15·11	3·66	250·3	1·000	76·7
9	3 14	21 46	29 10	336·2	68·4	15·00	3·69	252·4	1·009	88·1 L.Q
10	3 57	21 46	32 56	335·3	66·8	14·94	3·72	248·5	0·994	99·4
11	4 49	21 56	37 33	335·5	64·6	14·93	3·72	240·3	0·961	110·7
12	5 48	22 11	42 35	336·7	67·5	14·98	3·69	249·1	0·996	122·2
13	6 53	22 32	47 36	339·1	67·2	15·06	3·68	247·3	0·989	133·5
14	8 01	22 53	52 00	342·5	68·3	15·17	3·65	249·3	0·997	145·1
15	9 10	23 12	55 19	347·0	68·7	15·31	3·60	247·3	0·989	157·1
16	10 22	23 33	57 26	352·3	70·6	15·46	3·53	249·2	0·996	169·3
17	11 36	23 54	58 01	358·2	69·7	15·62	3·50	244·0	0·976	−178·2 N.M
18	12 50	0 14	56 56	4·3	71·5	15·77	3·45	246·7	0·986	+165·3
19	14 07	0 37	54 08	10·1	73·3	15·91	3·41	250·0	0·999	152·2
20	15 25	1 01	49 44	15·3	75·7	16·03	3·38	255·9	1·023	138·8
21	16 43	1 27	44 04	19·6	76·4	16·12	3·36	256·7	1·026	125·2
22	18 03	1 55	37 18	22·8	74·3	16·20	3·33	247·4	0·989	115·2
23	19 15	2 17	30 36	24·4	78·5	16·24	3·32	260·6	1·041	97·8 F.Q
24	20 16	2 24	25 27	24·6	75·3	16·27	3·32	250·0	0·999	84·1
25	21 04	2 20	21 47	23·2	75·2	16·29	3·31	248·9	0·995	70·4
26	21 42	2 04	19 36	20·3	74·5	16·28	3·32	247·3	0·989	56·8
27	22 10	1 37	18 46	16·0	75·7	16·25	3·32	251·3	1·004	43·2
28	22 32	1 03	18 43	10·7	74·8	16·17	3·33	249·1	0·996	29·9
29	22 53	0 28	19 04	4·7	75·0	16·06	3·37	252·8	1·010	16·7
30	23 11	23 51	19 45	358·5	76·8	15·92	3·40	261·1	1·044	+ 3·7 F.M.

Table 1. (Continued) List of the observations (see bottom for explanation)

(1) 1958	(2) UT hr/min	(3) t hr/min	(4) h deg./min	(5) q deg.	(6) T_A °K	(7) R min	(8) $\psi(R)$	(9) T_M °K	(10) $T_M/\bar{T}_M$	(11) P deg.
July 1	23 29	23 16	20 37	352·5	71·2	15·75	3·42	243·5	0·973	− 9·1
2	23 48	22 44	21 40	347·1	71·6	15·58	3·52	252·0	1·007	21·6
3										
4	0 10	22 17	23 02	342·7	69·8	15·39	3·57	249·2	0·996	33·8
5	0 38	21 59	25 03	339·2	69·4	15·23	3·61	250·5	1·001	45·7
6	1 10	21 47	27 34	336·8	—	15·10	3·65	—	—	57·3
7	1 51	21 45	31 06	335·5	67·4	15·01	3·68	248·0	0·992	68·7
8	2 40	21 52	35 27	335·3	66·1	14·96	3·70	244·6	0·978	80·0 L.Q.
9	3 35	22 04	40 14	336·1	68·0	14·96	3·70	251·6	1·006	91·3
10	4 37	22 21	45 16	338·0	67·6	15·01	3·68	248·8	0·994	102·7
11	5 45	22 44	50 06	341·1	67·0	15·11	3·67	245·9	0·983	114·2
12	6 53	23 04	53 54	344·9	69·4	15·25	3·61	250·5	1·001	125·9
13	8 06	23 27	56 42	350·0	67·0	15·42	3·56	238·5	0·954	138·0
14	9 18	23 46	57 56	355·7	68·2	15·60	3·51	239·4	0·957	150·4
15	10 32	0 06	57 34	1·8	70·0	15·80	3·45	241·5	0·966	163·2
16	11 49	0 28	55 28	7·8	73·4	15·97	3·40	249·6	0·998	−176·5 N.M.
17	13 09	0 53	51 35	13·5	73·7	16·12	3·36	247·6	0·990	+170·0
18	14 31	1 21	46 05	18·3	77·3	16·25	3·33	257·4	1·030	156·1
19	15 51	1 47	39 37	21·9	76·8	16·31	3·32	255·0	1·019	142·1
20	17 05	2 08	32 55	24·0	74·0	16·33	3·31	244·9	0·979	128·1
21	18 12	2 23	27 06	24·7	76·3	16·32	3·32	253·3	1·012	114·2
22	19 05	2 23	22 48	23·8	74·3	16·28	3·32	246·7	0·986	+100·4 F.Q.

Mean of 73 values: $\bar{T}_M = 250{\cdot}20$

Columns—(1) Date; (2) Universal time; (3) t = hour angle; (4) h = elevation (altitude); (5) q = parallactic angle = position angle of moon's axis = angle between moon's drifting path and horizon; (6) T_A = aerial temperature, corrected for atmospheric absorption; (7) R = apparent radius of moon; (8) $\psi(R)$ = "correcting function" for transforming T_A to T_M. (cf. Section IV of the text); (9) T_M = temperature at the centre of the moon's disk; (10) $T_M/\bar{T}_M$; (11) P = phase of the moon (0° = full moon, −90° = last quarter, ±180° = new moon, +90° = first quarter). The result of May 15 has been discarded because of imperfect working of the radio telescope.

($t=0$ at full moon); t_0 is introduced to account for a possible time shift of radio radiation maximum after optical full moon.

According to this formula, the isothermal curves on the moon's surface are no longer assumed to coincide with the curves of constant selenographic longitude, but with the straight lines normal to the moon's equator $\xi'=\text{const}$. This assumption is believed to be sufficient for our purposes. The exact form of the distribution function at radio wavelengths is unknown; moreover, here the amplitude a of the variations with time is generally so small that the moon radiates rather as a disk of nearly uniform brightness. Taking $(1-\xi'^2/R^2)^{\frac{1}{4}}$ for the variation of radiation temperature with selenographic latitude, we have a difference of less than 1 per cent in aerial temperature in comparison with the case of uniform brightness.

The daily times of the observations have been so chosen (Section 3) that the magnetic plane of the aerial was parallel to the moon's equator. The aerial-fixed co-ordinate system $\xi'\eta'$, therefore, has only a parallel shift against the moon-fixed system $\xi\eta$ during a passage of the moon. Supposing for simplicity that the moon passes the aerial exactly in the direction of the moon's equator, i.e. along the horizontal line $\xi=\xi'=0$,* the aerial temperature during a passage can be written as

$$T_A(\eta)=\frac{(1-\beta_a)}{\pi\alpha\beta}\int_{-\infty}^{+\infty}\int T_s(\xi'\eta')\exp\left\{-\frac{\xi^2}{\alpha^2}-\frac{(\eta-\eta')^2}{\beta^2}\right\}d\xi'd\eta' \qquad (9)$$

where $T_s(\xi'\eta')$ is the function described above. It is not possible to give an exact evaluation of this integral; we have made an approximate evaluation by series. For that moment when the principal aerial direction points to the moon's centre ($\eta=0$)—this was always marked in our recordings—the calculation yields (cf. Appendix)

$$\frac{T_A(0)}{T_0(1-\beta_a)}=\frac{R^2}{\alpha\beta}\sum_{n=0}^{\infty}C_n\left\{A_1(n)\left[1-\frac{1}{2(n+2)}\frac{R^2}{\beta^2}\right]-A_2(n)\frac{R^2}{\alpha^2}\left[1-\frac{1}{2(n+3)}\frac{R^2}{\beta^2}\right]\right\}+a\cos\Omega(t-t_0)\times\frac{R^2}{\alpha\beta}\sum_{n=0}^{\infty}C_n\left\{B_1(n)\left[1-\frac{n+3}{(2n+5)(2n+6)}\right]-B_2(n)\frac{R^2}{\alpha^2}\cdot\left[1-\frac{n+4}{(2n+7)(2n+8)}\frac{R^2}{\beta^2}\right]\right\} \qquad (10)$$

The formulae for the coefficients of the expansion are also given in the Appendix. The apparent radius of the moon varies with time by about 20 per cent; its value is to be taken from an astronomical yearbook for every observation. For the observing station we have then

$$R=R_{\text{yearbook}}+0{\cdot}257'\sin h$$

The convergence of the series (10) depends upon the ratio of the moon's radius to the stray parameters α, β of the aerial main lobe; in the present case the series still converges very well. We used a constant average moon radius $R=15{\cdot}75'$ in all terms of the expansion, the influence of which on the final result is small. Taking $\alpha=24{\cdot}6'$, $\beta=19{\cdot}5'$ (6a), and $\beta_a=0{\cdot}25$ (6b), we get numerically

$$T_A(0)=0{\cdot}75\,T_0\frac{R^2}{\alpha\beta}\left\{\left[1{\cdot}01-0{\cdot}25\left(\frac{R^2}{\alpha^2}+\frac{R^2}{\beta^2}\right)\right]+0{\cdot}79\,a\cos\Omega(t-t_0)\right\} \qquad (10a)$$

We should like to emphasize again that, strictly speaking, this relation applies to the aerial temperature at that moment when the principal aerial direction points to the centre of the moon's disk. In the general case, there is no need for this aerial temperature to be identical with the maximum aerial temperature for a passage.

Now we are faced with the problem to find such values of T_0, a and t_0, that the observed aerial temperatures (Fig. 3) are represented as well as possible by relation (10a), where t is reckoned from full moon and R is also a function of t. Starting with $a=0$ as a first approximation, we got immediately a very good agreement between observation and calculation.

* As a matter of fact, in our observations the moon's path can be inclined up to about $\pm25°$ against its equator.

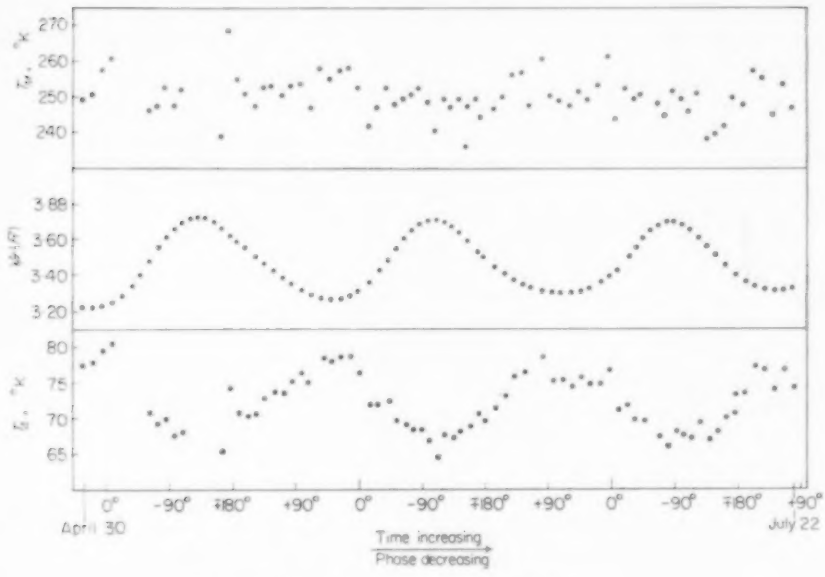

Fig. 3. Bottom: Aerial temperatures T_A.
Middle: Correcting function $\Psi(R)$.
Top: Radiation temperatures of the moon $T_M = T_A \cdot \Psi(R)$.

We have, therefore, $T_s = T_0$, and the moon's radio radiation temperature at 21 cm is constant all over the moon's equator. From (10a) we get with $a = 0$:

$$T_M = T_0 = \Psi(R) \cdot T_A = \left\{ 0{\cdot}75 \frac{R^2}{\alpha\beta} \left[1{\cdot}01 - 0{\cdot}25 \left(\frac{R^2}{\alpha^2} + \frac{R^2}{\beta^2} \right) \right] \right\}^{-1} \cdot T_A \qquad (11)$$

The "correcting function" $\Psi(R)$ was calculated for every observation; it is plotted in Fig. 3. From Fig. 3 it can be seen that the variations with time of the functions T_A and $\Psi(R)$ are nearly symmetrical.

Multiplying the seventy-three individual values of T_A by the corresponding values of $\Psi(R)$ (cf. Table 1) and taking the mean of the products, we get

$$\overline{T_M} = T_0 = 250{\cdot}2^\circ\mathrm{K} \pm \begin{cases} 2 \text{ per cent relatively} \\ 12 \text{ per cent absolutely} \end{cases} \qquad (12)$$

The deviations $(T_M - \overline{T_M})/\overline{T_M}$, expressed as percentages, are plotted in Fig. 4 against phases of the moon. There is no indication of a perodic effect in these deviations. Since positional errors of the radio telescope work always in the direction of lowering the resulting temperatures, the true radiation temperature of the moon may possibly be 1–2°K higher than (12). As opposed to the relative accuracy of ± 2 per cent, an estimation of the calibration errors for aerial temperature and aerial[15] yields a value of ± 12 per cent for the absolute uncertainty of our result.

We have tacitly regarded the moon as a black body, at least for microwaves. As a matter of fact, radar observations have shown that the reflection coefficient of the moon has very small values for microwaves and is doubtlessly smaller than the amount $r = 1 - \varepsilon = 0{\cdot}1$ which was used by Piddington and Minnett in the reduction of their measurements.

5. DISCUSSION OF THE RESULT

Observations of the moon's radio radiation have been made by various authors; the measurings cover the wavelength interval from

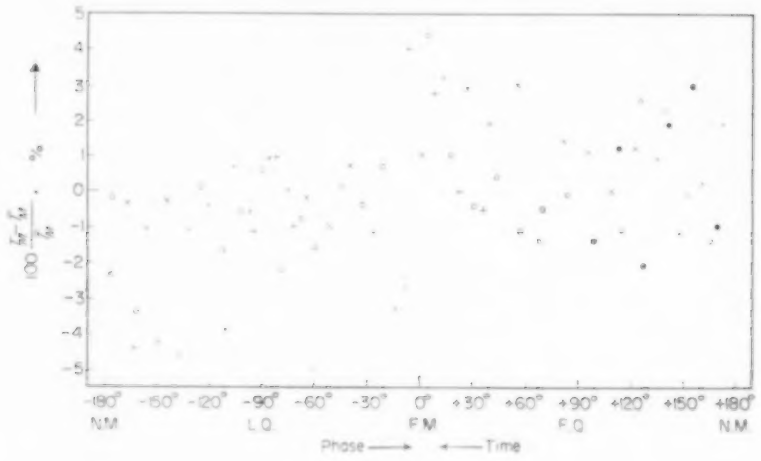

Fig. 4. Deviations of the moon's radiation temperatures T_M from the mean radiation temperature T_0=250·2 °K, given in per cent
+ 1. Lunation 1958 April 30–May 18
× 2. Lunation 1958 May 18–June 17
○ 3. Lunation 1958 June 17–July 16
● 4. Lunation 1958 July 16–July 22
71 per cent of all deviations are within ± 2%.

8 mm to 75 cm. The principal qualitative results of these observations are given in Table 2.

A variation of the radiation temperature at the centre of the moon's disk during a lunation has with certainty hitherto been found only by observers working at shorter wavelengths (8 mm and 1·25 cm). A variation of the radiation temperature during a lunar eclipse has been observed in the infra-red only. In this connexion it may be mentioned that the lunar eclipse of 13/14 June 1957 was observed with the Stockert radio telescope at 21 cm during its proper duration and during the two preceding and the two following hours. The measurements were made by recording drift curves as well as with optical guiding. No measurable variation of the thermal radio radiation was found. This result is in agreement with that of Gibson[6] at 8 mm. The variation of the thermal infra-red radiation during a lunar eclipse is about as strong as during a lunation.[2, 3, 4]

On the theoretical side, Jaeger[8, 9] made a thorough investigation of Wesselink's one layer model[1] and of Piddington–Minnett's two layer model of the moon's surface. It was found that the thermal microwave radiation is influenced by one more material constant, the attenuating constant for the respective wavelength. A penetrating limit x for microwaves is defined by $\alpha_m x = 1$. Conversely it is to be assumed that the essential part of the moon's thermal radiation at a certain wavelength has its origin at a depth which approximately equals the penetrating limit. Various authors have given the following penetrating limits:

Observer	Wavelength	Penetrating limit
Gibson	8 mm	3·37 cm
Troitzky	1·25 cm	3·3 cm
Piddington	1·25 cm	40 cm
Troitzky	3·2 cm	8·7 cm

Table 2. Results of various observers

Observer	Wavelength	Variation of radiation temp.		Mean radiation temperature at equator
		Eclipse	Lunation	
Pettit and Nicholson[2, 3, 4]	8–14 μ	yes	yes	245°K (212°K)[1]
Gibson[6]	8 mm	no	yes	180°K[2]
Piddington and Minnett[10]	1·25 cm	—	yes	249°K (with $\epsilon = 0{\cdot}9$)
Troitzky and Khaikin[5]	3·2 cm	—	no	170°K
Akabane[18]	10 cm	—	yes[3]	
Mezger and Strassl	20·5 cm	no	no	250°K
Westerhout[17]	21 cm	—	—[4]	245°K
Denisse and Le Roux[12]	33 cm	—	no	208°K
Seeger, Westerhout and Conway[11]	75 cm	—	no	185°K

Remarks:

(1) The value 212°K for the mean radiation temperature has been calculated by Wesselink from infra-red observations during a lunar eclipse.

(2) In Gibson's paper no reduction of aerial temperature T_A to main lobe temperature T_H is given. We have $T_A = (1-\beta_s)\,T_H$, where β_s = stray factor of aerial. For Gibson's parabolic aerial, β_s may be assumed to be about 0·3, the resulting radiation temperature of the moon would be 275°K.

(3) As far as can be seen from Akabane's paper, the variation with time of the moon's apparent diameter has not been taken into account in his reductions. With due account of that variation (the times of the observations are not fully given in the paper) we may conclude that the rate T_{max}/T_{min} of the moon's radiation temperature may come out to be about 1·25, instead of 1·50 as given by the author. Moreover, since there is considerable scattering in the author's measurements, it seems to us that a constant radiation temperature of the moon at 10 cm would not be incompatible with Akabane's results.

(4) Westerhout's observations have been made on a single day only.

Our result, constancy of the moon's radiation at 21 cm, cannot help to decide which of the models gives the truer picture of the moon's surface. Obviously, the radio radiation at wavelengths of about 20 cm and longer originates in layers so far beneath the surface that the periodic heat waves are completely attenuated there. At a depth $x=l=2\pi/\rho$,[1] the so-called "heat wavelength", the fundamental wave of the surface temperature distribution is attenuated to 2×10^{-3} of its amount. This heat wavelength gives us a lower limit for the depth where the moon's decimeter radio radiation has its origin. The limiting cases of the models which have hitherto been taken into consideration, are one layer models with the values $(k\rho s)^{-1}=120$ and $(k\rho s)^{-1}=1000$. For these models, the heat wavelength and, accordingly, the lower limit for the emitting layer is calculated to be 5 cm and 14·5 cm, respectively.

Our value of 250°K for the radiation temperature at the centre of the moon's disk is in good agreement with the values of most of the other observers. The values of Troitzky and Akabane seem hardly to be real. Perhaps the decline of measured radiation temperatures with lower frequencies is due to the difficulties in isolating the moon's radiation from underground radiation.

Acknowledgments—With a part of the observations we were helped by Dr. Grahl and Messrs. Schäfer and Schnakenburg. Our special thanks are due to Prof. F. Becker for stimulating and furthering the work.

APPENDIX
EVALUATION OF THE CONVOLUTION INTEGRAL (9)

The passage of the moon through the aerial diagram is mathematically represented as a convolution of the aerial diagram (6a) with the distribution of the radiation temperature T_s on the moon's disk:

$$T_A(\xi,\eta)=\frac{(1-\beta_e)}{\pi\,\beta}\int_{-\infty}^{+\infty}\int T_s(\xi'\eta')\exp.\left\{-\frac{(\xi-\xi')^2}{\alpha^2}-\right.$$

$$\left.-\frac{(\eta-\eta')^2}{\beta^2}\right\} \qquad (13)$$

For T_s we took the formula (Section IV)

$$T_s(\xi,\eta)=T_0\left(1-\frac{\xi^2}{R^2}\right)^{\frac{1}{4}}\left\{1+a\left[\cos\Omega(t-t_0)\cdot\times\right.\right.$$

$$\left.\left.\times\left(1-\frac{\eta^2}{R^2}\right)+\sin\Omega(t-t_0)\right]+\ \ldots\ \right\}$$

We restrict ourselves to passages of the moon parallel to the $\eta-$axis; the convolution, therefore, is working in the $\eta-$co-ordinate alone. Integrating over ξ we get

$$I_\xi(\eta)=2\int_0^{R(1-\eta^2/R^2)^{1/2}}d\xi\left(1-\frac{\xi^2}{R^2}\right)^{\frac{1}{4}}\exp(-\xi^2/\alpha^2)=2R\sum_{n=0}^{\infty}C_n$$

$$\left\{\frac{1}{2n+1}\left(1-\frac{\eta^2}{R^2}\right)^{n+1/2}-\frac{1}{2n+3}\,\frac{R^2}{\alpha^2}\left(1-\frac{\eta^2}{R^2}\right)^{n+3/2}\right\}$$

$$\text{with}\quad C_n=\frac{\Gamma(\frac{1}{4}+1)}{n!\,(\frac{1}{4}+1-n)}$$

Here the expansions

$$\exp(-\xi^2/\alpha^2)=1-\frac{\xi^2}{\alpha^2}+\ \ldots$$

$$\text{and}\quad\left(1-\frac{\xi^2}{R^2}\right)^{\frac{1}{4}}=\sum_{n=0}^{\infty}C_n\left(\frac{\xi}{R}\right)^{2n}$$

are used. With $\eta/R=y$ we get for the convolution integral:

$$T_A(y)/T_0(1-\beta_e)=\frac{R}{\pi\,\beta}\int_{-\infty}^{+\infty}dy'\exp\left\{-\frac{R^2}{\beta^2}(y-y')^2\right\}$$

$$I_\xi(y')[1+a\{(1-y'^2)^{\frac{1}{2}}\cos\Omega(t-t_0)+y'\sin\Omega(t-t_0)\}]$$

where $I_\xi(y')[1+a\{\ldots\}]$ is 0 for $y'>1$.

The last formula will be expressed as a Fourier integral. With[20]

$$\int_{-\infty}^{+\infty}dy'\exp\left\{-\frac{R^2}{\beta^2}(y-y')^2\right\}$$

$$\left\{\begin{array}{l}\cos xy=\beta/R\cdot\pi^{\frac{1}{2}}\exp(-x^2\beta^2/4R^2)\cos\ xy\\ \sin xy=\beta/R\cdot\pi^{\frac{1}{2}}\exp(-x^2\beta^2/4R^2)\sin\ xy\end{array}\right.$$

we get

$$\frac{T_A(y)}{T_0(1-\beta_e)}=\frac{2R^2}{\pi\,\beta}\sum_{n=0}^{\infty}C_n\left\{\frac{2\beta}{\pi^{\frac{1}{2}}R}\int_0^{\infty}dx\exp\left(-\frac{x^2\beta^2}{4R^2}\right)\times\right.$$

$$\left.\times[g_1(x)\cos xy+g_2(x)\sin xy]\right\}$$

The functions $g_1(x)$, $g_2(x)$ can be represented by combinations og Bessel functions.[19] The latter will be expanded in series and stopped after the second term. Then, integrals of the form

$$\int_0^\infty dx \exp(-\gamma^2 x^2)\, x^n \cos xy \quad (n=0, 2, \ldots)$$

$$\int_0^\infty dx \exp(-\gamma^2 x^2)\, x^n \sin xy \quad (n=1, 3, \ldots)$$

are to be evaluated; they can be given in terms of Hermite's polynomials or of hypergeometric series.[20] Finally, we get an expansion which for η/β, R/a, $R/\beta < 1$ can be used in the form

$$\frac{T_A(\eta)}{(1-\beta_s)T_0} = \frac{R^2}{a\beta}\exp\left(-\frac{\eta^2}{\beta^2}\right)\left[1-\frac{1}{4}\frac{R^2}{\beta^2}+\right.$$
$$\left.+\frac{1}{2}\frac{\eta^2}{\beta^2}\left(\frac{R^2}{\beta^2}-\frac{1}{6}\frac{R^2}{a^2}\right)\pm\ldots\right]+$$
$$+a\cos\Omega(t-t_0)\frac{R^2}{a\beta}\exp\left(-\frac{\eta^2}{R^2}\right)\frac{4}{3}\left[1-\frac{1}{5}\frac{R^2}{\beta^2}-\right.$$
$$\left.-\frac{4}{5}\frac{R^2}{a^2}+\frac{2}{5}\frac{R^2}{\beta^2}\frac{\eta}{\beta^2}\pm\ldots\right]+$$
$$+a\sin\Omega(t-t_0)\frac{R^2}{a\beta}\frac{\pi}{4}\frac{R^2}{\beta^2}\frac{\eta}{\beta}\left[1-\frac{5}{48}\frac{R^2}{a^2}-\right.$$
$$\left.-\frac{\eta^2}{\beta^2}\left(\frac{1}{3}-\frac{1}{16}\frac{R^2}{a^2}\right)-\frac{1}{6}\frac{\eta^4}{\beta^4}\pm\ldots\right] \quad (14)$$

We are especially interested in the case $\eta=0$; then the term with $\sin\Omega(t-t_0)$ vanishes, and we get

$$\frac{T_A(0)}{(1-\beta_s)T_0} = \frac{R^2}{a\beta}\sum_{n=0}^{\infty} C_n\left\{A_1(n)\left[1-\frac{1}{2(n+2)}\frac{R^2}{\beta^2}\right]-\right.$$
$$\left.-A_2(n)\frac{R^2}{a^2}\left[1-\frac{1}{2(n+3)}\frac{R^2}{\beta^2}\right]\right\}+$$
$$+a\cos\Omega(t-t_0)\frac{R^2}{a\beta}\sum_{n=0}^{\infty} C_n\left\{B_1(n)\times\right.$$
$$\times\left[1-\frac{n+3}{(2n+5)(2n+6)}\frac{R^2}{\beta^2}\right]-B_2(n)\frac{R^2}{a^2}\times$$
$$\left.\times\left[1-\frac{n+4}{(2n+7)(2n+8)}\frac{R_2}{\beta^2}\right]\right\} \quad (15)$$

For the coefficients of this expansion we have

$$C_n = \frac{\Gamma(\frac{1}{2}+1)}{n!\,\Gamma(\frac{1}{2}+1-n)}$$

$$A_1(n) = \frac{1}{2n+1}\cdot\frac{1}{2^{2n+1}}\cdot\frac{(2n+2)!}{[(n+1)!]^2}$$

$$B_1(n) = \frac{1}{\pi}2^{2n+5}\frac{[(n+1)!]^2(n+2)}{(2n+4)!(2n+3)}$$

$$A_2(n) = \frac{1}{2n+3}\frac{1}{2^{2n+3}}\frac{(2n+4)!}{[(n+2)!]^2}$$

$$B_2(n) = \frac{1}{\pi}2^{2n+7}\frac{[(n+2)!]^2(n+3)}{(2n+6)!(2n+3)}$$

The maximum of the drift curve is easier to observe than the aerial temperature at that moment when the principal direction of the aerial points exactly to the centre of the moon's disk. But the reduction of such observations by using the convolution integral (13) is more laborious than the case $\eta=0$ (15). Only for $a=0$ the two aerial temperatures become equal: $T_{A\max}=T_A(0)$. Taking $\alpha=24{\cdot}6'$, $\beta=19{\cdot}5'$ for the main lobe of the aerial, β_s (stray factor of aerial)$=$ 0·25, and assuming a constant apparent radius of the moon $R=15{\cdot}75'$ for all terms in (15) whose influence on the result is small, we get for the reduction of our measurements the numerical relation:

$$\frac{T_A(0)}{T_0} = 0{\cdot}75\,.\,\frac{R^2}{a\beta}\left\{\left[1{\cdot}01-0{\cdot}25\left(\frac{R^2}{a^2}+\frac{R^2}{\beta^2}\right)\right]+\right.$$
$$\left.+a\,.\,0{\cdot}79\cos\Omega(t-t_0)\right. \quad (16)$$

Here $T_A(0)$ is the observed aerial temperature, T_0 is the moon's radiation temperature at an equatorial point 90° from the subsolar point, a is the amplitude of the moon's temperature variation with time, Ωt_0 takes into account a possible phase shift between the electric and the optical full moon. The three parameters are to be so chosen that the observed aerial temperatures are represented by (16) as well as possible.

In our case, $a=0$, formula (16) reduces to

$$\frac{T_A(0)}{T_0} = 0{\cdot}75\,\frac{R_m^2}{a\beta}\left(1+\frac{\Delta R}{R_m}\right)^2\times$$
$$\times\left\{\left[1{\cdot}01-0{\cdot}25\,R_m^2\left(1\pm\frac{\Delta R}{R_m}\right)^2\left(\frac{1}{a^2}+\frac{1}{\beta^2}\right)\right\}\right. \quad (17)$$

where the mean radius of the moon is $R_m=15{\cdot}75'$ and the variations ΔR are at maximum $\Delta R=\pm 0{\cdot}65'$ during a lunation. From (16) or (17) we get the important result that the variation of the distance with time from the observer to the moon and, accordingly, the variation of the moon's apparent diameter does influence the result the more, the wider the aerial beam is. For R/a, $R/\beta \ll 1$ the observed aerial temperature is altered by ± 8 per cent during one lunation; in our case this alteration is smaller by the factor

$$\left\{1{\cdot}01-0{\cdot}25\left(\frac{R_m^2}{a^2}+\frac{R_m^2}{\beta^2}\right)\right\}=0{\cdot}745$$

i.e. ± 6 per cent at maximum.

REFERENCES

1. A. J. Wesselink, *Bull. Astr. Inst. Netherl.* **10**, 351 (1948).
2. E. Pettit and S. B. Nicholson, *Astrophys. J.* **71**, 102 (1930).
3. E. Pettit, *Astrophys. J.* **81**, 17 (1935).
4. E. Pettit, *Astrophys. J.* **91**, 408 (1940).
5. V. S. Troitzky and S. E. Khaikin, *Radio emission from the moon and the nature of its surface. IAU Symposium No. 4, Radioastronomy* p. 406–407. Cambridge University Press (1957).
6. J. E. Gibson, *Proc. Inst. Radio Engrs., N.Y.* **46**, 280 (1958).
7. *Institutsbericht der Radiosternwarte Stockert.* 15. 5. 1957.
8. J. C. Jaeger, *Austr. J. Phys.* **6**, 10 (1953).
9. J. C. Jaeger, *Proc. Camb. Phil. Soc.* **49**, 355–359 (1953).
10. J. H. Piddington and H. C. Minnett, *Austr. J. Sci. Res.* **2**, 63 (1949).
11. Ch. L. Seeger, G. Westerhout and R. C. Conway, *Astrophys. J.* **126**, 585 (1957).
12. J. F. Denisse and E. Le Roux, quoted in Ref. 11.
13. *Telefunkenztg.* **29**, Heft, 113 (1956).
14. P. G. Mezger, *Telefunkenztg.* **31**, 122 (1958).
15. P. G. Mezger, *Z. Astrophys.* **46**, 234 (1959).
16. P. G. Mezger, *Z. Instrumkde.* **11**, 219 (1958).
17. G. Westerhout, *Bull. Astr. Inst. Netherl.* **14**, 215 (1958).
18. K. Akabane, *Proc. Japan Acad.* **31**, 161; *Tokyo Astr. Obs. Rep.* No. 115 (1955).
19. W. Gröbner and N. Hofreiter, *Integraltafel*, Teil II. Springer, Wien (1950).
20. F. Oberhettinger, *Tabellen zur Fouriertransformation*. Springer, Berlin (1957).

Planet. Space Sci. Pergamon Press 1959. Vol. 1, pp. 227–237. Printed in Great Britain.

ARTIFICIAL ELECTRON CLOUDS—I

SUMMARY REPORT ON THE CREATION OF ARTIFICIAL ELECTRON CLOUDS IN THE UPPER ATMOSPHERE

F. F. MARMO,* L. M. ASCHENBRAND* and J. PRESSMAN*
Geophysics Research Directorate, Air Force Cambridge Research Center,
L. G. Hanscom Field, Bedford, Massachusetts

(*Received* 21 *April* 1959)

Abstract—A systematic study has been initiated for the purpose of better understanding the problems associated with the creation of artificial electron clouds in the upper atmosphere. A series of eight rocket experiments has been performed whereby artificial electron clouds were produced between 70 km and 130 km. The ground-based detection networks that were employed are discussed, and included is a method of correlating both optical and radio-radar data. This affords a new dimension for propagation and upper atmospheric studies. This paper, the first of a series, is devoted to summarizing the overall concepts, methods and techniques, and operating procedures employed in this study. It includes tabulated summaries of the various optical and radio-radar detection data in addition to some scientific uses of artificial electron clouds. The subsequent papers of this series offer detailed discussion and conclusions pertaining to much of the data outlined here.

1. BACKGROUND AND EVOLUTION

A series of eight successful experiments has been performed in which chemical constituents have been released into the upper atmosphere with the aid of vertical probe rockets for the purpose of creating artificial electron clouds. These exploratory experiments have established the foundation of a new technique of study of physical and chemical processes associated with the earth's upper atmosphere. A substantial amount of qualitative and quantitative data has been obtained from each of these experiments pertinent to the studies of upper atmospheric winds, diffusion, microscopic cross-section values (electron attachment, ion-electron recombination, charge exchange, etc.), chemical consumption, expansion of high-pressure gases into an attenuated atmosphere, electromagnetic propagation research and implications, ionospheric research, thermo-chemical and explosive effects, etc.

The intent in submitting this preliminary report is concisely to present the experimental facts, methods of detection and overall results of all the experiments to date. A series of papers covering detailed considerations of the associated chemical and physical processes as well as the interpretation of the extensive data that was accumulated is in preparation. It is anticipated that subsequent papers will appear in this journal in the immediate future. Another scientific paper covering the details of all the experimental procedures and the optical and radar ground-based instrumentation is in preparation. This series will also concern itself with logical extensions of this area of research as described in suggested experiments and methods of approach.

The first of these experiments, conducted in March 1956, in which 18 lb (275 moles) of nitric oxide gas was released from high-pressure containers at an altitude of 95 km has been previously reported.[1] The success of this experiment whereby an artificial electron cloud with an initial average density of about 4×10^6

* Presently associated with Geophysics Corporation of America, 700 Commonwealth Avenue, Boston 15, Massachusetts.

electrons per cm² was detected for more than 10 min by radar techniques indicated that it would be feasible to use other contaminants to create artificial electron clouds at various altitudes with a wide range of densities, time duration, size, shape and other parameters. Logically, a systematically planned series of experiments was initiated in order to study the basic characteristics and effects of electron clouds with certain predetermined characteristics.

The sequence and eventual evolution of the series performed was based on the examination of results and the quest for specific geophysical and electromagnetic propagation data.

Examination of the photo-ionization cross-section data of various constituents and the character of the solar flux and other parameters indicated that the alkali metal elements as a family offered a particularly high potential for obtaining high density, long-lived electron clouds at altitudes between 70 and 200 km with presently available techniques. In addition, it was felt advantageous to keep this systematic study confined to one given chemical family; this affords many advantages. Thus, it was decided to utilize only the alkali metals (Cs, K and Na) throughout these initial experiments. The alkali metal vapors have characteristic, very low ionization potentials (2400 Å to 3200 Å) which fall into the spectral region where the solar photon flux averages about 5×10^{12} photons/Å cm² sec. Since cesium possesses the lowest ionization potential of the family, an Aerobee rocket experiment was performed in September 1957, whereby 110 moles was scheduled to be released at an altitude of about 120 km. The experiment was unsuccessful in that the material was not released due to mechanical failure of both the primary and back-up release mechanisms.

Previous scheduling had called for a release of potassium vapor during the month of November 1957. There was no opportunity to reschedule the unsuccessful cesium experiment due to relatively difficult delivery problems; therefore, it was decided to continue the original schedule. A successful release of a payload containing 153 moles of potassium was accomplished from an Aerobee at 121 km. This flight occurred at about 0932 MST on 19 November 1957; it is represented by entry number 1 in Table 1. The electron cloud

Table 1. Summary of Upper Atmospheric Artificial Ionization Experiments Conducted at Holloman Air Force Base in New Mexico

No.	Date	Study constituent	Moles	Approx. release time (MST)	Release altitude (km)	Vehicle
1	19 Nov. 1957	Potassium	153	0932	121	Aerobee
2	20 May 1958	Cesium + 10% sodium	Cs-43	0245	101	Nike-Cajun
3	21 May 1958	Cesium + 2% sodium	Cs-46	0434	128	Nike-Cajun
4	22 May 1958	Sodium	61	0432	116	Nike-Cajun
5	15 Sept. 1958	Cesium	27	0934	82	Nike-Cajun
6	16 Sept. 1958	Cesium	28	0933	69	Nike-Cajun
7	18 Sept. 1958	Cesium	30	0953	91	Nike-Cajun
The following experiment was performed but was unsuccessful due to mechanical failure:						
A	19 Sept. 1957	Cesium	110	0930	—	Aerobee
The following was the initial experiment previously reported:						
B	12 March 1956	Nitric oxide	300	1415	95	Aerobee

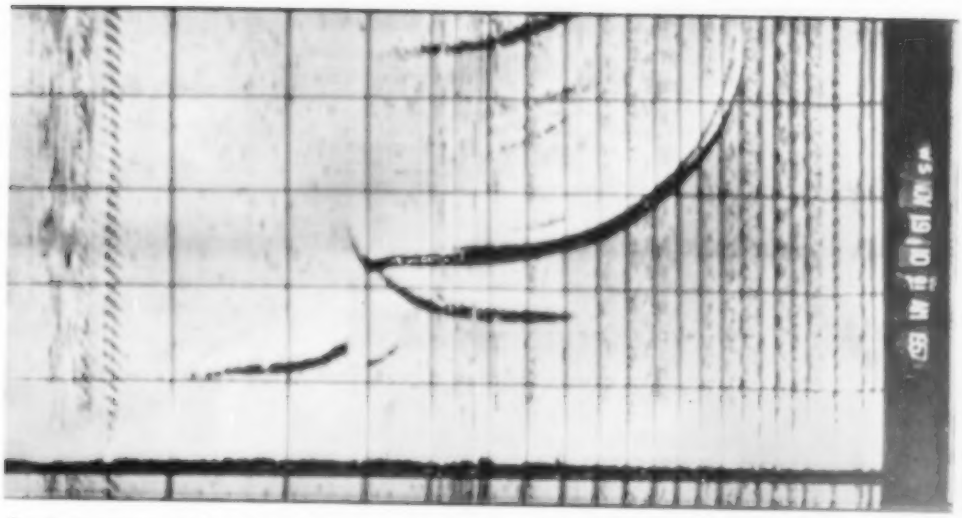

Fig. 1. Ionogram obtained 30 min. after chemical release as recorded by *C*-3 vertical ionosonde located at White Sands Proving Ground, New Mexico, for experiment conducted in November 1957. This display depicts the slant range vs. maximum frequency. Each altitude marker represents 100 km, whereas the frequency scale goes from 1 to 25 Mc s. The artificial cloud is shown between the normal *E*-and *F*-regions at about 170 km slant range. The maximum frequency return is about 8 Mc s.

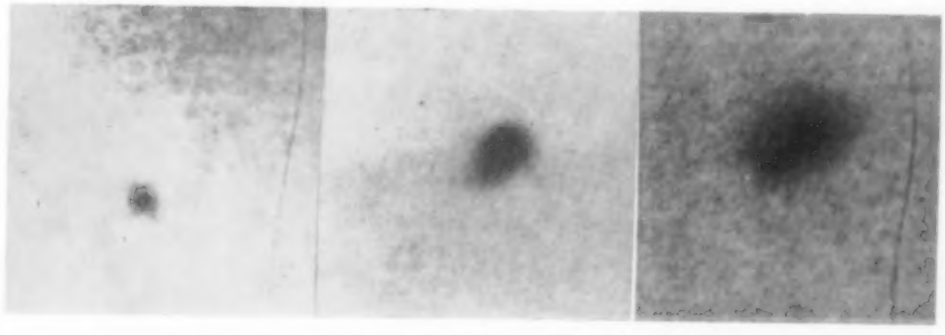

Fig. 2. Photographs taken from television screen of Lumicon depicting the dynamics of cloud formation for experiment conducted 21 May 1958. The picture (a) was obtained 2 sec. after chemical release, (b) and (c) after 1 min. and 2 min., respectively.

to face p. 229

formed from this experiment was readily detected by conventional radar techniques. Fig. 1 depicts one of the more interesting representative pieces of data. This result is an ionogram obtained from a *C*-3 vertical ionosonde located at White Sands Proving Grounds, New Mexico, and clearly shows the detection of the man-made cloud lying between the normal *E*- and *F*-layer (at about 170 km slant range) at 30 min after chemical release.

The interpretation of the results pertinent to the ionized cloud which was formed in this experiment suggested that some additional process to photo-ionization was responsible for the initial electron production. The chemical nature of the experimental method indicated that the effect could be due to thermal ionization. In order to examine this important effect, an experiment was devised in which atomic cesium would be released during the night-time hours to eliminate the role of solar photo-ionizing flux. The choice of the element arose from the consideration that at a given temperature within the range considered, cesium should produce considerably more thermal electrons than other constituents of the alkali metal family; thus, a maximum type effect could be anticipated. In addition, since this was a night-time release, it was considered possible to produce an easily visible and photographed cloud. Some of the obvious advantages gained by optical detection are accurate determination of release altitudes by triangulation optics, correlation of radar returns as a function of cloud size and shape, determination of yield and chemical rates, wind and diffusion data, and spectral characteristics of the emission. The method employed for rendering the cloud visible was to "dope" the cesium release with about 10 per cent sodium so that the latter would react in a chemiluminescent manner with the ambient atomic oxygen in the upper atmosphere (maximum number density at about 100 km). The chemistry and physics associated with the release of sodium vapor in a filament fashion in the upper atmosphere has been reported by Bedinger *et al.*[2] One additional feature should be mentioned here. It was anticipated that a systematic study of the type described here could require a large number of rockets. The result of the 17 November Aerobee flight suggested the feasibility of utilizing the smaller Nike-Cajun two-stage rocket. The advantages obtained include lower cost, ease of handling at launching, solid fuel and superior trajectory characteristics. However, it is clear that for maximal-type electron clouds the sacrifice of larger payload is recognized. The Aerobee's instrumented payload is capable of carrying aloft about 3 times more constituent. In spite of this, it was decided to utilize the Nike-Cajun vehicle whenever feasible. This will be the case in all subsequent probes reported in this series. The successful release of this cesium–sodium mixture was accomplished from a Nike-Cajun rocket at an altitude of 101 km at the dark pre-dawn hour of 0245 MST on 20 May 1958. The electron cloud created was detected by radar; the cloud was assumed to be due to thermal ionization. It was clearly visible to the naked eye, and photographic and spectral data was obtained for as long as 6 min. Interpretation of the optical data presents the possibility of a study of the cloud dynamics *versus* time, as well as information pertaining to chemical consumption, kinetics of the reactions involved, and some of the physical processes previously mentioned.

The next group of experiments of the series was concerned primarily with the correlation of optical and radar data from ionized clouds as formed by solar ionization of alkali metal vapor.

This could conveniently be accomplished by creating a light-emitting photographic cloud, preferably one that emits in the visible. The method of rendering the released contaminant visible is based upon the detectability of sodium resonance radiation against a morning twilight sky background.[2] Again, if we merely "doped" the chemical payload of cesium compound with a small amount of sodium, an easily observable cloud would be formed. A morning twilight release was adopted since it was essential that the cloud be solar illuminated for an extended period and that a reduced intensity sky background for the early part of the experiment exist. Two different experiments were performed as part of this phase in solar induced

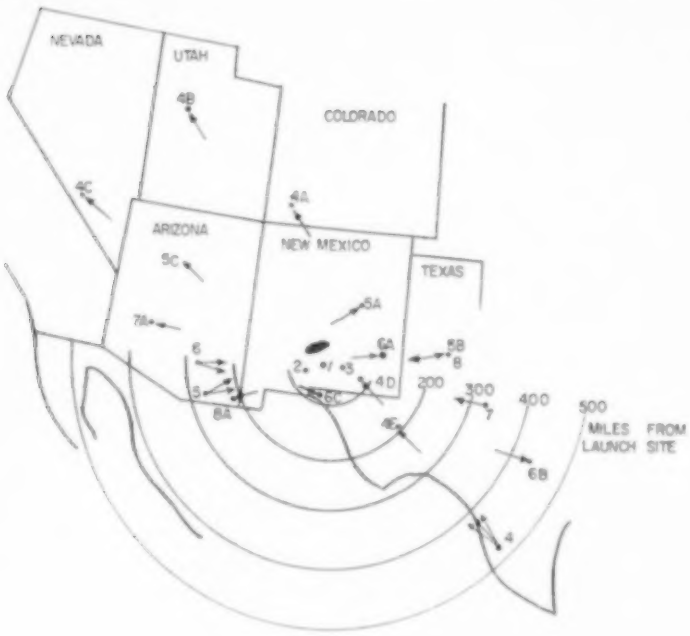

No.	Location	Equipment	Type*
1	Launch site—HAFB and Alamagordo, New Mexico	(A) 70 kW pulsed radar 23·1 Mc/s, 45 kW—40·7 Mc/s	B
		(B) Radars 100 kc—1·8 kW, 6 Mc/s—2·1 kW, 20·8 Mc/s—28 kW	B
		(C) HAFB frequency monitor station—TV channels	F
2	White Sands Proving Ground, New Mexico	(A) C-3 vertical ionosonde 10 kW—1–25 Mc/s	B
		(B) Dovap net 1 kW—36·94 Mc/s, 125 W—73·88 Mc/s	F
		Doran net 1·4 kW—132·48 Mc/s, 200 W—264·96 Mc/s	
		(C) Acoustical sounding	F
3	Sacramento Peak, New Mexico	(A) Cossor portable ionosonde 1 kW—1·6–20 Mc/s	B
4	Laredo, Texas, to Durango, Colorado	Transmitter 1·2 mW—201 Mc/s	F
	Nevada site	(A) Receiver 201 Mc/s	F
	Utah site	(B) Receiver 201 Mc/s	F
	White's City, New Mexico	(C) Receiver 201 Mc/s	F
	Fort Stockton, Texas	(D) Receiver 201 Mc/s	B
		(E) Receiver 201 Mc/s	B
5	Fort Huachuca, Arizona to Encino, New Mexico	Transmitter 10 kW—810 Mc/s, 50 W—13·56 Mc/s	F
	Lubbock, Texas	(A) Receivers 810 Mc/s and 13·56 Mc/s	F
	Williams AFB, Arizona	(B) Receivers 810 Mc/s and 13·56 Mc/s	F
6	(Radio amateur 2 and 6 m net)	(C) Receiver 810 Mc/s	B
	Tucson, Arizona, to Roswell, New Mexico	Transmitter 50·01 Mc/s (6 m) and 144·01 Mc/s (2 m), 70 kW Radar 23·1 Mc/s	F
	Austin, Texas	(A) Receiver 50·01 Mc/s	B
	El Paso, Texas	(B) Receiver 144·01 Mc/s	F
		(C) Receiver 144·01 Mc/s	F

7	Phoenix, Arizona, to Midland, Texas	Transmitter 100 kW—55·26 Mc/s (A) Receiver 55·26 Mc/s	F F
8	Lubbock, Texas, to Douglas, Arizona	Transmitter 216 kW—211·24 Mc/s (A) Receiver 211·24 Mc/s	F F

* B = Back scatter, F = Forward scatter

Fig. 3. Location and description of ground-based instrumentation used for ionization detection of artificial electron clouds. Arrows designate either transmitting and/or receiving station.

ionization. A release of a mixture of cesium and sodium (2 per cent) was conducted at 128 km on 21 May 1958, and following that, a payload consisting entirely of sodium compound was released at 116 km on 22 May 1958. Both experiments were successful in that they afforded the opportunity of providing good photographic and spectral coverage for over 8 min. Fig. 2 shows a series of three pictures obtained on the 21 May experiment using a light amplifying unit (Lumicon) capable of obtaining series photographs. The first picture was obtained 2 sec after release time and the latter two show the cloud development after 1 and 2 min, respectively.

The expansion characteristics are clearly indicated and the utilization for data of this type is obvious.

The radar results from the former release provided positive results for as long as 19 min, resulting in valuable correlated radar and optical data. The results of the sodium release were uniform in that all operating stations reported negative radar results. This negative result appears to be in agreement with the deduced relative photo-ionization probabilities of Cs, K and Na. This further indicates as expected that thermal ionization does not play an important role for sodium as far as production of a detectable artificial electron cloud is concerned.

The last series of experiments in this program was conducted on September 1958, and pertained to the study of altitude effect of ionized cloud formation. These flights were to investigate the conclusion that there probably exists some lower altitude below which the generation of a detectable, high-density, long-lived, solar-induced artificial electron cloud cannot be achieved; this conclusion was based on arguments of rate of photo-ionization electron production, recombination, electron attachment processes and chemical consumption of contaminant. The following approach was taken. The first experiment was to be conducted at 80 km. If positive radar detection results were obtained, a similar release at 70 km would be attempted. If the latter were positive then a release at 60 km would be performed. However, if the results of the 70 km release proved to be negative, a release at 90 km would be attempted in order to complete this investigation of the altitude dependence of generation of artificial electron clouds. The actual releases were performed in succession at 82, 69 and 91 km, respectively, since a negative result was obtained with the 69 km release of cesium.

2. EXPERIMENTAL FACTS

Table 1 is a tabulation of the pertinent data pertaining to all the experiments conducted at Holloman Air Force Base, New Mexico, for the purpose of creating ionized clouds in the upper atmosphere.

The basic engineering techniques concerning the release of alkali metal vapors involved a stainless steel canister so designed and constructed as to be employed within the requirements of payload, configuration of nose cone, high acceleration and adaptability to the rocket body and instrument package.

The alkali metal compounds used for the experiments were all nitrates; a discussion of the chemistry will be covered in a future paper. The alkali metal nitrates were intimately mixed with aluminium granules, and the chemical mix was then sealed in the steel canister. The actuation of the release mechanism was accom-

Table 2. Summary of Results by Detection of Ionization Characteristics of Electron Clouds.
The times refer to the maximum positive identification time reported.

M = min
S = sec
Neg. = no detection during proper equipment performance
— = equipment not in operation
X = no detection due to mechanical failure or lack of communication
All designations pertinent to equipment conform with tabulation in Fig. 3

Flight no.	Detection equipment results																		Remarks
	1A	1B	1C	2A	2B	3A	4A	4B	4C	4D	4E	5A	5B	5C	6A	6B	6C	7A	8A	
1	29S —	—	X	30M	X X	—	2½S	—	—	—	—	—	X	—	—	—	X	—	—	1A: 23·1 Mc/s 1A: 49·9 Mc/s
2	90S —	2½M	X	3M	60S 9S 6S Neg	—	—	7S	9S	—	—	2S Neg	Neg Neg	—	8M	4S	4M	Neg	Neg	1B: 6 Mc/s 5A–5B: 810 Mc/s 5A–5B: 13·56 Mc/s
3	— 20S	Neg	X	19M	10S 4S 2S Neg	—	—	3S	2S	—	—	1S Neg	2S Neg	—	15S	3S	Neg	Neg	Neg	Same as flight two

Table 2 (Continued)

4	Neg ——	Neg	X	Neg	2S Neg Neg Neg	—	—	Neg	Neg	—	—	Neg Neg	Neg Neg	—	Neg	Neg	Neg	Neg	Neg	Same as flight two
5	Neg 4·3S	Neg Neg Neg	—	24M	X	20M	—	—	—	—	—	Neg	—	Neg	Neg	Neg	Neg	—	—	1A: 23·1 Mc/s at Tucson 1A: 40·7 Mc/s
6	Neg 1½S	Neg Neg Neg	—	Neg	X	X	—	—	—	Neg	2S	Neg	—	Neg	Neg	Neg	Neg	—	—	Same as flight five
7	2M 54S	Neg 4M Neg	—	7M	X	2M	—	—	—	3·5S	3·5S	1S	—	Neg	Neg	Neg	Neg	—	—	Same as flight five

Note: Column 1B is split into 3 sections for flights 5, 6 and 7 (100 kc, 6 Mc/s, 20·8 Mc/s).
Column 2B is split into 4 sections for flights 2, 3 and 4 (36·94 Mc/s, 73·88 Mc/s, 134·88 Mc/s, 264·96 Mc/s).

plished by an accurate timer which ignited two squibs imbedded in an igniter mix. The altitudes of release were determined by several independent techniques including optical triangulation, slant-range radar measurements, rocket-borne timer in conjunction with trajectory data, etc. In all cases, the altitude determinations were in excellent agreement.

3. EXPERIMENTAL RESULTS

3.1. *Ionization detection*

An extensive and elaborate network of radar-type equipment was located throughout the southwestern part of the United States. The map and index depicted in Fig. 3 show the locations of all the ground-based ionization detection equipment and a brief description of their performance capabilities. The list is divided into categories, *i.e.* equipment used to study back-scatter effects and those used to test forward-scatter results.

It is worth noting that the radio amateur nets consisted of a group of approximately 650 participants located within a radius of 700 miles from the launch site. An article published in QST magazine[3] helped co-ordinate the effort. Although this method of group participation did produce some interesting positive results, the difficulties encountered in communication from launch site, abnormal hours of flight time in certain time belts, and changes of flight data and hour curtailed the effort in obtaining a maximal effect.

The compilation in Table 2 provides data obtained by the various ionization detection instrumentation on all the flights. These data attempt to give the maximum time of detection. It should be recognized that all the ground-based equipment was not used on any one experiment. The omission of an entry means that the equipment was not in operation at that time; an "X" signifies that equipment was manned but no results were obtained because of mechanical failure or lack of adequate communication of launch time and duration of positive results; and "negative" means that no results were detected during proper performance of the equipment. Further explanatory remarks and notes are encompassed in the tabulation.

3.2. *Optical detection*

The aims and requirements for the use of optical detection have been pointed out already. Table 3 provides a brief description of the equipment used and the respective geographic locations. Table 4 provides the information pertinent to the maximum time duration that gave positive results using optical techniques listed in the previous Table. Calibrated exposure times were obtained and fast film was used wherever applicable.

4. SOME SCIENTIFIC USES OF ARTIFICIAL ELECTRON CLOUDS

It is clear that there are many possible scientific uses of artificial electron clouds. Some of these possibilities are outlined below in a general fashion. Many of these have been successfully executed in the discussed series of experiments; others are in the process of development. It is felt to be of value to list the several possibilities with a very brief summary of the salient features. Although the list does not pretend to be exhaustive, it is sufficiently comprehensive for illustration of the scope involved.

4.1. *Winds*

Winds and wind shear may be obtained through the entire height range of creation of the artificial electron clouds. Experimentally, radar systems giving azimuth and slant range with time would be adequate. This radar wind system can be in the form of a net or incorporated into a single unit. The use of doppler or phase techniques to obtain winds offer alternative schemes. In general, those methods utilized to measure meteor drift and ionospheric irregularities may be modified and adapted, except that measurements are no longer restricted to heights of meteors or ionospheric irregularities.

In addition, the use of experiments with properly "doped" contaminants to give strongly visible clouds permits a close calibration and correlation of the radio-radar techniques for use

Table 3. Location (from Launch Site) of Ground-based Optical Detection Equipment

No.	Location from launch site	Equipment
1	(A) 29·7 mi N—0·6 mi E (B) 0·4 mi N—0·6 mi E (C) 33·5 mi S—1·5 mi W	Three sites, each having two astro ballistic cameras (f/2·5 lens) located on HAFB–WSPG range
2	35 mi SW	Baker-Nunn satellite tracking camera (f/1 20-in. aperture)
3	20 mi E	Light amplifying unit (Lumicon) used with an 85 mm f/1·4 lens
4	15 mi E	Multicamera spectrograph consisting of 6 each 35 mm cameras fitted with appropriate narrow band pass and other filters
5	(A) 30 mi N—50 mi W (B) 7 mi N—25 mi E (C) 80 mi N—57 mi W	Three sites, each having a 4 in.×5 in. press camera (f/2·8 lens)
6	15 mi E	Photometer with ½ degree field of view appropriately fitted with filter and sensitive phototube
7	15 mi E	Beattie-Coleman Varitron 35 mm recording camera
8	15 mi E	Spectrograph equipped with Schmidt optical system

Table 4. Summary of Results of Optical Data Obtained for May 1958 Series of Nike-Cajun Experiments

M = min S = sec — = equipment not in use

All designations pertinent to equipment conform with tabulation in Table 3

Flight no.	Detection equipment results								Remarks
	1	2	3	4	5	6	7	8	
2	6 M	25 S	40 S	6 M	6 M	4½ M	—	6 M	1, 4, 6: time exposure
3	X	2 S	6 M	3½ M	15 S	—	2 M	—	1: insufficient data provided 2: used yellow filter 3: used narrow band filter
4	X	45 S	12 M	6 M	15 S	—	4 M	—	Same remarks as flight 3

NOTE: Photometer and spectrograph could not be used in flights 3 and 4 due to hour of firing and subsequent sky background intensity.

under those conditions for determining winds when the clouds are not visible.

4.2. *Diffusion and related processes*

The data from radio-radar reflections from the cloud can be applied to determinations of the diffusion coefficients; the methods employed are similar to those used in meteor trail studies. In addition, it is possible to obtain data concerning the changing shape of the cloud with time and hence the variation of diffusion with direction. Here, again, value of the correlation with optical coverage is re-emphasized.

Some of the problems in which the above data can be of value include: the magnetic field alignment of ionization, the importance of ambi-polar diffusion and the relative importance of molecular versus turbulent diffusion. Information on the latter is intimately related to the energy spectrum associated with the turbulent eddies in the atmosphere.

4.3. *Atomic and molecular cross sections*

Examination of the dynamic equations for the controlling processes involved in the formation of these clouds indicates the several atomic and molecular processes involved. It is clear that by judicious experimental design one or several of these processes can be minimized or maximized for conveniently examining the process of interest. Some of the processes whose cross-section may be evaluated include: photo-ionization, photodetachment, recombination, attachment, charge transfer and chemical reaction cross-sections. It should be mentioned that a wide latitude of experimental control is available. For example, this latitude derives from the choice of chemical contaminant, altitude, payload, geometry of release and magnitude of photon flux (night, twilight or day), including the use of atmospheric screening regions (*e.g.* ozone) to filter unwanted radiations. Other controls exist, but the above suffices to illustrate the extent of the latitude available.

4.4. *Ionospheric structure*

Since the natural ionosphere serves as a background against which experiments of artificial electron clouds are performed it can be expected that there will be compound interactions between the artificial electron clouds and the ambient ionospheric plasma. For example, in these experiments it has been noted that multiple reflections from the artificial cloud to the various ionospheric strata have been observed. In addition, cusping of the low-frequency end of the echo from the artificial cloud (as illustrated in Fig. 1) can be utilized to obtain information regarding the electron density gradients existent in the natural ionosphere. With the use of more sophisticated coverage it is felt that other, perhaps more subtle, phenomena may be uncovered.

4.5. *Tool for electromagnetic propagation research*

At present, controversies exist related to the propagation of electromagnetic radiation via electron distributions in the atmosphere. The artificial electron cloud offers the opportunity of setting up a controlled target of appropriate design characteristics in order to check various theories of scattering, reflection, etc., of naturally or artificially present electron distributions in the atmosphere. One of the unique characteristics of this tool is the possibility of obtaining simultaneous optical and radar data thus affording a new dimension in experimental propagation studies.

4.6. *Measurements of atmospheric parameters*

The atmospheric parameters of pressure, density and temperature certainly invoke some degree of control over the initial size of the electron cloud and its subsequent behavior with time. A detailed understanding of the physics and dynamics of the cloud should offer an opportunity for improving our knowledge concerning these aforementioned parameters.

4.7. *Expansion of high-pressure gases into an attenuated atmosphere*

The dynamics of the fast initial expansion phase of the released gas can be examined by conventional detection schemes. Similar related problems have been studied by other techniques but are often limited to those regimes where

the mean free paths involved are smaller than the geometrical dimensions of the system. Here, the opportunity exists for examining this phenomena under a wide varying range of mean free paths. Again, optical coverage, when possible, affords valuable correlation data.

4.8. *Thermochemical phenomena*

In many instances the creation of artificial electron clouds utilizes complicated chemical systems in order to produce atoms, molecules and/or ion electron pairs. In many cases the system in question is not capable of satisfactory analysis by conventional methods. However, it is often possible to obtain radio-radar and optical data on electron clouds which give experimental information as to the processes which have occurred in the selected reaction. The identification and yield determination of the final products is then used for elucidation of the chemical and thermal processes involved. This method is illustrated in a future paper associated with the thermal production of ion electron clouds.

5. CONCLUSIONS

This series of experiments has served to establish the fact that artificial electron clouds provide a new, fertile tool for research in the fields of upper atmospheric studies and electromagnetic propagation techniques. Several peripheral scientific areas can also benefit from findings associated with electron cloud studies. The detailed justification of this viewpoint will be offered by the subsequent papers of this series which analyze the results obtained to date.

REFERENCES

1. F. F. Marmo, J. Pressman, L. M. Aschenbrand, A. S. Jursa and M. Zelikoff, *J. Chem. Phys.* **25**, 187 (1956).
2. J. F. Bedinger, E. R. Manring and S. N. Ghosh, *J. Geophys. Res.* **63**, 19 (1958).
3. O. G. Villard and R. S. Rich, *QST Magazine*, American Radio Relay League, Hartford, Conn., May (1957).

Acknowledgements—We gratefully acknowledge the active support of the following, who were an asset to the success of the experiments of this series:

Mr. C. B. Moore, Arthur D. Little Co., Cambridge, Massachusetts.

Professor O. G. Villard, Dr. P. Gallagher and associates of the Radio Propagation Laboratories of Stanford University, Palo Alto, California.

Personnel of AEPG, Fort Huachuca, Arizona; Smyth Associates, Inc., San Diego, California; Land-Air Corporation, Alamagordo, New Mexico; Laredo Test Site, Laredo, Texas; White Sands *C*-3 Ionospheric Station, White Sands Proving Ground, New Mexico; and participating radio amateurs who assisted in detection networks.

Dr. R. W. Knecht, National Bureau of Standards, Boulder, Colorado.

R. Sturm, physicist, Friez Instrument Division, Bendix Aviation Corp., Baltimore, Maryland.

Personnel of Geophysics Research Directorate of Air Force Cambridge Research Center, Bedford, Massachusetts, for their support in instrumentation and launch preparation.

Planet. Space Sci. Pergamon Press 1959. Vol. 1, pp. 238–248. Printed in Great Britain.

A REPORT ON THE SYMPOSIUM ON THE USE OF SPACE VEHICLES AT THE FALL 1958 URSI MEETING

W. C. HOFFMAN

Rand Corporation, Santa Monica, California
Author now at Hughes Research Laboratories, Malibu, California

(*Received* 2 *March* 1959)

During the Fall 1958 URSI meeting at Pennsylvania State University a symposium, under the chairmanship of A. H. Shapley, was held on "The Use of Space Vehicles." Other members of the panel were:

O. K. Garriott, Stanford University
R. A. Helliwell, Stanford University
C. G. Little, CRPL*
W. Pfister, AFCRC†
Mrs. R. Sagalyn, AFCRC†
J. C. Seddon, NRL‡

The panel members had all actually proposed experiments involving radio instrumentation of space vehicles to the Working Group on Satellite Ionospheric Measurements (WGSIM) of the USNC–IGY** Technical Panel on the Earth Satellite Program. These proposals were in turn forwarded to the Space Science Board of the National Academy of Sciences for action.

A. H. Shapley opened the meeting by introducing the panel and inviting active audience participation in the discussion. After pointing out that we are now approximately one year into the Space Age, Shapley reviewed the recent history of satellite radio experiments. Originally the U.S. IGY program had allowed for no ionospheric radio or propagation experiments because weight limitations permitted transmission only at about 100 Mc/s, a frequency not sufficiently affected by the ionosphere. The advent of the Sputniks with transmissions at 40 Mc/s and 20 Mc/s provided opportunities for this type of experiment and soon afterward WGSIM was established and several organizations participated in the IGY program for Satellite Ionospheric Measurements. Meantime preliminary plans were being developed for research with satellites in the post IGY era, and during the early summer of 1958 a circular letter was sent out to URSI Commissions 3, 4 and 5 encouraging contributions and descriptions of possible experiments. It was during this period that the National Academy of Sciences established the Space Science Board. Several *ad hoc* committees were also set up, among others, one for ionospheric measurements. The latter had the responsibility for exchanging ideas and information on satellite ionospheric experiments and for investigating possible experiments with new satellite vehicles, no restriction on weights or orbits of such vehicles being assumed.

The symposium was conducted on the following plan: Five classes of experiments would be discussed, a short, five-minute introduction for each type being given by the panel members directly concerned, after which the subject would be thrown open to discussion by any interested member of the audience. The five classes of experiments and the speakers for each were (1) VLF satellite measurements (R. A. Helliwell and C. G. Little), (2) ion probes (J. C. Seddon and Mrs. Sagalyn), (3) Faraday

* Central Radio Propagation Laboratory, Boulder, Colorado.

† Air Force Cambridge Research Center, Bedford, Massachusetts.

‡ Naval Research Laboratory, Washington 25, D.C.

** U.S. National Committee—International Geophysical Year.

rotation measurements (C. G. Little and J. C. Seddon), (4) topside ionospheric sounders (W. Pfister and O. Garriott), (5) studies of anomalous propagation (W. Pfister and O. Garriott).

(1) R. A. Helliwell opened the discussion on the VLF satellite by describing an experiment based on receiving and demodulating in the satellite a 15·5 kc/s signal transmitted from the surface of the earth (station NSS, Annapolis). A 30 msec pulse would be transmitted every second from the ground station, the transmission delay being governed by the whistler mode with group velocity $v_g = 2c(ff_H)^{1/2}/f_p$. For a satellite overhead at 1000 km altitude the transmission delay would be about 13 msec. A spin stabilized satellite in a 1000 km circular orbit is envisioned. The geomagnetic field lines and the ionospheric stratification both influence the received signal. Variations in time delay and amplitude will be measured on the earth at both ends of the path as well as in the satellite. Thus the distribution of ionization above the $F2$ peak as well as the structure of large ionospheric irregularities can be determined as the satellite moves along its orbit. Broadband and multifrequency transmissions may be a possibility.

C. G. Little described the VLF satellite proposal evolved by Owen Storey at CRPL to obtain information on the local electron density. In this experiment VLF CW transmissions from a ground station would be received by a satellite having a dipole antenna (electric dipole) along its long axis and a loop antenna (magnetic dipole) feeding into a separate VLF receiver, at right angles to the dipole antenna. Under free space conditions and proper orientation, the dipole would receive only E, the loop only H, from the ground transmitter. The satellite will be spun about an axis in the plane of the magnetic loop in the manner indicated in Fig. 1.

The free space impedance is given by $Z_0 = E/H$. In the ionosphere the local impedance Z_l is given by Z_0/μ, where μ is the local real refractive index, so that values of the ionospheric refractive index can be measured. The voltage vs. time record for the loop antenna will have an appearance similar to that

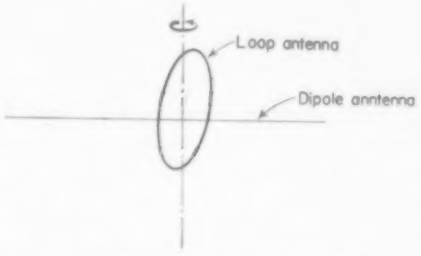

Fig. 1. Crossed antenna configuration for CRPL VLF satellite.

shown in Fig. 2, due to the spin modulation (the ratio of maximum and minimum deflection being twice the spin rate). A similar record will be obtained from the dipole antenna. Comparison of the two records, after proper allowance has been made for the spin modulation, then enables one to estimate the local impedance Z_l and so the corresponding refractive index. In a sense such a satellite would constitute an ion density probe.

W. Pfister noted that there was no apparent frequency restriction in such a system and suggested that frequencies as high as 5 Mc/s could be employed up to the vicinity of the F-layer peak. R. A. Helliwell agreed that the same method is apparently applicable at any frequency such that the local refractive index

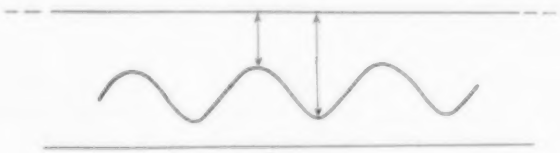

Fig. 2. Voltage vs. time record for the loop antenna.

is proportional to the impedance, but observed that the sensitivity of the system is the crux of the matter.

R. S. Lawrence described a VLF satellite experiment which, unlike those already described, was intended to record cosmic noise on a broadband basis. Such observations would yield information on cosmic noise at frequencies below the ionospheric cutoff and the fashion in which cosmic noise radiation is absorbed as it travels downward through the ionosphere. This information would be of considerable value in radio astronomy, and in fact Lilley at Yale University has taken an active part in formulating this experiment. C. G. Little agreed on the value of exospheric cosmic noise measurements, but noted that such an experiment might measure a G-condition rather than the local electron density. W. Pfister commented that Lilley was proceeding with this experiment under AFCRC GRD sponsorship and at the time of the symposium was mainly devising instrumentation, with no particular vehicle specified. Two or three frequencies in the band 2–5 Mc/s will be monitored by comparing the cosmic noise level with the internal receiver noise and by properly calibrating the antennas. Pfister observed that this is not a simple experiment. In answer to a question of R. S. Lawrence concerning the possible use of frequencies below 2 Mc/s, Pfister stated that such transmission would have to make use of the extraordinary mode and so would complicate matters by the necessity of taking into account guidance by the geomagnetic field.

Helliwell noted, in answer to a question of S. A. Bowhill concerning propagation along the geomagnetic field, that in a spherically stratified medium the wave normal eventually must line up with the geomagnetic field vector, this feature marking the essential difference between a columnar and a spherically stratified medium. H. Poeverlein noted that the angle of arrival and polarization of whistlers change during reception, and Helliwell agreed that multiple columns of ionization which might act as multiple whistler paths would result in a complicated signal. Helliwell agreed with R. S. Lawrence that it would be useful to record field strength at the satellite and noted that additional measurements, sufficient to determine the satellite orientation and to calibrate instruments, would be necessary. A. J. Dessler noted that hydromagnetic waves will constitute a factor compromising ELF* reception above 300 km altitude. Helliwell replied that observations of exospheric hydromagnetic phenomena will be reserved for a later experiment making use of a broadband receiver. W. C. Hoffman observed that a good method for determining instantaneous satellite orientation could be based on referring the satellite axis to the direction of the local geomagnetic field through the use of a satellite-borne magnetometer, as in Sputnik III. Shapley stated a combination of VLF receiver and magnetometer in the satellite is envisioned for later experiments. S. A. Bowhill noted that in the VLF experiment described by C. G. Little the requirements on spin along the axis of the dipole can be relaxed by employing additional dipoles together with commutated channels. H. Poeverlein raised the question as to how important an effect the longitudinal component of the electric vector would have on the Storey experiment. Helliwell stated that the orbital elements of the VLF satellite would require careful study. An orbital inclination which would coincide with the magnetic meridian through station NSS† would be desirable but not essential. W. C. Hoffman stated that a possible alternative to the 1000 km circular orbit would be a fairly eccentric orbit with $i=78°$ and a high apogee, low perigee. The apogee would be such as to be tangent to the geomagnetic field line emanating from station NSS at its farthest point from the earth. The low perigee would reduce the power required for radio transmission from satellite to ground, if the information received near apogee could be stored until the low point of the orbit is reached.

(2) The panel meeting then turned to a discussion of the second type of satellite ionospheric experiment, that of ion probe, for which there were several approaches. J. C. Seddon outlined the NRL work in determining local ion density by measuring the beat frequency

* extremely low frequency
† Annapolis, Maryland.

between two CW rocket-borne transmitters at 7·75 Mc/s and the sixth harmonic thereof. The probe work as such was recently reactivated under the direction of R. Bordeaux when sufficient staff became available. One of the most severe difficulties of the phase beat experiments is caused by antenna detuning, the antenna impedance undergoing even more drastic changes below the ionosphere than in it. Recent results using the configuration shown in Fig. 3 have been encouraging.

The antenna capacity C plus the insulator capacity is determined in free space, and ΔC is then measured by the equipment diagrammed in Fig. 4. The plasma frequency f_p, which is proportional to the local electron density, can then be determined from the equation

$$n^2 = \frac{C - \Delta C}{C},$$

where $n^2 = 1 - (f_p/f)^2$. The system is calibrated by varying the load and capacitance of a dummy antenna. The capacity as a function of time has the appearance shown in Fig. 5.

The bottom curve represents the predicted variation based on experience with phase beat experiments. The top curve gives what is actually observed and shows large excursions modulated at not twice the rocket roll rate, as might be expected, but at exactly the roll rate. One can get 150 V on the 15 ft antennas up to 230 km altitude, and the plasma frequency can be measured in terms of the capacitance. These values should be multiplied by $3{\cdot}0 \pm 0{\cdot}3$ to get the right answer, due to the shielding

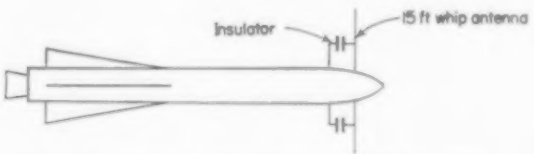

Fig. 3. Antenna rocket configuration for NRL phase beat experiment.

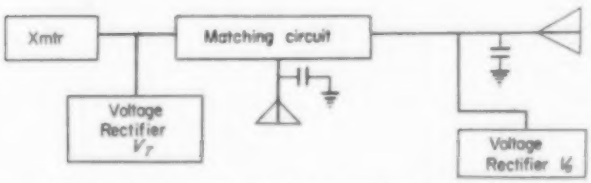

Fig. 4. Internal capacity measuring equipment in NRL rocket.

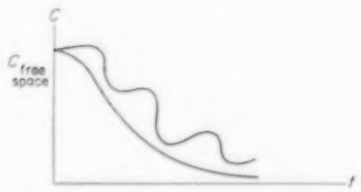

Fig. 5. Capacitance of the system as a function of time.

effect of the positive ion sheath around the antenna.

Seddon described the technique recently employed by Massey for British measurements of local electron density above Woomera utilizing the Skylark rocket. The warhead of the rocket was electrically insulated from the main body and the inductance capacity of the system was used to set the frequency of an oscillator. The conductivity and dielectric constant in the vicinity of the rocket change with the local electron density and collision frequency. From measurements of the frequency and amplitude of the oscillator one can determine the electron density.

Seddon suggested that any proposed probe be installed on a small rocket and calibrated in flight by means of the following procedure: Let the rocket-borne transmitter ordinarily feed a low power (1 V) signal to the antenna to get away from the factor of 3. Telemeter on high frequency and low power the oscillator voltage V_i and the antenna voltage V_a. During the flight the r.f. antenna voltage would be occasionally jumped to 150 V and corresponding spot readings of electron density at altitude would be obtained by the usual NRL phase beat method. This will provide the calibration of the probe system. In between times one can calibrate. The probes and associated low frequency oscillator and frequency multipliers are installed in the nose and the output is telemetered back at the tenth harmonic of the carrier frequency.

Mrs. R. Sagalyn then described the proposed AFCRC satellite probe, based on the probe theory of Langmuir and Mott-Smith. The technique is similar to the Soviet probe on Sputnik III which consists of a reticulated spherical ion trap insulated from the satellite itself. The AFCRC configuration will appear as in Fig. 6.

Fig. 6. AFCRC ion probe.

The sensing element consists of a spherical condenser mounted approximately 18 in. from the satellite surface. The magnitude of the potential difference between the electrodes and the polarity of the central collection electrode can be adjusted so that all ions or electrons entering the outer sphere will be collected.

Along the satellite orbit the thermal velocity of positive ions is about one-tenth the satellite velocity. The positive ion current to the probe can therefore be expressed

$$i = ne\pi r^2 v f(V)$$

where n is the positive ion density, e the charge per ion, r the radius of the outer sphere, v the velocity of the satellite. The value of the function $f(V)$ depends on the potential of the outer sphere with respect to the undisturbed plasma. It can be determined from the analysis of the current voltage curve obtained by periodically sweeping the voltage on the outer sphere with respect to the satellite surface.

When the voltage between the electrodes is large enough to collect on the negative inner sphere all positive ions which enter the probe, the positive ion density can be evaluated from the relation:

$$i = ne\pi r^2 v f(V)\,\alpha$$

where α is the experimentally determined transmission factor for the outer sphere.

Because the thermal velocities of the electrons are much larger than the satellite velocity, the expression for the electron current is more complicated. If the satellite capacity is much larger than the capacity of the probe, then the potential of the satellite can also be determined from the analysis of the current voltage curve described above. By suitable programming of the sweep voltages and adjusting the polarity of three probes mounted on a satellite, local ion and electron densities, electron temperatures and satellite potential can be obtained simultaneously from this experiment.

Schmerling suggested that a simple probe could be based on measurement of the antenna impedance which undergoes a catastrophic drop at the plasma frequency. Five or six small (mW power) oscillators with an equal number of small loop or dipole antennas could cover

the required frequency range adequately. Seddon agreed with Schmerling in principle but pointed out that the probe system he had described would have adequate dynamic range if only two frequencies are used. For example, the 7·75 Mc/s probe measured an electron density of $1{\cdot}7\times10^{5}$ electrons/cm^{3} with no difficulty, and a reduction in frequency greatly improves the sensitivity.

R. Bordeaux described a first generation ion probe under construction at NRL. This instrument consists essentially of a Langmuir probe plus a retarding potential. The device is illustrated in Fig. 7.

Fig. 7. First-generation NRL ion probe.

Another mode in which the collector grid might be operated is to ground it to the satellite skin rather than the collector plate load. For the first configuration the volt ampere curve to the shield will have a form similar to that shown in Fig. 8.

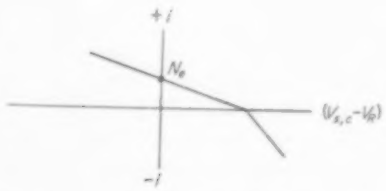

Fig. 8. Characteristic curve for the shield voltage.

A second generation probe, which is being developed by W. R. Bennett at NRL, will consist of substantially the same configuration but with several wire grids maintained at different potentials as shown in Fig. 9.

Such a device will yield information on the various types of ions involved, since, if several mass numbers are present, there will be corresponding plateaus in the voltage vs. current characteristic. Mrs. Sagalyn and R. Bordeaux discussed the effect of the time duration of the frequency sweep upon the variations in apparent electron density. Bordeaux stated that while the sweep duration might be as much as 1/2 sec for a vertically fired rocket, it would be a good deal faster on a satellite, say, 0·1 sec. E. Mueller noted that due to the satellite spin the probe reading would consist of a crude average over several turns, the value being proportional to the satellite velocity multiplied by the cosine of the spin angle. It might be somewhat risky, he felt, to bet 5 million dollars on the precision of such a method. The effect of any paint upon the satellite surface might be to build up as much as several volts static charge, since paints are ordinarily good insulators.

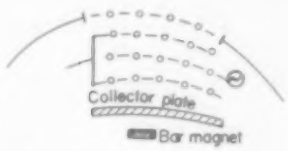

Fig. 9. Advanced NRL ion probe.

Bordeaux cited the Soviet probe experience to the effect that the vehicle potential is low when no high power transmitters are being operated. He also noted the importance of avoiding the situation where the ion chamber faces into the vacuum pocket behind the satellite and stated that this possibility could be avoided by locating one ion chamber on the satellite axis perpendicular to the spin axis. Mrs. Sagalyn responded that two diametrically opposed probes on the vehicle will also avoid any troubles with the vacuum pocket.

W. Pfister said that he was speaking for Spencer of the University of Michigan, who was unable to be present, and proceeded to describe a Langmuir bipolar (or Spencer) type of satellite probe. The bipolar probe rocket already flown is constructed in the shape of a dumbbell, with the electrical characteristics indicated in Fig. 10. The voltage vs. current characteristic is shown in Fig. 11. With such

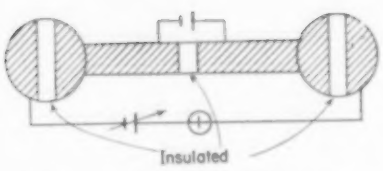

Fig. 10. Langmuir bipolar (Spencer) rocket borne ion probe.

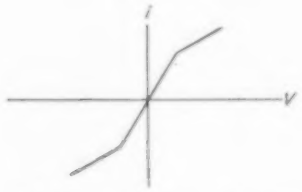

Fig. 11. Voltage vs. current characteristic for Langmuir bipolar ion probe.

a device one can measure electron temperature and ion density, but to determine electron density the probe would have to be unsymmetrical. The satellite bipolar probe would be constructed on the basis of the same principle but would not necessarily have the same shape. E. Mueller commented that there will be no definite electron temperature, and the high energy tail of fast electrons may play an important role.

(3) The third type of satellite experiment involved Faraday rotation of the radio signal emitted from a satellite. C. G. Little went into the background of the phenomenon and described some experimental techniques, both developed and proposed. The Faraday rotation is given by the expression

$$\varphi = \frac{1}{2\pi} \frac{e^3}{m^2 f^2 c^2} \int NH \cos\Theta \, dl \quad \text{(radians)}$$

or, assuming quasi longitudinal propagation at 20 Mc/s,

$$\varphi = 6 \times 10^{-11} \int NH \cos\Theta \, dl$$

Though the rotation rate can readily be measured, it is in general impossible to determine the number of complete rotations. One way (which cannot be used in the majority of passes) of determining the total number of rotations is to identify the period when propagation from the satellite is quasi transverse. This period is marked by a relatively steady signal and two linearly polarized components rather than two circularly polarized ones. When the transition to quasi longitudinal propagation occurs the signal will be modulated at the Faraday rotation rate, and the number of rotations can be determined by counting back to the time when propagation ceased to be quasi transverse. Another way of resolving the ambiguity is to install two transmitters in the satellite which are separated 1 to 3 Mc/s in frequency. At least one proposal suggests the use of 2 CW transmitters radiating linear polarized signals from the same antenna at 38 and 40 Mc/s.

Little described another type of experiment which is based on the differential absorption undergone by the ordinary and extraordinary components, the absorption of the extraordinary component exceeding that of the ordinary by the factor $(f+f_L)^2/(f-f_L)^2$. In high latitudes the total differential absorption along the path may amount to as much as 10–20 per cent. The proposed method, then, involves measuring the difference between the intensity of the ordinary and extraordinary wave. The technique appears promising and should make it possible to monitor the size of absorbing irregularities (down to 100 km in size) at high latitudes and thus offers considerable advantage over the use of an ionosonde for this purpose.

J. C. Seddon then described NRL experience relative to Faraday rotation. At 7·75 Mc/s it was possible to measure down to 10^3 electrons/cm^3 or less in the *D*-region. Pitch and yaw of the rocket will bring about a phase modulation of the signal due to changing antenna orientation. During the day, at 100 km altitude, Faraday rotation does not work. The modulation is irregular and the nulls are spotty, apparently due to irregularities in the *E*-region. At higher frequencies (46·5 Mc/s) the use of the technique is satisfactory. Seddon described a night rocket flight intended to sound a

"spread F" condition. The roll rate of the rocket was determined in the lower ionosphere, but in the spread F the apparent rotation rate was erratic, so that if a small altitude increment is used, a negative value may be obtained for the electron density. This is apparently due to rapid electron density changes with time. At the peak of the trajectory, however, a longer time is available for measurement, and an average value of electron density could be determined. At 234 km it was found to give a value of $6{\cdot}4 \times 10^5$ electrons/cm^3, but this could easily be in error by a factor of two or three.

S. J. Bauer described the theory and techniques developed by F. B. Daniels of USASRDL* and himself in connection with Faraday rotation of the satellite signal. Bauer's expression for the Faraday rotation is as follows:

$$\varphi \sim f^{-2} \int_{h_1}^{h_2} BN \cos\Theta \sec\delta \, dh$$

where h_1 and h_2 are the lower and upper limits of the ionosphere and δ is the zenith angle. Below 1000 km altitude one can take B outside the integral sign, and the expression for the rate of change of Faraday rotation becomes (h_s denoting the satellite altitude)

$$\frac{d\varphi}{dt} \sim f^{-2} B \left\{ \frac{\partial (\cos\Theta \sec\delta)}{\partial t} \int_{h_1}^{h_s} N\,(h)\, dh + \cos\Theta \sec\delta \, N\,(h_s) \frac{dh_s}{dt} \right\}$$

The second term inside the parentheses is zero at apogee and perigee and also vanishes for a circular orbit, but in general cannot be neglected at an arbitrary point of the orbit. The presence of two unknowns, the local electron density at the satellite and the integrated electron density over the entire path requires simultaneous observations at at least two stations. Bauer showed slides of the term $\cos\Theta \sec\delta$ and its time derivative for 35° and 65° orbits, the fading rate as a function of time in terms of the contribution of the integrated electron density, the local electron density, as well as the sum of the two. The last slide had an appearance like that of Fig. 12.

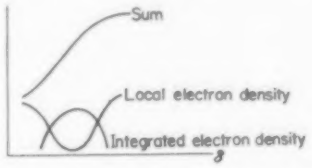

Fig. 12. Local vs. integrated electron density.

British observations of the fading rate give a value for $\int_{h_1}^{h_s} N\,dh$ of 19×10^{12} electrons/cm^2 for a satellite passage at about 450 km height. This value seems to be much too high in view of the fact that the integrated electron density up to the $F2$ maximum obtained from vertical sounding data was about 5×10^{12} electrons/cm^2. Since the observed fading rate results from the combined effects of both the integrated and the local electron density (as indicated by the close resemblance of the observed fading rate curve to the theoretical curve of Daniels and Bauer), the estimated integrated electron density up to the satellite would be of the order of $8\text{–}9 \times 10^{12}$ electrons/cm^2 and the local electron density at the satellite about $4\text{–}5 \times 10^5$ electrons/cm^3. This indicates that for orbits having appreciable eccentricity, both the local and integrated contributions must be taken into account. R. R. Arendt noted that the second term in Dr. Bauer's expression contains the radial velocity $\sec\delta \frac{dh_s}{dt}$ and that in full generality two more terms containing time derivatives of $N\,(h)$ and B, respectively, should be included. The plot of the fading period t between two successive nulls vs. zenith angle is U-shaped in a nonionized medium. The presence of the radial velocity term introduces a dimple into this curve (Fig. 13) for an overhead passage. This behavior has been noted with respect to the radio signal from Explorer IV. Arendt

* U.S. Army Signal Research and Development Laboratory, Fort Monmouth, N.J.

further noted that at altitudes above 1000 km strong hydromagnetic effects could be expected, so that the situation should not be regarded as that prevailing in free space.

Fig. 13. Fading period for an overhead passage.

S. Weisbrod commented that the results of his theoretical work showed that when the geomagnetic field and direction of wave propagation are regarded as constant over the path, the integral expression for the Faraday rotation reduces simply to the retardation in the group velocity. He therefore suggested that a beacon could be incorporated in the satellite to measure $\int N\,dh$ to the same order of accuracy as the Faraday rotation method.

S. A. Bowhill noted that the satellite spin and the Faraday rotation combined give sum and difference frequencies and higher harmonics thereof. The extraordinary and ordinary components will often interfere in the same way. C. G. Little recounted his experience at a high latitude station using crossed dipoles aimed at the zenith. Switching between them enabled one to distinguish between the ordinary and extraordinary components. Little emphasized the desirability of looking only at the portion of the sky where circular polarization prevailed.

G. H. Millman suggested the use of two bistatic radars at frequencies f_1 and f_2 to determine $\int N\,dh$. H. P. Hutchinson of USARSDL agreed with Bowhill that spin rotation is a considerable problem, and outlined his experience in trying to determine the slant range of 1957 β based on comparison of observed and computed Doppler frequencies. W. W. Berning pointed out that curvature of the orbit and uncertainty in the orbital elements could introduce appreciable error into Hutchinson's method, but Hutchinson felt that these effects could be minimized since the slant range is determined by only a small portion of the orbit near the zenith.

(4) The symposium then turned to a consideration of the topside sounder, by which is meant a miniaturized satellite borne ionosonde looking downward at the ionosphere from above. W. Pfister led off with a description of "the ionosphere that we will have to deal with." The Soviet satellite experiments yield a value of 10^4 electron/cm^3 at an altitude of 2000 km. This corresponds to an absorption of 1 neper for an operating frequency of 12 Mc/s and an altitude of 1000 km. Thus a peak pulse power of 20–50 W would be required for a satellite borne transmitter at this altitude. An important distinction between a ground based ionosonde and one in a rapidly moving satellite is that sweeping the frequency is unnecessary in the satellite. A series of fixed frequencies in the range 1–15 Mc/s will do just as well. A CW topside sounder, operating by measuring the beat note between separated frequencies, requires a smooth ionosphere, but the ionosphere is even less smooth above the $F2$ peak than below. Vertical drift motions and ionospheric tilts grow more pronounced with altitude. One type of topside sounder experiment which has been proposed is the use of a net of sounders on the ground to interrogate the satellite at spot frequencies as it passes over. Such a technique would not, however, make full use of the motion of the satellite.

E. R. Schmerling agreed on the use of fixed frequencies. Although the ground-based ionosonde records are taken on a continuously swept frequency basis, when the h'–f records are reduced, they are sampled at a discrete interval of 2 Mc/s. Schmerling suggested that peak power limitations on the satellite transmitter could be circumvented to some extent through the use of photographic integration at a rate of, say, 10 pictures/sec. It was further noted that in the determination of electron density from h'–f records it is necessary to fix the bottom point fairly accurately by means of the plasma frequency at this level. With respect to the latter point, Pfister commented that, for a satellite orbit below 2000 km altitude, transmission of a 1 Mc/s signal will pick up the minimum plasma frequency, and determination at one ground based location is sufficient.

T. E. Van Zandt commented that in determining the plasma frequency at satellite altitude, signals at the lower frequencies will be heavily absorbed. Van Zandt mentioned a method for determining true heights from *O* and *X* traces recently developed by Owen Storey. The method should also be applicable to satellite transmissions, with proper inversion of the geometry. This technique, Van Zandt felt, might also be made the basis of a good electron density probe, which would be relatively immune to the effects of spin and the ion sheath surrounding the satellite.

W. C. Hoffman pointed out that a theoretical program of research in methods for reducing the h'–f records obtained by the satellite ought to be carried out simultaneously with the development of hardware. In 1956, Karp and Schmoys* laid down the foundations of an analytical method for determining the full electron density profile, including valleys, from ionosonde observations taken both above and below the ionosphere. Extension of the Karp–Schmoys theory now, so as to have available a practically usable technique for reduction of the joint satellite ground station h'–f records when the topside sounder is flown, ought to be worthwhile.

G. J. Gassmann, who had been a member of the *ad hoc* group concerned with the topside sounder, then spoke. The first satellite should contain fairly elaborate equipment, with simplification of the instrumentation taking place as experience grew. Measurements at 2, 4, 6, 8 10 and 12 Mc/s will be carried out on a routine basis, with a few seconds' transmission at each frequency. The estimated radiated power required on the satellite is of the order of 10 W, allowing a one-way absorption of 4dB since transmission through the *D*-region is not required and only cosmic noise is present. The antenna offers a difficult problem. It cannot be a dipole, and since the plasma frequency of the medium is of the order of 5 Mc/s, it is important to avoid detuning the antenna. For this reason, a resistively terminated antenna similar to that for ground stations will have to be employed. Measurements should be made during both magnetically quiet and disturbed days, over a variety of seasons and during a period of sunspot minima. Due to the equatorial bulge one must expect tremendous focusing effects (sometimes as great as ± 30 dB) in sunlight near the equator.

R. W. Knecht was present at the same *ad hoc* committee meeting, and described a simple experiment based on transmission of a single frequency, say, 6 Mc/s. Due to power limitations, soundings would be made only over ground based ionosonde stations. A frequency which is "too high" might be included to obtain calibration of distance. With such a system one might get totally unexpected answers. Several ingenious hardware schemes have been proposed, among others one which will automatically optimize the transmission frequency of the sounder in the presence of a plasma.

(5) The final symposium topic was concerned with propagation anomalies in radio transmission from satellite vehicles. O. K. Garriott led off by describing the recent Stanford experience in reception of the antipodal signals first noticed by H. W. Wells. During the first three weeks of Sputnik III reception on 20 Mc/s the antipodal signal was received on 13 occasions, with negative results on 5 other passes. During this period the satellite altitude exceeded the altitude of the *F*2 maximum near the antipodal point. The morning, or low, passes were much less successful, the antipodal signal being received on only two occasions. If Wells' explanation of the antipodal signal is correct, a change in Doppler shift would be expected as the "ghost" satellite passed nearby. Stanford's observations do show a Doppler shift (consistent with the azimuth of arrival) but no *change* in Doppler shift during an antipodal passage. The direction of arrival, as determined by means of a rotating Yagi antenna, was between south and southeast on all afternoon or evening antipodal observations. The radio signal travels in the dark hemisphere during the early part of its passage, and it is believed that the ionospheric tilts to the southeast of the receiving location, set up by sunset conditions, are an important factor in this type of trans-

* *J. Geophys.* **61**, 183 (1956); *cf. N.Y.U. Inst. Math. Sci. Rep.* EM-82.

mission. Garriott also briefly discussed the extended range reception of satellite signals at many different locations on the earth's surface. Reports of such extended range transmission have been quite frequent on 20 Mc/s, less so on 40 Mc/s and have occurred only once on 108 Mc/s.

S. A. Bowhill asked whether there was a standard reference frequency employed during the overhead passages, and Garriott replied that this was supplied by a local oscillator at the receiving station. The use of the local oscillator permitted a Doppler shift to be measured which was consistent with the observed direction of arrival.

W. J. Ross asked why the antipodal point is important if tilt *F* transmission is the crux of the matter, and noted that focusing does not occur simply because of the existence of one tilt. Garriott replied that the antipode is the only point such that a signal originating there will reflect from an intermediate tilt no matter what its bearing from the transmitter may be. W. W. Berning noted that antipodal transmission might also rise from a *G* condition at an altitude of the order of 900 km and described an occasion when the Doppler shift on a satellite signal which had been undergoing considerable fading was being monitored. As the satellite rose above 900 km altitude an abrupt decrease occurred in the frequency of fading.

R. W. Knecht asked whether anyone had a good explanation for the extended range transmissions observed from high latitude stations and cited the case of Ice Island where reception had been accomplished for 12–14 hr continuously. W. Pfister said that there seemed to be no valid explanation as yet, and that it was mainly a phenomenon of the Arctic and the Antarctic regions. The longest continuous signal received to date lasted for a period of 17 hr. His group has attempted to repeat the long range observations made with Sputnik I at Thule and will try soon also at Ice Island. However, the transmitter in Sputnik III is weaker than in I and results have mainly been negative. M. Katzin referred to F. H. Dickson's Ice Island observations and said that later study indicated that some of the earlier reports may now be doubtful. H. Busch stated that the reception was not completely continuous, and on many records of signal strength the period of reception became progressively longer as the latitude of the receiving station increased, especially for high inclination orbits. Knecht observed that the extended range reception at high latitudes was somewhat surprising, since in general one expects the electron density to be higher, the nearer the equator. Pfister said that a possible mode might involve trapping of the signal above the peak of the *F*-layer with return to the earth possible in the polar regions because of the relative transparency of the ionosphere there. P. Green suggested that the whole phenomenon might simply be the result of the fact that, statistically, the satellite is more often than not near the arctic.

A. H. Shapley then concluded the meeting by stating that the afternoon's discussion would serve as a basis for recommendations to URSI Commission III and, thence, to the National Academy of Sciences' Space Science Board. The Space Science Board, which includes WGSIM, is acting in an advisory capacity to NASA.* Proposals to NASA for satellite ionospheric experiments are referred by that organization to the Space Science Board. Those who may wish to participate in future study group meetings are requested to inform A. H. Shapley or Dr. R. C. Peavey, Secretary to the Space Science Board, USNC–IGY, National Academy of Science, of their interest. Shapley stated that one of the prime concerns of the WGSIM and the Space Board is to broaden the participation in space research. Shapley then adjourned the meeting.

* National Aeronautics and Space Administration, Washington 25, D.C.

Planet. Space Sci. Pergamon Press 1959. Vol. 1, pp. 249–251. Printed in Great Britain.

INTERNATIONAL NEWS

SECOND MEETING OF THE *ad hoc* COMMITTEE ON CONTAMINATION BY EXTRA-TERRESTRIAL EXPLORATION

(The Hague, 9-10 March 1959)

LIST OF PARTICIPANTS

Convenor: PROFESSOR MARCEL FLORKIN

Representatives

IAU	DR. J. ROSCH
IUGG	PROFESSOR J. BARTELS
IUPAP	DR. DONALD J. HUGHES
IUBS	DR. P. ALEXANDER
IUPS	PROFESSOR W. O. FENN
IUB	PROFESSOR J. ROCHE

Observers: PROFESSOR P. SWINGS; PROFESSOR H. C. VAN DE HULST

SUMMARY RECOMMENDATIONS

CETEX was established in 1958 by ICSU to meet once to find out if the problem of contamination of extra-terrestrial objects by space vehicles represents a real problem. The report of this meeting which was held in May 1958 was that in the committee's view there is a real possibility that early experiments might spoil subsequent research. The committee therefore proposed to ICSU that a code of conduct be drawn up for space research with particular reference to the allocation of priorities and sequences of different experiments. CETEX stressed that such a report would require the active participation by experts, especially from the field of rocket technology. ICSU accepted this recommendation and at its general meeting in Washington in October 1958 asked CETEX to hold a second meeting. At the same time ICSU requested the National Academies of the U.S.A. and U.S.S.R. to assist CETEX with experts in rocket technology and with prepared documents. CETEX at its second meeting held at The Hague in March 1959 was able only to start its assigned task because the complexities of the problem made it impossible for the necessary detailed technical information to be available.

In the interval between the first and second meetings COSPAR has been formed by ICSU to co-ordinate world-wide space research and this new body enjoys the support of the American and Russian Academies. CETEX feels that the detailed functions proposed for its second meeting form an integral and important part of the duties of COSPAR and at this meeting CETEX confined itself to the general formulation of the problem and review of its initial report which has been slightly modified.

General principles governing space research

1. Space research offers a challenge and opportunities which should appeal to the most imaginative minds. The greatest encouragement must be given to novel and unconventional approaches and no proposal should be sanctioned which would hamper the experimenters freedom of action unless there are compelling reasons. On the other hand equally imaginative thinking is required when considering possible complications which can follow a particular type of experiment. Surprises are certain and unlikely possibilities must be borne in mind when dealing with the problem of contamination which is better defined as the problem of reducing the risk whereby one experiment may spoil the situation for other subsequent enquiries. The question of deciding whether such a conflict is likely to arise can best be dealt with by a committee or working group engaged in planning or advising on scientific experiments.

2. Ideally scientists should be asked to inform COSPAR as early as possible of each space experiment which is envisaged and of the methods to be used in its execution. The broadly based committee of COSPAR containing scientists from all disciplines may be able to see much more clearly than the space research specialists possible conflicts introduced by such experiments and may be able to suggest ways of overcoming these difficulties.

3. There are a number of obvious and necessary experiments which are bound to be done and here the COSPAR working group dealing with experiments may be able to suggest priorities. While it may not be possible to avoid all types of contamination a proper sequence can ensure that the collection of data is not thereby hindered. For example CETEX recommends positively that no "soft" landing, which requires the release of large quantities of gases, should be made on the moon until experiments have been successfully carried out—or at last all reasonable attempts made—to determine the nature of the moon's atmosphere.

4. In view of the great uncertainties which face space research, all operations which are not capable of conveying meaningful scientific data are to be discouraged even if they do not appear to carry with them a known source of contamination. Risks with the unexpected must be taken as otherwise no space exploration is possible but such risks must be justified by the scientific content of the experiment.

Contamination endangering physical and chemical studies

1. *The moon's atmosphere.* The moon's atmosphere contains only a small amount of matter (it is estimated at less than 100 tons) and is therefore extremely vulnerable to contamination. The release on the surface of any amount of volatile material (having a molecular weight of greater than 60) within this range of magnitude such as might be given off from explosions for marking purposes or to slow down the vehicle for "soft" landings is likely to remain on the moon. Another factor which a change in the lunar atmosphere might bring about is an upset in the thermal equilibrium and careful computation will be required before the magnitude of this effect can be assessed. The possibility that the impact of a rocket vehicle may itself be sufficient to alter the atmosphere by releasing trapped gases was rejected because the moon surface must occasionally be subject to bombardment by heavy meteorites.

The release of any chemical marker on the moon's surface is therefore objectionable if it involves tons of material. If it has to be done, a flare releasing material quite unlike that normally present in the lunar atmosphere should be used so that in subsequent investigations it can be clearly recognized as a contaminant introduced by man. Both in this connection and because of increased ease in detection a flare produced by sodium should be considered for this purpose. The sodium-*D* lines could be detected at low intensities if a monochromator is used to cut out scattered light of other wavelengths. Probably the quantity of material required to be visible through a telescope, though not to the naked eye, would be insufficient to cause serious contamination of the atmosphere.

The possibility that a flare of this type might disturb the lunar atmosphere due to the ionization of the sodium atoms by sunlight has been considered, but such an effect is unlikely to persist for long periods.

From the foregoing it is clear that detailed exploration can very easily modify the lunar atmosphere which should, if at all possible, be studied spectroscopically from either earth or moon satellites. An accidental hit by a vehicle which has failed to orbit would probably not be serious, since the moon's surface must occasionally be subject to bombardment by heavy meteorites and the release of trapped gases by impact will not therefore cause a departure from natural conditions.

2. *Moon dust.** The chemical composition of the dust on the moon's surface is of the greatest interest to a wide range of sciences. Knowledge of changes of composition at different levels would also be informative but may be difficult to interpret since bombardment by meteorites is likely to disturb the dust. For this reason mixing of some of the dust by rocket impact is unlikely to result in the loss of information.

The suggestion has been made in the recent scientific literature that there are unstable structures of a high free-energy content (i.e. containing a high concentration of free radicals) on the moon, which may be caused to react explosively on coming into contact with organic substances from the earth. The suggestion has therefore been made that great care be taken to exclude organic substances from space vehicles likely to impact on the moon. The committee could not support the view that such a hazard existed since such free radical structures would be triggered off by any impact which caused intimate mixing. Meteorites or solar corpuscular radiation would act as a fuze and initiate an explosive chain reaction.

The man-made object would do no more harm in this respect.

Radioactivity

A serious danger of spoiling the moon's dust will come from nuclear explosions. These will release fission products which under the conditions of extreme vacuum will enter the moon's atmosphere and be rapidly distributed. These radioactive atoms will be in a highly reactive form and on coming into contact with moon dust may form involatile compounds. In this way the whole surface of the moon may acquire additional radioactivity which may interfere with subsequent radiochemical analyses that could be of the greatest value in particular for problems relating to the history of the moon. The explosion of a fusion device is likely to be more serious than that of a fission bomb since the former will give rise mainly to volatile radioactive products, notably tritium, whereas the bulk of the volatile fission products are rare gases which will not combine with the moon dust. However, the range of the small particles by which fission bomb

*The possibility that valuable information concerning cosmic dust may be lost by disturbing the moon's surface has been considered but is unlikely to be serious. Analysis of the moon's dust can only provide a very incomplete picture of cosmic dust because many of the constituents will be volatilized by solar radiation.

activity is spread is likely to be very great on the moon and a serious danger of contamination would undoubtedly arise.

Although the relative extent of the contamination of the planets from a nuclear explosion would be very much smaller than in the case of the moon it may nonthe-less be sufficient to interfere with detailed radio chemical analyses under certain conditions. Also the effect of introducing radioactivity on another planet where there may be entirely different levels of background radiation from those found on earth could greatly influence any form of life found there. Although the objections against nuclear explosions on Mars and Venus may not be as compelling as in the case of the moon, they are nevertheless justified until more information is available.

Biological contamination

Recommendation for immediate action. The sterilization of space vehicles to prevent the spreading of spores and other terrestrial mirco-organism in the solar system is likely to present a number of technical problems that may not be easy to solve. CETEX suggests that COSPAR initiate a study immediately of the methods by which the inside of space vehicles can be sterilized, bearing in mind the presence of delicate instruments that must not be damaged. As soon as possible methods should be published by which this can be achieved it should be urged that all space probes be sterilized in this way. Although CETEX feels that the possibility that life can persist on the moon is sufficiently remote to justify being neglected, all moon probes should be sterilised so that the difficult techniques of sterilization may be worked out in practice.

The outside of space vehicles need not be sterilized since exposure to the unfiltered solar radiation during flight will destroy all micro-organisms which have settled on the shell. The need for sterilization is only temporary. Mars and possibly Venus need to remain uncontaminated only until study by manned space ships becomes possible.

1. *Contamination of the moon by living cells.* There is no reasonable possibility by which the introduction of cells such as spores or bacteria might give rise to life on the moon of the same type (i.e. containing DNA) as on earth which might confuse later investigators. There are no cells on earth which grow or multiply in the absence of water and at the high vacuum of the moon no water can exist on its surface.

2. *Contamination of Mars and Venus.* There is a possibility of biological contamination of these planets since there is a reasonable probability that the conditions on Mars are such that some terrestrial organisms might grow. Carbon compounds, light for photosynthesis and probably water and nitrogen are all available. It is therefore of the greatest importance that space vehicles should not land either accidentally or deliberately on Mars (and possibly also Venus) unless all precautions have been taken to exclude living organisms from them. Otherwise the most challenging of all planetary studies, that of extra-terrestrial life, may be put in jeopardy. The same precautions in regard to the development of complex molecules which have been dealt with in respect of lunar contamination in paragraph 4 below apply equally to both Mars and Venus.

3. *Panspermia hypothesis.* The suggestion that moon dust might help in evaluating the hypothesis that dissemination of life in the cosmos occurred by transport of forms of life in the cosmic dust must be rejected because solar radiation (in high vacuo) would decompose "biospores" just as it decomposes cosmic dust. The possibilities by which a spore might travel through space inside meteorites involve so many improbabilities that they do not justify special consideration at this stage.

4. *The development of complex molecules.* The basic problem concerning the origin of life is how complex molecules (on the earth they are based on carbon) came to be built up and become replicated. It is conceivable that the interior of the moon dust may provide some valuable clues in this direction. It is not beyond the bounds of possibility that some "pre-life" processes may be occurring on the moon and these may be similar or different from those which had taken place on earth. If there are such processes then the introduction of "foreign" macromolecules from the earth may cause a serious upset in the lunar processes. The earth macromolecules may under lunar conditions act as templates and provide new foci for "pre-life" growth. If such events were started indiscriminately all over the moon the pattern might be distorted. It is important to emphasize that living cells are not envisaged for this process and that in this connection a dead bacterium from an aseptic rocket would be as harmful as a live one. The occurrence of any such growth reactions is remote and does not justify the imposition of any irksome restrictions on lunar exploration, but where reasonably possible it should be borne in mind. A simple precaution against endangering future studies might be to limit the areas of landings on the moon and thereby to localize the effects—if any—of terrestrial templates.

Planet. Space Sci. Pergamon Press 1959. Vol. 1, pp. 253–258. Printed in Great Britain.

LOW FREQUENCY ELECTROMAGNETIC RADIATION ASSOCIATED WITH MAGNETIC DISTURBANCES

G. R. A. ELLIS

Upper Atmosphere Section, CSIRO Camden, N.S.W.

(*Received* 16 *April* 1959)

Abstract—Continuous observations of the amplitude and spectrum of naturally occurring radiation in the band 2–40 kc/s have been made during the period June to December 1958 near Sydney, Australia. A large number of isolated noise bursts lasting for some hours were detected. The intensity ranged from 6×10^{-19} to 6×10^{-17}W m^{-2} (c/s)$^{-1}$ at 4·6 kc/s. Three main types of bursts were identified and classified on a basis of their spectra which usually extended from 3 to 5 kc/s, 4 to 8 kc/s and 2 to 30 kc/s, respectively. Major bursts, which were always of the latter two types, were clearly associated with strong auroral and magnetic activity and some showed a reproducible sequence of amplitude variation lasting about 36 hours. On three occasions, a detailed correspondence between the intensity of the noise and of simultaneously occurring red oxygen airglow was observed. Theories of the origin of the noise are discussed.

1. INTRODUCTION

It has been known for many years that it is possible to detect, at times, continuous atmospheric radio noise at kilocycle frequencies, in addition to the more usual impulsive atmospherics and whistling atmospherics[1]. In a loud speaker the noise sounds like smooth hiss with a bandwidth of several kilocycles and a centre frequency of 3 or 4 kilocycles[2, 3].

Previous observations of the noise have been hampered by the difficulty of recording it in the presence of interference from atmospherics and electric mains. As a result, existing reports are of strong outbursts detected during routine intermittent recording of whistlers in the same frequency band. No continuous observations have been reported, so there is little information on the time variation of the noise.

Its origin is not yet understood but is thought to lie in the interaction between auroral particle streams and the plasma of the outer atmosphere[4, 5]. Such VLF noise may thus prove to be a phenomenon analogous to solar radio noise, but generated in a more accessible region.

2. EXPERIMENTAL TECHNIQUE

Except at remote places the ambient noise level due to radiation from power lines and from lightning is sufficient to mask many bursts of VLF noise if simple integration is used in the recording system. However, as this interference differs from the continuous noise by being largely impulsive, it may be reduced considerably by a recorder which rejects impulses. Two possible methods are to cancel repetitive impulses with a time delay filter (a method which would be of use for mains interference only) and, more generally, to use a partly unidirectional integrating recorder of the type which has been applied to reduce atmospherics interference with cosmic noise observations[6].

In the present investigation the second method proved adequate. Otherwise the equipment was similar to that used for routine observations of whistling atmospherics[7]. The antenna was a six turn vertical loop with an area of 100 square metres connected to a wide band amplifier. The amplitude of continuous noise in a band 800 c/s wide at 4·6 kc/s was traced with a pen recorder having a charging time constant of 20 sec and a discharge time constant of 0·01 sec. The spectrum of the noise between 2 kc/s and 40 kc/s was recorded with a spectrum analyser of the frequency scanning type. Its frequency resolution was 600 c/s and

scanning rate 6/sec, the records being made on film moving at 3 in./hr. Also, tape recordings were made of selected noise bursts for later analysis.

The sensitivity of the fixed frequency recorder for signal equal to noise was 0·005 μV m^{-1} (c/s)$^{-1}$ at 4·6 kc/s. With the antenna connected the effective ambient noise level was approximately 0·010/μV/m during the day and 0·02/μV/m during the night. The average ambient noise level was about 20 dB higher. The receiving equipment was situated at Camden, New South Wales (geomagnetic latitude 42°S), 42 miles from Sydney.

3. OBSERVATIONS

(a) *4·6 kc/s*

From the beginning of observations in June 1958 frequent distinct noise bursts lasting for a few hours and many times stronger than the background were recorded at 4·6 kc/s. Altogether 90 bursts occurred between June and December, those in September being listed in Table 1. The noise amplitude varied between 0·016 and 0·16 μV m^{-1} (c/s)$^{-1}$, corresponding flux densities ranging from 6×10^{-19} to 6×10^{-17} Wm^{-2} (c/s)$^{-1}$.

Table 1. List of Noise Bursts Recorded in September 1958

Date	Local time	Peak field-strength μV^{-1} (c/s)$^{-1}$	Frequency range kc/s
3/9/58	2150-0040	0·02	4–5
4/9/58	0130-0700	0·06	3–5·5
4/9/58	1000-2300	0·04	5–8
			7–10
			3–5
5/9/58	0020-0230	0·04	4–5·5
5/9/58	0830-2340	0·1	3–10
6/9/58	1400-0200	0·2	2–30
7/9/58	1800-2000	0·04	3–7
7/9/58	2230-0040	0·016	3–5
8/9/58	1700-2030	0·18	4–20
9/9/58	2330-0110	0·02	3–10
10/9/58	0350-0510	0·02	3·5–5·5
12/9/58	1900-1915	0·012	No record
17/9/58	0430-0500	0·024	No record
25/9/58	2210-0150	0·04	No record
26/9/58	1800-0100	0·1	No record

A comparison with magnetic data showed that all major magnetic storms were accompanied by extended series of noise bursts or noise storms which sometimes lasted for 48 hr. The latter occurred on or following all days for which the daily *K*-index (Watheroo) exceeded 30 (Fig. 1). On the rare occasions on which the magnetic storm was associated with an aurora visible from Camden, the noise bursts began at about the same time as the aurora. On the average they followed the magnetic sudden commencement after an interval of $6\cdot5\pm2\cdot7$ hr (ten cases). Fig. 2(d) shows the record obtained during the auroral event of 9th July 1958. During three noise storms the amplitude fluctuations followed a reproducible sequence lasting 36 hr with a 27-hr interval between a long burst lasting several hours and a much weaker burst (Fig. 2a, b, c). Two of these records showed remarkable similarity in the minute to minute variations.

Since it is known that in the night airglow in sub-auroral latitudes the red oxygen line (6300 Å) is strongly correlated with magnetic activity[8], it might be expected that the airglow would also correlate with noise bursts. This was found to be so and an examination of Camden records for the 53 nights when both airglow and noise equipment were operating showed that both airglow and noise were recorded during the same hours on 18 nights. On 27 nights neither was recorded and on 6 nights noise was recorded in the absence of airglow. On 2 nights airglow was recorded without noise. The detailed relation between the noise and airglow intensities was not usually close. A strong noise burst could be accompanied by weak airglow and vice versa. However, on three occasions the records showed the same minute to minute variation, strongly suggesting a common cause between the processes originating the two phenomena. Figs. 3(a) and 3(b) show two records of simultaneous noise and airglow. Since it was likely that the noise may have propagated long distances beneath the ionosphere it was not

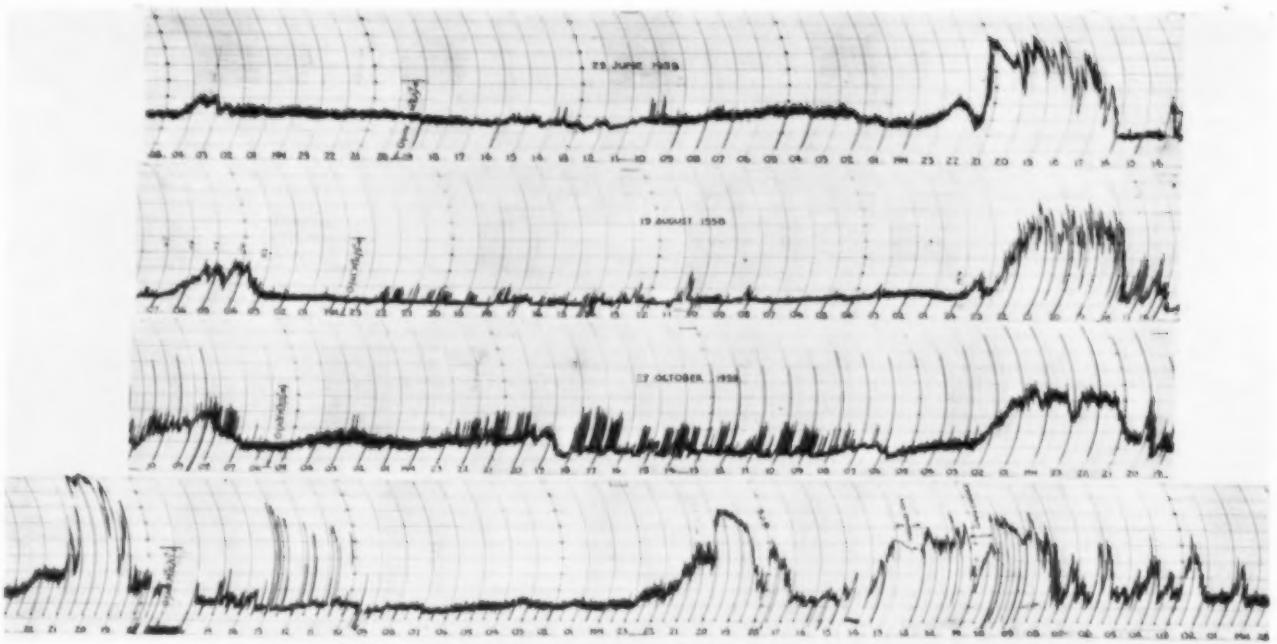

Fig. 2 (a, b, c). Reproducible sequence of amplitude variation observed during periods of magnetic activity.
Fig. 2 (d). Record obtained during the auroral event of July 9, 1959. The aurora was first seen at Camden at 0030 hours on the 9th July.

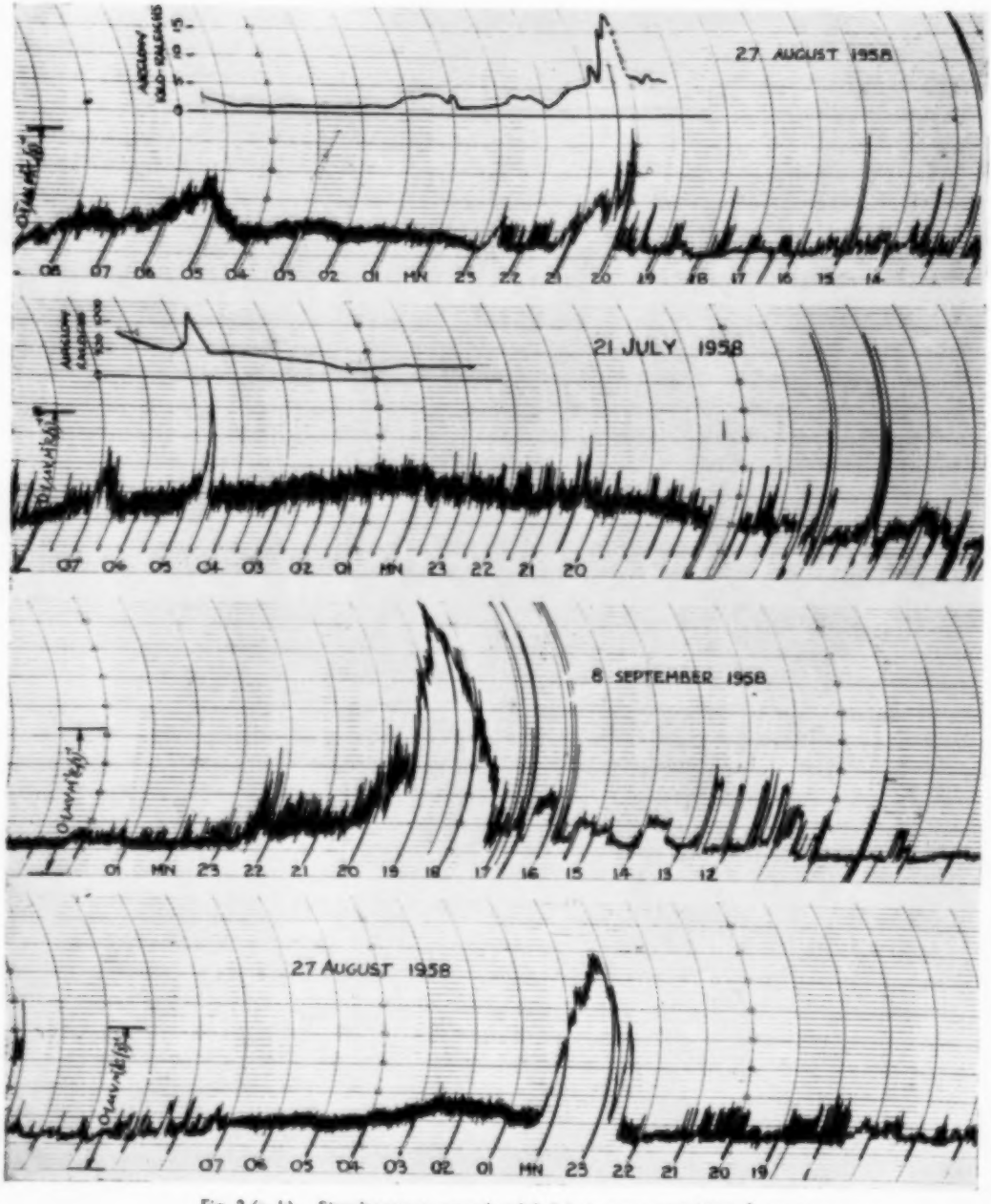

Fig. 3 (a, b). Simultaneous records of 4·6 kc/s noise and 6300 Å airglow.
Fig. 3 (c, d). Typical examples of short duration noise bursts.

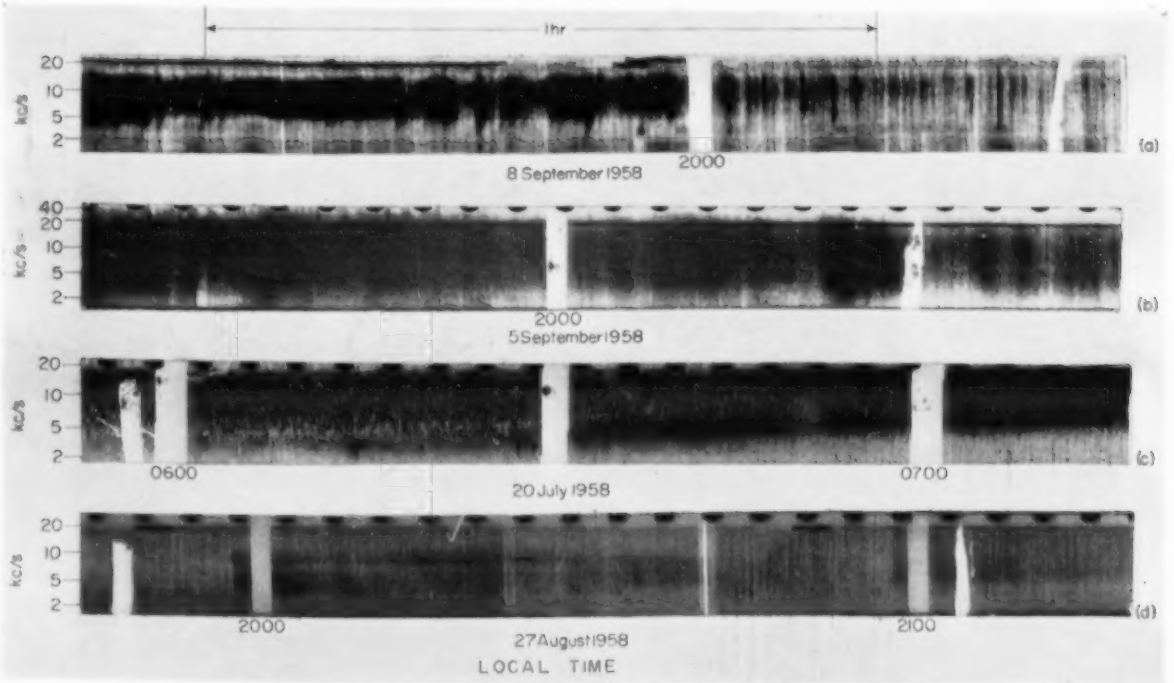

Fig. 6 (a, b). Wide band noise spectra.

Fig. 6 (c). Spectrum with a rising frequency characteristic.

Fig. 6 (d). Spectrum of airglow burst of figure 3 (b).

Reprinted in 2551

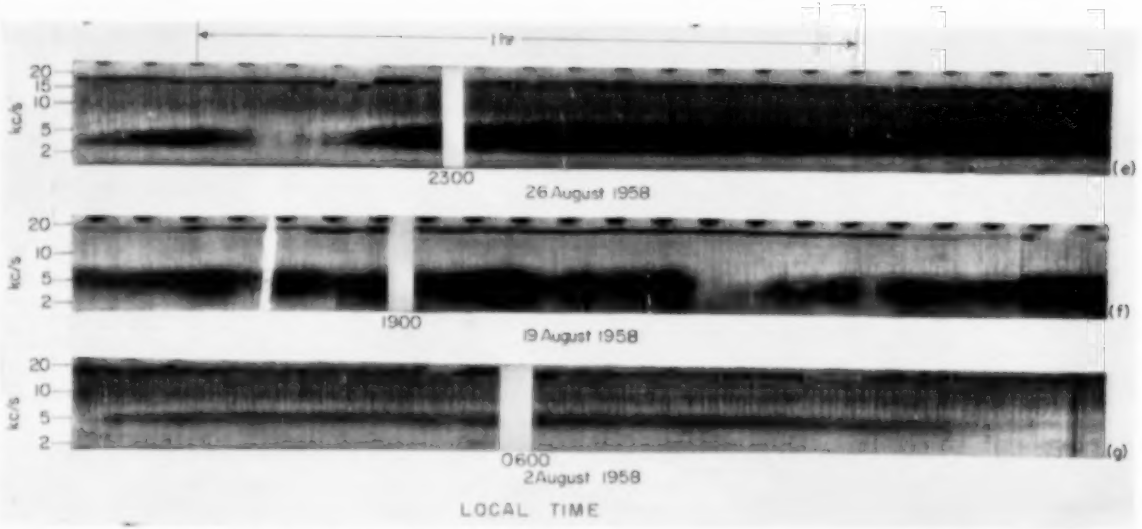

Fig. 6 (e). Spectrum of burst of Fig. 3 (c).

Fig. 6 (f). Typical medium bandwidth spectrum obtained during noise storm.

Fig. 6 (g). Constant frequency narrow bandwidth spectrum.

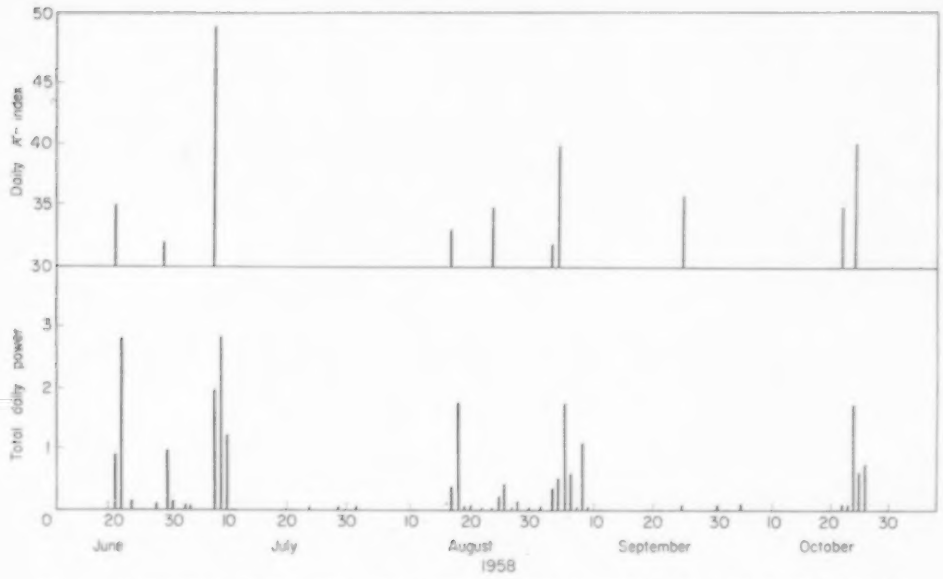

Fig. 1. Comparison of the total noise power received in each 24-hr period with days for which the daily *K*-index (Watheroo) exceeded 30.

surprising to record noise in the absence of airglow.

The majority of noise bursts recorded during the period June to December were not clearly associated with magnetic activity and were of short duration, usually lasting for less than 3 hr (Fig. 4). Figs. 3(c) and 3(d) show two examples. Such examples all occurred at night and only rarely was there more than one burst during any one night. Noise bursts recorded during the daylight hours were always associated with auroral activity. The diurnal variation of the starting time of all bursts is shown in Fig. 5.

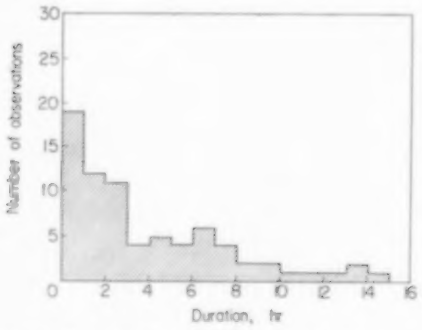

Fig. 4. Duration of individual noise bursts.

During one auroral daylight noise storm the loop antenna was rotated to see if it were possible to determine the direction of arrival of the radiation. The amplitude fell to 0·6 of its maximum value when the null of the loop was bearing 186° magnetic. It may prove possible therefore to locate the region where the radiation is fed into the ionosphere–earth duct.

(b) *Spectrum observations*

Although the spectrum analyser was not so sensitive a detector of noise as the fixed frequency recorder, sufficient spectra were accumulated to show that there were three distinct classes with different frequency limits (Table 2). Wide band bursts extending on the

Table 2:

Number of observations	Centre frequency kc/s	Bandwidth kc/s
5	16	26
7	6·1	4·1
14	4·1	1·7

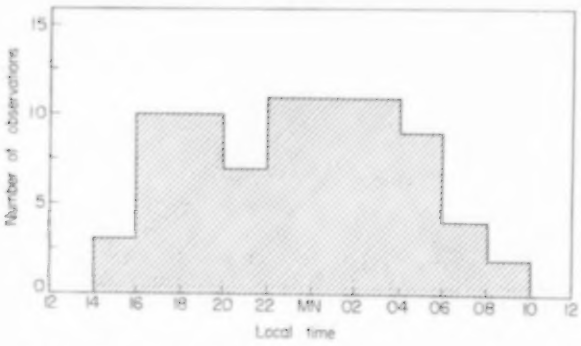

Fig. 5. Diurnal variation of starting time of noise bursts.

average from 2 to 29 kc/s were recorded only during major magnetic storms.

These usually showed large fluctuations in amplitude with an almost constant spectrum and were sometimes followed by a succession of very short isolated wide band bursts (Figs. 6(a) and 6(b)). Figs. 6(c), 6(d) and 6(e) show examples of a second class of spectrum in the range 4–10 kc/s. These also occurred on magnetically active days but were more variable in spectral profile than the wide band bursts. Some showed a gradual increase in frequency and bandwidth with time (Fig. 6c). Another type (Fig. 6d), obtained during the airglow burst of Fig. 3(b), showed several peaks between 5 and 10 kc/s. A significant feature is the almost simultaneous onset of the burst at all frequencies, the 5 kc/s components beginning about 15 sec after the 10 kc/s components. Fig. 6(a) shows the spectrum of the burst of Fig. 3(d). The spectrum of Fig. 6(f) was obtained during the extended auroral noise storm and resembles the wide band spectra in its absence of spectral features. The cloudy appearance of the record is due to large amplitude variations without change in spectral profile

Finally, the most common type of spectrum was of narrow bandwidth, usually 1 or 2 kc/s, centred at about 4 kc/s. The intensity and spectrum remained remarkably constant during bursts of this type (Fig. 6g). On the 4·6 kc/s recorder these narrow bandwidth bursts were brief and show no clear association with magnetic activity.

4. DISCUSSION

With the small amount of information so far available, any discussion of the origin of terrestrial VLF noise bursts must be largely speculative. Nevertheless, over the last few years a considerable effort has been expended on the essentially similar problem of explaining solar radio noise bursts. These are generally believed to originate in the interaction between fast streams of charged particles and the plasma of the solar corona, and suggested mechanisms include plasma oscillations, gyro and synchrotron radiation and Čerenkov radiation[9, 10].

Similarly, one might expect that the interaction between auroral particle streams and the plasma of the outer atmosphere of the earth would also produce radio noise. The gyro frequency and plasma frequency in this region are such that the wave frequency of noise generated by any of the above processes would be in the kilocycle to megacycle range rather than tens or hundreds of megacycles as for the sun. The main difference lies in the position of the observer and an acceptable process for the terrestrial case must provide for the propagation of the radiation inwards through the plasma to the ground instead of outwards through the solar corona. Since the critical penetration frequency of the *F*-region is much higher than the wave frequency of VLF noise, this means that the terrestrial process must produce "extraordinarily" polarised radiation instead of the "ordinary" polarisation favoured in the solar case.

Specifically associated with the X-mode are

the gyro or synchrotron process and the Čerenkov process, the former because it involves the gyration of charged particles round the geomagnetic field lines and the latter because it requires a refractive index greater than unity.

Gyro radiation is synchrotron radiation emitted by non-relativistic particles at the gyro frequency and its harmonics[10]. However, only the fundamental frequency may propagate to the ground without encountering an infinite refractive index at the level where the wave frequency is equal to the gyro frequency. At frequencies of a few kc/s the region of emission of gyro radiation would necessarily be at a distance of several tens of thousands of km from the earth.

Čerenkov radiation, on the other hand, is emitted by charged particles when the resolved component of particle velocity equals the phase velocity in some direction. For the X-mode the refractive index

$$n^2 = 1 + f_0^2/(ff_H \cos\theta - f^2)$$

where f_0 = plasma frequency, f_H = gyro frequency = $eH/(2\pi Mc)$ and f = wave frequency. If θ represents the propagation angle and V the particle velocity, for particles travelling in the direction of the magnetic field the coherence condition for Čerenkov emission is

$$C^2/V^2 = n^2 \cos^2\theta,$$

θ = propagation angle (see text)

V = particle velocity

Where $f \ll f_H$ and $f \ll f_0$, substituting the expression for refractive index gives

$$f = (V^2 f_0^2 \cos\theta)/(C^2 f_H). \qquad (1)$$

A given frequency may be generated by the Čerenkov process under a wide variety of conditions of particle speed, plasma frequency and magnetic field intensity. For example, with a particle speed of the order of 10^4 km/sec, equation (1) may be satisfied at wave frequencies less than 10 kc/sec in most regions of the outer atmosphere. However, the persistence of the observed narrow spectral band at about 4 kc/s over long periods suggests strongly that it is generated in circumstances which do not vary, and for this type of burst, at least, the gyro radiation hypothesis seems more likely. If the geomagnetic field at great distances still approximates that of a dipole, the gyro frequency would be 4 kc/s at about 6 earth radii from the centre of the earth. It is a remarkable coincidence that this is the region where particle streams from the sun should be stopped by the geomagnetic field[11].

If narrow band noise bursts are due to gyro radiation from this region then it would be expected that the noise would be fed into the ionosphere earth duct over a narrow range of geomagnetic latitudes. In the gyro region ($f \sim f_H$) the refractive index varies with propagation angle in such a way that there is no guiding of the ray almost along the field lines as is the case, familiar in whistler propagation, when $f \ll f_H$[1]. Guiding would not become effective until the radiation had penetrated to lower levels with a gyro frequency several times the wave frequency, and the latitude at which the radiation would reach the ground would be expected to be somewhat less than with guiding throughout.

On this hypothesis the high frequency components of the wide bandwidth bursts recorded during strong magnetic activity would be generated at smaller distances from the earth, where the gyro frequency is higher, and would enter the ionosphere at lower latitudes. On the other hand, the minute to minute correlation between airglow and noise intensities on a few occasions suggests that these bursts are not generated in a region remote from the ionosphere. This receives support from the records of the airglow bursts of Figs. 3(b) and 3(a) where the high frequency components began slightly before the lower frequencies. On the gyro hypothesis a group of particles penetrating the exosphere could be expected to excite the lower frequency components first. If these bursts are generated by the Čerenkov process, there would not be the same association between latitude and frequency as for the gyro process.

Another phenomenon thought to be related to VLF noise is "dawn chorus" which usually

takes the form of rapidly rising whistles in the 5 to 10 kc/s band, the time scale being of the order of tenths of a second.

Gallet[5] has suggested that discrete, well spaced groups of charged particles entering the ionosphere may produce dawn chorus by a process analogous to the generation of radio noise in a travelling wave tube when the particle velocity equals the phase velocity of propagation. In a three-dimensional medium this is the same as the Čerenkov process[12] and his theory predicts well the rapidly rising frequency characteristic of dawn chorus. Randomly spaced groups of particles with a spacing less than a wavelength (about 6 km) would be expected to produce dawn chorus, without separation between the individual bursts, which would be recorded on the equipment described here as medium bandwidth VLF noise.

The 36 hr sequence of amplitude fluctuations illustrated in Figs. 3(a), 3(b) and 3(c) implies that the process of interaction between a solar stream and the exosphere may on occasions be reproducible to an extent remarkable in such a large scale phenomenon. However, to interpret the detailed amplitude fluctuations during the sequence as time variations may be misleading since they could be caused, at least in part, by the rotation of the observer with the earth past an interaction region almost constant in position in Right Ascension. The observed 27-hr interval between the two bursts would then be produced mainly by the 24-hr period of rotation necessary to bring the observer back to the vicinity of the interaction region. It would be possible to test this idea with simultaneous observations at different longitudes.

The observed intensity of the noise—about 10^{-16}W m^{-2} (c/s)$^{-1}$—is several orders of magnitude greater than would be expected on a basis of Čerenkov emission[4] or gyro emission by single particles. This discrepancy is not considered serious however since coherent emission by closely spaced groups of particles[13] could increase the intensity to the observed levels.

REFERENCES

1. L. R. O. Storey, *Phil. Trans. Roy. Soc.* A **246**, 113 (1954).
2. R. A. Helliwell, *Low Frequency Propagation Studies*, part I. Stanford University (1956).
3. M. J. Watts, *J. Geophys. Res.* **62**, 199 (1957).
4. G. R. Ellis, *J. Atmos. Terr. Phys.* **10**, 302 (1957).
5. R. M. Gallet and R. A. Helliwell, *VLF Symposium*, Boulder, Colorado, 23–25 Jan. 1957, Paper 20 (1957).
6. G. Reber and G. R. Ellis, *J. Geophys. Res.* **61**, 1 (1956).
7. L. R. O. Storey, *Radio Physics Laboratory Report*, Ottawa 23-4-3 (1957).
8. R. A. Duncan, private communication.
9. L. Marshall, *Astrophys. J.* **124**, 469 (1956).
10. R. Q. Twiss and J. A. Roberts, *Aust. J. Phys.* **11**, 424 (1958).
11. D. F. Martyn, *Nature, Lond.* **167**, 92 (1951).
12. J. R. Pierce, *J. Appl. Phys.* **26**, 627 (1955).
13. J. V. Jelly, *Cerenkov Radiation and its Applications*, p 45. Pergamon Press, London (1958).

Planet. Space Sci. Pergamon Press 1959. Vol. 1, pp. 259-264. Printed in Great Britain.

ATMOSPHERIC DENSITIES FROM SATELLITES AND ROCKET OBSERVATION

K. W. CHAMPION* and R. A. MINZNER†

(*Received* 16 *April* 1959)

Abstract—Atmospheric densities deduced from high altitude rocket flights have a large variability of which a large percentage is undoubtedly due to measurement errors. Prior to the IGY, the available density data gave reasonable support to the ARDC Model Atmosphere. Satellite data which at first appeared to be inconsistent with rocket data are now seen to be continuous with the average of presently available rocket derived densities. The current data suggest the revision of the 1956 ARDC Model to lower densities near 100 km altitude and demand higher densities above 160 km (a twenty fold increase at 500 km). The revised altitude distribution of density implies (1) lower temperatures at 90 km and (2) temperature-altitude gradients between 105 and 160 km (two times the molecular-scale-temperature gradient of the 1956 ARDC Model). Density-altitude and temperature-altitude profiles for a revised model atmosphere are discussed.

1. INTRODUCTION

The first atmospheric density data from observations on Russian satellites suggested that there might be a discrepancy between densities deduced from satellite data and those measured by rockets. Thus, results of rocket measurements of densities have been investigated to determine their relative accuracy and likely errors. Also, a study has been made of the assumptions involved in calculating atmospheric density from satellite orbit data. In addition, densities have been calculated from more recent orbital data of all satellites launched prior to September 1958. The total atmospheric density data as of the above date suggest the need for a revision of current atmospheric models. A 1959 version of the ARDC Model Atmosphere has been defined and its density–altitude profile computed. An extension of this model to 5 earth's radii is in reasonable agreement with Chapman's solar-corona model.

* Physics Department, Tufts University, Medford, Massachusetts, and Geophysics Research Directorate, Air Force Cambridge Research Center, Bedford, Massachusetts.

† Work initiated while at Geophysics Research Directorate, Air Force Cambridge Research Center, Bedford, Mass. Mr. Minzner is presently with Geophysics Corporation of America, 700 Commonwealth Avenue, Boston 15, Mass.

2. ROCKET DATA

The results of rocket measurements above 170 km′ are considered first. Although a number of rockets have been fired to measure densities at these altitudes, data has, so far, been published for relatively few flights. An early experiment by Horowitz and LaGow[7] at White Sands (11.00 a.m., 7 August 1951) used a rocket instrumented with a Phillips ionization gauge. Unfortunately, the amplitude of the spin-modulated density-measuring signal during much of the flight was of the order of 1 per cent of a rapidly changing total gauge signal, resulting in low accuracy. The mean values of up- and down-leg data can be seen in Fig. 1. The experimenters' estimate of error is a factor of two.

The results of four high-altitude rocket firings at Fort Churchill, Canada, are also shown. One of these (11.21 p.m., 20 November 1956) reported by Townsend and Meadows[21] was a winter night (WN) flight of a Bennet type mass spectrometer. The results of this flight were found to be reliable at lower altitudes, but near 200 standard geopotential kilometers (km′), the experimenters' own estimate of error is a factor of three, as indicated in the figure. In addition, the mass spectrometer did not record the density of either hydrogen or helium, and since the flight was made during an aurora,

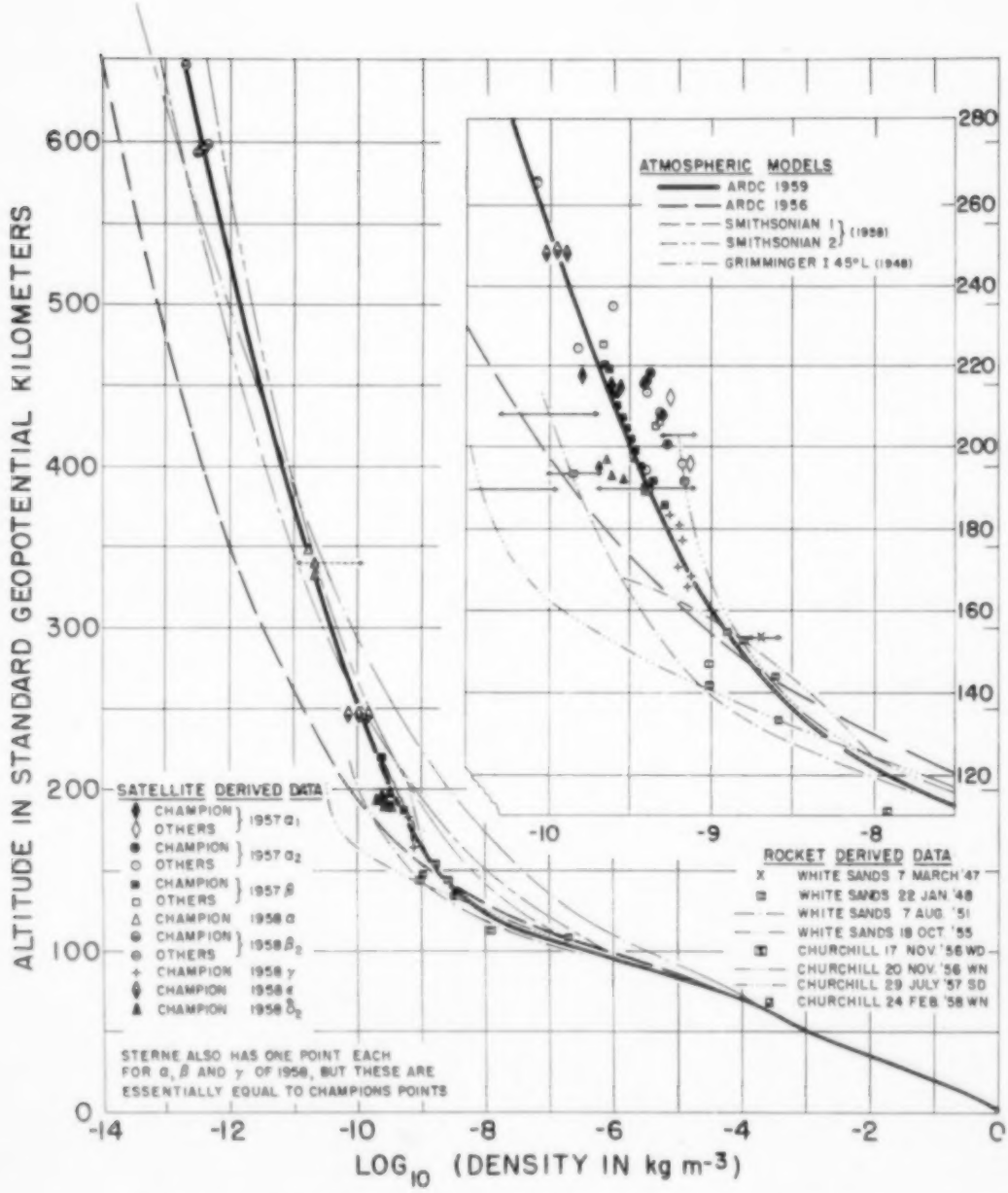
ALTITUDE IN STANDARD GEOPOTENTIAL KILOMETERS
LOG10 (DENSITY IN kg m-3)
ATMOSPHERIC MODELS
ARDC 1959
ARDC 1956
SMITHSONIAN 1 } (1958)
SMITHSONIAN 2 }
GRIMMINGER I 45°L (1948)
SATELLITE DERIVED DATA
CHAMPION } 1957 σ1
OTHERS }
CHAMPION } 1957 σ2
OTHERS }
CHAMPION } 1957 β
OTHERS }
CHAMPION 1958 α
CHAMPION } 1958 β2
OTHERS }
CHAMPION 1958 γ
CHAMPION 1958 ε
CHAMPION 1958 σ2
STERNE ALSO HAS ONE POINT EACH FOR α, β AND γ OF 1958, BUT THESE ARE ESSENTIALLY EQUAL TO CHAMPIONS POINTS
ROCKET DERIVED DATA
WHITE SANDS 7 MARCH '47
WHITE SANDS 22 JAN '48
WHITE SANDS 7 AUG. '51
WHITE SANDS 18 OCT. '55
CHURCHILL 17 NOV. '56 WD
CHURCHILL 20 NOV. '56 WN
CHURCHILL 29 JULY '57 SD
CHURCHILL 24 FEB. '58 WN

Fig. 1. Atmospheric density data supporting the ARDC model atmosphere 1959.

the proportion of these gases (and, in particular, protons) at higher altitudes may not have been negligible. The low densities above 140 km′ should, therefore, not be considered too seriously. The other three high altitude firings, in which the instrumentation consisted of Phillips and other types of gauges, were reported by LaGow, Horowitz and Ainsworth[8]. The first of these occurred during a winter day (WD) (11.00 a.m., 17 November 1956) but the rocket tumbled badly, and the error in measurement may be a factor of two or more. Only one data point has been reported for that rocket flight to date. The second of these flights (4.00 p.m., 29 July 1958) occurred during a summer day (SD). The rocket attitude and telemeter data of this flight were both excellent. The graph shows that this measurement gave the highest density recorded on any rocket flight at these altitudes. The error in the density measurement may be about ± 30 per cent. The preliminary results from the third one of these flights, fired on a winter night (1.00 a.m., 24 February 1958) shows an error of about ± 50 per cent. Neglecting the unreliable data of 20 November 1956, the average of rocket data near 200 km′ is about 5 times higher than the ARDC Model 1956[10], and suggests an upward revision of the density of the Model in this region.

Densities from three earlier rocket flights are considered along with densities from the more recent flights in the 110 to 170 km′ region and these data are also shown in Fig. 1. Byram, Chubb and Friedman[1] reported densities derived from X-ray photon counter data obtained during an aerobee flight on 18 October 1955, 3.50 p.m. at White Sands Proving Grounds. These densities tend to be rather high, especially between 140 and 150 km′ and have an unusual altitude variation. The scatter in the X-ray counting rate versus altitude, however, suggests errors of more than a factor of two in these densities. Other considerations may also increase the error of these data. The other two flights are reported by Havens, Koll and LaGow[6], and together yielded nine scattered density points between 109 and 158 km′ from Phillips gauge measurements on *V*-2 rockets, one point from the flight of 7 March 1947 and eight points from the flight of 22 January 1948. No accuracy is listed for these data*, but they are probably subject to considerable error due to a lack of altitude correction and the relatively crude techniques used at that time.

The rocket flights of 7 August 1951, 20 November 1956 and 29 July 1957 previously discussed in regard to high altitude densities also provide data in this lower altitude region, and while the accuracy of some of these data may be poor at the higher altitudes, the accuracy should improve at lower altitudes. At 200 km′ altitude, the data show a spread of about a factor of twenty. A large part of this variation is probably due to inaccuracy of the measurements at this altitude. Between 120 and 130 km′, however, the spread of these data is within a factor of two and, together with the other rocket density data in this altitude region, fall considerably below the ARDC Model Atmosphere 1956, suggesting the need for lowering of the density of the ARDC Model in this region.

3. SATELLITE DATA

Densities computed from satellite observations are shown in Fig. 1. These consist of those values computed by one of the authors (Champion) plus those published values of other authors available at the end of 1958. The latter consist of data presented by Groves[4], Harris and Jastrow[5], Mullard Observatory[11], Priester *et al.*[12], Royal Aircraft Establishment[13], Schilling and Whitney[14], Schilling *et al.*[15], Sterne[16] and, finally, Sterne and Schilling[20].

The calculations reported herein have been made using the equation developed by Sterne and the orbital data supplied by Air Force Cambridge Research Center Project "Space Track", Project "Vanguard" and Smithsonian Astrophysical Observatory. Sterne's equation relates the density to the rates of change of

* The pressures from which these densities are derived "may be in error by a factor of two" according to Havens *et al.*[6] These authors also show a single point at about 109 km for a flight of 21 November 1950, but no further mention of it is made in their paper and it is not given in Fig. 1 of this paper.

period, orbital parameters and physical data of the satellite. The physical data are: A, the effective cross-sectional area; M, the mass; and C_D, the drag coefficient. There is some spread of the computed densities, but all values derived from satellites, extending from 170 to 650 km′, are higher than densities of the ARDC Model Atmosphere at corresponding altitudes. The departure is small at 170 km′, but increases with increasing altitude.

It is of interest to consider both the assumptions involved in the satellite density calculations, and also the probable errors of the results. Most previous investigators had used one-quarter of the total surface area for the effective cross-sectional area presented by a satellite in flight. This is accurate for a sphere, and approximate for other shaped objects if randomly oriented. The orientation of a non-stabilized satellite over a long enough period of time will probably not deviate very much from random. Neither a cylinder spinning about its axis nor a stabilized satellite will be randomly oriented, however, and the effective cross-sections of such bodies may differ by as much as a factor of ten from the value used above. The appropriate range of densities obtained from Explorer I (1958 α) data, for the limiting cases of the satellite moving side-on (lower density) and end-on (higher density) near perigee, is indicated by the horizontal dashed arrow on Fig. 1. The range for the other Explorer satellites (1958 γ and 1958 ε) is the same, for Sputnik II and III (1957 β and 1958 δ1) it is somewhat smaller.

The value 2 used for the drag coefficient C_D was also investigated. Values of C_D were calculated for various geometric figures, including cones, cylinders and truncated cones, either with fixed or random orientations. The exact values require a correction in the range 20 per cent to 25 per cent to the value of AC_D for the Explorers and Sputnik II.

There is some doubt about the densities derived from orbital data of Sputnik I rocket (1957 α1) and Sputnik II. This results from the fact that the values of M/A have not been published for these satellites. The data on Fig. 1 have been calculated with values of M/A chosen so that the densities agree with those obtained from Sputnik I data. However, data from Sputnik III and its rocket suggest that the correct value of M/A for the rockets may be as low as half this value. If this is so, the densities for 1957 α1 and 1957 β1 should be reduced by a factor of two. This then raises the paradox that Sputnik I and its rocket give different densities. A partial explanation of this paradox may be that the sheath of charge around a satellite has a given thickness at a specified altitude, and that its effect (on drag due to ions) is proportionally greater with smaller satellites, giving an apparently larger density. This could also apply to Vanguard I (1958 β2).

The possibility of seasonal variation of density has been investigated by plotting the satellite perigee latitudes as a function of time and comparing the density points. Preliminary results suggest that densities calculated from satellite data may be lower in the summer than in the winter at these altitudes. This statement is very tentative as later data may not confirm it, or the apparent difference in density may be due to some other reason, for example, variation in the amount of ionization of the atmosphere or in the photoelectric effect on the satellite. It is considered probable, in any case, that a significant percentage of the atmospheric gas at high altitudes is in the form of ions.

4. ATMOSPHERIC MODEL

Neglecting the possible temporal or latitude variations, the estimated mean values of satellite-derived densities tend to lie on a smooth curve, shown in Fig. 1, starting at a point approximately 20 times higher than the 1956 ARDC Model at 600 km′, gradually coming closer to that model with decreasing altitude and crossing it at about 153 km′. Between 170 and 200 km′, these satellite-derived densities agree well with the mean value of rocket-derived data. The extrapolation of this curve below 153 km′ again departs from the ARDC Model 1956 but agrees well with rocket data between 130 and 140 km′ which, in turn, suggest a rapid change in slope of the mean value of the density curve in the

region around 125 km′, bringing the curve smoothly back to the ARDC Model below 90 km′.

The apparent inconsistencies[9, 14, 17] between satellite and rocket data suggested by the first satellite densities from Sputnik I and II orbits and the rocket data available at the end of 1958, have essentially vanished in the light of the additional rocket and satellite data. The new concept of values of upper atmosphere densities brought about by these data have made it mandatory to revise the 1956 ARDC Model Atmosphere. This has been accomplished (by Minzner) through the computation of a new molecular-scale-temperature function of geopotential altitude (T_M of H) consistent with the observed densities. This molecular-scale-temperature function was deduced by numerical methods starting with the 1956 ARDC Model temperature at 53 km, well within the altitude range of good agreement between computed and observed densities. A series of molecular-scale-temperature gradients were selected intuitively each operating upward from this initial point, and corresponding densities were computed for reasonable altitude increments. That gradient yielding the best fit to the data was adopted up to such an altitude where the data demanded a change in gradient. Starting at a point slightly below this altitude, the trial process was repeated. Such a method is necessary, for, unlike the case of the temperature–pressure–altitude relationship, the molecular-scale-temperature (T_M) may not be explicitly determined from the slope of the density altitude function; a first approximation of the value of T_M may, however, be so determined.

Starting at 53 km′ and upward, the value of the negative gradient of T_M is increased from that of the 1956 Model so that the second minimum in the T_M of H function between 79 and 90 km′ has a value of about 165·7°K instead of 196·86°K. This lower value of T_M is necessary to produce the 50 per cent reduction in density in the 105 km′ region from that of the ARDC Model 1956 as required by existing rocket data. The decrease in density from that of the ARDC Model 1956 is very small at the lower altitudes being only 2 per cent at 80 km′. Above about 105 km′ the difference in density between the two models decreases with altitude as the density curve of the new model rapidly moves toward and crosses the 1956 Model at about 153 km′. This rapid change in the slope of the new log ρ versus H curve dictates a doubling of the value of dT_M/dH to 20°K/km′ between 105 and 160 km′, followed by a rapid reduction of this value to 3·5°K/km′ above 200 km′.

An extension of this model from 600 km′ to 5 earth's radii (about 32,000 geometric kilometers) using values of dT_M/dH consistent with a constant value of dT/dZ equal to 3·18°K/km and mean molecular weight decreasing to 1 yields values of mass density which are in good agreement with Chapman's solar-corona values[2] at this distance from the earth. Even if these values should prove to be in agreement with future observations, however, it is unlikely that the hydrostatic equation and related temperatures alone will explain the mechanisms producing such densities.

The heavy solid line of the Fig. 2 depicts the density–altitude profile of the 1959 ARDC Model Atmosphere. This is compared with the density curves of the ARDC Model 1956, the Smithsonian Models 1 and 2[19], and the Grimminger[3] Model 1 45°L, in the same figure.

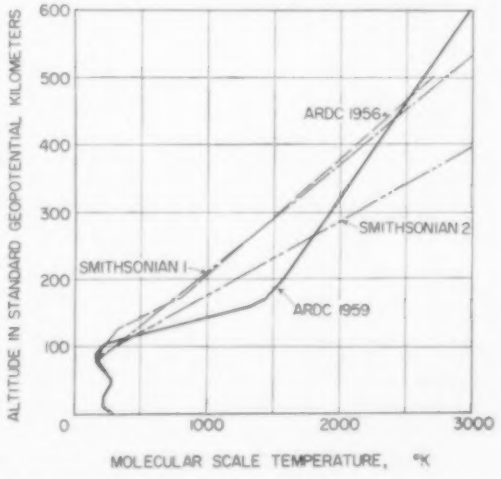

Fig. 2. Comparison of temperature–altitude functions for various atmospheric models.

The Grimminger Model was calculated theoretically before any rocket data were available and yielded densities about 25 times too high at 150 km′ compared with rocket data. The definition of the upper half of the 1956 ARDC Model was determined from theoretical considerations before there were any satellite density data and at a time when the only published rocket density data above 100 km′ consisted of the ten scattered density points.

These were from rocket flights of 7 March 1947, 27 January 1948 and 21 November 1950 between the altitudes of 109 and 158 km′, plus one density point at 219 km′ from the flight of 7 August 1951. The densities of the ARDC Model 1956 appear to be satisfactory at 150 km′, but are about one twentieth of the observed values at 500 km′ and 2 times the observed values near 100 km′. The Smithsonian density models were devised to pass through early data points obtained from Sputnik I and II and correspond to two different assumed single temperature gradients. The densities of these models are reasonably accurate above 200 km′, but their authors admit that these models do not account for atmospheric features between 100 and 170 km′ and are obviously unsuitable in this region.

5. CONCLUSIONS

Satellite and rocket derived density data are in agreement with each other. The value of $d \log \rho / dH$ decreases much more rapidly above 105 km than previously expected. The proposed 1959 ARDC Model, which departs from the 1956 Model above 53 km′, accounts for density data available at the beginning of 1959. The related molecular-scale-temperature function suggests a great warming region between 105 and 170 km′. Other temperature-altitude functions, differing slightly in detail from the one selected, might have been used without seriously changing the computed density curve. The major aspects, however, of lower temperatures in the 90 km′ region and higher gradients with correspondingly higher temperatures in the 105 to 160 km′ regions are mandatory gross aspects of the new T_M of H curve as compared with that of the 1956 model.

REFERENCES

1. E. T. Byram, T. A. Chubb and H. Friedman, pp. 211–16 in *The Threshold of Space* (M. Zelikoff, editor). Pergamon Press, New York (1956).
2. S. Chapman, *Smithson. Contrib. Astrophys.* **2**, 1–12 (1957).
3. G. Grimminger, *Analysis of Temperature, Pressure and Density of the Atmosphere Extending to Extreme Altitudes*. RAND Corporation, Santa Monica (1948).
4. G. V. Groves, *Nature, Lond.* **181**, 1055 (1958).
5. I. Harris and R. Jastrow, *Science* **127**, 471 (1958).
6. R. J. Havens, R. T. Koll and H. E. LaGow, *J. Geophys. Res.* **57**, 59–72 (1952).
7. R. Horowitz and H. E. LaGow, *J. Geophys. Res.* **62**, 57–78 (1957).
8. H. E. LaGow, R. Horowitz and J. Arnsworth, *IGY Rocket Rep. Ser.* No. 1, 38–46 (1958).
9. R. A. Minzner, *Trans. Amer. Geophys. Un.* **39**, 525 (abstract) (1958).
10. R. A. Minzner and W. S. Ripley, *The ARDC Model Atmosphere 1956*. ASTIA Document 110233 (1956).
11. Mullard Radio Astronomy Observatory Staff, Cambridge, *Nature, Lond.* **180**, 879 (1957).
12. W. Priester, H. G. Bennewitz and P. Lengruesser. *Radiobeobachtungen des ersten kuenstlichen Erdsatelliten*. Westdeustcher Verlag, Koeln u. Opladen (1958).
13. Royal Aircraft Establishment Staff, Farnborough, *Nature, Lond.* **180**, 937 (1957).
14. G. F. Schilling and C. A. Whitney, *Spec. Rep. Smithson. Astrophys. Obs., Cambridge* No. 18, 13–22 (1958).
15. G. F. Schilling, C. A. Whitney and B. M. Folkart, *Spec. Rep. Smithson. Astrophys. Obs., Cambridge* No. 14, 32–34 (1957).
16. T. E. Sterne, *Spec. Rep. Smithson. Astrophys. Obs., Cambridge* No. 11, 18–22 (1958).
17. T. E. Sterne, *Physics of Fluids* **1**, 165–170 (1958).
18. T. E. Sterne, *Science* **127**, 1245 (1958).
19. T. E. Sterne, B. M. Folkart and G. F. Schilling, *Spec. Rep. Smithson. Astrophys. Obs., Cambridge* No. 7 (1957). Reprinted in *Smithson. Contrib. Astrophys.* 275–280 (1958).
20. T. E. Sterne and G. F. Schilling, *Spec. Rep. Smithson. Astrophys. Obs., Cambridge* No. 3 (1957). Reprinted in *Smithson. Contrib. Astrophys.* 207–210 (1958).
21. J. W. Townsend, Jr. and E. B. Meadows, *Ann. Géophys.* **14**, 117 (1958).

Planet. Space Sci. Pergamon Press 1959. Vol. 1, pp. 265–276. Printed in Great Britain.

CHARACTERISTICS OF THE RADIATION EMERGING FROM THE TOP OF A RAYLEIGH ATMOSPHERE—I

INTENSITY AND POLARIZATION

K. L. COULSON*

Meteorology Department of the University of California, Los Angeles

(*Received* 13 *March* 1959)

Abstract—S. Chandrasekhar's solution of the equation of radiative transfer in a medium scattering according to Rayleigh's law has been used for an extensive series of computations of the scattered and diffusely reflected radiation directed outward from the top of a plane stratified model of the atmosphere. The results are discussed in two parts, the first of which deals with the intensity, degree of polarization, plane of polarization and the neutral points of the scattered and diffusely reflected radiation. Part II (see following article) will be a discussion of the upward flux, integrated over the hemisphere, as a function of wavelength of the incident radiation, and of the albedo of the atmospheric model for an energy distribution of the incident light similar to that of the extra-terrestrial solar spectrum. The results are compared with similar quantities for the diffusely scattered radiation from the sunlit sky.

1. INTRODUCTION

The exact solution of the equation of radiative transfer in a medium scattering according to Rayleigh's law, as developed by S. Chandrasekhar[1, 2], has been used to compute the characteristics of the scattered and diffusely reflected radiation directed outward from the top of a model atmosphere, the model corresponding in many respects to the sunlit portion of the earth's atmosphere. All of the Stokes parameters, by which the radiation is described completely, have been determined as a function of sun elevation, depression and azimuth of the observed direction, optical thickness of the medium and reflectivity of the underlying ground surface. These Stokes parameters were then used to compute the total relative intensity and the entire polarization field of the upward radiation, the latter consisting of the degree of polarization, the orientation of the plane of polarization and the behavior of the neutral points (shown for the first time to exist in the upward radiation, as they were already known to exist in skylight). By introducing the known spectral energy distribution of solar radiation, the absolute intensity as a function of wavelength was determined for various values of sun elevation, direction of observation and surface reflectivity. Further, a double integration with respect to azimuth and depression angles gave the upward flux for any wavelength interval, and an additional integration with respect to wavelength gave the total upward flux of the scattered and diffusely reflected solar radiation. Finally, approximation methods were used to determine the earth's planetary albedo due to scattering in the clear atmosphere, and standard colorimetric methods were used to determine the dominant wavelength and excitation purity of the scattered light.

It has been necessary to divide the discussion of these data into two parts, Part I to deal with the relative intensity and the field of polarization, and Part II (see this volume, p. 277) to discuss the other features mentioned above. The most important results included in Part I are thought to be the following:

(1) The basic primary Rayleigh scattering pattern for a single particle is evident throughout the results, but the additional effects of multiple scattering and attenuation are of major importance for all but the smallest optical thicknesses.

* Presently affiliated with The Stanford Research Institute, Menlo Park, California.

(2) The intensity of the scattered light generally increases with increasing optical thickness, increasing sun elevation and decreasing angular depression of the observed direction.

(3) The surface reflectivity is much more important in determining the radiation emerging from the top of the atmosphere than it is for the skylight.

(4) The degree of linear polarization of the scattered light is of about the same magnitude as that of skylight, and the plane of polarization is quite analogous to that of the skylight.

(5) Three neutral points occur in the upward radiation. Their positions and behavior are analogous to those of the Babinet, Brewster and Arago points of skylight.

2. STOKES PARAMETERS FOR THE MODEL

The problem is the following: Parallel neutral radiation of net flux πF per unit time, unit frequency interval and unit area, normal to its direction of propagation, is assumed incident on the top of a plane parallel Rayleigh atmosphere of finite optical thickness*. The type of source is immaterial, but we assume it to be the sun. The atmosphere is assumed to be bounded at the top by a perfect vacuum and at the bottom by a surface which is uniform and of infinite extent in the horizontal. The reflectivity of this ground surface is assumed to have an arbitrary fixed value A, which satisfies the condition $0 \leqslant A \leqslant 1$. If $A=0$, the ground is a perfect absorber and all radiation incident on it is removed from the system. If $A \neq 0$, a part of the radiation incident on the ground is returned to the system. It is assumed that this radiation is reflected according to Lambert's law, i.e. the reflected radiation is completely unpolarized and of uniform intensity in the outward hemisphere. It is required to find the intensity and state of polarization of the radiation emerging from the top of this model atmosphere.

The direction of propagation of the incident light is defined by the zenith angle θ_0 and azimuth φ_0 of the sun; for the light emerging from the top of the atmosphere the corresponding coordinates are the nadir angle θ and the azimuth taken with respect to that of the sun, $\varphi_0 - \varphi$. For convenience, $\mu_0 = \cos\theta_0$ and $\mu = \cos\theta$ are used as the directional parameters, instead of θ_0 and θ.

For no ground reflection ($A=0$), the intensity components I_l and I_r, parallel and perpendicular, respectively, to the vertical plane in the azimuth of the observed point, and the Stokes parameter U were computed from the expressions†:

$$I_l(\tau, \mu, \varphi, \mu_0, \varphi_0) = \frac{3}{32}\frac{\mu_0 F}{\mu_0+\mu}\{\psi(\mu)[\psi(\mu_0)+\chi(\mu_0)] + 2\varphi(\mu)[\varphi(\mu_0)+\zeta(\mu_0)] - \xi(\mu)[\xi(\mu_0)+\sigma(\mu_0)] - 2\eta(\mu)[\eta(\mu_0)+\theta(\mu_0)] - 4\mu\mu_0(1-\mu^2)^{\frac{1}{2}}(1-\mu_0^2)^{\frac{1}{2}} \times [x^{(1)}(\mu)\,x^{(1)}(\mu_0) - y^{(1)}(\mu)\,y^{(1)}(\mu_0)]\cos(\varphi_0-\varphi) - \mu^2(1-\mu_0^2)[x^{(2)}(\mu)\,x^{(2)}(\mu_0) - y^{(2)}(\mu)\,y^{(2)}(\mu_0)] \cos 2(\varphi_0-\varphi)\}. \quad (1)$$

$$I_r(\tau, \mu, \varphi, \mu_0, \varphi_0) = \frac{3}{32}\frac{\mu_0 F}{\mu_0+\mu}\{\chi(\mu)[\psi(\mu_0)+\chi(\mu_0)] + 2\zeta(\mu)[\varphi(\mu_0)+\zeta(\mu_0)] - \sigma(\mu)[\xi(\mu_0)+\sigma(\mu_0)] - 2\theta(\mu)[\eta(\mu_0)+\theta(\mu_0)] + (1-\mu_0^2)[x^{(2)}(\mu)\,x^{(2)}(\mu_0) - y^{(2)}(\mu)\,y^{(2)}(\mu_0)]\cos 2(\varphi_0-\varphi)\}. \quad (2)$$

$$U(\tau, \mu, \varphi, \mu_0, \varphi_0) = \frac{3}{32}\frac{\mu_0 F}{\mu_0+\mu}\{4\mu_0(1-\mu^2)^{\frac{1}{2}}(1-\mu_0^2)^{\frac{1}{2}} \times [x^{(1)}(\mu)\,x^{(1)}(\mu_0) - y^{(1)}(\mu)\,y^{(1)}(\mu_0)]\sin(\varphi_0-\varphi) + 2\mu(1-\mu_0^2)[x^{(2)}(\mu)\,x^{(2)}(\mu_0) - y^{(2)}(\mu)\,y^{(2)}(\mu_0)] \times \sin 2(\varphi_0-\varphi)\}. \quad (3)$$

The quantities $x^{(i)}$ and $y^{(i)}$, $(i=1, 2, 3, 4)$ are solutions of a pair of non-linear integral equations developed by Chandrasekhar. Two pairs of these so-called x and y functions appear explicitly in the above equations. The other two pairs combine with a set of constants to form the eight functions $\psi(\mu)$, $\varphi(\mu)$, $\chi(\mu)$, $\zeta(\mu)$, $\xi(\mu)$, $\eta(\mu)$, $\sigma(\mu)$, $\theta(\mu)$ (the "scattering functions"). For a given optical thickness, both the x and y functions and the scattering functions depend only on μ or μ_0.

If the underlying surface is assumed to reflect, by Lambert's law of reflection, a given fixed fraction A of the radiation on it, then the

* For a definition of optical thickness see p. 12 of Chandrasekhar[2].

† The fourth Stokes parameter, V, vanishes in a Rayleigh atmosphere.

intensities I_e and I_r are augmented, respectively, by the additional intensities

$$I_e^*(\tau, \mu, \mu_0) = \tfrac{1}{4} \frac{A\mu_0}{1 - A\bar{s}} \gamma_e(\mu) [\gamma_e(\mu_0) + \gamma_r(\mu_0)]. \quad (4)$$

$$I_r^*(\tau, \mu, \mu_0) = \tfrac{1}{4} \frac{A\mu_0}{1 - A\bar{s}} \gamma_r(\mu) [\gamma_r(\mu_0) + \gamma_r(\mu_0)]. \quad (5)$$

Since the reflected radiation is assumed to be isotropic, the azimuth does not enter (4) and (5). The quantity $\bar{s}$ is a function only of the optical thickness, and the $\gamma_i[i = e, r]$ are functions of both the optical thickness and the zenith angle.

The functions in the above expressions are available in tabular form, and were obtained for the present work from Sekera and Ashburn[12] for optical thickness $\tau = 0{\cdot}02$, $0{\cdot}05$, $0{\cdot}10$; from Sekera and Blanch[13] for $\tau = 0{\cdot}15$, $0{\cdot}25$, $1{\cdot}0$; and from Chandrasekhar and Elbert[2] for $\tau = 0{\cdot}50$.

3. RELATIVE INTENSITY

3.1. *Intensity in sun's vertical*

In the following the relative intensity will be taken to mean the total intensity $I = I_e + I_r$ of the radiation emerging from the top of the model atmosphere, with the incident flux assumed to have the value π, F being taken as unity.

The general effect of optical thickness is seen in the curves of Fig. 1, in which the intensity is plotted as a function of direction in the sun's vertical for three values of optical thickness. The increase of intensity near the horizons is a fairly characteristic feature of the radiation field, although exceptions do occur, as will be seen in a later diagram. The intensity increases with an increase of optical thickness, but not as rapidly as does the number of scattering centers, which is the same as saying that the average scattering efficiency decreases with increasing optical thickness. This is easily explained by considering the attenuation of the incident and scattered radiation during their traverse of the scattering medium. A particle is, on the average, illuminated by less intense incident radiation for large optical thickness[7], and the scattered radiation is attenuated more before emerging from the atmosphere.

It is interesting to note the relative importance of multiple scattering in the intensity for the different optical thicknesses. The intensity

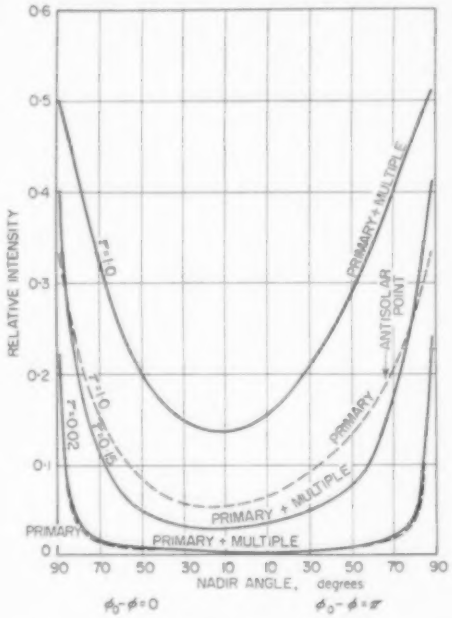

Fig. 1. Relative intensity for three different values of optical thickness as a function of direction in the sun's vertical. Dashed curves are primary scattering only; solid curves include higher order scattering ($\mu_0 = 0{\cdot}40$, $A = 0$).

of the primary scattered light is easily shown to be[9, 10]

$$I_p = \frac{F}{4} P(\psi) \frac{\mu_0}{\mu + \mu_0} \left[1 - e^{-\tau\left(\frac{1}{\mu} + \frac{1}{\mu_0}\right)}\right], \quad (6)$$

where ψ is the scattering angle and $P(\psi)$ is the phase function determining the angular distribution of the scattered light. If we compute I_p for the Rayleigh phase function

$$P(\psi) = \tfrac{3}{4}(1 + \cos^2\psi)$$

and optical thickness $\tau = 0{\cdot}02$ and $1{\cdot}0$, we obtain the dashed curves of Fig. 1. It is seen that for $\tau = 0{\cdot}02$ multiple scattering is of minor

importance, but for large optical thickness multiple scattering plays a major role, as shown by the curves for $\tau = 1{\cdot}0$. As τ increases further, the effect of multiple becomes dominant, and as $\tau \to \infty$ the intensity I_p in (6) approaches asymptotically to a constant value which is only a relatively small fraction of the total intensity of the scattered light.

The effect of optical thickness is shown explicitly by Fig. 2, in which the intensity as a function of optical thickness is given for low and moderate sun elevations at eight different directions in the sun's vertical. The negative fourth power dependence on wavelength for

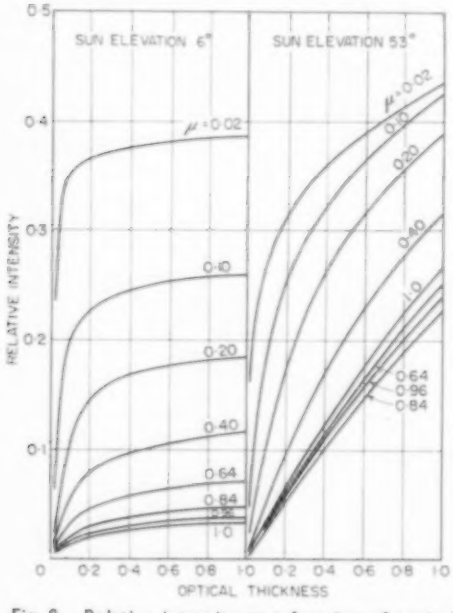

Fig. 2. Relative intensity as a function of optical thickness, for two sun elevations and eight different directions in the sun's vertical ($\varphi_0 - \varphi = 0$, $A = 0$).

primary scattering is responsible for the sharp increase at small optical thickness, particularly pronounced for low sun elevation. Attenuation effects entering at larger values of optical thickness cause the change of slope of the curves, the change being most marked, as would be expected, for long pathlengths of both the incident and scattered radiation.

The effect of sun elevation on the intensity of the scattered light is shown by the curves of intensity, at eight different depression angles

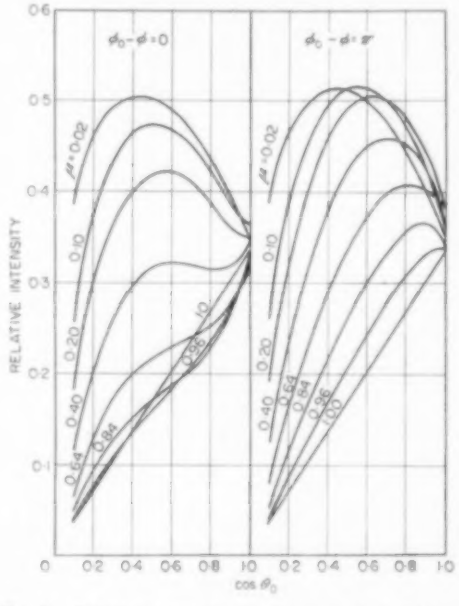

Fig. 3. Relative intensity for large optical thickness as a function of sun elevation, for eight different directions in the sun's vertical ($\tau = 1{\cdot}0$, $A = 0$).

and at the azimuths of the sun and antisolar point, in Fig. 3. As the sun elevation changes, two effects tend to oppose each other resulting in a smaller change of intensity of the diffusely scattered light than might be expected. First, the flux incident on a unit horizontal surface at the top of the atmosphere is directly proportional to $\cos \theta_0$. But the pathlength through the medium, and consequently the number of scatterers encountered by the incident ray, is inversely proportional to $\cos \theta_0$. If attenuation of the incident and scattered light were entirely negligible, the two effects would exactly compensate each other and the intensity of the light scattered at a given scattering angle would be independent of sun elevation. The actual dependence, most pronounced for the case of large optical thickness shown by Fig. 3, is directly attributable to attenuation effects.

The reflectivity of the underlying surface is very important in determining the characteristics of the radiation emerging from the top of the model atmosphere. For the case of small optical thickness and moderate or high surface reflectivity, the emergent light is principally that reflected from the surface directly, the effect of scattering being very minor by comparison. The plot of intensity as a function of depression angle in the sun's vertical for three different values of surface reflectivity, reproduced in Fig. 4, shows that

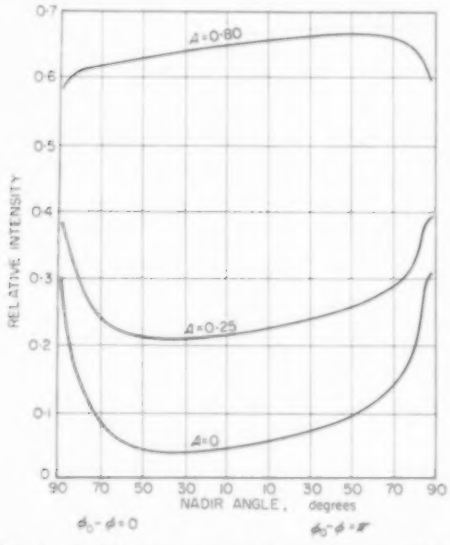

Fig. 4. Relative intensity as a function of direction in the sun's vertical, for moderate optical thickness, sun elevation 53° and three values of surface reflectivity ($\tau = 0{\cdot}15$, $\mu_0 = 0{\cdot}80$).

even for moderate optical thickness the surface-reflected light may constitute the major part of the emergent light. For higher optical thickness the reflectivity is relatively less dominant but still very important, even for optical thickness $\tau = 1{\cdot}0$.

The decrease of intensity in the regions near the horizon is a characteristic feature for all optical thicknesses for the strong "internal" source represented by a surface reflectivity of $A = 0{\cdot}80$. It is only for the case of large optical thickness that the "internal" source represented by scattering alone is sufficiently strong to cause the darkening of the region near the horizon. (It should be pointed out that the theory is not applicable right at the horizons, because of the assumption of a plane parallel atmosphere. Consequently the computations were stopped at $\mu = 0{\cdot}02$, corresponding to a point 1·1° below the horizons.)

3.2. *Intensity over entire downward hemisphere*

The intensity at different azimuths over the downward hemisphere has much the same distribution as it does in the sun's vertical. For cases in which the horizon is bright at the solar and antisolar azimuths, it is bright at other azimuths also, although the relative intensity is somewhat less at the 90° azimuth than in the sun's vertical. The intensity distribution over the entire downward hemisphere, for large optical thickness and zero surface reflectivity, is shown in Fig. 5. The diagram is supposed to represent one half of the downward hemisphere, the circumference being the horizon, and distance toward the center representing angular distance below the horizon (angular depression) on a linear scale. The maximum does not appear at the antisolar point, as it would for only primary scattering, but is shifted toward the antisolar horizon. The increased number of scatterers toward the horizon more than compensates for the intensity decrease expected by the Rayleigh phase function. The darkening near the horizon, which was mentioned in the previous section, is evident at and near the antisolar azimuth. The darkest band follows roughly the pattern indicated by the Rayleigh phase function, although the minimum is shifted somewhat toward the nadir because of the plane stratified distribution of the scatterers.

For smaller optical thickness the region near the horizon is everywhere the brightest part, but otherwise the pattern is similar to that shown. Surface reflection, being assumed independent of azimuth, does not change the distribution with azimuth very much, but serves principally to increase the magnitude of the intensity. High reflectivity, however, does produce an intensity

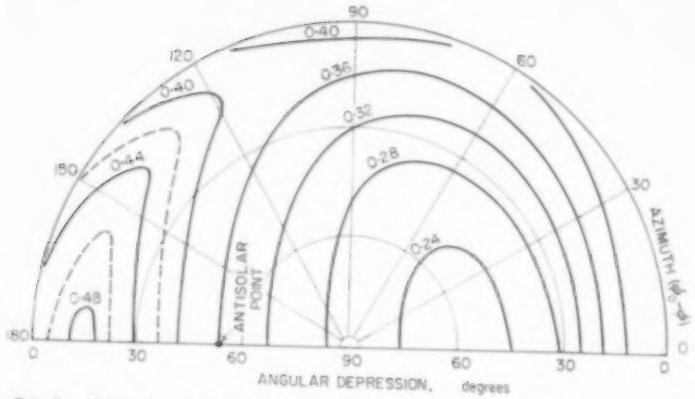

Fig. 5. Distribution of relative intensity over the downward hemisphere, for large optical thickness and sun elevation 53° ($\tau = 1{\cdot}0$, $\mu_0 = 0{\cdot}80$, $A = 0$).

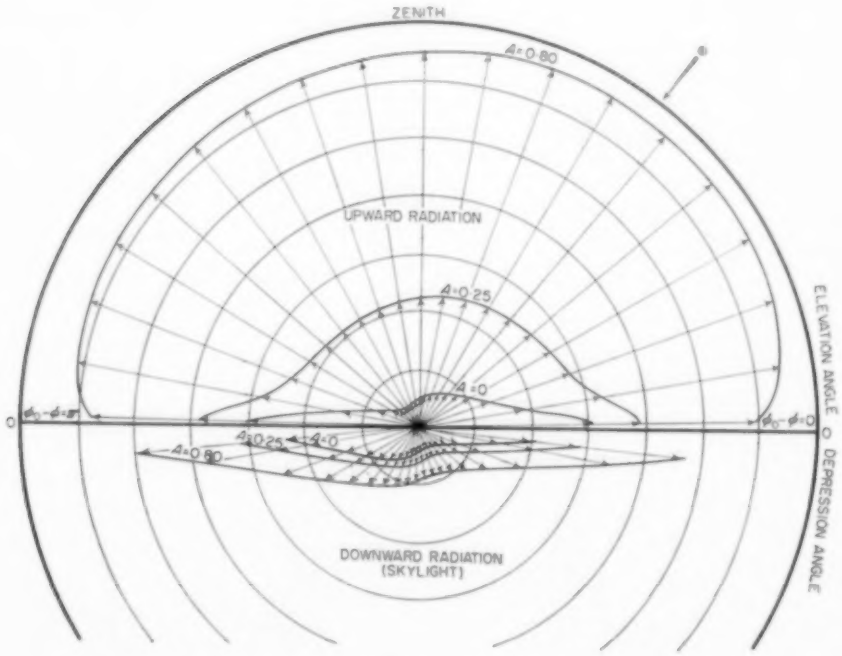

Fig. 6. Distribution of intensity of the light emerging from the top of the atmosphere and of the skylight as a function of direction in the sun's vertical, for moderate optical thickness, sun elevation 53° and three values of surface reflectivity ($\tau = 0{\cdot}15$, $\mu_0 = 0{\cdot}80$, $A = 0$, $0{\cdot}25$, $0{\cdot}80$). The sun's position is indicated by ← ⊙.

maximum below the horizons, as discussed above.

3.3. *Comparison with intensity of skylight*

The intensities of the sky radiation as determined by Sekera and collaborators[12, 13] may be very advantageously used for comparison, since they are based on the same theory. They are the more valuable for this purpose since they have been found to agree in many important respects with actual conditions in a clear atmosphere, and thereby lend further credibility to the theory.

A typical example of the intensity distribution, for both the skylight and the light emerging from the top of the model atmosphere of optical thickness $\tau=0{\cdot}15$, is given in Fig. 6 for a sun elevation of $53{\cdot}1°$ and for three different values of surface reflectivity. The similarity of the curves representing the upward and downward streams of light for $A=0$ is attributable directly to scattering according to the Rayleigh phase function, the minimum occurring at about 90° from the direction of the sun in each case. For $\tau\to 0$ the two streams must be identical, and for larger values of τ multiple scattering and attenuation effects cause the upward intensity to be the greater. Surface reflectivity is seen to have a much greater influence on the intensity of the upward radiation than on the intensity of skylight.

An equivalent scattering diagram for $\tau=1{\cdot}0$ is reproduced as Fig. 7. Downward scattering of the surface-reflected light by the large number of scatterers greatly increases the intensity of the skylight, while the intensity of the upward radiation is increased mainly by scattering of the direct incident radiation,

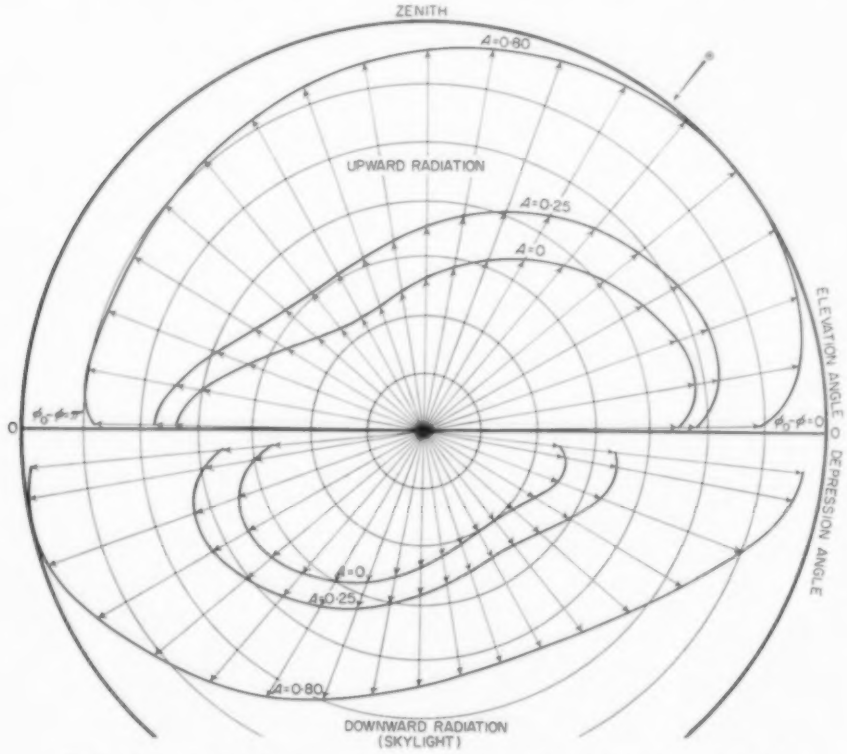

Fig. 7. Same as Fig. 6 except for large optical thickness ($\tau=1{\cdot}0$, $\mu_0=0{\cdot}80$, $A=0, 0{\cdot}25, 0{\cdot}80$).

surface reflectivity being much less important here than it is for smaller values of optical thickness.

4. DEGREE OF POLARIZATION

The degree of polarization of the diffuse skylight has been studied quite extensively by Sekera and collaborators during the last few years[11, 14, 5] both by actual measurements and by the theory developed by Chandrasekhar. Since the same principles apply for the diffuse light directed upward from the top of the atmosphere, it is reasonable to expect the degree of polarization to follow the same general pattern as that found for skylight. Such is indeed found to be the case, but some important differences occur also.

The degree of linear polarization is given by

$$P=[(I_r-I_e)^2+U^2]^{\frac{1}{2}}/(I_r+I_e) \tag{7}$$

for the case of surface reflectivity $A=0$, and by

$$P=[(I_r+I_r^*-I_e-I_e^*)^2+U^2]^{\frac{1}{2}}/(I_r+I_r^*+I_e+I_e^*) \tag{8}$$

for $A\neq 0$.

In the sun's vertical $U=0$, and (7) and (8) simplify, respectively, to

$$P=(I_r-I_e)/(I_r+I_e) \tag{9}$$

and

$$P=(I_r+I_r^*-I_e-I_e^*)/(I_r+I_r^*+I_e+I_e^*). \tag{10}$$

For convenience, the degree of polarization given by (9) or (10) is represented as either positive or negative; in (7) or (8) P is considered positive.

The general characteristics of the polarization distribution can be seen from Fig. 8, in which the degree of polarization is plotted as a function of the nadir angle, for three different optical thicknesses. The high degree of polarization for small optical thickness results from the predominance of primary scattering. Conversely, the much greater number of scatterers for large optical thickness results in greater multiple scattering and a consequent decrease of the polarization. For the same reason, the angular distance of the neutral points from the antisolar point increases with optical thickness.

For the case of no ground reflection the degree of polarization is almost independent of

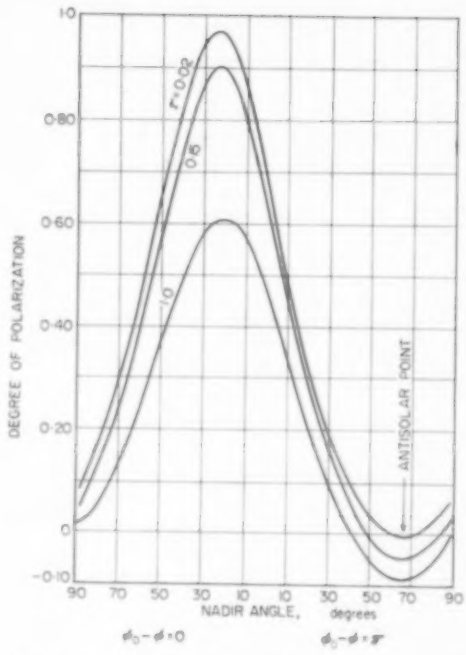

Fig. 8. Degree of polarization as a function of direction in the sun's vertical, for sun elevation 24° and three different values of optical thickness ($\tau=0{\cdot}02, 0{\cdot}15, 1{\cdot}0$; $\mu_0=0{\cdot}40$; $A=0$).

sun elevation, but its angular distribution shifts with the sun's position. The maximum is always located at approximately 90° to the direction of the sun, and there is slight negative polarization in the vicinity of the antisolar point. The increased number of scattering centers near the horizon decreases the polarization slightly in that region with respect to that at the nadir, thereby creating a slight asymmetry of polarization around the 90° point and tending to shift the maximum toward the nadir. This effect is very minor, however, and results in a shift of only a degree or two at most.

The degree of polarization of the light upward from the top of the atmosphere is more affected by surface reflectivity than is that of the skylight. The numerator of (8) or (10) is determined almost entirely by the scattered light, since the light reflected from the ground is assumed to be neutral. The denominator, how-

ever, is simply the total intensity. As was shown in the previous section, the total intensity is very sensitive to the reflectivity of the surface, and the degree of polarization is therefore sensitive to surface reflectivity. Typical curves of the degree of polarization as a function of direction in the sun's vertical are given in Fig. 9, for large optical thickness

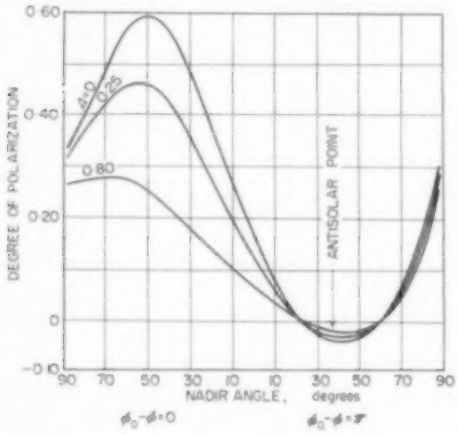

Fig. 9. Degree of polarization as a function of direction in the sun's vertical, for large optical thickness, sun elevation 53° and three different values of surface reflectivity ($\tau=1{\cdot}0$, $\mu_0=0{\cdot}80$, $A=0, 0{\cdot}25, 0{\cdot}80$).

and three values of surface reflectivity. It is seen that for the case of $A=0{\cdot}80$ the maximum is less than half that for $A=0$, and its position is shifted by as much as 10° from the normal position. The addition of unpolarized light reflected from the surface could not be expected to change the positions of the neutral points much, and indeed it does not.

A much greater effect of surface reflectivity is shown by a similar diagram for small optical thickness, reproduced as Fig. 10. Here the degree of polarization is very small throughout most of the sun's vertical, being greatly decreased by the intense but unpolarized reflected light for both $A=0{\cdot}25$ and $A=0{\cdot}80$. It is only for the long pathlengths near the horizon, in which the scattering is considerable and the reflected light is strongly attenuated, that the

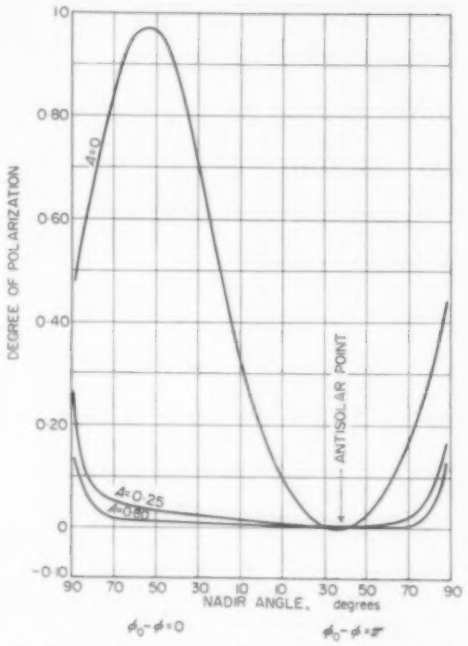

Fig. 10. Degree of polarization as a function of direction in the sun's vertical, for small optical thickness, sun elevation 53° and three different values of surface reflectivity ($\tau=0{\cdot}02$, $\mu_0=0{\cdot}80$, $A=0, 0{\cdot}25, 0{\cdot}80$).

degree of polarization approximates its value for $A=0$.

The distribution of the degree of polarization over the downward hemisphere is shown in Fig. 11 for the case of moderate optical thickness and zero surface reflectivity. The maximum is seen to be located in a band about 90° from the antisolar point, with very small polarization over a region near the antisolar point. Both these features are attributable to the Rayleigh scattering pattern directly. The pattern for higher and lower optical thicknesses is generally the same as that shown, but the maximum is somewhat greater for small optical thickness and less for large optical thickness. The whole pattern shifts its position as the sun elevation changes, maintaining the same relative position with respect to the direction of the antisolar point as that shown. For the sun at the zenith the pattern must be independent of azimuth,

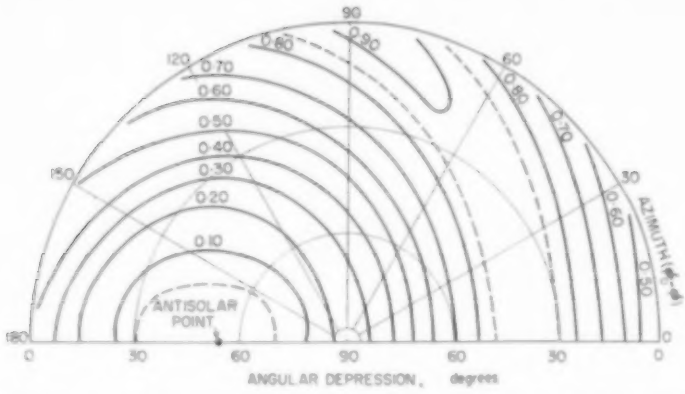

Fig. 11. Distribution of the degree of polarization over the downward hemisphere, for moderate optical thickness and sun elevation 53° ($\tau=0{\cdot}15$, $\mu_0=0{\cdot}80$, $A=0$).

with a neutral point at the nadir and the maximum degree of polarization extending around the horizon.

By comparing these figures with equivalent diagrams for skylight[5, 11] it is seen that the degree of polarization of the scattered light emerging from the top of the atmosphere has almost exactly the same character as that of skylight under the same conditions, except that the position of the sun for skylight is replaced here by the position of the antisolar point. Ground reflection, however, has a much greater effect here than it has for skylight.

5. PLANE OF POLARIZATION

If only the primary scattering is considered, as in the original Rayleigh theory, the plane of polarization has a simple orientation, being everywhere normal to the plane containing the directions of the antisolar point and the observed point. The angle can then be computed from an expression easily derived from spherical trigonometry. In this case the plane of polarization in the sun's vertical is everywhere normal to the plane of the sun's vertical, except in the direction of the antisolar point. In that direction the light is neutral, so no plane of polarization exists. Outside the sun's vertical the plane is defined everywhere. This case has been discussed by Coulson and Sekera[14] for skylight.

If multiple scattering is taken into account, many of the features in the orientation of the plane of polarization are similar to those of simple primary scattering, but some additional features appear. The distribution of the plane of polarization over the downward hemisphere for moderate optical thickness and moderate sun elevation is given in Fig. 12. Neutral points occur above and below the antisolar point (or below the antisolar point and below the sun for very low sun elevations), the antisolar point itself being no longer a neutral point. In the region between the neutral points $I_r<I_t$ (negative polarization), and the plane of polarization is in the sun's vertical. Outside this region everywhere in the sun's vertical $I_r>I_t$, and the plane of polarization is normal to the sun's vertical. For regions other than the sun's vertical the orientation of the plane of polarization is similar to that for primary scattering, although multiple scattering does produce minor angular shifts.

From the above remarks it can be seen that the orientation of the plane of polarization for this case of the light emerging from the top of the model atmosphere is almost identical with that for the case of skylight, except that the directions of the sun and antisolar point are interchanged. The changes of the plane as a function of optical thickness and sun elevation are also essentially the same as for skylight,

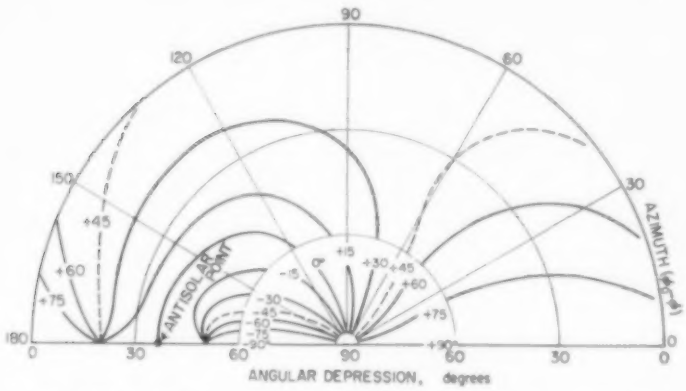

Fig. 12. Distribution of the plane of polarization over the downward hemisphere, for moderate optical thickness and sun elevation 53° ($\tau=0{\cdot}15$, $\mu_0=0{\cdot}80$, $A=0$). Positive angles indicate the plane to lie in the first and third quadrants; negative angles indicate the second and fourth quadrants of a cartesian co-ordinate system.

which have already been described by Coulson and Sekera[14].

6. NEUTRAL POINTS

The positions of the neutral points of skylight have been studied probably more extensively than any other feature of skylight polarization, from both observational and theoretical viewpoints[4, 6, 8, 11, 14]. The present investigation shows that the neutral points of the light emerging from the top of the model atmosphere are completely analogous to those of skylight, with the interchange of direction of sun and antisolar point. The angular distances between the neutral points and the antisolar point as a function of sun elevation is given, for three different optical thicknesses, in Fig. 13. The equivalent positions for the neutral points of skylight (Babinet and Brewster points) are given for $\tau=1{\cdot}0$, for comparison. It is seen that the behavior is essentially the same, although there is a slight difference of relative position for low sun elevations. The intervals of μ_0 at which the present computations were made are too large adequately to define the behavior of the point appearing beneath the sun for low sun elevations (i.e. the point equivalent to the Arago point of skylight), but the computations show

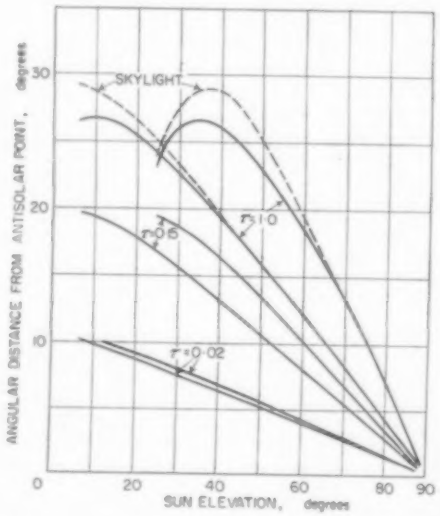

Fig. 13. Angular distance between the antisolar point and the neutral points as a function of sun elevation, for three different optical thicknesses. The upper of the solid curves for each optical thickness is for the point above the antisolar point, and the lower one is for the point below the antisolar point. Positions of the neutral points of skylight are included for $\tau=1{\cdot}0$, in which case the reference is the sun.

that it does exist, and the few values of its position which are available indicate its behavior to correspond closely to that of the Arago point.

REFERENCES

1. S. CHANDRASEKHAR, *Astrophys. Journ.* **106,** 152–216 (1947); **107,** 48–72 (1948).
2. S. CHANDRASEKHAR, *Radiative Transfer.* Clarendon Press, Oxford (1950).
3. S. CHANDRASEKHAR and D. D. ELBERT, *Trans. Amer. Phil. Soc.* (N.S.) **44,** 643–728 (1954).
4. S. CHANDRASEKHAR and D. D. ELBERT, *Nature, Lond.* **167,** 51–55 (1951).
5. K. L. COULSON, *Sci. Rep. Air Force Cambridge Research Center* No. 4, Contr. AF 19(122)-239 (1952).
6. K. L. COULSON, *Sci. Rep. Air Force Cambridge Research Center* No. 7, Contr. AF 19(122)-239 (1954).
7. D. DEIRMENDJIAN, *Sci. Rep. Air Force Cambridge Research Center* No. 1, Contr. AF 19(122)-239 (1952).
8. C. DORNO, *Met. Z.* **36,** 109, 181 (1918).
9. A. HAMMAD, *Astrophys. J.* **108,** 338–346 (1948).
10. A. HAMMAD and S. CHAPMAN, *Phil. Mag.* **28,** *Ser.* 7, 99–110 (1939).
11. Z. SEKERA, *Handbuch der Physik, Bd.* 48, Springer, Berlin (1957).
12. Z. SEKERA and E. V. ASHBURN, *Nav. Ordn. Rep. Inyokern* No. 2061 (1953).
13. Z. SEKERA and G. BLANCHE, *Sci. Rep. Air Force Cambridge Research Center* No. 3, Contr. AF 19(122)-239 (1952).
14. Z. SEKERA *et al.*, *Final Rep. Air Force Cambridge Research Center,* Contr. AF 19(122)-239 (1955).

Planet. Space Sci. Pergamon Press 1959, Vol. 1, pp. 277–284. Printed in Great Britain.

CHARACTERISTICS OF THE RADIATION EMERGING FROM THE TOP OF A RAYLEIGH ATMOSPHERE—II

TOTAL UPWARD FLUX AND ALBEDO

K. L. COULSON*

Meteorology Department, University of California, Los Angeles

(*Received* 13 *March* 1959)

Abstract—The solution of the equation of radiative transfer in a medium exhibiting Rayleigh scattering, as developed by S. Chandrasekhar, has been used for an extensive series of computations[3] of the characteristics of the scattered and diffusely reflected radiation emerging from the top of an atmospheric model which corresponds in many respects to the sunlit portion of the earth's atmosphere. The first part of this two-part discussion dealt with the intensity, degree of polarization, plane of polarization and the neutral points of the emergent light as functions of sun elevation, direction in the downward hemisphere, optical thickness of the model atmosphere and reflectivity of the underlying surface. This second part is concerned with the upward flux obtained by an integration of the intensity over the entire hemisphere, for the incident radiation (a) being independent of wavelength or (b) having the spectral distribution of the extra-terrestrial solar radiation. Integration with respect to wavelength in the latter case, together with an approximation for the sphericity of the atmosphere, yields a value of 7·6 per cent for the earth's planetary albedo due to scattering by the clear atmosphere. An approximation for ozone absorption decreases the computed albedo to 6·9 per cent.

1. INTRODUCTION

Parallel unpolarized radiation of net flux πF per unit area normal to its direction of propagation is assumed incident on the top of an idealized atmosphere from a direction specified by the sun's zenith angle θ_0. The atmospheric model is characterized by being (a) uniform and infinite in the horizontal (b) non-absorbing (c) composed of scattering centers which are small compared to the wavelength of the light and (d) of finite optical thickness. Further, the upper boundary is a perfect vacuum and the lower boundary is a Lambert reflector with an arbitrarily fixed reflectivity A $(0 \leqslant A \leqslant 1)$. The problem in this second part of a two-part discussion[2] is to determine the flux of scattered and diffusely reflected radiation directed upward from the top of the model atmosphere and obtain an estimate of the earth's planetary albedo due to scattering by the clear atmosphere.

* Presently affiliated with The Stanford Research Institute, Menlo Park, California.

2. TOTAL OUTWARD FLUX

2.1. *Relative flux (incident radiation independent of wavelength)*

It is possible to determine very simply the total integrated flux of radiation proceeding in the outward direction from the top of the model atmosphere for a given inward flux incident on the top of the atmosphere, and thereby compute both the monochromatic reflectance of the atmosphere and the reflectance integrated with respect to wavelength. The first of these quantities will be called the *reflectance* and the second the *albedo*.

The total outward flux from the top of the atmosphere in unit frequency interval and unit time is given by

$$D_\nu = \int_0^{\pi/2}\int_0^{2\pi} I(\theta, \varphi) \sin\theta \cos\theta \, d\theta \, d\varphi = \int_0^1 \int_0^{2\pi} I(\mu, \varphi) \, \mu d\mu d\varphi. \quad (1)$$

where φ and θ are the azimuth and nadir angles, respectively, and $\mu = \cos\theta$. The intensity I is in general a function of both μ and φ, but it can

be expressed as a sum of three terms, the first of which is independent of azimuth and the other two are functions of azimuth only in a cosine relation. Thus

$$I(\mu, \varphi) = I^{(0)}(\mu) + f^{(1)}(\mu, \mu_0)\cos(\varphi_0 - \varphi) + f^{(2)}(\mu, \mu_0)\cos 2(\varphi_0 - \varphi). \quad (2)$$

If the integration indicated in (1) is carried out, the azimuth dependent terms vanish, and (1) becomes

$$D_\nu = 2\pi \int_0^1 I^{(0)}(\mu)\, \mu d\mu. \quad (3)$$

Now if the light incident on the atmosphere is neutral, $I^0(\mu)$ can be expressed as

$$I^{(0)}(\mu) = \frac{3}{16\mu}(S_{ee}^{(0)} + S_{er}^{(0)} + S_{re}^{(0)} + S_{rr}^{(0)})F, \quad (4)$$

where the $S_{ij}^{(0)}$ $(i, j = e, r)$ are elements of an azimuth independent scattering matrix†, functions of both μ and μ_0. For a net incident flux πF (3) reduces to

$$D_\nu = \pi F \mu_0 \left[1 - \frac{\gamma_e(\mu_0) + \gamma_r(\mu_0)}{2}\right]. \quad (5)$$

where the $\gamma_i(\mu_0)$, $(i = e, r)$ are the same as those discussed in part I[2], and are available in tabular form. (5) represents the total flux of monochromatic radiation emerging from the top of the atmosphere, for the case of no ground reflection.

If ground reflection is taken into account, there is an additional stream of light of intensity I^* emerging from the top of the atmosphere and, if we assume incoherency of the streams, the intensities are additive. The intensity I^* can be expressed in terms of the scattering matrix and an additional matrix involving the γ_i $(i = e, r)$. The azimuth dependence again vanishes on integration, and the total flux of the radiation reflected by the ground which emerges from the top of the atmosphere can, for the case of neutral incident light, be expressed as

$$D^* = \pi F \frac{A\mu_0}{1 - A\bar{s}}\left[\frac{\gamma_e(\mu_0) + \gamma_r(\mu_0)}{2}\right]. \quad (6)$$

† See p. 276 of Chandrasekhar[1].

Here A is the reflectivity of the ground and $\bar{s}$ is a known function of only the optical thickness.

On adding (5) and (6), we obtain the total radiative flux D_ν emerging from the top of the atmosphere, in unit time and unit frequency interval, as

$$D_\nu = \pi F \mu_0 \left[1 - \left(\frac{\gamma_e(\mu_0) + \gamma_r(\mu_0)}{2}\right)\left(\frac{1 - A}{1 - A\bar{s}}\right)\right]. \quad (7)$$

This is for an incident flux of $\pi F \mu_0$ units of energy on a unit horizontal area at the top of the atmosphere, in unit time and unit frequency interval. D_ν will be called the total relative monochromatic flux, when $F = 1$.

Curves of the total relative monochromatic flux emerging from the top of the atmosphere as a function of wavelength, for various sun elevations and values of surface reflectivity, are given in Fig. 1. A great change of flux with wavelength is seen for the scattered light only $(A = 0)$, particularly for high sun elevations $(\mu_0 = \cos\theta_0 = 0{\cdot}80,\ 1{\cdot}0)$. The effect of attenuation of the light for the various sun elevations is apparent from a comparison with the curve $(X's)$ computed from the relation

$$D_\nu = (\text{Const.}) \times (\lambda^{-4}), \quad (8)$$

where the constant was evaluated for $\mu_0 = 1{\cdot}0$ at wavelength $\lambda = 8000$ Å. Physically it shows the flux which would result from primary Rayleigh scattering if there were no attenuation of either the incident or scattered light. The opposing effects of changing sun elevation and the corresponding changing atmospheric pathlength of the incident radiation exactly compensate each other, so the curve is valid for all sun elevations.

The change of flux with wavelength is greatly decreased for $A = 0{\cdot}25$, and practically eliminated for $A = 0{\cdot}80$, by the influence of surface reflectivity in the long wavelengths. The great transparency of the atmosphere for these long wavelengths is evidenced by both the small attenuation during two traverses of the total depth of the atmosphere and the small flux scattered upward by the atmosphere itself.

By dividing the values of the upward flux D_ν contained in Fig. 1 by the incident flux we obtain the reflectance of the atmospheric model as a function of wavelength. Thus

$$R_\nu = D_\nu / \pi F \mu_0. \tag{9}$$

Some typical results for various sun elevations and surface reflectivities are given in Table 1. The values show an increase of reflectance with decrease of wavelength at all sun elevations for the case of $A=0$, the increase being most pronounced for high sun elevations. Ground reflection increases the reflectance at all wavelengths, but, as expected, the increase is greatest at wavelengths for which the atmospheric transparency is greatest. It is interesting to note that, for high surface reflectivity ($A=0{\cdot}80$) and high sun elevations ($\mu_0=0{\cdot}80$, $1{\cdot}0$), the effect of the atmosphere is actually to decrease the reflectance of the atmosphere–ground system by a small amount over a wide range of wavelengths.

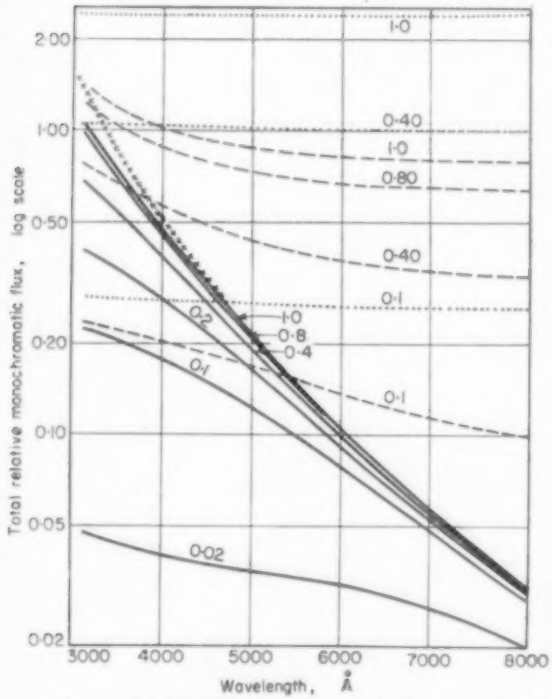

Fig. 1. Total relative monochromatic flux emerging from the top of the atmosphere as a function of wavelength, for various sun elevations and three values of surface reflectivity: $A=0$ (solid curves), $A=0{\cdot}25$ (dashed curves) and $A=0{\cdot}80$ (dotted curves). Curves are labeled with values of μ_0. A curve (x) for primary Rayleigh scattering and no attenuation is included for comparison.

2.2. *Absolute flux (incident radiation a function of wavelength)*

In the discussion thus far F has been assumed to be unity. It is of interest to see the characteristics of the flux emerging from the top of the model atmosphere, if we assume the incident flux has the same variation with wavelength as the solar radiation does have at the outside of the atmosphere. The most recent data available on the extra-terrestial flux $F_{0\nu}$ of solar radiation have been summarized by Nicolet[15] and tabulated at 100 Å intervals by Deirmendjian[6]. These data have been used for computations of the total absolute monochromatic flux J emerging from the top of the model atmosphere. Values of J_ν for $A=0$ have been plotted as a function of wavelength for five different sun elevations in Fig. 2. A pronounced shift of the maximum toward longer wavelengths with decreasing sun elevation is seen, the first major maximum being suppressed entirely at the lowest sun elevation.

Two important features can be deduced by comparing the solid curves of Fig. 2 with equivalent curves for skylight. One such curve for skylight, as given by Deirmendjian and Sekera[7], is included in the diagram. First, the scattered light emerging from the top of the atmosphere would tend more toward violet than the skylight, the difference being most pronounced for low sun elevations. Secondly, the total flux of scattered light directed upward from the top of the atmosphere must be at least as great as the total flux of scattered light directed downward from the bottom of the atmosphere. It is only for the limiting case of $\tau \to 0$ that the two fluxes are equal; otherwise the upward flux is the greater.

It is interesting to compare the flux of the emergent radiation with that of the incident radiation, both being integrated over a specified

Table 1. Reflectance of the Atmospheric Model at Various Wavelengths, for Representative Values of Sun Elevation and Surface Reflectivity.

A	μ_0	λ 3150 Å	4000	5000	6000	7000	8000
0	0·02	0·754	0·638	0·565	0·503	0·430	0·325
0	0·10	0·705	0·552	0·396	0·247	0·154	0·094
0	0·40	0·550	0·304	0·152	0·079	0·044	0·024
0	0·80	0·400	0·181	0·085	0·039	0·022	0·013
0	1·00	0·345	0·148	0·068	0·033	0·017	0·009
0·25	0·02	0·791	0·712	0·665	0·625	0·574	0·494
0·25	0·10	0·752	0·643	0·536	0·427	0·362	0·319
0·25	0·40	0·623	0·445	0·345	0·298	0·276	0·285
0·25	0·80	0·492	0·347	0·293	0·271	0·260	0·257
0·25	1·00	0·450	0·322	0·280	0·264	0·256	0·255
0·80	0·02	0·922	0·910	0·904	0·896	0·885	0·865
0·80	0·10	0·918	0·892	0·866	0·842	0·826	0·815
0·80	0·40	0·860	0·830	0·812	0·805	0·803	0·800
0·80	0·80	0·811	0·798	0·798	0·798	0·798	0·799
0·80	1·00	0·794	0·792	0·794	0·796	0·798	0·799

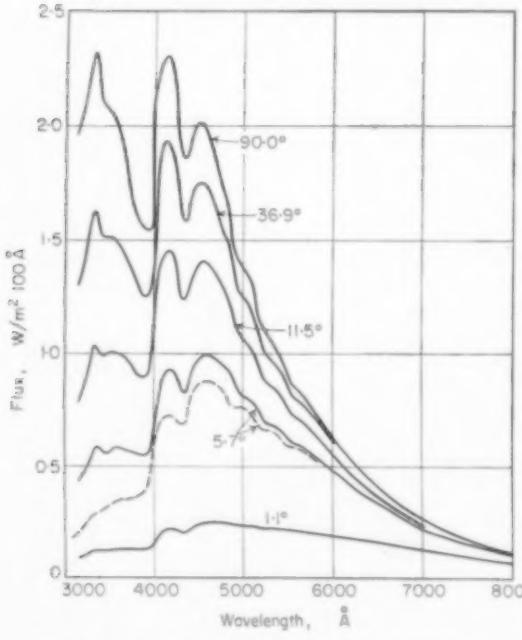

Fig. 2. Absolute monochromatic flux from the top of the model atmosphere as a function of wavelength, for zero surface reflectivity and five different sun elevations ($\mu_0 = 1{\cdot}0$, 0·40, 0·20, 0·10 0·02; $A = 0$). Dashed curve is for sky radiation at sun elevation 5·7°, as given by Deirmendjian and Sekera [7].

wavelength interval. The first of these will be denoted J, with a subscript to indicate the surface reflectivity, and the second by F_0, for the range 3200 Å$\leqslant\lambda\leqslant$8000 Å in both cases. The ratio J/F_0 is the *albedo*. Data for both J and F_0 are given for six different sun elevations in Table 2. The values were obtained by integration of the area under the appropriate curves on diagrams such as that of Fig. 2. The extra-terrestrial flux F_0 given for the range 3200 Å$\leqslant\lambda\leqslant$8000 Å is 769·9 W/m² for normal incidence or about 55 per cent of the solar constant (1391 W/m²)*. The dominating influence of surface reflectivity for the higher sun elevations, and its much smaller influence for the lower sun elevations, is shown by the values of both J and a in the table. The change of albedo with sun elevation is very pronounced for scattering alone ($A = 0$), but for high surface reflectivity the small amount of scattering at high sun elevations is largely compensated by the strong reflected component. In fact the values of albedo at the highest sun elevations show that for $A = 0{\cdot}80$ the atmosphere actually

* This value of the solar constant is somewhat higher than the commonly accepted value of 1353 W/m², but it agrees closely with that obtained by Johnson[13] and is the one used by Deirmendjian and Sekera[7]. Its use here makes these data directly comparable with theirs.

Table 2. Values and Comparisons of the Total Absolute Flux for 3200 Å$\leqslant\lambda\leqslant$8000 Å at Six Different Sun Elevations* (Units of flux: W/m^2)

Sun elevation	1·1°	5·7°	11·5°	23·6°	53·1°	90·0°
F_0	15·4	77·0	154·0	307·9	615·8	769·9
$(J)_0$	8·0	25·0	34·3	44·0	48·9	51·8
$(J)_{25}$	9·7	37·1	62·4	103·6	179·9	214·8
$(J)_{80}$	13·7	65·9	128·3	249·6	488·6	609·6
$(\alpha)_0$	0·519	0·325	0·223	0·143	0·079	0·067
$(\alpha)_{25}$	0·630	0·482	0·405	0·336	0·292	0·279
$(\alpha)_{80}$	0·890	0·856	0·833	0·811	0·793	0·792
$(F_{0g})_0$	7·4	52·0	119·7	263·9	566·9	718·1
$(F_{0g})_{25}$	7·6	53·2	122·1	272·4	581·2	740·1
$(F_{0g})_{80}$	8·5	55·5	128·5	291·5	636·0	801·5

* F_0 : Incident flux on horizontal surface at top of atmosphere.

$(J)_A$: Emergent flux through horizontal surface at top of atmosphere. (Subscript A represents value of surface reflectivity: 0, 0·25 or 0·80).

$(\alpha)_A$: $\dfrac{(J)_A}{F_0}$ = Albedo: ratio of emergent to incident flux.

$(F_{0g})_A$: Flux incident on horizontal surface at ground.

decreases the emergent flux, making the albedo slightly less than the reflectivity of the surface itself.

The effect of scattering of the very intense reflected radiation can be seen in the values of the flux $(F_{0g})_A$ incident on the ground given in the table. The increase of (F_{0g}) for $A\neq 0$ over that for $A=0$ represents the amount of the reflected radiation which is scattered back to the surface in the form of diffuse skylight. This leads to the apparent paradox of the flux incident on the surface, at high sun elevations and $A=0{\cdot}80$, being greater than the flux incident at the outside of the atmosphere. The values given are, of course, for the flux downward only, and not a net flux at the surface, so the paradox is only apparent. But it does point up very graphically the great importance of surface reflectivity.

3. ESTIMATE OF PLANETARY ALBEDO BY MOLECULAR SCATTERING

We can now arrive at a rough estimate of the earth's planetary albedo due to molecular scattering. Integration under curves such as those of Fig. 2 gives the upward flux due to scattering of the radiation wavelengths 3200 Å$\leqslant\lambda\leqslant$8000 Å for different sun elevations. The ratio of this outward flux to the incident flux for this spectral region is plotted (solid curve of Fig. 3) as a function of sun elevation. An estimate of the effect of scattering of wavelengths above 8000 Å and below 3200 Å can be obtained as follows. Taking the latter first, since only about 2·3 per cent[13] of the total energy lies in the region below 3200 Å, any overall errors introduced by that portion must be small. In view of the high albedo for the short wavelengths let us say that one half of the energy is scattered back directly: (0·50) (0·023) (1391 μ_0) = 16 μ_0 W/m^2. The situation is more serious for the long wavelengths; about 42 per cent of the incident energy lies in the region beyond 8000 Å. However, even the wavelengths 7500–8000 Å require very long pathlengths for appreciable scattering and the amount of scattering decreases rapidly with increasing wavelength. A reasonable value of albedo due to scattering alone would be 1 per cent or 2 per cent for the long wavelengths, and

probably closer to 1 per cent. Then the emergent flux by scattering of the long wavelengths would be (0·01) (0·42) (1391 μ_0) = 58 μ_0 W/m². By combining these fluxes with the flux obtained by direct integration for the middle spectral region, we obtain the albedo shown by the dashed curve of Fig. 3 for the entire solar spectrum.

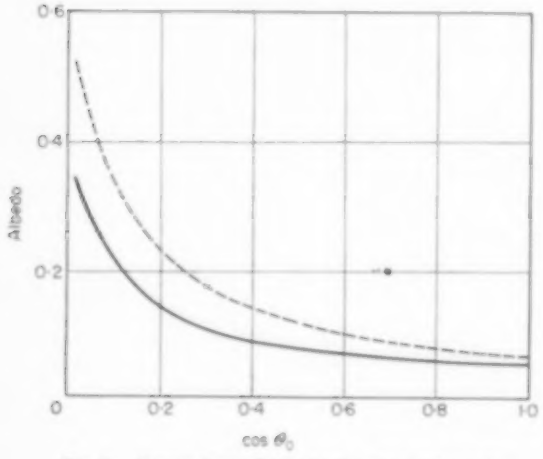

Fig. 3. Approximated albedo for the entire solar spectrum (solid curve) and computed albedo for the spectral range 3200 Å $\leqslant \lambda \leqslant$ 8000 Å (dashed curve) as a function of sun elevation ($A = 0$).

The discussion so far has been for the case of a plane parallel atmosphere and is not directly applicable to the earth's atmosphere. We can, however, obtain an approximation for a spherical atmosphere by dividing the total area of the disc which intercepts the sun's rays into narrow concentric rings, and considering the sun elevation constant and the atmosphere plane parallel for a given ring. We can then determine the incident and emergent fluxes for a given ring and combine them to give the albedo. If we let the total area of the disc be unity, the total flux incident on the disc is simply the solar constant C, and the flux incident on the ith ring of fractional area Δa_i is $F_i = C\ \Delta a_i$. Evidently $\sum_{i=1}^{n} \Delta a_i = 1$. The emergent flux from the ring is $a_i F_i = a_i C\ \Delta a_i$, a being the albedo, and the emergent flux from the whole disc is $\sum_{i=1}^{n} C a_i \Delta a_i$. Then, by definition, the albedo for the total disc is

$$a = \left(\sum_{i=1}^{n} C a_i \Delta a_i\right)/C.$$

If the limits of the rings are defined in terms of the angles listed in the first column of Table 3, the sun elevations in column two can be used as representative of the respective rings. The incident flux for the rings is given in column four, and the product of incident flux and albedo, obtained from Fig. 3, gives the emergent flux for the rings, listed in the last column of Table 3. Then the ratio of the total emergent flux to the total incident flux is the total albedo, given at the bottom of the table.

A value of 7·6 per cent for the planetary albedo due to molecular scattering is obtained by the above approximation to the spherical atmosphere.

Comparison of the computations with measurements[4, 8] is not very realistic unless atmospheric absorption is taken into account. The slight absorption of solar radiation in the various bands of water vapor and carbon dioxide can be neglected for present purposes. Most of the absorption of solar radiation occurs in the Hartley and Huggins bands of ozone, the absorption in the Chappius bands being small except for low sun elevations. Dave and Sekera[5] have computed the effect of ozone absorption on the total skylight, under the assumption that the ozone is concentrated in a layer above the atmosphere and therefore absorbs only the downward-directed incident radiation. If we assume the same percentage change of the radiation scattered upward as they computed for skylight, and compute the additional absorption for the upward traverse through the ozone layer, then we can recompute the fluxes analogous to those of Table 3 and find the albedo for the more realistic case. The value of albedo obtained by this method is 6·9 per cent.

Fritz[9] used Fowle's data for Washington, D.C., for estimating the contribution of molecular scattering to the albedo of the earth, and obtained a value of 8 per cent for the mean albedo due to atmospheric scattering. The 6·9

per cent obtained from the computations would decrease his estimate of the planetary albedo by about 1 per cent. In view, however, of the approximations involved in the computed value and the rough estimations made by Fritz, the 1 per cent does not seem significant. Kano[14] has made a determination of the planetary albedo by means of Chandrasekhar's theoretical development, entirely independent of the work reported here, and obtained 6·6 per cent for the albedo of the cloudless atmosphere. He accounted for ozone absorption in a different manner, which is probably responsible for the slight discrepancy between his value and the 6·9 per cent obtained here.

Table 3. Approximation of Earth's Planetary Albedo due to Atmospheric Scattering. The Disc of the Earth, as Seen from the Sun, was Divided into Concentric Rings and the Sun Elevation for Each Ring was Considered Constant

Angular limits of rings	Sun elevation for ring	Fraction of total area of disc	Incident flux (W/m^2)	Albedo of ring	Emergent flux (W/m^2)
0·0° to 8·6°	5·7°	0·02235	31·09	0·200	6·22
8·6° to 17·6°	11·5°	0·06908	96·09	0·139	13·36
17·6° to 30·3°	23·6°	0·16311	226·89	0·095	21·55
30·3° to 45·0°	36·9°	0·24546	341·43	0·074	25·27
45·0° to 60·0°	53·1°	0·25000	347·75	0·060	20·86
60·0° to 78·5°	66·9°	0·21025	292·46	0·055	16·09
78·5° to 90·0°	90·0°	0·03975	55·29	0·053	2·93
		Total flux	1391·00		106·28
				Albedo	7·6 per cent

4. DISCUSSION

The problem of the scattering of radiation by the molecules of the air is only one part of the larger and more complicated problem of the radiative transfer in a turbid atmosphere. But it is a necessary and very important part. One of the most fruitful lines of attack on the more general problem for the turbid atmosphere has been to study the deviations of measured values of intensity and degree of polarization from those computed for a pure molecular atmosphere, and ascribe the deviations to the effects of large particles in the actual atmosphere. Previous investigations of this type have dealt with the skylight, but, as far as is known, none have attempted to described the light directed upward from the top of the atmosphere.

Even this first part of the whole problem is still not completely solved, however. The sphericity of the atmosphere has not yet been successfully introduced into the exact theory of radiative transfer, so the theory is not entirely applicable to a planetary molecular atmosphere. It is highly desirable that efforts be directed toward developing the equations to take sphericity into account. Of perhaps even more import is the lack of knowledge of the reflectivity of the ground. It is evident that surface reflectivity is a major factor in the radiative problem, particularly for the radiation emerging from the top of the atmosphere.[10, 11, 12] The importance of seeing or photographing features of the earth's surface from outside the atmosphere instills a sense of urgency into this phase. A great many measurements of the radiation reflected from various types of surfaces are needed, such measurements to include both the intensity and the state of polarization of the reflected light. Once the measurements are available, their inclusion into the theory is not difficult.

Finally, radiative absorption by the atmospheric constituents, both gaseous and particulate, must be included for an adequate solution

to the problem of radiative transfer in a real atmosphere.

Acknowledgment—The work reported here was sponsored, in part, by the Air Force Cambridge Research Center, and machine time for the computations was made available, without charge, by the Western Data Processing Center, University of California. The author is particularly grateful to Professor Zdenek Sekera for his original suggestion of the problem and his supervision throughout the work.

REFERENCES

1. S. CHANDRASEKHAR, *Radiative Transfer*. Clarendon Press, Oxford (1950).
2. K. L. COULSON, *Planet. Space Sci.* **1** (1959).
3. K. L. COULSON and Z. SEKERA, *Tables Related to Rayleigh Scattering of Light in a Plane Parallel Atmosphere*. Univ. of California Press (In press.)
4. A. DANJON, Chap. 15 in *The Earth as a Planet* (Edited by F. P. KUIPER). Univ. of Chicago Press (1954).
5. J. V. DAVE and Z. SEKERA, *J. Met.* **16**, 211–212 (1959).
6. D. DEIRMENDJIAN, private communication (1958).
7. D. DEIRMENDJIAN and Z. SEKERA, *Tellus* **6**, 382–398 (1954).
8. J. DUBOIS, *Bull. Astr., Paris* **13**, 193–196 (1947).
9. S. FRITZ, *J. Met.* **6**, 277–282 (1949).
10. S. FRITZ, *Bull. Am. Met. Soc.* **29**, 303–312 (1948).
11. S. FRITZ, *Bull. Am. Met. Soc.* **31**, 25–27 (1950).
12. C. T. HOLLIDAY, Chap. 14 in *The Earth as a Planet* (Edited by F. P. KUIPER). Univ. of Chicago Press (1954).
13. F. S. JOHNSON, *J. Met.* **11**, 431–439 (1954).
14. M. KANO, *Pap. Met. Geophys., Tokyo* **9**, 113–122 (1958).
15. M. NICOLET, *Ann. Astrophys.* **14**, 249–265 (1951).

Planet. Space Sci. Pergamon Press 1959. Vol. 1, pp. 285–290. Printed in Great Britain.

LINES OF FORCE OF THE GEOMAGNETIC FIELD IN SPACE

E. H. VESTINE and W. L. SIBLEY

The RAND Corporation, Santa Monica, California

(*Received* 7 *April* 1959)

Abstract—The lines of force of the geomagnetic field at various latitudes and longitudes in the northern hemisphere are approximately traced to their intersections with the earth's surface in the southern hemisphere, using an electronic computer and the first nine Gauss coefficients. Those lines leaving the average northern auroral zone are traced to their intersection of the geomagnetic field with the earth's surface. These points of intersection are found to be very nearly at the average southern auroral zone deduced from auroral observations and from magnetic measurements of disturbance. It is concluded, therefore, that the geomagnetic field has stability and a simple character even at distances as great as about 6 earth radii above the earth, measured in the equatorial plane, even during auroral displays. It is also concluded that solar streams at such times do not seriously distort the field lines connecting the auroral zones.

In various geophysical research problems it may be desirable to know the path of the line of geomagnetic force leaving the ground in the southern hemisphere up to its point of entry in the northern hemisphere. In particular, as in auroral and magnetic observations, it may be of interest to place observing stations on the ground at either end of such a line of force. This problem has been previously considered by Block and Herlofson[1], who computed some results for actual magnetic observatories, using data for the year 1922. The present study continues this work, using more recent data, and broadens the scale of coverage, especially for lower latitudes.

The present memorandum summarizes, in preliminary form, the locations of intersections with the earth's surface of lines of force of the geomagnetic field over a world-wide grid of points. The information is approximate but will be supplemented later by more precise estimates based on more elaborate calculations for use in the study of geophysical problems such as whistlers and the aurora. In particular, it is planned to estimate lines of force for certain Arctic and Antarctic stations of the International Geophysical Year.

The geomagnetic field within the atmosphere and beyond resembles that of a short bar magnet at the earth's center with its axis about 12° off the axis of rotation. The strength of the magnetic field has been decaying for the past 125 years at a rate suggesting a half life of about 2000 years, though this rate of decay seems to be slowing up in recent years. The hypothetical magnetic dipole at the earth's center intersects the earth's surface at 78·5°N latitude, 291·0°E, a point near Etah, Greenland. This is the position of the pole now adopted internationally.

The magnetic potential of the geomagnetic field may be written

$$V = a \sum \sum [g_n^m \cos m\lambda + h_n^m \sin m\lambda] P_n^m(\cos\theta)\left[\frac{a}{r}\right]^{n+1} \qquad (1)$$

where r, θ, λ are the spherical coordinates of the point, a is the mean radius of the earth, $P_n^m(\cos\theta)$ is the normalized associated Legendre polynomial of Schmidt. The coefficients in the series are usually fitted by least squares to the magnetic survey data, using terms up to and including $n=6$.

The centered dipole referred to above has the representation

$$V_1 = g_1^0 \cos\theta + g_1^1 \sin\theta \cos\lambda + h_1^1 \sin\theta \sin\lambda \qquad (2)$$

where θ is the colatitude.

Instead of a centered dipole there may be used instead the eccentric dipole, a dipole located at the magnetic center of the earth. Its northern pole was at latitude 80·1°N, λ = 277·3°E, in 1922.

Then the geomagnetic potential may be written

$$V=[g_1^0\cos\theta+(g_1^1\cos\lambda+h_1^1\sin\lambda)\sin\theta]\,r^{-2}+ \\ +[0{\cdot}25\,g_2^0(3\cos 2\theta+1)+(g_2^1\cos\lambda+h_2^1\sin\lambda)\times \\ \times\sqrt{\tfrac{3}{2}}\sin 2\theta+(g_2^2\cos 2\lambda+h_2^2\sin 2\lambda)\sqrt{\tfrac{3}{2}}\sin 2\theta]\,r^{-3} \qquad (3)$$

where λ is the longitude east of Greenwich, θ the colatitude (polar angle) measured from the geographic north pole, r the distance from the earth's center, with the radius of the earth as the unit of length.

Values of the g's and h's for 1958 were extrapolated from the values of Vestine and Lange[2] for 1945. The results gave, in units of 10^{-4} c.g.s.:

$$\begin{array}{lll} g_1^0=-3053 & & \\ g_1^1=-207 & h_1^1=587 & \\ g_2^0=-152 & & \\ g_2^1=\ 296 & h_2^1=-193 & \\ g_2^2=\ 162 & h_2^2=35 & \end{array}$$

If, instead of polar co-ordinates, use be made of right-handed Cartesian axes with origin 0 at the earth's center—the 0x-axis through the meridian 90° West of Greenwich, and in the equatorial plane, the 0y-axis through the Greenwich meridian, and the 0z-axis through the north pole—there results

$$x=-r\sin\theta\sin\lambda$$
$$y=r\sin\theta\cos\lambda$$
$$z=r\cos\theta$$

The equations of the lines of force are

$$\frac{dx}{ds}=\frac{\partial V}{\partial x}\,|\text{grad } V|^{-1}\ \text{etc.} \qquad (4)$$

where s is the arc distance measured along the line of force. Thus, equation (1) becomes

$$V=(Px+Qy+Rz)\,r^{-3}+(Ax^2+By^2+Cz^2+ \\ +Dxy+Exz+Fyz)\,r^{-5} \qquad (5)$$

and

$$\begin{array}{lll} P=587 & Q=\ 207 & R=\ 3053 \\ A=\ 68 & B=-220 & C=\ 152 \\ D=\ 59 & E=-334 & F=-\ 513 \end{array}$$

From equation (5)

$$r^3\frac{\partial V}{\partial x}=3\alpha\frac{x}{r}-P+\left[(5\beta-2A)\frac{x}{r}-D\frac{y}{r}-E\frac{z}{r}\right]r^{-1}$$
$$r^3\frac{\partial V}{\partial y}=3\alpha\frac{y}{r}-Q+\left[(5\beta-2B)\frac{y}{r}-D\frac{x}{r}-F\frac{z}{r}\right]r^{-1}$$
$$r^3\frac{\partial V}{\partial z}=3\alpha\frac{z}{r}-R+\left[(5\beta-2C)\frac{z}{r}-E\frac{x}{r}-F\frac{y}{r}\right]r^{-1} \qquad (6)$$

with

$$\alpha=P\frac{x}{r}+Q\frac{y}{r}+R\frac{z}{r} \qquad (7)$$

$$\beta=A\left(\frac{x}{r}\right)^2+B\left(\frac{y}{r}\right)^2+C\left(\frac{z}{r}\right)^2+D\frac{xy}{r^2}+ \\ +E\frac{xz}{r^2}+F\frac{yz}{r^2} \qquad (8)$$

The differential equations of the field lines are thus equation (4) and (6).

An electronic computer (Johnniac) was used to integrate the paths of the lines starting at $s=0$ at the ground in step lengths of 100 km. The consistency of results was better than 50 km.

Also computed was the greatest height h (to the nearest 100 km or better) to the line of force.

The results found are indicated in Table 1, which lists values for lines terminating at ground level every 10° of latitude from 60°N to 0°S latitude and at 30° intervals in longitude.

Figure 1 summarizes the principal results of Table 1. The dipole fitting the geomagnetic field best is located at about 16°N, 149°E longitude about 350 km away from the earth's center. Although equation (3) includes the quadrupole terms in P_2^2, there is a tendency to symmetry about the off-center or eccentric dipole[3].

In Fig. 2 the average southern auroral zone estimated by Vestine and Snyder[4] from

Table 1. Latitudes and Longitudes of Points of Intersection of Lines of Force in Southern Hemisphere when Line Enters Earth at Latitudes $\phi \leqslant 60°$N, at Longitudes $\lambda = 0°$, 30° . . . . 330°E; also Maximum Height h of Line above Earth's Surface

North ϕ	$\lambda = 0°$		h (km)	$\lambda = 30°$		h (km)	$\lambda = 60°$		h (km)	$\lambda = 90°$		h (km)
	South ϕ	λ		South ϕ	λ		South ϕ	λ		South ϕ	λ	
60°	54·67	36·01	15292	46·97	52·60	11690	43·11	72·56	10610	41·31	95·30	10488
50	44·58	25·57	7226	36·56	44·77	5573	33·48	67·56	5219	32·30	93·40	5260
40	33·88	18·29	3470	25·75	39·37	2607	23·63	64·26	2500	23·16	92·11	2567
30	23·17	12·61	1540	14·92	35·56	1064	13·69	62·18	1039	13·86	91·23	1092
20	12·86	7·73	536	4·33	32·76	289	3·71	60·93	284	4·33	90·60	311
10	3·20	3·16	83									

North ϕ	$\lambda = 120°$		h (km)	$\lambda = 150°$		h (km)	$\lambda = 180°$		h (km)	$\lambda = 210°$		h (km)
	South ϕ	λ		South ϕ	λ		South ϕ	λ		South ϕ	λ	
60°	40·49	118·58	10661	41·19	140·20	11339	44·82	159·12	13502	52·45	175·47	19082
50	31·30	119·72	5270	31·38	144·12	5410	34·76	165·73	6245	43·04	184·89	8651
40	21·99	120·31	2531	21·44	146·65	2515	24·47	170·41	2878	33·22	191·73	4095
30	12·54	120·48	1049	11·43	148·24	1003	14·19	173·95	1168	23·38	197·23	1828
20	2·91	120·35	282	1·42	149·24	249	4·05	176·83	318	13·74	202·04	656
10										4·42	206·57	113

North ϕ	$\lambda = 240°$		h (km)	$\lambda = 270°$		h (km)	$\lambda = 300°$		h (km)	$\lambda = 330°$		h (km)
	South ϕ	λ		South ϕ	λ		South ϕ	λ		South ϕ	λ	
60°	64·15	191·20	31376	78·74	216·76	46938	81·74	346·41	40863	66·88	20·18	24345
50	56·22	204·54	13762	71·65	239·11	19844	73·96	324·26	18207	58·50	5·85	11473
40	47·52	213·36	6728	63·51	248·67	9887	65·57	316·57	9336	49·39	357·02	5833
30	38·64	220·10	3324	55·12	254·23	5193	57·13	312·23	5014	40·01	350·48	2960
20	29·81	225·90	1513	46·63	258·34	2669	48·69	308·96	2637	30·93	344·80	1383
10	21·15	231·28	540	38·03	261·91	1229	40·16	306·14	1253	22·35	339·40	515

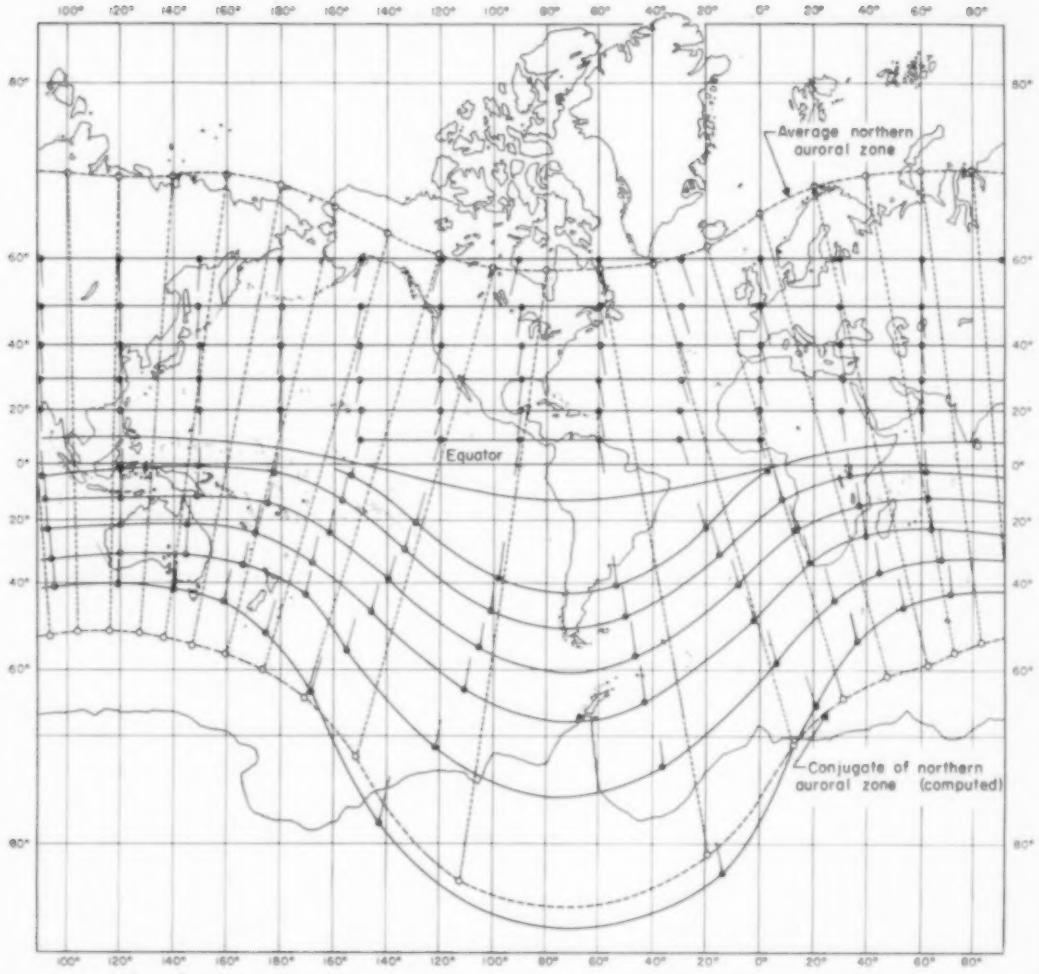

Fig. 1. Approximate intersections of lines of force of the geomagnetic field with the earths surface, northern and southern hemispheres, based on first 9 Gauss coefficients.

observation is shown. This is compared with that given by the southern intersection of the geomagnetic field lines with a spherical surface at height 100 km above the earth, in the case where these field lines originate at the northern average auroral zone.

The northern curve of maximum auroral frequency is that for observations made at ground level and is that deduced using Fritz's results to 1870, auroral observations of the First and Second International Polar Years 1882–83 and 1932–33, respectively, with the precision enhanced somewhat by the use of geomagnetic disturbance data in certain regions[3]. This precision of determination of the average maximum curve is unlikely to be much better than a degree of latitude or so, because the individual auroral displays actually range over a number of degrees of latitude and appear as transient phenomena. Hence the agreement in the calculated and estimated auroral zones to about 2° noted here lends

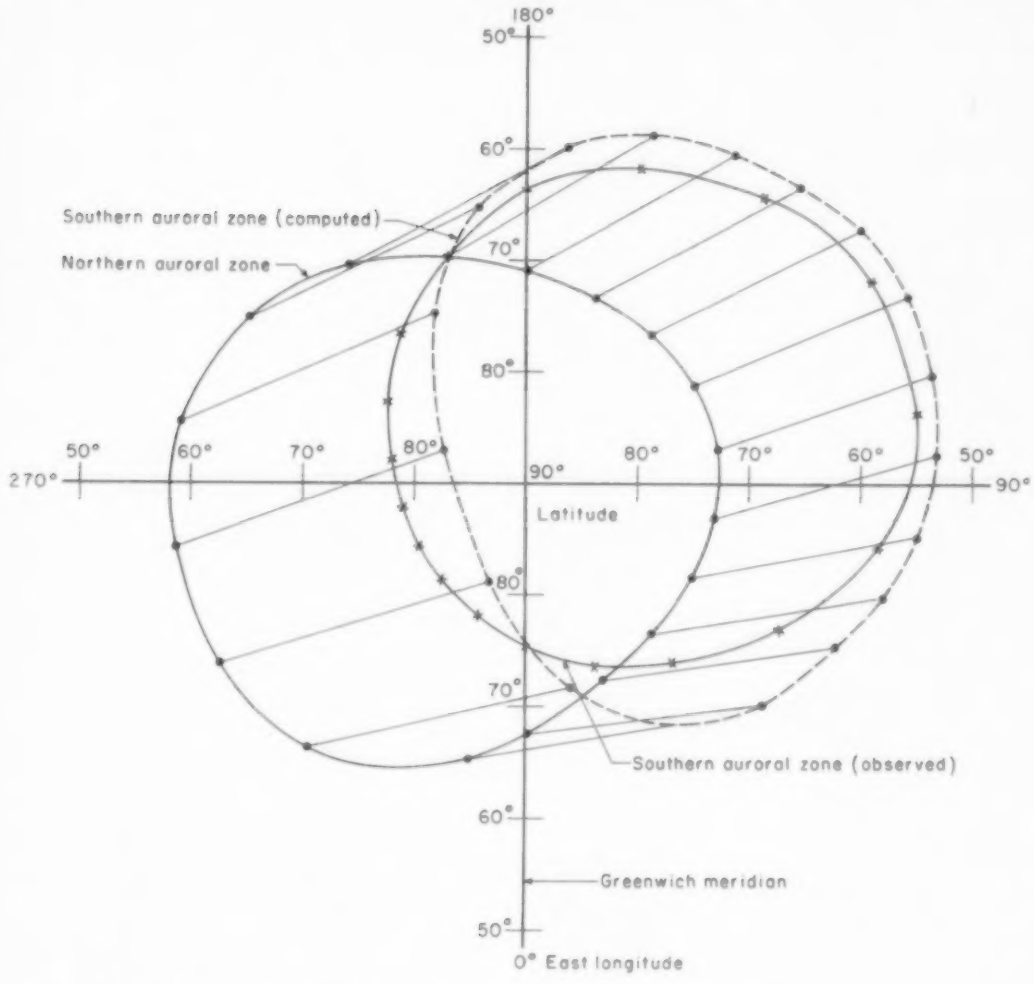

Fig. 2. Average northern and southern auroral zones as seen from above north pole.

added credence to the view, often expressed, that auroral displays in the northern and southern auroral zones are interlinked via the lines of force of the geomagnetic field. In fact Stormer[6] early suggested this possibility and actually computed trajectories of particles moving rapidly back and forth between the northern and southern auroral zones. More recently Singer[7, 8] has extended these calculations, using rough but useful approximate methods in connection with his model of magnetic storms and aurora and in his discussion of the earth's radiation belts high in the atmosphere, discovered from the U.S. earth satellite observations[9]. If the soft auroral particles represent transitory leakages of charge from the trapping region of the geomagnetic field, his results would also indicate, as Alfvén and others have shown, an eastward drift of electrons and westward drift of positive particles, mainly in the direction $F_\wedge$ grad F. For this reason the auroral zone is not a circle

but an oval, and average curves of auroral frequency will change in shape as the magnetic pole is approached. Since one can scarcely imagine that the lines of force entering close to the northern dipole can exist at many earth radii with a pattern resembling that of a simple dipole, it seems likely that auroral arcs seen near the dipole are variable in direction. In fact, Vegard and Krogness[10] and Currie[11] showed many years ago that the average direction of homogeneous auroral arcs as seen from stations well inside the auroral zone was inclined in angle to that expected from symmetry relative to the average curve of maximum auroral frequency. The average directions of these arcs was found to be very nearly perpendicular to the horizontal magnetic disturbance vector[12]. This can thus be explained on the basis of drift of charge and flow of current, or by the conduction of electric current horizontally along the auroral arc. The data of the IGY should afford interesting opportunities to check these possibilities. Study of these problems is not simple because other effects undoubtedly complicate the picture. Thus leakage of charge into the lower ionosphere may occur, for instance, during magnetic bays, giving rise to electric forces caused by penetration of protons and electrons to unequal depths.

The present result also shows that the lines of force of the geomagnetic field between the auroral zones probably have stability and a well defined simple character even in the equatorial belt out to a radial distance of the order 6 earth radii. It is also probable that solar streams do not ordinarily disrupt the geomagnetic field much closer to the earth. In other words any kinks in the field lines probably do not disrupt the motions of auroral particles travelling between the northern and southern auroral zones.

New analyses of Soviet and American charts for 1955 are under way which should provide better values. It is also hoped to include higher order terms in equation (1) possibly up to $n=6$. There are also plans to make some tabulations of the geometric field at distances up to about 10 earth radii in a form suited to geophysical and space studies.

REFERENCES

1. L. Block and N. Herlofson, Numerical Integration of Geomagnetic Field Lines, *Tellus* **8**, 210–214 (1956).
2. E. H. Vestine, I. Lange, L. Laporte and W. E. Scott, The Geomagnetic Field, Its Description and Analysis, *Publ. Carneg. Instn.* 580 (1947).
3. S. Chapman and J. Bartels, *Geomagnetism*, Vol. 2, pp. 648–659. University Press, Oxford (1940).
4. E. H. Vestine and E. J. Snyder, *Terr. Magn. Atmos. Elect.* **50**, 105–124 (1945).
5. E. H. Vestine, *Terr. Magn. Atmos. Elect.* **49**, 77–102 (1944).
6. C. Stormer, *Arch. Sci. Phys. Nat.* 140 pp. (1907).
7. S. F. Singer, *Trans. Amer. Geophys. Un.* **38**, 175–190 (1957).
8. S. F. Singer, *Phys. Rev. Letters* **1**, 171–173, 181–183 (1958).
9. J. A. van Allen, G. H. Ludwig, E. C. Ray and C. E. McIlwain, IGY Satellite Report Series No. 3; *Proc. Nat. Acad. of Sci.*, 73–92 (1958).
10. L. Vegard and O. Krogness, *Geophys. Publ.* **1**, No. 1 (1920).
11. B. W. Currie, *Terr. Magn.* **42**, 105–107 (1937).
12. E. H. Vestine, *Terr. Magn.* **43**, 261–282 (1938).

Planet. Space Sci. Pergamon Press 1959. Vol. 1, pp. 291–305. Printed in Great Britain.

ARTIFICIAL ELECTRON CLOUDS—II

GENERAL CONSIDERATIONS

F. F. MARMO,* J. PRESSMAN* and L. M. ASCHENBRAND*

Geophysics Research Directorate, Air Force Cambridge Research Center,
L. G. Hanscom Field, Bedford, Massachusetts

(*Received* 24 *April* 1959)

Abstract—This is the second in a series of papers which deals with the creation of artificial electron clouds by the ejection of proper contaminants into the upper atmosphere. It presents those general considerations which are common to the several papers to follow. A square-well model is used to describe the distribution of the ejected contaminant immediately after the fast initial expansion. The diffusion equation is applied to this model and the salient features are noted. Basic equations are applied to this simplified model to describe the electron generative and decay processes on a term-by-term basis, in order to ascertain the relaxation times involved for the several interrelated problems. Chemical consumption of the alkali metal contaminant by reaction with the ambient species is found to be negligible above 95 km. It is concluded that for generation methods similar to those outlined here the practical altitude limits of generation of long lived electron clouds is between about 70 and 200 km; chemical consumption determines the lower while the diffusion process establishes the upper limit.

1. INTRODUCTION

The feasibility of the formation of an artificially created electron cloud was first demonstrated on 12 March 1956[1]. This was accomplished by the release of approximately 18 pounds (275 moles) of nitric oxide gas from high pressure spheres which were carried aloft by an Aerobee rocket at an altitude of 95 km above Holloman Air Force Base, New Mexico. This experiment was projected as the result of a new laboratory determination of the photo-ionization cross-sections of nitric oxide[2]. The Lyman alpha (1215 Å) cross-section in particular was found to be 2×10^{-18} cm^2; a value about 25 times higher than was previously estimated by Bates and Seaton[3]. It was, therefore, possible to ascribe the formation of the natural *D*-layer of the earth's atmosphere to the photo-ionization of NO by the solar Lyman alpha radiation[4]. The March 1956 experiment served to strengthen this hypothesis, since an artificial electron cloud with an average density of about 4×10^6 electrons/cm^3 was created and detected for more than 10 minutes by radar techniques.

The success of the original electron cloud experiment initiated a systematic study of the physical, geophysical, chemical and engineering problems associated with the generation and properties of artificial electron clouds. Seven additional rocket experiments were performed between September 1957 and September 1958, in which artificial electron clouds were created by release of alkali metals into the upper atmosphere.

The extensive experimental data obtained have been summarized and a general discussion presented in the first paper of this series[5]. The experimental procedures and instrumentation have been described[6]. In this paper we present the theoretical structure required for the analysis of the various experiments to be considered in forthcoming publications.

Although the generation of a dense ($n_e > 10^6$ electrons/cm^3) electron cloud, by release of a contaminant at a predetermined altitude and time of day is a simple concept, the analysis and control of the processes involved is quite complex. The situation is further complicated by the interdependence of many processes and

* Presently associated with Geophysics Corporation of America, 700 Commonwealth Avenue, Boston 15, Massachusetts.

their dependence upon ill-defined or poorly known parameters. For example, the processes of generation of electrons can include thermochemical, photoionization, shock phenomena and photodetachment. Electron decay processes involve recombination, electron attachment and ion–electron kinetics among others. Further, these many processes are intimately related and vary in a complex manner and degree with such parameters as altitude of release, ambient or contaminant temperature, available solar flux, atmospheric composition, etc. This interplay of processes is further complicated by dynamic phenomena such as diffusion, shear and atmospheric turbulence which continually alter the problem with time. Chemical production of the contaminant (alkali metals for this study), the method of ejection and subsequent chemical consumption of contaminant by the active ambient species introduce other problems. Finally, the very practical considerations of engineering and cloud detection methods involve problems of still another nature.

2. GENERAL CONSIDERATIONS

(a) *Model concept*

The formulation of the mathematics associated with the phenomena discussed here is somewhat dependent upon the choice of model concept. It is supposed that the chemical contaminant is contained (or produced) under very high pressures (order of thousands of p.s.i.) and instantaneously released into the upper atmosphere (pressures of millimeters to microns). This gaseous contaminant is considered to expand very rapidly upon release and assume a given initial size and density distribution.

Initial size (and distribution) is taken to prevail after the instantaneous directed expansion and before the onset of significant diffusive. wind shear, magnetic or eddy effects, i.e. perhaps seconds after release (this is taken as $t=0$). Further, the initial size that the contaminant cloud assumes is described by a dilution factor. It is assumed that the cloud assumes ambient temperature but not necessarily ambient density. Thus, if ambient density prevails, the dilution factor is taken as unity. A contaminant density less than ambient is described by an appropriate dilution factor, i.e. 2 per cent of the ambient density is associated with a dilution factor of 0·02.

One can consider several models for the initial distribution, each applicable to some degree. Gaussian, parabolic, linear or square-well models have been examined. It can be shown that the square-well model is a good one; other choices do not profoundly alter the derived conclusions.

Immediately following the initial burst ($t=0$), the relatively slow expansion process due to the diffusion forces is considered to perturb the initial homogeneous distribution (square-well) and produce a Gaussian-like distribution of the neutrals, ions and electrons.

This model can be described mathematically by

$$\partial\psi/\partial t = D\nabla^2\psi \tag{1}$$

where $\psi(\mathbf{r}, t)$ is the normalized electron density and $\mathbf{r}$ the position vector of interest.

Assuming isotropic distribution and the initial conditions

$$\psi(\mathbf{r}, t)=1 \quad \text{where } r<a$$
$$\psi(\mathbf{r}, t)=0 \quad \text{where } r>a$$

Consider

$$y=(a-r)/(2\sqrt{Dt}); \quad Z=(r+a)/(2\sqrt{Dt})$$

For the case $r<a$

$$\psi(\mathbf{r}, t)=\phi+\frac{1}{\sqrt{\pi}}\int_0^y \exp(-\xi^2)\,d\xi \tag{2}$$

where

$$\phi=\frac{1}{\sqrt{\pi}}\left[\frac{\sqrt{Dt}}{r}\{\exp(-z^2)-\exp(-y^2)\}+\int_0^z \exp(-\xi^2)\,d\xi\right]$$

For $r>a$ we write

$$\psi(\mathbf{r}, t)=\phi-\frac{1}{\sqrt{\pi}}\int_0^y \exp(-\xi^2)\,d\xi \tag{3}$$

Maximum density occus at $r=0$ and is given by

$$\psi(0, t)=\frac{2}{\sqrt{\pi}}\left[\int_0^x \exp(-\xi^2)\,d\xi-\chi\exp(-\chi^2)\right] \tag{4}$$

where

$$\chi = a/(2\sqrt{Dt})$$

This expression is readily evaluated with the aid of tables of the well-known error function and its derivatives.

Clearly, the variation of mass and density with time and radial distance from the center can be determined. We choose to consider only the behavior of the maximum density ($r=0$) with time since it will be of value to determine the magnitude of the relaxation time required to observe any significant decrease of this data[7]. Thus, for order of magnitude considerations, this is essentially constant for several minutes. Similar calculations for the other models considered show that similar relaxation times prevail. This factor results in considerable simplification of some of the problems encountered. It should be mentioned here that experimental observations have indicated that dilution factors greater than 50 are usual under these experimental conditions.

More complex models that necessarily include some of the parameters omitted from the simplified considerations (magnetic effects, wind shear, eddy-size spectrum, etc.) will be developed whenever applicable and necessary in later papers of this series.

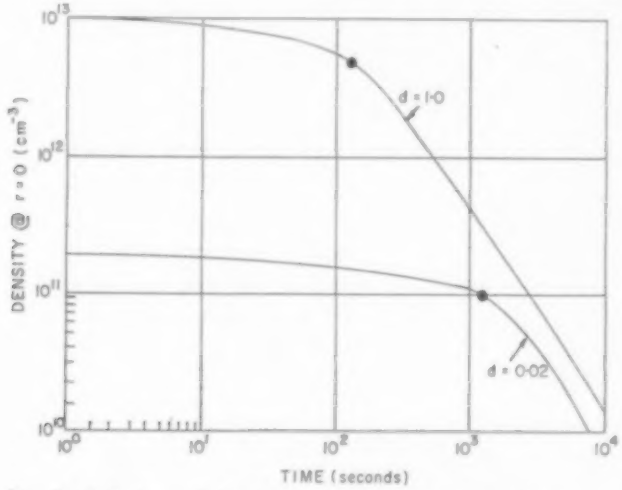

Fig. 1. Behaviour of density (0,t) and associated $t_{\frac{1}{2}}$ (shown by solid circles). Plot is for 3×10^{25} particles at 100 km where the diffusion coefficient is taken to be 13 m²/sec. Upper curve is for dilution factor, d, of unity whereas the lower curve is for $d=0{\cdot}02$.

density (see Fig. 1). Two important parameters controlling the rate of decrease are the diffusion coefficient and initial size (as varied by the mass of material, method of release, dilution factor, etc.). Fig. 1 is a plot of the center density $n(0,t)$ vs. time. The solid circles indicate $t_{\frac{1}{2}}$, the time needed to decrease the initial density by a factor of 2 for the release of 50 moles (3×10^{25} particles) of constituent at 100 km with dilution factors of 0·02 and unity. The $t_{\frac{1}{2}}$ values are of the order of $1{\cdot}4\times10^3$ and 10^2 sec, respectively. The value for D of 13 m²/sec was taken from empirical meteor

(b) *Basic equations*

Using the adopted model the following governing equations are applied in order to examine the behavior of the ionized cloud system as a function of time. Consider the differential equation of the time variation of electron and ion densities.

$$dn_e/dt = q - \alpha_r n_e N^+ - \beta n_e + \delta N^- + \gamma N^- \quad (5)$$

which describes the net rate of production of electrons. The production rate of free electrons, cm^3/sec, by photoionization is given by

$$q = \int \sigma n_c I d\nu \tag{5a}$$

where

n_c = number of contaminant particles per cm^3,
I = solar flux, photons/cm^2 sec wave number,
σ = atomic photoionization cross-section, cm^2.

Recombination is indicated as

$$\alpha_r n_e N^+ \tag{5b}$$

where

α_r = ion electron recombination coefficient, cm^3/sec (here taken as radiative),
n_e = density of electrons, cm^{-3}
N^+ = positive ion density, cm^{-3}. In addition
N^- = negative ion density, cm^{-3}.

The coefficients of the remaining terms are defined as follows:

$\beta_1 = \eta_1 [o]$
$\beta_2 = \eta_2 n [o_2]$
η_1 = two-body electron attachment coefficient, cm^3/sec
η_2 = three-body electron attachment coefficient, cm^6/sec
n = ambient particle density
$\delta = \int \rho I d\nu$
ρ = photodetachment cross-section in cm^2
$\gamma = \kappa n$
κ = coefficient of collisional detachment cm^3/sec.

We can also write

$$dN^-/dt = -\alpha_i N^+ N^- + \beta n_e - \delta N^- - \gamma N^- \tag{6}$$

where α_i = coefficient of mutual neutralization by negative and positive ions (cm^3/sec) including three-body recombination. We assume the net space charge as zero at all times so that

$$N^+ = n_e + N^- \tag{7}$$

According to the above equations the net electron production rate depends on a complex relationship between the processes of generation and decay. Several experimental parameters encountered in this series of experiments varied over a wide range: for example, the altitudes, solar ionizing fluxes, atmospheric composition (with altitude variation), the methods of contaminant release, etc. The time constants or relaxation times involved for the various processes may vary correspondingly. Therefore, the general solutions of these overall equations would yield little data of immediate value. On the other hand, it is illuminating to treat the various processes independently to ascertain the various time constants involved and the departure (if any) from equilibrium for the various terms. This approach often yields a justification for neglecting various processes for given experimental conditions. This method is adopted here for further discussion of the terms in the differential equation.

(c) *Photo-electron generation, q*

The production of electrons is considered to be due only to the process of photoionization of the released constituent at altitude. According to equation (5a), the rate of production, q, is large when σ, the overall photoionization cross-section, is large, and also when the local contaminant particle density, n_c, and the available ionizing flux are large. In considering an isolated ionized cloud in the upper atmosphere, the phenomena of diffusion or possible wind and turbulent effects are working against any buildup of a high electron density. In order to achieve the required high rate of electron production, the chemical contaminant under study must possess a low ionization potential (large solar ionizing flux) and a large photoionization cross-section (preferably throughout

Table 1. Tabulation of σI Data for Various Elements

Element	I. P. (eV)	At. Wt.	σI
Cesium	3·87	132·91	$6{\cdot}5 \times 10^{-4}$/sec
Lithium	5·36	6·94	$1{\cdot}38 \times 10^{-4}$
Rubidium	4·16	85·48	$1{\cdot}06 \times 10^{-4}$
Potassium	4·32	39·10	$1{\cdot}85 \times 10^{-5}$
Sodium	5·12	22·99	$1{\cdot}01 \times 10^{-5}$
Magnesium	7·61	24·32	$3{\cdot}6 \times 10^{-6}$
Barium	5·10	137·36	$2{\cdot}07 \times 10^{-6}$
Calcium	6·09	40·08	$1{\cdot}4 \times 10^{-6}$
Beryllium	9·28	9·01	$1{\cdot}6 \times 10^{-7}$

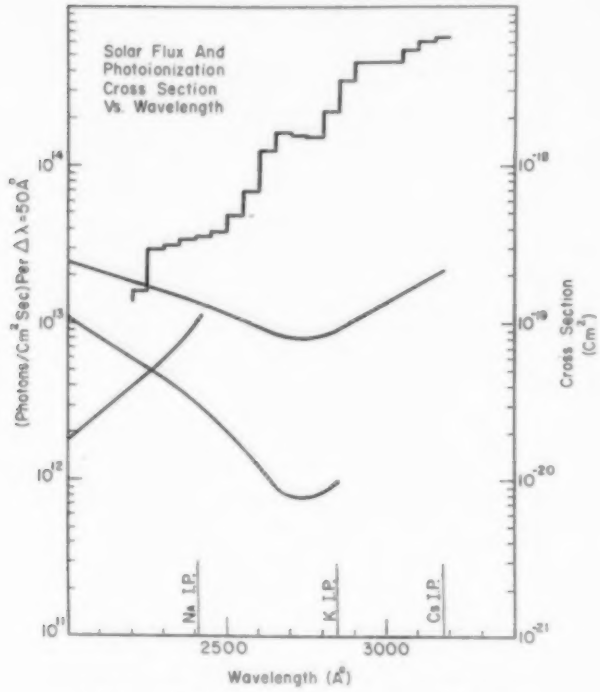

Fig. 2. Plot of the solar flux outside the atmosphere in units of $\Delta\lambda = 50$ Å, photons/cm² sec and photoionization cross-sections of the alkali metals between 2000 and 3200 Å. The ionization potentials are included.

an extended spectral range). The probability of photoionization per particle is defined as $p = \int \sigma I d\nu$ and has been determined here for a representative group of elements which were considered for experimentation. These are shown in Table 1, where the tabulated probability values were obtained in the following manner. The photon flux, I, above the atmosphere was averaged over 50 Å intervals[9] for the wavelength region from 2200 Å to 3200 Å. Data on intensity of vertically incident solar radiation below 2200 Å was obtained from a recent publication by Watanabe[9]. The photoionization cross-sections, σ, of various elements have been reported by Weissler[10]. Fig. 2 shows the average ($\Delta\lambda = 50$ Å) available photoionizing solar flux throughout the spectral range 2000 Å to 3200 Å and the observed photoionization cross-sections of three alkali metals, Cs, K and Na. To determine the probability of photoionization per particle, the products ($\Delta\sigma \cdot \Delta I$) were summed over the 2200-3200 Å region. Deduced or extrapolated values in the wavelength region 1600 Å to 2200 Å were obtained for a particular element (wherever applicable) and added to the longer wavelength contribution.

The data shown in Table 1 were useful in the choice of possible contaminants for the experimental program. Additional considerations such as engineering feasibility, costs, availability, photoionization cross-section data, physical and chemical characteristics were also important. For an initial systematic study the utilization of a family of elements offers advantages since the results may easily be correlated.

The alkali metals (cesium, sodium and potassium) were chosen for initial investigation.

In this series, neutral Na was used as a "doping agent" for cesium experiments to make visible the twilight release of contaminant[5]. This was possible because Na possesses a strong resonance line at about 5890 Å. Similar possibilities exist for other neutral species (Ba, Li, etc.). In addition, the interesting possibility of rendering the positive ions (in the ion–electron cloud) visible should be further explored. For example, it may be valuable to consider Ba and Ca twilight releases and optically detect the subsequent resonance radiation emitted from the neutrals and positive ions. The dynamics of the ions and neutrals can thus be compared. Combinations of contaminants can also be utilized for controlling the emission intensity ratio of various neutral and ionized species.

According to equation (5a), to determine the rate of electron production, the photoionization probability must be multiplied by the proper value of the contaminant particle density n_c. Since under these experimental conditions the contaminant can absorb only a small fraction of the incident solar radiation, the photoionization probability is relatively independent of the complex behavior of the clouds, whereas n_c is strongly dependent. However, the question of what value of n_c to utilize for determining q is difficult, since in practice the local $n_c(r, t)$ varies with time in a complex manner. The complexity is ascribed to the effect of diffusion, wind shear, eddy-size spectrum, initial cloud size and shape, and chemical reactivity with ambient atmospheric constituents, etc. By imposing certain assumptions and conditions it is possible to obtain a working approximation for $n_c(r, t)$. For example, we assumed, previously, the square-well distribution and found for a dilution factor of 0·02 a contaminant density of $2\times10^{11}/\text{cm}^3$ at $r=0$, which we showed to be essentially constant for the order of minutes (Fig. 1). For a cesium contaminant, therefore, the initial photoionization rate, $q_0 \simeq 1{\cdot}3\times10^6/\text{cm}^3$ sec.

(d) *Electron–ion recombination*

We now wish to determine the relaxation times associated with the attainment of equilibrium when only the processes of electron production, q, and recombination, α_r are considered. For this purpose, it is valuable to consider realistic parameters. Unfortunately, a serious discrepancy exists between theoretical and experimental determinations of electron–ion recombination rates. For example, a common type of recombination occurs when the excess energy of electron–ion recombination is given off in the form of radiation. Quantum mechanical calculations[11] predict a coefficient for this type of radiative recombination of the order of 10^{-12} cm^3 sec^{-1}, but these do not agree even in order of magnitude with experimental determinations. The extent of the discrepancy is shown in Table 2 where some experimental values from recent recombination measurements are given; the values are observed to vary between 10^{-6} to 10^{-10} cm^3 sec^{-1} (indicating processes other than radiative recombination).

The process we limit ourselves to here is described by

Table 2. Experimental Determinations of Recombination Rates for Cesium

Alkali metal	Reference	Electron temperature (°K)	Pressure (mm Hg)	Method	(cm^3/in sec)	Electron density
Cs	Mohler[12]	1300	$1\text{–}10\times10^{-2}$	optical cont. spectrum cesium arc	$3{\cdot}6\times10^{-10}$	$1{\cdot}8\times10^{12}$
Cs	Mohler	1200	$1\text{–}10\times10^{-2}$	probes in arc	$3{\cdot}4\times10^{-10}$	1×10^{12}
Cs	Donderad and Holt[13]	1400	0·32–0·68	microwave	$3{\cdot}5\times10^{-7}$ $1{\cdot}21\times10^{-6}$	10^{12}

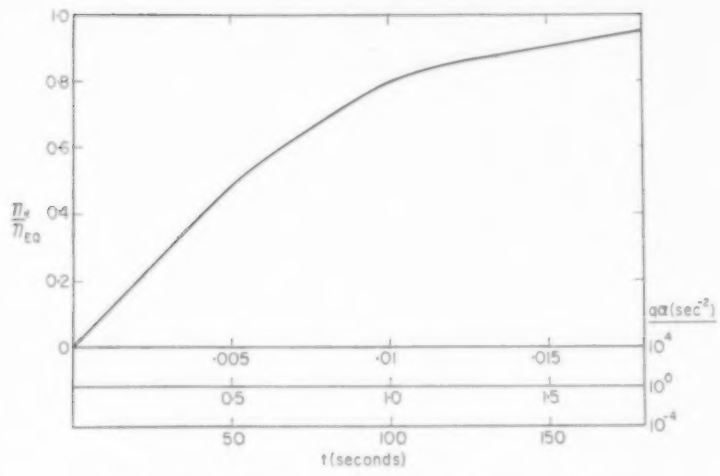

Fig. 3. Time behaviour of n_e/n_{eq} for $q\alpha$ values of from 10^{-4} to 10^4 sec^{-2}.

$$dn_e/dt = q - \alpha_r n_e^2 \tag{8}$$

Integration and rearrangement of this equation yields the following expression:

$$n_e/n_{eq} = \mathrm{Tanh}\,(q\alpha_r)^{\frac{1}{2}}t$$

where

$$n_{eq} = (q/\alpha_r)^{\frac{1}{2}}$$

and

$$q\alpha_r = (\sigma I)N\alpha_r \tag{9}$$

In Fig. 3 we have evaluated equation (9) as a function of time for $q\alpha_r$ between 10^{-4} to 10^4 sec^{-2}. It can be shown that this is a representative range of $q\alpha_r$ values to explore if one considers a release altitude range of between 70 to 200 km and incorporates the uncertainty in the value of α_r. For illustration, this latitude can be sharply reduced if we choose to employ certain values for specific experiments reported in this series so that we can then establish the relaxation times for the attainment of close approach to equilibrium. For example, we can choose a value of about 10^{-10} cm^3 sec^{-1} for α_r, consider a release in the close vicinity of 100 km and again apply a dilution factor of 0·02. For this case, the $q\alpha_r$ value is about 2×10^{-4} sec^{-2}. Thus, according to Fig. 3, the time constants involved for $t_{\frac{1}{2}}$ (for $n_e/n_{eq} = 0{\cdot}5$) is about a minute or so. This time is to be compared to those shown in Fig. 1, where for only 50 moles of contaminant $t_{\frac{1}{2}}$ is about 25 min for diffusion.

(e) *Electron-attachment considerations*

We consider now the time constants for electron attachment processes for the conditions encountered in electron cloud production. Only the processes of attachment to 0_2 and 0 are considered.

The coefficient adopted for three-body attachment of thermal electrons to molecular oxygen is 5×10^{-30} cm^6/sec from drift tube measurements by Chanin *et al.*[14]. This value was substantially corroborated by a theoretical calculation by Dubs and Sen[15] who used the data from a nuclear explosion. Their theoretical value was $4{\cdot}2 \times 10^{-30}$ cm^6/sec for thermal electrons.

The value of the two-body attachment coefficient to atomic oxygen has been recently obtained by using the principle of detailed balancing to determine the radiative attachment cross-section from the experimentally determined photodetachment cross-section[16]; near thermal energies the coefficient varies from $1{\cdot}2$ to $1{\cdot}37 \times 10^{-15}$ cm^3 per sec. A value of

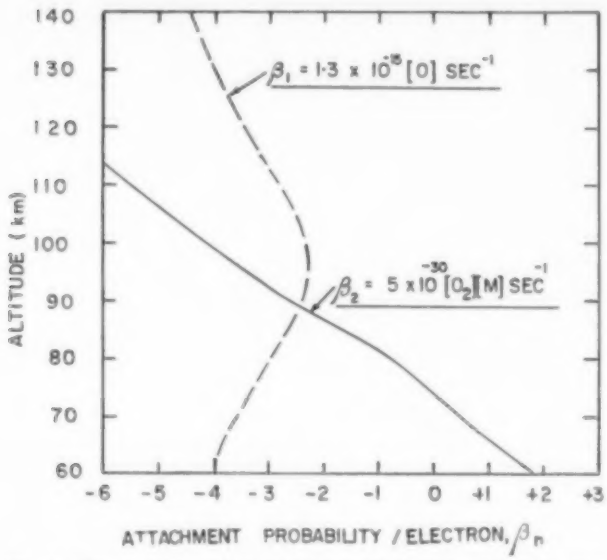

Fig. 4. The variation of the electron attachment probability per electron, β, with altitude for the two processes: two-body atomic and three-body molecular oxygen attachment.

1×10^{-15} cm^3/sec has been adopted in this paper. Finally, on the basis of recent findings[14] consideration of two-body attachment of thermal electrons to molecular oxygen has been excluded.

The process discussed here is described by

$$dn_e/dt = (\sigma I)\, n_e - \beta n_e \qquad (10)$$

where the terms have been previously defined. Integration and rearrangement of this expression give the simple relationship

$$n_e/n_{eq} = 1 - e^{-\beta t} \qquad (11)$$

Since the definitions of β incorporate the particle density of either 0_2, and/or 0 and M, it is, of course, sensitively dependent on altitude and ambient composition. These factors are taken into account in Fig. 4, where the values of β as a function of altitude are indicated separately for both the three-body molecular and two-body atomic oxygen attachment processes. The largest β values from about 60 to 130 km vary between $10^2 - 10^{-4}$ sec^{-1}. The plot clearly shows that at about 90 km $\beta = 10^{-2}$ sec^{-1} and that above this altitude the two-body (atomic oxygen) process predominates. At lower altitudes it is the three-body (molecular oxygen) attachment which is important. Fig. 5 is a plot of n_e/n_{eq} versus time for representative β values between 10^{-2} to 10^2 sec^{-1}.

From the form of equation (11) it can be seen that Fig. 5 may be used to determine the relaxation time required for the value of n_e/n_{eq} to attain a value of $1 - 1/e$ or 0·63. This is accomplished simply by taking the reciprocals of the β values given on the abscissa. For example, at an altitude of about 100 km this time constant is already of the order of 500 sec or over 8 min. It is noted that short relaxation times are encountered below about 80 km.

It is interesting to note the experimental latitude that exists here. The relaxation times associated with β are independent of contaminant mass, σ, I and n_e. This is not the case for ion–electron recombination. Proper experimental planning can utilize this fact in probes designed to isolate or minimize the role of one process.

(f) *Photodetachment-processes*

Previous discussion has been concerned with the problem associated with the probability of

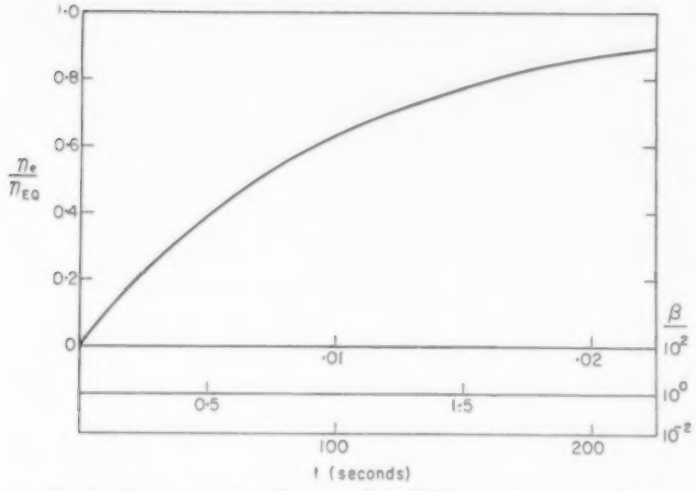

Fig. 5. Time variation of n_e/n_{eq} for photoionization production and electron attachment processes. The parameter β, the probability of attachment per negative ion, varies from 10^{-2} to 10^2.

electron attachment to molecular and/or atomic oxygen to form negative ions. Further consideration must be applied to the history of these negative molecular and/or atomic ions. Since the species O_2^- and O^- absorb the solar radiation, there exists a subsequent detachment of the electrons to form neutral species. The present approach is concerned with the rates of photodetachment without any consideration of atmospheric attenuation or absorption of entering radiation. The equation describing the photodetachment process has been given in Section 2(b). The appropriate flux, I, can be computed from published data of the solar radiation[8]. The spectral region of interest is in the relatively long wavelength radiations. For the case of atomic oxygen photodetachment, a rate of 1·4 per negative ion/sec at noon in the upper atmosphere has been determined[16]. The analogous value for molecular oxygen has been computed here by utilizing solar radiation data[8] and applying the known absorption cross-section values[18]. Then, numerical integration yields a value of 0·40 negative ion/sec at noon in the upper atmosphere.

Thus, if one considers a constant rate of production, with electron attachment and detachment as the only other processes, the governing equation is

$$dn_e/dt = q + \delta N^- - \beta n_e \qquad (12)$$

where electron photodetachment contributes to the production of electrons rather than decay. The solution to this equation is given in (17) where the negative ion–electron equilibrium is treated.

3. CHEMICAL CONSUMPTON PROCESSES

It is important in these experiments to determine the role of competitive chemical processes in the consumption of the released contaminant by ambient atmospheric constituents. For this purpose it is necessary to compare two rates, namely, that at which the ejected alkali metal vapor is chemically consumed by ozone or atomic and/or molecular oxygen to the net rate of production of electrons. The X^+ ion is considered chemically inert and not considered further here. The chemical processes considered are

$$X + 0 + M = X0 + M \qquad (13)$$

$$X + 0_2 + M = X0_2 + M \qquad (14)$$

$$X + 0_3 = X0 + 0_2 \qquad (15)$$

where X represents the alkali metal. Reactions involving atomic and molecular nitrogen are considered less probable. It is also unlikely that the two-body reaction involving X and 0_2 need be considered[19]. The rate coefficients for the above three reactions are taken as 1×10^{-32} cm^6 sec^{-1} [20], 5×10^{-30} cm^6 sec^{-1} [21] and $1{\cdot}5 \times 10^{-11}$ cm^3 sec^{-1} [20], respectively. Serious consideration of reaction (15) can be dismissed simply on the question of the available mass of ozone within the volume containing the contaminant, X. Ozone is present only in parts per million in the atmosphere at the experimental altitudes; therefore, there is not enough mass to consume a significant portion of the contaminant, regardless of the rate of consumption under experimental conditions encountered. On the other hand, it is quite possible to have at least the equivalent number of 0_2 and/or 0 within the physical volume occupied by the contaminant and to suffer complete consumption of the alkali metal in time. The assumption is made that there is an excess of available ambient constituent as compared to the contaminant. Experimentally, this is probably the case, since an over-expansion resulting in a decrease of contaminant density by a factor of 50 ($d = 0{\cdot}02$) below ambient is achieved. In addition, the growth of the cloud with time implies that it encompasses more mass of ambient constituent with time whereas the total number of contaminant atoms decrease with time.

Fig. 6 is a plot of altitude versus time with two curves describing the variance of $t_{\frac{1}{2}}$, that time necessary to achieve one-half completion of reaction or depletion of contaminant. The plot was obtained by considering the three-body reactions of equations (13) and (14) using the ambient densities of 0_2 and 0 at the various altitudes and the total number density at these altitudes for the third body M. Fig. 7 depicts the variation of number density of the constituents of interest and the total density as a function of altitude[22]. The $t_{\frac{1}{2}}$ for consumption is insensitive to the number density of alkali metal so long as the assumption of excess combining constituent over contaminant is preserved. In Fig. 6 it is shown that even for altitudes as low as 90 km hundreds of seconds

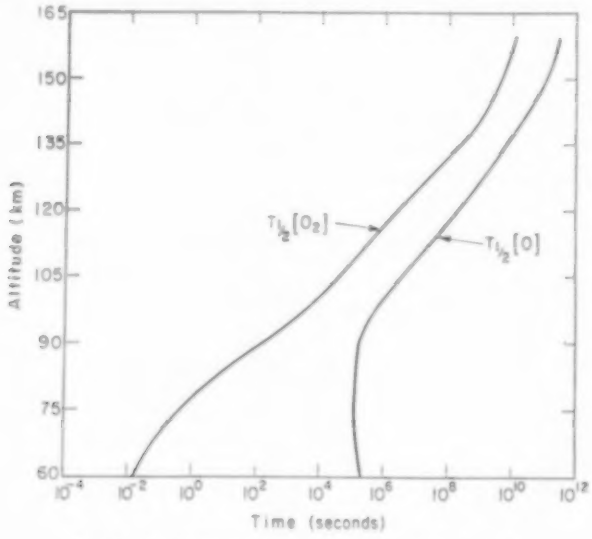

Fig. 6. Altitude variation of alkali metal half-life by atomic and molecular oxygen chemical consumption processes.

are required for 50 per cent consumption, whereas at an altitude of 60 km only about 10^{-2} sec is required. Thus, it is apparent that the times associated with significant chemical

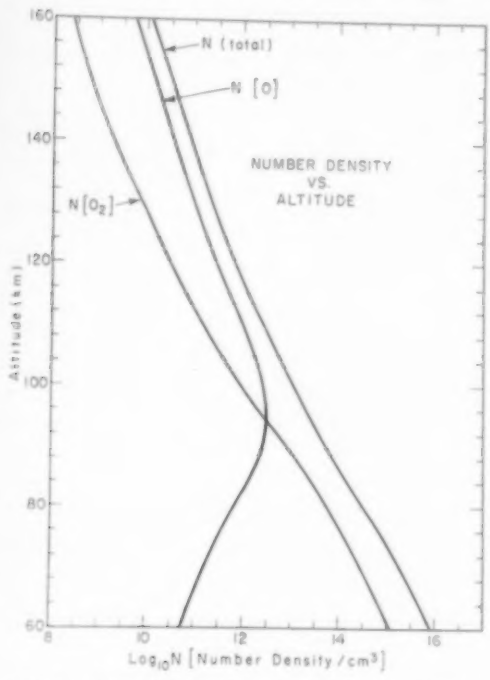

Fig. 7. Number density vs. altitude of various atmospheric constituents (after Minzner and Ripley [22]).

consumption of contaminant should be compared to the time factors considered significant for the other processes discussed earlier. Accordingly, above about 100 km the consumption process is ignored.

4. ALTITUDE OF RELEASE

We consider now the qualitative behavior of the electron cloud as a function of altitude. It will be seen that the experimental goals will determine the release altitude.

We divide the altitude range into two categories. Upper altitudes are defined as those above which electron attachment (and subsequent negative ion kinetics) can be ignored compared to processes such as diffusion and recombination. This is taken to be above about 90–100 km. At lower altitudes, negative ion kinetics are significant. It will be shown that the practical altitudes for artificial electron cloud generation fall between 70 km and 200 km, if we assume that the primary purpose is the creation of a radio–radar detectable cloud (electron density considerably above ambient) for the order of minutes.

The following discussion assumes the release of 50 moles of cesium vapor (3×10^{25} particles), photoionization probability of $6{\cdot}5\times10^{-4}$/sec and a dilution factor of 0·02.

(a) *Upper altitude considerations*

For the upper altitudes (above 100 km) electron attachment is slow compared to recombination or diffusion. Hence, in the following we omit references to attachment and the follow-on processes of detachment and mutual neutralization. We calculate q for 200 km to be approximately 10^5 cm^3/sec (see Table 3) and take α_r even to be 10^{-10} cm^3/sec; then it can be seen from Fig. 3 that the time, $t_{\frac{1}{2}}$, to approach the recombination equilibrium is of the order of 300 sec. Diffusion, however, works against the

Table 3. Rate of Production of Photo-Electrons for Various Altitudes

(d is the Dilution Factor)

H (km)	q	
	$d=1{\cdot}0$	$d=0{\cdot}02$
100	$1{\cdot}06\times10^{10}$	$2{\cdot}1\times10^{8}$
150	$2{\cdot}9\times10^{7}$	$6{\cdot}0\times10^{5}$
200	$6{\cdot}6\times10^{6}$	$1{\cdot}3\times10^{5}$

establishment of this equilibrium in two ways. First, q, decreases rapidly by diffusion of the contaminant material and secondly, the generated electrons suffer depletion by the diffusion process. From the analysis of the square-well model we deduce the following decay time relationship for the center point density: $t_{\frac{1}{2}}=a^2/(4{\cdot}4D)$, $t_{0{\cdot}1}=2{\cdot}02t_{\frac{1}{2}}$, $t_{0{\cdot}01}=4{\cdot}6t_{\frac{1}{2}}$ where $t_{\frac{1}{2}}$, $t_{0{\cdot}01}$ and $t_{0{\cdot}1}$ represent the times for the center density to fall to one-half, one-tenth and one-hundredth of its original value. For 200

km, in Table 4, we obtain a value of $t_{\frac{1}{2}}$ for diffusion to be about 70 sec. Thus, no significant approach to recombination equilibrium will be achieved since by 300 sec the contaminant density is down to 0·01, i.e. part of its original value. In addition, the original electron density itself will have been depleted by a factor of 0·01. Hence, for the values selected, the achievement of an electron density of 10^6 for the order of minutes seems marginal at best.

In addition, this calculation is sensitive to the selected value of the diffusion coefficient, D. The value of D chosen was not that obtained by graphical extrapolation of the empirical diffusion coefficients[7] used in the lower regions. Such an extrapolation would yield a value of D which is larger by a factor of 300. Rather, the calculation was made on the basis of the ratio of pressure and temperature at 200 km–100 km as determined by satellite observations[23]. These conclusions are further weakened since even the mechanism of diffusion has not been established for this case. We further note that if D is larger by only a factor of two it seems that it would be quite unlikely to achieve $n_e > 10^6$ for any reasonable period of time. Therefore, while the calculations are somewhat uncertain they do indicate that production of practical electron clouds above 200 km is unlikely.

Table 4. Values Used in Upper Altitude Determination*

H (km)	n (particles/cm³)		a (particles/cm³)	q (electrons/cm³ sec)	D (meters²/sec)
	$d=1·0$	$d=0·02$	$d=0·02$	$d=0·02$	
150	$4·4\times10^{10}$	$8·8\times10^{8}$	2×10^{5}	$5·8\times10^{5}$	$1·9\times10^{4}$
200	$1·0\times10^{10}$	2×10^{8}	$3·2\times10^{5}$	$1·2\times10^{5}$	$1·1\times10^{5}$

* All symbols have been defined in the text.

(b) *Lower altitudes*

We will not attempt to deal, at length, with the lower altitudes (70 to 90 km) since this will be treated in detail in another paper. For completeness, we briefly summarize here some of the conclusions of that study[17]: (1) the photoionization production rate decreases by about a factor of 100 with increasing altitude, (2) the probability of photodetachment remains relatively constant, (3) the rate of chemical consumption is altitude sensitive with rapid consumption at the lowest altitude, (4) diffusion is not significant, (5) the electron attachment process is affected strongly by altitude variation, with the three-body reaction rate becoming dominant with decreasing altitudes. Finally, it is shown that it is not practical to achieve long lived dense electron clouds below about 70 km.

Here it is pertinent to consider the importance of electron attachment. We introduce the negative ion-to-electron ratio, $\lambda = N^-/n_e$. The time required for establishment of the electron–negative ion equilibrium is of importance. If we restrict the processes to those of electron production, attachment and photodetachment we obtain the following equations:

$$N^- = \beta q/(\beta+\delta)^2\,[(\beta+\delta)\,t - 1 + e^{-(\beta+\delta)t}] \quad (16)$$

and

$$n_e = qt - N^- \quad (17)$$

For $(\beta+\delta)\,t > 1$ the following approximation holds

$$N^- = \beta qt/(\beta+\delta)$$

and

$$n_e = \delta qt/(\beta+\delta)$$

hence

$$\lambda = \beta/\delta \quad (18)$$

Since $\delta \simeq 1$, at all altitudes equilibrium is reached in the order of seconds and at lower altitudes within a fraction of a second. The assumption that λ is a constant is justified by the fast rate of the attachment equilibrium relative to the other processes. A further consequence is that $\beta \simeq \lambda$, so that Fig. 4 is directly

applicable for obtaining λ-values. Hence, λ has a real meaning in our discussion.

There are two main processes for the formation of negative ions; the three-body 0_2 attachment and the two-body 0 attachment. From Fig. 4 it is clear that the three-body attachment process is the dominant one below 90 km, whereas the two-body process is important above this altitude.

As a consequence of the formation of the negative ions, a variety of processes involving negative ions become possible. These include collisional detachment, associative detachment, and mutual neutralization of positive and negative ions.

Collisional detachment is still not effective at 70 km because of the small coefficient ($2{\cdot}4\times10^{-17}$ cm^3/sec)[25]; associative detachment is not effective because of the low concentration of atomic oxygen. From Fig. 6 we obtain a value of only 10 for λ at 70 km. In the following section the n_{eq} is analyzed as a function of varying height. If we use Case III of Section 5, we find that

$$n_{eq}=\left(\frac{1{\cdot}4\times10^{9}}{10^{2}\alpha_i}\right)^{\frac{1}{2}}=\left(\frac{1{\cdot}4\times10^{7}}{\alpha_i}\right)^{\frac{1}{2}}$$

If we let $\alpha_i=10^{7}-10^{-9}$ we obtain

$$n_{eq}=1{\cdot}2\times10^{7}-1{\cdot}2\times10^{8}$$

so that reasonable concentrations may still be established despite the increasing role of attachment at lower altitudes. This leads to the conclusion that at 70 km electron attachment does not preclude the possibility of generating useful electron clouds. On the other hand, Fig. 6 indicates that for chemical consumption of alkali metals at 70 km the $t_{\frac{1}{2}}$ is much less than one second; it is considered here that this establishes the lower limit.

5. VARIATION OF EQUILIBRIUM ELECTRON DENSITY WITH ALTITUDE

In this section we examine the behavior of the equilibrium electron density, n_{eq}, with altitude. It is shown to vary with different powers of n_e for several cases. We assume the following: (1) λ is established rapidly, (2) diffusion and chemical consumption are negligible, (3) a high degree of dilution of the contaminant species.

We have the well known relationship

$$\frac{dn_e}{dt}=\frac{q}{1+\lambda}-(\alpha_r+\lambda\alpha_i)\,n_e^2 \tag{19}$$

The equilibrium value is given by

$$n_{eq}=\left[\frac{q}{(1+\lambda)\,(\alpha_r+\lambda\alpha_i)}\right]^{\frac{1}{2}} \tag{20}$$

We have further set $\lambda=\beta/\kappa n+\delta=\beta/\delta$ since the term κn in the denominator is much less than δ for altitudes above 35 km for reasonable values of κ (about 10^{-17} cm^3/sec)[25]. Further, since $\delta\simeq1$, $\beta\simeq\lambda$ and we use the numerical values interchangeably from Fig. 4. Thus, the crossover in two-body and three-body attachment rates corresponds to a value of $\lambda=7\times10^{-3}$. We shall first consider only the case of three-body attachment and altitudes below 90 km. Thus we have

$$\lambda=(\eta_2 n^2)/5\delta \tag{21}$$

where the concentration of 0_2 is taken to be $n/5$. In addition, $q=pdn_e$ at all altitudes and $\alpha_r\ll\alpha_i$[24].

We now examine equation (20) employing three different cases corresponding to various relationships which may exist between the parameters involved.

Case I. This is the case where

$$\lambda\ll1 \text{ and } \alpha_r>\lambda\alpha_i$$

then

$$n_{eq}=\left(\frac{q}{\alpha_r}\right)^{\frac{1}{2}}=\left(\frac{pd}{\alpha_r}\right)^{\frac{1}{2}}n_e^{\frac{1}{2}};\ n_{eq}\sim n_e^{\frac{1}{2}} \tag{22}$$

Case II is where

$$\lambda<1 \text{ and } \alpha_r<\lambda\alpha_i$$

and

$$n_{eq}=\left(\frac{q}{\lambda\alpha_i}\right)^{\frac{1}{2}}=\left(\frac{5pd\delta}{\eta_2}\right)n_e^{-\frac{1}{2}};\ n_{eq}\sim n_e^{-\frac{1}{2}} \tag{23}$$

For Case III we have

$$\lambda>1 \text{ and } \alpha_r\ll\lambda\alpha_i$$

which yields

$$n_{eq}=\left(\frac{q}{\lambda^2\alpha_i}\right)^{\frac{1}{2}}=\frac{5\delta}{\eta_2}\left(\frac{pd}{\alpha_i}\right)^{\frac{1}{2}}n_e^{-3/2};\ n_{eq}\sim n_e^{-3/2} \tag{24}$$

Thus we obtain three distinct regions in which the relationships between n_{eq} and n_e are indicated above.

There is another possibility for the case $\lambda < 1$. A two-body reaction which depends upon the relative value of λ and the ratio α_r/α_i, may come into play. If $\lambda > \alpha_r/\alpha_i$ for the region of the atmosphere where the two-body processes dominates (above 90 km), we have a similar situation to Case II which we call Case IV.

$$\lambda = \eta_i [\mathrm{o}]/\delta$$

and

$$n_{eq} = \left(\frac{q}{\lambda \alpha_i}\right)^{\frac{1}{2}} = \left(\frac{pd\delta}{\eta_1 \alpha_i}\right)^{\frac{1}{2}} \left(\frac{n}{[\mathrm{o}]}\right)^{\frac{1}{2}} \qquad (25)$$

To illustrate, let us assume some values and consider the consequences.

Let $\alpha_r = 10^{-10}$ cm^3 sec^{-1}, and $\alpha_i = 10^{-7}$ cm^3 sec^{-1}, thus $\alpha_r/\alpha_i = 10^{-3}$. Then, if we extract λ values from Fig. 4 we conclude that: Case I applies above 110 km; Case IV applies from 110–90 km; Case II applies from approximately 90–75 km; and Case III below 75 km. If $\alpha_r/\alpha_i = 10^{-2}$ then Case I holds above 90 km; Case II holds 90–75 km and Case III from 75 km down. Case IV is not applicable.

The above arguments reveal the interesting variation of the equilibrium electron concentration, n_{eq}, with altitude. We should note again that we have omitted diffusion and chemical consumption considerations. This point is somewhat elaborated in a future paper of this series[17].

6. CONCLUSION

The performance and interpretation of electron cloud experiments involves solutions of a number of physical and engineering problems, including some of considerable complexity. On the other hand, the fact that a link exists, between experiments of this kind and an extended spectrum of physical processes, implies that considerable information pertaining to the phenomena concerned can be obtained with the proper development of the theoretical and experimental techniques. Paper I[5] of this series outlines some of these areas.

The scientific areas discussed in this work have been considerably simplified and consequently suffer in general applicability and exactness. For example, the utilization of a square-well model with a given mass of gas release allowed simplification of the mathematics employed. Although other models yield similar results, the approach is highly restrictive.

The influence of several parameters upon the overall dynamics of the cloud composed of neutrals, electrons, positive and negative ions have been ignored. These include the effects of wind and wind shear, magnetic-interaction, shock formation and the varying nature of the diffusion mechanism (molecular, transitional, turbulent, ambipolar, eddy-size spectrum). Indeed, consideration of the complex behavior of the initial expansion and its interaction (or degree of mixing) with the ambient atmosphere has been deferred until later. These are extremely important considerations and are critical for the studies as will be recognized as the series progresses.

The various kinetic and dynamic problems associated with the production and decay of the several possible species have been limited to daytime, solar-illuminated conditions. The limitations imposed by this restriction have been discussed in the text. However, some of the conclusions presented change radically when night-time experiments are considered.

In conclusion, this discussion has served to illustrate the general scope of the problem and the roles of the various processes and phenomena encountered. Several of the pertinent problems have been defined and qualitatively discussed. Further, it has been shown that several suitable contaminants are available for utilization as atmospheric contaminants; in some cases optical detection of the ions can be anticipated. Finally, it has been established that for the experimental methods employed, the altitude limits for the generation of long lived, dense artificial electron clouds are between 70–200 km. The lower limit is determined by the chemical consumption rate whereas the upper altitude limit is diffusion-controlled.

REFEFRENCES

1. F. F. Marmo, J. Pressman, L. M. Aschenbrand, A. S. Jursa and M. Zelikoff, *J. Chem. Phys.* **25,** 187 (1956).
2. K. Watanabe, F. F. Marmo and E. C. Y. Inn, *Phys. Rev.* **91,** 1155 (1953).
3. D. R. Bates and M. J. Seaton, *Proc. Phys. Soc. London* **B63,** 129 (1950).
4. K. Watanabe, F. F. Marmo and J. Pressman, *J. Geophys. Res.* **60,** 513 (1955).
5. F. F. Marmo, L. M. Aschenbrand and J. Pressman, *Planet. Space Sci.* **1,** 227 (1959).
6. L. M. Aschenbrand, F. F. Marmo and J. Pressman, *Electron clouds—VI,* to be published.
7. T. R. Kaiser, *Meteors,* p. 19. Pergamon Press, London (1955).
8. P. R. Gast, Handbook of Geophysics for Air Force Designers, AFCRC (1957).
9. K. Watanabe, *Advances in Geophysics,* vol. 5, p. 174 (1958).
10. G. L. Weissler, *Handbuch der Physik,* Bd. 21, S. 332. Springer, Berlin (1956).
11. E. C. G. Stueckelberg and P. M. Morse, *Phys. Rev.* **36,** 16 (1930).
12. F. L. Mohler, *J. Res. Bur. Stand.,* **10,** 771 (1933).
13. P. Donderad and E. H. Holt, *Handbuch der Physik,* Bd. 21. Springer, Berlin (1956).
14. L. M. Chanin, A. V. Phelps and M. A. Biondi, *Phys. Rev. Letters* **2,** 34 (1959).
15. C. W. Dubs and H. K. Sen, *11th Annual Gaseous Electronics Conference, New York, Oct. 1958.*
16. L. M. Branscomb, D. S. Burch, S. J. Smith and S. Geltman, *Phys. Rev.* **111,** 504 (1958).
17. J. Pressman, F. F. Marmo and L. M. Aschenbrand, *Electron Clouds—VII, Planet. Space Sci.,* to be published.
18. D. S. Burch, S. J. Smith and L. M. Branscomb, *Phys. Rev.* **112,** 171 (1958).
19. J. F. Bedinger, E. R. Manring and S. N. Ghosh, *J. Geophys. Res.* **63,** 19 (1958).
20. D. M. Hunten, *J. Atmos. Terr. Phys.,* **5,** 144 (1954).
21. C. E. H. Bawn and A. G. Evans, *Trans. Farad. Soc.,* **33,** 1571 (1937).
22. R. A. Minzer and W. S. Ripley, *Air Force Surveys in Geophysics* No. 86, AFCRC (1957).
23. R. A. Minzner, private communication.
24. D. K. Bailey, *The Nature of the Ionosphere, Proc. Inst. Radio Engrs., N.Y.,* special issue, p. 255 (February 1959).
25. A. P. Mitra and R. E. Jones, *J. Geophys. Res.,* **59,** 391 (1954).

Planet. Space Sci. Pergamon Press 1959. Vol. 1, pp. 306–318. Printed in Great Britain.

ARTIFICIAL ELECTRON CLOUDS—III

RELEASE OF ATOMIC POTASSIUM AT 121 km

F. F. MARMO*, L. M. ASCHENBRAND* and J. PRESSMAN*

Geophysics Corporation of America, Boston 15, Massachusetts

(*Received* 12 *June* 1959)

Abstract—This paper reports the results of the first successful rocket seeding experiment expressly designed for the generation of an optimum type artificial electron cloud. The analysis and interpretation of the data was successfully accomplished by assigning the initial ionization to thermal effects after which solar photoionization of the released contaminant predominates. This was achieved by the daytime Aerobee release of atomic potassium at an altitude of 121 km.

A best fit of experimental data was dependent on varying sensitivity and extent of several parameters. These include D_e, the effective diffusion coefficient; c, the thermal ionization efficiency; r_0, the initial half width of the electron cloud and the chemical yield. Approximate values for these are deduced.

C-3 ionosonde data on the change in cloud slant range with time was utilized to obtain a measure of the horizontal wind velocity at about 121 km; this value is about 78 m/sec.

Extrapolation of the obtained information was employed in order to ascertain the feasibility of utilizing other type rocket carriers for experiments of this kind. This also afforded the opportunity to deduce the order of magnitude results which should have been obtained by the release of cesium from an Aerobee, an experiment attempted earlier by the authors which mechanically failed. The interesting results also serve to suggest several new rocket experiments.

1. INTRODUCTION

Paper I[1] of this series presents a concise summary of data obtained in eight rocket experiments associated with the production of artificial electron clouds while Paper II[2] discusses the general considerations pertinent to a systematic study of this nature. This, the third in the series, is concerned with the presentation, analysis and interpretation of the data obtained for the initial experiment designed expressly for the generation of an optimum artificial electron cloud in the upper atmosphere. The successful experiment was performed by the daytime release of atomic potassium at an altitude of 121 km. The remainder of this section is devoted to a brief discussion related to the planning involved in the experimentation.

Paper II included the reasons for restricting this initial study to the three alkali metals, namely, cesium, potassium and sodium. In addition, it was indicated that the photoionization probabilities per atom for these contaminants were $6{\cdot}5\times10^{-4}$/sec, $1{\cdot}9\times10^{-5}$/sec and $1{\cdot}0\times10^{-5}$/sec, respectively. Thus, other things equal, it appears that cesium is most suitable of these for the generation of a maximal type artificial electron cloud. On this basis, the constituent was chosen for the initial attempt in this study for the generation of dense electron clouds in the upper atmosphere.

Important to this intial attempt was the determination of the optimum altitude of chemical release. The term optimum is relative since it is dependent upon the electron density–time factors regarded attainable for the experiment. For example, it was felt that one could strive for a cloud which displayed an

* Original work was performed when authors were employed at Geophysics Research Directorate, Air Force Cambridge Research Center, Hanscom Field, Bedford, Mass.

This work has been supported in part under contract U.S. Army Signal Corps DA36-039-SC-78925.

electron density in excess of 10^7 electrons/cm^3 for a period of more than 30 min or about 2×10^3 sec. Thus, with this sample criterion, the rôles of chemical consumption, electron attachment, recombination, diffusion, chemical yield and cloud dynamics had to be considered in order to determine the most advantageous release altitude. For this initial attempt little was known of the various factors involved, and in some cases little more than crude estimates could be employed. For example, the chemical yield was arbitrarily taken to be 100 per cent, and the maximum of the initial contaminant density was assumed to be equal to that of the ambient atmosphere at the altitude of release. In addition, the question of chemical consumption (as discussed in Paper II) at a release altitude of greater than 100 km was considered a negligible effect. Above this altitude, the daylight rôle of electron attachment and photodetachment processes could be ignored. Thus, a programmed release altitude of greater than 100 km was in order. To arrive at a practical upper limit one must consider the rôle of recombination at some altitude above 100 km utilizing the above assumptions and criteria. If this is done (cf. Paragraph 1*d* of Paper II), an upper-limit estimate of about 130 km seems to be reasonable. This would imply that, for the case of cesium, the rate of apparent electron density loss at this altitude becomes primarily diffusion-controlled.

Thus, for optimum probability of success, based on the order of magnitude arguments above, a cesium release at about 130 km was considered a good choice for the initial attempt of this kind. Accordingly, the first experiment devised for generation of a long-lived dense artificial electron cloud was performed on 19 September 1957, when 110 moles of cesium nitrate in a chemical mix was carried aloft by an Aerobee rocket and was to be released in the form of atomic cesium at 130 km. Unfortunately, both the primary and alternate initiating and release mechanisms failed to function at altitude. A second cesium compound payload was not readily available, so it was decided to perform the identical experiment utilizing the second best of the chemicals considered, potassium. It was considered advantageous to alter the choice of release altitude down to 120 km, since the photoionization probability of potassium is only $1{\cdot}9 \times 10^{-5}$/sec. Accordingly, the altitude at which the process becomes diffusion-controlled is reduced. Preliminary calculations indicated a high probability of success with this element, albeit a more reduced probability when compared to cesium. In addition, some apparent advantages of utilizing potassium were as follows: the chemical nitrate is very inexpensive, readily available and weighs less per mole than the cesium compound. These factors are considered to be relatively important for the planning of an extensive rocket study.

Notwithstanding that in retrospect it was found that several of the above assumptions did not apply (especially the assumed yield), the successful generation of a detectable artificial electron cloud was achieved by the release of atomic potassium at 121 km.

In addition to obtaining valuable information regarding winds, diffusion constants and mechanisms, chemical yield, reaction temperature, etc., it was found that the data could be scaled accordingly to predict the result of an identical release of sodium and/or cesium. These interesting results indicated the possibility of utilizing a smaller, more reliable, much less expensive carrier as the Nike-Cajun.

2. EXPERIMENTAL TECHNIQUES

Chemically, the primary experimental requirement was for the production and release of the elemental alkali metal within a very short period of time, since it was desirable to achieve a well defined release of contaminant at the predetermined altitude. A method of producing alkali metal vapor was devised which incorporated these requirements. The employed chemical reaction was that between the alkali metal nitrate and finely divided aluminum powder.

It was ascertained by prior ground tests that a low constant pressure reaction was not suitable in that it reacted too slowly and inefficiently. On the other hand, if the reaction

was permitted to proceed in a confining volume the resultant effect was a very vigorous release of alkali metal vapor which ruptured the cannister (static rupture pressure of about 250 atm).

In order to instrument the Aerobee rocket carrier, a stainless steel container with the proper dimensions was fabricated. It measured 11·5 in. in height and diameter with a wall thickness of $\frac{3}{16}$ in., so the available volume was 1120 in^3 or about 17·5 l. It was fabricated with a $\frac{1}{2}$ in. thick steel flanged cover which was attached in such a manner as to rupture at approximately the same burst pressure as the container. Consideration of the strength of the container was important since it was desirable to contain the reaction for an appreciable fraction of one second or so following ignition by the squib arrangement. However, the possibility of rupture before complete reaction was considered to be serious, and in fact, it is later suggested that rupture did occur before 10 per cent reaction had been completed. The reactants used consisted of 153 gm moles of potassium nitrate and 407 moles of aluminum granules of 60 micron maximum particle size. The loaded cannister weighed about 51·0 kg.

In spite of the inherent shortcomings in this type of chemical release, it was utilized in this initial experiment and proved effective. The chemical, physical and mechanical considerations associated with this type of release are discussed next.

3. CHEMISTRY OF CONTAMINANT RELEASE METHOD

In addition to the several difficulties encountered in the chemical method employed, it is clear that several different possible reaction paths can be employed to accomplish the generation of the alkali metal. In spite of this, some useful information is derived by the following simplified considerations.

Preliminary inspection of these various reaction paths indicated that an excess of Al should result in a higher probability for the successful generation of the alkali metal. Further, simple thermochemical calculations indicated that the confined reaction could not produce temperatures above about 4000 °K. Consequently, since the critical temperature of Al is taken to be greater than 4500°K some unreacted aluminum may exist in the condensed phase (if at equilibrium). On the other hand, it can be shown that the aluminum suboxides probably exist primarily in the gaseous form. Thus, the overall reaction is considered to be represented by

$$407\ \mathrm{Al} + 153\ \mathrm{KNO_3} = 153\ \mathrm{K}\ (g) + 76{\cdot}5 n_2\ (g) + \sum_i n_i$$

where

n_1 = moles $\mathrm{Al_2O}$ (g),
n_2 = moles AlO (g),
n_3 = moles $\mathrm{O_2}$ (g),
n_4 = moles O (g),
n_5 = moles Al (c),
n_6 = moles $\mathrm{Al_2O_3}$ (c)

and (c) means condensed, (g) gaseous phase.

The ideal gas law is assumed, and the following equilibria are considered to hold simultaneously:

$$\mathrm{Al_2O_3}\ (c) = 2\ \mathrm{Al}\ (c) + \tfrac{3}{2}\mathrm{O_2} \quad \text{and} \quad P_{\mathrm{O_2}} = K_1^{\frac{3}{2}} \tag{1}$$

$$\mathrm{Al_2O_3}\ (c) = 2\ \mathrm{AlO}\ (g) + \tfrac{1}{2}\mathrm{O_2} \qquad P_{\mathrm{AlO}} = K_2^{\frac{1}{2}} K^{-\frac{1}{2}} \tag{2}$$

$$\mathrm{Al_2O_3}\ (c) = \mathrm{Al_2O}\ (g) + \mathrm{O_2} \qquad P_{\mathrm{Al_2O}} = K_3 K_1^{-\frac{1}{2}} \tag{3}$$

$$\mathrm{O_2}\ (g) = 2\mathrm{O}\ (g) \qquad P_{\mathrm{O}} = K_4^{\frac{1}{2}} K_1^{\frac{1}{4}} \tag{4}$$

It is assumed that the activities of the condensed constituents are independent of pressure. Additional considerations show that the produced number of moles of gaseous AlO, $\mathrm{O_2}$ and O are negligible as compared to the other gaseous constituents and can be safely neglected in the following. The conservation of mass relation now becomes (N equals the total moles):

$$N_{\mathrm{Al}} = 2n_6 + 2n_1 + n_5 = 407$$
$$N_{\mathrm{O}} = 3n_6 + n_1 = 459$$

and from these relations and other data presented the number of moles of the several product constituents can be calculated.

Thereafter, the various K_n and P_n are determined from tabulated free energy values[3] at various temperatures near the expected reaction temperature (1500°K to 4000°K). The heat content of the products are determined as a function of temperature; the heat of reaction as a function of the amount of reaction products. From these data, heat balance techniques can be applied with the result that the temperature of reaction is estimated to be about 3500°K for complete reaction confined within the 17·5 l. vessel. However, when the sum of the partial pressures of the gaseous components is obtained, it is found that the cannister pressure is greater than 5000 atm. The cannister static burst pressure was about 250 atm, thus even if one assumes that it can tolerate a relatively instantaneous pressure of 1000 atm, it appears as if the cannister ruptures before complete reaction is achieved. A crude estimate of somewhat less than 10 per cent reaction seems reasonable. It should be noted that this situation also renders the calculated temperature as unreliable, however, it is felt that the above arguments do offer some overall qualitative conclusions. In fact, later discussion of *C*-3 radar returns indicate a yield of only 3 per cent and a temperature of release of about 3500°K. A later paper of this series[4] deals with the optical determination of yields in this type experiment, and this approach also indicates a chemical yield of no greater than 10 per cent in each case studied.

An Aerobee rocket carrying the KNO_3–Al mix was launched at 0929:56 MST on 19 November 1957 at HAFB, W. Alamogordo, New Mexico. At 111 sec after launch, the constituent was successfully released at an altitude of 121 km.

4. EXPERIMENTAL PROBES

Shortly after release of the chemical contaminant at this altitude, a highly ionized electron cloud was detected and reported.

The various experimental radar probes are individually discussed here for later reference pertinent to interpretation of experimental data. For this particular experiment a total of six significant radar techniques was utilized. These included the following: (1) a 70 kW Stanford University operated radar located at Alamogordo, New Mexico, (2) a forward-scatter probe of the transmission from the high frequency pulsed radar facility at Laredo, Texas, (3) the White Sands Proving Ground *C*-3 vertical incidence ionosonde facility, (4) the Ft. Huachuca, Arizona, 800 Mc transmitter monitored at Lubbock, Texas, (5) the Dovap missile tracking facility at White Sands Proving Ground, and (6) a radio amateur net dispersed within an 800 mile radius around the launch site.

The Stanford University probe is a 70 kW pulsed radar tunable at frequencies near 17·3 Mc, 23·1 Mc, 30·6 Mc, 40·6 Mc and 49 Mc. Since at least one minute is required to change a frequency setting, it was decided to start operating on 23·1 Mc since the initial electron density was expected to be of the order of 10^7 electrons/cm^3. Subsequent shift of frequencies was to be dictated by observed returns and application of proper judgment. The frequency of 23·1 Mc was utilized throughout the potassium experiment discussed here.

The Laredo transmitter radiates 1·2 MW pulsed power into each of two three-degree beams directed over the launch site. In the operation reported here, the Laredo transmissions were monitored by Smythe Associates at Durango, Colorado.

The *C*-3 ionosonde is located at the White Sands Proving Ground, New Mexico. It is a vertical incidence radar with a 10 kW pulsed output and sweeps a continuously variable frequency band of between 1 and 25 Mc. The ionosonde is normally programmed to take probe soundings routinely each 15 min. These are recorded on 35 mm film and exposed to reduction at the National Bureau of Standards Laboratory at Boulder, Colorado. One feature of this instrument is that it can be made to operate continuously by sweeping the 1–25 Mc band within 15 sec, and in this way it is possible to obtain up to four soundings per minute.

Programming for the several rocket flights reported in this series was generally as follows:

ionograms were obtained at the rate of 1/min for about 30 min before planned launch time to within 2 min of launch. Thereafter, the *C*-3 was operated on a continuous scan basis (four soundings per min) for a varying period of time depending on the observed and anticipated results. For the potassium experiment in particular, this period was for about 10 min after launch, and the operation was repeated at about 15 min after launch for another 10 min.

The Ft. Huachuca facility consists of an 800 Mc c-W transmission with 10 kW power. This transmission which was beamed toward the launch site was monitored for forward-scatter at Lubbock, Texas. This operation produced no reliable results. No signal at Lubbock could be associated with the formation of an electron cloud. The time factors involved in this initial utilization of the Ft. Huachuca facility and the incapacity of calibration under the conditions probably accounted for the lack of results.

The Dovap system is utilized for missile tracking at White Sands Proving Ground, New Mexico. It consists of a network of receiving stations giving recorded Doppler amplitude information on the transmitted signals of 36·94 Mc and 73·88 Mc with power of 1·5 kW and 125 W, respectively.

The amateur net consisted of several hundred radio amateurs located within an 800 mile radius of the launch site. An invitation to amateurs to participate in this series of ionospheric probes was publicized.[5] Briefly, a zone number was assigned to each participating station depending on where the station was located, and identifying call letters were also assigned. An attempt was made for the various amateurs (in one zone) to make contact with another zone so located as to test forward-scatter. The frequency range varied from 14 to 148 Mc.

Unfortunately, analysis of data from both the Dovap and amateur nets yielded no conclusive data. The interpretation of the Dovap data was made difficult by the presence of continual interference returns from many scattering points in the area. The inconclusiveness of the amateur reports was ascribed to poor communication between the launch site and the amateurs.

5. EXPERIMENTAL RESULTS

Figure 1 shows several representative ionograms taken on 19 November 1957. No. 1 was taken at 1 min prior to release (while the rocket was airborne). The horizontal lines are in hundreds of kilometers while the vertical lines show the frequencies, and the normal *E*- and *F*-layer responses are apparent. No. 2 (15 sec scan, starting at 0931:45) depicts the onset of ionization at 12 Mc as shown by the horizontal line at about 142 km (slant range) extending as far out as 25 Mc. No. 3 (scan starting at 0932:00) clearly makes the establishment of the ionized cloud. The initial height of the cloud formation was several kilometers above the normal *E*- but below the normal *F*-regions. Two resulting effects are noticeable in No. 4 which is the ionogram taken about 30 min after release. One effect is the upward cusping of the echo signal from both the lower and higher frequency sweep. The other effect is the low frequency cut off for reflections from the electron cloud. These effects are due to the fact that the electron cloud is embedded in the upper *E*-region. If the true height of release is known, these observations can be utilized to determine the electron content within the ionospheric region in question.

On the original *C*-3 records many multiple echoes were observed throughout the time of the programmed experiment. The three traces taken at release time plus 18, 20 and 22 min are shown in Fig. 2. The multiple echoes which were definitely ascribed to the presence of the electron cloud are obvious. The presence and behavior of these multiples have been related to processes other than normal diffusion. It was concluded that after a period of 10 min the cloud has expanded in horizontal diameters to values of hundreds of meters, and its shape was roughly that of a very flat spheriod. In addition, there probably was some cloud breakup at this time. It is clear that a better

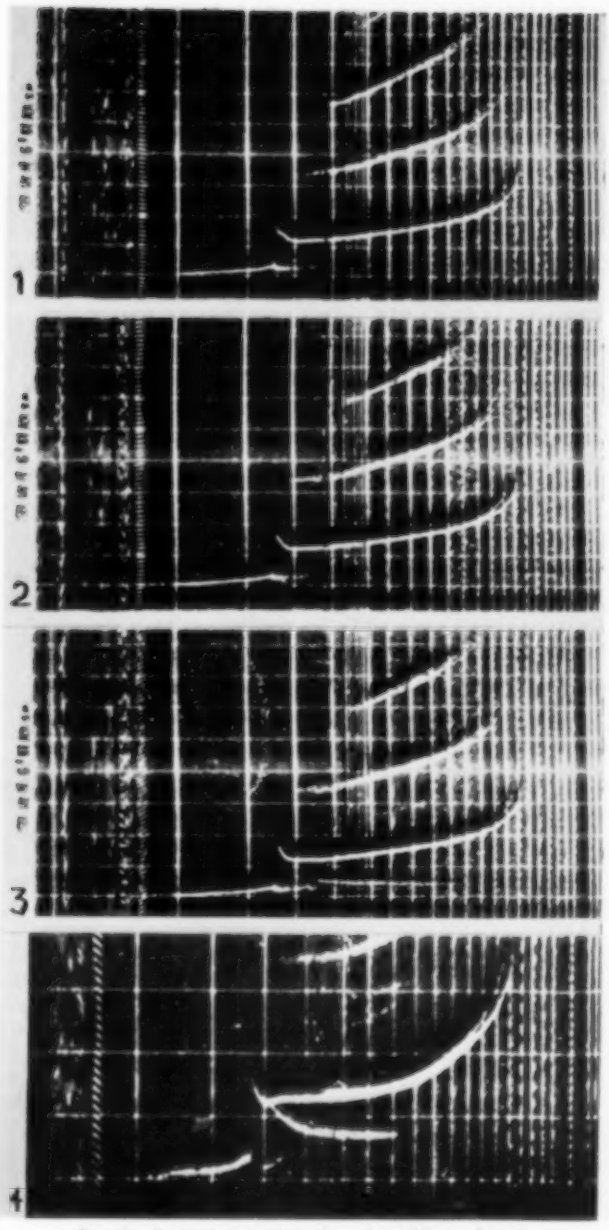

Fig. 1. Ionograms taken by the White Sands Proving Ground C-3 Ionospheric Sounder depicting No. 1—while the rocket was airborne prior to release, No. 2—just after release and onset of ionization (0931 : 45 scan), No. 3—established identification of ionization (0932·00 scan) and, No. 4 effect 30 min. after release.

[facing p. 310

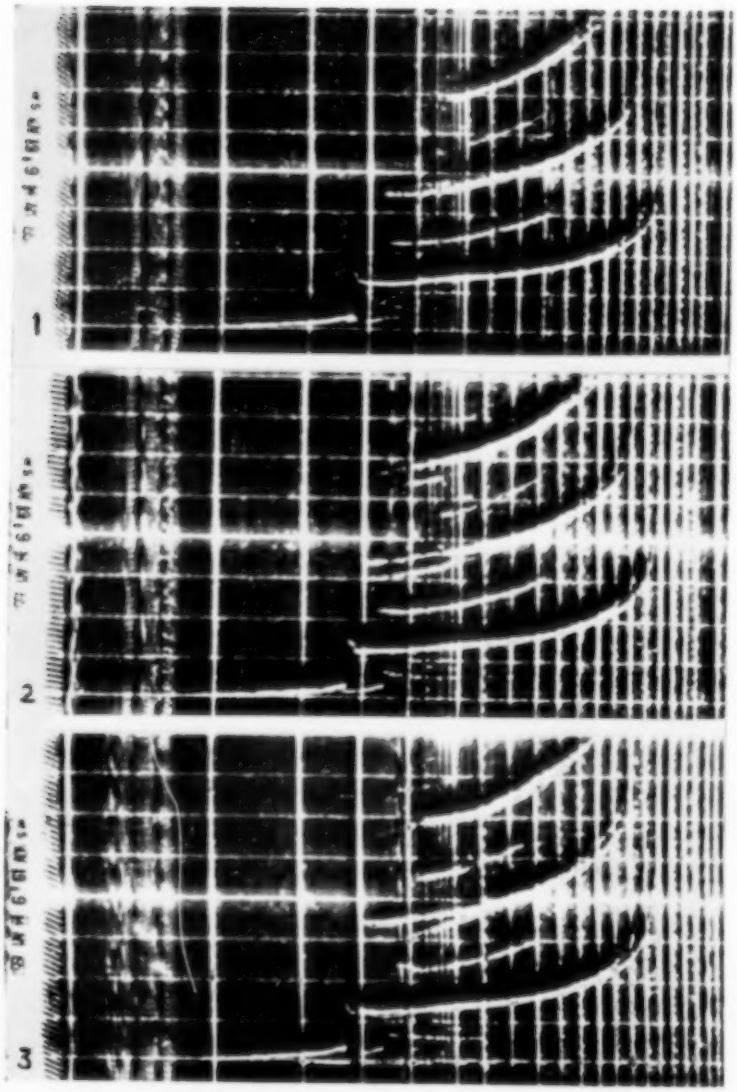

Fig. 2. Ionograms taken at 18, 20 and 22 min after constituent release. Evidence of Cloud effect as depicted by multiple echoes in each frame is apparent.

(facing p. 311)

interpretation of the data could be accomplished if the electron cloud were visible or photographable in order to correlate the radar and optical behavior with time. This was not accomplished here, but this is accomplished in the twilight releases discussed in Paper V[4] of this series.

Fig. 3 depicts the echo amplitude vs. time (*A* scan) plot of the Stanford University 70 kW radar located at Alamogrodo, New Mexico. The original record indicated some fluctuations in the amplitude which have been averaged out in the figure for simplification; however, the general contour has been preserved. Concerning

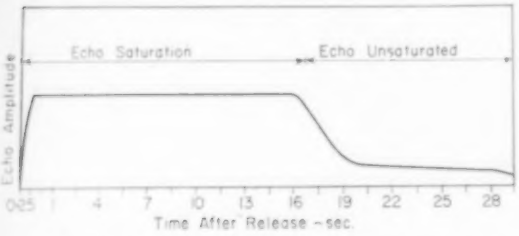

Fig. 3. Plot of echo amplitude versus time after release of constituent from data obtained by the Stanford University 70 kW radar.

this record the following can be stated. It represents a positive detection of the appearance of a reflecting cloud at the proper height (*B* scan gave 120 km) and time (launch time plus 111 sec). Thus, this return is undoubtedly associated with the formation of the artificial electron cloud. In addition, the saturated echo duration of about 17 sec indicated that the initial (first 17 sec) electron density was probably greater than $N_e = 6{\cdot}6 \times 10^6$ electrons per cm^3. Since the total 23·1 Mc was observed up to 30 sec, this density persisted at least for about 30 sec after release time. The relatively short duration of the unsaturated signal seems to indicate a rapid drop in critical frequencies. This effect can possibly be ascribed to normal diffusion. The *C*-3 ionosonde records, discussed later, support the observation of rapid drop in initial critical frequencies.

The results of the Laredo-Durango forward scatter experiment were considered positive on the basis of the record obtained by Smythe Associates at Durango, Colorado. This record indicated a saturated signal lasting for about 2½ sec for the 207 Mc transmission from Laredo, Texas. The timing of the observed echo (0931:48·5) corresponds with the data from the other probes described here. Accordingly, this represents transmission of a 207 Mc signal beyond line of sight, in fact for a distance of about 855 miles (Laredo–Durango).

Figure 4 shows the time variation of the slant range of the electron cloud as obtained from the *C*-3 ionosonde data. The range point represent averages of the four soundings taken during each minute. The smooth variation of the range with time for this 8 min period is strong support for the presence of a simple electron cloud. From the initial slant range of about 142 km, the increase in range is presumably due to ionospheric winds assumed to be horizontal, moreover, the contribution of vertical drifts is probably negligible. The relative radial velocity is 43 m/sec, and the initial height of the cloud formation is taken at 121 km. Simple geometric considerations show that if the cloud is drifting directly away from the *C*-3 ionosonde, its direction and average velocity are towards the northeast at 76 m/sec. If the cloud were moving at right angles to the plane which contains the station and the clouds initial position, the average velocity is 160 m/sec. An attempt to obtain the intermediate best geometric fit from these two extreme cases indicates that most likely the wind direction was towards the northeast with an average velocity of between 76 and 80 m/sec. These values are consistent with wind velocity data at an altitude of 95 km of 60 m per sec deduced from the nitric oxide release experiment[6], and wind determinations of 36 miles per sec at 119 km using a sodium release technique[7].

The results of the *C*-3 ionosonde (and the 23·1 Mc radar) are depicted in Fig. 5. The maximum frequency return associated with the cloud (and the corresponding electron density, backscatter assumed) is plotted against the time after contaminant release. According to the

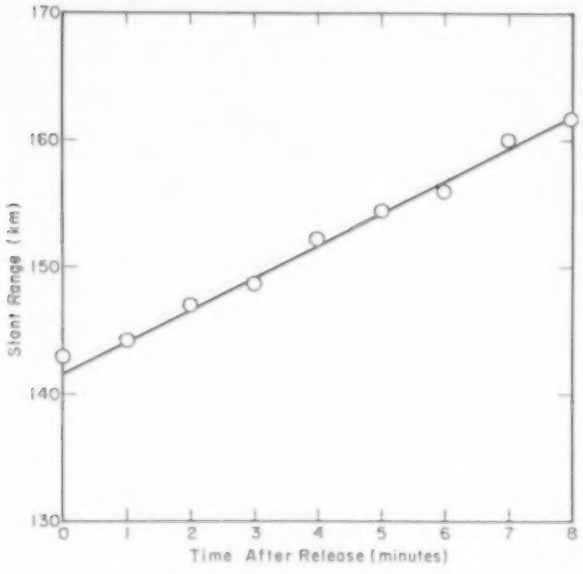

Fig. 4. Time variation of the slant range of the electron cloud versus time as obtained from the C-3 ionogram data.

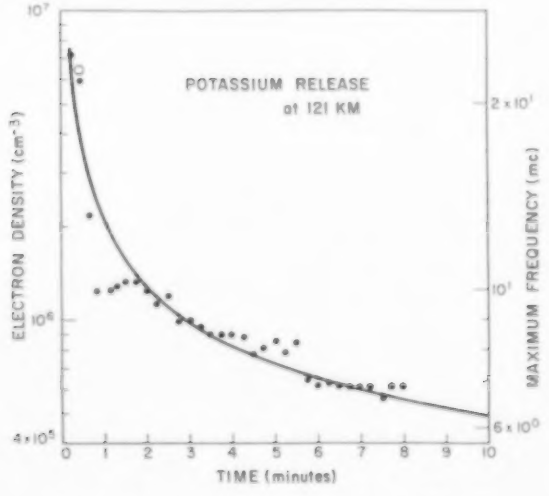

Fig. 5. Theoretical fit to the maximum frequency return versus time after release of constituent as obtained from the C-3 ionograms.

records, the contaminant release time occurred between the 0931:45 and 0932:00 MST ionograms. This corresponds to the time interval of launch time plus 105 to 120 sec. The actual release was verified by independent methods (ground monitor of timer) to be at 111 sec after launch. It is considered that the data shown in Fig. 5 is the most meaningful and reliable of the total. Also, it can be analyzed and interpreted in a manner which proves to be consistent with general theory. Thus, the analysis of these data is more detailed and follows.

6. ANALYSIS OF *C*-3 IONOSONDE DATA

As mentioned, the *C*-3 ionosonde data were considered to be the most meaningful and compatible to analysis. For ready comparison the data from the 23·1 Mc radar are represented by the open circle (Fig. 5) at 30 sec. This section outlines the method employed for the analysis of the data and the results obtained thereof. Subsequently, some of the experimental parameters obtained are extrapolated and applied to some hypothetical experiments revealing interesting results.

(*a*) *Dominant electron density decay processes*

For the proper choice of mathematical model it is important to ascertain which process or processes contribute significantly to the time rate of decay of electron density. An earlier discussion based upon the experimental parameters expected to be encountered led to the conclusion that diffusion was the dominant decay process. This was based on several assumptions not all of which were found to hold in retrospect to the subsequent findings from the analysis contained in this section. However, in those instances where only little agreement was found between some initial assumptions and an experimentally determined parameter the direction of disagreement was such as to strengthen the basis of the initial assumptions. Hence, the mathematical model selected still considers diffusion as the only effective electron density decay process in this experiment. Finally, it is demonstrated that the validity of this choice is further supported by the excellent agreement obtained between theory and observed data.

(*b*) *Mathematical model, Gaussian distribution*

Paper II of this series[2] employed a model which assumed an initial squarewell, homogeneous distribution which became Gaussian in time; this was used to facilitate the introductory discussions associated with the various interrelated processes encountered in the generation of artificial electron clouds. In most cases the general conclusions were similar to those which could have been derived from other initial distributions including the three dimensional Gaussian. The latter model is adopted for analysis here, since now the mathematics is facilitated without any loss in physical significance.

(*c*) *Optical size of cloud, Gaussian half width*

The electron cloud is not considered to be a relatively efficient radar reflector unless it has a diameter of greater than a few wavelengths; at 6 Mc the associated wavelength is about 50 m. An estimate of the electron cloud initial size is obtained as follows:

Data were available concerning the observed optical sizes (initial) of "doped" contaminant visible rocket twilight releases performed under cloud generation and release conditions similar to those employed here (see experiments 3 and 4 of Paper I[1]). In particular these were performed at 128 km and 116 km with somewhat smaller payloads (Nike-Cajun rockets). For our purpose, the observed optical widths were adjusted to an intermediate altitude release at 121 km, where an optical radius of about 600 m is suggested (after proper adjustment of varying payload). From this optical radius one can then obtain the corresponding Gaussian half-width r_0 of 200 meters by a method described in a forthcoming paper by the authors on the general optical behavior of resonance radiation clouds. Since many uncertainties exist in this method for estimating the proper Gaussian half-width, a range of between 100–300 m radius is considered here. Three consequences of this estimated r_0-value

are as follows. First, the rate of change in the cloud electron density is relatively insensitive to the adopted range of r_0-values in that no significant observable difference is apparent with the substitution of 100 or 300 m. Second, for such large r_0-values the cloud size criterion (radar reflector) is achieved essentially at release time (within a fraction of one sec). Third, the time behavior of the required radar cross section essentially duplicates the center point electron density decay. This latter factor is utilized in the mathematical treatment that follows:

(*d*) *Mathematical analysis*

The following analysis based on prior discussion was found to yield the best fit to the experimental data.

The general equation is

$$\frac{\partial n_e}{\partial t} = q + D_2 \nabla^2 n_e \tag{5}$$

where n_e = the electron density,
q = the photoionization rate of electron production,
D_2 = the ambipolar diffusion coefficient.

We assume that

$$q = \frac{\sigma N}{\pi^{3/2}(4D_1 t + r_0^2)^{3/2}} \exp - \left(\frac{r^2}{4D_1 t + r_0^2}\right) \tag{6}$$

where σ = the photoionization probability per atom,
N = total number of contaminant particles,
D_1 = the diffusion coefficient associated with the neutrals.

Further, the fit is considerably improved when the following initial condition is imposed

$$n_e(r, 0) = \frac{cN}{\pi^{3/2} r_0^3} \exp - \left(\frac{r}{r_0}\right)^2 \tag{7}$$

where c is found to be about 5×10^{-4} and can be interpreted as the thermal ionization efficiency if initial thermal ionization is assumed.

If $D_1 = D_2$, then the general solution is

$$n_e(r, t) = \frac{N[1 - \exp(-kt)] + Nc}{\pi^{3/2}(4D_e t + r_0^2)^{3/2}} \exp - \left(\frac{r^2}{4D_e t + r_0^2}\right) \tag{8}$$

where D_e is an effective diffusion coefficient discussed later. Finally, since the criterion for utilizing center-point densities has been established, the use of the solution of $n_e(0, t)$ is appropriate.

(*e*) *Experimentally determined parameters*

The best agreement to the observed *C*-3 data was obtained with the following values:

$\sigma = 1{\cdot}9 \times 10^{-5}$/sec,
$D_e = 2{\cdot}2 \times 10^7$ cm^2/sec,
$N = 3 \times 10^{24}$ particles, or 5 moles,
$r_0 = 100$–300 m,
$c = 5 \times 10^{-4}$

(listed in order of suggested decreasing reliability of determined magnitude). The result is depicted in Fig. 5.

It may appear that a large degree of flexibility is available for proper fitting in view of the several parameters involved. It is suggested that this is not the case, in fact the requirement of utilizing several reasonable values simultaneously for proper fit can serve to make a proper fit highly restrictive. This seems to be the case here. For example, although it is felt that the values of r_0 and c are not too well established, they are probably correct to within a factor of two or three. Regardless, it can be shown that in either case, both these parameters affect only the very early behavior of the decreasing electron density. For example, from equation (8) the r_0 effect is only significant for $t < r_0^2/4D$. Representative values indicate that these times are earlier than any analysed here. Physically, this implies that the initial shape affects only the early data with little effect on the later measurements. Accordingly, for this case, the choice of r_0 (within the range indicated) is not too critical in fitting the data. For the c-values case, it is readily shown that the cross over point (from thermal to photoionization processes) is at $t = c/\sigma$. Again one concludes that the effect is restricted to relatively early data. It is clear, however, that the early data cannot be matched with any value far removed from 5×10^{-4}; it is only emphasized here that the importance is

restricted to early times. The validity of assuming initial thermal ionization and this c-value are established in Paper IV[8] of this series.

The σ-value of $1{\cdot}0\times10^{-5}$/sec was derived from published experimental data[9] and is considered to be the most reliable of the several parameters employed. Consequently, this value is not subject to variation here, and this results in another restriction of apparent flexibility. There remains the consideration of the remaining two parameters, N and D_e, the total number of contaminant particles and the effective diffusion coefficient, respectively. Concerning N, earlier discussion (Section 3) indicated a chemical yield of less than about 10 per cent could be expected. Reference to thermally achieved total initial electrons indicates a relatively low chemical yield for any reasonable c-values. Only by imposing a c-value of less than about $1{\cdot}6\times10^{-4}$ could yields greater than 10 per cent be permitted. Thermochemical considerations indicate that this is not too likely. Again, further evidence for expectation of a poor chemical yield is given in a future publication[4] in which the optical method employed shows yields of the order of a few per cent for alkali metal contaminant releases employing chemical techniques analogous to those employed here. However, even if a chemical yield of only a few per cent is anticipated, it still remains to ascertain if it is compatible with using a reasonable value for D_e, the effective diffusion coefficient, and the subsequent obtaining of a good experimental fit.

For reasons to be discussed in the following Section, it is expected that D_e should lie somewhere between the ambipolar and neutral diffusion coefficients. The latter two have been determined theoretically[10] and at 120 km the respective values are $8{\cdot}2\times10^{6}$ cm^2/sec and $5{\cdot}5\times10^{7}$ cm^2/sec. For a reasonable trial value an intermediate value of about 3×10^{7} cm^2/sec is appropriate. Corroboration for this initial choice is again found in Paper V where the visible photographic clouds yielded cloud dynamics data that suggest, for early times (first several minutes), prevailing non-turbulent diffusion; thus, the calculated values of molecular diffusion are supported. Considering all the peripheral data which must be dovetailed into this analysis, it is particularly illuminating to experience a best fit of the experimental data with parametric values for D_e and N of $2{\cdot}2\times10^{7}$ cm^2/sec and $3{\cdot}0\times10^{24}$ (5·0 moles which correspond to about 3 per cent chemical yield).

(f) Some comments on diffusion

In the original formulation, two different D's were employed, the ambipolar and the neutral diffusion coefficients, D_2 and D_1, respectively. For mathematical expediency, these were regarded as identical while in fact they are quite different. Actually, a best fit was achieved by using a value of D_e which was intermediate between the two.

In the early phases of the cloud life (thermal ionization) the dominant diffusive forces are presumably ambipolar. Some time after the cross-over point ($t=c/\sigma$) the dominant diffusion process reflects the joint influence of the neutrals (continuously photoionized) and the generated ion–electron pairs. Thus, it is expected that the observed coefficient would increase in time from initially ambipolar to some effective value, D_e, intermediate between D_2 and D_1. This D_e is what is computed from the data that best indicates a good fit.

The above discussion implies that the diffusion process throughout the time of observation was primarily molecular. This is not necessarily the case. For example, neither turbulent diffusion is ruled out nor a diffusion mechanism that changes with time (i.e. transition from molecular to turbulent). In addition, turbulent diffusion itself can vary with time as the size of the cloud moves into different zones of the turbulent size spectrum. The rates associated with the various regimes are not well known. The data reported here are of little value for definitive statements regarding the complex diffusive effects mentioned. It is sufficient to state that from these data (and peripheral data discussed) it is felt that the

diffusive forces are probably dominantly molecular in view of the agreement obtained with estimated magnitudes of the appropriate molecular diffusion coefficients. Valuable information concerning diffusive mechanisms and rates can be obtained by the judicious choice of rocket experimentation. Some examples are offered here.

Electron clouds created under nighttime conditions or in twilight, when the ozone shadow has effectively absorbed out the ionizing component, will diffuse under ambipolar diffusion and can be utilized to measure the ambipolar coefficient. Those clouds created under other conditions can be utilized to measure D_e, the effective diffusion coefficient, which is intermediate between the neutral and ambipolar diffusion coefficient.

Additionally, the appropriate doping and suitable optical detection techniques can be utilized very effectively to study the diffusion coefficients of contaminants of different masses (Cs, Ba, Na, Li, etc.) and reactivity with the atmospheric species.

The possibility of determining the dynamics associated with the ions and neutrals simultaneously is afforded by the high altitude twilight release of contaminants that resonate in the visible or photographic region for both the neutral and ionized species. Barium and calcium are examples. These data would be valuable in determining the dominant diffusive mechanism (molecular, ambipolar, turbulent, effective, etc.).

It should be added that for the successful interpretation of the above experiments quite careful optical requirements must be met.

7. ESTIMATED EFFECTIVENESS OF SOME PROJECTED EXPERIMENTS

The three curves in Fig. 6 are intended to offer crude estimates of the predicted time behavior of the maximum frequency backscatter for the hypothetical 121 km Nike-Cajun release of the three alkali metals, cesium, potassium and sodium. The figure was derived in an attempt to ascertain the feasibility of utilizing the less expensive, more reliable,

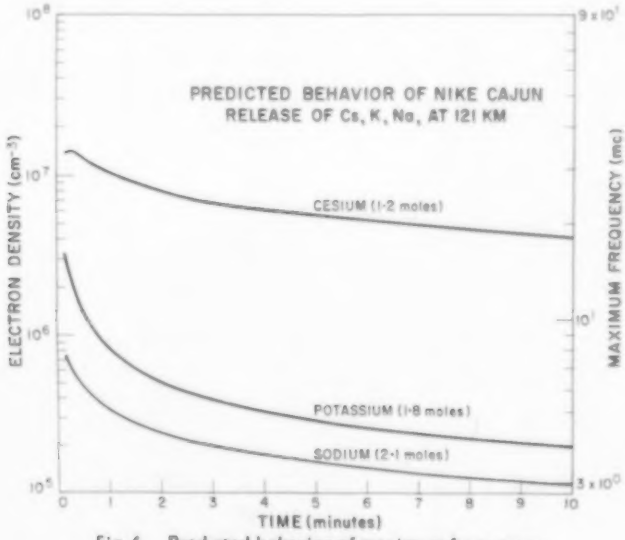

Fig. 6. Predicted behavior of maximum frequency versus time of Nike-Cajun release of cesium, potassium and sodium at 121 km for chemical and thermal ionization yields of only 3% and 0·1%, respectively. The curves serve to indicate the potential capability of an improved system.

available solid fuel rockets for the generation of artificial electron clouds and related experiments. The results have been obtained by extrapolation of the information obtained from the analysis of the 121 km Aerobee potassium release. The assumptions employed, anticipated accuracy and the limitations imposed for further extrapolation are discussed below.

First, the overall assumption is made that the same values of the parameters apply here as those determined from the potassium experiment; D_e, c, r_0, altitude of release (121 km) and chemical yield (3 per cent). The c-value of cesium and sodium do not differ markedly from the intermediate potassium value of 5×10^{-4}. Further, the reduced mass effect on the observed D_e is considered negligible for cesium or sodium when compared to potassium (intermediate in atomic weight). The assumption of similar chemistry, based on the fact that we deal here with a chemical family of elements, leads to the values of N shown in Fig. 6 for each element (after proper adjustment for payload). The σ-values are considered fixed and obtained from Table 1 in Paper II[2]. Admittedly, this treatment is not too rigid, but it is found to lead to interesting conclusions which have been confirmed in later experiments (Paper V, VI[4]). The restriction of electron density loss mechanism attributed only to diffusion is inherent in these arguments, and caution must be exercised in extrapolations to those experimental conditions that are somewhat removed from the assumed ones.

Since the experiments discussed here occur within the ionosphere, a criterion for successful experimentation may be defined as the capability of generating an artificial electron cloud with electron densities of at least 5×10^5 to 10^6 electrons/cm^3 persisting at least several minutes. Reference to Fig. 6 shows that, even for this minimal type cloud formation, the potassium and sodium cases are at best borderline, whereas for cesium it is apparent that, with present capabilities, a Nike-Cajun release at about 120 km could result in an effective artificial electron cloud.

In Table 1 are some values for the predicted time duration of backscatter of the discrete frequencies 100, 50 and 25 Mc. For approximate forward-scatter beyond line of sight capability it is valid to multiply f_{max} by a factor of 4 or 5 for an assumed symmetrical trans-

Table 1. Predicted Values for f_{max} vs. Time Duration (Δt) by release of Cesium at 121km in Aerobee (A) and Nike-Cajun (N-C)

f_{max} (Mc)	$\Delta t_{(A)}$	$\Delta t_{(N-C)}$
100	<15 sec	<1 sec
50	~ 1 min	<1 sec
25	>10 min	~ 3 min

mitter–cloud–receiver geometry. In addition to the Nike-Cajun release, analogous expectation values are included for the attempted Aerobee cesium (about 100 moles) experiment of September 1957, which failed. Although these projections are based on a somewhat approximate treatment, they do indicate the high potential of the system especially since such poor chemical yield (3 per cent) and relatively low thermal ionization efficiency (5×10^{-4}) values were employed.

On the basis of these findings, it is valid to conclude that the capability of performing certain Nike-Cajun (or similar payload vehicles) electron cloud experiments has been established. It was this reasoning, in fact, which led to the subsequent use of Nike-Cajuns exclusively on all future experiments reported in this series.

REFERENCES

1. F. F. Marmo, L. M. Aschenbrand and J. Pressman, *Planet. Space Sci.* **1**, 227 (1959).
2. F. F. Marmo, J. Pressman and L. M. Aschenbrand, *Planet. Space Sci.* **1**, 291 (1959).
3. *Thermodynamic Properties of the Elements, Advances in Chemistry Series* No. 18, p. 37, American Chemical Society (1956).
4. F. F. Marmo, J. Pressman, L. M. Aschenbrand and E. R. Manring, *Electron Clouds—V and VI, Planet. Space Sci.*, to be published.
5. O. G. Villard and R. S. Rich, *QST Magazine*,

American Radio Relay League, Hartford, Conn., May (1957).
6. F. F. MARMO, J. PRESSMAN, L. M. ASCHENBRAND, A. S. JURSA and M. ZELIKOFF, *J. Chem. Phys.* **25**, 187 (1956).
7. E. R. MANRING, J. F. BEDINGER, H. B. PETTIT and C. B. MOORE, *J. Geophys. Res.* **64**, 187 (1956).
8. J. PRESSMAN, F. F. MARMO and L. M. ASCHENBRAND, *Planet. Space Sci.*, to be published.
9. G. L. WEISSLER, *Handbuch der Physik*, Bd. 21, S. 332. Springer, Berlin (1956).
10. A. DALGARNO, private communication.

Planet. Space Sci. Pergamon Press 1959. Vol. 1, pp. 319–324. Printed in Great Britain.

ELECTRO-HYDROMAGNETIC WAVES IN A FULLY IONIZED GAS—I

K. D. COLE

Antarctic Division, Department of External Affairs, Melbourne

(*Received* 12 *June* 1959)

Abstract—Transport equations are used to determine coefficients which are generalizations for any frequency of electric field of the parallel, Pedersen and Hall conductivities in a fully ionized gas.

These coefficients are used in an investigation of the propagation of weak electromagnetic and hydromagnetic waves of all frequencies across a homogeneous and constant magnetic field in a rarefied fully ionized gas. For propagation perpendicular to the magnetic field it is found for all frequencies

(i) $$\frac{\omega^2}{k^2} = c^2 \frac{\tau\left(\frac{V^2}{c^2}\omega_p^2 - \omega^2\right) + i\omega}{\tau(\omega_p^2 - \omega^2) + i\omega},$$

(ii) $$\frac{1}{2}\rho\,|v|^2 = V^2 \cdot \frac{|k|^2}{\omega^2} \cdot \frac{|h|^2}{8\pi},$$

where $V^2 = H^2/4\pi\rho$ and v, h are the perturbations of the velocity, magnetic field. Similar relationships are deduced for propagation at any angle to the field for frequencies greater than about 10 times the gyrofrequency of electrons.

The theory is applied to discuss transmission of disturbance across the interplanetary medium, the temperature of the solar corona and the earth's outer atmosphere, the emission of non-thermal solar radio noise, cosmic radio noise and the anomalous emission of light from shock fronts.

1. THE CONDUCTIVITIES

The equation of motion of electrons in a fully ionised gas in which viscosity, the gradient of pressure of electrons and gravitation can be neglected is (c.f. reference 1) in e.m.u.

$$n\,m\frac{d\mathbf{v}}{dt} = -\frac{ne}{c}(\mathbf{E} + \mathbf{v}\times\mathbf{H}) + \mathbf{P}, \qquad (1)$$

where

n = number of electrons per cm^3
$\mathbf{v}$ = average velocity of electrons
e, m = charge, mass of an electron
$\mathbf{E}$ = electric field
$\mathbf{H}$ = magnetic field
c = velocity of light
$\mathbf{P}$ = total momentum transferred to the electrons per unit volume per unit time by collision with ions.

For small electric fields, the mean time (τ) between collisions of an electron with ions can be considered as approximately independent of the field and $\mathbf{P} = -nm\mathbf{v}/\tau$. Thus equation (1) becomes

$$m\left(\frac{d\mathbf{v}}{dt} + \frac{\mathbf{v}}{\tau}\right) = -\frac{e}{c}(\mathbf{E} + \mathbf{v}\times\mathbf{H}). \qquad (2)$$

Let it be assumed that $\mathbf{E}$ is a small perturbation of the form $\mathbf{E} = \mathbf{E}_0 \exp i\omega t$; then solutions of equation (2) of the form $\mathbf{v} = \mathbf{v}_0 \exp i\omega t$ can be found, where

$$m\mathbf{v}_0\left(i\omega + \frac{1}{\tau}\right) - \frac{e}{c}(\mathbf{E}_0 + \mathbf{v}_0\times\mathbf{H}). \qquad (3)$$

Neglecting the current due to the movement of ions, the conduction current ($\mathbf{j}$) is given by

$\mathbf{j}=ne\mathbf{v}/c$. This is equivalent to assuming the average velocity of ions to be zero. In general

$$\mathbf{j}=s_0\mathbf{E}_{//}+s_1\mathbf{E}_{\perp}+s_2\frac{\mathbf{H}\times\mathbf{E}_{\perp}}{|H|}, \tag{4}$$

where $\mathbf{E}_{//}$, $\mathbf{E}_{\perp}$ are components of $\mathbf{E}$ parallel, perpendicular to $\mathbf{H}$. Hence from equation (3) we derive

$$\left.\begin{aligned} s_0&=\frac{ne^2\tau}{mc^2}\,\frac{1}{1+\iota\omega\tau},\\ s_1&=\frac{ne^2\tau}{mc^2}\,\frac{1+\iota\omega\tau}{(1+\iota\omega\tau)^2+p^2\tau^2},\\ s_2&=\frac{ne^2\tau}{mc^2}\,\frac{p\tau}{(1+\iota\omega\tau)^2+p^2\tau^2}, \end{aligned}\right\} \tag{5}$$

where $p=\dfrac{He}{mc}$ is the gyrofrequency of electrons.

When $\omega\tau\longrightarrow 0$, s_0, s_1, s_2 reduce to the well known parallel conductivity σ_0, the Pedersen conductivity σ_1 and the Hall conductivity σ_2, respectively. The real part of s_0 is the parallel "conductivity" as deduced by Mitra[2] for an alternating electric field; this is applicable when $\omega\tau<<1$. The real parts of s_1 and s_2 are the conductivities deduced by Chapman and Cowling[3] for an alternating electric field; again these are applicable when $\omega\tau<<1$.

It is to be noted, from equations (5), that when $\omega>>p$, $s_0\approx s_1$ and $s_2\approx 0$. That is, for such frequencies the medium can be regarded as approximately isotropic in conductivity. For lower frequencies the medium must be regarded as anisotropic.

1.1. *Joule heating*

Because of the nature of the coefficients s_0, s_1, s_2 there are in general phase differences between the field $\mathbf{E}$ and the current $\mathbf{j}$. In order to formulate a physically meaningful expression for the rate of joule heating it is convenient to work[4] with the real parts of the expressions for $\mathbf{E}$ and $\mathbf{j}$. We denote the real part of a complex quantity A by $R(A)$, the complex conjugate by A^*, and the amplitude or modulus by $|A|$. The time average of the product $R(A_1)\,.\,R(A_2)$ is equal to $\frac{1}{2}R(A_1A_2^*)$.

If an electric force $R(e\mathbf{E})$ maintains a velocity $R(\mathbf{v})$ of electrons in spite of collisions then the electric force does work at the rate of $R(e\mathbf{E})\,.\,R(\mathbf{v})$ per electron per sec. Hence the time average rate of production of joule heat (Q) per unit volume is given by

$$\begin{aligned} Q&=[nR(e\mathbf{E})\,.\,R(\mathbf{v})]_{av.}=[R(\mathbf{j})\,.\,R(\mathbf{E})]_{av.}=\\ &=\frac{1}{2}R(s_0\mathbf{E}_0^2\cos^2\varphi+s_1\mathbf{E}_0^2\sin^2\varphi), \end{aligned} \tag{6}$$

where φ is the angle between the electric field $\mathbf{E}$ and the magnetic field $\mathbf{H}$. We may also express Q in terms of the current as follows

$$\begin{aligned} Q&=1/s^*[R(\mathbf{j})\,.\,R(\mathbf{j})]_{av.}\\ &=1/2s^*\{|s_0|^2\mathbf{E}_0^2\cos^2\varphi+[|s_1|^2+\\ &\qquad+|s_2|^2]\mathbf{E}_0^2\sin^2\varphi\}. \end{aligned} \tag{7}$$

Thus $$s^*=\frac{|s_0|^2\cos^2\varphi+[|s_1|^2+|s_2|^2]\sin^2\varphi}{R(s_0)\cos^2\varphi+R(s_1)\sin^2\varphi}. \tag{8}$$

From equation (8) it is seen that when $\varphi=0$, $s^*=|s_0|^2/R(s_0)$ and when $\varphi=\dfrac{\pi}{2}$, $s^*=[|s_1|^2+|s_2|^2]/R(s_1)$. When $\omega\tau<<1$ this last result becomes $\sigma_3=\sigma_1+\sigma_2^2/\sigma_1$ which result[5, 6] is independent of the angle φ.

The expressions for s_0, s_1, s_2, s^* are derived for a fully ionized gas. The same formulae will also apply approximately to any gas in which the conductivity can be attributed principally to electrons. Thus they also apply to a lightly ionized dense gas. In general for a partially ionized gas a total conductivity component is the sum of the respective conductivity components from each ion separately.

For later use in this paper we introduce here a third conductivity s_3 defined by $s_3=s_1+s_2^2/s_1$. From (5) it follows that $s_3=s_0$ for a fully ionized gas.

In discussing hydromagnetic wave phenomena in terms of transport equations[7], one is restricted by the use of the coefficients σ_0, σ_1, σ_2, σ_3 to frequencies much smaller than the collision frequency of electrons. The use of the coefficients s_0, s_1, s_2, s_3 deduced above enables extension to all frequencies of electromagnetic and hydromagnetic waves in a fully ionized gas.

2. ELECTRO-HYDROMAGNETIC WAVES

By analogy with Piddington's[6] work, the equation governing the rates of change of the field vectors in a conducting medium in which the resident magnetic field is homogeneous and constant is (under conditions specified below)

$$\nabla^2\mathbf{H}=4\pi s\left\{\frac{\partial\mathbf{H}}{\partial t}-\operatorname{curl}\mathbf{v}\times\mathbf{H}\right\}+c^{-2}\frac{\partial^2\mathbf{H}}{\partial t^2}, \quad (9)$$

where $\mathbf{v}$ is the momentum per unit mass of the medium. If the medium is incompressible[7] then

$$\frac{\partial^2\mathbf{v}}{\partial t^2}+\frac{V^2}{H^2}\frac{\partial}{\partial t}(\mathbf{H}\times\operatorname{curl}\mathbf{H})=0, \quad (10)$$

where $V=H/\sqrt{4\pi\rho}$ (the Alfvén velocity).

If the field vectors vary with frequencies much greater than the gyrofrequency of electrons p, say $\omega\gtrsim 10\,p$, the medium can be regarded as isotropic in conductivity. Hence we can put $s=s_0$ and equation (9) applies for all directions of propagation at these frequencies. For propagation orthogonal to the magnetic field at any frequency we put $s=s_3$ (c.f. reference 6). But for a fully ionized gas $s_3=s_0$, so the equation is unchanged.

We now seek solutions of (9), (10) for $\mathbf{v}$ and small perturbations, $\mathbf{h}$ of the vector $\mathbf{H}$, of the form $\exp\iota(\omega t-k\xi)$. We choose rectangular cartesian coordinates with the z-axis in the direction of $\mathbf{H}$ and the x-axis in the plane made by the wave normal 0ξ and $\mathbf{H}$. Denote by ψ the angle between 0ξ and $\mathbf{H}$. Following the method of Piddington[7] we find from equations (8) and (10) the relationships between the perturbations, viz.,

$$v_z=\frac{V^2}{H}\frac{k}{\omega}\frac{h_x}{\cos\psi}, \quad (11a)$$

$$v_x=\frac{4\pi s_0\iota\omega+k^2-\dfrac{\omega^2}{c^2}}{-4\pi s_0\iota k\cos\psi H}h_z, \quad (11b)$$

$$v_y=-\frac{V^2}{H}\frac{k}{\omega}\cos\psi h_y, \quad (12a)$$

$$v_y=\frac{4\pi s_0\iota\omega+k^2-\dfrac{\omega^2}{c^2}}{-4\pi s_0\iota k\cos\psi H}h_y, \quad (12b)$$

$$v_z=0, \quad (13)$$

$$\frac{h_z}{h_x}=\tan\psi. \quad (14)$$

Equations (11) and (12) correspond to two different waves, the extraordinary ray and the ordinary ray respectively (c.f. reference 7). From equations (11a) and (11b) it follows that

$$\frac{\omega^2}{k^2_{(\text{extraord.})}}=c^2\frac{V^2\varepsilon+\iota}{c^2\varepsilon+\iota}, \quad (15)$$

where $\varepsilon=\dfrac{4\pi s_0}{\omega}$. From equations (12a) and (12b) it follows that

$$\frac{\omega^2}{k^2_{(\text{ord.})}}=c^2\frac{V^2\varepsilon\cos^2\psi+\iota}{c^2\varepsilon+\iota}. \quad (16)$$

Consider the special case of $\psi=\pi/2$ and in particular the extraordinary ray. The following is seen from equation (15)

(*i*) As $\varepsilon\longrightarrow 0$, i.e. as $s_0\longrightarrow 0$ or $\omega\longrightarrow\infty$, $\dfrac{\omega}{k}\longrightarrow c$; it is usual to call these waves electromagnetic.

(*ii*) As $\varepsilon\longrightarrow\infty$, i.e. as $s_0\longrightarrow\infty$ or $\omega\longrightarrow 0$, $\dfrac{\omega}{k}\longrightarrow V$; it is usual to call these waves hydromagnetic.

It is suggested that the term electro-hydromagnetic (e.h.m.) waves be used in the general case.

Substituting for V^2 and s_0, equations (15), (16) become

$$\frac{\omega^2}{k^2_{(\text{extraord.})}}=c^2\frac{\tau(\beta^2\omega_p{}^2-\omega^2)+\iota\omega}{\tau(\omega_p{}^2-\omega^2)+\iota\omega}, \quad (17)$$

$$\frac{\omega^2}{k^2_{(\text{ord.})}}=c^2\frac{\tau(\beta^2\cdot\cos^2\psi\cdot\omega_p{}^2-\omega^2)+\iota\omega}{\tau(\omega_p{}^2-\omega^2)+\iota\omega}, \quad (18)$$

where $\beta=\dfrac{V}{c}$, $\omega_p=\left(\dfrac{4\pi ne^2}{m}\right)^{\frac{1}{2}}$,

the plasma frequency.

The main features of these expressions can be illustrated by considering the limiting case $\tau\longrightarrow\infty$. Equation (17) then reduces to

$$\frac{\omega^2}{k^2}=c^2\frac{\beta^2\omega_p{}^2-\omega^2}{\omega_p{}^2-\omega^2}. \quad (19)$$

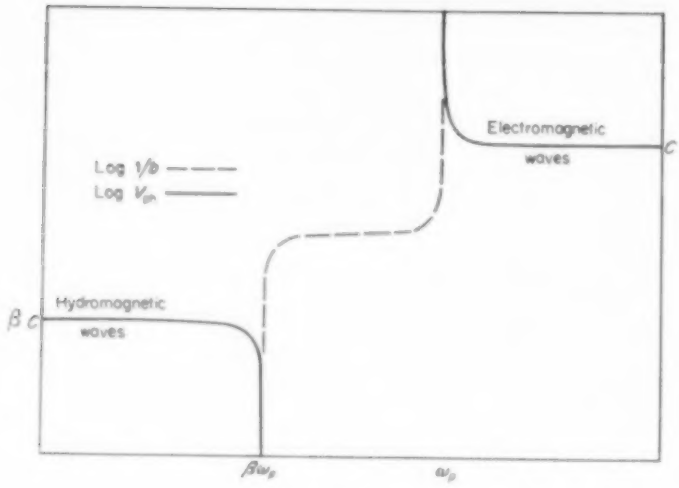

Fig. 1. The propagation of e.h.m. waves orthogonal to a homogeneous magnetic field in a fully ionized gas with $\tau \to \infty$. Plot of the logarithm of phase velocity (V_{ph}) and attenuation distance $1/b$ against the logarithm of frequency. V_{ph} and $1/b$ are infinite outside of ranges drawn.

Writing k in the form $k = a - ib$ where a and b are real, $V_{ph} = \dfrac{\omega}{a}$ is the phase velocity of the wave and $1/b$ is the exponential attenuation distance. The mode of variation of these quantities is illustrated qualitatively in Fig. 1. It is seen that at frequencies between $\beta\omega_p$ and ω_p the disturbance is a stationary wave.

2.1. *Energy partition*

Consider the special case of $\psi = \pi/2$. It follows from equations (11) to (14) that $h_x = h_y = v_y = 0$, and

$$\frac{1}{2}\rho\,|v_x|^2 = V^2 \cdot \frac{|k|^2}{\omega^2}\,\frac{|h_z|^2}{8\pi}. \qquad (20)$$

The appropriate dispersion relation is equation (17). Equation (20) shows that with e.h.m. waves in a fully ionised gas there is associated not only a magnetic energy of disturbance but also a kinetic one. *This is true not only for frequencies usually called hydromagnetic but also for those usually called electromagnetic (i.e. optical and radio).*

For completeness let the electric energy of disturbance $\left(\dfrac{|E|^2}{8\pi}\right)$ be introduced. Since curl $\mathbf{E} = -\dfrac{1}{c}\dfrac{\partial \mathbf{h}}{\partial t}$, then $\dfrac{|E|^2}{8\pi} = \dfrac{\omega^2}{|k|^2} \cdot \dfrac{1}{c^2}\,\dfrac{|h|^2}{8\pi}$.

Thus for propagation orthogonal to the magnetic field in a fully ionized gas

$$\frac{1}{2}\rho\,|v|^2 = V^2\,\frac{|k|^2}{\omega^2}\,\frac{|h|^2}{8\pi} = V^2c^2\,\frac{|k|^4}{\omega^4}\,\frac{|E|^2}{8\pi}. \qquad (21)$$

This relationship shows the partition of energy over the entire range of frequencies.

When $\dfrac{\omega}{k} = c$, i.e. for waves usually called electromagnetic,

$$\frac{1}{2}\rho|v|^2 = \beta^2\,\frac{|h|^2}{8\pi} = \beta^2\,\frac{|E|^2}{8\pi}. \qquad (22)$$

When $\dfrac{\omega}{k} = V$, i.e. for waves usually called hydromagnetic

$$\frac{1}{2}\rho|v|^2 = \frac{|h|^2}{8\pi} = \frac{1}{\beta^2}\frac{|E|^2}{8\pi}. \qquad (23)$$

Consider now the general case of propagation at any angle ψ to the magnetic field **H**. For frequencies $\omega \lesssim 10\,p$, the medium can be regarded as isotropically conducting and equations (9) to (18) describe this case. The partition of energy for the ordinary and extraordinary components may be calculated from equations (11) and (12) and curl $\mathbf{E} = -1/c\,.\,\partial\mathbf{h}/\partial t$.

For frequencies $\omega \lesssim 10\,p$, the medium is anisotropically conducting and the equations describing propagation at these frequencies in any direction but orthogonal become complicated. The relevant equations can be shown by the method of Piddington[6] to be

$$\nabla^2\mathbf{H} - \frac{s_2}{s_1}\frac{\partial}{\partial z}\left(\operatorname{curl}\mathbf{H} - c^{-2}\frac{\partial\mathbf{E}}{\partial t}\right) = 4\pi s_3\left\{\frac{\partial\mathbf{H}}{\partial t} - \operatorname{curl}\mathbf{v}\times\mathbf{H}\right\} + c^{-2}\frac{\partial^2\mathbf{H}}{\partial t^2}, \qquad (24)$$

together with equation (10), and

$$\operatorname{curl}\mathbf{E} = -\frac{1}{c}\frac{\partial\mathbf{H}}{\partial t}. \qquad (25)$$

In principle these three equations can be solved as above* and the dispersion relationship is obtained by eliminating the variables h_x, h_y, h_z, v_x, v_y, v_z and E_x, E_y, E_z.

3. APPLICATIONS

3.1. *Geomagnetic disturbance*

Let us make the assumption that at some time during a solar disturbance e.h.m. waves of all frequencies are simultaneously emitted. Such an event would appear at the earth as a dispersed train of e.h.m. waves. The high frequencies would arrive with the velocity c and the low frequencies with the velocity V. We take the average V across the sun–earth space to be 10^8 cm per sec corresponding to a 2 day delay.

If the sun has a magnetic field of strength 1G at its surface and this field decreases inversely as the square[8] of the distance from the sun, the average field between the sun and the earth may be of the order of 10^{-3} G. This would make the proton density of order 1 per cm.^{3} A density of this order is indicated by extrapolation of outer atmosphere electron density obtained by whistler[9] and micropulsation[10] studies. (These conflict with estimates made by other means[11].)

It is known[2] that a typical large magnetic storm involves a disturbance of order 100 gammas averaged over the whole earth. However this may be the result of only weak hydromagnetic waves in the nearby interplanetary medium for, on account of the convergence of the lines of force of the earth's field, there may be considerable magnification of such disturbances.

Corpuscular bombardment of the earth does not necessarily imply corpuscular emission by the sun. The propagation of an e.h.m. wave at right angles to a magnetic field ensures that the velocity perturbation of the medium is in the direction of wave motion. It follows from equations (11a) and (14) that for the extraordinary ray, when $\psi = \pi/2$ and for the hydromagnetic frequencies, $v_x = Vh_z/H$. Hence with $V = 10^8$ cm per sec and $h_z/H = 0{\cdot}1$, $v_x = 10^7$ cm per sec. Thus weak waves can give rise to particle velocities of the order of those associated with auroras.[12]

3.2. *The temperature of the solar corona*

For propagation along a magnetic field it follows from equations (11) to (14) that

$$\frac{1}{2}\rho|v_\perp|^2 = V^2\frac{|k|^2}{\omega^2}\frac{|h_\perp|^2}{8\pi}, \qquad (26)$$

where the subscript $\perp$ indicates perturbations perpendicular to the resident magnetic field. It is assumed that by far the greatest amount of radiation from the sun is at frequencies such that $\omega/k \approx c$.

Now in localised areas of the sun magnetic fields of 100 G and more are not uncommon. A particle density of 2×10^8 per cm^3 in such regions gives $V \approx 0{\cdot}1c$. The magnetic energy of disturbance is given by $S/2c$ where S is the flux of electromagnetic energy per second.

* This is the subject of a further paper in preparation.

The kinetic energy of disturbance can be represented in terms of an equivalent temperature T, viz. $\frac{3}{2}nkT = \frac{1}{2}\rho|v_\perp|^2$. It follows that

$$T = \frac{SV^2}{3c^3nk}. \tag{27}$$

Using $n = 2 \times 10^8$ per cm^3, $s = 6 \times 10^{10}$ ergs per cm^2 per sec, $V = 0{\cdot}1c$, we have $T \approx 10^6$ °K.

3.3. *Temperature in the earth's outer atmosphere*

We assume the earth's atmosphere to be fully ionized at great heights. The spectrum of radiation emitted by the sun is divided roughly into two blocks (see Fig. 1). We denote the flux associated with the electromagnetic block by S_E (the solar constant) and that with the hydromagnetic block by S_H. Using the partition equations (22) and (23) it follows that the temperature equivalent of the kinetic energy of disturbance associated with the total solar radiation is

$$T = \frac{1}{3nk}\left\{\frac{S_E V^2}{c^3} + \frac{S_H}{V}\right\}. \tag{28}$$

S_E is known to stay approximately constant. Providing V remains reasonably steady the contribution to temperature in the outer atmosphere by the electromagnetic block will also be steady. However, it seems likely that S_H will be subject to considerable fluctuations and this will reflect in T. Unfortunately considerable uncertainty on the variation of the density of the outer atmosphere precludes evaluation of T as a function of height. However equivalent temperatures of order $10^{4\cdot5}$°K at 5 earth radii appear likely.

3.4. *Generation of radio and optical frequency noise*

Equation (21) implies that whatever frequencies appear in the spectrum of velocity of matter moving across a magnetic field in a fully ionized gas also appear in the electromagnetic field. It is suggested that the violent deceleration of matter across magnetic fields is responsible for the production of non-thermal solar radio noise and for a substantial part of the radio noise emitted by galactic emitters. It is suggested also that a similar explanation may account for the anomalous production of light at shock fronts.[13]

3.5. *Cosmic radio noise*

Consider a radio source situated in a direction from the earth orthogonal to the interplanetary magnetic field. Fig. 1 represents approximately the behaviour of the interplanetary medium. It will be seen that there will be a missing band of frequencies from the spectrum of the emitter. The lower limit of this band will be $\beta\omega_p$ and the upper will be set by the distance of the emitter from the earth. Since vast distances are involved, it is highly likely that this upper limit will be just less than ω_p. Since $\beta\omega_p$ is proportional to H, and ω_p is proportional to $n^{\frac{1}{2}}$, it may be possible to find experimentally values of the interplanetary magnetic field and electron density by locating this missing band of frequencies.

Acknowledgement—The author thanks Dr. F. Jacka, Chief Physicist, of this Division for his critical reading of the original draft of this paper, for clarifying discussions on some applications of the theory, and for considerable help in improving the presentation.

REFERENCES

1. L. Spitzer, *Physics of Fully Ionized Gases*. Interscience Publishers, New York (1956).
2. S. K. Mitra, *The Upper Atmosphere*. The Asiatic Society, Calcutta (1953).
3. S. Chapman and T. G. Cowling, *The Mathematical Theory of Non Uniform Gases*. 2nd Ed. University Press, Cambridge (1953).
4. J. A. Stratton, *Electromagnetic Theory*. McGraw-Hill, New York (1941).
5. T. G. Cowling, *Mon. Not. R. Astr. Soc.* **116**, 114 (1956).
6. J. H. Piddington, *Mon. Not. R. Astr. Soc.* **114**, 638 (1954).
7. J. H. Piddington, *Mon. Not. R. Astr. Soc.* **115**, 671 (1955).
8. L. Block, *Ark. Fys.* **14**, 179 (1958).
9. G. McK. Allcock, private communication (1958).
10. T. Obayashi and J. A. Jacobs, *Geophys. J.* **1**, 53 (1958).
11. I. S. Shklovsky, *Planet. Space Sci.* **1**, 63 (1959).
12. G. I. Galperin, *Planet. Space Sci.* **1**, 71 (1959).
13. A. Kantrowitz, *Gas Dynamics of Cosmic Clouds*. North Holland Publishing Co., Amsterdam (1955).

Planet Space. Sci. Pergamon Press 1959. Vol. 1, pp. 325–332. Printed in Great Britain.

THE ASSOCIATION OF SOLAR RADIO BURSTS WITH AURORAL STREAMS

A. MAXWELL, A. R. THOMPSON and G. GARMIRE

Radio Astronomy Station of Harvard College Observatory, Fort Davis, Texas

(*Received* 16 *June* 1959)

Abstract—Slow drift (Type II) radio bursts from the sun are believed to be caused by a primary disturbance moving outward through the solar atmosphere with a velocity of about 1000 km/sec. Analysis of the 2 years, 1956 October 1 through 1958 September 30, over the sunspot maximum shows that 45 per cent of these bursts are associated with the subsequent occurrence of terrestrial auroræ and magnetic storms. The mean delay between the radio bursts and the terrestrial disturbances is 33 hr, which is in good accord with the velocity for the disturbing source as deduced from the radio data. Investigation of the properties of the individual slow drift bursts and their association with other solar radio and optical phenomena reveals no completely conclusive criteria to explain why only 45 per cent of the bursts are geomagnetically important. The geomagnetic effects are enhanced, however, if the bursts occur near the equinoxes and if they are accompanied by a flare of importance 2 or 3, or by continuum (Type IV) radiation.

In the reverse association, with radio data available for an average 14 hr daily, it is shown that at least 60 per cent of magnetic storms are preceded, within 4 days, by a slow drift burst.

1. INTRODUCTION

It has for some years been suggested that the generation of certain types of radio bursts in the solar atmosphere is associated with the emission of auroral corpuscular particles from the sun.[1, 2] This paper is concerned specifically with the relation of the slow drift (spectral Type II) bursts to the emission of auroral streams and the occurrence of geomagnetic storms. The spectral properties of the slow drift bursts strongly suggest that they, alone amongst the various types of radio bursts, originate from the passage of such streams through the solar atmosphere.

Two examples of the slow drift bursts are shown in Fig. 1. These were recorded with sweep frequency equipment at Fort Davis, Texas, covering the range 100–580 Mc/s,[3] and are typical of an average of thirty such bursts recorded yearly at Fort Davis during the solar maximum. The dominant characteristic of this type of burst is its gradual drift towards the lower end of the frequency spectrum. This is consistent with an origin due to a disturbance moving outwards through the solar corona, and exciting emission from levels of progressively lower plasma frequency. The observed rate of change of frequency together with the present estimates of the electron density in the corona indicate a velocity of about 1000 km/sec for the exciting agency.[4] This figure has recently been verified by the interferometer measurements of Wild, Sheridan and Trent[5], which also confirm that the different frequencies originate at different heights in the solar atmosphere, as the above emission mechanism requires.

A velocity of 1000 km/sec corresponds to a time of travel of 42 hr for a direct path between the sun and the earth, and is approximately that assigned to auroral particles. The velocity of the particles has been derived, in the past, from the time delay which exists beween the occurrence of a large solar flare or large solar radio burst of unspecified spectral classification and the onset of a terrestrial magnetic storm.[6, 7] Since the origin of the slow drift bursts is assigned to a disturbance moving outwards through the solar atmosphere with a velocity of approximately 1000 km/sec, it is plausible to

assume that this disturbing agency may be the auroral corpuscular particles, or at least a shock wave associated with their ejection. For this reason, one might expect to find a definite relation between the slow drift bursts and subsequent terrestrial magnetic storms.

The radio data described in this paper were recorded with sweep frequency receivers, covering the range 100–580 Mc/s, at the Radio Astronomy Station of Harvard College Observatory, Fort Davis, Texas. A preliminary account of this work was given at the I.A.U.-U.R.S.I. symposium on radio astronomy in Paris, August 1958.[8]

2. SLOW DRIFT BURSTS AND THE PLANETARY MAGNETIC INDEX

We first investigate the relation of geomagnetic activity to slow drift bursts alone, without reference to any associated phenomena such as solar flares. The radio data cover 95 per cent of the period sunrise to sunset at Fort Davis for the 2 years 1956 October 1 through 1958 September 30. During this time sixty slow drift bursts were recorded. The 3 hr planetary magnetic index Kp has been used as the index of the influx of auroral particles in the vicinity of the earth.

The comparison of the occurrence of the slow drift radio bursts with the onset of terrestrial magnetic activity has been carried out by the superposed epoch method, the occurrence of the radio bursts being taken as the zero reference time, and the three hourly magnetic character figures within the range -3 to $+7$ days being plotted about the time of the radio burst. The result is shown in Fig. 2, in which the ordinate gives values of Kp averaged over the sixty bursts, and the abscissa shows time relative to the bursts. The curve shows a clear rise in geomagnetic activity following the occurrence of the slow drift radio bursts. (A similar result was found by Roberts[9] for the Ap-index of magnetic activity). The first peak in magnetic activity occurs approximately 12–24 hr after the slow drift bursts and a second peak occurs at approximately 48–60 hr. These time delays are in reasonable accord with the velocity deduced for the disturbing agent which gives rise to the slow drift bursts, and one may logically conclude that the slow drift bursts are related to the terrestrial magnetic storms.

It will also be seen from Fig. 2 that a further rise in magnetic activity commences on the day $+4$ after the slow drift bursts. This may be

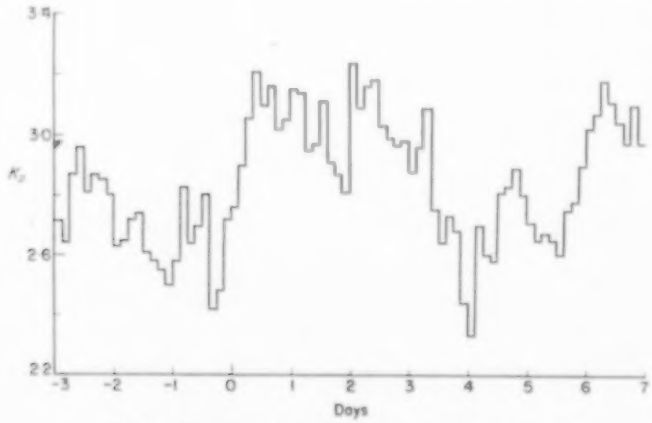

Fig. 2. Superposed epoch diagram of the variation of the planetary magnetic index, Kp, about the occurrence of slow drift radio bursts. The average Kp for the period 1956, October 1 to 1958, September 30, was 2·76.

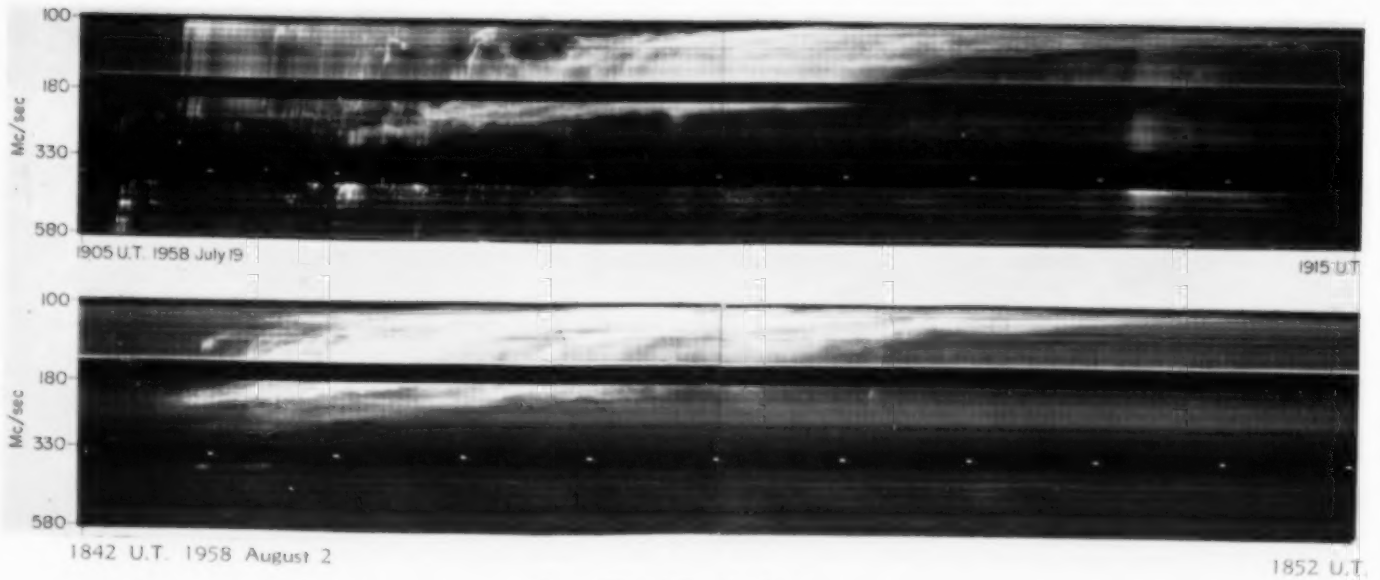

Fig. 1. Slow drift radio bursts.

Upper. 1958, July 19, 1907–1915 U.T. This burst was associated with a class 2+ flare, a class 3 short wave fadeout, and was followed by a magnetic storm.

Lower. 1958, August 2, 1843–1852 U.T. This burst was accompanied by a class 3+ short wave fadeout, but was not accompanied by a flare nor followed by a magnetic storm.

associated with the fact that slow drift bursts tend to recur within a period of about 5 days. The time distribution of the sixty bursts is shown in Fig. 3, from which it will be seen that approximately 50 per cent of the bursts were followed by a second slow drift burst within this period.

We now consider the relation of the slow drift radio bursts to well defined magnetic "storms", in contrast to their general association with the planetary geomagnetic indices. For this purpose we have defined a magnetic storm as a disturbance in which the mean Kp is greater than or equal to five for a period of not less than 12 hr. This is a rigorous definition which excludes all minor magnetic disturbances; on the other hand, it includes 98 per cent of periods when auroral radio echoes were recorded at the Jodrell Bank Experimental Station, England. Under this criterion 45 per cent of all slow drift bursts were followed by geomagnetic storms. If we adopt a slightly

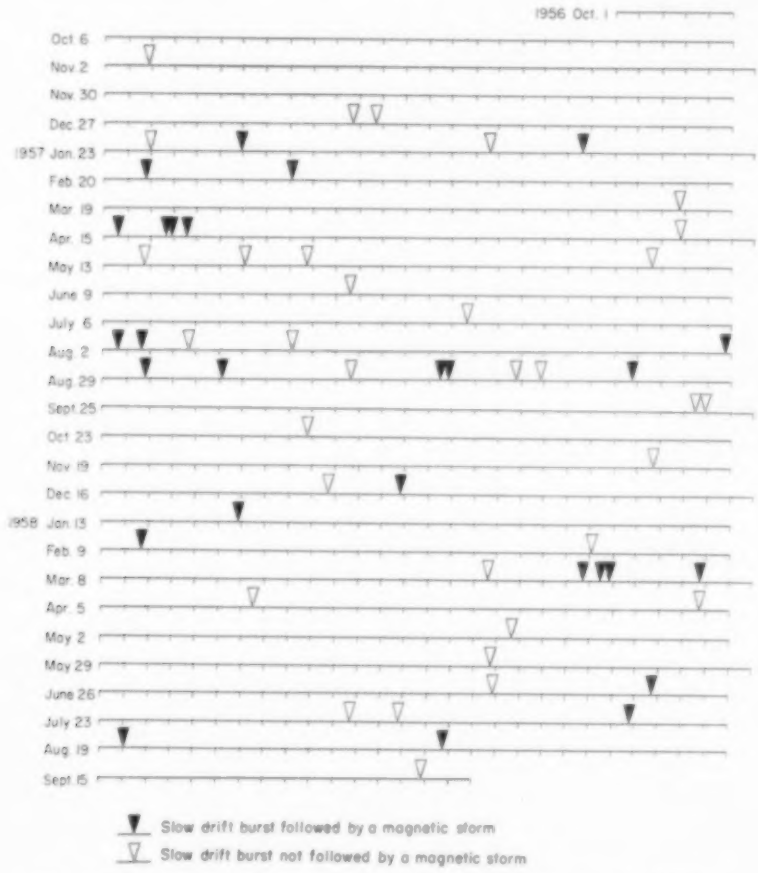

Fig. 3. Distribution of slow drift bursts recorded at Fort Davis, Texas, during 1956, October 1 to 1958, September 30, plotted as a function of the synodic rotation of the sun.

▼ denotes slow drift burst followed by geomagnetic storm.

▽ denotes slow drift burst not followed by geomagnetic storm.

different criterion for magnetic storms—activity preceded by a "sudden commencement"—we still find about 45 per cent of slow drift bursts associated with such storms, although in this case we have a slightly different set of bursts.

We further note, from Fig. 3, that 80 per cent of the slow drift bursts associated with magnetic storms occurred in the 3 month periods surrounding the equinoxes.

The reverse association, that of the magnetic storms with slow drift bursts, has also been investigated. During the 2 years 1956 October through 1958 September, sixty-one magnetic storms occurred. Of these, 60 per cent were preceded within 4 days by a slow drift burst recorded either at Fort Davis or Sydney, Australia. The combination of the Australian data with those from Fort Davis increases the mean daily period of spectral radio observations for the days preceding each storm to 14 hr. However, without complete radio data it is impossible to estimate how near to 100 per cent the true association lies.

3. THE TIME DELAY BETWEEN SLOW DRIFT BURSTS AND THE ONSET OF MAGNETIC STORMS

The cases of slow drift bursts associated with magnetic storms are listed in Table 1, from which it is possible to investigate in more detail the time delay between the two phenomena. Here the magnetic storms conform to the definition given in the previous section, and the onset of a storm is taken as the mid-point of the first 3 hr interval for which the value of Kp is 5 or greater. A radio burst is considered to be associated with a storm only when the time delay between the burst and the storm does not exceed 4 days. The delay times listed in Table 1 show a considerable spread, but tend to fall within two groups, 12–24 hr and 36–60 hr, which correspond to the two peaks in Fig. 3. The interpretation is complicated by the tendency of the bursts to recur within a period of a few days, so that in some cases a storm is associated with more than one burst. Furthermore, the radio observing hours cover only 50 per cent of each day, so that the data are incomplete.

The mean time delay between the slow drift bursts and magnetic storms listed in Table 1 is 33 hr, and this must be considered the best single value which the present data yield. It should also be noted that the magnetic storms referred to in this paper occurred near sunspot maximum, and are not of the recurrent type associated with solar M-regions.

4. ASSOCIATION OF SLOW DRIFT BURSTS WITH OTHER SOLAR PHENOMENA

Seventy per cent of the slow drift bursts were preceded by a group of intense fast drift bursts.[4] It is therefore of interest to enquire whether the association of the fast drift bursts with the slow drift bursts bears any relation to subsequent geomagnetic acitvity. Investigation of this point shows that those slow drift bursts which have an associated fast drift group have the same association with Kp variations as those which do not. This is not unexpected, since the fast drift bursts themselves bear no relation to magnetic activity;[9] they occur in very large numbers, and 25 per cent are correlated with occurrence of all flares.[10]

Seven of the sixty slow drift bursts were followed within a period of 15 min by intense wide band continuum radiation, sometimes known as Type IV radiation.[5] This type of activity is one of the most spectacular of solar radio phenomena, often covering a band several hundred Mc/s wide, and lasting for periods of several hours. Of the seven slow drift bursts associated with continuum radiation, five were followed by magnetic storms. If we now examine all cases of continuum radiation with duration greater than 5 min, regardless of whether they were associated with slow drift bursts or not, we find 29 days during the 2 year period on which continuum radiation was observed. Seventeen of these instances were followed by magnetic storms, but in thirteen out of the seventeen cases slow drift bursts were also recorded at Fort Davis within the four days preceding the magnetic storm. This again suggests that the slow drift bursts are the predominating influence with regard to geomagnetic activity.

Table 1. Time Delays between Slow Drift Bursts and Magnetic Storms

Start of slow drift burst	Associated radio bursts	Start of magnetic storm: mid point of 3 hr range for first $K_p \geqslant 5$	Radio auroral echoes	Delay between slow drift burst and magnetic storm
1957 Jan. 28 2351 U.T.		1957 Jan. 29 1330 U.T.	R	13·5 hr
Feb. 12 1546	III	Feb. 13 1030	R	18·5
Feb. 21 2008		Feb. 23 1930	R	47·5
Feb. 28 0017		Mar. 2 0130	R	49·0
Apr. 15 1401		Apr. 17 1330		47·5
		Apr. 18 1630	R	74·5
Apr. 17 1846	III	Apr. 18 1630	R	21·5
Apr. 17 2032	III IV	Apr. 18 1630	R	20·0
Apr. 18 1304	III	Apr. 18 1630	R	3·5
Aug. 2 1438	III	Aug. 3 1630		26·0
Aug. 3 1724	III	Burst occurred during storm		
Aug. 28 2022	III	Aug. 29 1930		23·0
		Aug. 31 1630		68·0
Aug. 30 2214	III IV	Aug. 31 1630		18·5
		Sept. 2 0430	R	54·5
Sept. 3 0036		Sept. 4 1330	R	37·0
1957 Sept. 12 1516	III IV	1957 Sept. 13 0130	R	10·0
		Sept. 14 0730		40·0
Sept. 12 2150	III	Sept. 13 0130	R	3·5
		Sept. 14 0730		33·5
Sept. 20 2121	III	Sept. 21 1030	R	13·0
Dec. 28 2230	III IV	Dec. 31 0430	R	54·0
1958 Jan. 18 2257	III	1958 Jan. 20 2230		47·5
Feb. 10 1911	III	Feb. 11 0130	R	6·5
Mar. 28 1837		Mar. 30 1330		43·0
Mar. 29 1452	III	Mar. 30 1330		22·5
Mar. 29 1630		Mar. 30 1330		21·0
Apr. 2 1955	III IV	Apr. 4 1930	R	47·5
July 19 1907	III	July 21 1630		45·5
Aug. 14 2158	III	Aug. 17 0730	R	57·5
Aug. 20 0046	III	Aug. 22 0130	R	48·5
Sept. 2 2108	III	Sept. 3 1030	R	13·5
		Sept. 4 1330	R	40·5

This table lists only those slow drift bursts which were followed by magnetic storms within a period of 4 days. A magnetic storm is defined as a period for which the mean K_p index is $\geqslant 5$ for not less than 12 hr. The second column in the table indicates whether the slow drift burst was accompanied by fast drift bursts (III) or continuum radiation (IV), and the fourth column whether auroral echoes (R) were recorded at Jodrell Bank during the magnetic storm.

In cases where optical observations were available, about 90 per cent of the slow drift bursts were associated with flares of importance ≥ 1,[10] and the bursts followed by magnetic storms tended to be associated with flares of importance 2 and 3. Thus, the distribution of magnetically effective bursts with flares of importance 1−, 1, 2 and 3, was 2, 4,

8 and 3, respectively, whereas the distribution of the magnetically non-effective bursts was 3, 11, 4 and 1.

Examination of the commencement of the radio bursts relative to the *start* of the flares shows the radio bursts to be delayed by an average of 7 min. This holds for the magnetically effective bursts as well as the magnetically non-effective bursts. A delay of 7 min, it will be remarked, is approximately the time taken by a disturbance travelling at 1000 km/sec to reach the coronal radio emitting levels, if it traverses the chromospheric optical levels at the starting time of the flare.

Examination of the commencement of the radio bursts relative to the *maximum* phase of the flare shows that, for the twenty-four cases where adequate optical data were available, the onset of the burst preceded the flare maximum in eleven cases, of which seven were followed by geomagnetic storms. For the thirteen bursts succeeding flare maximum, four were followed by geomagnetic storms. However, it must be noted that there is often a wide discrepancy in the estimates of optical observers for the time of flare maximum. As slow drift bursts tend to cluster about flare maximum within a period of ± 5 min, it is often difficult, therefore, to be certain whether the radio burst preceded or succeeded the maximum. This result may be compared with that of Dodson and Hedeman[7] who studied the association of solar flares and radio bursts with magnetic activity. Their analysis covered the period 1949 January–1956 April, and the radio bursts were recorded on single frequency equipments. They found that solar flares preceded by "major early bursts" were followed in most cases by an increase in geomagnetic activity approximately 2·5 days later. It is not certain to what spectral classification the "major early bursts" belong. However, intense bursts with the time duration of a few minutes, as they are described to be, must almost certainly be slow drift bursts or intense groups of fast drift bursts. The results of the present analysis show that, as regards geomagnetic activity, it is the slow drift bursts which are of importance.

Examination of the distribution across the solar disk of the flares associated with slow drift bursts shows that those flares with radio bursts followed by magnetic storms were nearly uniformly distributed in heliographic longitude; the flares and radio bursts not followed by magnetic storms were also uniformly distributed across the disk. The heliographic distribution of the thirty-six flares which were unambiguously associated in time with the occurrence of slow drift bursts is shown in Fig. 4.

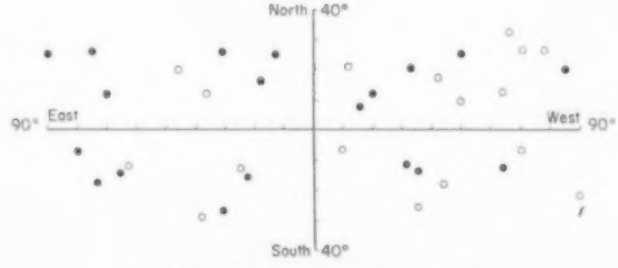

Fig. 4. The heliographic distribution of flares associated with slow drift bursts: ● followed by geomagnetic storm; ○ not followed by geomagnetic storm.
The correlation of the bursts and flares is in time only; radio position measurements are not available.

5. DISCUSSION

From the evidence reviewed above, we conclude that slow drift (Type II) bursts result from the emission of the auroral corpuscular streams from the sun or from an associated shock front, and that they are causally associated with the occurrence, approximately 30 hr later, of terrestrial magnetic storms and displays of the aurora. It does not necessarily follow that the radio bursts are associated only with the first front of the stream, as there is a tendency for more than one slow drift burst to precede a given magnetic storm. The velocity of the primary disturbing agent which causes the bursts is of the order of 1000 km/sec, and this is in good accord with the mean time delay of 33 hr between the bursts and the terrestrial disturbances.

Only 45 per cent of slow drift bursts are followed by magnetic storms. We must therefore enquire whether there are any radio characteristics of the slow drift bursts, or unusual optical characteristics of the associated visible phenomena, which would give us an indication as to the reason why only 45 per cent of the bursts are followed by geomagnetic disturbances. One might anticipate that an examination of the slopes of the slow drift bursts would resolve this problem, a low slope indicating that the outward travelling disturbance may not have sufficient energy to escape from the solar atmosphere. However, this investigation yields no conclusive result; the slope of individual bursts is often indeterminate within a factor of two, and in 85 per cent of cases best estimates lie within the range 10–40 Mc/s per min (at a frequency of 125 Mc/s). Further evidence on this point may become available when sweep frequency observations are extended to the lowest possible frequencies. The observing band 100–580 Mc/s corresponds to radio signals emitted from the height range approximately 500–50 000 km in the solar atmosphere, and therefore yields no information about deceleration of an outward moving disturbance as it traverses the outer corona.

It has been shown that the presence or absence of fast drift bursts in association with the slow drift bursts is immaterial. It has also been shown that the occurrence of continuum (Type IV) radiation is also apparently not an essential controlling factor, since it accompanies only 12 per cent of slow drift bursts. The latter, however, are nearly always magnetically effective.

In examining the optical evidence, we have noted that the slow drift bursts which are magnetically effective tend to be associated with flares of high importance. A number of these flares are accompanied by ejective prominences, as indicated by accompanying sprays, surges and the sudden disappearance of filaments. But the available data are insufficient to permit any useful statistical comment on the existence of optical criteria which immediately and conclusively determine the geomagnetic importance of slow drift bursts. Comparison of the time of occurrence of slow drift bursts with the start and maximum phases of the associated flares gives no additional information.

The long search for substantive evidence concerning the existence and nature of the so called auroral corpuscular streams has as yet yielded few direct results. Spectral radio observations, which monitor the radio emissions from the outer regions of the solar atmosphere do, however, provide strong supporting evidence for the outward passage of such streams from the sun.

Acknowledgements—The work described in this paper forms part of a program of research supported by financial assistance from the U.S. Air Force Cambridge Research Center, through the offices of the Sacramento Peak Observatory. The authors are indebted to Mr. C. D. Watkins of the Jodrell Bank Experimental Station, England, for providing the auroral radio data, and to Mr. J. P. Wild, CSIRO Division of Radiophysics, Australia, for additional solar radio data.

REFERENCES

1. R. Payne-Scott, D. E. Yabsley and J. G. Bolton, *Nature, Lond.* **160**, 256 (1947).
2. J. P. Wild, *Aust. J. Sci. Res.* A **3**, 399 (1950).
3. A. Maxwell, G. Swarup and A. R. Thompson, *Proc. Inst. Radio Engrs., N.Y.* **46**, 142 (1958).

4. A. MAXWELL and A. R. THOMPSON, in preparation.
5. J. P. WILD, K. V. SHERIDAN and G. H. TRENT, *Paris Symposium on Radio-Astronomy*, p. 176. Stanford University Press (1959).
6. H. W. NEWTON, *Mon. Not. R. Astr. Soc.* **103**, 244 (1943).
7. H. W. DODSON and E. R. HEDEMAN, *J. Geophys. Res.* **63**, 77 (1958).
8. A. R. THOMPSON, *Paris Symposium on Radio-Astronomy*, p. 210. Stanford University Press (1959).
9. J. A. ROBERTS, *Paris Symposium on Radio-Astronomy*, p. 194. Stanford University Press (1959).
10. G. SWARUP, P. H. STONE and A. MAXWELL, in preparation.

Planet Space. Sci. Pergamon Press 1959. Vol. 1, pp. 333–342. Printed in Great Britain.

THE PHOTOLYSIS OF NITROUS OXIDE IN THE FAR ULTRAVIOLET

W. E. GROTH and H. SCHIERHOLZ

Institut für Physikalische Chemie, Universität Bonn

(*Received* 23 *June* 1959)

Abstract—The photolysis of nitrous oxide has been studied in a flow system using xenon resonance radiation at 1470 and 1295 Å and krypton resonance radiation at 1236 and 1165 Å. The average quantum yields with regard to decomposed nitrous oxide, nitrogen and higher oxides of nitrogen were found to be larger in the experiments using the longer wave lengths than in the experiments using the 1236 and 1165 Å radiation. The ratio of the quantum yield with respect to oxygen and nitrogen was found to be lower in the experiments with the resonance radiation of xenon than in the experiments with the resonance radiation of krypton.

From the data obtained, it can be assumed that at the xenon resonance radiation the initial absorption of a light quantum leads to the production of nitrogen molecules and oxygen atoms. At the shorter wave lengths, the initial absorption act probably proceeds in a dual manner. It is supposed that both the splitting of nitrous oxide into nitrogen molecules and oxygen atoms and into nitrogen atoms and nitric oxide occurs at this radiation.

1. INTRODUCTION

The photolysis of nitrous oxide has been investigated by several authors from different points of view. The investigations of Macdonald[1], Noyes[2], and Briner and Karbassi[3] were carried out in the near ultraviolet. Macdonald extended the investigations of Berthelot and Gaudechon[4] as well as of Regener and Warburg[5]. In his experiments, the first measurements of the quantum yield of the photolysis of nitrous oxide were carried out. Noyes intended to determine the nature of the primary reaction which follows the absorption of a light quantum. Briner and Karbassi investigated the photochemical decomposition of nitrous oxide in the pressure interval between 5 and 40 atm.

As Adel has shown, nitrous oxide is a minor constituent of the earth's atmosphere[6] and since nitrous oxide certainly plays a rôle in the photochemical equilibrium of the earth's atmosphere[7], its photodecomposition in the far ultraviolet light is of interest in aeronomy.

The photolysis of nitrous oxide at 1470 as well as 1236 Å (and 1165 Å) has been studied by Zelikoff and Aschenbrand[8]. In the experiments carried out with the longer wavelengths these authors used a lamp of the type described by Dacey and Hodgins[9]. The body of this lamp consisted of a quartz tube of extremely thin walls and the xenon resonance line at 1470 Å was supposed to penetrate this quartz wall. In contrast to this assumption, an investigation of the transparency of several sorts of quartz glass in the spectral range between 1470 and 1750 Å[10] has shown that quartz glass is practically non-transparent for the 1470 Å radiation and that quartz tubes of 0·05 to 0·1 mm wall thickness are useful as lamp bodies at wave lengths greater than 1550 Å. This conclusion has recently been verified in this laboratory by the investigation of the transmission of fused silica of extreme thinness[11].

For this reason it seemed possible that the dissociation of nitrous oxide investigated by Zelikoff and Aschenbrand was not due to the 1470 Å radiation but to the relatively intensive lines at about 1550 and 1650 Å which were observed in our experiments with a low voltage xenon lamp[12] and which were caused by impurities present in the gas filling of the lamp. Therefore it was intended to reproduce the

experiments of Zelikoff and Aschenbrand by means of a radiation source which emitted practically exclusively the xenon resonance lines. It was also intended to extend the investigations to a larger pressure interval. The experiments of Zelikoff and Aschenbrand with the xenon resonance lines were carried out in the pressure range between 1·7 mm Hg and 5·6 mm Hg; their experiments at 1236 and 1165 Å (krypton resonance lines) were carried out between 1·27 and 49·5 mm Hg. In the present experiments, the pressure interval between 20 and 670 mm Hg was investigated. In contrast to the previous investigations in a static system, our experiments were carried out in a flow system.

2. EXPERIMENTAL TECHNIQUE AND ANALYTICAL PROCEDURES

The nitrous oxide was tank gas for medical purposes manufactured by Bayer-Werke, Leverkusen. The gas was purified by adsorption on silica gel and subsequent desorption.

The experiments were carried out in the apparatus shown in Fig. 1.

The photolysis of N_2O occurred in the reaction cell R which was situated in front of the lithium fluoride window of a low voltage lamp.[12] The 1470 and 1295 Å radiation was produced by the xenon resonance lines whereas the 1236 and 1165 Å radiation was due to the krypton resonance lines. The application of a magnetic field of several 1000 G to the part of the lamp before the LiF window caused a three-to-fourfold increase of the quantum efficiency. The intensity of the lines at about 1550 and 1650 Å due to impurities was essentially reduced by this magnetic field as is shown by Fig. 2.

The quantum efficiency of the lamp was determined from the amount of ozone formed when rapidly flowing oxygen passed the window of the lamp.

During the experiments nitrous oxide was stored in trap F_3. Its vapour pressure was regulated by a temperature bath and was controlled by a quartz spiral gauge M_1.

After having passed the capillary S serving as a flow resistance, the irradiated gas mixture was collected in trap F_1 which was cooled with liquid air.

Nitrogen and oxygen formed during the experiments were pumped off from the gas mixture cooled to 56°K, collected in a Toepler pump and pumped into a manometer system of known volume. The amount of the non-condensable gases was determined volumetrically.

Condensable gases were frozen out at 56°K in F_1 and distilled into a bulb of known volume connected with a quartz gauge. The total amount of the condensable gases was determined volumetrically.

Mercury was kept from the high vacuum line and all parts of the apparatus in contact with nitrous oxide or with gas mixtures containing higher oxides of nitrogen by liquid air traps. Ground joints and stopcocks which were in contact with higher oxides of nitrogen were greased with fluorinated grease.

The ratio of nitrogen and oxygen was determined mass-spectrometrically. The determination of very small concentrations of nitric oxide and nitrogen dioxide in a gas mixture consisting mainly of nitrous oxide was not possible by means of a conventional mass spectrometer (Atlas-Werke, Bremen, type *CH4*). In very rough measurements which had a more qualitative character a field emission mass spectrometer[13] was used. Experiments were carried out to investigate the possibility of analysing gas mixtures containing nitrous oxide, nitric oxide and nitrogen dioxide by gas chromatographic methods.

The determination of the ratio of nitrous oxide and the sum of nitrogen dioxide and nitric oxide is possible, but no column and no combination of columns could be found by which a separation of all three gases was obtained. The gas fractions due to nitric oxide and nitrogen dioxide appeared at the same place of the chromatogram. Experiments to separate N_2O, NO and NO_2 by a molecular sieve (Linde Air Products Comp., type *x*13) showed that NO could penetrate, while N_2O and NO_2 are absorbed in the column. However, mixtures of N_2O and NO with small NO concentrations were quantitatively absorbed in this column.

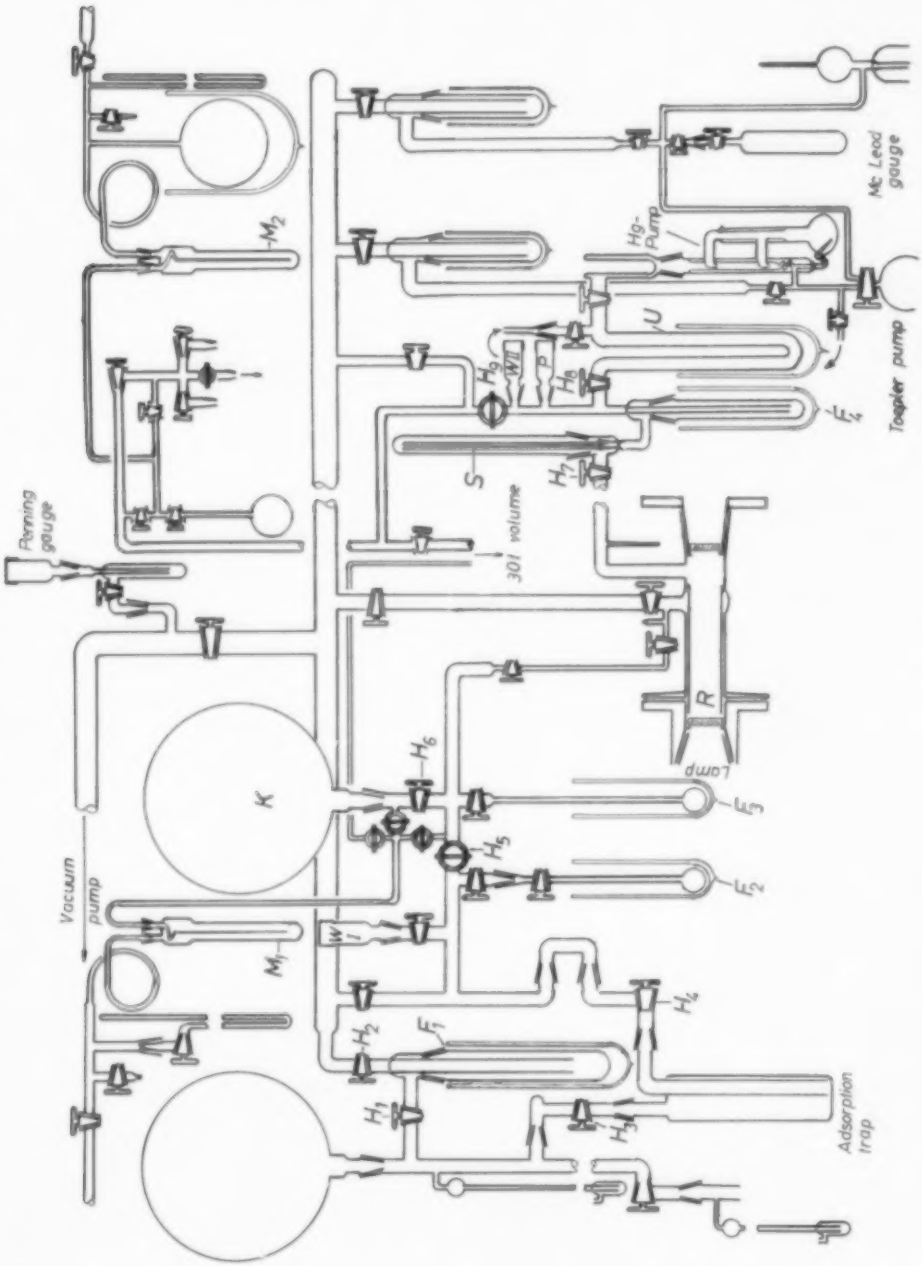
Penning gauge
Vacuum pump
M2
M1
K
H6
H5
H4
H2
H1
H3
F1
F2
F3
F4
W1
W2
P
S
R
U
Lamp
301 volume
Hg-Pump
Mc Leod gauge
Toepler pump
Adsorption trap

Fig. 1.

In the finally adopted analytical procedure, the separation of nitrous oxide on the one hand and nitrogen dioxide and nitric oxide on the other hand was carried out with an aluminium oxide column containing 3 per cent water. It was found by Greene and Pust[14] that nitrogen dioxide reacts with water absorbed on a molecular sieve quantitatively according to

$$2\,NO_2 + H_2O = HNO_2 + HNO_3$$

$$3\,HNO_2 = HNO_3 + H_2O + 2\,NO.$$

It can be assumed that similar conditions existed in the aluminium oxide column.

The calculation of the quantities of NO_2 and NO formed in the photolysis of nitrous oxide was performed by the combination of these measurements with the equation which is derived from the material balance of the decomposition of N_2O:

$$N_{N_2O} = N_{N_2} + 1/2\,N_{NO} + 1/2\,N_{NO_2} = 2\,N_{O_2} + 2N_{NO_2} + N_{NO}. \qquad (1)$$

The quantity of nitrogen and oxygen was determined mass-spectrometrically. By gas chromatographic methods the ratio of higher oxides of nitrogen and nitrous oxide was determined and the total amount of condensable gases was known from volumetric measurements.

3. EXPERIMENTAL RESULTS

The results of the photochemical decomposition of nitrous oxide by the resonance wavelength radiation of xenon at 1470 and 1295 Å are given in Table 1. These experiments were carried out in a pressure interval between 20 mm Hg and 670 mm Hg at flow velocities between 16 and 740 ml/min. At higher pressures and at high flow velocities, the total throughput of N_2O amounted up to 20 l. NTP. In these cases the concentration of the reaction products was extremely low and a direct analysis of the higher oxides of nitrogen was not possible.

In these experiments, the mixtures of nitrogen, oxygen and higher oxides of nitrogen were collected at liquid air temperature. Since nitric oxide reacts at this temperature with molecular oxygen to form nitrogen dioxide[15], it was assumed that in the gas mixtures, the higher oxides of nitrogen consisted mainly of nitrogen dioxide and that nitric oxide was present only in negligible amounts. On this

Table 1. Experimental Results Using Renon Resonance Radiation at 1470 and 1295 Å

Pressure in the reaction cell (mm Hg)	Velocity of gas flow (ml/min)	Quantum yields				
		Φ_{N_2}	Φ_{O_2}	$\frac{\Phi_{O_2}}{\Phi_{N_2}}$	Φ_{NO_2} (calc.)	Φ_{N_2O} (calc.)
650	51	1·74	0·16	0·092	0·95	2·22
670	45	1·38	0·25	0·181	0·56	1·66
494	261	1·54	0·12	0·078	0·87	1·98
511	250	1·34	0·08	0·059	0·79	1·73
361	740	1·50	0·15	0·100	0·80	1·90
307	400	1·37	0·14	0·120	0·72	1·73
650	16	1·48	0·15	0·105	0·89	1·92
660	23	1·18	0·18	0·153	0·55	1·45
20·2	28	1·14	0·12	0·105	0·60	1·44
27·5	23	1·27	0·16	0·126	0·63	1·58
Averages		1·40 ±0·06	0·15 ±0·01	0·11 ±0·01	0·74 ±0·05	1·76 ±0·08

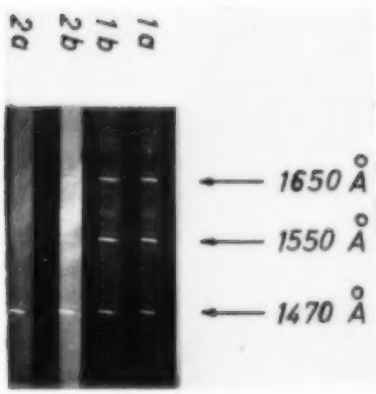

Fig. 2.

[facing p. 335]

assumption the quantum yield with regard to nitrogen dioxide and with regard to nitrous oxide can be calculated from the quantum yields with regard to nitrogen and oxygen by the following equation:

$$\phi_{N_2O} = \phi_{N_2} + 1/2\,\phi_{NO_2} = 2\,\phi_{O_2} + 2\,\phi_{NO_2}. \quad (2)$$

The values shown in column 6 and 7 of Tables 1 and 2 were calculated in this manner.

The quantum yields with respect to nitrous oxide, nitrogen and higher oxides of nitrogen are very similar to the values published by Zelikoff and Aschenbrand (see above table).

	Present results	Zelikoff and Aschenbrand
ϕ_{N_2O}	1·76 (±0·08)	1·70 (±0·07)
ϕ_{N_2}	1·40 (±0·06)	1·44 (±0·11)
$\phi_{\text{higher oxides of nitrogen}}$	0·74 (±0·05)	0·67 – 0·82 (experiments in the pressure range between 4·6 and 5·6 mm Hg)

In the experiments of Zelikoff and Aschenbrand the higher oxides of nitrogen consisted only of nitric oxide. The gas mixtures finally resulting from our experiments contained mainly higher oxides of nitrogen in the form of nitrogen dioxide. The quantum yields with respect to oxygen found in our experiments should therefore be markedly smaller than the values given by Zelikoff and Aschenbrand. As is shown in Table 1 the average quantum yield with respect to oxygen was 0·15, the value given by Zelikoff and Aschenbrand is 0·50. The experiments carried out with the krypton resonance radiation (1236 and 1165 Å) are summarized in Table 2.

A direct comparison of these values with the measurements of Zelikoff and Aschenbrand is not possible since these authors gave no quantum yields but reported the ratios of nitrous oxide decomposed with respect to the dissociation products. The average ratio with respect to nitrogen formed, which was 1·12, compares fairly well with our value of 1·23. This correspondence was less precise for the ratio with respect to the higher oxides of nitrogen. From the work of Zelikoff and Aschenbrand an average value of 2·35 was obtained, whereas in this investigation a ratio of

Table 2. Experimental Results Using Krypton Resonance Radiation at 1236 and 1165 Å

Pressure in the reaction cell (mm Hg)	Velocity of gas flow (ml/min)	Quantum yields				
		ϕ_{N_2}	ϕ_{O_2}	$\frac{\phi_{O_2}}{\phi_{N_2}}$	ϕ_{NO_2} (calc.)	ϕ_{N_2O} (calc.)
549	34	1·18	0·20	0·170	0·52	1·44
311	56	1·29	0·20	0·155	0·59	1·58
23	50	1·35	0·23	0·170	0·59	1·68
24	50	1·09	0·18	0·165	0·49	1·34
23	50	1·04	0·12	0·115	0·53	1·30
41	35	1·19	0·19	0·160	0·55	1·46
20	29	1·18	0·21	0·178	0·51	1·44
20	29	1·14	0·19	0·167	0·51	1·40
42	26	1·21	0·28	0·229	0·43	1·42
Averages		1·18 ±0·03	0·20 ±0·01	0·167 ±0·01	0·52 ±0·02	1·45 ±0·04

2·8 was found. However, the values from the individual measurements of Zelikoff and Aschenbrand vary between 1·75 and 3·88 so that our values lie well within their range of variation.

Further experiments at low pressures were carried out, allowing the direct determination of the higher oxides of nitrogen.

The analysis of a gas mixture resulting from the irradiation of nitrous oxide by the krypton resonance radiation was carried out by a field emission mass spectrometer. In the condensable gas only nitrogen dioxide was found; a detection of nitric oxide in this gas mixture was not possible by this method. Experiments analysed by gas chromatographic and mass-spectrometric methods are summarised in Table 3.

Table 3.

Experimental Results
Mass Spectrometric (MSA) and Gas Chromatographic Analysis (GCA)

Wavelength (Å)	Pressure (mm Hg)	Velocity of gas flow (ml/min)	ϕ_{O_2} ϕ_{N_2} determined by MSA		ϕ_{NO_2} ϕ_{NO} determined by GCA		$\frac{\phi_{O_2}}{\phi_{N_2}}$	$\frac{\phi_{NO_2}}{\phi_{N_2}}$	$\frac{\phi_{NO}}{\phi_{N_2}}$
1470 (1295)	20·2	28	1·14	0·12	0·57	0·10	0·11	0·50	0·09
1470 (1295)	27·5	23	1·27	0·16	0·61	0·08	0·13	0·48	0·06
1236 (1165)	20·0	29	1·18	0·21	0·48	0·03	0·18	0·41	0·03
1236 (1165)	20·3	29	1·14	0·19	0·47	0·12	0·17	0·41	0·10

The nitrous oxide pressures were high enough to ensure that at least 99 per cent of the radiation emitted was absorbed in a layer of 1 cm thickness. The total amount of gas irradiated in these experiments varied from 70 to 100 ml NTP; concentrations of higher oxides of nitrogen produced by photolysis varied from 0·5 to 1 per cent.

Table 4.

Average Results Obtained from the Photolysis of Nitrous Oxide with the Resonance Radiations of Xenon and Krypton

	1470 (1295) Å	1236 (1165) Å
ϕ_{O_2}/ϕ_{N_2}	0·11	0·17
ϕ_{NO_2}/ϕ_{N_2}	0·49	0·41
ϕ_{NO}/ϕ_{N_2}	0·08	0·06
ϕ_{N_2}	1·40	1·18
ϕ_{O_2}	0·15	0·20
ϕ_{NO_2}	0·68	0·48
ϕ_{NO}	0·11	0·07
ϕ_{N_2O}	1·8	1·46

The average values from the experiments summarised in the Tables 1, 2 and 3 are given in Table 4.

As Table 4 indicates, the photolysis of nitrous oxide follows two different reaction paths for each of the two radiation regions.

The experiments did not permit any conclusion whether the nitrogen dioxide found in the gas mixtures was the product of a secondary process occurring at the temperature of liquid air or whether the formation of nitrogen dioxide followed the primary process of the photochemical dissociation of nitrous oxide.

In two experiments carried out with the 1236 and 1165 Å radiation the freezing out of the reaction products was avoided. The irradiated gas was collected in a 30 l. volume at room temperature. The analysis of these gas mixtures was carried out by a field-emission mass spectrometer.

The data of these experiments are given in Table 5. In both experiments, the intensity of

Table 5. Experimental Data and Results of two Experiments Evaluated by a Field Emission Mass Spectrometer (Irradiated Gases were kept at Room Temperature)

Calibration spectra of N_2O, NO and mixtures of N_2O with NO_2 and N_2O with NO

Mass	Intensities and intensity ratios of the peaks (in arbitrary units)															
	N_2O		NO		$N_2O + NO_2$ 12.43 : 1				$N_2O + NO_2$ 64.7 : 1				$N_2O + NO$ 1.16 : 1			
	Intensity	Intensity rel. to base peak	Intensity	Intensity rel. to base peak	Total intensity measured	Intensity of the peaks due to NO_2	Intensity rel. to base peak of NO_2	Sensitivity of NO_2 rel. to base peak of N_2O	Total intensity measured	Intensity of the peaks due to NO_2	Intensity rel. to base peak of NO_2	Sensitivity of NO_2 rel. to base peak of N_2O	Total intensity measured	Intensity of the peaks due to NO	Intensity rel. to base peak of NO	Sensitivity of NO rel. to base peak of N_2O
	Mass spectrum after elimination of the N_2O spectrum															
46	32 000 50000	1			24 000				23 000				15000			
47	170 200	0.0049 0.0038			2400	2284	1	1.3	720	608	1	1.6				
30	260 272	0.007 0.0047	160000	1	9 000	8820	3.9	4.8	1500	1450	2.4	4	72 000	71 900	1	4.1
31	3		1000	0.006	50	47	0.02	0.0024	15	12	0.02	0.0034	200	197	0.003	0.015

Background: Mass 47 = 13, Mass 30 = 36, Mass 31 = 3

Data and results of the experiments

Quanta emitted 5.8×10^{19}

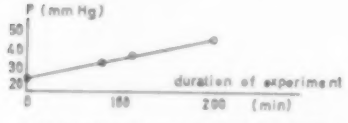

Total quantity of gas irradiated: 556 ml nTP
Average flow velocity 55 ml/min

Quanta emitted 5.4×10^{19}

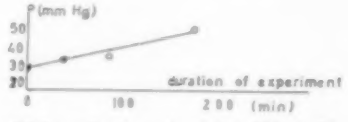

Total quantity of gas irradiated: 557 ml nTP
Average flow velocity 56 ml/min

Mass spectrum of the gas irradiated

Mass	Total intensity measured (arbitrary units)	Intensity after elimination of the N_2O spectrum (arbitrary units)
45	24 000	
47	155	49
30	329	102

Mass spectrum of the gas irradiated

Mass	Total intensity measured (arbitrary units)	Intensity after elimination of the N_2O spectrum (arbitrary units)
45	30 000	
47	186	44
30	312	96

Intensity ratio of the masses 30 and 47 in the resulting mass spectrum after elimination of the N_2O spectrum:

2.1 2.2

the peak corresponding to mass 47* exceeded clearly the isotopic intensity due to the $14_{N_2}18_O1_H{}^+$-ion and it can be assumed that this surplus intensity was due to the NO_2H^+-ion. This assumption was substantiated by the fact that no surplus intensity could be tested when the same gas mixture was analysed in the presence of mercury vapour.

In order to ensure that nitrogen dioxide found in these gas mixtures was not a secondary product, formed by oxidation of nitric oxide by molecular oxygen, the decrease of the oxygen concentration was observed in mixtures of nitric oxide and oxygen at partial pressures as low as 0·5 mm Hg and argon at a pressure of about 20 mm Hg.

As was shown by these experiments, the reaction rate of the oxidation of nitric oxide with molecular oxygen at low partial pressures of nitric oxide and oxygen and in the presence of relatively high concentrations of an inert gas is very low. After a reaction time of 8 h about 3·5 per cent of the oxygen initially present had reacted.

4. DISCUSSION

The results may be summarized as follows:

(1) When flowing nitrous oxide was photolysed by 1470 and 1295 Å radiation and also by 1236 and 1165 Å radiation, the decomposition products were oxygen, nitrogen, nitrogen dioxide and nitric oxide.

(2) When nitrous oxide was photolysed by the xenon resonance radiation (1470 and 1295 Å) a quantum yield of 1·8 with regard to nitrous oxide was obtained. When the krypton resonance radiation (1236 and 1165 Å) was used, a quantum yield of 1·46 was found.

(3) The ratio of the quantum yield of oxygen to the quantum yield of nitrogen in the experiments with the 1470 and 1295 Å radiation was 0·11, with the 1236 and 1165 Å radiation this ratio was 0·17.

In the photochemical decomposition of nitrous oxide the possible primary reactions are given by equations (1) and (2):

$$N_2O + h\nu = N_2 + O \quad (1)$$

$$N_2O + h\nu = NO + N \quad (2)$$

Since the observed quantum yield with regard to N_2O was greater than unity, the products of the primary reaction must react with nitrous oxide. Such reactive products are oxygen atoms which are formed by reaction (1). These oxygen atoms can react with nitrous oxide:

$$O + N_2O = 2\,NO \quad (3)$$

$$O + N_2O = N_2 + O_2 \quad (4)$$

Although the work of Noyes[2] as well as of Kistiakowsky and Volpi[16] has shown that oxygen atoms in the ground state do not react with nitrous oxide at a detectable rate, it must be concluded from the experiments of Friedman and Bigeleisen[17] that a reaction of oxygen atoms in an electronically excited state (^1S) or of high kinetic energy with nitrous oxide is possible. A reaction of nitrogen atoms with nitrous oxide was not observed by Kistiakowsky and Volpi[16] and by Kaufman and Kelso[18].

It can be assumed that the nitrogen dioxide observed in the photolysis of nitrous oxide in a flow system has been formed by reaction (5):

$$NO + O + M = NO_2 + M \quad (5)$$

The rate of the oxidation of nitric oxide by molecular oxygen at low partial pressures of

* An investigation of the properties of ions formed by field emission[13] has shown that from molecules with even numbers of electrons such as H_2O, N_2, A and CO_2 almost exclusively the ions H_3O^+, N_2H^+, AH^+ and CO_2H^+ appear in the mass spectrum of the field emission mass spectrometer, provided a proton-donating substance is present.

In the vicinity of the extremely strong electrical field present in the neighbourhood of the ionizing tungsten tip, small, unavoidable traces of water cause reactions of the following sort:

$$A + H_2O = AH^+ + OH + e^-$$

In the mass spectrum of molecules with odd numbers of electrons such as NO both the hydride ions and the parent ions appear. In the case of nitric oxide the ion NO^+ with mass 30 was predominant, in the case of NO_2 both the $NO_2{}^+$-ion with mass 46 and the NO_2H^+-ion with mass 47 were present with comparable intensities. The peak due to the latter ions was used exclusively for the mass spectroscopic determination of NO_2.

nitric oxide and oxygen in the presence of relatively high concentrations of a third non-reacting gas is very slow. The amount of NO_2 formed in this way in the time between the photolytical experiment and the analysis of the sample would have been small and not detectable by our analytical methods.

The nitrogen dioxide formed by reaction (5) was removed from the reaction region fast enough so that its subsequent destruction by oxygen atoms through the reaction

$$NO_2 + O = NO + O_2 \qquad (6)$$

can have taken place only to a small extent.

In accordance with our observations that NO_2 was formed in the photolysis of N_2O, Kaufmann, Gerri and Bowman[19] have demonstrated the presence of NO_2 as an intermediate product in the thermal decomposition of N_2O by the observation of chemiluminescence. The quantum yield with respect to nitrous oxide in the experiments with the 1236 and 1165 Å radiation was found to be smaller than in experiments with longer wavelengths. In the first case a relatively smaller number of energetic oxygen atoms was formed than in the second case.

That means, in the photolysis with the 1236 and 1160 Å radiation, reaction (2) has a markedly more important role than in the photolysis with the 1470 and 1295 Å radiation.

Nitrogen atoms produced by reaction (2) react with NO according to reaction (7)[18]

$$N + NO = N_2 + O \qquad (7)$$

This process causes a decrease of the quantum yield with respect to higher oxides of nitrogen. Therefore the photochemical decomposition of N_2O by 1470 and 1295 Å radiation may be explained by the following reaction scheme:

$$N_2O + h\nu = N_2 + O \qquad (1)$$
$$O + N_2O = 2\,NO \qquad (3)$$
$$O + N_2O = N_2 + O_2 \qquad (4)$$
$$NO + O + M = NO_2 + M \qquad (5)$$
$$NO_2 + O = NO + O_2 \qquad (6)$$
$$O + O + M = O_2 + M \qquad (8)$$

Reactions (2) and (7) could not be excluded, however, the experiments show that they are not of great importance in this case. In the case of photolysis of N_2O with 1235 and 1165 Å radiation these reaction must be included:

$$N_2O + h\nu = N_2 + O \qquad (1)$$
$$N_2O + h\nu = NO + N \qquad (2)$$
$$O + N_2O = 2\,NO \qquad (3)$$
$$O + N_2O = N_2 + O_2 \qquad (4)$$
$$N + NO = N_2 + O \qquad (7)$$
$$NO + O + M = NO_2 + M \qquad (5)$$
$$NO_2 + O = NO + O_2 \qquad (6)$$
$$O + O + M = O_2 + M \qquad (8)$$
$$N + N + M = N_2 + M \qquad (9)$$

The primary steps of these reaction mechanisms are identical with those given by Zelikoff and Aschenbrand. There is a possibility that ozone may have been formed and may have participated in the oxidation reactions.

Acknowledgement—We gratefully acknowledge the helpful assistance of Dr. H. D. Beckey with the analysis of the products on his field emission mass spectrometer.

This work was sponsored by the European Office, Air Research and Development Command, under Contract Nr. AF 61(514)-1079.

REFERENCES

1. J. Y. Macdonald, *J. Chem. Soc.* p. 1 (1928).
2. W. A. Noyes, Jr., *J. Chem. Phys.* **5**, 807 (1937).
3. D. Briner, H. Karbassi, *Helv. Chim. Acta* **28**, 1204 (1945).
4. D. Berthelot and F. H. Gaudechon, *C. R. Acad. Sci., Paris* **150**, 1517 (1910), cited in reference (1).
5. E. Regener and E. Warburg, *S.B. Preuss. Akad. Wiss.* 1228 (1904), cited in reference (1).
6. A. Adel, *Astrophys. J.* **88**, 186 (1938); **90**, 627 (1939); **93**, 509 (1941), cited in reference (7).
7. D. R. Bates and A. Witherspoon, *Mon. Not. R. Ast. Soc.* **112**, 101 (1952).
8. M. Zelikoff and L. M. Aschenbrand, *J. Chem. Phys.* **22**, 1680 (1954); *idem* **27**, 123 (1957).
9. J. R. Dacey and J. W. Hodgins, *Canad. J. Res.* **28B**, 90 (1950).

10. W. GROTH and H. v. WEYSSENHOFF, *Z. Naturf.* **11a**, 165 (1956).
11. C. BARTH, private communication (unpublished results).
12. W. GROTH, *Z. Elektrochem. angew. phys. Chem.* **45**, 262 (1939).
13. H. D. BECKEY, *IV. International Kongress für Elektronenmikroskopie, Berlin* 1958. Springer, Berlin (in press).
14. S. A. GREENE and H. PUST, *Analytical Chem.* **30**, 1039 (1958).
15. F. C. HENRIQUES, A. B. F. DUNCAN and M. A. NOYES, Jr. *J. Chem. Phys.* **6**, 518 (1938).
16. G. B. KISTIAKOWSKY and G. G. VOLPI, *J. Chem. Phys.* **27**, 1141 (1957).
17. L. FRIEDMAN and J. BIGELEISEN, *J. Amer. Soc.* **75**, 2215 (1953).
18. F. KAUFMAN and J. R. KELSO, *J. Chem. Phys.* **28**, 510 (1958).
19. F. KAUFMAN, N. J. GERRI and R. E. BOWMAN, *J. Chem. Phys.* **25**, 106 (1957).

Planet Space. Sci. Pergamon Press 1959. Vol. 1, pp. 343–346. Printed in Great Britain.

IONIZING RADIATION DETECTED BY PIONEER II

A. ROSEN, P. J. COLEMAN, Jr. and C. P. SONETT

Space Technology Laboratories, Los Angeles 45, California

(*Received* 14 *May* 1959)

Abstract—The total ionizing component of cosmic radiation was measured up to an altitude of 1550 km. An upper bound to the ratio of average-to-minimum specific ionization was determined by comparing the ionization with the count-rate observations from the Explorer IV satellite. This result implied that protons are the predominant species which gave rise to the observed ionization.

Pioneer II was launched from Cape Canaveral, Florida, on November 7, 1958, and attained a maximum altitude of 1550 km. The payload contained an ionization chamber to measure the total ionizing component of cosmic radiation flux[1]. Ion chamber data were received during the first half hour of flight. The measured radiation levels are plotted versus altitude (see Fig. 1). The declination and longitude of the vehicle's position are given for each data point. Reportedly, the level of solar activity was low during the flight and unusual magnetic and corpuscular disturbances were absent. However, solar activity was moderate a few days prior to the flight.

The ionization chamber consisted of an aluminium-walled vessel, filled with spectroscopically pure argon to a pressure of 13·6 atm. The volume of the chamber was 43 cm³ and the areal density of the cylindrical walls was 400 mg/cm². The ends of the cylinder were slightly thicker in order to attain the necessary structural strength. The areal density of the ends was 1200 mg/cm². The shell of the vehicle accounted for another 50 mg/cm² of shielding so that the minimum areal density traversed by a particle before reaching the sensitive volume of the chamber was 450 mg/cm². The solid angle subtended by the 1200 mg/cm² ends of the cylinder was 1 steradian. An additional amount of shielding due to the presence of a miscellany of electronic components, structure, and a retrorocket accounted for a solid angle of 1·5 steradians. For this solid

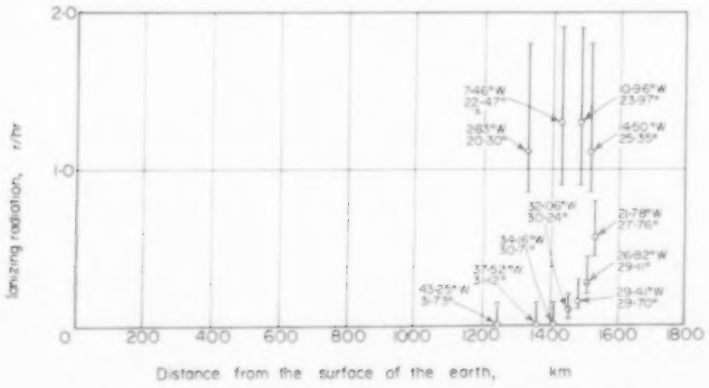

Fig. 1. Pioneer II. Ionizing radiation versus altitude including longitude and north latitude.

angle the shielding corresponded to an average areal density of 20 gm/cm^2.

The electronics was basically a design utilized for the CsI scintillation count-rate meter in Explorer IV[2]. A d.c. electrometer amplifier, with a range of 1000 r/hr, drove a subcarrier oscillator which, in turn, modulated the transmitter. Since the circuit was temperature dependent, in-flight calibration was provided by the substitution of a known voltage for the ionization chamber output. The duty cycle consisted of 180 sec of ionization chamber data followed by 20 sec of calibration voltage. With this calibration voltage on the input, the subcarrier frequency varied with the temperature of the circuit. Thus, by measuring the subcarrier frequency of the calibration signal, the effective temperature of the circuit could be determined.

Calibration of the ion chamber, itself, was accomplished by utilizing a Co^{60} source located at the Radiology Department of the UCLA Medical Center. Several sources of error were considered in determining the range of error to be assigned to each data point. Some of these sources lay in the drift and nonlinearity of the subcarrier oscillator in the vehicle, the demodulating equipment on the ground and the recording apparatus. The asymmetry of the error flags is due to the fact that the output was, approximately, a logarithmic function of the radiation level. This relationship was used so that the instrument would have a comparatively large dynamic range.

The significance of the information on ionizing radiation which was gathered during the brief life of Pioneer II lies in the fact that it clearly indicates an increase of such radiation with decreasing north latitude. At the apogee of the orbit, in the altitude range of 1500 to 1550 km, the vehicle traversed 7° of latitude. Thus for an essentially constant altitude, the variation of ionization with latitude was observed. Fig. 2 shows the variation of ionization with latitude when the chamber was located at 1525 ± 25 km. altitude.

Further, it is possible to obtain a bound for the average specific ionization of the observed radiation at this altitude by combining the results of this experiment with those of other satellites. Such correlations generally involve special consideration relating to the possibility

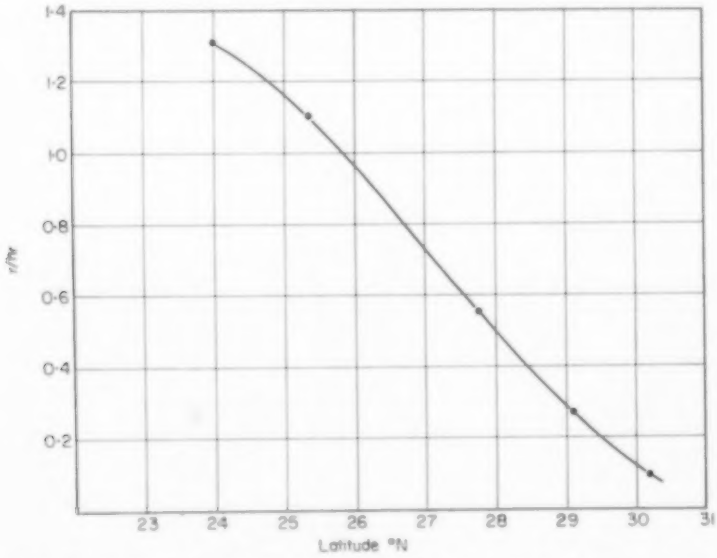

Fig. 2. Pioneer II. Ioniziation versus latitude at an altitude of 1525 ± 25km.

of temporal variation of the intensity in the interval between the two measurements, differences in the positions of the two experiments and differences in the shielding of the detectors. The earth satellite, Explorer IV, was well suited for such a correlation because it was in orbit at the same time that ionization data was gathered, and it traversed the same region of space as Pioneer II. A partial summary of the data gathered by instruments on the Explorer IV satellite has been presented by van Allen[2]. The counting rates from two Geiger tubes were used to determine the contours of equal counting rates. One tube was shielded by a minimum of 1·2 gm/cm² for certain directions and a maximum of 5·0 gm/cm² for other directions. The counting rate reported for this tube at an altitude of 1550 km, 20° N geomagnetic latitude, and 80° W geographic longitude was 1200 count/sec.*

In using these data for a determination of average specific ionization, differences in the positions of the two vehicles were considered. At the altitude of 1550 km, the coordinates of Pioneer differed from the Explorer in longitude only, and consideration of the trapping mechanism indicates that the counting rates are almost independent of geomagnetic longitudes but are strongly dependent on geomagnetic latitudes. Thus, it was expected that 1200 c/s would be the count rate reported in the Explorer satellite when its position was the same as the position of Pioneer. Verification of this expectation was obtained by a cursory check of some of the unreduced tapes of Explorer IV. This check revealed that the count rate was between 1000 and 2000 counts/sec† and further substantiates the fact that the counting rates are strongly dependent on geometric latitudes alone.

The minimum shielding around the ionization chamber was 450 mg/cm². Since the minimum shielding around the Geiger tube was 1·2 gm/cm², it was possible for low-energy particles to penetrate the ionization chamber without triggering the Geiger tube. This led to an upper bound of 5 for the ratio of average-to-minimum specific ionization.

In order to arrive at this value, the average specific ionization σ was determined by use of $\sigma = I/J_0$* where J_0 is the total number of particles crossing a sphere of unit cross sectional area, and I is the ionization within the sphere[3].

The upper bound of σ occurred for the maximum value of I and the minimum value of J_0. These variables would become extreme values if all the radiation was sufficiently hard to penetrate 5 gm/cm² shielding, but not hard enough to penetrate 20 gm/cm² shielding. In this case, the omnidirectional geometrical factor was 0·705 cm² and, assuming an efficiency of 85 per cent for detection of the radiation, the omnidirectional intensity[2]

$$J_0 = 1200/0{\cdot}85 \times 0{\cdot}705 = 2000 \text{ c/s}.$$

Maximum value of I was obtained by observing that 12 per cent of 4π solid angle was completely shielded from radiation. Increasing the maximum value of I by 12 per cent yields 1·45 r/hr. Thus,

$$\frac{I}{I_m} = 6{\cdot}86 \times 10^3 \frac{1{\cdot}45}{2000} = 4{\cdot}97.$$

It is interesting to note that this value of specific ionization implies that β (the ratio of the velocity of the particles to the velocity of light) of the particles responsible for the ionization is approximately 0·45. Such a low value for β excludes the singly-charged small-mass particles as the predominant species which gave rise to the observed ionization, because these particles would not have sufficient energy to penetrate the walls of the ionization chamber at its minimal areal density. For example, an electron with a β ratio of 0·45 has less than 80 keV kinetic energy. Thus it is more likely that

* Geomagnetic coordinates were determined from the 1955 *Dip Equator*, U.S. Navy Hydrographic Office.

† C. E. McIlwain, verbal communication.

* This formula may be related to roentgen per hour by noting that 1 r/hr = $5{\cdot}8 \times 10^5$ ion pair/sec cm³ air STP, and that for a sphere of unit cross sectional area (vol = 0·77 cm³) $I = 0{\cdot}77 \times 5{\cdot}8 \times 10^5$ r. Thus, $\sigma/\sigma_m = 6{\cdot}86 \times 10^3$ r/J_0, where J_0 has units of count/cm² sec, and σ_m, the minimum specific ionization in air, is taken as 65 ion pair/cm air STP.

the more massive particles, probably protons with an average energy of 120 MeV, are the predominant species which gave rise to the observed ionization.

REFERENCES

1. A. Rosen, C. P. Sonett, P. J. Coleman, Jr. and C. E. McIlwain, *J. Geophys. Res.* **64**, 709 (1959).
2. J. A. van Allen, C. E. McIlwain and G. H. Ludwig, *J. Geophys. Res.* **64**, 271 (1959).
3. H. V. Neher, "Recent Data on Geomagnetic Effects", *Progress in Cosmic Ray Physics*, Vol. IV, p. 245. North Holland Publishing Co., Amsterdam, Holland (1952).

ERRATUM

A. S. JURSA, Y. TANAKA and F. J. LEBLANC, Nitric Oxide and Molecular Oxygen in the Earth's Upper Atmosphere, *Planet. Space Sci.*—**1,** 161 (1959).

The '*P*' and '*R*' designations for the rotational lines in the 5–0 band of O_2 should be reversed throughout the text and in the figures: *P* (15) *R* (13) should read *R* (15) *P* (13), etc.